Analytical characterization of semi-synthetic cannabinoids in Forensics: Detection, metabolism and synthetic origin

Inauguraldissertation

der Philosophisch-naturwissenschaftlichen Fakultät

der Universität Bern

vorgelegt von:

Willi Schirmer

Leiter der Arbeit:

Prof. Dr. Wolfgang Weinmann

Institut für Rechtsmedizin, Universität Bern

Prof. Dr. Stefan Schürch

Departement für Chemie, Biochemie und Pharmazie, Universität Bern

Analytical characterization of semi-synthetic cannabinoids in Forensics: Detection, metabolism and synthetic origin

Inauguraldissertation

der Philosophisch-naturwissenschaftlichen Fakultät

der Universität Bern

vorgelegt von:

Willi Schirmer

Leiter der Arbeit:

Prof. Dr. Wolfgang Weinmann

Institut für Rechtsmedizin, Universität Bern

Prof. Dr. Stefan Schürch

Departement für Chemie, Biochemie und Pharmazie, Universität Bern

Von der Philosophisch-naturwissenschaftlichen Fakultät angenommen.

Bern, 07. Nov. 2025

Der Dekan

Prof. Dr. Jean-Louis Reymond

"Suchen heißt ein Ziel haben. Finden aber heißt frei sein, offen stehen, kein Ziel haben."

Hermann Hesse (1877 -1962), *Siddhartha*

Dedicated to my father Willi Schirmer senior,
to Ilios, and to my dear friend Rouven K.

Acknowledgments

First and foremost, I want to thank my mentor Prof. Dr. Wolfgang Weinmann for accepting me as his PhD student. I am very grateful that I had the opportunity for doing research in these exciting projects at the Institute of Forensic Medicine in Bern. I am highly acknowledging the fact that I was very free in chosing my projects and forming my own collaborations while he was always available for supporting and guiding me. I also want to thank him for giving me the possibility to present my research in various national and international conferences and meetings of The International Association of Forensic Toxicologists (TIAFT), the Society of Toxicology and Forensic Chemistry (GTFCh) and the Swiss Society of Forensic Medicine (SGRM). I grew confident during these conferences, he introduced me to a lot of people, he helped me in establishing an own scientific network and always gave me the opportunity to "network" with other colleagues after the conference talks. I know that this is not a matter of course! The independency and his simultaneous support during the three and a bit years helped me to grow as a researcher and as a human. He gave me a lot during this time and I hope he received something back!

Secondly, I want to thank my supervisor from the Department of Chemistry, Biochemistry and Pharmaceutical Sciences (DCBP), Prof. Dr. Stefan Schürch, for giving me the opportunity in doing a PhD of Science. Without him, I would not have been able to do what I have grown to love so much. He was always open for my concerns and supported me everytime with his guidance. I am very grateful for the scientific discussions and the feedback he gave me.

I am very grateful to Dr. Götz Schlotterbeck for kindly agreeing to serve as the external referee, it is very appreciated. I also want to share my thanks to Prof. Dr. Christoph von Ballmoos, who is gratefully acknowledged for serving as the head of the examination committee.

I want to thank Prof. Dr. Volker Auwärter and Dr. Julia Kaudewitz from the University Medical Center Freiburg for the collaborative work during my first year as a PhD student. Furthermore, I am also very grateful for the interesting discussions during the conferences and the possibility to visit your lab and learn there. My thanks are therefore also shared to Martin Scheu and Annette Zschiesche for their help during the visit.

I would like to thank Dr. Martina Vermathen, Dr. Ilche Gjuroski and Prof. Dr. Julien Furrer from the DCBP for the collaboration we have started. I learned a lot during this time and I am very grateful for the discussions and work you have put in our project. It is astonishing what kind of spectra you can measure from homeopathic amounts of substance!

I am very grateful that I got the opportunity doing a part of my research in the United States. My thanks goes to the Vice-Rectorate International and Academic Careers of the University of Bern for granting me the "UniBE Short Travel Grant for (Post)Docs", which covered for my stay abroad. I learned a lot during the eight weeks at the Center for Forensic Research and Education near Philadelphia and was given a very warm welcome. Great thanks goes to Dr. Alex Krotulski, Sara Walton and Dr. Barry Logan for working with me during this time and introducing me to the staff. I have met a lot of great people there, my thanks goes to the staff too for the help in and outside the laboratory.

I would also like to thank Lisa Höfert from the University of Leipzig for the ongoing cooperation we have established and for the fruitful discussions at various conferences. Many thanks goes to Christian Bissig from the Zurich Forensic Science Institute for sending me reference material and for the many scientific discussions. I would also like to thank Dr. Sebastian Hamer and Dr. Folker Westphal from the Bureau of Criminal Investigation Schleswig-Holstein for the discussions at the Mosbach conference in 2025. Furthermore, I would like to thank Dr. Benedikt Pulver from the University Medical Center Freiburg for the discussions and inputs he shared with me at various conferences. Furthermore, I want to thank Dr. István Ujváry from iKem BT for the scientific exchange. My gratitude goes to Prof. Dr. Henrik Gréen from Linköping University for the discussions.

Many thanks goes to the group of Forensic Toxicology and Chemistry in Bern for welcoming me as one of you, for helping me in the lab and with the instruments, and for the countless talks with everyone of you. Thanks goes to Dr. Stefan König, Dr. Marie Martin, Andreas Längin, Petra Kindler, Severine Krönert, Sidonia Guggisberg, Anita Iannone, Thomas Wüthrich, Alain Broillet, Luiz Faccani, Simon Vonarburg and Nadja Utiger. I also want to thank my colleagues who endured me during this time and for the countless scientific and not-so-scientific discussions. Thanks goes to Dr. Frederike Stöth, Gaia Alluisetti, Joel Brügger and Severin Zemp. My special thanks goes to my colleague Matthias Bantle, with whom I spent most of my time during my research work. Thank you for all the conversations and memories, one could not wish for a better colleague!

I would also like to take this opportunity to express my gratitude the generosity of the Institute of Forensic Medicine in Bern for its generosity in approving and financing the various conference meetings. My gratitude goes to Antoinette Angehrn, Merita Wohlgensinger, Sarah Menge and to our director, Prof. Dr. Christian Jackowski.

My thanks go to Isabelle Mösch, who I have supervised during her practical training in our lab. I know you learned a lot during this time and I wish for you the very best, wherever your future paths will take you. Thank you very much for your help during my projects, you did very well. Do not be afraid to express yourself, you are a formidable student, thank you!

I also want to share my thanks to Dr. Pascal Küpfer, Denise Morgenegg, Therese Schneuwly-Schär and Adrian Schindler from the DCBP. I enjoyed giving practical courses for the chemists and the pharmacists, not so much for the medical students. I would also like to thank the numerous students, which I have supervised in the lab, I hope you still remember something from the courses. I had a great time teaching you sense and non-sense! Thank you for the beer and farewell cards, they were very much appreciated!

Further thanks goes to Dr. Remo Arnold and Alain Rieder for the regular discussions during lunch.

A big thank you is dedicated to Heinz Laska and Thomas Fuhrer, who encouraged me in my early years in going further and studying chemistry. Thank you very much, I never regretted this decision!

I am very grateful to Dr. Vanessa Hofmann for proof-reading my thesis and correcting my English. Thank you very much for the countless occasions you have made endurable, especially during monotonous speaches at different meetings and conferences. I very much enjoyed our discussions, especially these after the conference talks, which were catalyzed by EtOH. Thank you!

Rainer Winkler is acknowledged for the entertainment in the last few years, I want to thank Tom, Flo, Oli and Arthur for their accompaniment during our pilgrimage. Further thanks goes to my close friends Erico, Shpetim, Simi, Mischu, Auer, Koni, Jan, Annika, Cedi, Tobi, Fabri, Robin, Cindy and another Koni for the countless discussions and the time we have spent and enjoyed together. Furthermore, I want to thank Linda Kuster for her support. Ulimately, I want to thank my siblings Ivo "Kiki" and Solida "Solibous", and my dear mother for their unconditional support and love through all these years. Thank you!

Abstract

In mid 2022, hexahydrocannabinol (HHC) emerged as an unregulated, legal substitute for cannabis. HHC is a hydrogenated derivative of the main psychoactive compound found in cannabis, Δ^9-tetrahydrocannabinol (Δ^9-THC), which also shows psychoactive effects in human. It was therefore commonly abused and set new challenges for forensic investigators due to its novelty. Prior 2023, only scarce information about the detection and metabolism of HHC were available. After the regulation of HHC in Switzerland in April 2023, other semi-synthetic cannabinoids emerged, which were even more potent, such as hexahydrocannabiphorol (HHCP) or Δ^9-tetrahydrocannabiphorol (Δ^9-THCP). These potent successors shared the same core structure, but they have a longer side chain. Distributors of these products claim that they are obtained from the cannabis plant or from extracted cannabidiol (CBD). Two distinct products were investigated to get an insight into the synthetic procedures. A product that was declared as pure HHCP wax (**Publication I**) and a vape pen, which contained 10% Δ^9-THCP according to the labeling (**Publication II**).

After initial GC-MS analysis of the HHCP wax, it was found that this recreational product contained several compounds with mass spectra similar to or indistinguishable from HHCP. Six compounds were isolated from the wax using flash column chromatography and their structures were elucidated by NMR. Besides the main compound (9*R*)-HHCP, the side products *iso*-HHCP, *cis*-HHCP, *abn*-HHCP, and two α,β-unsaturated ketone intermediates were identified. The isolated products were derivatized using *R*- and *S*-mosher acid chloride and analyzed by GC-MS. Besides *iso*-HHCP, the isolated compounds were enantiopure. Furthermore, a fraction was collected that contained bisalkylated cannabinoids, which are common side products in total synthetic approaches for the synthesis of phytocannabinoids. The presence of the intermediates indicated that a derived route from Tietze et al. for the synthesis of HHC has been used.

The vape pen, which contained Δ^9-THCP was analyzed by GC-MS and it was found that this product contained several compounds with mass spectra similar to or indistinguishable from Δ^9-THCP. Besides Δ^9-THCP, the vape pen liquid contained cannabiphorol (CBP), cannabidiphorol (CBDP), Δ^8-THCP, and 5-heptylresorcinol, which were confirmed by comparison with reference standards. Additionally, four other compounds were tentatively identified by comparison with mass spectra from THC analogs, these were 8-oxo-Δ^9-THCP, *cis*-Δ^9-THCP, 7,8-dihydrocannabidiphorol, and 6a,10a-dihydrocannabiphorol. Furthermore, the vape pen liquid also contained a fraction with bisalkylated cannabinoids, which are commonly found in total synthetic approaches of phytocannabinoids. The compounds Δ^9-THCP and 5-heptylresorcinol were isolated from the vape pen by flash column chromatography. The isolated Δ^9-THCP was derivatized with mosher acid chloride and it was found that this compound was enantiopure, too. The presence of 5-heptylresorcinol, a homolog of olivetol, indicates that this product was synthesized by using a total synthetic approach

as olivetol is a known precursor for the total synthesis of Δ^9-THC. It is however unclear which other starting material has been used as several terpenes can be used for the total synthesis. This vape pen liquid contained various unspecified terpenes, presumably for olfactory and sensory reasons.

In order to prove the abuse of new emerging substances, analytical targets have to be identified, which are the abundant and characteristic metabolites of these new compounds. As another topic, this thesis describes the identification of Phase I and II metabolites of the semi-synthetic cannabinoids HHC (**Publication III**), HHCP (**Publication IV**), and tetrahydrocannabidiol (H4CBD, **Publication V**) in human urine. These studies involved one or two volunteers who ingested a small amount of the semi-synthetic cannabinoids and collected urine over the course of up to three days. The Phase I and II metabolites were identified using LC-QqTOF. The Phase I metabolites were also analyzed after trimethylsilylation with *N*-methyl-*N*-(trimethylsilyl)trifluoroacetamide (MSTFA), and sensitive detection methods for the Phase I metabolites were developed using LC-QqLIT.

For HHC, it was found that the most abundant Phase I metabolites were side chain hydroxylated metabolites. The main metabolite was tentatively identified as 4'OH-HHC. Besides 4'OH-HHC, both epimers of 11-OH-HHC have been found to be abundant metabolites and therefore good analytical targets. The epimers of 11-nor-9-carboxy-HHC (HHC-COOH) and (8*R*,9*R*)-8-OH-HHC were identified as minor metabolites. Further metabolites with hydroxylation positions on the alicyclic moiety or on the side chain were detected but their structures were not elucidated. The detected Phase II metabolites were glucuronides of HHC and its hydroxylated structures.

In the case of HHCP, the identified Phase I metabolites were mainly mono- and bishydroxylated metabolites. Hydroxylation was observed on the alicyclic moiety and/or the side chain. The bishydroxylated Phase I metabolites were more abundant than the monohydroxylated metabolites, indicating that cannabinoids with a longer side chain undergo further metabolisation. The most abundant Phase I metabolites of HHCP were two bishydroxylated metabolites, which showed a hydroxylation position on the side chain and another one on the alicyclic moiety of the molecule. Phase II metabolites were glucuronides of HHCP, which were formed to a lesser extent, and the glucuronides of Phase I metabolites. After HHCP ingestion, the urine samples were tested negative with homogeneous enzyme immunoassay tests designed for Δ^9-THC. This indicates that positive cases for HHCP might remain undetected in routine case work.

After the ingestion of H4CBD, deglucuronidated urine samples revealed several hydroxylated Phase I metabolites in high abundance, and bishydroxylated and carboxylated Phase I metabolites in low abundance. The carboxylated metabolites 7-COOH-H4CBD and 5"COOH-H4CBD, as well as the hydroxylated metabolites (1*R*,6*R*)-6-OH-H4CBD, (1*R*,6*S*)-6-OH-H4CBD, 2"OH-H4CBD and both epimers of 7-OH-H4CBD were tentatively identified. The Phase II metabolites were glucuronides of

H4CBD and of its Phase I metabolites. ESI+ product ion mass spectra of H4CBD and its side chain hydroxylated Phase I metabolites showed very uncommon fragmentation patterns. In some cases, loss of both oxygens from the resorcinol unit was observed. The corresponding Phase II metabolites showed degradation of the glucuronide moiety to form furanyl radical cations. This emphasises the necessity that mass spectra of newly emerging compounds and their metabolites have to be investigated carefully as they might not just show shifted signals in respect to a well-known derivative.

With the emergence of new semi-synthetic cannabinoids, detection methods have to keep up to date. **Publication VI** describes the development and validation of a qualitative screening method for the detection of semi-synthetic cannabinoids in human blood by LC-QqTOF. This method covers 24 different phyto- and semi-synthetic cannabinoids with recovery rates ranging from 87-118%, matrix effects ranging from 24-93% and limits of detection ranging from 0.8-16 ng/mL. During the development of this method, it was observed that more hydrophobic analytes showed non-specific binding to glass vials, which led to diminished or even complete loss of detection signals. The initially used glass vials did not show this behavior for the analysis of phytocannabinoids and their metabolites, and finally switching to polypropylene vials solved this issue. Further preanalytically investigations should be carried out, as this issue can occur when physiological samples are stored in unsuitable containers with the consequence of analyte loss remaining unnoticed.

Contents

1 Introduction

1.1 Cannabis and phytocannabinoids

Cannabis is a flowering plant from the family of the *Cannabaceae*, which were already present in Central Asia near the Altai Mountain about 12'000 years ago. From there, it found its way all around the world through domestication.[1,2] Cannabis was versatily used. The flowers provided by unfertilized female plants (ganja sinsemilla, marijuana) or their resin glands (charas, hashish) were used for medicine and mind-altering drugs. Seeds of the cannabis plant were used for the production of oil as well as food or animal feed. The stems of the plant deliver long, resiliant fibers and were used for cordage to provide tows and ropes, or were formed to a pulp for the production of paper. The leaves were used as fodder and mulch.[3,4] Today, cannabis is mostly associated with recreational drug consumption because it is the globally most widely used illicit drug. The United Nations Office on Drugs and Crime (UNODC) states that 244 million people have used cannabis in 2024, roughly 4.6% of the worlds population aged between 15 and 64.[5] According to the European Union Drug Agency (EUDA), formerly known as the European Monitoring Centre for Drugs and Drug Addiction (EMCDDA), it is estimated that 24 million people in the European Union (EU) used cannabis in 2024, which is 8.4% of the EU population aged between 15 and 64. Furthermore, it is estimated that approximately 1.5% of the adult European population are daily or almost daily cannabis consumers.[6] In Switzerland, 7.6% of the population aged between 15 and 64 have consumed cannabis in 2022.[7]

To date, cannabis remains prohibited for recreational use in most countries worldwide. Only nine countries and some US States have legalized the recreational use of cannabis. Switzerland does not belong to these countries, but the use of cannabis is decriminalized. Cannabis is legal if the content of Δ^9-THC is below 1.0% by dry weight.[8] However, possession of up to 10 g of cannabis with a higher Δ^9-THC content is considered legal as long it is only carried and not consumed.[9,10]

Currently, over 550 different compounds have been identified in the cannabis plant. Of these, 125 are classified as cannabinoids, which are terpenophenolic compounds. Since they originate from the plant, they are commonly referred to as phytocannabinoids.[11,12] The two most abundant phytocannabinoids are Δ^9-tetrahydrocannabinol (Δ^9-THC), which is the main psychoactive compound in the plant, and cannabidiol (CBD), which does not show psychoactive properties. In the plants, they occur mainly as their inactive precursors Δ^9-tetrahydrocannabinolic acid A (Δ^9-THC acid A) and cannabidiolic acid (CBDA), which are decarboxylated by heat.

Δ^9-THC was first discovered from the acidic catalyzed cyclization of CBD using either diluted HCl in EtOH or H_3PO_4 in EtOH. The same reaction using CBD with dry pyridinium HCl resulted

in another THC isomer; Δ^8-THC.[13] The structures of the THC isomers were not initially determined correctly, but it transpired that the THC isomers prepared by Adams et al. were in fact Δ^9-THC and Δ^8-THC.[14] Structural elucidation relied on degradation studies before nuclear magnetic resonance spectroscopy (NMR) was invented and established. It was in 1964 when Gaoni and Mechoulam elucidated the structure of Δ^9-THC, the main psychoactive compound in cannabis.[15] The psychotropic effects of pure Δ^9-THC were later shown on different animal models. The observed effects included severe motor disturbances, reduced aggression, drowsiness and reduced spontaneous movement activity.[16–18] The content of Δ^9-THC in cannabis for recreational use rose significantly over the years. ElSohly et al. reported that the content of Δ^9-THC in cannabis from the United States rose from ∼4 % in 1995 to ∼12 % in 2014, while the content of CBD decreased from 0.28 % to below 0.15 % in a similar time frame, resulting in a change of the Δ^9-THC to CBD ratio from 14 to 80 times.[19] Recently, the same group reported that the Δ^9-THC and CBD content did not change significantly from 2013 to 2022 in cannabis samples confiscated in the United States.[20] Similar observations have been made in Switzerland. The mean content of Δ^9-THC in marijuana samples analyzed between 1981 and 1985 was 1.4%, whereas cannabis samples analyzed between 2002 and 2003 showed a mean Δ^9-THC content of 12.9%.[21] Until 2023, the mean content of Δ^9-THC in confiscated marijuana samples from Switzerland remained similar.[22] High contents of Δ^9-THC, and high Δ^9-THC to CBD ratios are associated with the development of psychotic symptoms after consumption.[23] However, abother study shows that CBD does not attenuate the psychotic symptoms of Δ^9-THC.[24] Nevertheless, the occurence of developing psychotic symptoms in individuals who consume cannabis is significantly higher when cannabis with a high Δ^9-THC content is consumed.[25]

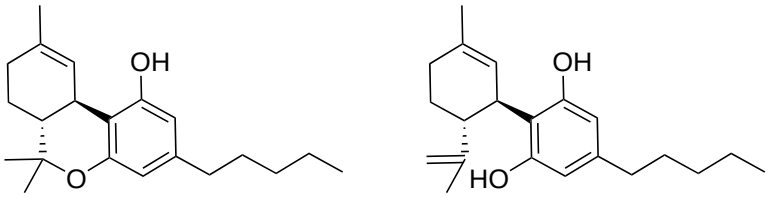

Figure 1: Chemical structures of Δ^9-THC (left) and CBD (right).

In contrary to Δ^9-THC, CBD does not show euphoriant effects. It was first in 1940 when CBD was isolated by two research groups working independently on Minnesota wild hemp and Egyptian hashish.[26,27] It was recognized that, unlike cannabinol (CBN), CBD has two phenol groups and therefore no pyran structure. The proposed structure was based on degradational studies. Adams et al. mentioned that not all structural features of CBD could be assigned with certainty.[28] It was not until 1963 when Mechoulam and Shvo elucidated the correct structure of CBD by NMR.[29]

1.2 Semi-synthetic cannabinoids

In order to mimic the psychoactive effects of Δ^9-THC from the cannabis plant (*Cannabis sativa* L.) other unregulated compounds emerged. Semi-synthetic cannabinoids are a class of compounds that do share the dibenzopyran structure of Δ^9-THC. The first of these compounds were obtained after derivatization of Δ^9-THC. The Δ^9-THC was either isolated directly from the cannabis plant or obtained after acidic catalyzed cyclization of CBD, which is extractable from CBD-rich cannabis.

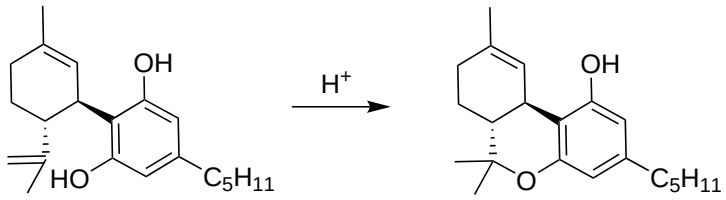

Figure 2: Acidic catalyzed cyclization of CBD to Δ^9-THC.

In 2023, Ujváry and the EUDA reported about the emergence of hexahydrocannabinol (HHC) and related substances. HHC first appeared in Europe (Ireland) in May 2022 and has been identified in 70% of the EU Member States by December 2022. It was sold openly as a legal substitute for marijuana and products containing Δ^9-THC.[30,31]

Since the emergence of semi-synthetic cannabinoids, many methods have been published for the analysis of these compounds and their metabolites. The most applied methods for the analysis are using LC-MS/MS approaches.[32–54] GC-MS and GC-MS/MS approaches have also been widely used for the analysis of semi-synthetic cannabinoids.[47–60] Super critical fluid chromatography coupled to a diode array detector (SFC-DAD) and liquid chromatography coupled to electrochemical detection (LC-ECD) have also been used for the chromatographic analysis of HHC.[61,62] Different immunoassay techniques (HEIA, EMIT, ELISA) have been applied to investigate the cross-reactivity of semi-synthetic cannabinoids and some of their metabolites in Δ^9-THC specific assays.[42–45,63–67]

Even though Δ^8-THC is internationally regulated due to the United Nations Single Convention on Psychotropic Substances from 1971, it is frequently encountered in the United States as a replacement for marijuana and products containing Δ^9-THC.[68] The Agricultural Improvement Act of 2018 (Farm Bill 2018) legalized the sale of cannabis products, which do have a content of below 0.3% Δ^9-THC by dry weight.[69] This definition has a loophole, as cannabis products for the recreational use can be sold legally as long as the product mainly contains Δ^8-THC or other plant-derived cannabinoids that have a psychoactive effect.[70] Due to its scheduling in the United Nations Single Convention on Psychotropic Substances from 1971, Δ^8-THC was not frequently encountered as a psychoactive substitute for cannabis outside the United States. Outside the United States, Δ^8-THC is found as its acetate ester (Δ^8-THC acetate, Δ^8-THC-O) and other esters such as its methyl carbonate, as these compounds circumvent the narcotics law in certain countries.

1.2.1 Legal situation in Switzerland

In Switzerland, salts, esters, ethers, carbamates and stereoisomers of drugs, which are listed in the Narcotics Schedule Ordinance (BetmVV-EDI) are treated like the drug itself and therefore illegal. Furthermore, all other THC isomers, like the minor phytocannabinoid Δ^8-THC, are regulated in Switzerland and therefore no grey market has evolved for THC isomers, or their esters and ethers. As mentioned before, Switzerland legalized CBD products with a content of below 1.0% Δ^9-THC in 2011.[8] Even though CBD does not induce psychoactive effects after consumption, it can be used as a precursor for the synthesis of THC isomers. With the emergence of HHC, CBD was used as starting material for the synthesis. HHC was not banned until March 31, 2023, when the Narcotics Schedule Ordinance (BetmVV-EDI) was revised. With the ban of HHC, other semi-synthetic cannabinoids like Δ^9-tetrahydrocannabiphorol (Δ^9-THCP) or hexahydrocannabiphorol (HHCP) emerged on the grey market, which were legal at that time. This was quickly changed with another revision of the Narcotics Schedule Ordinance (BetmVV-EDI) in October of the same year. In this revision, a group listing was enacted for compounds sharing the dibenzopyran structure of THC.

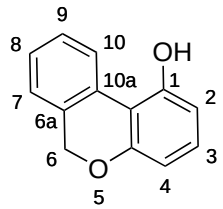

Figure 3: General structure for semi-synthetic cannabinoids as drawn in the Swiss Narcotics Schedule Ordinance (Verzeichnis e, Nr. 303, Synthetische Cannabinoide 2, BetmVV-EDI).

This group list includes all compounds derived from the general structure shown in Figure 3, regardless of the degree of hydrogenation of the non-phenolic benzene ring, and which are substituted with any alkyl groups at the positions 3, 6 and 9. Compounds that are additionally substituted with alkyl-, alkoxy-, hydroxygroups or halogens are also included in this listing.

1.2.2 Health concerns

Reports from intoxication cases with HHC state that they are similar to those of cannabis. Like THC, HHC can induce psychosis in predisposed individuals. The adverse effects range from mild to severe.[6,71–73] Referring to a French study, only 5% of the 26 reported HHC intoxications were classified as severe.[74] A Czech study investigated 196 cases of poisoning with HHC (185 cases) and HHCP (11 cases) and reported that 6% of the poisonings were critical.[75] Severe poisonings are especially known from intoxications with semi-synthetic cannabinoids that contain a prolonged alkyl chain. In June 2024, an outbreak of 31 non-fatal, but severe poisonings have been reported in Hungary. These poisonings were linked to the consumption of gummies containing tetrahydrocannabioctyl isomers (THC-C8). The patients were reported to be in comatose conditions for several days.[76,77] Consumption of HHCP has lead to serious poisonings in Japan and Denmark.[78,79] Also in Denmark, severe poisonings were reported after the consumption of hexahydrocannabioctyl (HHC-C8). In one of the presented cases, a young man was brought to hospital after his father found him unconscious and with froth around his mouth. The man remained comatose for two days and woke up on the third. He showed cognitive and motor impairment for six days and gradually, but not fully regained his functions. The man was discharged after 17 days and reported on a follow-up visit two and a half months after the discharge that he felt fatigued and sluggish for 2-3 weeks after his discharge.[65] Lethal poisonings connected to semi-synthetic cannabinoids were only reported from e-cigarette, or vaping, product use associated lung injury (EVALI). This injury is caused by inhalation of ketene, which is formed through pyrolysis of acetate esters and is therefore not directly linked to the toxicity of the cannabinoids.[80] These vaping products did not only contain acetates of THC and semi-synthetic cannabinoids, but also vitamin E acetate (α-tocopherol acetate).[81–83] Vitamin E acetate is used as an additive to thicken vaping liquids.[84] Even though vitamin E is known as radical scavenger, the consumption of vitamin E shows no beneficial impact on the occurence of lung cancer.[85,86]

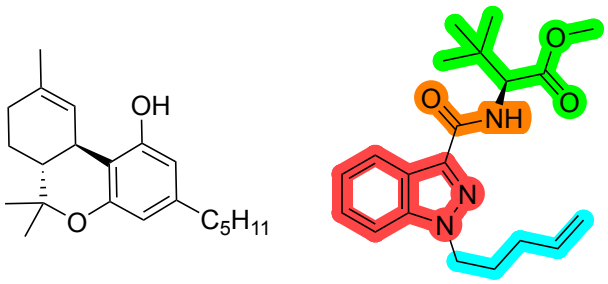

Figure 4: Left: Structure of Δ^9-THC. Right: Structure of MDMB-4en-PINACA, as an example for a synthetic cannabinoid with its structural motifs: linked group (green), tail (blue), core (red), linker (orange).

Due to lacking regulation of these compounds, consumers might unknowingly ingest mislabeled and uncharacterized products.[35,46,60,87–90] To date, no fatal intoxications were reported from the sole use of semi-synthetic cannabinoids. This is contrary to the use of synthetic cannabinoids, which has lead to deaths from overdosing.[91,92] The most synthetic cannabinoids are not structurally related to

phytocannabinoids and are usually potent full agonists on the CB_1 and CB_2 receptors.[93,94] Their structure and naming convention can be described as a connection of four units: a linked group, a tail, a core and a linker.[95] An example is depicted on the right side of Figure 4.

1.2.3 Synthesis of semi-synthetic cannabinoids from CBD or THC

Δ^8-THC, Δ^9-THC and *iso*-THCs

Distributors of products containing semi-synthetic cannabinoids claim that the psychoactive compounds within their products are synthesized from a natural cannabis source, usually CBD.[96] This is likely true for semi-synthetic cannabinoids containing a pentyl side chain as the common THC isomers Δ^8-THC and Δ^9-THC are obtained from CBD after a single step under acidic catalysis. Δ^8-THC occurs only in trace amounts in the plant and is likely synthesized from CBD and not extracted from the plant. Studies have found that Δ^8-THC products contain *iso*-THCs, which are bridged cyclization products of CBD with the cyclic double bond instead of the *iso*-propenylic double bond.[97,98] The *iso*-THCs have first been described as side products after the acid catalyzed cyclization of CBD to Δ^8-THC and Δ^9-THC.[99] The *iso*-THCs have never been described as natural compounds in cannabis and are commonly found in Δ^8-THC products, indicating that these products were made from CBD.

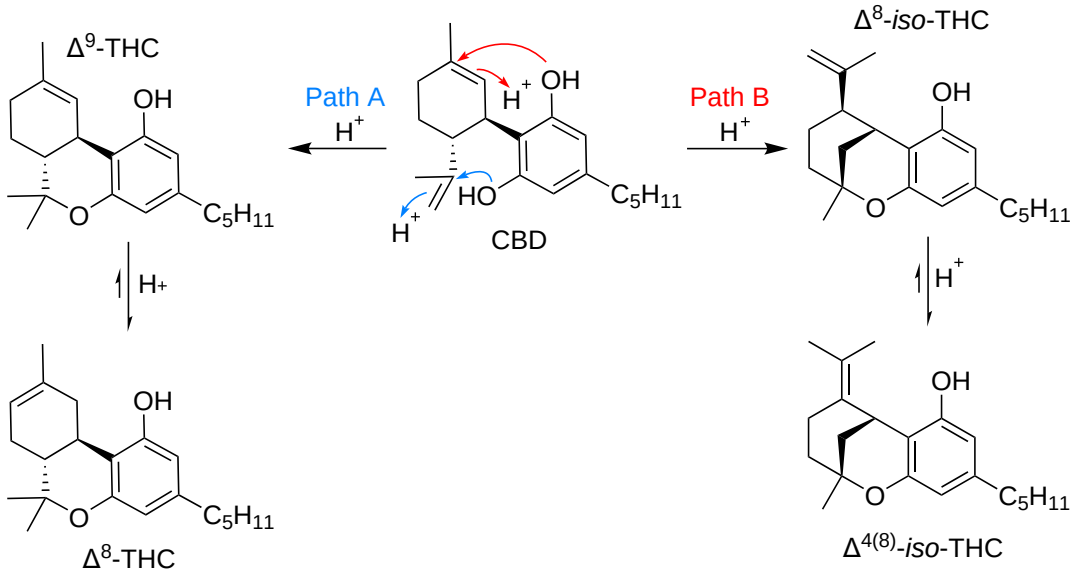

Figure 5: Path A: Acidic catalyzed cyclization of CBD to Δ^9-THC and isomerization to Δ^8-THC. Path B: Acidic catalyzed cyclization of CBD to Δ^8-*iso*-THC and isomerization to $\Delta^{4(8)}$-*iso*-THC.

THC esters and ethers

Outside Switzerland, esters and ethers of Δ^8-THC and Δ^9-THC are popular substitutes for cannabis. The most widespread ester is Δ^9-THC acetate, its synthesis was first described by Gaoni and Mechoulam in 1968 by Einhorn acylation of Δ^9-THC using acetic anhydride under pyridine catalysis.[99] Other THC esters are also obtained via the Schotten-Baumann method or a modification of it. It was recently reported that the propionyl and butanoyl esters of Δ^9-THC emerged on the recreational drug market in Japan.[53] The most recent THC ester is Δ^9-THC methylcarbonate, its synthesis is not described in literature but it can be assumed that it is obtained by acylation with dimethyl dicarbonate under base catalysis, similar to the analog Δ^9-THC *tert*-butylcarbonate.[100] The esters of THC are prodrugs, which are active after enzymatic hydrolysis to THC.[18,101]

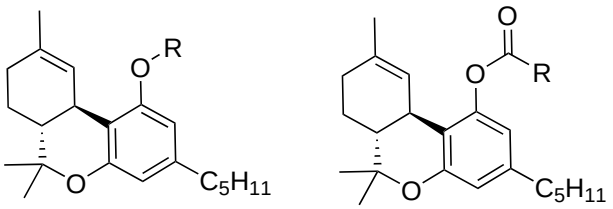

Figure 6: General structure for THC ethers (left) and esters (right). The Δ^9-THC derivatives are depicted.

Ethers of THC are probably not active.[101–103] Contrary to the respective esters, the ethers are not readily hydrolyzed *in vivo*. They are however easily obtained by alkylation of the phenol with an alkyl halide under basic conditions.[103,104] In 2024, Δ^8-THC methyl ether (Δ^8-THC-OMe) was firstly encountered as a designer drug in Sweden.[6]

Other THC derivatives

In early 2025, new THC analogs were reported bearing an allyl or a propenyl group on C2 of the aromatic ring.[55] These compounds are likely products obtained from THC allyl ether after Claisen rearrangement.[105] The synthesis of THC allyl ether is described in the literature.[104]

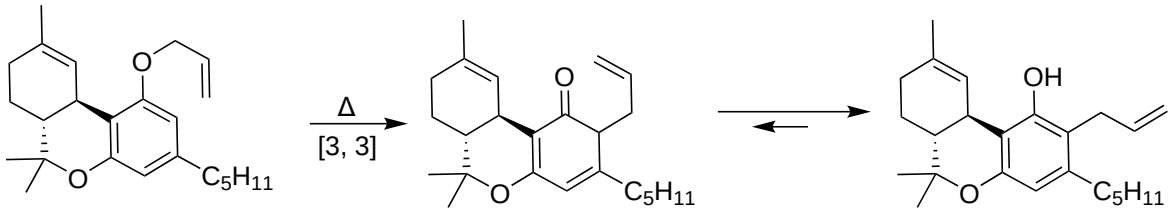

Figure 7: Claisen rearrangement of Δ^9-THC allyl ether to *o*-allyl-Δ^9-THC.

Hydrohalogenated and halogenated derivatives of THC were reported in 2024. The hydrohalogenated THC derivatives 9-chloro-HHC and 9-bromo-HHC were found in Germany and Switzerland.[106] The derivative 9-chloro-HHC potentially lacks any cannabimimetic effects and was first described in literature as an intermediate for the conversion of Δ^8-THC to Δ^9-THC.[107] Since they potentially lack

cannabimimetic activities, one can assume that their purpose is masking illicit THC and recover Δ^9-THC in a later stage. They can also be used for the synthesis of other THC derivatives.

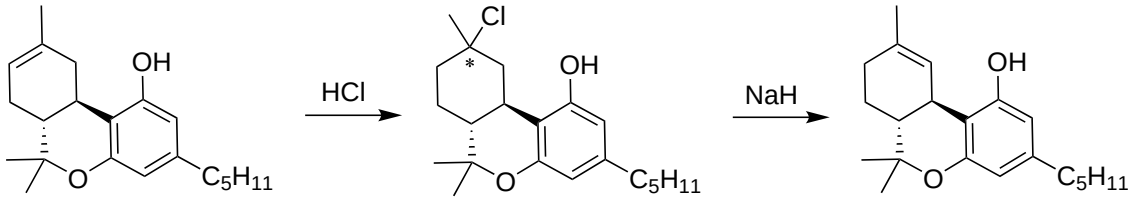

Figure 8: Conversion of Δ^8-THC to Δ^9-THC by addition and subsequent elimination of HCl.

In 2025, mono- and bischlorinated analogs of HHC were reported, which were chlorinated on the aromatic ring.[54] Aromatic halogenation of CBD or Δ^9-THC to mono-, and bishalogenated derivatives can be achieved by the action of a potassium halide and *m*-chloroperoxybenzoic acid (*m*-CPBA) on the cannabinoid in methylene chloride by using 18-crown-6 ether as phase transfer catalyst.[108,109] For the synthesis of monofluorinated cannabinoids another approach using *N*-fluoropyridinium triflate can be used.[110] Some of these halogenated THC derivatives show cannabimimetic effects.[109,111]

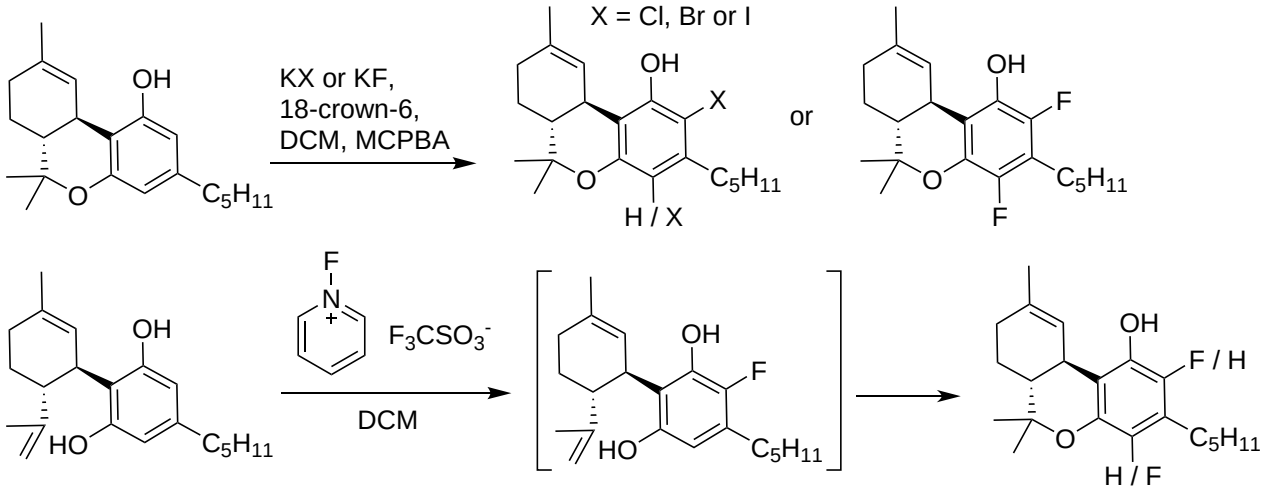

Figure 9: Top: Aromatic mono- and bishalogenation of Δ^9-THC. Bottom: Aromatic monofluoration of CBD and subsequent cyclization to 2-fluoro-Δ^9-THC and 4-fluoro-Δ^9-THC.

HHC and H4CBD

A reason for the rapid rise of HHC is surely its facile synthesis. It is easily obtained by catalytic hydrogenation of THC isomers, mainly from a mixture of Δ^8-THC and Δ^9-THC.[61,112,113] Tetrahydrocannabidiol (H4CBD) is also easily obtained by hydrogenation using CBD as starting material.[61] A recent study has shown that HHC and H4CBD are the most frequently encountered semi-synthetic cannabinoids in recreational products.[35] HHC and H4CBD are obtained as epimeric mixtures of (9*R*)- and (9*S*)-HHC, or (1*R*)- and (1*S*)-H4CBD, respectively. The diastereomeric ratio in HHC depends on the used ratio of THC isomers in the starting material, and on reaction conditions like temperature, and the choice of catalyst or solvent.[61,112,113]

1.2.4 Total synthetic approaches to semi-synthetic cannabinoids

The semi-synthetic approaches that start from CBD or THC as starting material allow modifications of the structure on the phenolic groups, the initial double bond or even on the aromatic ring in rare cases. Alterations on the pentyl side chain of the aromatic rings cannot be introduced at reasonable cost. Distributors still claim that homologs of the previously discussed compounds can be obtained by "fortifying the carbon side chain" of CBD or other obscure explanations. It is assumed that these claims are made for two reasons: First, a loophole in the Agricultural Improvement Act of 2018 (United States) allows the sale of cannabis products as long as the Δ^9-THC content is below 0.3% of the dry weight and as long these products contain hemp derived ingredients. Secondly, it seems to be more advantageous for marketing purposes to claim that a synthetic drug is derived from natural ingredients obtained from hemp rather than being produced in a laboratory.

For the total synthesis of Δ^8-THC or Δ^9-THC, olivetol is the most frequently used starting material. The first stereoselective synthesis of Δ^8-THC and Δ^9-THC was described in 1967. Condensation of olivetol and (–)-verbenol under acidic catalysis using *p*-toluenesulfonic acid (*p*-TSA) leads to an intermediate, which gives enantiopure Δ^8-THC after treatment with BF_3. Addition of HCl and subsequent elimination of HCl with NaH gives the enantiopure Δ^9-THC.[114] A reaction scheme is shown in Figure 10.

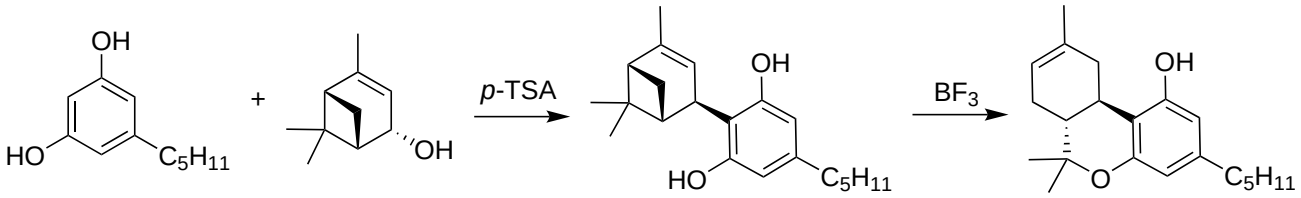

Figure 10: Δ^8-THC synthesis from olivetol and (–)-verbenol. The isomerization of Δ^9-THC to Δ^8-THC is not shown.[114]

Another enantiopure approach by Petrzilka uses *p*-mentha-2,8-dien-1-ol as chiral starting material, which reacts with olivetol to CBD and subsequentally to Δ^8-THC under *p*-TSA catalysis.[115] Using $BF_3{\cdot}Et_2O$ instead of *p*-TSA leads to Δ^9-THC in a single step.[116] Reaction schemes for the *p*-mentha-2,8-dien-1-ol approaches are shown in Figure 11.

Many other approaches are known for the synthesis of THC isomers. Some use a chiral terpenoid like the examples shown in Figures 10 and 11. Some of the terpenoids, which have succesfully been used in the synthesis of THC isomers have been described as natural occurring compounds in the cannabis plant. Other approaches use asymmetric catalysis to obtain the natural THC enantiomers in high yield. The review article of Bloemendal, van Hest and Rutjes gives an overview of synthetic approaches to THC.[117] Further synthesis strategies for the synthesis of saturated cannabinoids like HHC are discussed by Docampio-Palacios et al.[118]

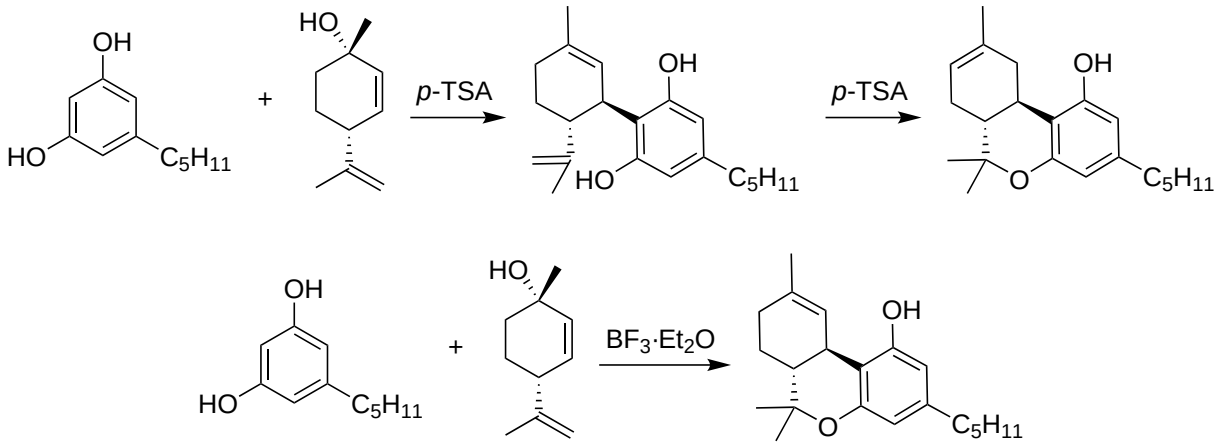

Figure 11: Top: Δ^8-THC synthesis from olivetol and *p*-mentha-2,8-dien-1-ol.[115] Bottom: Δ^9-THC synthesis from olivetol and *p*-mentha-2,8-dien-1-ol.[116]

Homologs of Δ^8-THC, Δ^9-THC and HHC

In 2024, Tanaka and Kikura-Hanajiri reported the occurrence of HHCP in Japan, which was found in vaping liquids.[52] The synthetic methods for Δ^8-THC and Δ^9-THC can be altered to obtain the respective homologs. Since the homologs only differ in the length of the side chain, the olivetol used for the THC synthesis can be exchanged for any 5-alkylresorcinol in order to obtain the desired THC homolog.[119]

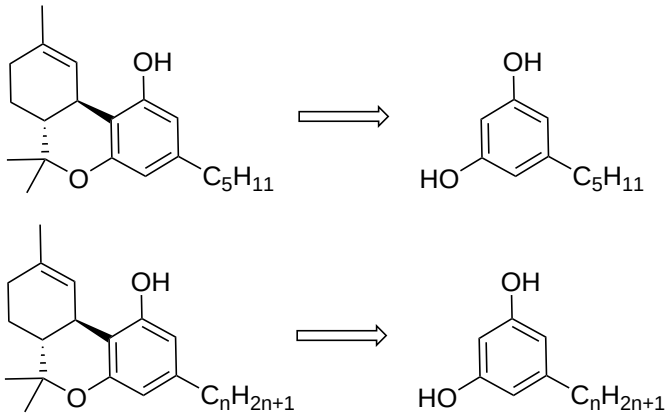

Figure 12: Top: Total synthetic approach to Δ^9-THC from olivetol. Bottom: Total synthetic approach to Δ^9-THC homologs using olivetol homologs as starting material.

In a recent study, the potency of Δ^9-THC homologs with a varying chain length from pentyl to octyl were determined using a β-arrestin-2 recruitment assay. It was found that the potency increased to a maximum for the heptyl derivative Δ^9-THCP. The same behavior was also found for the Δ^8-THC homologs, where Δ^8-THCP was the most potent compound.[120] Similar observations were made in dog ataxia tests with homologs of $\Delta^{6a(10a)}$-THC and HHC ranging from a methyl to an octyl side chain with the exclusion of the ethyl homologs. In both series the most potent compounds were the hexyl homologs $\Delta^{6a(10a)}$-THCH and HHCH.[121,122]

An approach to (9R)-HHC and its homologs is depicted in Figure 13. The Tietze route starts from (R)-citronellal and a 5-alkylcyclohexa-1,3-dione. Aldol condensation of these products leads to an intermediate, which can undergo a Hetero-Diels-Alder reaction to form the dibenzopyran skeleton as an α,β-unsaturated ketone. This cyclization is stereocontrolled through the chiral methyl group from the citronellal moiety leading to the (6aR,10aR)-configuration of the newly formed stereo centers, the same configuration is found in natural Δ^9-THC. Oxidation of the α,β-unsaturated ketone results in the (9R)-HHC homolog. Starting from (S)-citronellal instead, would not lead to (9S)-HHC homologs with a (6aR,9S,10aR)-configuration, but to the enantiomers of (9R)-HHC homologs with a (6aS,9S,10aS)-configuration.[123] A similar one-pot reaction to the homologs of (9R)-HHC uses (R)-citronellal and olivetol derivatives as starting material.[124]

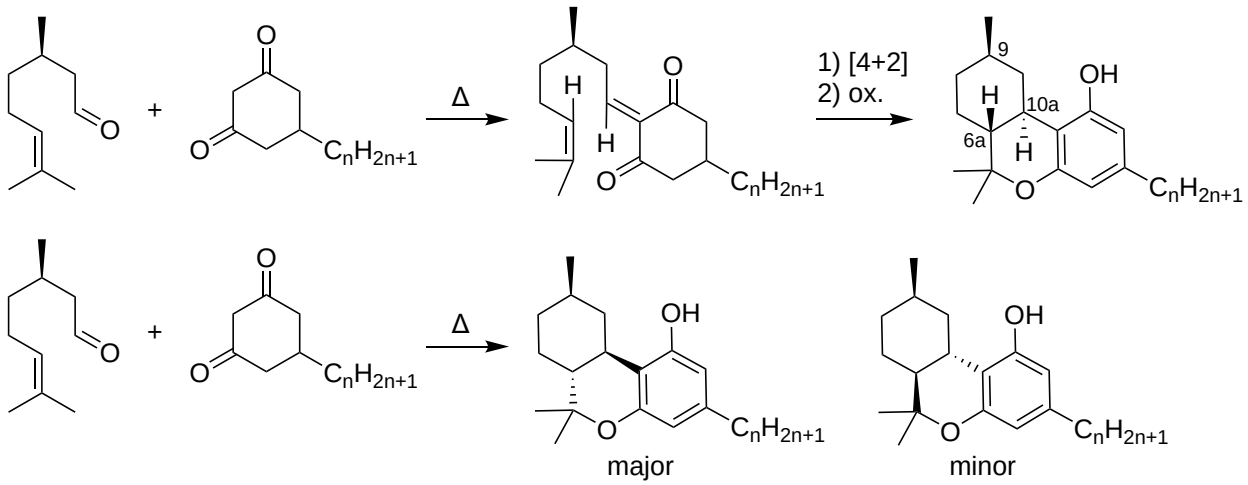

Figure 13: Top: Total synthetic approach to (9R)-HHC and its homologs using the Tietze synthesis.[123] Bottom: Possible explanation for the minor products with (6aS,9R,10aS)-configuration, which are enantiomers of the (9S)-HHC homologs.

Incomplete stereocontrol at the newly formed stereocenters C6a and C10a leads to *cis*-isomers and to the unnatural *trans*-configuration (6a*S*,10a*S*) (see minor product Figure 13). Besides the lack of stereocontrol at the centers C6a and C10a, other possible side reactions lead to abnormal cannabinoids, in which the position of the phenol and the alkyl side chain are exchanged. These compounds are physiologically inactive and have never been described in the cannabis plant.[125] The occurence of *abn*-CBN and *abn*-Δ^8-THC have been described in the total synthesis of CBN and Δ^8/Δ^9-THC.[119] Another possible side reaction is the occurence of bisalkylated compounds, which emerge if two terpene precursors condense with a single olivetol moiety. They have never been described in the plant, but are well-known side products in total synthetic approaches for Δ^9-THC and its analogs.[119,126,127] An overview of possible side products in the synthesis of THC homologs is depicted in Figure 14.

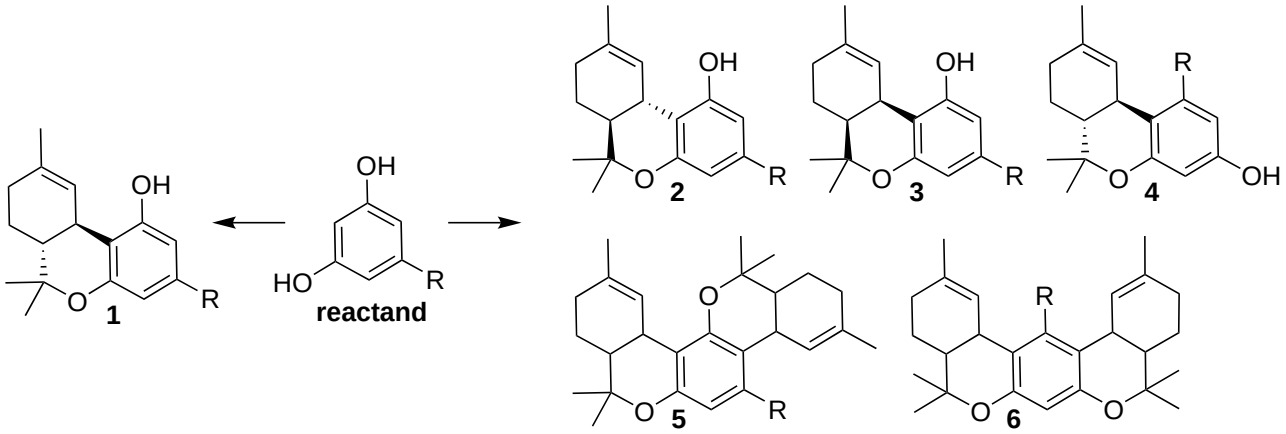

Figure 14: Synthesis of Δ^9-THC homologs from olivetol homologs and undesired side reactions. **1**: (-)-*trans*-Δ^9-THC homolog (desired product), **2**: Unnatural enantiomer of **1** ((+)-*trans*-Δ^9-THC homologs), **3**: (±)-*cis*-Δ^9-THC homologs (both enantiomers), **4**: *abn*-Δ^9-THC homologs (abnormal cannabinoids), **5** and **6**: bisalkylated cannabinoids (stereo centers not defined).

1.3 Metabolism of Δ^9-THC and CBD

Semi-synthetic cannabinoids are structurally related to Δ^9-THC and CBD. It is therefore expected that their metabolic fate is similar to the aforementioned phytocannabinoids. Allylic oxidation of Δ^9-THC by the action of the cytochrome P450 enzymes CYP2C and CYP3A leads to the main metabolites 11-OH-Δ^9-THC and 11-nor-9-carboxy-Δ^9-THC (11-COOH-THC). Allylic oxidation at C8 also takes place leading to the two epimers (8*S*)-OH-Δ^9-THC and (8*R*)-OH-Δ^9-THC. Oxidations on other positions occur as well, involving the pentyl side chain and the olefinic carbons. The side chain hydroxylated metabolites oxidize further to oxo-metabolites that can undergo oxidative degradation of the side chain to form carboxylated metabolites. Epoxidation of the olefinic bond and subsequent hydrolysis results in the formation of 9,10-bishydroxylated metabolites. Phase II metabolites of Δ^9-THC are mainly glucuronidated species, but conjugates with fatty acids, amino acids, glutathione and sulphate have also been observed.[128–130]

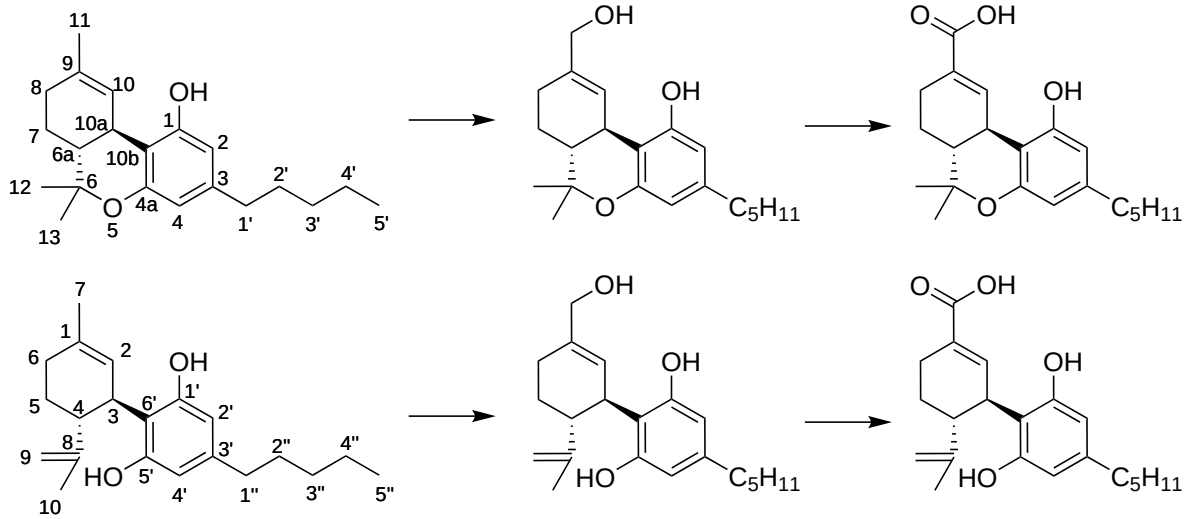

Figure 15: Top: Metabolism of Δ^9-THC to its metabolites 11-OH-Δ^9-THC and 11-COOH-Δ^9-THC. Bottom: Metabolism of CBD to its metabolites 7-OH-CBD and 7-COOH-CBD.

The human *in vivo* metabolism of CBD is similar to that of Δ^9-THC (see Figure 15).[131] In an earlier study, CBD metabolites were identified by GC-MS in the urine of a dystonic patient who received 600 mg CBD each day. The most abundant metabolite of CBD was CBD glucuronide. 7-COOH-CBD was also found in high abundance, this metabolite is formed after allylic oxidation, similar to the formation of 11-COOH-Δ^9-THC from Δ^9-THC. Other abundant metabolites are further oxidation products of 7-COOH-CBD, bearing hydroxyl groups on the side chain and on the *iso*-propenyl group, either after allylic oxidation on C10 or after epoxidation and hydrolysis. Other abundant metabolites are formed after oxidative degradation of the side chain.[132] Side chain hydroxylated metabolites of CBD have been found from *in vitro* metabolism experiments of CBD after incubation with human liver microsomes.[133] The same side chain hydroxylated metabolites have previously been identified from animal studies involving CBD.[134]

1.3.1 Metabolism of (9*R*)-HHC in animal hepatic microsomes

Prior 2023, data on the *in vivo* or the human metabolism of HHC did not exist. The only existing metabolism data were from *in vitro* experiments of (9*R*)-HHC using hepatic microsomal preparations of five different animal models; mouse, rat, guinea pig, rabbit and hamster.[135,136] Eight different hydroxylated metabolites of (9*R*)-HHC were identified; 11-OH-(9*R*)-HHC, (8*S*, 9*S*)-8-OH-HHC, (8*R*, 9*S*)-8-OH-HHC, 4-OH-(9*R*)-HHC, and hydroxylations on all five carbons of the pentyl side chain besides 2'OH-(9*R*)-HHC were found. No information were given about the epimers of 1'-, 3'- or 4'OH-(9*R*)-HHC. The *in vitro* metabolism of (9*R*)-HHC in these hepatic microsomes is very similar to those of Δ^9-THC and Δ^8-THC. It is noteworthy that the amount of the 11-OH metabolite is much less abundant than in the THCs, where it is the main metabolite in all species besides hamster, presumably because this position is not allylic in HHC. Furthermore, the 2'OH metabolite was not found for (9*R*)-HHC, but the aromatic 4-OH metabolite was identified. The epimers of the 7-OH metabolites were only found after incubation with Δ^8-THC, probably because the carbon C7 is allylic in Δ^8-THC. Allylic oxidation by cytochrome P450 is a favored metabolic pathway as the allylic C-H bond strength is low in energy.[137]

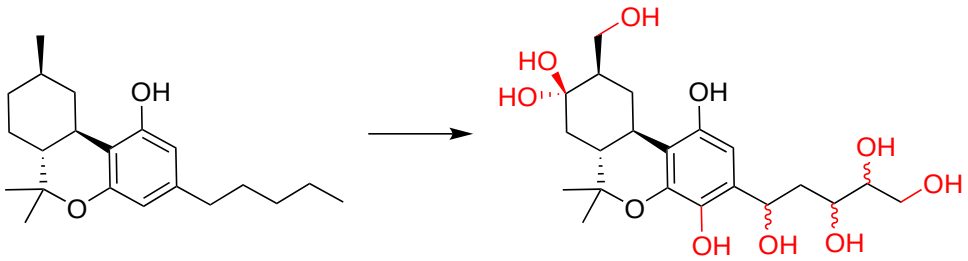

Figure 16: Monohydroxylated metabolites of (9*R*)-HHC found after *in vitro* metabolism with hepatic microsomes from five different animals.[135,136] Only one of the red drawn hydroxy groups is present for each of the eight discovered metabolites.

1.3.2 Metabolism of semi-synthetic cannabinoids

With the emergence of HHC and other semi-synthetic cannabinoids on the recreational drug market, studies have been conducted investigating their metabolism. Forensic-toxicological proof of consumption can only be determined if abundant and characteristic metabolites of the semi-synthetic cannabinoids are known, these can serve as analytical targets. Among the studies, which will be presented later (**Publications III**, **IV** and **V**), research has been conducted investigating the metabolism of HHC and other semi-synthetic cannabinoids. In several studies the metabolites of HHC were identified from physiological samples after controlled administration or from real cases.[36,49] The metabolism of HHC and other semi-synthetic cannabinoids was also investigated from rat samples (urine and feces) and from *in vitro* experiments with pooled human liver S9 fraction, hepatocytes, and liver microsomes.[37,38,50,138] The same HHC metabolites have been found as described in the previous animal studies.[135,136] The major metabolites were 4'OH-HHC, 5'OH-HHC, (8*R*, 9*R*)-8-OH-HHC, 11-OH-HHC and 11-COOH-HHC. It was found that 11-COOH-HHC is also a

metabolite of Δ^9-THC.[39,51] Other groups have shown that the pharmacokinetics of HHC and its metabolites are similar to those of Δ^9-THC and its metabolites, as evidenced by the analyses of oral fluid, serum, and urine samples from volunteers who ingested HHC orally or by inhalation, as well as from rat brain and blood.[45,58,139]

1.4 Mass spectrometry of cannabinoids

In order to understand the fragmentation patterns of semi-synthetic cannabinoids and their metabolites, understanding the fragmentation behavior of phytocannabinoids and their metabolites is crucial. The electron impact (EI) mass spectra of phytocannabinoids and their metabolites, but also of HHC and its hypothetical metabolites are very well understood. The fragmentation mechanisms were evaluated by studying the EI mass spectra of the cannabinoids and several deuterated analogs. It was found that many derivatives, such as the trimethylsilyl (TMS) ethers and esters, have a negligible effect on the fragmentation pathways as they are directed by charge localization distant from the derivatized group. The following reviews give a deep insight into the EI fragmentation behavior of phytocannabinoids and some of their derivatives.[140–143] Fragmentation mechanisms of the cannabinoids under electrospray ionization (ESI) is not that well understood. Several fragmentation mechanisms have been proposed but they have not been fully verified by analyis of various isotope labeled analogs. In fact, fragmentation mechanisms of Δ^9-THC and its metabolites were only elucidated by comparison with a single deuterated analog (Δ^9-THC-D_3), which is commonly used as internal standard for the quantification of Δ^9-THC.[144]

1.4.1 Characteristic fragment ions of THC isomers (EI)

The fragmentation pathway of the THC isomers are similar and lead to some very characteristic ions. Understanding their formation is crucial for identifying their analogs and locating metabolically added functions. A common reaction observed in EI spectra of THC isomers and their TMS derivatives is the loss of a methyl radical, mechanisms are shown in Figure 17. From EI spectra of deuterium labeled THC analogs, it was found that 68% of the ion *m/z* 371 (TMS derivative of *m/z* 299) in Δ^9-THC TMS ether was formed after elimination of a methyl radical from C11. Similar observations were seen for the underivatized Δ^9-THC (see Figure 17, top).[145,146] In Δ^8-THC TMS ether, most of the formed ion *m/z* 371 results from loss of a methyl radical from one of the *gem*-dimethyl groups at C12 or C13 (see Figure 17, bottom).[145,147] In both cases elimination of a methyl radical from the TMS group played a minor role for the formation of the ion *m/z* 371.[145]

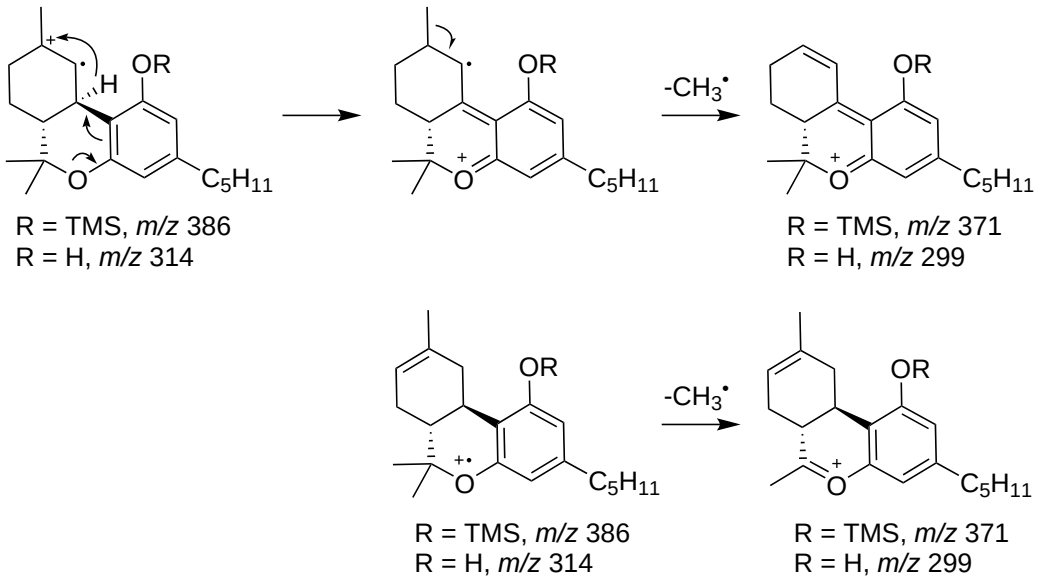

Figure 17: Formation of the ion *m/z* 299 (*m/z* 371 for TMS derivative) in EI spectra of THC isomers. Top: Loss of a methyl radical from C11 in Δ^9-THC. Bottom: Loss of a methyl radical from C12 in Δ^8-THC.

Two different pathways have been suggested for the formation of the ion *m/z* 271. A mechanism in which the *gem*-dimethyl group is eliminated as an *iso*-propyl radical and subsequent ring contraction could lead to the abundant fragment ion *m/z* 271 (see Figure 18, bottom).[140,141] This mechanism involves the abstraction of a hydrogen radical from C10a, which is not supported from deuterium labeled experiments. Another pathway was therefore formulated, which is consistent with observations from deuterium labeled experiments (see Figure 18, top). This mechanism involves the elimination of ethene from the alicyclic moiety and loss of a methyl radical from the *gem*-dimethyl group.[145,147]

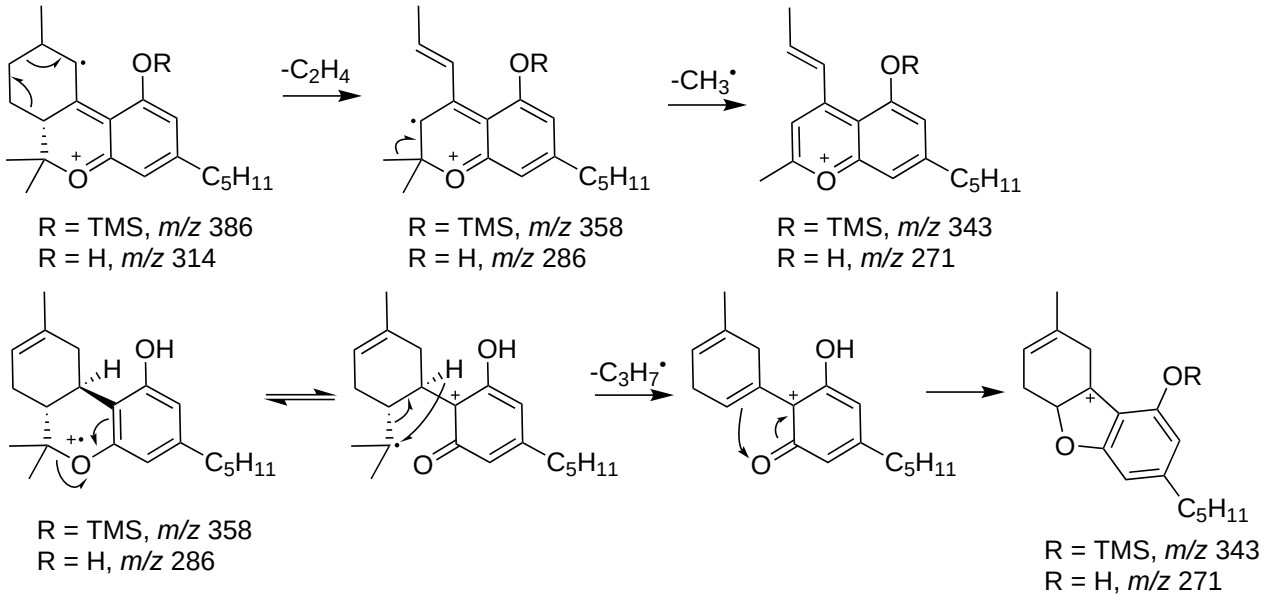

Figure 18: Formation of the ion *m/z* 271 (*m/z* 343 for TMS derivative) in EI spectra of THC isomers. Top: Loss of ethene and a methyl radical in Δ^9-THC. Bottom: Loss of an *iso*-propyl radical in Δ^8-THC.

Another common fragment ion in the EI spectra of THC isomers is the ion *m/z* 258, which is formed after fragmentation of the side chain through a McLafferty rearrangement (see Figure 19).[140,145] This ion is not shifted in THC homologs with a different side chain. It does not appear in the EI spectrum of THC ethyl homologs as these ions do not possess the structural requirement for a McLafferty rearrangement. Usually, further loss of a methyl radical is observed leading to the formation of the ion *m/z* 243.

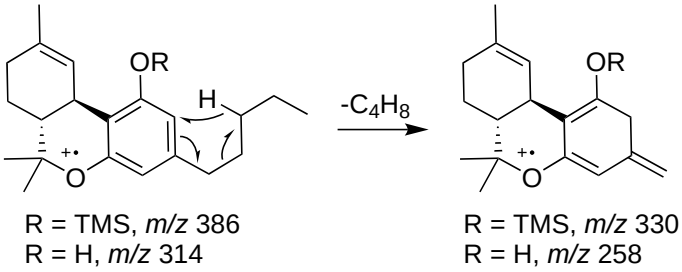

Figure 19: Formation of the ion *m/z* 258 (*m/z* 330 for TMS derivative) in EI spectra of THC isomers after loss of *n*-butene through a McLafferty rearrangement.

The ion *m/z* 231 is another abundant fragment ion in the EI spectra of THC isomers. Its formation in Δ^8-THC can be explained from the elimination of isoprene after a Retro-Diels-Alder reaction, and subsequent elimination of a methyl radical from the *gem*-dimethyl group (see Figure 20).[145] Another mechanism that leads to the same chromenylium ion was proposed, which was not initiated by a Retro-Diels-Alder reaction. This mechanism also contributes to the formation of the chromenylium ion *m/z* 231. It is supported through the abundance of the ions *m/z* 231, 232 and 234, which are found when all six *gem*-dimethyl protons are deuterium labeled. A fragmentation mechanism is shown in the literature.[147]

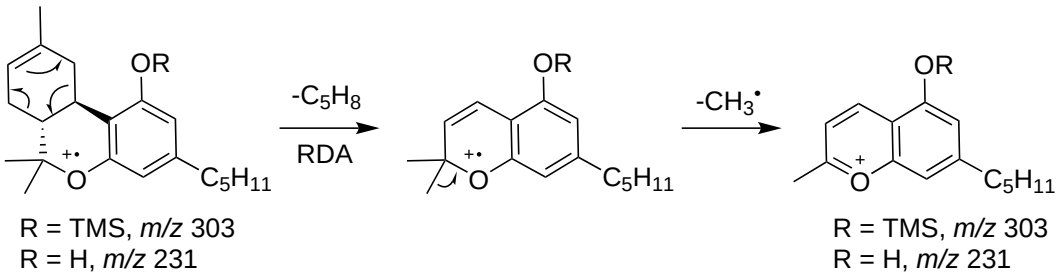

Figure 20: Formation of the ion *m/z* 231 (*m/z* 303 for TMS derivative) in the EI spectrum of Δ^8-THC.

A last characteristic fragment ion is the ion *m/z* 193. Its formation is seen in the EI spectra of THC isomers, HHC, CBD, cannabigerol (CBG), *iso*-THCs and in some of their abnormal isomers. The formation of this ion was only elucidated for CBG and *abn*-CBG through deuterium labeling.[148] Fragmentation mechanisms leading to this ion have been proposed for CBD and HHC.[140,142] The ion *m/z* 193 is a benzylium ion, which is already stable, and rearranges to an even better stabilized tropylium ion (see Figure 21).

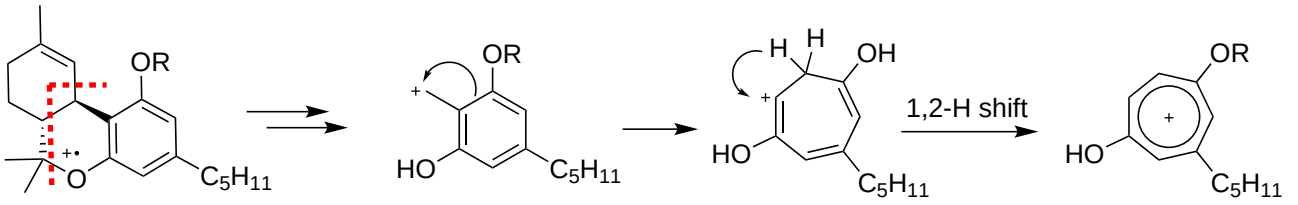

R = TMS, *m/z* 386
R = H, *m/z* 314

R = TMS, *m/z* 265
R = H, *m/z* 193

R = TMS, *m/z* 265
R = H, *m/z* 193

R = TMS, *m/z* 265
R = H, *m/z* 193

Figure 21: Formation and stabilization of the ion *m/z* 193 (*m/z* 265 for TMS derivative) in the EI spectrum of Δ^9-THC.

1.5 Structure-Activity Relationship of Cannabinoids

The psychoactive effects of Δ^9-THC and other cannabinoids are linked to their interaction at the CB_1 receptor.[149] The first structure-activity relationships (SAR) of cannabinoids were conducted in the early 1940s using dog ataxia tests. Good correlation has been found between the relative potency in the dog ataxia test and psychoactive effects in human.[102,150] The mouse tetrad assay is another animal model, which correlates well with the psychoactive potency of cannabinoids in human. This assay consists of four individual tests: analgesia, sedation, catalepsy, and sedation. Presence of these responses is indicative for a compound with cannabimetic effects and agonistic activity at CB_1.[102,150] It was furthermore found that the static ataxia was blocked when the dogs received the CB_1 antagonist rimonabant in addition to Δ^9-THC.[151] Rimonabant also attenuates the effects of Δ^9-THC in human, including the psychoactive effects.[152] The responses in the mouse tetrad assay were clearly attenuated when the mice received rimonabant in addition to Δ^9-THC.[153] This indicates that the static ataxia in dogs as well as the responses in the mouse tetrad assay, and the psychoactive effects in human are caused through action on the CB_1, however it is very likely that different cellular pathways are responsible for these effects.[150]

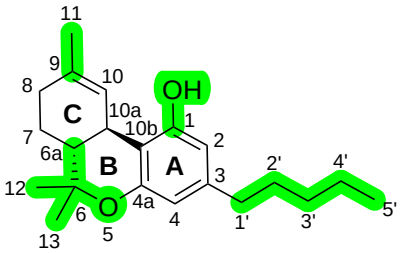

Figure 22: SAR of dibenzopyran cannabinoids. The major CB_1 and CB_2 pharmacophores are highlighted (methyl group C11, B-ring, phenol and side chain).[154]

Since the early 1940s, THC served as scaffold for the investigation of cannabimimetic effects. Even though, the exact structure of the main psychoactive compound in cannabis (Δ^9-THC) was not known until 1963.[29] The dibenzopyran core structure was known and served as template for further studies (see Figure 22). The first SAR studies used different cannabis extracts, racemic homologs of $\Delta^{6a(10a)}$-THC and epimeric homologs of HHC.[121,122,155] Even though it was known that $\Delta^{6a(10a)}$-THC was not the isomer found in THC, it was used for the early investigations.[121] Presumably because it exists as enantiomers and not as a diastereomeric mixture, which facilitated the synthesis.

Nonetheless, the early SAR investigations lacked stereochemically pure compounds, which made interpretation difficult. It was known that the levorotatory $\Delta^{6a(10a)}$-THC ((9*R*)-enantiomer) are physiologically active, because the dextrorotatory compounds did not show any activity in animals, while the racemic did.[156] It was later shown that the (6a*R*,10a*R*)-configuration is required for the psychoactive effects of Δ^9-THC and its derivatives.[157] Modifications on the structural motifs in THC isomers lead to the discovery of the pharmacophores. The earlier studies were performed using different animal models, which correlated well with psychoactive effects in human. Later SAR studies determined the affinities (K_i) or the potencies (EC_{50}) at the cannabinoid receptors CB_1 and CB_2, which were discovered in 1988 and 1993, respectively.[158,159] Affinities however, do not necessarily reflect physiological effects as antagonistic ligands are affine too. In fact, EC_{50} values do also not correlate with *in vivo* potency entirely as different mechanisms are responsible for the observed effect in the assay and *in vivo*.[160] This is also true for semi-synthetic cannabinoids.[161] Furthermore, these assays do not consider the pharmacokinetics as cannabimimetic ligands have to interact with the CB_1 receptors in the brain to show psychoactive effects.[162] The following alterations on the structure of THC discuss the effects in different animal models or the affinity on CB_1, as action on this receptor is responsible for the psychoactive effects of cannabinoids.

1.5.1 Alterations on Ring A

The alkyl group at C3 shows the largest influence on the affinity to CB_1 receptors. At least three carbons are necessary to show cannabimimetic effects, the optimal length for affinity is between five and eight carbons.[102,154] Branching of the alkyl chain shows an influence on the affinity. Methylation at C1' or C2' substantially increases the affinity, while a methyl group on C3' or C4' decreases the affinity. Inserting a methyl group each at C1' and C2' showed even greater affinity at CB_1. The absolute configuration of these newly formed stereocenters has a negligible influence on the affinity. Bismethylation at C1' avoids the issue with designing diastereoselective reactions or tidious separation of them and they show similar affinities at CB_1.[163–166] Branched analogs with a methyl group on the last carbon of the side chain showed no activity, as seen for the *iso*-pentyl and *iso*-hexyl compounds.[167] Up to five-membered alicyclic groups, as well as a dioxolane or dithiolane group on C1' show no decline in CB_1 affinity.[168–170] The analogs with a desaturated alkyl chain show similar CB_1 affinities as their saturated counterparts.[171–173] Some bulky hydrocarbon substituents like bornyl, 1-adamantyl and 1-naphthyl show stronger affinities at CB_1 than the pentyl analogs.[174–176] Some derivatives are depicted in Figure 23. These derivatives show greater affinity at CB_1 than Δ^8-THC.

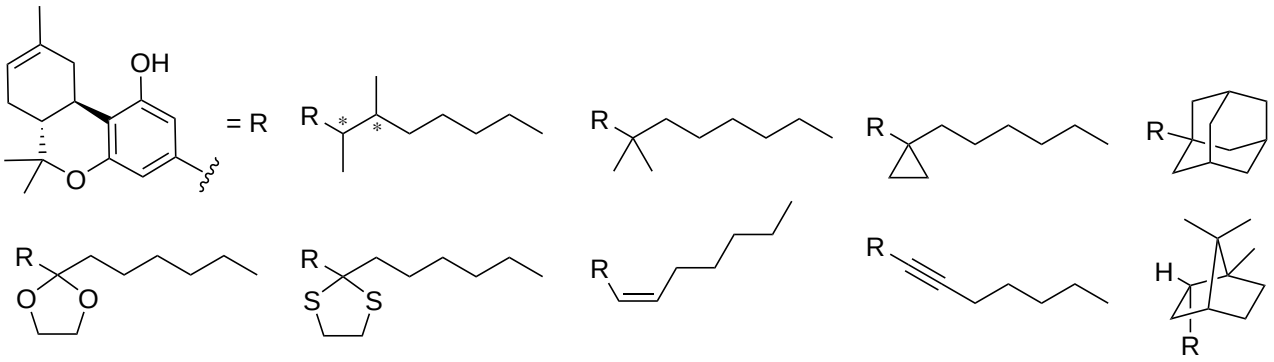

Figure 23: Discussed examples of side chain altered derivatives of Δ^8-THC. Apart from the bornyl derivative (bottom right), it is known that these compounds act agonistic at CB_1.

Tetracyclic analogs of Δ^8-THC show that the conformer with greater CB_1 affinity is the one in which the alkyl group is oriented away from the phenol, the lateral conformer shows a sharp decline in affinity (see Figure 24).[177,178] The preferred orientation of the side chain in the binding pocket can be seen in molecular dockings of Δ^9-THC or its derivative AM11542 with the CB_1 receptor.[179]

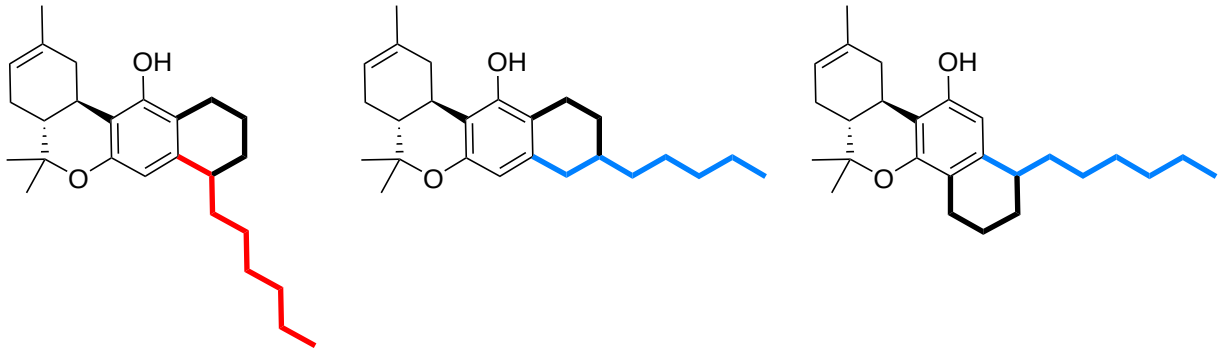

Figure 24: Tetracyclic Δ^8-THC analogs with a fixed alkyl chain. The lateral conformers (blue isomers) show a sharp decline in CB_1 affinity while the isomer that is oriented away from the phenol (red isomer) shows high CB_1 affinity.[178]

The potency declined when the side chain was replaced with an *n*-hexoxy group.[180] Replacement of the carbons C2' and C3' with an ester function showed similar CB_1 affinities like the corresponding alkyl analogs. This is also true when C1' is further functionalized with methyl groups or a cyclobutyl group. The resulting carboxylic acids after *in vivo* hydrolysis through esterases are inactive.[181] Longer carboxylic acids are very weak ligands at CB_1.[182] Similar nitriles, halogenalkanes, amides and hydrazides are well tolerated and show strong affinities at CB_1.[182–187] Secondary amines like morpholin or imidazole, as well as phenol ethers can also be used to terminate the alkyl chain and retain strong CB_1 affinities.[183,186,187] Furthermore, hydroxylation, halogenation, methylation or ethylation at C2 retains cannabimimetic activity. Alkylation at C4 or bishalogenation at C2 and C4 diminishes cannabimimetic activity.[101,109] A phenol group at C1 or a predrug which liberates the phenol *in vivo* seems to be necessary for CB_1 affinity.[102] Interistingly, by methylation of the phenol group or desoxygenation, compounds can be obtained that are strong ligands for CB_2 but barely active for CB_1.[188,189] Replacement of the phenol with an amino group leads to a drop of cannabimietic activity, while substitution with thiol, methylamine or dimethylamine entirely shut

the activity down.[190] The phenol group at C1 forms a hydrogen bond with a serine residue within the binding site of the CB_1 receptor and therefore contributes significantly to the affinity.[179]

1.5.2 Alterations on Ring B

Alterations on Ring B usually lead to decreased potency or inactivity. Changing the *gem*-dimethyl group at C6 to a *gem*-diethyl or *gem*-dipropyl group showed also a sharp drop in potency.[191] Replacing the pyran ring with an oxepane ring decreases the activity drastically, regardless of the presence or position of the *gem*-dimethyl group. Replacement of the *gem*-dimethyl group with an oxo-group results to basically inactive compounds.[192,193] Substitution of the pyran oxygen with an NCH_3 group shut the activity entirely down.[194] Replacement of the pyran oxygen with a NH group and removal of a methyl group from the *gem*-dimethyl moiety can be seen in levonantradol, which is significantly more potent than Δ^9-THC.[195] Levonantradol also exhibits further alterations on the A- and C-Ring, it is therefore not clear to which extent the alterations in the B-ring contribute on its potency. Removal of the B-ring and replacement of the methyl group at C9 with (3*R*)-OH leads to the potent CB_1 agonist CP 47,497.[196] Its C8 homolog, also named Cannabicyclohexanol, was among the first synthetic cannabinoid detected on the recreational product, which was found in the herbal blend mixture 'Spice'.[197] Further functionalisation on the cyclohexanol leads to CP 55,940, which has become the ligand of choice in investigating the endocannabinoid system due to its subnanomolar affinities for CB_1 and CB_2.[198] Some active THC analogs with alterations on the B-ring are depicted in Figure 25.

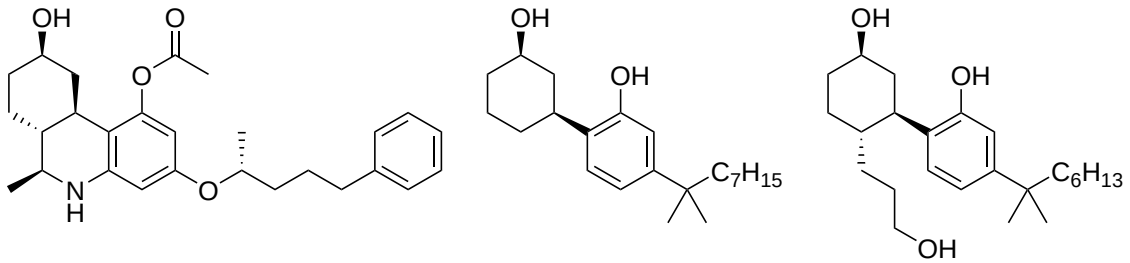

Figure 25: Active THC analogs with alterations on the B-ring. Besides alterations on the B-ring, these compounds show alterations on the side chain and a replacement of the C11 methyl group. Levonantradol (left), Cannabicyclohexanol (middle), CP 55,940 (right).

1.5.3 Alterations on Ring C

Some of the double bond isomers of THC are active at CB_1 and show psychoactive effects. Besides the natural Δ^9-THC, the isomers Δ^8-THC, (9*R*)-$\Delta^{6a(10a)}$-THC and $\Delta^{9(11)}$-THC (exo-THC) are potentially psychoactive.[103] From binding studies one might expect that (9*R*)-Δ^7-THC is psychoactive.[199] The other epimer (9*S*)-Δ^7-THC was reported to be inactive, but later studies with the epimers of Δ^7-THC have shown that both epimers show affinity to the CB_1 receptor.[200,201] Pharmacological investigations are nonexistent for the epimers of Δ^{6a}-THC, a synthetic pathway for the (9*R*) epimer is described in the literature.[202] There is also no pharmacological data on the epimers of Δ^{10}-THC,

but the synthesis is described as well in the literature.[203] The different THC isomers and HHC are shown in Figure 26.

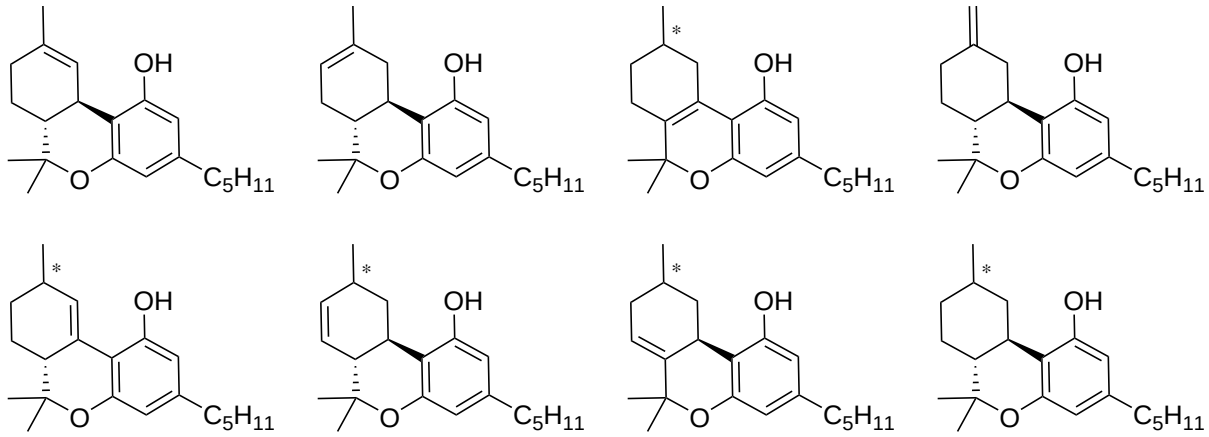

Figure 26: Isomers of THC and HHC. Top: Δ^9-THC, Δ^8-THC, $\Delta^{6a(10a)}$-THC (two enantiomers), $\Delta^{9(11)}$-THC. Bottom: Δ^{10}-THC (two epimers), Δ^7-THC (two epimers), Δ^{6a}-THC (two epimers), HHC (two epimers).

Displacement of the methyl group at C9 to C8 or C10, or the removal of the methyl group showed a significant drop in cannabimimetic potency.[167,191] Removal of the alicyclic ring (Ring C) also leads to a sharp drop in potency.[204] Addition of a second methyl group at C9 or C8 leads to a drop in potency, as did the replacement of the methyl group at C9 with an ethyl group. Whereas the addition of a second methyl group at C7 showed only a slight drop in potency. The hydroxylated Δ^9-THC derivatives that are hydroxylated on C11 and C8 show cannabimimetic potency, the epimer (8*S*)-OH-Δ^9-THC was reported to be slightly active.[205] Further oxidation to the aldehydes showed that only 11-oxo-Δ^9-THC had cannabimietic potency.[102] Hydroxylation at position C8 or C10 of HHC can lead to cannabimimetic compounds. Of the investigated diastereomers only (8*S*,9*R*)-8-OH-HHC and (9*S*,10*S*)-10-OH-HHC showed activity. Both are potential metabolites of the less potent (9*S*)-HHC epimer.[205] Substitution of the methyl group C11 with a hydroxy group in HHC leads to an active compound, the (9*R*)-OH epimer.[206] Further oxidation to an oxo group retains cannabimimetic potency as seen in Nabilone.[207] Replacement of Ring C and the methyl group at C9 with a cycloheptenyl group ((*abeo*)-$\Delta^{6a(10a)}$-THC) leads to potency drop.[208] Replacing Ring C with a cyclopentenyl group showed no cannabimimetic activity.[209] Later experiments with derivatives of the potent dimethylheptylpyran (DMHP) showed that replacement of the Ring C with cyclopentenyl and methylcyclopentenyl, as well as dihydrothiophenyl, methyldihydrothiophenyl and dihydrothiopyran rings retained the cannabimimetic potency.[210,211] If Ring C is replaced with different unsaturated nitrogen heterocycles like tetrahydropyridines, dihydropyrroles or azabicyclooctenes, the resulting compounds lose some potency.[212] Elimination of Ring C and connection of a pyridine ring at position C10a retains some activity as seen in Nonabine.[102] Substitution of C9 with nitrogen can retain activity as seen in the compound Abbott-40174.[212] Replacing Ring C with an azepane, *N*-methylazepane or caprolactam ring can retain some cannabimetic potency.[213] Some active CB_1 ligands with alterations on Ring C are shown in Figure 27.

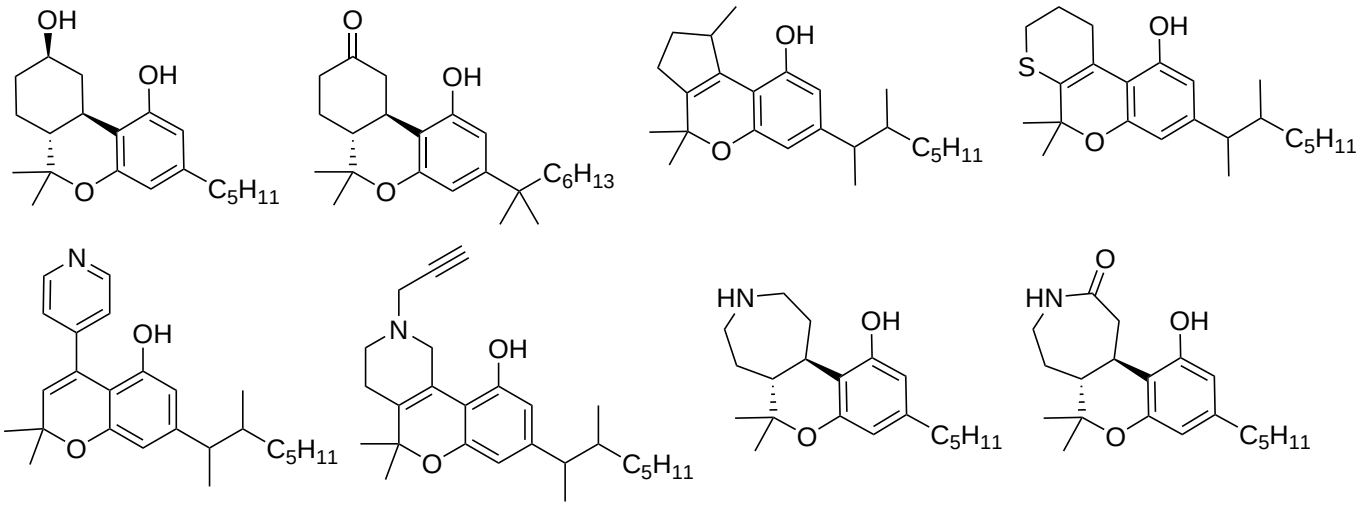

Figure 27: Active THC analogs with alterations in Ring C.

As to date, most of the novel cannabimimetic drugs are compounds that derived from another scaffold and are known as synthetic cannabinoids or synthetic cannabinoid receptor agonists (SCRAs). These compounds were initially developed to increase the polarity in order to become potential medication drugs.[154] Besides their potency, another reason for their popular rise as new psychoactive substance is clearly their facile synthesis. These compounds like JWH-018, initially found in the herbal blend mixture 'Spice', or the more recent MDMB-4en-PINACA do not share the stereoselectivity issues of phytocannabinoids and semi-synthetic cannabinoids. The obtained compounds are either achiral or the stereocenter is already present in a cheap precursor like *tert*-leucine in case of MDMB-4en-PINACA.[214,215] Further information about SAR studies of cannabinoids can be found in the literature.[102,154,216]

2 Results

2.1 Publication I

Isolation and characterization of synthesis intermediates and side products in hexahydrocannabiphorol

Schirmer W., Gjuroski I., Vermathen M., Furrer J., Schürch S., Weinmann W.
Drug Testing and Analysis, **2024**, *17*(4), 531-543
DOI: 10.1002/dta.3759

Description of own contribution

I have initialized and conceptualized this study. Afterwards, I have isolated the compounds, performed the GC-MS experiments and elucidated the structures of the isolated compounds. Dr. Ilche Gjuroski performed the NMR experiments of the isolated compounds. Prof. Dr. Julien Furrer, Dr. Martina Vermathen and Dr. Ilche Gjuroski verified the elucidated structures. Dr. Martina Vermathen, Prof. Dr. Wolfgang Weinmann and Prof. Dr. Stefan Schürch helped to finalize the manuscript. Dr. Stefan König measured the samples for the LC-QqTOF experiments and Isabelle Mösch helped with the GC-MS quantification of (9*R*)- and (9*S*)-HHCP in the HHCP product.

Description of novelty

This research paper describes the first investigation, which has shown that semi-synthetic cannabinoids with an alkyl chain length other than pentyl are made through total synthesic approaches. In this work, the synthesis intermediates and side products of HHCP, the heptyl homolog of HHC, were investigated. It was found that the manufacturers of this HHCP product partially followed a derived route from the synthesis of HHC described by Tietze et al.[123]

Reprint permission

Received: 17 April 2024 | Revised: 17 June 2024 | Accepted: 18 June 2024
DOI: 10.1002/dta.3759

RESEARCH ARTICLE

WILEY

Isolation and characterization of synthesis intermediates and side products in hexahydrocannabiphorol

Willi Schirmer[1,2] | **Ilche Gjuroski**[2] | **Martina Vermathen**[2] | **Julien Furrer**[2] | **Stefan Schürch**[2] | **Wolfgang Weinmann**[1]

[1]Institute of Forensic Medicine, Forensic Toxicology and Chemistry, University of Bern, Bern, Switzerland

[2]Department of Chemistry, Biochemistry and Pharmaceutical Sciences, University of Bern, Bern, Switzerland

Correspondence
Willi Schirmer, Institute of Forensic Medicine, Forensic Toxicology and Chemistry, University of Bern, Murtenstrasse 26, Bern 3008, Switzerland.
Email: willi.schirmer@irm.unibe.ch

Abstract

After the Swiss ban of hexahydrocannabinol (HHC) in March 2023, other semisynthetic dibenzopyran cannabinoids emerged on the Swiss gray market. Hexahydrocannabiphorol (HHCP) was the most prominent of them due to its potent cannabimimetic effects, as anecdotal reports from recreational users suggest. In October 2023, a class wide ban of dibenzopyran cannabinoids was introduced in Switzerland to prevent new similar substances from entering the drug market. Various vendors in online shops claim that HHCP is made from CBD, even though they possess different alkyl chain lengths. An HHCP sample was analyzed by gas chromatography coupled to mass spectrometry (GC-MS), showing that a mixture of molecules with the same or a similar molecular mass as HHCP was present. Six different substances could be isolated from this sample using column chromatography. Four phenols ((9*R*)-HHCP, *iso*-HHCP, *cis*-HHCP, and *abn*-HHCP) and two ketones (possible intermediates to (9*R*)-HHCP and *abn*-HHCP) were identified by various nuclear magnetic resonance spectroscopy (NMR) techniques. (9*S*)-HHCP was obtained in an impure fraction. In addition, a fraction was obtained that showed characteristic molecular and fragment ions consistent with bisalkylated products from the synthesis of similar compounds. The presence of abnormal cannabinoids (*abn*-HHCP) and bisalkylated cannabinoids is a confirmation that this sample was produced purely synthetically as initially suspected, as these compounds have not been reported in *Cannabis*. Chiral derivatization of the phenols with Mosher acid chlorides showed that only *iso*-HHCP was present as a scalemic mixture, indicating a good stereocontrol of this synthetic procedure.

KEYWORDS
cannabis, hexahydrocannabinol (HHC), hexahydrocannabiphorol (HHCP), isomeric cannabinoids, Mosher ester

1 | INTRODUCTION

Hexahydrocannabiphorol (HHCP, also named HHCp, HHC-P, or HHC-C7) is a synthetic cannabinoid with a dibenzopyran structure like tetrahydrocannabinol (THC). Like hexahydrocannabinol (HHC) before it was banned, HHCP was also sold as a legal alternative to THC in Switzerland. On October 9, 2023, Switzerland issued a group-wide ban on cannabinoids with a dibenzopyran structure, placing HHCP

and structurally similar compounds under control. This was in response to the legal dibenzopyran-cannabimimetics emerging on the gray market after the ban of HHC on March 31, 2023.[1]

The aim of this work was to identify stereoisomers, synthesis side products, precursors, or the absolute configuration of the HHCP epimers in a product obtained from a German vendor to get an insight about the HHCP on the market. The claim that HHCP and similar dibenzopyran cannabinoids are synthesized from CBD with an alkyl side chain other than pentyl should be verifiable. A synthetic route from CBD is unlikely, as it involves a homologation step of a pentyl chain without functional groups. Synthetic approaches for dibenzopyran cannabinoids from the literature start with a 5-alkylresorcinol or a 5-alkylcyclohexane-1,3-dione with the desired chain length. It is also possible to isolate Δ^9-tetrahydrocannabiphorol (THCP), a minor cannabinoid, from a *Cannabis* strain with higher THCP content and hydrogenate that fraction to obtain HHCP. This, however, is unlikely since the THCP content is still very low, making the process very costly.[2] To the authors' knowledge, neither the potency nor the affinity of HHCP towards the human cannabinoid receptor 1 (hCB_1) is known yet, but anecdotal reports from users suggest that it is more potent than THC. Concerning THCP, it is known that the affinity towards hCB_1 in vitro is 30 times higher than for THC.[3]

2 | MATERIALS AND METHODS

2.1 | Chemicals and reagents

The HHCP sample was bought from an online shop in Germany (52% (9*R*)-HHCP and 21% (9*S*)-HHCP, gas chromatography coupled to mass spectrometry (GC-MS) area-% (not quantified)). *N*-methyl-*N*-trimethylsilyltrifluoracetamide (MSTFA) (≥98.5%), 4-(dimethylamino) pyridine (DMAP) (≥99%), (*R*)-(−)-α-Methoxy-α-(trifluoromethyl)-phenylacetyl chloride ((*R*)-MTPA-Cl), (*S*)-(+)-α-Methoxy-α-(trifluoromethyl)-phenylacetyl chloride ((*S*)-MTPA-Cl), and the alkane standard (C7-C40, 1,000 µg/ml) were purchased from Sigma-Aldrich (Buchs, Switzerland). (9*R*)-HHCP, (9*S*)-HHCP, cannabidiphorol (CBDP), and cannabiphorol (CBP) were purchased from Cayman Chemical (Ann Arbor, United States). Ethyl acetate (EtOAc) (for liquid chromatography), *n*-hexane (for analysis), Na_2SO_4 sicc. (for analysis, Reag. Ph. Eur.), and dichloromethane (DCM) (for analysis, Reag. Ph. Eur.) were from Grogg Chemie (Stettlen, Switzerland). Methanol (MeOH) (≥99.9%) was from Carl Roth (Karlsruhe, Germany). Silica gel 60 (0.015–0.04 mm) from Macherey-Nagel (Önsingen, Switzerland) was used. Deuterated chloroform, $CDCl_3$ (99.80% D), was purchased from Eurisotop (St.-Aubin Cedex, France) and used as solvent for the nuclear magnetic resonance spectroscopy (NMR) measurements.

2.2 | Chiral derivatization solutions

(*S*)-MTPA-Cl or (*R*)-MTPA-Cl (5 µl) was diluted with 495 µl dry DCM. The solution was kept over Na_2SO_4 sicc.

2.3 | DMAP solution

DMAP (10 mg) was dissolved in 1 ml dry DCM. The solution was kept over Na_2SO_4 sicc.

2.4 | Column chromatographic separation

A part of the HHCP sample (250 mg) was separated on silica gel starting from *n*-hexane: EtOAc (100:1, V:V) as eluent.[4] The polarity of the eluent was stepwise increased to pure EtOAc. Collected fractions were analyzed by GC-MS. Pure fractions containing the same product were unified and evaporated to dryness.

2.5 | GC-MS analysis

The isolated samples were analyzed using an 8890 gas chromatograph with a 7693A autosampler coupled to a 5977B mass selective detector (Agilent, Basel, Switzerland). Data were acquired with MassHunter Workstation GC/MS Data Acquisition (Version 10.1.49) and analyzed with Enhaced ChemStation (F.01.03.2357) (Agilent). Chromatography was performed on a 5% phenylmethylsiloxane column (HP-5 ms Ultra Inert, 30 m, 250 µm i.d., 0.25 µm film thickness; Agilent J&W). Helium was used as a carrier gas with a constant flow of 1 ml/min. The injection volume was 1 µl in pulsed splitless mode. Oven temperature started at 70°C for 3 min and was ramped with 15°C/min to 290°C and held for 19 min, resulting in a total separation time of 36.7 min. The source temperature was set to 230°C, and the quadrupole temperature was 150°C. EI mass spectra were obtained with an ionization energy of 70 eV. Depending on the experiment, the scan range was set from *m/z* 35 to 450, from *m/z* 35 to 650, or from *m/z* 35 to 800.

2.6 | NMR analysis

The NMR spectra were recorded on Bruker Avance II and Avance NEO spectrometers operating at resonance frequencies of 400.33 and 500.13 MHz for ^{1}H nuclei and 100.66 and 125.76 MHz for ^{13}C nuclei, respectively (Bruker BioSpin AG, Fällanden, Switzerland). The instruments are equipped with a 5 mm dual (^{1}H/^{13}C) probe (400 MHz) and a 1.7 mm triple (^{1}H/^{13}C/^{31}P) TXI microprobe (500 MHz) both with z-gradient coils. All measurements were carried out at room temperature ($T = 298$ K). Acquisition and processing of the spectra were done using the Bruker software TopSpin versions 4.1.4 and 4.0.9. ^{1}H chemical shifts were referenced to the residual ^{1}H resonance of $CDCl_3$ ($\delta^1H = 7.264$ ppm), and ^{13}C chemical shifts were referenced through the ^{13}C resonance of $CDCl_3$ (set to $\delta^{13}C = 77.5$ ppm).

One- and two-dimensional NMR experiments were performed using the Bruker pulse program library (the names of pulse programs are given in brackets). 1D proton spectra were acquired using the standard one-pulse experiment with a 30° flip angle (*zg30*). For structure elucidation, the following 2D experiments were applied: ^{1}H-^{1}H-

COSY using magnitude mode with gradients and purge pulses (*cosygpppqf*), ^{1}H-^{13}C-HSQC with carbon multiplicity editing and echo-antiecho acquisition mode (*hsqcedetgpsisp2.3*), ^{1}H-^{13}C-HMBC with low-pass J-filter to suppress one-bond correlations and magnitude acquisition mode (*hmbclpndqf*), and ^{1}H-^{1}H-NOESY in phase sensitive mode using a mixing time of 300 ms (*noesygpphpp*).

^{1}H and ^{13}C chemical shift prediction was performed using the ChemDraw software, version 20.0.0.41 (PerkinElmer Informatics, Inc.), and used to support resonance assignments.

3 | RESULTS AND DISCUSSION

3.1 | Purity of the sample

The HHCP sample was diluted to 100 mg/L and analyzed by GC-MS. Besides (9*R*)-HHCP and (9*S*)-HHCP, several substances were detected with the same molecular ion of *m/z* 344 and the same fragment ions, indicating the presence of isomers. Other compounds in the sample showed a molecular ion of *m/z* 346. The total ion current chromatogram of a sample solution is shown in Figure 1. The absence of palmitic acid and stearic acid is a hint that no plant extract might have been used for the synthesis. Unpublished casework showed that these fatty acids are present in HHC samples deriving from natural CBD. A fraction with Kováts indices of 2,900–3,400 was collected. This fraction contained numerous compounds with molecular ions of *m/z* 480 and 482. XIC of the fragment ion *m/z* 395 from the HHCP sample is included in Supporting Information S104.

3.2 | Identification of components by NMR

Six different components were isolated by column chromatography including (9*R*)-HHCP. They are shown in Figure 2. Structural elucidation was determined using various NMR-experiments. The isolated compounds are described in order of column chromatographic elution; the NMR spectra are found in Supporting Information S1–S58.

3.2.1 | Structure elucidation of compound **1**

^{1}H-NMR revealed two aromatic protons in *meta*-orientation (H-8 and H-10) and a phenolic proton. The methyl groups appear as a singlet (H-12), two doublets (H-14 and H-15), and a triplet (H-7′), which is different to the methyl groups of HHCP, as they appear as two singlets, a doublet, and a triplet. This indicates another structure of the terpenoid moiety than in HHCP. The correlations in the 2D-NMR spectra indicate an *iso*-propyl group (COSY cross peak between H-13 and H-14, 15) and a bicyclic structure. HMBC correlates the bridged carbon at position C5 to both *iso*-propyl CH_3-protons (H-15/C-5 and H-14/C-5). In addition, NOE cross peaks are detected between H-5 and H-15, H-6 and H-15, H-11, and between H-4 and H-14.

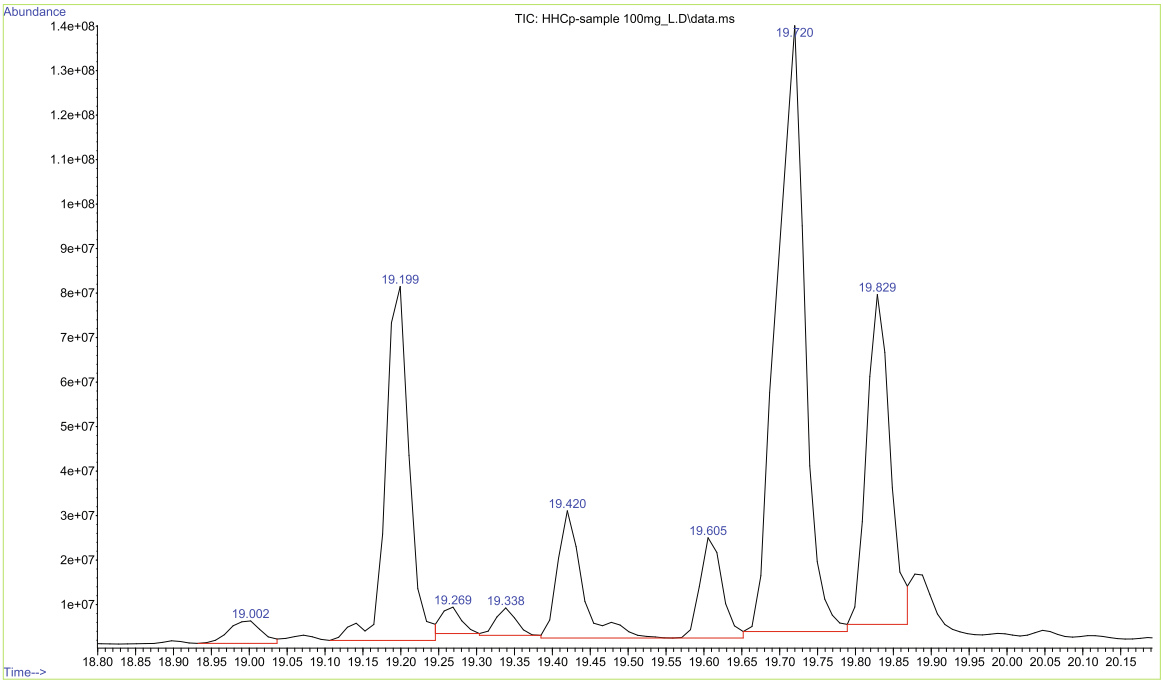

FIGURE 1 TIC of the HHCP sample (γ = 100 mg/L). Other compounds besides the isolated compounds **1**–**6** are present.

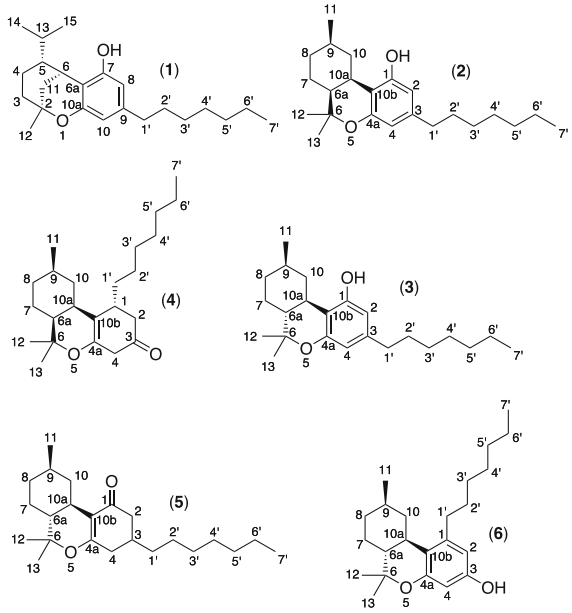

FIGURE 2 Isolated compounds *iso*-HHCP (**1**), *cis*-(9*R*)-HHCP (**2**), (9*R*)-HHCP (**3**), precursor to *cis*-*abn*-HHCP (**4**), precursor to (9*R*)-HHCP (**5**), and *abn*-HHCP (**6**).

H-5 and H-6 only yield weak NOE. This leads to the structure of *rel*-(2*S*,5*R*,6*S*)-9-heptyl-5-isopropyl-2-methyl-3,4,5,6-tetrahydro-2*H*-2,6-methanobenzo[*b*]oxocin-7- ol (*iso*-HHCP, dihydro-*iso*-THCP). The protons (H-14 and H-15) of the *iso*-propyl group are diastereotopic due to the chiral centers. The non-equivalency of methyl shifts in branched, chiral *iso*-propyl moieties has been reported in the literature.[5,6] The pentyl-homolog of compound **1**, *iso*-HHC, shows the same non-equivalency of these particular methyl groups.[4,6–9] The ^{1}H and ^{13}C resonance assignments are summarized in Table 1. The NMR spectra of compound **1** are found in Supporting Information S1–S12.

3.2.2 | Structure elucidation of compounds **2** and **3**

In the ^{1}H-NMR spectrum of compound **2**, two aromatic protons (H-2′ and H-4′) in *meta*-position could be identified. In addition, four methyl groups were identified appearing as a doublet (H-11), two singlets (H-12 and H-13), and a triplet (H-7′) as in (9*R*)-HHCP. Correlations in the 2D-spectra indicated a constitution like in HHCP. The shifts are very similar to (9*R*)-HHCP but change notably in proximity of the stereogenic centers. NOESY spectrum indicates that the stereochemistry at C10a differs from (9*R*)-HHCP; a cross peak correlates proton H-10a to proton H-9; a *trans*-diaxial orientation of these two protons might be the reason. The protons (H-10a and H-6a) are correlated by NOESY, indicating a *cis*-configuration of this compound. Compound **2** was identified as *rel*-(6a*S*,9*R*,10a*R*)-3-heptyl-6,6,9-trimethyl-6a,7,8,9,10,10a-hexahydro-6H-benzo[*c*]chromen-1-ol (*cis*-HHCP). The NMR spectra of compound **2** are found in Supporting Information S13–S23.

Compound **3** is (9*R*)-HHCP; this was confirmed by GC-MS using a reference standard. The ^{1}H- and ^{13}C-NMR shifts of this compound are in accordance to the literature.[4] The ^{1}H and ^{13}C resonances of compounds **2** and **3** are summarized in Table 2. The NMR spectra of compound **3** are found in Supporting Information S24–S28.

TABLE 1 ^{13}C- and ^{1}H shifts of *iso*-HHCP (**1**) in $CDCl_3$.

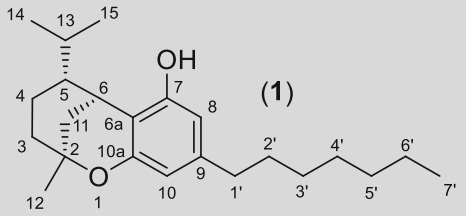

Nr.	δ(^{13}C)/ppm	δ(^{1}H)/ppm
Phenolic H	-	4.49 (s, br 1H)
1	-	-
2	74.8	-
3	41.0	1.98 (m, 1H) 1.48 (m, 1H)
4	23.6	1.06 (ddd, J = 12.9, 4.4 Hz, 1H) 1.59 (td, J = 13.2, 4.9 Hz, 1H)
5	51.3	1.26 (m, 1H)
6	30.3	3.40 (dt, J = 3.5 Hz, 2.5 Hz 1H)
6a	109.4	-
7	153.9	-
8	106.9	6.09 (d, J = 1.5 Hz, 1H)
9	143.4	-
10	108.9	6.26 (d, J = 1.4 Hz, 1H)
10a	158.5	-
11	38.5	1.78 (m, 2H)
12	29.6	1.34 (s, 3H)
13	30.3	1.40 (m, 1H)
14	21.6	0.75 (d, J = 6.6 Hz, 3H)
15	23.8	1.12 (d, J = 6.3 Hz, 3H)
1′	36.6	2.45 (m, 2H)
2′	31.8	1.57 (m, 2H)
3′	30.3	1.30 (m, 2H)
4′	30.4	1.26 (m, 2H)
5′	32.7	1.27 (m, 2H)
6′	23.5	1.29 (m, 2H)
7′	15.2	0.88 (m, 3H)

TABLE 2 ^{13}C- and ^{1}H shifts of cis-(9R)-HHCP (**2**) and (9R)-HHCP (**3**) in $CDCl_3$.

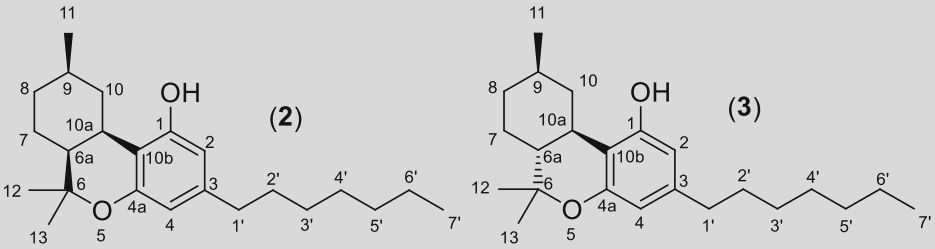

	cis-HHCP (2)		(9*R*)-HHCP (3)	
Nr.	δ(^{13}C)/ppm	δ(^{1}H)/ppm	δ(^{13}C)/ppm	δ(^{1}H)/ppm
Phenolic H	-	4.65 (s, 1H)	-	5.88 (m, 1H)
1	156.6		155.1	-
2	110.5	6.25 (d, J = 1.8 Hz, 1H)	110.1	6.31 (d, J = 1.8 Hz, 1H)
3	143.0	-	142.8	-
4	108.6	6.06 (d, J = 1.8 Hz, 1H)	108.3	6.11 (d, J = 1.8 Hz, 1H)
4a	156.6	-	156.7	-
5	-	-	-	-
6	76.9	-	77.6	-
6a	42.8	1.49 (ddd, J = 9.0 5.3, 4.1 Hz, 1H)	49.6	1.51 (m, 1H)
7	23.9	1.27 (m, 1H)	28.4	1.14 (m, 1H)
		1.78 (m, 1H)		1.87 (m, 1H)
8	35.9	0.94 (m, 1H)	36.0	1.11 (m, 1H)
		1.65 (ddt, J = 12.8, 6.7, 3.1 Hz, 1H)		1.89 (m, 1H)
9	27.9	1.19 (m, 1H)	33.2	1.66 (m, 1H)
10	38.2	1.09 (m, 1H)	39.3	0.82 (m, 1H)
		3.13 (dq, J = 13.2, 2.6 Hz, 1H)		3.17 (dt, J = 13.0, 3.2 Hz, 1H)
10a	32.0	3.27 (ddd, J = 4.3, 4.3, 4.3 Hz, 1H)	35.8	2.53 (td, J = 11.1, 2.9 Hz, 1H)
10b	108.6	-	110.9	-
11	23.1	0.84 (d, J = 6.5 Hz, 3H)	22.9	0.99 (d, J = 6.6 Hz, 3H)
12	26.1	1.23 (s, 3H)	19.3	1.10 (s, 3H)
13	27.2	1.36 (s, 3H)	28.0	1.43 (s, 3H)
1′	36.2	2.43 (dd, J = 9.0, 6.7 Hz, 2H)	35.8	2.44 second order
2′	31.7	1.56 second order	31.3	1.56 (m, 2H)
3′	30.2	1.27 (m, 2H)	29.7	1.33 (m, 2H)
4′	30.2	1.29 (m, 2H)	29.7	1.33 (m, 2H)
5′	32.4	1.29 (m, 2H)	32.2	1.32 (m, 2H)
6′	23.9	1.27 (m, 2H)	22.9	1.32 (m, 2H)
7′	14.9	0.88 (t, J = 7.2 Hz, 3H)	14.5	0.93 (t, J = 7.0 Hz, 3H)

3.2.3 | Structure elucidation of compounds **4** and **5**

Compound **4** showed no aromatic or olefinic protons in the ^{1}H-NMR. HMBC revealed the presence of a ketone and an olefin. Since no olefinic protons were found, a tetrasubstituted olefin was concluded. The four methyl groups consist of two singlets (H-12 and H-13), a doublet (H-11), and a triplet (H-7′) like in HHCP. Further correlations in the 2D-NMR spectra lead to a dibenzopyran structure like in HHCP. The COSY correlation (H-1 and H-1′) and the HMBC correlations (H-2 and C-3, H-4, and C-3) indicate that the positions of the substituents at C-1 and C-3 are exchanged in comparison to (9*R*)-HHCP. NOESY crosspeaks were found between H-10a and H-11, indicating a *trans*-diaxial relation between them, and a correlation between H-10a and H-6a, indicating a *cis*-relation between the

respective carbons C-10a and C-6a. No NOESY crosspeak was detected between H-1′ and H-10, indicating the same configuration at the atoms C-10a and C-1′. The opposite configuration on these two carbons should lead to shorter distances between the attached hydrogens and therefore to a positive NOESY correlation. The correlations lead to the structure of *rel*-(1*R*,6a*S*,9*R*,10a*R*)-1-heptyl-

TABLE 3 ^{13}C- and ^{1}H shifts of the ketones **4** and **5** in $CDCl_3$.

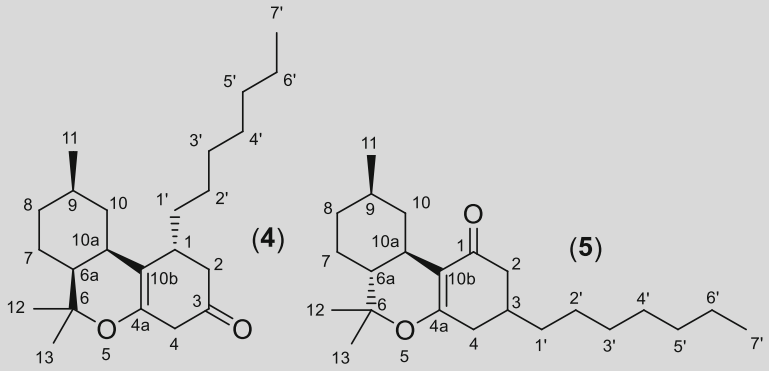

	Compound 4		Compound 5	
Nr.	δ(^{13}C)/ppm	δ(^{1}H)/ppm	δ(^{13}C)/ppm	δ(^{1}H)/ppm
1	33.6	2.07 (m, 1H)	199.6	-
2	44.4	2.26 (m, 1H) 2.43 (dd, J = 15.8, 4.7 Hz, 1H)	44.8	2.22 (m, 1H) 2.47 (m, 1H)
3	199.7	-	33.3	1.55(m, 1H)
4	36.0	2.23 (m, 1H) 2.35 (m, 1H)	36.3	2.24 (m, 1H) 2.32 (m, 1H)
4a	171.3	-	171.1	-
5	-	-	-	-
6	80.2	-	81.8	-
6a	41.6	1.43 (ddd, J = 12, 5, 5 Hz, 1H)	49.4	1.23 (m, 1H)
7	23.3	1.0 (m, 1H) 1.71 (m, 1H)	28.1	1.04 (m, 1H) 1.73 (m, 1H)
8	35.0	0.85 (m, 1H) 1.65 (m, 1H)	36.3	1.00 (m, 1H) 1.81 (m, 1H)
9	20.6	1.03 (m, 1H)	26.4	1.20 (m, 1H)
10	36.1	0.91 (m, 1H) 2.95 (dd, J = 13.4, 2.8 Hz, 1H)	39.0	0.45 (q, J = 11.7 Hz, 1H) 2.84 (dq, J = 12.8, 3.4 Hz, 1H)
10a	29.9	2.85 (m, 1H)	34.3	2.07 (m, 1H)
10b	111.2	-	114.9	-
11	22.9	0.81 (d, J = 6.4 Hz, 3H)	23.1	0.90 (d, J = 7.2 Hz, 3H)
12	26.1	1.20 (s, 3H)	20.6	1.06 (s, 3H)
13	26.4	1.31 (s, 3H)	28.0	1.34 (s, 3H)
1′	35.4	1.36 (m, 2H)	35.8	1.37 (m, 2H)
2′	27.2	1.28 (m, 2H)	29.9	1.27 (m, 2H)
3′	30.0	1.25 (m, 2H)	27.8	1.27 (m, 2H)
4′	30.0	1.26 (m, 2H)	27.6	1.27 (m, 2H)
5′	32.5	1.27 (m, 2H)	32.5	1.26 (m, 2H)
6′	23.0	1.29 (m, 2H)	23.2	1.28 (m, 2H)
7′	14.6	0.88 (t, J = 7.0 Hz, 3H)	14.7	0.88 (t, J = 6.5 Hz, 3H)

6,6,9-trimethyl-2,3,4,6,6a,7,8,9,10,10a-decahydro-1*H*-benzo[*c*]chromen-3-one. The NMR spectra of compound **4** are found in Supporting Information S29–S37.

^{1}H-NMR of compound **5** showed that this compound does not contain any aromatic or olefinic protons. HMBC signals in the lower field can be seen indicating an olefin and a ketone. Considering the dibenzopyran structure of HHCP, it was assumed that the oxo group is located where the phenol would otherwise be found. The olefin is located where the aromatic and heterocyclic rings are fused, resulting in a tetrasubstituted olefin. Two singlets (H-12 and H-13) on similar positions like in the ^{1}H-NMR spectrum of (9*R*)-HHCP are present, which are likely the geminal methyl groups. The other methyl groups are overlaid around 0.9 ppm. Spin–spin-multiplicity (doublet H11 and triplet H7′) indicates that they are bound to a R_2CH group and a RCH_2 group, respectively, like in HHCP. The correlations in the 2D-NMR lead to the structure of *rel*-(6a*R*,9*R*,10a*R*)-3-heptyl-6,6,9-trimethyl-2,3,4,6,6a,7,8,9,10,10a-decahydro-1*H*-benzo[*c*]chromen-1-one. No NOESY crosspeak was found between H-10a and H-6a, indicating a *trans*-configuration. No crosspeak was found between H-10a and H-11 but one between H-10a and H-9. Stereochemistry at position C-3 could not be determined. The ^{1}H and ^{13}C resonances of compounds **4** and **5** are summarized in Table 3. NMR spectra of compound **5** are found in Supporting Information S38–S44.

3.2.4 | Structure elucidation of compound **6**

^{1}H-NMR revealed the presence of two aromatic protons with the same multiplicities and coupling constant as in HHCP indicating *meta*-orientation of the protons. Multiplicity of the methyl groups is the same as in HHCP (two singlets [H-12 and H-13], a doublet [H-11], and a triplet [H-7′]); these signals were assigned to the same methyl groups. The correlations in the 2D-NMR spectra indicate that the positions of the heptyl-group and the phenol are exchanged. A correlation between protons H-1 and H-1′ and between H-1 and H-10b are seen in the HMBC spectrum. NOESY shows that H-1′ of the heptyl chain and H-10 are in close proximity confirming that structure. Protons H-11 and the proton at H-10a show a NOESY crosspeak indicating *trans*-diaxial orientation of these two protons. The missing crosspeak between protons H-10a and H-6a indicates a *trans*-configuration of the molecule leading to the molecule *rel*-(6a*R*,9*R*,10a*R*)-1-heptyl-6,6,9-trimethyl-6a,7,8,9,10,10a-hexahydro-6*H*-benzo[*c*]chromen-3-ol. ^{1}H-NMR spectrum looks similar to the homolog *cis-abn*-HHC.[10] The ^{1}H and ^{13}C resonances of compound **6** are summarized in Table 4. NMR spectra of compound **6** are found in Supporting Information S45–S58.

TABLE 4 ^{13}C- and ^{1}H shifts of *abn*-HHCP (**6**) in $CDCl_3$.

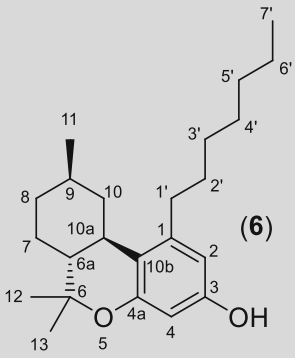

	Compound 6	
Nr.	δ(^{13}C)/ppm	δ(^{1}H)/ppm
Phenolic H	-	4.31 (very broad)
1	143.8	-
2	109.1	6.27 (d, *J* = 2.6 Hz, 1H)
3	154.9	-
4	102.1	6.14 (d, *J* = 2.7 Hz, 1H)
4a	155.3	-
5	-	-
6	76.6	-
6a	51.4	1.52 (m, 1H)
7	32.1	1.30 (m, 1H)
		1.65 (m, 1H)
8	23.8	1.53 (m, 1H)
		1.68 (m, 1H)
9	28.3	2.13 (dtd, *J* = 7.3, 4.7, 2.4 Hz, 1H)
10	39.4	1.38 (m, 1H)
		2.22 (m, 1H)
10a	30.9	2.65 (td, *J* = 11.2, 2.6 Hz, 1H)
10b	117.5	-
11	18.6	1.16 (d, *J* = 7.2 Hz, 3H)
12	27.5	1.05 (s, 3H)
13	18.5	1.36 (s, 3H)
1′	33.5	2.55 (ddd, *J* = 9.6, 7.0, 2.8 Hz, 2H)
2′	31.3	1.60 (m, 2H)
3′	29.6	1.33 (m, 2H)
4′	29.6	1.33 (m, 2H)
5′	22.8	1.31 (m, 2H)
6′	22.8	1.31 (m, 2H)
7′	14.1	0.90 (t, *J* = 6.7 Hz, 3H)

3.3 | Mass spectrometric elucidation

3.3.1 | Formation of HHCP mass fragments

The mass spectra of (9*R*)-HHCP and (9*S*)-HHCP are indistinguishable. Figure 3 shows the mass spectrum of (9*R*)-HHCP. Their major ions are the molecular ion (*m/z* 344), loss of a propyl radical from the *gem*-dimethyl group ($[M\text{-}C_3H_7^{\bullet}]^+$, *m/z* 301), loss of *n*-hexene from the side chain after McLafferty rearrangement ($[M\text{-}C_6H_{12}]^{+\bullet}$, *m/z* 260, base peak), and the tropylium ion ($[M\text{-}123^{\bullet}]^+$, *m/z* 221). Some minor ions like the loss of a methyl radical ($[M\text{-}CH_3^{\bullet}]^+$, *m/z* 329) and the ion *m/z*

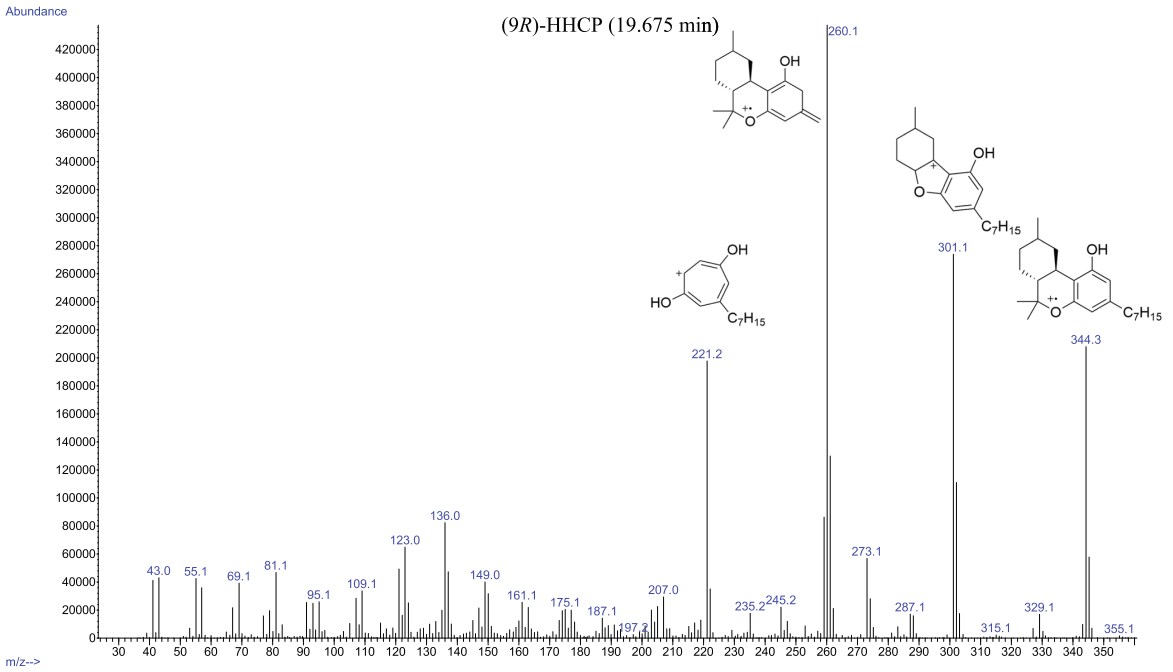

FIGURE 3 Mass spectrum of (9*R*)-HHCP with the structures of the most abundant ions.

136 from the alicyclic moiety are also visible. The fragmentation mechanisms are in analogy to other well characterized cannabinoids.[11–13]

An alkane standard (C7-C40) was measured, and the Kováts index[14] of the isolated compounds and the references were calculated according to van den Dool and Kratz.[15] The data are summarized in Table 5. A chromatogram of the alkane standard is included in Supporting Information S59.

3.3.2 | Mass spectrum of compound **1**

The mass spectrum of compound **1** consists of only a few ions with high intensity: the molecular ion ($[M]^{+\bullet}$, *m/z* 344), loss of *n*-hexene from the side chain ($[M\text{-}C_6H_{12}]^{+\bullet}$, *m/z* 260), and loss of a *iso*-hexyl radical ($[M\text{-}C_6H_{13}^{\bullet}]^{+}$, *m/z* 259, base peak).[16] Other fragments with lower abundance like the tropylium ion at *m/z* 221 and loss of a methyl radical at *m/z* 329 are also present. Mass spectrum is similar to the pentyl analog *iso*-HHC described in literature. The ions *m/z* 221, 301, and 344 are shifted by +28 (ethylene) in comparison to the ions of *iso*-HHC. The ion *m/z* 260, which results from the McLafferty rearrangement, is the same.[4]

3.3.3 | Mass spectrum of compound 2

This compound shows the same fragments with the same abundances as (9*R*)-HHCP and (9*S*)-HHCP. NMR data imply a *cis*-configuration of the hydrogens at C6a and C10a. By comparison with (9*R*)- and (9*S*)-*cis*-HHC from the literature, it is observable that the according fragments were found. The fragments *m/z* 344, 301, and 221 are shifted by +28 due to the longer alkyl chain of compound **2** ($+C_2H_4$), and the fragment *m/z* 260 remains identical because this fragment ion results from the fragmentation of the alkyl chain.[7]

TABLE 5 Chromatographic data and relevant ions of the isolated compounds and reference compounds.

Name	RT/min	RRI	Relevant ions
Compound **1**	19.12	2,615	344, 260, 259, 221
Compound **2**	19.18	2,623	344, 301, 260, 221
Compound **3**	19.68	2,692	344, 301, 260, 221
Compound **4**	18.62	2,537	346, 331, 303
Compound **5**	18.96	2,591	346, 303, 247
Compound **6**	19.58	2,679	344, 329, 301, 260, 137
(9*R*)-HHCP	19.68	2,692	344, 301, 260, 221
(9*S*)-HHCP	19.80	2,708	344, 301, 260, 221
CBP	20.88	2,835	338, 323, 238
CBDP	19.51	2,670	342, 327, 274, 221
Δ^9-THCP	19.99	2,732	342, 327, 299, 259, 243

Note: Spectra are included in Supporting Information S60–S70.
Abbreviations: RRI, relative retention index (Kováts index); RT, Retention time.

3.3.4 | Mass spectrum of compound 3

The isolated compound **3** is (9*R*)-HHCP. The same retention time and mass spectrum were obtained as from the reference compound.

3.3.5 | Mass spectrum of compound 4

Comparison of the mass spectrum of compound **4** with a mass spectrum from a similar molecule lacking the heptyl chain revealed that the main fragments are shifted by the mass of heptylene (C_7H_{14}, *m/z* 98). The relative abundances of the main peaks are similar to those reported in the literature.[17] These fragment ions occur therefore from the fragmentation of the tricyclic moiety. The most abundant fragments are the molecular ion ($[M]^{+\bullet}$, *m/z* 346), loss of a methyl radical ($[M\text{-}CH_3^{\bullet}]^+$, *m/z* 331), and loss of a propyl radical from the *gem*-dimethyl group ($[M\text{-}C_3H_7^{\bullet}]^+$, *m/z* 303, base peak). In addition, loss of a heptyl radical can also be observed ($[M\text{-}C_7H_{15}^{\bullet}]^+$, *m/z* 247). A mechanism for this reaction is shown in Figure 4.[18]

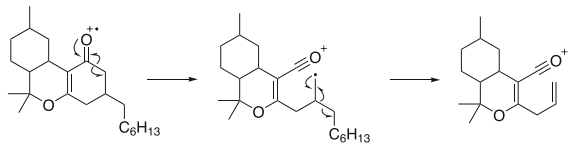

FIGURE 4 Fragmentation mechanism for the loss of a heptyl radical from compound **4**.

3.3.6 | Mass spectrum of compound 5

The same fragments appear as in compound **4** with *m/z* 303 as base peak. Slight changes in the abundances of the characteristic fragment ions are observed. The same fragmentation mechanisms can occur as in compound **4**.

3.4 | Chiral derivatization

Compounds **1**–**6** were derivatized in presence of the acylation catalyst DMAP with either (*R*)-MTPA-Cl or (*S*)-MTPA-Cl to their respective Mosher esters. A solution of (9*R*)-HHCP, (9*S*)-HHCP, or of one of the compounds **1**–**6** ($\gamma = 1$ mg/ml, 10 µl, dry DCM) was evaporated to dryness. DMAP solution ($\gamma = 10$ mg/ml in dry DCM, 10 µl), dry DCM (50 µl), and either (*R*)-MTPA-Cl or (*S*)-MTPA-Cl solution ($\sigma = 10$ ml/l in dry DCM, 10 µl) were added to the residue. The solutions were incubated at 50°C for 15 h overnight. The samples were evaporated to dryness, and the residue was dissolved in 50 µl EtOAc and analyzed by GC-MS. An impure sample fraction containing (9*S*)-HHCP was derivatized with a similar protocol using 20 µl of a sample solution ($\gamma = 1$ mg/ml) and 20 µl (*R*)-MTPA-Cl or (*S*)-MTPA-Cl ($\sigma = 10$ ml/L). The Mosher esters of the isolated compounds and the references (9*R*)-HHCP and (9*S*)-HHCP are summarized in Table 6. (*S*)-MTPA esters are the products of derivatization with (*R*)-MTPA-Cl and vice versa.

The (*S*)-MTPA and (*R*)-MTPA esters of one enantiomer of compound **1** ((2*S*,5*R*,6*S*)-*iso*-HHCP) are the enantiomers of the (*R*)-MTPA and (*S*)-MTPA esters of the other enantiomer of compound

TABLE 6 Chromatographic data and relevant ions of the (*R*)- and (*S*)-MTPA esters of the isolated compounds and reference compounds.

Name	RT/min	RRI	ee	Relevant ions
(*S*)-MTPA ester of **1**	24.58	3,131	72%	560, 475, 273, 189
(*S*)-MTPA ester of **1***	25.00	3,127	-	560, 475, 273, 189
(*R*)-MTPA ester of **1**	25.06	3,159	82%	560, 475, 273, 189
(*R*)-MTPA ester of **1***	24.50	3,156	-	560, 475, 273, 189
(*S*)-MTPA ester of **2**	24.81	3,145	100%	560, 517, 485, 327, 189
(*R*)-MTPA ester of **2**	25.24	3,170	100%	560, 514, 485, 327, 189
(*S*)-MTPA ester of **3**	26.25	3,224	100%	560, 517, 485, 327, 189
(*R*)-MTPA ester of **3**	25.69	3,197	100%	560, 517, 485, 327, 189
(*S*)-MTPA ester of **6**	30.04	3,387	100%	560, 517, 343, 315, 274, 189
(*R*)-MTPA ester of **6**	30.08	3,389	100%	560, 517, 343, 315, 274, 189
(*S*)-MTPA ester of (9*S*)-HHCP from sample	27.27	3,274	100%	560, 517, 485, 327, 189
(*S*)-MTPA ester of (9*S*)-HHCP from sample	27.04	3,262	100%	560, 517, 485, 327, 189
(*S*)-MTPA ester of (9*R*)-HHCP	26.30	3,227	100%	560, 517, 485, 327, 189
(*R*)-MTPA ester of (9*R*)-HHCP	25.77	3,201	100%	560, 517, 485, 327, 189
(*S*)-MTPA ester of (9*S*)-HHCP	27.43	3,281	100%	560, 517, 485, 327, 189
(*R*)-MTPA ester of (9*S*)-HHCP	27.16	3,268	100%	560, 517, 485, 327, 189

Note: Spectra included in Supporting Information S73–S102. Enantiomeric excess was calculated from GC-MS area-% of the Mosher esters.
Abbreviations: **1***, enantiomer of compound **1**; ee, enantiomeric excess; RRI, relative retention index (Kováts index); RT, retention time.

1 ((2*R*,5*S*,6*R*)-*iso*-HHCP). The enantiomeric Mosher esters have the same retention time (see Table 6). Relative intensities of the Mosher esters to each other are reversed when compound **1** is esterified with (*S*)-MTPA-Cl instead of (*R*)-MTPA-Cl. This indicates that compound **1** is a scalemic mixture. An enantiomeric excess of 72–82% was calculated from GC-MS area-%. The Mosher esters of both enantiomers of compound **1** are shown in Figure 5.

Chiral derivatization revealed that the epimers of HHCP in the sample were enantiopure. Comparison with reference standards showed that the HHCP epimers in the sample were indeed (9*R*)-HHCP and (9*S*)-HHCP and not their unnatural enantiomers ((6a*S*,9*S*,10a*R*)- and (6a*S*,9*S*,10a*S*)-HHCP).

3.5 | Mass spectra of high-molecular impurities

A fraction was collected that contained several compounds with molecular ions of *m/z* 480 and 482. Some molecules with a molecular ion of *m/z* 480 (base peak) showed the ions $[M\text{-}15^{\bullet}]^{+}$, $[M\text{-}43^{\bullet}]^{+}$, $[M\text{-}84]^{+\bullet}$, and $[M\text{-}123^{\bullet}]^{+}$, indicating that similar fragments are generated as in HHCP. These compounds are sideproducts resulting from a second alkylation on the cyclic diketone. Fragmentation patterns are shown in Figure 6.

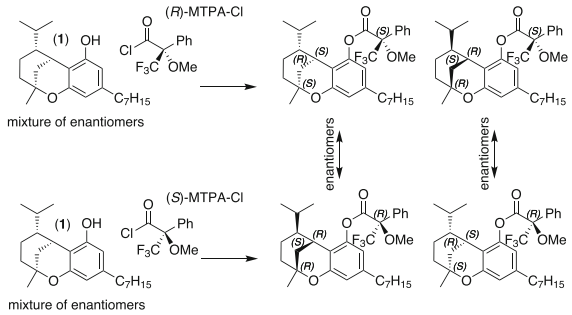

FIGURE 5 Formation of (*S*)-MTPA- (top) and (*R*)-MTPA esters (bottom) of compound **1** and its enantiomer. Two pairs of enantiomers are formed.

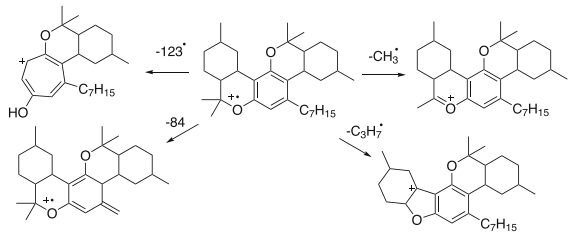

FIGURE 6 Fragmentation of the bisalkylated product shown on an *ortho*,*para*-disubstituted molecule.

Two different substitution patterns for the bisalkylation are plausible, which are shown in Figure 7. Each of the molecules possesses six stereogenic centers, which would lead to a total of 48 enantiomeric pairs and 4 *meso* compounds, explaining the crowded extracted ion chromatogram. It can be expected that the fragmentation patterns are similar.

In addition, bisalkylated *iso*-cannabinoids might also be formed. Some of the molecules with a molecular ion of *m/z* 480 show the fragments $[M\text{-}15^{\bullet}]^{+}$, $[M\text{-}84]^{+\bullet}$, and $[M\text{-}85^{\bullet}]^{+}$, which are the same losses as observed for compound **1**. Substituted *iso*-HHCPs are therefore likely structures, which add even more complexity in the extracted ion chromatogram. They are shown in Figure 8.

Such bisalkylated compounds are known side products from the synthesis of other cannabinoids. Houry et al.[19,20] described a double condensation product from the reaction of olivetol with limonene or α–pinene in the presence of phosphorous oxychloride. Millimaci et al.[8] described that bis-addition can occur from the reaction of 4-isopropyl-1-methylcyclohex-2-en-1-ol with olivetol under acidic conditions. Similar observations were made from the synthesis of THC from olivetol with menthadienol under acidic conditions leading to a disubstituted olivetol.[21]

3.6 | Trimethylsilylation of the high-molecular weight fraction

The fraction, which contained the high-molecular weight impurities, was evaporated to dryness and dissolved in 500 µl EtOAc. At 90°C, 100 µl of this solution and 100 µl MSTFA were incubated for 40 min. The solution was then evaporated to dryness and dissolved in 1 ml EtOAc; this was repeated without MSTFA. The samples were measured by GC-MS. The silylated sample showed peaks with molecular

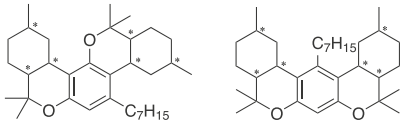

FIGURE 7 *o*-,*p*-disubstitution pattern (left) and *o*-,*o*-disubstitution pattern (right). Stereogenic centers are marked with an asterisk (*ortho*- and *para*- refer to the carbon-rest in relation to the position of the heptyl group).

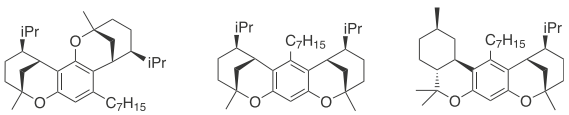

FIGURE 8 Examples of disubstituted bridged molecules. *o*,-*p*-disubstitution (left) and *o*-,*o*-disubstitution (mid) and a mixed form (right).

ions, which would fit to mono- and disilylation (*m/z* 554, 626). The extracted ion chromatograms of the derivatized and underivatized sample from *m/z* 480 were identical, indicating that these compounds do not have reactive groups (Supporting Information S105 and S106). The silylated molecules are possibly TMS-enol ethers of intermediates prior Hetero-Diels-Alder cyclization. An interesting ion of *m/z* 429 can be seen in the mass spectra of compounds with a molecular ion of *m/z* 554. This ion might result from the fragmentation of the citronellyl-sidechain; a mechanism is provided in Figure 9. The same loss of 125 can be seen in an underivatized sample with the ion *m/z* 482; this molecule is not present after derivatization with MSTFA (24.94 min). Some monoalkylated compounds with *m/z* 346 also show the acylium ion from the loss of 125 amu; the tricyclic ketones **4** and **5** do not.

3.7 | Potential synthetic route to HHCP and side products

The presence of the two α,β-unsaturated ketones **4** and **5** is a strong hint that this HHCP sample was synthesized from 5-heptylcyclohexa-1,3-dione. Knoevenagel condensation of this diketone with (*R*)-citronellal, subsequent Hetero-Diels-Alder reaction, and aromatization leads to enantiopure (6a*R*,9*R*,10a*R*)-HHCP.[22] An alternative aromatization to olivetol derivatives using catalytic amounts of iodine in dimethylsulfoxide was shown recently.[23] This sequence with citral A or B as aldehyde would lead to cannabichromephorol (CBCP) and not Δ^9-THCP, since the 6π-electrocyclization would be the preferred pathway and not the Hetero-Diels-Alder reaction.[24] The presence of the so-called abnormal or *ortho* substitution pattern (compounds **5** and **6**), where the alkyl chain and the phenol or ketone change position might also be explained by this reaction sequence. The α,β-unsaturated ketones **4** and **5** are intermediates in this sequence and deliver the desired phenols after oxidation. A plausible pathway to the ketones **4** and **5** is shown in Figure 10.

The presence of *iso*-HHCP (compound **1**) can occur from cyclization of CBDP with the cyclic olefin and subsequent hydrogenation of the double bond (see Figure 11). Derivatization of compound **1** with (*R*)- and (*S*)-MTPA-Cl revealed that this compound is scalemic, which means that the precursor was scalemic as well, a mixture of (+)-and (−)-*trans*-CBDP for instance, therefore confirming that not a natural substance was used to synthesize this sample. Partial racemization seems unlikely due to lack of acidic protons at the stereogenic centers. It is not known how and if CBDP was formed in this process. CBDP was not detected in the sample.

Chiral derivatization revealed that the isolated phenols besides compound **1** were enantiopure. Compounds **2** and **3** are the *cis* and *trans* products of the intramolecular Hetero-Diels-Alder reaction of condensed (*R*)-citronellal (see Figure 12). Due to the diastereoselectivity of the reaction, the respective *trans*-product of (*S*)-citronellal should be (6a*S*,9*S*,10a*S*)-HHCP, the enantiomer of (9*R*)-HHCP.[22] This product was not found. A chiral analysis of the impure fraction containing (9*S*)-HHCP revealed that this fraction contained only (9*S*)-HHCP and not its enantiomer (6a*S*,9*R*,10a*S*)-HHCP. The latter could have been a plausible side product if only (*R*)-citronellal was used to prepare this sample, as their stereochemistry at this position is identical.

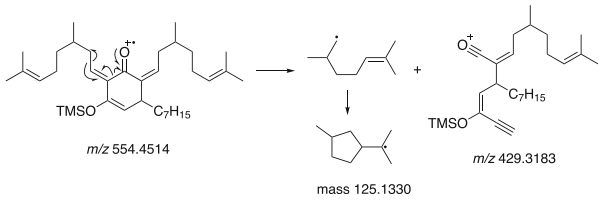

FIGURE 9 Fragmentation mechanism of the TMS-enol ether with an *m/z* 554 to the ion *m/z* 429.

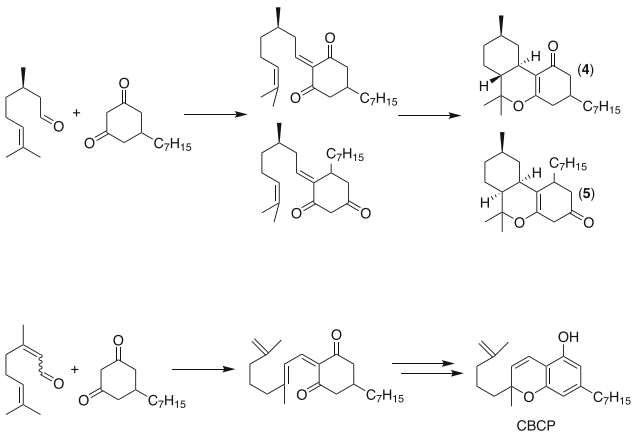

FIGURE 10 Top: plausible synthetic pathway to the α,β-unsaturated ketones **4** and **5** starting from (*R*)-citronellal. Bottom: same reaction pathway using *E*- or *Z*-citral as the aldehyde leads to CBCP.

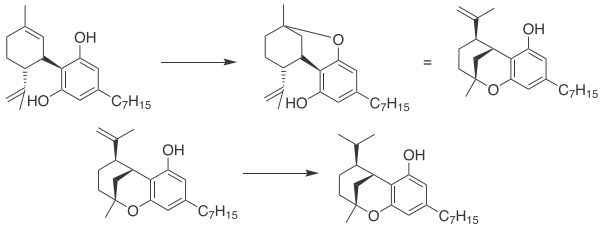

FIGURE 11 Cyclization of natural occurring (−)-*trans*-CBDP with subsequent hydrogenation to compound **1** would only deliver enantiopure (2*R*,5*S*,6*R*)-9-heptyl-5-isopropyl-2-methyl-3,4,5,6-tetrahydro-2*H*-2,6-methanobenzo[*b*]oxocin-7-ol.

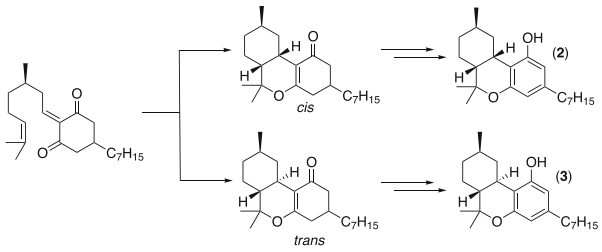

FIGURE 12 Plausible formation of compounds **2** and **3** ((9*R*)-HHCP) from the condensed (*R*)-citronellal adduct.

4 | CONCLUSIONS

The impurity profile and the isolated compounds from the analyzed HHCP sample lead to the conclusion that this sample was made synthetically. To the authors' knowledge, neither (9*R*)-HHCP nor (9*S*)-HHCP has yet been found in *Cannabis*. Disproportionation from naturally occurring Δ^9-THCP is plausible, but the by-product of this reaction, cannabiphorol, was not found in the sample. It is not known for certain how this sample was prepared, but the sample contained unnatural stereoisomers (*cis*-HHCP), unnatural regioisomers (*abn*-HHCP), and higher condensed molecules similar to side products from the total synthesis of similar cannabinoids. The isolated ketones are most probably unreacted intermediates from chemical synthesis (precursors of (9*R*)-HHCP and *cis-abn*-HHCP) as they are not known to be intermediates from the cannabinoid biosynthesis. The chosen pathway allowed acceptable stereocontrol of the centers C6a and C10a. Most of the impurities in the sample could not be isolated in an acceptable purity for structure elucidation. Due to their fragmentation behavior, they are probably isomers of the isolated compounds. Unreacted starting material was not found, which makes it difficult to understand which synthetic route was chosen. It is very likely that this sample is a mixture of different synthetic batches from different synthetic routes. The presence of (9*S*)-HHCP cannot be explained by the proposed pathway, and the presence of ketones **4** and **5** cannot be explained by a pathway starting from an olivetol homolog. It is assumed that not every manufacturer uses the same pathway to synthesize HHCP and similar compounds but CBD as starting material is certainly not one of these.

ACKNOWLEDGMENTS

Remo Arnold from the University of Bern is acknowledged for the help and material he provided for the column chromatography. Christian Bissig from the Forensic Institute of Zurich is acknowledged for the fruitful discussions concerning semisynthetic cannabinoids.

ORCID

Willi Schirmer https://orcid.org/0009-0004-5579-2217
Martina Vermathen https://orcid.org/0000-0002-0796-1643
Julien Furrer https://orcid.org/0000-0003-2096-0618
Stefan Schürch https://orcid.org/0000-0001-5109-4623
Wolfgang Weinmann https://orcid.org/0000-0001-8659-1304

REFERENCES

1. Schweizerische Eidgenossenschaft. Verordnung des EDI über die Verzeichnisse der Betäubungsmittel, psychotropen Stoffe, Vorläuferstoffe und Hilfschemikalien (Betäubungsmittelverzeichnisverordnung, BetmVV-EDI) vom 30. Mai 2011 (Stand am 9. Oktober 2023), https://www.fedlex.admin.ch/eli/cc/2011/363/de
2. Bueno J, Greenbaum EA. (−)-*trans*-Δ^9-Tetrahydrocannabiphorol content of *Cannabis sativa* inflorescence from various chemotypes. *J. Nat. Prod.* 2021;84(2):531-536. doi:10.1021/acs.jnatprod.0c01034
3. Citti C, Linciano P, Russo F, et al. A novel phytocannabinoid isolated from *Cannabis sativa* L. with an *in vivo* cannabimimetic activity higher than Δ^9-tetrahydrocannabinol: Δ^9-Tetrahydrocannabiphorol. *Sci. Rep.* 2019;9(1):20335. doi:10.1038/s41598-019-56785-1
4. Tanaka R, Kikura-Hanajiri R. Identification of hexahydrocannabinol (HHC), dihydro-*iso*-tetrahydrocannabinol (dihydro-*iso*-THC) and hexahydrocannabiphorol (HHCP) in electronic cigarette cartridge products. *Forensic. Toxicol.* 2023;42(1):71-81. doi:10.1007/s11419-023-00667-9
5. Sorensen TS. On the non-equivalence of isopropyl CH_3 nuclear magnetic resonance signals. *Can. J. Chem.* 1967;45(13):1585-1588. doi:10.1139/v67-256
6. Tonelli AE, Schilling FC, Bovey FA. Conformational origin of the nonequivalent ^{13}C NMR chemical shifts observed for the isopropyl methyl carbons in branched alkanes. *J. Am. Chem. Soc.* 1984;106(4):1157-1158. doi:10.1021/ja00316a079
7. Arnone A, Merlini L, Servi S. Hashish: synthesis of (+)-Δ^4-tetrahydrocannabinol. *Tetrahedron.* 1975;31(24):3093-3096. doi:10.1016/0040-4020(75)80154-2
8. Millimaci AM, Trilles RV, McNeely JH, Brown LE, Beeler AB, Porco JA Jr. Synthesis of Neocannabinoids using controlled Friedel-crafts reactions. *J. Org. Chem.* 2023;88(18):13135-13141. doi:10.1021/acs.joc.3c01362
9. Gaoni Y, Mechoulam R. The *iso*-tetrahydrocannabinols. *Israel J. Chem.* 1968;6(5):679-690. doi:10.1002/ijch.196800086
10. Inoue T, Inoue S, Sato K. Lewis acid catalyzed reaction of o-[1-(alkylthio)alkyl]phenols: the generation and reaction of *o*-quinonemethides and applications to cannabinoid synthesis. *Bull. Chem. Soc. Jpn.* 1990;63(6):1647-1652. doi:10.1246/bcsj.63.1647
11. Vree TB. Mass spectrometry of cannabinoids. *J. Pharm. Sci.* 1977;66(10):1444-1450. doi:10.1002/jps.2600661025
12. Harvey DJ, Brown NK. Electron impact-induced fragmentation of the trimethylsilyl derivatives of monohydroxy-hexahydrocannabinols. *Biol. Mass Spectrom.* 1991;20(5):292-302. doi:10.1002/bms.1200200510

13. Budzikiewicz H, Alpin RT, Lightner DA, Djerassi C, Mechoulam R, Gaoni Y. Massenspektroskopie und ihre Anwendung auf strukturelle und stereochemische Probleme—LXVIII: Massenspektroskopische Untersuchung der Inhaltstoffe von Haschisch. *Tetrahedron*. 1965; 21(7):1881-1888. doi:10.1016/S0040-4020(01)98657-0
14. Kováts E. Gas-chromatographische Charakterisierung organischer Verbindungen. Teil 1: Retentionsindices aliphatischer Halogenide, Alkohole, Aldehyde und Ketone. *Helv. Chim. Acta*. 1958;41(7):1915-1932. doi:10.1002/hlca.19580410703
15. van den Dool H, Kratz PD. A generalization of the retention index system including linear temperature programmed gas–liquid partition chromatography. *J. Chromatogr. A*. 1963;11:463-471. doi:10.1016/S0021-9673(01)80947-X
16. Terlouw JK, Heerma W, Burgers PC, et al. The use of metastable ion characteristics for the determination of ion structures of some isomeric cannabinoids. *Tetrahedron*. 1974;30(23-24):4243-4248. doi:10.1016/S0040-4020(01)97415-0
17. Fernandes S, Rajakannu P, Bhat SV. Efficient catalyst for tandem solvent free enantioselective Knoevenagel-formal [3+3] cycloaddition and Knoevenagel-hetero-Diels–Alder reactions. *RSC Adv*. 2015;5(83): 67706-67711. doi:10.1039/C5RA09865C
18. Vandewalle M, Schamp N, de Wilde H. Studies in organic mass spectrometry III 1, 3-cyclohexanediones. *Bull. Soc. Chimiques Belg*. 1967; 76(1-2):111-122. doi:10.1002/bscb.19670760112
19. Houry S, Mechoulam R, Fowler PJ, Macko E, Loev B. Benzoxocin and benzoxonin derivatives. Novel groups of terpenophenols with central nervous system activity. *J. Med. Chem*. 1974;17(3):287-293. doi:10.1021/jm00249a006
20. Houry S, Mechoulam R, Loev B. Benzoxocin and benzoxonin derivatives. Novel groups of terpenophenols with central nervous system activity. *Correction J. Med. Chem*. 1975;18(9):951-952. doi:10.1021/jm00243a020
21. Petrzilka T. Chemie synthetischer hanfderivate. *B Schweiz Akad. Med*. 1971;27. doi:10.5169/seals-307854
22. Tietze LF, von Kiedrowski G, Berger B. Stereo- and Regioselective synthesis of enantiomerically pure (+)- and (−)-Hexahydrocannabinol by intramolecular cycloaddition. *Angew. Chem. Int. Ed. Engl*. 1982; 21(3):221-222. doi:10.1002/anie.198202212
23. Hurem D, Macphail BJ, Carlini R, Lewis J, McNulty J. A catalytic, oxidative synthesis of olivetol, methyl olivetolate and orthogonally protected methyl ether derivatives. *SynOpen*. 2021;5(1):86-90. doi:10.1055/a-1440-9732
24. Tietze LF, Kiedrowski GV, Berger B. A new method of aromatization of cyclohexenone derivatives; synthesis of cannabichromene. *Synthesis*. 1982;1982(8):683-684. doi:10.1055/s-1982-29902

SUPPORTING INFORMATION

Additional supporting information can be found online in the Supporting Information section at the end of this article.

How to cite this article: Schirmer W, Gjuroski I, Vermathen M, Furrer J, Schürch S, Weinmann W. Isolation and characterization of synthesis intermediates and side products in hexahydrocannabiphorol. *Drug Test Anal*. 2025;17(4): 531-543. doi:10.1002/dta.3759

2.2 Publication II

The Identification of Synthetic Impurities in a Vape Pen Containing Δ^9-Tetrahydrocannabiphorol Using Gas Chromatography Coupled with Mass Spectrometry

Schirmer W., Schürch S., Weinmann W.
Psychoactives, **2024**, *3*(4), 491-500
DOI: 10.3390/psychoactives3040030

Description of own contribution

I have initialized and conceptualized this study. Afterwards, I have isolated the compounds and performed the GC-MS experiments. Prof. Dr. Wolfgang Weinmann and Prof. Dr. Stefan Schürch corrected the manuscript and helped to finalize it.

Description of novelty

This research paper describes the identification of synthetic side products and 5-heptylresorcinol, a suspected precursor, in a vape pen containing Δ^9-THCP. 5-Heptylresorcinol is the heptyl homolog of olivetol, which is a listed substance in Switzerland since August 1, 2020, (BetmVV-EDI, Verzeichnis f, Nr. 112) as it can be used for the total synthesis of Δ^9-THC. Similar side products were found as described in **Publication I**, but another synthetic route was used for the total synthesis of Δ^9-THCP. The side products were tentatively identified by comparison of their mass spectra with those of the homologs described in the literature.

Reprint permission

psychoactives

MDPI

Article

The Identification of Synthetic Impurities in a Vape Pen Containing Δ^9-Tetrahydrocannabiphorol Using Gas Chromatography Coupled with Mass Spectrometry

Willi Schirmer [1,2,*], Stefan Schürch [2] and Wolfgang Weinmann [1]

[1] Institute of Forensic Medicine, Forensic Toxicology and Chemistry, University of Bern, Murtenstrasse 26, 3008 Bern, Switzerland
[2] Department of Chemistry, Biochemistry and Pharmaceutical Sciences, University of Bern, Freiestrasse 3, 3012 Bern, Switzerland
* Correspondence: willi.schirmer@irm.unibe.ch

Abstract: Δ^9-Tetrahydrocannabiphorol (Δ^9-THCP, THCP) a psychoactive cannabinoid recently found in *Cannabis sativa* L., is widely used as a legal marijuana substitute. THCP is encountered in sprayed Cannabis, edibles, and vape liquids. The distributors of such products claim that the THCP in use originates from a natural source. The legal status of this substance varies from country to country. THCP and similar cannabinoids with a dibenzoyprane structure have been banned in Switzerland since October 2023. A vape liquid, which contains 90% THCP and 10% terpenes according to the distributor, was analyzed by gas chromatography coupled with mass spectrometry (GC-MS). Besides CBP, CBDP, Δ^9-THCP and Δ^8-THCP and some terpenes, other compounds were found which probably result from a synthetic procedure. This sample contained 5-heptylresorcinol, the heptyl homologue of olivetol, a common precursor for the synthesis of tetrahydrocannabinol (THC). Bisalkylated compounds (*m/z* 476) were found as a result of the reaction of one equivalent of 5-heptylresorcinol with two equivalents of (+)-*p*-mentha-1,8-dien-4-ol or another precursor. Similar bisalkylated compounds are known as undesired side products of the synthesis of THC. The sample contained unidentified isomers of Δ^9-THCP, presumably abnormal cannabinoids (*abn*-Δ^9-THCP; *abn*-Δ^8-THCP) and *iso*-cannabinoids (*iso*-THCP). Chiral derivatization with Mosher acid chlorides revealed that the Δ^9-THCP in the sample was enantiopure.

Keywords: tetrahydrocannabiphorol; THCP; semi-synthetic cannabinoids; GC-MS; Mosher ester

Citation: Schirmer, W.; Schürch, S.; Weinmann, W. The Identification of Synthetic Impurities in a Vape Pen Containing Δ^9-Tetrahydrocannabiphorol Using Gas Chromatography Coupled with Mass Spectrometry. *Psychoactives* **2024**, *3*, 491–500. https://doi.org/10.3390/psychoactives3040030

Academic Editor: João Pedro Silva

Received: 30 August 2024
Revised: 8 October 2024
Accepted: 10 October 2024
Published: 12 October 2024

1. Introduction

The emergence of hexahydrocannabinol (HHC) on the European gray market for cannabimimetic new psychoactive substances (NPS) in mid 2022 and its regulation by various European countries has led to new and unregulated entries with a similar structure on the drug market [1]. HHC can be synthesized from cannabidiol (CBD)-rich extracts of *Cannabis* by acidic cyclization to a mixture of Δ^8- and Δ^9-tetrahydrocannabinol (Δ^8- and Δ^9-THC) and subsequent hydrogenation [2]. It is therefore known as a semi-synthetic cannabinoid. This term is also used for unregulated successors, which share the dibenzopyran structure of THC even though they are not synthesized from natural cannabinoids. One of the semi-synthetic cannabinoids which followed HHC is Δ^9-tetrahydrocannabiphorol (Δ^9-THCP), the heptyl homolog of Δ^9-THC. Δ^9-THCP was recently found as a trace cannabinoid in Cannabis [3]. Its low amount makes it unprofitable for isolation from the natural source, and it is not possible to use a synthetic procedure from a more abundant cannabinoid like CBD [4]. However, manufacturers of semi-synthetic cannabinoid products still claim that a natural Cannabis source was used to make these products. A previous work showed that hexahydrocannabiphorol (HHCP) is probably made synthetically. Isolated

and characterized intermediates and side products led to the conclusion that the analyzed HHCP sample was made from 5-heptyl-1,3-cyclohexadione and citronellal [5].

Due to the unregulated distribution of Δ^9-THCP in the form of vape pen liquids, sprayed hemp, and candies and concerns about the usage of such products, some countries have placed Δ^9-THCP under control, including Germany, Switzerland, France, and Japan [6–9]. This work presents an analysis of a THCP vape pen to determine the origin of its psychoactive ingredient.

1.1. Prevalence of Semi-Synthetic Cannabinoids

To date, statistical data on the prevalence of semi-synthetic cannabinoids on a global perspective are lacking. Recently, data from Denmark were reported [10]. The United Nations Office on Drugs and Crime (Vienna, Austria) reported that the number of countries in North America, South America, Europe, and Southeast Asia reporting semi-synthetic cannabinoids has increased since the first emergence of HHC in late 2021 [11]. The European Union Drugs Agency (Lisbon, Portugal) reported that the market of semi-synthetic cannabinoids can be associated with the legalization of hemp in the United States and the global surplus of CBD from hemp, which can be used for the synthesis of THC isomers and HHC [12]. Semi-synthetic cannabinoids, which cannot be made from CBD, entered the market when countries first started to regulate HHC.

1.2. Health Issues of Semi-Synthetic Cannabinoids

The intoxications associated with THCP are not yet reported, but they are reported for other semi-synthetic cannabinoids. Most intoxication reports due to semi-synthetic cannabinoids are from the consumption of HHC. The effects of HHC intoxication are similar to those of THC intoxication [13,14]. Two cases were recently reported where HHCP was taken. A case of a 20-year-old man with no relevant medical history was reported who orally ingested several drops of an inhalation liquid containing HHCP. He lost his ability to articulate, hallucinated, and vomited twice, after which his friend contacted the ambulance. He received intravenous fluids for maintenance and for facilitating external drug elimination. The patient continued hallucinating on the second day and was able to communicate approximately 26 h after drug administration. On the third day, he received oral intake. Intravenous infusions were stopped on the fourth day as the man reacted well to oral intake. The man was discharged at the fifth day. No blood pressure fluctuations or arrhythmias requiring a medical intervention were observed [15]. Another case described HHCP intoxication in a 19-year-old man who consumed cannabis flowers which were labeled as having 9% HHCP. A part of it was cooked in butter and oil and was then mixed into food, which he ate. The man also smoked some of the flowers and went to sleep two hours after ingestion. The next morning, the man was in a panicked state and had difficulty breathing, and his friend called an ambulance for him. He was taken to a psychiatric emergency room due to suspected psychosis. The man fell into a deep sleep and woke up approximately 50 h after ingestion. He was discharged after two and a half days. During his stay, severe impaired consciousness, tachycardia, and bradycardia with accompanying hypotension were noticed [16].

To this day, no fatal cases from the use of semi-synthetic cannabinoids have been reported. Some semi-synthetic cannabinoids are partial agonists at the human CB_1 receptor [17,18], but this might not be the case for future entries in the market. The cases involving HHCP, an analog of THCP, show that consumers are impaired for several days after consumption.

1.3. Synthetic Routes to Δ^9-THCP and Homologs

The first synthesis of Δ^9-THCP and other THC homologs was described by Adams et al. starting from a corresponding 5-alkylresorcinol and ethyl 4-methyl-2-oxocyclohexane-1-carboxylate [19] or pulegone [20]. Petrzilka used (+)-*p*-mentha-2,8-dien-1-ol and a corresponding 5-alkylresorcinol for the synthesis of various Δ^8-THC homologs. The addition of HCl and the subsequent elimination of HCl with potassium *tert*-amylate afforded Δ^9-THC

Psychoactives **2024**, *3* 493

homologs [21]. The Petrzilka reaction sequence was used for the synthesis of Δ^9-THCP in a recent US patent [22].

Several methods for the synthesis of Δ^9-THC using a chiral terpenoid and olivetol are known. Substituting olivetol for a homolog should deliver the desired Δ^9-THC homolog. Enantiopure verbenol [23], carene epoxides [24], and *cis*-chrysanthenol [25] have also been used with olivetol for the synthesis of Δ^9-THC. Using 5-heptylresorcinol should lead to Δ^9-THCP. Other approaches to Δ^9-THC are summarized in a recent review article [26].

In Switzerland, olivetol is regulated and listed as a precursor substance in the Narcotics List Ordinance [7]. However, the homologs of olivetol that can be used as precursors for THC homologs are not listed in the Swiss Narcotics List Ordinance. Neither olivetol nor its homologs are listed as precursor substances in the United Nations Convention against Illicit Traffic in Narcotic Drugs and Psychotropic Substances 1988 [27].

2. Materials and Methods

2.1. Chemicals and Reagents

The THCP vape pen analyzed in this work was an evidence object confiscated by Swiss customs. It was labeled as having 90% THCP and 10% terpenes. The alkane standard (C7-C40, 1000 µg/mL), (*R*)-(-)-α-Methoxy-α-(trifluoromethyl)-phenylacetyl chloride ((*R*)-MTPA-Cl), (*S*)-(+)-α-Methoxy-α-(trifluoromethyl)-phenylacetyl chloride ((*S*)-MTPA-Cl), and 4-(dimethylamino)pyridine (DMAP) (≥99%) were purchased from Sigma-Aldrich (Buchs, Switzerland). The reference standards Δ^9-THCP, cannabidiphorol (CBDP), cannabiphorol (CBP), and 5-heptylresorcinol were purchased from Cayman Chemical (Ann Arbor, United States). Ethyl acetate (EtOAc) (≥99.9%), *n*-hexane (≥99.9%), sodium sulfate sicc. (Na_2SO_4) (for analysis, Reag. Ph. Eur.), and dichloromethane (DCM) (Reag. Ph. Eur.) were purchased from Grogg Chemie (Stettlen, Switzerland). Methanol (MeOH) (≥99.9%) was purchased from Carl Roth (Karlsruhe, Germany). Silica gel 60 (0.015–0.04 mm) from Macherey-Nagel (Önsingen, Switzerland) was used for the isolation of Δ^9-THCP by preparative column chromatography. An e-liquid sample containing Δ^8-THCP was used for the identification of Δ^8-THCP. This sample was donated to us by Christian Bissig from the Forensic Institute of Zürich (Zürich, Switzerland).

2.1.1. Sample Preparation for Untargeted Analysis

The cannabinoid references and 5-heptylresorcinol references were diluted with EtOAc to a concentration of 10 mg/L or 50 mg/L, respectively, prior to analysis by gas chromatography coupled with mass spectrometry (GC-MS). The mass spectra are shown in the Supplementary Information.

The eluted fractions from preparative column chromatography were measured undiluted. The fraction containing high-molecular-weight impurities was evaporated to dryness, redissolved in 500 µL of EtOAc and measured by GC-MS. The chromatogram and mass spectra of the fraction with high-molecular-weight impurities are included in the Supplementary Information.

2.1.2. DMAP Solution

A DMAP solution (γ = 10 mg/mL in dry DCM) was used as the acylation catalyst for the chiral derivatization. The solution was stored over dry Na_2SO_4.

2.1.3. Chiral Derivatization Solutions

Mosher acid chloride solutions (σ = 10 µL/mL in dry DCM) were used for the preparation of (*S*)- and (*R*)-Mosher esters of Δ^9-THCP. The solutions were stored over dry Na_2SO_4.

2.1.4. Sample Preparation Mosher Ester

The isolated Δ^9-THCP was derivatized to (*S*)- and (*R*)-Mosher esters to determine the absolute configuration and enantiopurity of this compound. An enantiopure reference standard of Δ^9-THCP was derivatized accordingly for comparison. The derivatization

process was described in a previous publication [5]. In brief, a 1 mg/mL solution of Δ^9-THCP in dry DCM was aliquoted into a vial and evaporated to dryness under a stream of nitrogen; 10 µL of a DMAP solution, 50 µL of dry DCM, and 10 µL of either (*R*)-MTPA-Cl or (*S*)-MTPA-Cl solution were added to the residue. The vials were capped, and the solutions were incubated at 50 °C for 12 h. After derivatization, the samples were evaporated to dryness, redissolved in 50 µL EtOAc, and analyzed by GC-MS. The chromatograms and spectra of the Mosher esters are included in the Supplementary Information.

2.2. GC-MS Analysis

Untargeted analysis was performed using a previously published method [5]. The isolated Δ^9-THCP, the cannabinoid and 5-heptylresorcinol references, and the Mosher esters were analyzed using an 8890 gas chromatograph with a 7693A autosampler coupled with a 5977B mass selective detector (Agilent, Basel, Switzerland). MassHunter Workstation GC/MS Data Acquisition (Version 10.1.49) was used for data acquisition, and Enhanced ChemStation (F.01.03.2357) was used for data analysis (both from Agilent). A 5% phenylmethylsiloxane column was used for chromatography (HP-5 ms Ultra Inert, 30 m, 250 µm i.d., 0.25 µm film thickness; Agilent J&W). Helium with a constant flow of 1 mL/min was used as carrier gas. The injection volume was 1 µL in pulsed splitless mode. The thermal oven program started at 70 °C and was held for 3 min; the temperature was then ramped to 290 °C at a rate of 15 °C/min and held for 19 min for a total separation time of 36.7 min. The quadrupole temperature was set to 150 °C, and the source temperature was set to 230 °C. Electron impact (EI) mass spectra were measured with an ionization energy of 70 eV. Measurements were performed in scan mode using a range from *m/z* 35 to 800.

3. Results

3.1. GC-MS Analysis of Vape Pen Liquid

The cartridge of the vape pen was cracked, and 30 mg of the liquid was removed and dissolved in 10 mL of EtOAc for the GC-MS analysis. The total ion chromatogram (Figure 1) shows that this sample contained mostly Δ^9-THCP. Cannabidiphorol (CBDP), cannabiphorol (CBP), and 5-heptylresorcinol were identified using certified reference standards. Δ^8-THCP was identified by spectral comparison with the Cayman Spectral Library (v30052024) (99% match) and by comparison with a sample containing Δ^8-THCP. Besides the known cannabinoids, other compounds were present, which showed very similar mass spectra as the identified cannabinoids or as abnormal and *iso*-cannabinoids, which were isolated from an HHCP sample in a previous work [5]. The compounds are summarized in Table 1. The mass spectra are shown in the Supplementary Information.

Table 1. The chromatographic data, area percentages and relevant ions of the compounds found in the THCP vape pen. The area percentages were calculated from the total ion chromatogram.

Name	R_t/min	RRI	GC-MS Area%	Relevant Ions
5-Heptylresorcinol	15.22	1971	<1	208, 166, 137, 124
CBDP	19.46	2711	1	342, 327, 274, 221
Δ^8-THCP	20.00	2760	3	342, 299, 259
Δ^9-THCP	20.17	2774	56	342, 327, 299, 259
CBP	20.81	2837	7	338, 323, 238
THCP impurity A	19.76	2738	3	356, 341, 313, 286, 214
THCP impurity B *	19.86	2747	10	342, 327, 299, 259
THCP impurity C	20.43	2797	3	340, 325, 240
THCP impurity D	21.02	2858	2	340, 325, 297, 256

* Mass spectrum indistinguishable from Δ^9-THCP. Abbreviations: R_t: retention time; RRI: relative retention index (Kováts index).

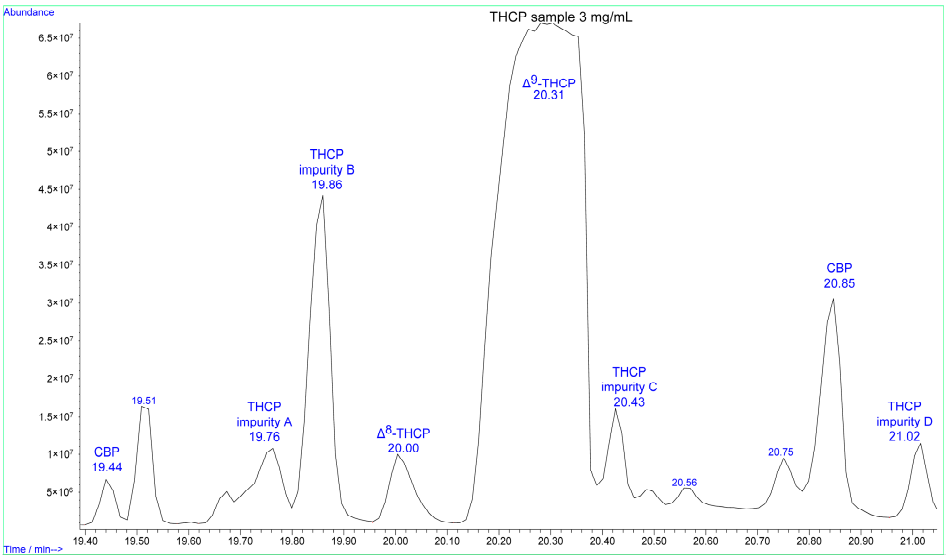

Figure 1. The total ion chromatogram of the THCP vape pen liquid diluted in EtOAc (γ = 3 mg/mL).

Additionally, some terpenes were identified by library hit (>90%) with the Wiley Registry 12th Edition/NIST 2020 Mass Spectral Library. The identified terpenes were α-humulene [28,29], β-myrcene [29], β-phellandrene [30], β-pinene [30], caryophyllene [28,29], and (*R*)-limonene [29], which are naturally found in *Cannabis sativa* L. besides other terpenes [31]. The spectra of the identified terpenes and comparison spectra from the library are included in the Supplementary Information.

3.2. Column Chromatographic Separation

A portion of the Δ^9-THCP vape liquid (300 mg) was separated on silica gel using a chromatography column. Mixtures of *n*-hexane with EtOAc were used as the mobile phase [32]. Pure *n*-hexane was first used as an eluent. The polarity of the eluent was continuously increased by switching to mobile phases with an increasing EtOAc content. Δ^9-THCP (m = 133.5 mg) was isolated, and the other cannabinoids and 5-heptylresorcinol were obtained as impure fractions usually with Δ^9-THCP present. An alkane standard (C7-C40) was measured to identify the Kováts indices of the identified compounds [33]. Their relative retention indices were calculated according to the method by van den Dool and Kratz [34]. A total ion chromatogram of the alkane standard is shown in the Supplementary Information.

3.3. Mass Spectrometric Elucidation of Δ^9-THCP

The mass spectrum of Δ^9-THCP shows similar fragmentation patterns as Δ^9-THC. The loss of a methyl radical ($[M\text{-}15^{\bullet}]^+$, *m/z* 327) forms the base peak of the mass spectrum. The ions resulting from the loss of a propyl radical from the *gem*-dimethyl group ($[M\text{-}43^{\bullet}]^+$, *m/z* 299) and the loss of *n*-hexene after McLafferty rearrangement ($[M\text{-}84]^{\bullet+}$, *m/z* 258) are also observed. The ion *m/z* 243 is formed after the loss of a methyl radical from the *gem*-dimethyl group and *n*-hexene from the side chain ($[M\text{-}15^{\bullet}\text{-}84]^+$). Another abundant ion is the *m/z* 259 ion, which forms after a reaction sequence, as shown in Figure 2. The same chromenylium ion *m/z* 259 is readily formed from Δ^8-THCP after the loss of a methyl radical and a Retro-Diels-Alder reaction [35].

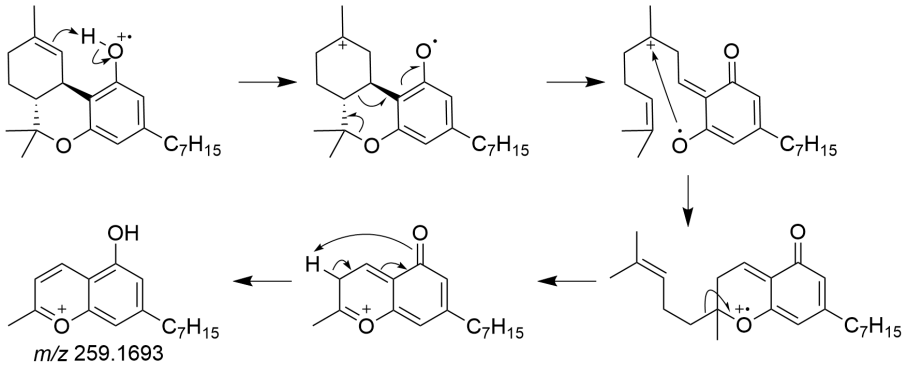

Figure 2. Fragmentation mechanism of the chromenylium ion *m/z* 259 from Δ^9-THCP.

3.4. Mass Spectrometric Elucidation of THCP Impurities

Impurity A shows some common fragmentation patterns of dibenzopyran cannabinoids. An oxo-derivative of THCP seems to be a plausible structure. The elimination of a methyl radical ($[M\text{-}15^{\bullet}]^+$, *m/z* 341) and the elimination of a propyl radical from the *gem*-dimethyl group ($[M\text{-}43^{\bullet}]^+$, *m/z* 313) are observed. The lower fragments could not be assigned.

Impurity B shows the same mass spectrum as Δ^9-THCP. Since the homolog Δ^9-THC and the analog (9*R*)-HHCP show identical mass spectra for their *cis*- and *trans*-isomers [5], it is assumed that the THCP impurity B is *cis*-Δ^9-THCP.

Impurity C has a similar mass spectrum to CBP. The ions are shifted by *m/z* 2, indicating that this compound possesses one degree of saturation more than CBP. 7,8-Dihydrocannabinol is a likely structure for impurity C. The base peak of the chromatogram is the ion after the loss of a methyl radical ($[M\text{-}15^{\bullet}]^+$, *m/z* 325). The fragment ion ($[M\text{-}43^{\bullet}]^+$, *m/z* 297) is not present. The high abundance of *m/z* 325 might be explained by the formation of an aromatic chromenylium ion locating the double bond between positions C6a and C10a. The double bond between C6a and C10a disfavors the formation of the $[M\text{-}43^{\bullet}]^+$ ion, as seen in the GC-MS spectrum of $\Delta^{6a,10a}$-THC [36].

6a,10a-dihydrocannabinol is a plausible structure for THCP impurity D. The mass spectrum of impurity D shows the molecular ion as the base peak ($[M]^{\bullet+}$, *m/z* 340). The loss of a methyl radical ($[M\text{-}15^{\bullet}]^+$, *m/z* 325) and a propyl radical from the *gem*-dimethyl group ($[M\text{-}43^{\bullet}]^+$, *m/z* 297) is seen. In addition, the loss of *n*-hexene after McLafferty rearrangement is also seen ($[M\text{-}84]^{\bullet+}$, *m/z* 256), confirming the heptyl side chain of this compound. Proposed structures for the impurities are shown in Figure 3. The mass spectra of the described THCP impurities are included in the Supplementary Information.

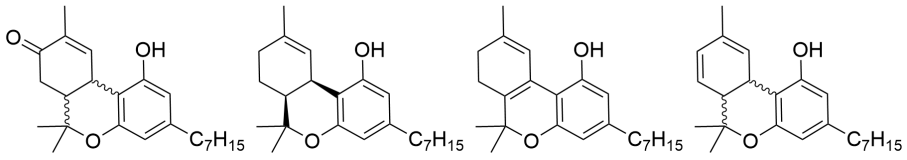

Figure 3. The proposed structures of the impurities found in the vape pen. From left to right: oxo-THCP (impurity A; the position of the oxo group is not determined), *cis*-Δ^9-THCP (impurity B), 7,8-dihydrocannabinol (impurity C), and 6a,10a-dihydrocannabinol (impurity D).

3.5. Mass Spectrometric Elucidation of High-Molecular-Weight Impurities

An impure fraction was isolated from the THCP sample, containing compounds with Kováts indices ranging from 3100 to 3600. These compounds showed fragmentation patterns, which were observed for Δ^9-THCP and its isomers. The molecular ion of most of these compounds is *m/z* 476, which would fit to bisalkylated cannabinoids. Bisalkylated

side products are known to be obtained from the synthesis of Δ^9-THC [21,37–39]. Similar bisalkylated products were found in a previous analysis of an HHCP sample [5]. The fragment ion *m/z* 461 occurs from the loss of a methyl radical; *m/z* 433 forms from the loss of a propyl radical. The chromenylium ion *m/z* 393 forms according to the mechanism shown for Δ^9-THCP in Figure 2. After the McLafferty rearrangement and the loss of *n*-hexene, the radical ion *m/z* 392 is formed. The fragmentation of an alicyclic ring leads to the tropylium ion *m/z* 355. The shown fragmentation reactions are commonly found in phytocannabinoids [35,40,41]. The structures for the proposed fragment ions are shown in Figure 4. Besides the discussed fragment ions, the mass spectra of the high-molecular-weight impurities showed an abundance of lighter fragment ions, but their structures could not be elucidated.

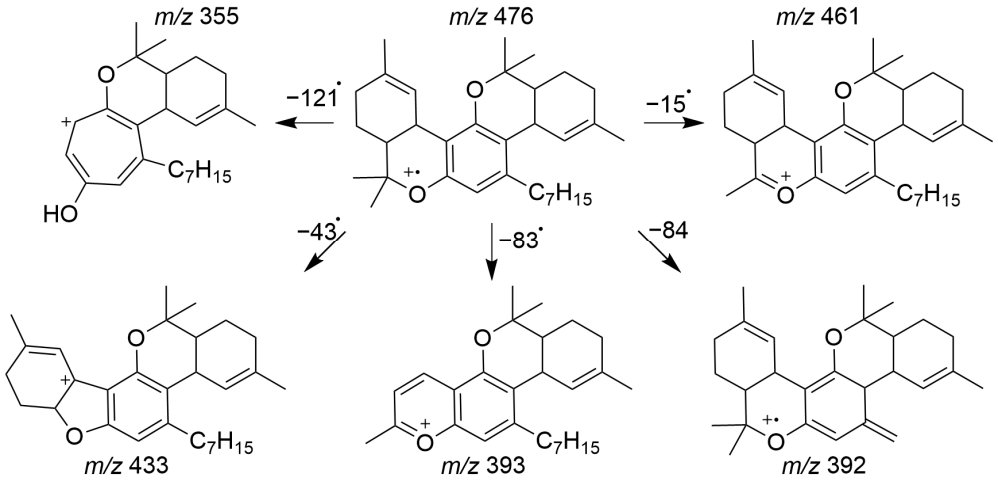

Figure 4. Proposed structures of some fragment ions found in mass spectra of high-molecular-weight impurities.

3.6. Stereoanalysis of Δ^9-THCP

The chromatograms of the (*R*)- and (*S*)-Mosher esters of the isolated Δ^9-THCP showed one peak with an *m/z* 558. No scalemic impurities were detected. The mass spectra and retention times matched with the Mosher esters of the reference compound, leading to the conclusion that the isolated Δ^9-THCP had a natural configuration ((6a*R*, 10a*R*)-Δ^9-THCP) and was enantiopure.

4. Discussion

The analyzed Δ^9-THCP vape pen consisted mainly of enantiopure (6a*R*, 10a*R*)-Δ^9-THCP. Isomeric compounds and derivatives were also present from which only Δ^8-THCP, CBP, and CBDP were unambiguously identified via library matching and comparison with the reference standards. This sample also contained 5-heptylresorcinol, which, to the authors' knowledge, does not occur naturally in Cannabis; it is likely an unreacted precursor for the synthesis of Δ^9-THCP. Several total syntheses of Δ^9-THC start from the homolog 5-pentylresorcinol, which is wider known as olivetol [26]. These methods share excellent stereocontrol of the newly formed stereocenters at positions 6a and 10a, which might explain why no scalemic impurity was found in the isolated Δ^9-THCP. THCP impurities A-D are likely synthetic side products of incomplete regiocontrol and diastereoselectivity, resulting in undesirable and mostly unnatural cannabinoids, including abnormal THCPs, *iso*-THCPs, *cis*-THCPs, or even hybrids. The vape pen also contained high-molecular-weight impurities, which are likely side products from a second alkylation on the resorcinol. Such side products are well known to be obtained from the synthesis of THC from olivetol [21,37–39].

The stated content of Δ^9-THCP of the vape pen does not match the results. The distributor stated that the composition of the liquid consists of 90% Δ^9-THCP and 10% terpenes. Watanabe et al. reported mismatches between the actual and stated contents of semi-synthetic cannabinoids in various vape pen liquids sold in Japan. Some of the products did not even contain the stated cannabinoid [42]. Pulver et al. drew the same conclusion after analyzing recreational products containing semi-synthetic cannabinoids in Germany [43].

5. Conclusions

The analysis of chemical impurities in synthetic drugs, e.g., semi-synthetic cannabinoids, provides information about the synthesis route and the starting material. Knowing the routes to certain drugs or drug classes gives the authorities the opportunity to control the illegal production of these substances. Similar to olivetol, which is used for the synthesis of THC, the control of olivetol homologs could be considered, as they are essential for the synthesis of semi-synthetic cannabinoids with a different chain length than CBD or THC.

Due to the low frequency of cannabinoids with an alkyl side chain other than pentyl and the low price of the products containing them, it can be expected that all semi-synthetic cannabinoids sold with a non-pentyl alkyl chain are of synthetic origin. The quality control of these products is rather low, as evidenced by the isomeric impurities. It can be assumed that these products contain impurities from the synthetic process such as solvents or catalysts. The regulation of semi-synthetic cannabinoids and olivetol homologs is highly recommended.

Supplementary Materials: The following supporting information can be downloaded at https://www.mdpi.com/article/10.3390/psychoactives3040030/s1, A Word document with figures of GC-MS chromatograms and the EI mass spectra of the compounds discussed in this article (S1–S37).

Author Contributions: Conceptualization, W.S. and W.W.; methodology, W.S.; investigation, W.S.; resources, W.W.; data curation, W.S.; writing—original draft preparation, W.S.; writing—review and editing, W.W. and S.S.; visualization, W.W.; supervision, W.W. and S.S. All authors have read and agreed to the published version of the manuscript.

Funding: This research received no external funding.

Institutional Review Board Statement: Not applicable.

Informed Consent Statement: Not applicable.

Data Availability Statement: The original contributions presented in this study are included in the article/Supplementary Materials; further inquiries can be directed to the corresponding author.

Acknowledgments: Severine Krönert from the Institute of Forensic Medicine Bern is acknowledged for her analytical help. Remo Arnold from the University of Bern is acknowledged for the material he provided for column chromatography. Christian Bissig from the Forensic Institute of Zürich is acknowledged for providing a reference sample, which included Δ^8-THCP.

Conflicts of Interest: The authors declare no conflicts of interest.

References

1. Ujváry, I.; Evans-Brown, M.; Gallegos, A.; Planchuelo, G.; de Morais, J.; Christie, R.; Jorge, R.; Sedefov, R. *Hexahydrocannabinol (HHC) and Related Substances*; European Monitoring Centre for Drugs and Drug Addiction (EMCDDA): Lisbon, Portugal, 2023. Available online: https://www.emcdda.europa.eu/publications/technical-reports/hhc-and-related-substances_en (accessed on 20 August 2024).
2. Russo, F.; Vandelli, M.A.; Biagini, G.; Schmid, M.; Luongo, L.; Perrone, M.; Ricciardi, F.; Maione, S.; Laganà, A.; Capriotti, A.L.; et al. Synthesis and pharmacological activity of the epimers of hexahydrocannabinol (HHC). *Sci. Rep.* **2023**, *13*, 11061. [CrossRef] [PubMed]
3. Citti, C.; Linciano, P.; Russo, F.; Luongo, L.; Iannotta, M.; Maione, S.; Laganà, A.; Capriotti, A.L.; Forni, F.; Vandelli, M.A.; et al. A novel phytocannabinoid isolated from *Cannabis sativa* L. with an in vivo cannabimimetic activity higher than Δ^9-tetrahydrocannabinol: Δ^9-Tetrahydrocannabiphorol. *Sci. Rep.* **2019**, *9*, 20335. [CrossRef] [PubMed]
4. Caprari, C.; Ferri, E.; Vandelli, M.A.; Citti, C.; Cannazza, G. An emerging trend in Novel Psychoactive Substances (NPSs): Designer THC. *J. Cannabis Res.* **2024**, *6*, 21. [CrossRef] [PubMed]

5. Schirmer, W.; Gjuroski, I.; Vermathen, M.; Furrer, J.; Schürch, S.; Weinmann, W. Isolation and characterization of synthesis intermediates and side products in hexahydrocannabiphorol. *Drug Test. Anal.* **2024**. [CrossRef]
6. Neue-Psychoaktive-Stoffe-Gesetz Vom 21. November 2016 (BGBl. I S. 2615), das Zuletzt Durch Artikel 1 der Verordnung Vom 21. Juni 2024 (BGBl. 2024 I Nr. 210) Geändert Worden ist. Available online: www.gesetze-im-internet.de/npsg/NpSG.pdf (accessed on 20 August 2024).
7. Schweizerische Eidgenossenschaft. Verordnung des EDI Über Die Verzeichnisse der Betäubungsmittel, Psychotropen Stoffe, Vorläuferstoffe und Hilfschemikalien (Betäubungsmittelverzeichnisverordnung, BetmVV-EDI) Vom 30. Mai 2011 (Stand am 9. Oktober 2023). Available online: https://www.fedlex.admin.ch/eli/cc/2011/363/de (accessed on 20 September 2024).
8. Agence Nationale de Sécurité du Médicament et des Produits de Santé. Available online: https://ansm.sante.fr/actualites/lansm-inscrit-de-nouveaux-cannabinoides-sur-la-liste-des-stupefiants (accessed on 20 September 2024).
9. Ministry of Health. Labour and Welfare of Japan. Available online: www.mhlw.go.jp/content/11126000/000791456.pdf (accessed on 20 September 2024).
10. Jørgensen, C.F.; Rasmussen, B.S.; Linnet, K.; Thomsen, R. Emergence of semi-synthetic cannabinoids in cannabis products seized in Eastern Denmark over a 6-year period. *J. Forensic Sci.* **2024**. [CrossRef] [PubMed]
11. United Nations Office on Drugs and Crime UNODC. *SMART Forensics Update, Beyond Plants: Semi-Synthetic Diversify the Cannabis Market*; United Nations Office on Drugs and Crime UNODC: Vienna, Austria, 2024; Volume 1.
12. European Union Drugs Agency EUDA. *EU Drug Market: New Psychoactive Substances-Distribution and Supply in Europe: Semi-Synthetic Cannabinoids*; European Union Drugs Agency EUDA: Lisbon, Portugal, 2024.
13. Labadie, M.; Nardon, A.; Castaing, N.; Bragança, C.; Daveluy, A.; Gaulier, J.-M.; El Balkhi, S.; Grenouillet, M. Hexahydrocannabinol poisoning reported to French poison centres. *Clin. Toxicol.* **2024**, *62*, 112–119. [CrossRef]
14. O'Mahony, B.; O'Malley, A.; Kerrigan, O.; McDonald, C. HHC-induced psychosis: A case series of psychotic illness triggered by a widely available semisynthetic cannabinoid. *Ir. J. Psychol. Med.* **2024**. [CrossRef]
15. Iketani, Y.; Morita, S.; Tsuji, T.; Noguchi, W.; Maki, Y.; Inoue, K.; Nakagawa, Y. A Case of Acute Intoxication from Sublingually Administering a Liquid Inhalation Product Containing a Marijuana Analoge. *Tokai J. Exp. Clin. Med.* **2024**, *49*, 128–132.
16. Reiter, N.; Linnet, K.; Østermark Andersen, N.; Rasmussen, B.S.; Klose Nielsen, M.; Eriksen, K.R.; Palmqvist, D.F. Svær forgiftning med semisyntetiske cannabinoider. *Ugeskr. Læger* **2024**, *186*, V04240241. [CrossRef]
17. Persson, M.; Kronstrand, R.; Evans-Brown, M.; Green, H. In vitro activation of the CB1 receptor by the semi-synthetic cannabinoids hexahydrocannabinol (HHC), hexahydrocannabinol acetate (HHC-O) and hexahydrocannabiphorol (HHC-P). *Drug Test. Anal.* **2024**. [CrossRef]
18. Janssens, L.K.; Van Uytfanghe, K.; Williams, J.B.; Hering, K.W.; Iula, D.M.; Stove, C.P. Investigation of the intrinsic cannabinoid activity of hemp-derived and semisynthetic cannabinoids with β-arrestin2 recruitment assays—And how this matters for the harm potential of seized drugs. *Arch. Toxicol.* **2024**, *98*, 2619–2630. [CrossRef] [PubMed]
19. Adams, R.; Loewe, S.; Jelinek, C.; Wolff, H. Tetrahydrocannabinol Homologs with Marihuana Activity. IX1. *J. Am. Chem. Soc.* **1941**, *63*, 1971–1973. [CrossRef]
20. Adams, R.; Loewe, S.; Smith, C.M.; McPhee, W.D. Tetrahydrocannabinol Homologs and Analogs with Marihuana Activity. XIII1. *J. Am. Chem. Soc.* **1942**, *64*, 694–697. [CrossRef]
21. Petrzilka, T.; Haefliger, W.; Sikemeier, C. Synthese von Haschisch-Inhaltsstoffen. 4. Mitteilung. *Helv. Chim. Acta* **1969**, *52*, 1102–1134. [CrossRef]
22. Linciano, P.; Citti, C.; Russo, F.; Luongo, L.; Iannotta, M.; Belardo, C.; Maione, S.; Vandelli, M.A.; Forni, F.; Gigli, G.; et al. Cannabis Extracts and Uses Thereof. US Patent US2022064090A1, 3 March 2022.
23. Mechoulam, R.; Braun, P.; Gaoni, Y. Stereospecific synthesis of (-)-Δ^1- and (-)-$\Delta^{1(6)}$-tetrahydrocannabinols. *J. Am. Chem. Soc.* **1967**, *89*, 4552–4554. [CrossRef]
24. Razdan, R.K.; Handrick, G.R.; Hashish, V. A stereospecific synthesis of (-)-Δ^1- and (-)-$\Delta^{1(6}$-tetrahydrocannabinols. *J. Am. Chem. Soc.* **1970**, *92*, 6061–6062. [CrossRef]
25. Razdan, R.K.; Handrick, G.R.; Dalzell, H.C. A one-step synthesis of (-)-Δ^1-Tetrahydrocannabinol from chrysanthenol. *Experientia* **1975**, *31*, 16–17. [CrossRef]
26. Bloemendal, V.R.L.J.; van Hest, J.C.M.; Rutjes, F.P.J.T. Synthetic pathways to tetrahydrocannabinol (THC): An overview. *Org. Biomol. Chem.* **2020**, *18*, 3203–3215. [CrossRef]
27. United Nations Convention against Illicit Traffic in Narcotic Drugs and Psychotropic Substances. 1988. Available online: https://www.incb.org/incb/en/precursors/1988-convention.html (accessed on 20 August 2024).
28. Simonsen, J.L.; Todd, A.R. 32. Cannabis indica. Part X. The essential oil from Egyptian hashish. *J. Chem. Soc.* **1942**, 188–191. [CrossRef]
29. Martin, L.; Smith, D.M.; Farmilo, C.G. Essential Oil from Fresh Cannabis Sativa and its Use in Identification. *Nature* **1961**, *191*, 774–776. [CrossRef]
30. Nigam, M.C.; Handa, K.L.; Nigam, I.C.; Levi, L. Essential oils and their constituents: XXIX. The essential oil of marihuana: Composition of genuine indian *Cannabis sativa* L. *Can. J. Chem.* **1965**, *43*, 3372–3376. [CrossRef]
31. Radwan, M.M.; Chandra, S.; Gul, S.; ElSohly, M.A. Cannabinoids, Phenolics, Terpenes and Alkaloids of Cannabis. *Molecules* **2021**, *26*, 2774. [CrossRef] [PubMed]

32. Tanaka, R.; Kikura-Hanajiri, R. Identification of hexahydrocannabinol (HHC), dihydro-*iso*-tetrahydrocannabinol (dihydro-*iso*-THC) and hexahydrocannabiphorol (HHCP) in electronic cigarette cartridge products. *Forensic Toxicol.* **2023**, *42*, 71–81. [CrossRef]
33. Kováts, E. Gas-chromatographische Charakterisierung organischer Verbindungen. Teil 1: Retentionsindices aliphatischer Halogenide, Alkohole, Aldehyde und Ketone. *Helv. Chim. Acta* **1958**, *41*, 1915–1932. [CrossRef]
34. van Den Dool, H.; Kratz, P.D. A generalization of the retention index system including linear temperature programmed gas—Liquid partition chromatography. *J. Chromatogr. A* **1963**, *11*, 463–471. [CrossRef]
35. Vree, T.B. Mass Spectrometry of Cannabinoids. *J. Pharm. Sci.* **1977**, *66*, 1444–1450. [CrossRef]
36. Claussen, U.; Fehlhabeer, H.W.; Korte, F. Haschisch—XI: Massenspektrometrische Bestimmung von Haschisch-Inhaltsstoffen-II. *Tetrahedron* **1966**, *22*, 3535–3543. [CrossRef]
37. Houry, S.; Mechoulam, R.; Fowler, P.J.; Macko, E.; Loev, B. Benzoxocin and benzoxonin derivatives. Novel groups of terpenophenols with central nervous system activity. *J. Med. Chem.* **1974**, *17*, 287–293. [CrossRef]
38. Houry, S.; Mechoulam, R.; Loev, B. Benzoxocin and benzoxonin derivatives. Novel groups of terpenophenols with central nervous system activity. Correction. *J. Med. Chem.* **1975**, *18*, 951–952. [CrossRef]
39. Millimaci, A.M.; Trilles, R.V.; McNeely, J.H.; Brown, L.E.; Beeler, A.B.; Porco, J.A., Jr. Synthesis of Neocannabinoids Using Controlled Friedel–Crafts Reactions. *J. Org. Chem.* **2023**, *88*, 13135–13141. [CrossRef]
40. Budzikiewicz, H.; Alpin, R.T.; Lightner, D.A.; Djerassi, C.; Mechoulam, R.; Gaoni, Y. Massenspektroskopie und ihre Anwendung auf strukturelle und stereochemische Probleme—LXVIII: Massenspektroskopische Untersuchung der Inhaltstoffe von Haschisch. *Tetrahedron* **1965**, *21*, 1881–1888. [CrossRef] [PubMed]
41. Harvey, D.J. Mass spectrometry of the cannabinoids and their metabolites. *Mass Spectrom. Rev.* **1987**, *6*, 135–229. [CrossRef]
42. Watanabe, S.; Murakami, T.; Muratsu, S.; Fujiwara, H.; Nakanishi, T.; Seto, Y. Discrepancies between the stated contents and analytical findings for electronic cigarette liquid products: Identification of the new cannabinoid, Δ^9-tetrahydrocannabihexol acetate. *Drug Test. Anal.* **2024**. [CrossRef] [PubMed]
43. Pulver, B.; Schmitz, B.; Brandt, S.D.; Auwärter, V. Chemical analysis of recreational products containing semi-synthetic cannabinoids in Germany. In Proceedings of the TIAFT2024 Conference, St. Gallen, Switzerland, 2–6 September 2024.

2.3 Publication III

Identification of human hexahydrocannabinol metabolites in urine

Schirmer W., Auwärter V., Kaudewitz J., Schürch S., Weinmann W.
European Journal of Mass Spectrometry, **2023**, *29*(5-6), 326-337
DOI: 10.1177/14690667231200139

Description of own contribution

Prof. Dr. Wolfgang Weinmann, Prof. Dr. Volker Auwärter, Dr. Julia Kaudewitz, and I have initialized and conceptualized this study. Dr. Julia Kaudewitz performed and interpreted the GC-MS/MS experiments. Dr. Stefan König measured the LC-QqTOF samples and I have analyzed and interpreted the LC-QqTOF data. I have performed the LC-QqLIT and GC-MS analysis, and interpreted the results. I have written the original manuscript. Prof. Dr. Wolfgang Weinmann, Prof. Dr. Stefan Schürch and Prof. Dr. Volker Auwärter have corrected the manuscript.

Description of novelty

Before its regulation, HHC was widely used as a legal substitute of cannabis. This research paper was among the first published investigations of the human *in vivo* metabolism of HHC and describes the identification of HHC and its metabolites after oral and inhalative consumption. The metabolites 4'OH-HHC and 11-OH-HHC have been proposed as analytical targets for the proof of HHC consumption. The carboxylated metabolites (9*R*)-11-nor-9-carboxy-HHC and (9*S*)-11-nor-9-carboxy-HHC were only found in trace amounts. Various methods have been developed for LC-MS/MS and GC-MS(/MS) to proof the consumption of HHC in forensic casework.

Reprint permission

In memoriam of Michael Przybylski

EJMS

European Journal of Mass Spectrometry
1–12

DOI: 10.1177/14690667231200139
journals.sagepub.com/home/ems
Sage

Identification of human hexahydrocannabinol metabolites in urine

Willi Schirmer[1,2], Volker Auwärter[3,4], Julia Kaudewitz[3,4], Stefan Schürch[2] and Wolfgang Weinmann[1]

Abstract

Hexahydrocannabinol (HHC) is a cannabinoid that has been known since 1940 but has only recently found its way into recreational use as a psychoactive drug. HHC has been used as a legal alternative to tetrahydrocannabinol (THC) in many countries, but first countries already placed it under their narcotic substances law. Our aim was to evaluate a reliable analytical method for the proof of HHC consumption by LC-MS/MS and GC-MS. We identified the two epimers of HHC and metabolites after HHC consumption by two volunteers (inhalation by use of a vaporizer and oral intake). LC-HR-MS/MS, LC-MS/MS and GC-MS with literature data (EI-MS spectra of derivatives) and reference compounds - as far as commercially available - were used for metabolite identification. Phase-II-metabolites (glucuronides) of HHC and OH-HHC were found in urine samples with LC-HR-MS/MS and LC-MS/MS. The main metabolite was tentatively identified with GC-MS as 4'OH-HHC (stereochemistry on C9 and C4' unknown). Another major side-chain hydroxylated metabolite found by LC-MS/MS could not be unambiguously identified. Both epimers of 11-OH-HHC were found in considerable amounts in urine. (8*R*, 9*R*)-8-OH-HHC was identified as a minor metabolite with GC-MS and LC-MS/MS. While (9*S*)-HHC was found in urine after oral intake and inhalation of HHC, the more psychoactive epimer (9*R*)-HHC was only found in urine after inhalation. Several other minor metabolites were detected but not structurally identified. We found that after oral or inhalative consumption the urinary main metabolites of a diastereomeric mixture of HHC are different from the respective, major Δ^9-THC metabolites (11-OH-Δ^9-THC and 11-nor-9-carboxy-Δ^9-THC). Although a sensitive LC-MS/MS and GC-SIM-MS method were set-up for the reference compounds (9*R*)-11-nor-9-carboxy-HHC and (9*S*)-11-nor-9-carboxy-HHC, these oxidation products were not detected in urine with these techniques. To further increase sensitivity, a GC-MS/MS method was developed, and the 11-nor-9-carboxy metabolites of HHC were confirmed to be present as minor metabolites.

Keywords

HHC, hexahydrocannabinol, metabolism, LC-MS/MS, GC-MS, GC-MS/MS, cannabinoid

Date received: 14 July 2023; accepted: 24 August 2023

Introduction

Hexahydrocannabinol (HHC) is a new psychoactive cannabinoid on the drug market. It was first synthesized and described by Roger Adams via hydrogenation of cannabis extracts.[1] It occurs naturally due to disproportionation of (-)-Δ^9-*trans*-tetrahydrocannabinol (Δ^9-THC) to cannabinol and hexahydrocannabinol.[2] HHC was found in small amounts in *Cannabis sativa*.[3] It can be synthesized from cannabidiol (CBD) in two steps after cyclization to Δ^8- or Δ^9-THC with subsequent hydrogenation.[4] It has to be noted that HHC marketed as cannabis substitute usually consists of a mixture of the epimers (9*R*)- and (9*S*)-HHC. (9*R*)-HHC possesses similar affinity towards hCB_1-receptor as Δ^9-THC and shows similar effects as Δ^9-THC *in vitro* and in various species *in vivo*. Detailed and further information about HHC can be found in the technical report from the EMCDDA and the recently published review on HHC.[5,6]

In mid 2022 HHC hit the Swiss market and was advertised as a legal but psychoactive alternative to THC until its ban in March 31, 2023. To our knowledge there has been no publication yet about the human metabolism of HHC. Our aim was to identify consumption markers for HHC in urine and to set up and present analytical methods for detection of HHC and its metabolites using LC-MS/MS or GC-MS(/MS) methods for target analysis. Enzymatic immunoassay for cannabinoids – with cross-reactivity for 11-nor-carboxy-Δ^9-THC and 11-OH- Δ^9-THC (and their phase-II-metabolites) resulted in positive results for up to 2 days after a single oral

[1]Forensic Toxicology and Chemistry, Institute of Forensic Medicine, University of Bern, Bern, Switzerland
[2]Department of Chemistry, Biochemistry and Pharmaceutical Sciences, University of Bern, Bern, Switzerland
[3]Forensic Toxicology, Institute of Forensic Medicine, Medical Center–University of Freiburg, Freiburg, Germany
[4]Faculty of Medicine, University of Freiburg, Freiburg, Germany

Corresponding author:
Willi Schirmer, Institute of Forensic Medicine, Forensic Toxicology and Chemistry, University of Bern, Murtenstrasse 26, 3008 Bern, Switzerland
Email: willi.schirmer@irm.unibe.ch

consumption of 20 mg HHC of a Δ^9-THC abstinent volunteer and up to 4 days after a single inhalation of HHC (15 mg vaped with a MIGHTY vaporizer), thus differentiation of HHC and THC-consumption is of forensic importance due to its different legal status and toxicological effects.

Materials and methods

Chemicals and reagents

Deionized water was produced with a Milli-Q® IQ 7000 system from Millipore (Billerica, USA). *N*-methyl-*N*-trimethylsilyltrifluoroacetamide (MSTFA) (≥ 98.5%), *n*-butyl acetate (*n*-BuOAc) (≥ 99.7%) and ammonium formate (≥ 99.0%) were purchased from Sigma-Aldrich (Buchs, Switzerland). Acetonitrile (MeCN) (≥ 99.9%) was purchased from Thermo Fisher Scientific (Reinach, Switzerland). Acetic acid (AcOH) (Reag. Ph. Eur.), formic acid (50%, in water) and ethyl acetate (EtOAc) (for liquid chromatography) were purchased from Grogg Chemie (Stettlen, Switzerland), methanol (MeOH) (≥ 99.9%) from Carl Roth (Karlsruhe, Germany). The internal standards (ISTD) (–)-Δ^9-*trans*-tetrahydrocannabinol-D_3, (±)-11-hydroxy-Δ^9-*trans*-tetrahydrocannabinol-D_3, (±)-11-nor-9-carboxy-Δ^9-*trans*-tetrahydrocannabinol-D_3 were purchased from Cerilliant (Round Rock, TX, USA). (8*S*, 9*S*)-8-hydroxy-hexahydrocannabinol, (8*R*, 9*R*)-8-hydroxy-hexahydrocannabinol, (8*R*, 9*S*)-8-hydroxy-hexahydrocannabinol, (9*R*)-11-hydroxy-hexahydrocannabinol, (9*S*)-11-hydroxy-hexahydrocannabinol, (9*R*)-11-nor-9-carboxy-hexahydrocannabinol and (9*S*)-11-nor-9-carboxy-hexahydrocannabinol were purchased from Cayman Chemical (Ann Arbor, USA). β-Glucuronidase (*Helix pomatia*) and the alkane standard (C7-C40, 1000 µg/mL) were purchased from Sigma-Aldrich (Buchs, Switzerland). Instant buffer I and β-glucuronidase (BGTurbo) from finden KURA and a homogenous enzyme immunoassay (HEIA) testkit 305UR for cannabinoids in urine from Immunalysis was also provided by Specialty Diagnostix (Passau, Germany). The vaporizer used for the self-administration of HHC was a MIGHTY vaporizer (STORZ & BICKEL GmbH, Tuttlingen, Germany). HHC was bought in online shops (66% (9*R*)-HHC for the vaped sample, 47% (9*R*)-HHC for the ingested sample, GC-MS area percentage).

Self-administration experiment. One of the authors vaped 15 mg HHC, another orally ingested 20 mg HHC. A urine sample was collected before the administration and urine samples were collected over a few days. The samples were stored at −20°C until analysis. An approval by an ethics committee is not required for self-experiments. After vaping 15 mg HHC mild cannabimimetic effects were reported by the volunteer which lasted for about two hours. No serious impairment was observed. The second volunteer reported no noticeable effects after oral ingestion of 20 mg HHC.

Internal standard for LC-QqLIT. The internal standard solution (ISTD) consists of 0.1 µg/mL (–)-Δ^9-*trans*-tetrahydrocannabinol-D_3, 0.1 µg/mL (±)-11-hydroxy-Δ^9-*trans*-tetrahydrocannabinol-D_3 and 0.5 µg/mL (±)-11-nor-9-carboxy-Δ^9-*trans*-tetrahydrocannabinol-D_3 in MeOH.

Reconstitution solution. The reconstitution solution was a mixture of MeCN in water (60 v%) containing formic acid (0.1 v%).

LC-QqTOF analysis. Samples were prepared as follows. 800 µL urine, 100 µL phosphate buffer pH 6 and 40 µL β-glucuronidase (from *Helix pomatia*) or 40 µL water were incubated for 4 h at 47 °C. 1 mL *n*-BuOAc was added and the mixture was shaken for 10 min and centrifuged for 10 min (13000 rpm (17190 *g*), 8 °C). The organic phase was transferred to an autosampler vial and evaporated to dryness under a stream of nitrogen at 50 °C. The residue was reconstituted with 100 µL reconstitution solution. A previously described screening method was used for the analysis.[7] A Dionex Ultimate 3000 HPLC system (Thermo Fisher Scientific, Reinach, Switzerland) coupled to a TripleTOF 5600 mass spectrometer was used (Sciex, Toronto, Canada). Data were acquired with Analyst TF software (version 1.7) and processed with Peak View (version 1.2.0.3) (Sciex, Toronto, Canada). Acquisition of mass spectra was performed in positive ionization mode with an IonDrive Turbo V ion source with TurboIonSpray probe. Samples were separated on a Kinetex C8 column, 50 × 2.1 mm, 2.6 µm, 100 Å (Phenomenex, Basel, Switzerland). A gradient method was used with water containing 0.1% formic acid (%v, mobile phase A) and MeCN containing 0.1% formic acid (%v, mobile phase B). The gradient was as follows: 0–1 min: 2.5% B, 1–7 min: 2.5%–97.5% B, 7–11 min: 97.5% B, 11–11.1 min: 97.5%–2.5% B, 11.1–14 min: 2.5% B. The injection volume was 2.5 µL and the flow rate was 0.35 mL/min. The LC-QqTOF instrument was operated in information dependend data acquisition (IDA) and in SWATH mode (sequential window acquisition of all theoretical mass spectra). For IDA a survey scan from *m/z* 100 to 950 was applied which triggered the acquisition of product ion mass spectra from *m/z* 50 to 950. For SWATH mode mass range from *m/z* 100 to 950 was scanned acquiring product ion spectra in windows of 35 Da from *m/z* 50 to 950. Collision energy with collision energy spread 35 ± 15 V was applied.

GC-MS analysis. For the references 50 µL of 10 µg/mL solutions were evaporated to dryness under a stream of nitrogen. The residue was dissolved in 25 µL MSTFA and 25 µL EtOAc, the mixture was incubated for 40 min at 90 °C. For sample solutions 1 mL urine, 200 µL instant buffer I and 50 µL β-glucuronidase (BGTurbo) were mixed and incubated for 15 min at 50 °C. To the mixture 500 µL *n*-BuOAc was added. The mixtures were shaken for 10 min and centrifuged for 10 min (13000 rpm (17190 *g*), 8 °C). The organic phase was collected and the extraction step was repeated with the same

conditions. The extracts were combined and evaporated to dryness under a stream of nitrogen at 50 °C. The residue was redissolved in 1 mL MeCN and diluted with 2 mL water. This solution was purified using solid phase extraction.

Chromabond® C18 cartridges (Macherey-Nagel, Önsingen, Switzerland) were conditioned with 2 mL MeOH and 2 mL AcOH (0.1 M) prior to loading the sample solution (3 mL) onto the cartridges. The cartridges were washed with 1 mL AcOH (0.1 M), 1 mL aqueous MeCN (40 v%) and optionally with 1 mL aqueous MeCN (70 v%). Samples were eluted with 1.5 mL MeCN, the eluate was transferred to an autosampler vial and evaporated to dryness under a stream of nitrogen at 70 °C. The residue was dissolved in 25 µL EtOAc and 25 µL MSTFA and incubated at 90 °C for 40 min. 1 µL of the reaction mixtures was injected for GC-MS analysis.

Samples were analyzed using a 8890 gas chromatograph with a 7693A autosampler coupled to a 5977B mass selective detector (Agilent, Basel, Switzerland), data were acquired with MassHunter Workstation GC-MS Data Acquisition (Version 10.1.49) and analyzed with Enhanced ChemStation (F.01.03.2357) (Agilent). Chromatography was performed on a 5% phenylmethylsiloxane column (HP-5 ms Ultra Inert, 30 m, 250 µm i.d., 0.25 µm film thickness; Agilent J&W). Helium was used as a carrier gas with a constant flow of 1 mL/min. The injection volume was 1 µL in pulsed splitless mode. The oven temperature started at 80 °C and was ramped with 10 °C/min to 300 °C and held for 1 min, resulting in a total separation time of 23 min. The source temperature was set to 230 °C and the quadrupole temperature to 150 °C. EI mass spectra were obtained with an ionization energy of 70 eV. The scan range was from *m/z* 40 to 650 with a scan speed of 1.562 s^{-1}.

GC-MS/MS analysis. One hundred µL of urine, 10 µL ISTD (0.25 µg/mL (–)-Δ^9-*trans*-tetrahydrocannabinol-D_3, 0.25 µg/mL (±)-11-hydroxy-Δ^9-*trans*-tetrahydrocannabinol-D_3 and 1.25 µg/mL (±)-11-nor-9-carboxy-Δ^9-*trans*-tetrahydrocannabinol-D_3 in MeOH) and 250 µL sodium hydroxide solution (10 M) were mixed and incubated for 15 min at 60 °C. To this mixture 750 µL AcOH (0.1 M) and 1 mL glacial AcOH were added and vortexed immediately. The solutions were used for solid phase extraction as described above for GC-MS. The eluate was evaporated under a stream of nitrogen at 60 °C. The residue was dissolved in 25 µL MSTFA. 1 µL was injected for GC-MS/MS analysis.

Samples were analyzed using a 7890B gas chromatograph with a 7693 autosampler coupled to a 7010 Triple Quadropole MS, operated by MassHunter Workstation B.07.05 (Agilent Technologies, Waldbronn, Germany). Chromatography was performed on a 5% phenylmethylsiloxane column (HP-5 ms Ultra Inert, 30 m, 250 µm i.d., 0.25 µm film thickness; Agilent J&W). The carrier gas was helium with a flow rate of 1 mL/min. The injection volume was 1 µL using splitless mode. The initial oven temperature was 160 °C, hold 0.5 min, ramped 40 °C/min to 280 °C, hold 5 min, ramped 20 °C/min to 310 °C, hold 5 min, resulting in a total time of 15 min. The injection port temperature was 250 °C with a transfer line temperature of 250 °C. The ion source temperature was set to 230 °C. Electronic ionization was employed with an energy of 70 eV. The collision gas was nitrogen. The transitions with corresponding collision energy of the multiple reaction monitoring (MRM) method are shown in Table 1.

LC-QqLIT analysis. For acquisition of mass spectra of the reference compounds, 2 µL of a 10 µg/mL solutions were mixed with 20 µL ISTD and evaporated to dryness under a stream of nitrogen and reconstituted in 200 µL reconstitution solution. The reference spectra are provided in the supplementary information. For the analysis of samples 200 µL urine, 20 µL ISTD, 80 µL instant buffer I and 40 µL β-glucuronidase (BGTurbo) were mixed together and incubated for 10 min at 50 °C. Then, 1 mL *n*-BuOAc was added and shaken for 10 min and centrifuged for 10 min (13000 rpm (17190 *g*), 8 °C). The upper organic phase was transferred to an autosampler vial and was evaporated to dryness under a stream of nitrogen at 50 °C. The residue was reconstituted in 200 µL reconstitution solution. A Dionex Ultimate 3000 HPLC system (Thermo Fisher Scientific, Reinach, Switzerland) was used, coupled to a QTrap 4500 mass spectrometer (Sciex, Toronto, Canada) equipped with an IonDrive Turbo V ion source with TurboIonSpray probe. Data was acquired and processed with Analyst TF software (version 1.7) and visualized with Peak View (version 1.2.0.3) (Sciex, Toronto, Canada). Mass spectra were acquired in positive ionization mode. Chromatographic separation was performed on a Luna Omega PS C18 column, 100 × 2.1 mm, 1.6 µm, 100 Å (Phenomenex, Basel, Switzerland) with the following conditions: gradient with mobile phase A (0.1% formic acid (% v)) and mobile phase B (MeCN containing 0.1% formic acid (%v)): 0–20 min: 35.0%–60.0% B, 20–25 min: 60.0%–97.5%, 25.0–26.0 min, 97.5% B, 26.0–26.1 min, 35.0% B with a flow rate of 0.4 mL/min and a column oven temperature of 40 °C. The injection volume was 1 µL. Spectra were acquired in positive ionization mode with a

Table 1. MRM method with the relevant transitions.

Q1 / Da	Q3 / Da	CE / eV	Name
388	332	10	**HHC MRM 1**
388	303	20	**HHC MRM 2**
373	265	15	**OH-HHC MRM 1**
373	249	15	**OH-HHC MRM 2**
490	329	15	**HHC-COOH MRM 1**
490	265	15	**HHC-COOH MRM 2**
490	434	15	**HHC-COOH MRM 3**
389	306	25	**THC-D_3 MRM 1**
374	308	20	**THC-D_3 MRM 2**
374	292	20	**OH-THC-D_3 MRM 1**
374	308	10	**OH-THC-D_3 MRM 2**
374	308	10	**THC-COOH-D_3 MRM 1**
491	300	30	**THC-COOH-D_3 MRM 2**

CE: collision energy, dwell time was 30 ms for the analytes and 10 ms for the internal standards.

biexperimental method involving multiple reaction monitoring and product ion scan. The curtain gas was set to 35.0 arbitrary units, the ion spray voltage was 4500 V, and the source temperature was 600 °C. Ion source gases 1 and 2 were set to 40.0 arbitrary units. A product ion scan of the precursor ion with *m/z* 333.2 was acquired from *m/z* 50–350 with a scan rate of 200 Da/s, a declustering potential of 120 V, an entry potential of 10 V, a collision energy of 30 V and an cell exit potential of 15 V were applied. The relevant transitions with corresponding potentials of the multiple reaction monitoring (MRM) method are shown in Table 2.

Results and discussion

LC-QqTOF analysis

A urine sample which was collected 2 h after oral ingestion of 20 mg HHC was analyzed by LC-QqTOF.

Table 2. MRM method with the relevant transitions.

Q1 / Da	Q3 / Da	DP / V	CE / V	CXP / V	Name
334.2	316.2	87	21	12	**11-OH-THC-D_3 MRM 1**
334.2	196.2	90	35	7	**11-OH-THC-D_3 MRM 2**
348.2	330.2	93	23	12	**THC-COOH-D_3 MRM 1**
348.2	302.2	102	28	12	**THC-COOH-D_3 MRM 2**
318.2	196.3	88	32	7	**THC-D_3 MRM 1**
318.2	123.0	88	32	7	**THC-D_3 MRM 2**
317.2	193.2	88	32	7	**HHC MRM 1**
317.2	123.2	100	43	8	**HHC MRM 2**
333.2	315.2	87	21	12	**OH-HHC MRM 1**
333.2	193.2	90	35	7	**OH-HHC MRM 2**
333.2	191.2	90	35	7	**OH-HHC MRM 3**
347.2	329.3	93	23	12	**HHC-COOH MRM 1**
347.2	301.2	102	28	12	**HHC-COOH MRM 2**
347.2	193.2	102	28	12	**HHC-COOH MRM 3**
347.2	191.2	93	23	12	**HHC-COOH MRM 4**
493.3	317.2	35	21	4	**HHC-Glu MRM 1**
493.3	193.3	35	21	4	**HHC-Glu MRM 2**
509.3	333.2	35	21	4	**OH-HHC-Glu MRM 1**
509.3	193.3	35	21	4	**OH-HHC-Glu MRM 2**

DP: Declustering potential, CE: collision energy, CXP: Cell exit potential. Dwell time was 20 ms for the glucuronides and 35 ms for all other transistions.

Figure 1 shows extracted ion chromatograms of HHC metabolites and their deglucuronidated products. The glucuronides were not cleaved quantitavely by β-glucuronidase. No further oxidation to carboxylic acids or dihydroxylated HHC was observed (extracted ion chromatograms are not shown). The characteristic fragment ions of the found metabolites are shown in Table 3. The characteristic fragments are discussed in the supplementary information, the respective mass spectra can also be found in the supplementary information.

The urine samples which were treated with β-glucuronidase prior to extraction showed several metabolites with *m/z* 333.2424 indicating hydroxylated HHC. Figure 2 shows the product ion spectrum of the most abundant metabolite M1. Collision induced dissociation of M1 result in product ions which are typical for HHC hydroxylated at the alicyclic part of the molecule (*m/z* 135.1168, *m/z* 153.1274 and *m/z* 193.1223). Additionally, product ions were detected which are typical for side-chain hydroxylated HHC (*m/z* 137.1325, *m/z* 191.1067 and *m/z* 209.1172), suggesting coelution of at least two compounds. It should be noted that this rapid screening method with the rather steep gradient did not resolve the epimers of HHC chromatographically, so coelution of multiple isobaric metabolites is also likely.

The presence of HHC was confirmed after deglucuronidation with comparison to a reference compound.

Product ion spectra of the metabolites were used for differentiation of some hydroxylation positions. Characteristic ions obtained by the fragmentation of HHC (see supplementary information) are altered by hydroxylation at various positions. Figure 3 shows the ions which are characteristic for the alicyclic-hydroxylated HHC. The ions with *m/z* 93.0699 and *m/z* 135.1168 are also found in the product ion spectrum of THC. In the case of OH-HHC these ions are likely formed by the dehydration reaction of *m/z* 153.1274 and *m/z* 111.0804 (see Figure 3), *m/z* 111.0804 was not found. Since the precursor ions corresponds to OH-HHC confusion with THC product ions is impossible. Metabolites which are likely hydroxylated at the alicyclic part of the molecule are the OH-HHC glucuronides M2 and M3 (see Figure 1). The deglucuronidated species M6 and M7 show the same fragment ions and likely originate from M2 and M3. M1

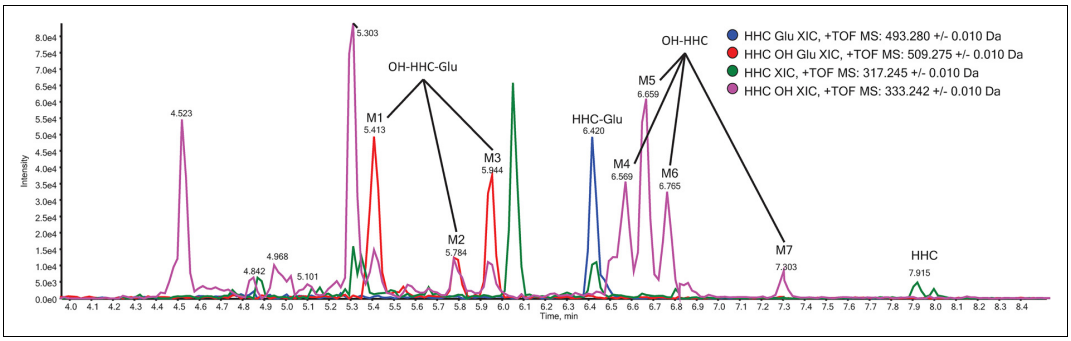

Figure 1. Ion chromatograms of HHC glucuronide, HHC-OH glucuronides (M1-M3) and their deglucuronidated species (M4-M7) in a urine sample 2 h after oral ingestion of 20 mg HHC. The glucuronides were only partially cleaved by β-glucuronidase.

Table 3. Retention time, molecular and fragment ions from HHC metabolites and their deglucuronidated products from the LC-QqTOF method.

Name	RT / min	$[M+H]^+$ / Da	Fragment ions / Da
M1	5.402	509.2793 (9.4 ppm)	333.2434, 315.2329, 259.1691, 193.1223, 191.1073, 137.1333, 135.1160
M2	5.778	509.2792 (9.2 ppm)	333.2423, 315.2256, 259.1692, 193.1208, 153.1263, 135.1102
M3	5.941	509.2754 (1.8 ppm)	333.2435, 315.2283, 259.1712, 193.1242, 135.1132
HHC-Glu	6.451	493.2785 (−2.2 ppm)	317.2477, 193.1222, 137.1320
M4	6.569	333.2442 (5.4 ppm)	315.2322, 259.1685, 209.1182, 191.1075, 137.1323
M5	6.659	333.2428 (1.2 ppm)	315.2322, 259.1697, 191.1075, 137.0583
M6	6.765	333.2394 (−9.0 ppm)	193.1223*
M7	7.303	333.2424 (0.0 ppm)	315.2313*, 193.1252*
HHC	7.915	317.2525 (15.8 ppm)	193.1223

The corresponding product ion spectra are shown in the supplementary material available.
*Ions observed in SWATH spectrum and are likely from the metabolite (M6 and M7).

seems to be a mixture of compounds since it shows fragment ions for both substitution patterns (Figure 3 and Figure 4).

Figure 4 shows ions which suggest hydroxylation at the pentyl side-chain. The ion with *m/z* 191.1067 results from the dehydration reaction of *m/z* 209.1172. Metabolites and deglucuronidated products which are likely side-chain hydroxylated are M4 and M5. M1 most likely consists of two OH-HHC glucuronides, one hydroxylated at the alicyclic part of the molecule and one at the side-chain.

GC-MS analysis

GC-MS analysis of the urine samples was performed after deglucuronidation, purification and derivatizion of the metabolites with MSTFA to the corresponding TMS derivatives. The obtained samples were ionzed by EI in the full scan mode (*m/z* 40–650). The extracted ion chromatogram of *m/z* 476, which is the molecular ion for OH-HHC TMS-derivatives, is shown in Figure 5. Full-scan spectra obtained for the found signals were compared to the list of characteristic ions (with relative ion abundances) of TMS derivatives of OH-HHCs from literature data or with reference compounds if available, reference spectra are provided in the supplementary information.[8] The presence of (8*R*, 9*R*)-8-OH-HHC could be confirmed by comparison of retention time and the EI-MS spectrum with a derivatized reference compound (metabolite G2). The main metabolite G7 was tentatively identified as a 4'OH-HHC by comparison of the relative ion abundances with literature data (stereochemistry at C9 and C4' are unknown).[8] The presence of the side-chain hydroxylated tropylium ion (*m/z* 353) and its fragment ion (*m/z* 263) after loss of TMSOH indicate that this metabolite is indeed a side-chain hydroxylated HHC. Harvey and Brown stated that 4'OH-HHC possesses a characteristic fragment ion with *m/z* 117, which is detected with a relative abundance of 21%. This characteristic ion derives from the elimination of $CH_3CHOTMS^+$, a possible mechanism is shown in Figure 6. We found a relative abundance of 25% for this ion.

This compound also fragments to an ion with *m/z* 263 which is the trimethylsilylated analogue of the characteristic ion with *m/z* 191 discussed in the LC-QqTOF part. However, due to the similarity of their fragmentation patterns, it is unclear which of the isomers was formed. A reference substance is not commercially available at this point. Furthermore, literature does not differentiate the epimers at the 4'OH position. Other compounds in Figure 5 (G1, G3, G4, G5) could not be assigned to hydroxylated structures due to lack of reference compounds and insufficient fit with the relative ion abundances found in the literature due to noise or coelution of unknown compounds from the biological matrix.

From our findings we can conclude that the epimers of HHC undergo a different metabolic pathway. The identification of (8*R*, 9*R*)-8-OH-HHC and absence of (8*R*, 9*S*)-8-OH-HHC in urine samples indicates that (9*R*)-HHC is not metabolized via hydroxylation at C8. The absence of (9*R*)-HHC in one sample after deglucuronidation might be an indicator that this epimer undergoes stronger metabolization during phase I metabolism. Both epimers of 11-OH-HHC were found (G6 and G8). Various peaks appear in the extracted ion chromatogram for *m/z* 476 with other characteristic ions described by Harvey and Brown for TMS-OH-HHCs which could not be structurally identified.[8] Extracted ion chromatograms for *m/z* 419, *m/z* 332 and *m/z* 145 show several peaks. These ions are

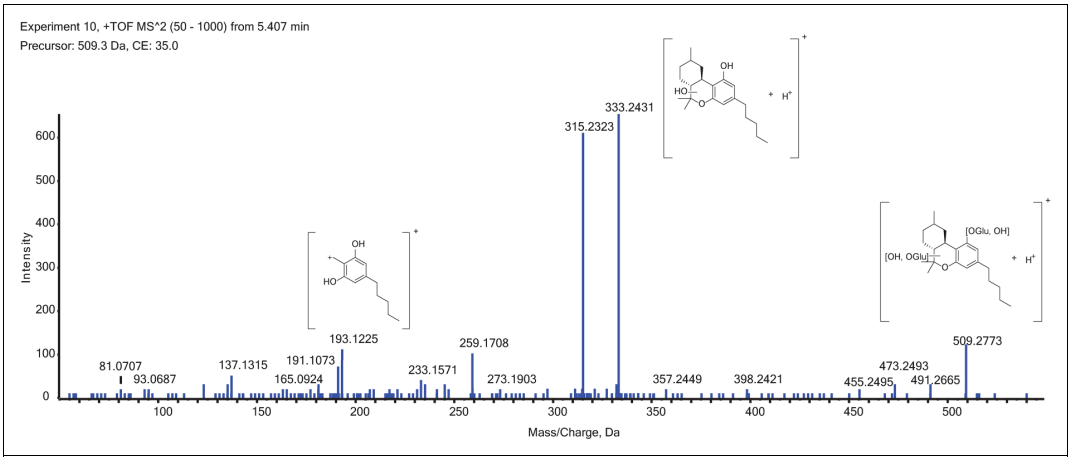

Figure 2. Product ion spectrum of *m/z* 509.3 at 5.407 min. The molecule ion can be seen at *m/z* 509.2773 (5.5 ppm), elimination of three water molecules are also visible (*m/z* 491.2665 (5.3 pm), *m/z* 473.2493 (- 8.7 ppm), *m/z* 455.2495 (14.7 ppm). Fragmentation of the glucuronide leads to protonated OH-HHC with *m/z* 333.2431 (−2.1 ppm). The ion with *m/z* 193.1225 (1.0 ppm) is characteristic for many phytocannabinoids.

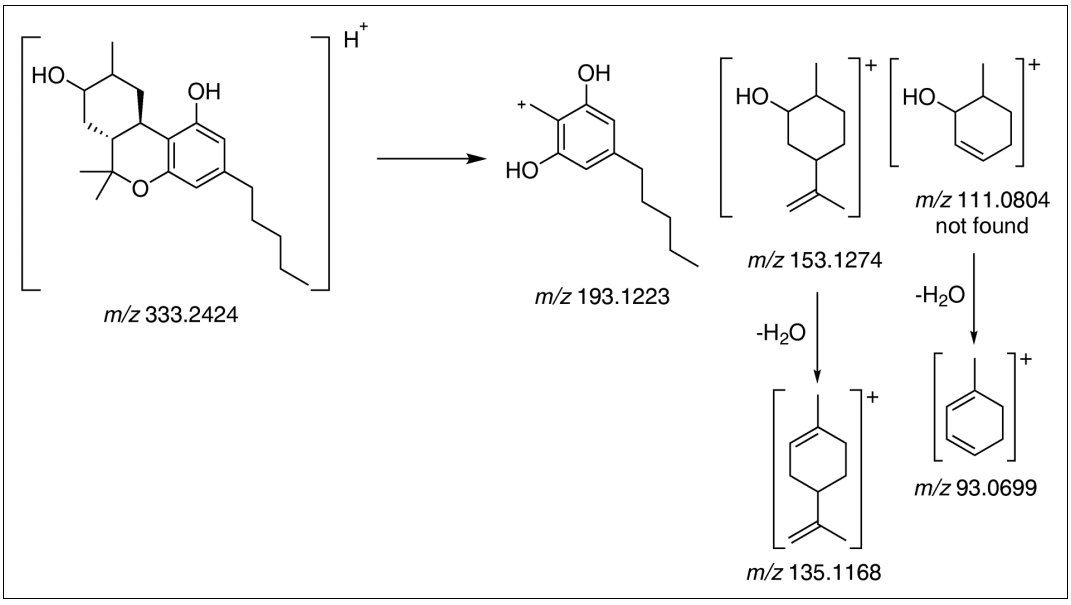

Figure 3. Characteristic product ions of OH-HHC are shown for the hydroxylation of the alicyclic part of the molecule. Hydroxylation position may change. As an example hydroxylation is shown at C8.

characteristic for 1'OH-HHC (*m/z* 419), 2'OH-HHC (*m/z* 145) and 3'OH-HHC (*m/z* 332), but these are the only ions which appear with high abundance in their EI-spectra.[8] Therefore their presence could not be proven. It is noteworthy that the epimers (9*R* and 9*S*) of 11-nor-9-carboxy-HHC can be distinguished via the abundance of the characteristic ion *m/z* 372. We assume that this ion is a radical cation which is formed after loss of CO and TMSOH. The postulated mechanism shown in Figure 7 requires a 1,3-diaxial orientation of the COOTMS group at position 9 and the hydrogen at position 10a (dibenzopyran numbering). This is only possible for (9*S*)-11-nor-9-carboxy-HHC, the 9*R* epimer cannot flip into the required conformation to perform the same reaction with the hydrogen at position 7 since HHC and its discussed metabolites are similar to *trans*-decalins and they cannot ring flip. The different mass spectra for the epimeric pairs of OH-HHCs, hydroxylated on the alicyclic moiety, could be explained with a similar mechanism leading to the ion *m/z* 371 after loss of TMSOH and a methyl radical.[8]

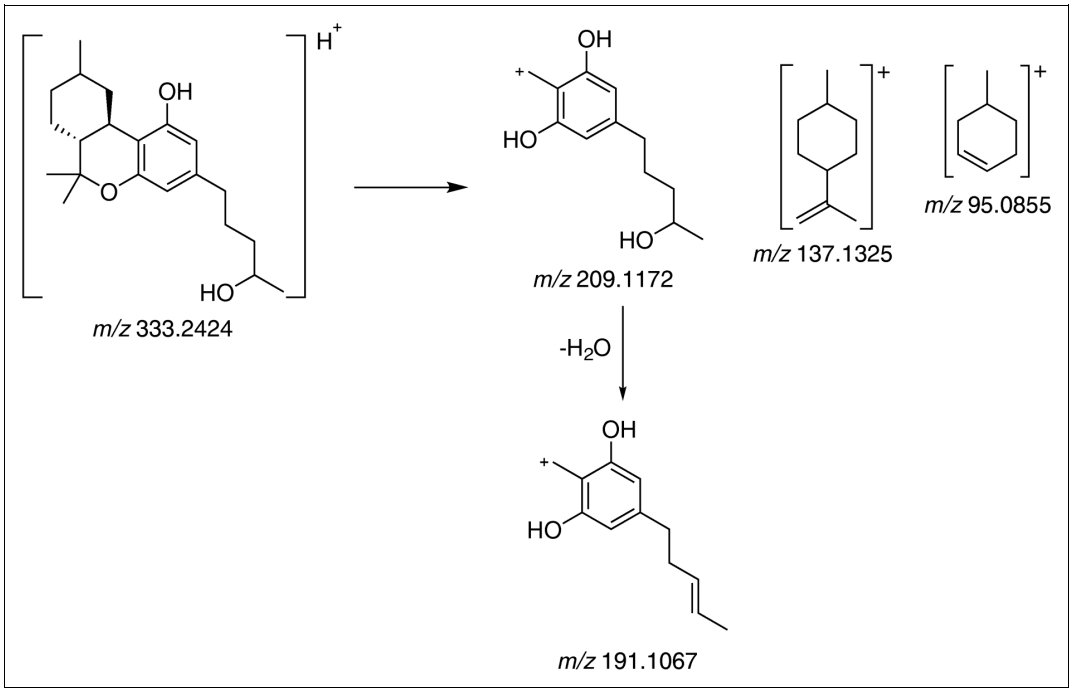

Figure 4. Characteristic product ions are shown of OH-HHC with the hydroxylation on the pentyl side chain of the molecule. As an example shown on the second last carbon of the side chain.

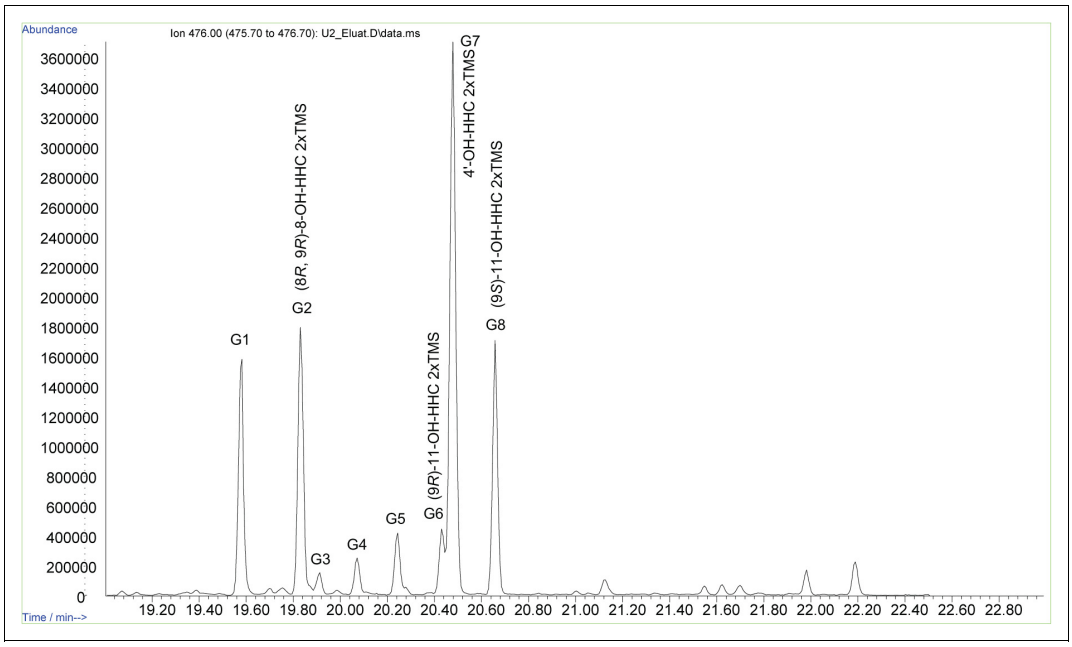

Figure 5. Extracted ion chromatogramm *m/z* 476 (OH-HHC 2×TMS) of a urine sample collected 2 h after oral ingestion of 20 mg HHC.

Table 4 shows the retention times, Kováts-indices[9] and characteristic ions of reference substances, compounds which have been identified by comparison with reference substances or have been tentavely identified according to the relative abundances of characteristic ions from the literature. For the determination of the Kováts-indices an

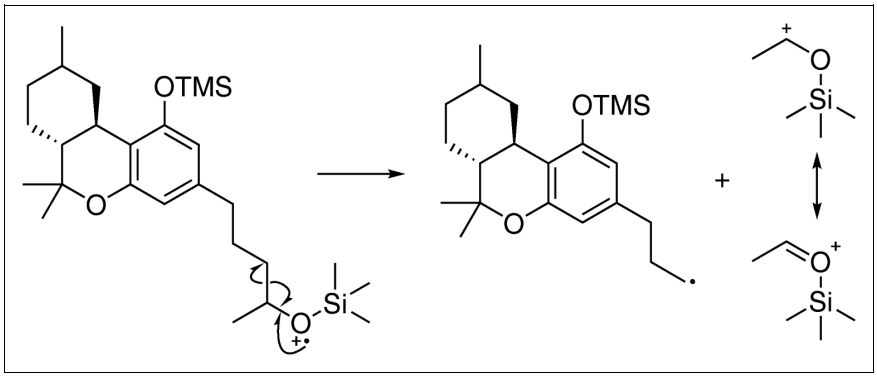

Figure 6. Mechanism for the formation of $CH_3CHOTMS^+$ (*m/z* 117) under EI condition. This fragment ion is characteristic for 4'OH-HHC.

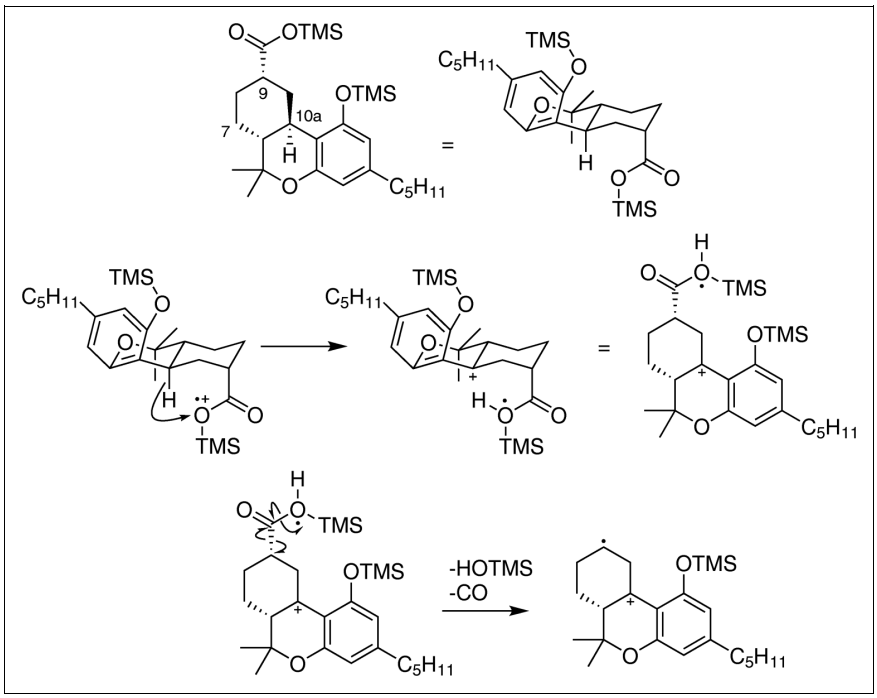

Figure 7. Reaction mechanism for the formation of the radical cation with *m/z* 372. This ion is characteristic for (9*S*)-11-nor-9-carboxy HHC since a 1,3-diaxial orientation of the hydrogen and the COOTMS group is required.

alkane standard (C7-C40) was measured with the same GC-MS method and was calculated according to van Den Dool and Kratz.[10]

Further investigations were performed for the detection of (9*S*)-11-nor-9-carboxy-HHC and (9*R*)-11-nor-9-carboxy-HHC. Urine samples were spiked with (±)-11-nor-9-carboxy-Δ^9-*trans*-tetrahydrocannabinol-D_3 as ISTD, treated with β-glucuronidase and loaded to SPE cartridges, washed with MeCN (40 v%) and eluted with pure MeCN. The evaporated eluates were derivatized as described above. For control, blank urine was spiked with 20 ng/mL each of (9*R*)-11-nor-9-carboxy-HHC and (9*S*)-11-nor-9-carboxy-HHC. The spiked urine and the urine samples after HHC consumption (oral intake and inhalation) were measured in SIM mode (*m/z* 490, 475, 448, 434, 329 and 265 for the 11-nor-9-carboxy HHCs. *m/z* 491, 476, 374 and 300 for the ISTD (±)-11-nor-9-carboxy-Δ^9-*trans*-tetrahydrocannabinol-D_3). With a limit of detection of approximately 10 ng/mL, none of the carboxy-metabolites could be detected in the respective urine samples from the volunteers. To further increase sensitivity, a GC-MS/MS method was applied, achieving a limit of detection below 2.5 ng/mL. Analyzing the urine sample with the highest response in the immunoassay test for cannabinoids after HHC inhalation with a vaporizer, taken 2 h post application, both epimers of 11-nor-9-carboxy-HHC were unambiguously

Table 4. Identification of HHC and metabolites as TMS derivatives with GC-MS. RT: retention time, RRI: relative retention index (Kováts-index).

Name	RT / min	RRI	Fragment ions (relative abundance) / Da
(9*R*)-HHC TMS	18.014	2349	388(85), 373(17), 345(60), 332(100), 303(31), 265(78)
(9*S*)-HHC TMS	18.536	2412	388(70), 373(20), 345(62), 332(100), 303(32), 265(57)
(8*R*, 9*R*)-8-OH-HHC 2xTMS	19.832	2576	476(100), 420(39), 371(46), 343(77), 303(43), 265(50)
(8*R*, 9*S*)-8-OH-HHC 2xTMS	19.902	2585	476(100), 420(41), 371(40), 343(52), 303(28), 265(38)
(8*S*, 9*S*)-8-OH-HHC 2xTMS	19.908	2586	476(6), 371(100)
(8*S*, 9*R*)-8-OH-HHC 2xTMS	20.237	2632	476(8), 371(100)
(9*R*)-11-OH-HHC 2xTMS	20.456	2660	476(100), 433(18), 420(60), 373(19), 343(40), 265(90)
4'OH-HHC 2xTMS	20.481	2663	476(100), 433(28), 332(45), 263(20), 117(25)
(9*S*)-11-OH-HHC 2xTMS	20.651	2685	476(89), 433(11) 420(33), 373(23), 371(100), 343(44), 265(65)
(9*S*)-11-nor-9-carboxy-HHC 2xTMS	21.004	2734	490(75), 475(29), 448(13), 434(43), 372(63), 329(100), 265(58)
(9*R*)-11-nor-9-carboxy-HHC 2xTMS	21.137	2753	490(97), 475(23), 448(29), 434(84), 372(10), 329(51), 265(100)

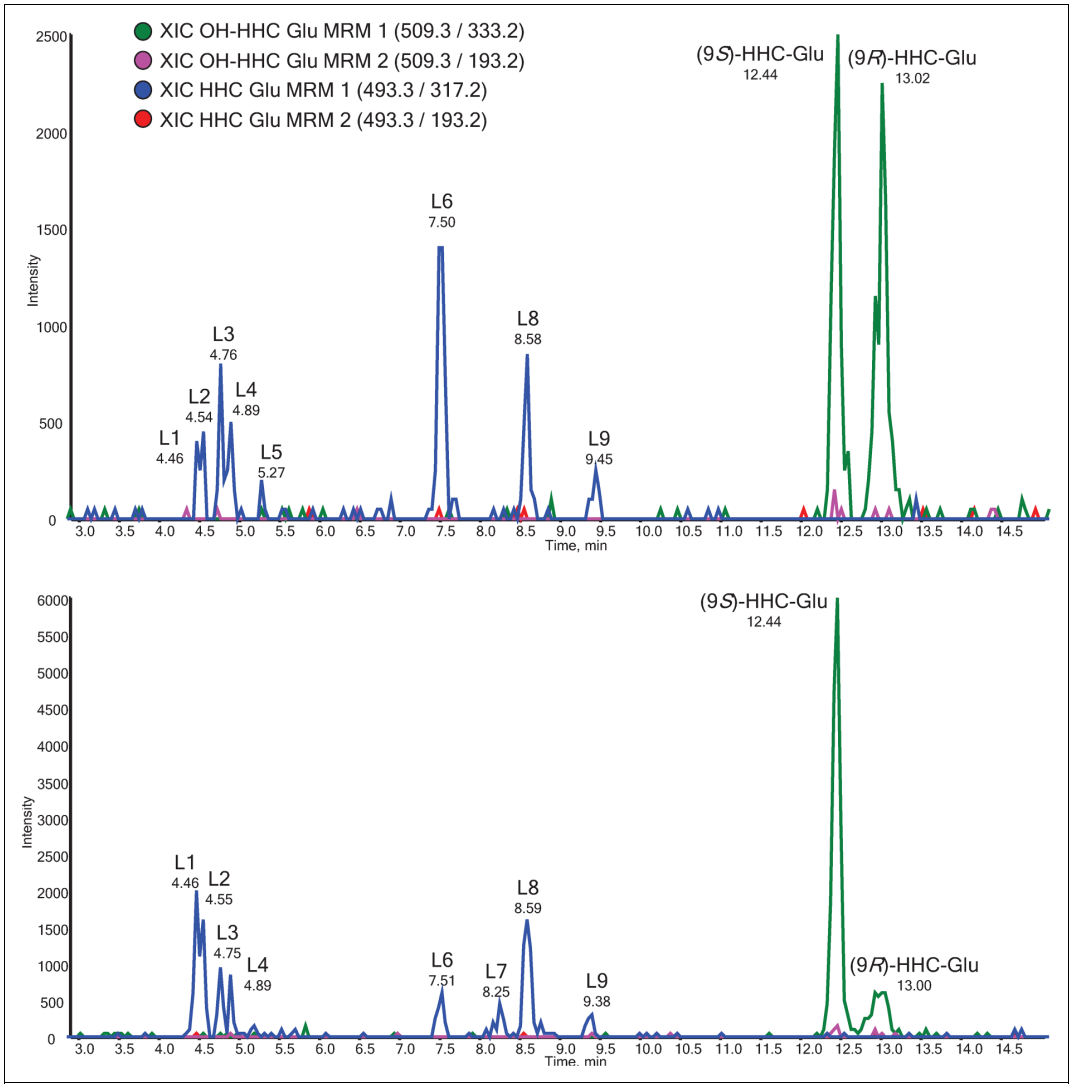

Figure 8. Extracted ion chromatograms for characteristic transitions of HHC glucuronide and OH-HHC glucuronide (L1-L9) in a urine sample 2 h after inhalative consumption of 20 mg HHC (top) and 2 h after oral ingestion of 20 mg HHC (bottom).

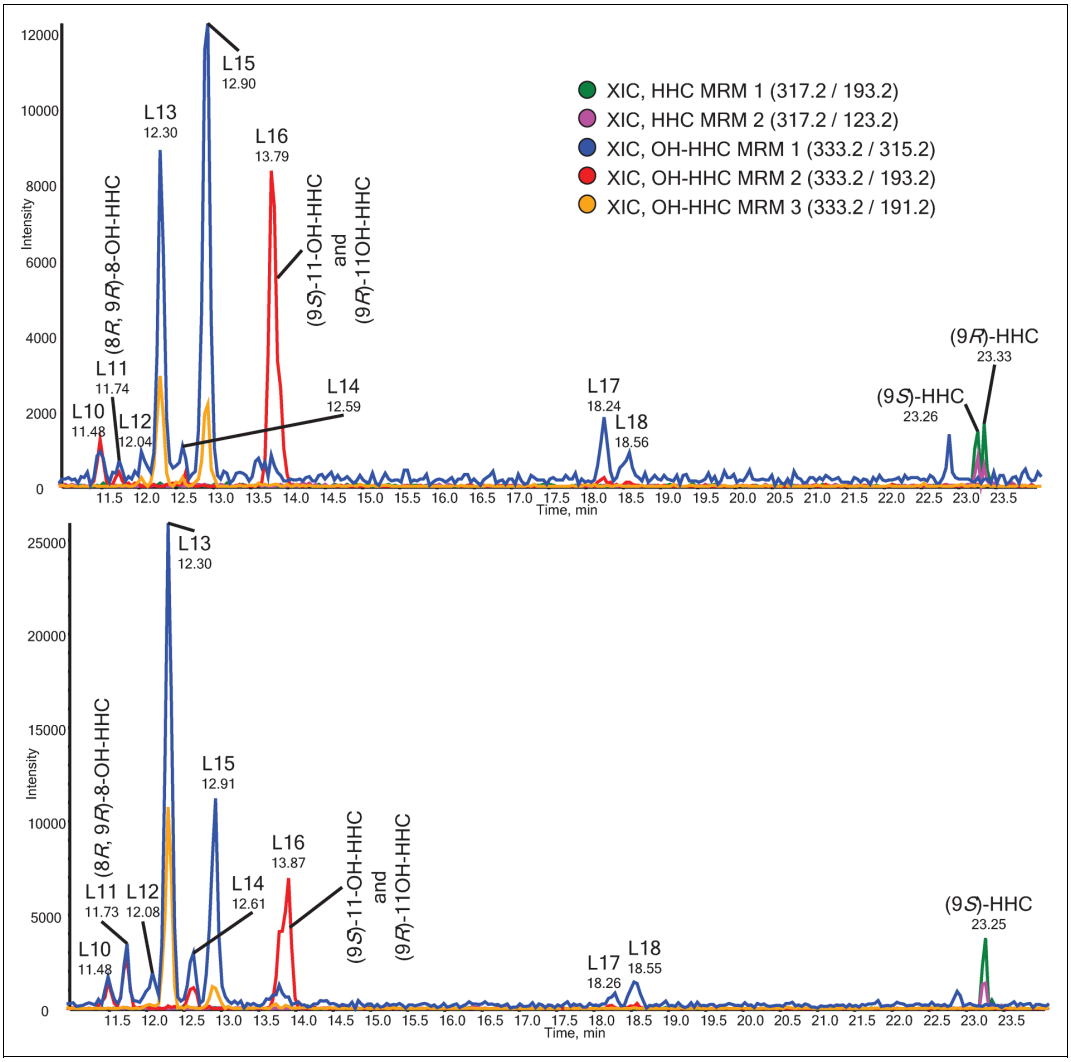

Figure 9. Extracted ion chromatograms for characteristic transitions of HHC and OH-HHC (L10-L18) in a deglucuronidated urine sample 2 h after inhalative consumption of 20 mg HHC (top) and in a deglucuronidated urine sample 2 h after oral ingestion of 20 mg HHC (bottom).

identified. Rough estimation of the concentration resulted in approximately 5 ng/mL for the 9*R* epimer with the 9*S* epimer showing lower abundance.

LC-QqLIT analysis

Several glucuronidated OH-HHCs and OH-HHCs have been detected in urine samples after HHC consumption. As an example, Figure 8 (top) shows a urine sample 2 h after inhalative consumption of 15 mg HHC. Eight different OH-HHC glucuronides (L1-L6, L8, L9) could be detected and both epimers of HHC glucuronide were present. A sample taken 2 h after oral ingestion of 20 mg HHC which was prepared in the same manner shows mainly the same metabolites as the urine sample after inhalative consumption (Figure 8 bottom). The intensity of the glucuronide L5 was very low in this case and another glucuronide L7 emerged which was not present after inhalative consumption. Interestingly, the intensity of (9*R*)-HHC glucuronide is much lower after oral uptake than after HHC inhalation.

In a second experiment, the urine samples were treated with β-glucuronidase prior to extraction. Figure 9 (top) shows such a treated urine sample 2 h after inhalative consumption of 15 mg HHC. Nine different OH-HHC (L10-L18) and both epimers of HHC were detected. The same metabolites were found in a urine sample after oral ingestion of 20 mg HHC as shown in Figure 9 (bottom). The only metabolite which was not found after deglucuronidation was (9*R*)-HHC. It is also observable that the relative composition of the metabolites is different for these two cases.

L11 has the same retention time as the reference compound (8*R*, 9*R*)-OH-HHC, the strong characteristic

Table 5. Retention time of available references and metabolites is shown from the LC-QqLIT method.

Name	RT / min	$[M+H]^+$ / Da	Fragment ions / Da	Identification
L1	4.46	509.3	333*	Present
L2	4.54	509.3	333*	Present
L3	4.76	509.3	333*	Present
L4	4.89	509.3	333*	Present
L5	5.27	509.3	333*	Present
L6	7.50	509.3	333*	Major metabolite after vaping
L7	8.25	509.3	333*	Only after oral consumption
L8	8.58	509.3	333*	Present
L9	9.44	509.3	333*	Present
L10	11.48	333.2	315, 193	Minor metabolite
(8*R*, 9*R*)-8-OH-HHC	11.71	333.2	315, 259, 193, 135	Minor metabolite L11
(8*S*, 9*S*)-8-OH-HHC	11.96	333.2	315, 259, 233, 193, 135	Not detected
(8*R*, 9*S*)-8-OH-HHC	12.03	333.2	315, 259, 193, 135	Not detected
L12	12.05	333.2	315	Minor metabolite
L13	12.28	333.2	315, 259, 191, 137	Main metabolite
(9*S*)-HHC glucuronide	12.48	509.3	317*	Present prior deglucuronidation
L14	12.58	333.2	315, 193	Minor metabolite
L15	12.90	333.2	315, 259, 209, 191, 137	Main metabolite
(9*R*)-HHC glucuronide	13.01	509.3	317*	Present prior deglucuronidation
(9*R*)-11-nor-9-carboxy-HHC	13.48	347.2	329, 301	Not detected
(9*R*)-11-OH-HHC	13.78	333.2	315, 259, 193, 135	Present
L16	13.83	333.2	259, 193, 135	Both epimers of 11-OH-HHC, major metabolite
(9*S*)-11-OH-HHC	13.88	333.2	315, 259, 193, 135	Present
(9*S*)-11-nor-9-carboxy-HHC	14.16	347.2	329, 301	Not detected
L17	18.25	333.2	315	Minor metabolite
L18	18.56	333.2	315	Minor metabolite
(9*S*)-HHC	23.24	317.2	193, 123	Present in both samples
(9*R*)-HHC	23.33	317.2	193, 123	Present in one sample (inhalative consumption)

Detected metabolites after enzymatic hydrolysis are indicated with "present". Product ion spectra were collected from ions with *m/z* 333.2 which correlate to hydroxylated HHC. The most intense product ions are given.
*No product ion spectra were measured for the glucuronides

transition of *m/z* 333.2 → *m/z* 193.2 is present in both analyses. L11 is therefore identified as (8*R*, 9*R*)-8-OH-HHC, which was also identified by GC-MS analysis. L12 has the same retention time as the reference compound (8*R*, 9*S*)-8-OH-HHC but the transition *m/z* 333.2 → *m/z* 193.2 was not observed for this metabolite. L12 could not be identified. L16 seems to be both epimers of 11-OH-HHC, the retention times and observed transitions are the same as in reference compounds. Both epimers of 11-OH-HHC were also identified with GC-MS. The metabolites L13 and L15 which are the main metabolites show a transition of *m/z* 333.2 → *m/z* 191.2 instead of *m/z* 333.2 → *m/z* 193.2 and are therefore likely side-chain hydroxylated OH-HHCs. This observation is in compliance with GC-MS analysis where the main metabolite was tentatively identified as one 4'OH-HHC diastereomer. Figure 8 (bottom) and Figure 9 (bottom), which show the same urine sample without and with deglucuronidation indicate that (9*R*)-HHC is extensively metabolized in this individual. It is however unclear if this is due to the different route of administration or due to other reasons. The same observation was made with GC-MS analysis.

The LC-QqLIT analyses showed that incomplete separation of OH-HHCs might have taken place during the LC-QqTOF screening since more metabolites were found with LC-QqLIT for *m/z* 333 and *m/z* 509 with reasonable product ions. The slower gradient was able to resolve the epimers of HHC and also showed that epimeric OH-HHCs could be resolved. The route of administration might have an impact on the metabolic profile of HHC due to different absorption rates and due to first pass effect.[11] Vaping of HHC leads to the same metabolites as oral ingestion of the compound. The only differences after inhalative consumption of HHC were that (9*R*)-HHC was still present after deglucuronidation and that the minor metabolite L7 was absent.

In contrast to the metabolism of Δ^9-THC, neither (9*R*)-11-nor-9-carboxy-HHC nor (9*S*)-11-nor-9-carboxy-HHC was identified as urinary main metabolite. However, the carboxy-metabolites can be regarded as minor metabolites, potentially accumulating after repeated use.

The composition of (9*R*)-HHC metabolites obtained by microsomal incubations from hepatic microsomes of various animals shows that hydroxylation of C11 is less favored than in THC. Side-chain hydroxylated metabolites of (9*R*)-HHC are generated in higher amounts but (9*R*)-11-OH-HHC was still the most dominant metabolite within all species.[12,13] In contrast to this study our findings indicate that a 4'OH-HHC and another presumably side-chain hydroxylated

HHC (metabolites L13 and L15) are the most abundant human metabolites of an epimeric mixture of HHC with regard to urine samples. It is unclear if only one of the HHC epimers is preferably hydroxylated at the side-chain Table 5.

Conclusions

After HHC consumption enzymatic immunoassays of urine samples were tested positive for cannabinoids. It is therefore important to confirm this result with mass spectrometric methods designed for the proof of HHC consumption.

Oxidation of the methyl group at C11 does not seem to be the major pathway in the human metabolism of HHC. However, position C11 is preferred for oxidative metabolism in Δ^9-THC due to the greater activity of the allylic C-H bond. The carboxylated metabolites ((9*R*)-11-nor-9-carboxy-HHC and (9*S*)-11-nor-9-carboxy-HHC) seem to be less useful for proof of HHC consumption. Instead HHC, (9*R*)-11-OH-HHC, (9*S*)-11-OH-HHC, 4'OH-HHC and their glucuronides can be used as target analytes by GC-MS or LC-MS/MS methods.

Further investigations are necessary to elucidate the differences in metabolism of the HHC epimers with respect to the epimer ratios in confiscated material and potential interindividual differences in humans.

Acknowledgments

Dr. Stefan König from the Institut of Forensic Medicine Bern is acknowledged for the measurement of the LC-QqTOF samples. Alain Broillet, Anita Iannone, Sidonia Guggisberg, Severine Krönert and Thomas Wüthrich from the Institute of Forensic Medicine Bern are acknowledged for their help with the analytic techniques used for this research.

Data availability statements

The data underlying this article are contained within the article or the supplementary material.

Declaration of conflicting interests

The authors declared no potential conflicts of interest with respect to the research, authorship, and/or publication of this article.

Funding

The authors received no financial support for the research, authorship, and/or publication of this article.

ORCID iDs

Willi Schirmer https://orcid.org/0009-0004-5579-2217
Volker Auwärter https://orcid.org/0000-0002-1883-2804

Supplemental material

Supplemental material for this article is available online.

References

1. Adams R, Pease DC, Cain CK, et al. Structure of cannabidiol. VI. Isomerization of cannabidiol to tetrahydrocannabinol, a physiologically active product. Conversion of cannabidiol to cannabinol. *J Am Chem Soc* 1940; 62: 2402–2405.
2. Garrett ER, Gouyette AJ and Roseboom H. Stability of tetrahydrocannabinols II. *J Pharm Sci* 1978; 67: 27–32.
3. Basas-Jaumandreu J and de las Heras FXC. GC-MS Metabolite profile and identification of unusual homologous cannabinoids in high potency Cannabis sativa. *Planta Med* 2020; 86: 338–347. 2020/02/13.
4. Seccamani P, Franco C, Protti S, et al. Photochemistry of cannabidiol (CBD) revised. A combined preparative and spectrometric investigation. *J Nat Prod* 2021; 84: 2858–2865.
5. Ujváry I. *Hexahydrocannabinol (HHC) and Related Substances.* 2023. European Monitoring Centre for Drugs and Drug Addiction (EMCDDA). https://www.emcdda.europa.eu/publications/technical-reports/hhc-and-related-substances_en.
6. Ujváry I. Hexahydrocannabinol and closely related semi-synthetic cannabinoids: A comprehensive review. *Drug Test Anal* 2023; 1-35.
7. Stöth F, Martin Fabritius M, Weinmann W, et al. Application of dried urine spots for non-targeted quadrupole time-of-flight drug screening. *J Anal Toxicol* 2023; 47: 332–337.
8. Harvey DJ and Brown NK. Electron impact-induced fragmentation of the trimethylsilyl derivatives of monohydroxy-hexahydrocannabinols. *Biol Mass Spectrom* 1991; 20: 292–302.
9. Kováts E. Gas-chromatographische charakterisierung organischer verbindungen. Teil 1: retentionsindices aliphatischer halogenide, alkohole, aldehyde und ketone. *Helv Chim Acta* 1958; 41: 1915–1932.
10. van Den Dool H and Dec. Kratz P. A generalization of the retention index system including linear temperature programmed gas—liquid partition chromatography. *J Chromatogr, A* 1963; 11: 463–471.
11. Huestis MA. Human cannabinoid pharmacokinetics. *Chem Biodiversity* 2007; 4: 1770–1804.
12. Harvey DJ and Brown NK. Comparative in vitro metabolism of the cannabinoids. *Pharmacol Biochem Behav* 1991; 40: 533–540.
13. Harvey DJ and Brown NK. In vitro metabolism of the equatorial C11-methyl isomer of hexahydrocannabinol in several mammalian species. *Drug Metab Dispos* 1991; 19: 714–716.

2.4 Publication IV

Identification of Hexahydrocannabiphorol Metabolites in Human Urine

Schirmer W., Schürch S., Weinmann W.
Drug Testing and Analysis, **2025**, *17*(9), 1681-1693
DOI: 10.1002/dta.3871

Description of own contribution

Prof. Dr. Wolfgang Weinmann and I have initialized and conceptualized this study. Dr. Stefan König measured the LC-QqTOF samples and I have analyzed and interpreted the LC-QqTOF data. I have performed and interpreted the LC-QqLIT and GC-MS experiments. Prof. Dr. Wolfgang Weinmann and Prof. Dr. Stefan Schürch have proof read the manuscript.

Description of novelty

After the regulation of HHC in Switzerland other semi-synthetic cannabinoids emerged on the Swiss drug market, including HHCP. This research paper describes the only investigation of the human *in vivo* metabolism of HHCP in urine after oral consumption. It was found that the urine samples showed no cross-reactivity for Δ^9-THC specific immunoassays. Several hydroxylated and bishydroxylated metabolites of HHCP, and their glucuronides have been discovered and tentatively identified. Contrary to the metabolism of Δ^9-THC or HHC, a significant amount of HHCP is bishydroxylated.

Reprint permission

Drug Testing and Analysis

WILEY

RESEARCH ARTICLE

Identification of Hexahydrocannabiphorol Metabolites in Human Urine

Willi Schirmer[1,2] | Stefan Schürch[2] | Wolfgang Weinmann[1]

[1]Institute of Forensic Medicine, Forensic Toxicology and Chemistry, University of Bern, Bern, Switzerland | [2]Department of Chemistry, Biochemistry and Pharmaceutical Sciences, University of Bern, Bern, Switzerland

Correspondence: Willi Schirmer (willi.schirmer@irm.unibe.ch)

Received: 4 October 2024 | **Revised:** 10 February 2025 | **Accepted:** 13 February 2025

ABSTRACT

Hexahydrocannabiphorol (HHCP) is an emerging semisynthetic cannabinoid, which has been known since 1942 from research of tetrahydrocannabinol (THC) analogs and homologs. After the ban of hexahydrocannabinol (HHC) in many European Countries HHCP emerged as a replacement among other similar compounds. First countries already placed HHCP under their narcotic substance law. The aim of this research was to identify human Phase I and II metabolites in urine after oral HHCP consumption. Enzymatic immunoassays of urine samples were tested negative for cannabinoids after a single oral consumption of 4-mg HHCP from a Δ^9-THC abstinent volunteer. The HHCP sample consumed in the self-experiment was purchased from an online store and analyzed beforehand using GC–MS. LC–HR-MS/MS and GC–MS after derivatization were used for the identification of metabolites. Hydroxylated metabolites were found with hydroxylation on the side chain or on the alicyclic part of the molecule. Bishydroxylated HHCP metabolites were found in similar abundance as the monohydroxy metabolites. All of the bishydroxylated metabolites besides a minor metabolite had a hydroxyl group on the side chain and another hydroxyl group on the alicyclic part of the molecule. In addition, the corresponding glucuronides were identified by LC–HR-MS/MS. The exact positions and stereochemistry of the hydroxylation sites could not be determined. Due to the extensive metabolism of HHCP and the lacking cross-reactivity of urine samples after consumption in Δ^9-THC specific immunoassays, it is recommended to include HHCP metabolites in routine screening methods. Monohydroxylated and bishydroxylated metabolites of HHCP and their respective glucuronides are suggested as forensic targets.

1 | Introduction

In 2022, a new class of new psychoactive substances with cannabimimetic effects emerged on the recreational market. These compounds are structurally related to Δ^9-tetrahydrocannabinol, the main psychoactive compound found in *Cannabis sativa* L. The first entries were synthesized from THC or cannabidiol (CBD), and these class of NPS are therefore known as semisynthetic cannabinoids. This terminology also remained for cannabimimetics, which are not synthesized from THC or CBD but share structural features with them [1, 2].

One of this synthetically made cannabinoids is hexahydrocannabiphorol (HHCP), which is found as an epimeric mixture of (9*R*)-HHCP and (9*S*)-HHCP in recreational products. As other semisynthetic cannabinoids, HHCP is sold as a legal and psychoactive alternative in countries that placed *Cannabis* and its psychoactive component THC under their narcotic substance law. Until the ban of hexahydrocannabinol (HHC) on March 31, 2023, HHCP was not widely used in Switzerland. This changed immediately after HHC was banned. In response to the market, a class wide ban on dibenzopyran cannabinoids, including HHCP, was enacted on October 9, 2023 [3].

According to anecdotal reports from users, HHCP is more potent and longer lasting than HHC or THC. Two recent cases from HHCP intoxications were reported but no fatalities. In both cases, the patients were hospitalized for several days after intoxication [4, 5]. The strong and enduring intoxication poses a safety risk for the consumers. The potency of the HHCP epimers were just recently investigated. Janssens et al. used a β-arrestin2 recruitment assay and Persson et al. used a G-protein coupled receptor functional assay [6, 7]. They reported that (9*R*)-HHCP is the more active epimer.

In contrast to HHC, HHCP cannot be synthesized from CBD even though various vendors from online shops claim that. GC–MS analysis of recreationally used HHCP shows many substances with the same molecular ion and fragment ions as HHCP. Probably resulting from stereoisomers and regioisomers during synthesis [2, 8, 9]. The poor manufacturing process and lacking quality standard of HHCP and similar semisynthetic cannabinoids, which do not derive from CBD poses a further risk to consumers.

To date, no method has been published that can detect HHCP and in particular its metabolites. Urine samples are usually measured beforehand using enzymatic immunoassay. From urine samples after the consumption of HHC is known that they show false positive signals for THC, probably due to structural similarities of the HHC and THC metabolites [10–15]. A study that evaluated cross-reactivity of 24 dibenzopyran cannabinoids in whole blood showed that the cross-reactivity of THC derivatives decline with the chain length. (9*R*)-HHCP and (9*S*)-HHCP were tested positive at 500 ng/mL but not at the next lower concentration of 20 ng/mL or below. An ELISA test kit from Immunalysis for THC and metabolites was used [16]. Another study compared the cross-reactivity of THC derivatives with different immunological screening tests in various biological matrices and showed no positive results for the HHCP epimers at a concentration of 250 ng/mL. In both studies, potential HHCP metabolites were not included [11, 16]. To the authors knowledge, no potential metabolites of the HHCP epimers are commercially available.

As to date, only a single study reported potential metabolites of (9*R*)-HHCP and (9*R*)-HHCP-O (HHCP acetate) from incubation experiments with human hepatocytes. They concluded that differentiation between HHCP and HHCP-O consumption is unlikely because ester hydrolysis of HHCP-O to HHCP occurs rapidly. Reported metabolic reactions of (9*R*)-HHCP in the incubation experiments were monohydroxylation, bishydroxylation, bishydroxylation with dehydrogenation (oxo-alcohols and carboxylic acids), trihydroxylation with dehydrogenation, and subsequent glucuronidation [17]. These reported HHCP metabolites are likely found in in vivo samples after the consumption of HHCP.

The presented study aimed to identify the metabolites of the semisynthetic cannabinoid HHCP in urine. A routine LC-QqTOF screening method was used for the determination of the metabolites and their fragments. With this routine method, not all of the isomeric metabolites could be resolved; therefore, a LC-QqLIT was developed for the separation. Additionally, a GC–MS method was developed for the identification of potential metabolic markers after derivatization with *N*-methyl-*N*-trimethylsilyltrifluoroacetamide (MSTFA).

1.1 | Chemicals and Reagents

HHCP was bought from a German online shop (47% (9*R*)-HHCP and 15% (9*S*)-HHCP, quantified by GC–MS (see Figure S1). Deionized water (18.2 MΩ·cm) was produced with a Milli-Q IQ 7000 system from Millipore (Billerica, MA, United States). Methanol (MeOH) (≥ 99.9%) was purchased from Carl Roth (Karlsruhe, Germany). Acetic acid (AcOH) (Reag. Ph. Eur.) and formic acid (50%, in water) were purchased from Grogg Chemie (Stettlen, Switzerland); *N*-methyl-*N*-trimethylsilyltrifluoroacetamide (MSTFA) (≥ 98.5%), *n*-butyl acetate (*n*-BuOAc) (≥ 99.7%), the alkane standard (C7–C40, 1000 µg/mL), and ammonium formate (≥ 99.0%) were purchased from Sigma-Aldrich (Buchs, Switzerland). Acetonitrile (MeCN) (≥ 99.9%) was purchased from Thermo Fisher Scientific (Reinach, Switzerland). Chromabond C18 SPE cartridges (3 mL, 500 mg) were from Macherey-Nagel (Önsingen, Switzerland). The internal standards (ISTDs) (−)-Δ^9-*trans*-tetrahydrocannabinol-D_3 (THC-D_3), (±)-11-hydroxy-Δ^9-*trans*-tetrahydrocannabinol-D_3 (11-OH-THC-D_3), and (±)-11-nor-9-carboxy-Δ^9-*trans*-tetrahydrocannabinol-D_3 (THC-COOH-D_3) were purchased from Cerilliant (Round Rock, TX, United States). The reference standards (9*R*)-HHCP and (9*S*)-HHCP were purchased from Cayman Chemical (Ann Arbor, MI, United States). Instant buffer I and β-glucuronidase (BGTurbo) from Finden KURA was used. A homogenous enzyme immunoassay (HEIA) testkit 305UR for cannabinoids in urine from Immunalysis was used. The buffer solution, the β-glucuronidase, and the HEIA testkit 305UR were provided by Specialty Diagnostix (Passau, Germany). For the LC-QqLIT analysis, an ISTD solution was used which consisted of 0.1-µg/mL THC-D_3, 0.1-µg/mL 11-OH-THC-D_3, and 0.5-µg/mL THC-COOH-D_3 in MeOH. A solution of MeCN in water (60%V) containing formic acid (0.1%V) was used for the sample reconstitution for LC-QqLIT and LC-QqTOF analysis.

1.1.1 | Recreational HHCP Product

The HHCP product for recreational use used in this study was analyzed in a previous study. Besides (9*R*)-HHCP and (9*S*)-HHCP, this sample contained unnatural regioisomers, unnatural stereoisomers, synthesis intermediates, and disubstituted heptylresorcinols from overalkylation. Five of the impurities and (9*R*)-HHCP were isolated, and their structure was elucidated with various NMR experiments. It was found that the (9*R*)-HHCP and (9*S*)-HHCP in this specific sample were enantiopure [9]. Both HHCP epimers were quantified in this recreational product using THC-D_3 as ISTD. The GC–MS method and instrument described in a previous publication was used [18]. This recreational HHCP product contained 47% (9*R*)-HHCP and 15% (9*S*)-HHCP by weight (see Figure S1).

1.1.2 | Self-Administration Experiment

In a self-experiment, a Δ^9-THC abstinent volunteer ingested 4 mg of a well-characterized HHCP sample by dissolving it in olive oil

on an evening. Cannabimimetic effects started approximately 1 h after ingestion and lasted for approx. 10 h. Drowsiness, dizziness, and uncomfortable sleep were experienced. Full recovery was achieved 14 h after ingestion. An approval by an ethics committee is not required for self-experiments. Urine samples were collected before administration and for up to three days after ingestion. The metabolites were analyzed in the urine samples 10 and 15 h after ingestion. The first urine sample was collected 10 h after the HHCP ingestion.

1.2 | LC-QqTOF Analysis

The sample pretreatment was performed according to Schirmer et al. with slight modifications to the deglucuronidation step [10]. Briefly, 800-µL urine, 20-µL ISTD, 100-µL instant buffer I, and 40-µL β-glucuronidase solution were incubated at 50°C for 10 min. One-milliliter *n*-BuOAc was added; the mixture was shaken for 10 min and centrifuged for 10 min (13,000 rpm [17,190×*g*], 8°C). Afterwards, the organic phase was transferred to an autosampler vial, evaporated to dryness under a stream of nitrogen at 50°C and reconstituted with 200-µL reconstitution solution for further LC–MS analysis. For the analysis of the glucuronides, 800-µL urine and 100-µL ammonium formate solution (10 M, aq.) were mixed. The solution was extracted using 1 mL of cold MeCN. The organic phase was separated, evaporated to dryness, and the residue was dissolved in 200-µL reconstitution solution. The same screening method with an LC-QqTOF instrument was used for the analysis as described previously. A Dionex Ultimate 3000 HPLC system (Thermo Fisher Scientific, Reinach, Switzerland) coupled to a TripleTOF 5600 mass spectrometer was used (Sciex, Toronto, Canada). Analyst TF software (Version 1.7) and Peak View (Version 1.2.0.3) (Sciex, Toronto, Canada) were used for data acquisition and processing. Mass spectra were measured in positive ionization mode with an IonDrive Turbo V ion source with TurboIonSpray probe. The curtain gas was set to 55.0 arbitrary units, the ion spray voltage floating was 5500 V, and the source temperature was 650°C. Ion Source Gases 1 and 2 were set to 55.0 arbitrary units. Chromatographic separation was performed on a Kinetex C8 column, 50×2.1 mm, 2.6 µm, 100 Å (Phenomenex, Basel, Switzerland). A gradient method was used consisting of Mobile Phase A (0.1% aqueous formic acid [%V]) and Mobile Phase B (MeCN with 0.1% formic acid [%V]) with the following gradient: 2.5% B, 1–7 min: 2.5%–97.5% B, 7–11 min: 97.5% B, 11–11.1 min: 97.5%–2.5% B, 11.1–14 min: 2.5% B. The injection volume was 2.5 µL, and the flow rate was 0.35 mL/min. The LC-QqTOF instrument was operated in information-dependent data acquisition (IDA) and in SWATH mode (sequential window acquisition of all theoretical mass spectra). For IDA a survey scan from *m/z* 100 to 950 was applied which triggered the acquisition of product ion mass spectra from *m/z* 50 to 950. For SWATH mode, a mass range from *m/z* 100 to 950 was scanned acquiring product ion spectra in windows of 35 Da from *m/z* 50 to 950. Collision energy with collision energy spread of 35 ± 15 V was applied for IDA and SWATH acquisition.

1.3 | LC-QqLIT Analysis

Reference solutions were prepared by mixing 2 µL of a 1-µg/mL solution and 20-µL ISTD. The solution was evaporated to dryness and reconstituted in 200-µL reconstitution solution. The extracts after deglucuronidation as described above were measured. A slightly changed protocol was used as described previously [10]. A Dionex Ultimate 3000 HPLC system (Thermo Fisher Scientific, Reinach, Switzerland) was used, coupled to a QTrap 4500 mass spectrometer (Sciex, Toronto, Canada) equipped with an IonDrive Turbo V ion source with TurboIonSpray probe. The curtain gas was set to 35.0 arbitrary units, the ion spray voltage was 4500 V, and the source temperature was 600°C. Ion Source Gases 1 and 2 were set to 40.0 arbitrary units. Data were acquired and processed with Analyst TF software (Version 1.7) and visualized with Sciex OS (Version 2.0.0.45330) (Sciex, Toronto, Canada). Chromatographic separation was performed on a Luna Omega PS C18 column, 100×2.1 mm, 1.6 µm, 100 Å (Phenomenex, Basel, Switzerland). A gradient method was used consisting of Mobile Phase A (0.1% aqueous formic acid [%V]) and Mobile Phase B (MeCN with 0.1% formic acid [%V]) with the following gradient: 0-25 min: 35%–60% B, 25.1–39 min: 70% B, 39.1%–41 min: 97.5% B, 41–41.1 min: 35% B. A flow rate of 0.4 mL/min and a column oven temperature of 40°C were applied. The injection volume was 1 µL. Spectra were acquired in positive ionization mode with a multiexperimental method involving multiple reaction monitoring (MRM) and two product ion scans in "enhanced product ion" (EPI) mode. The product ion scans of the precursors ion with *m/z* 361.2 and 377.3 were acquired from *m/z* 50 to 380 with a scan rate of 10,000 Da/s, a declustering potential of 120 V, an entry potential of 10 V, and a collision energy of 35 V were applied. The relevant transitions with corresponding potentials of the MRM method are shown in Table 1

1.4 | GC–MS Analysis

For measurement of the reference spectra, 50 µL of reference solutions ($\gamma = 10$ µg/mL) was evaporated to dryness under a stream of nitrogen. The residue was dissolved in 25-µL MSTFA and 25-µL EtOAc. The mixture was then heated to 90°C for 40 min; 1 µL of this solution was injected for GC–MS analysis. For measurement of sample solutions 1-mL urine, 200-µL instant buffer I and 50-µL β-glucuronidase (BGTurbo) were mixed and heated at 50°C for 15 min. The mixture was extracted with 500-µL *n*-BuOAc by shaking for 10 min and centrifuging for 10 min (13,000 rpm [17,190×*g*], 8°C). After separation, the organic phase was collected, and the extraction of the aqueous phase was repeated with 500-µL *n*-BuOAc. The organic phases were combined and evaporated to dryness under a stream of nitrogen at 50°C. The residue was dissolved in 1-mL MeCN and diluted with 2-mL water. The residue was further purified by solid-phase extraction on a VacMaster 20 (Biotage, Uppsala, Sweden). Conditioning of the C18 SPE cartridges was achieved with 2-mL MeOH and 2-mL AcOH (0.1 M) prior to loading the sample solution (3 mL) onto the C18 cartridges. After loading, the cartridges were washed with 1-mL AcOH (0.1 M), 1-mL aqueous MeCN (40%V), and 1-mL aqueous MeCN (70%V). The samples were eluted using 1.5-mL MeCN. The eluate was transferred to an autosampler vial, evaporated to dryness under a stream of nitrogen at 70°C, redissolved in 25-µL EtOAc and 25-µL MSTFA and heated at 90°C for 40 min. One microliter of this solution was injected for GC–MS analysis.

TABLE 1 | MRM transitions of the LC-QqLIT method.

Q1 (Da)	Q3 (Da)	DP (V)	CE (V)	CXP (V)	Name
334.2	316.2	87	21	12	11-OH-THC-D_3 MRM1
334.2	196.2	90	35	7	11-OH-THC-D_3 MRM2
348.2	330.2	93	23	12	THC-COOH-D_3 MRM1
348.2	302.2	102	28	12	THC-COOH-D_3 MRM2
318.2	196.3	88	32	7	THC-D_3 MRM 1
318.2	123.0	100	43	8	THC-D_3 MRM 2
345.3	221.2	88	32	7	HHCP MRM 1
345.3	123.0	100	43	8	HHCP MRM 2
361.3	343.3	87	21	12	OH-HHCP MRM1
361.3	221.2	90	35	7	OH-HHCP MRM2
361.3	219.1	90	35	7	OH-HHCP MRM3
377.3	359.3	87	21	12	2OH-HHCP MRM1
377.3	341.3	90	35	7	2OH-HHCP MRM2
377.3	219.1	90	35	7	2OH-HHCP MRM3

Note: A dwell time of 20 ms for every transition was applied.
Abbreviations: CE: collision energy, CXP: cell exit potential, DP: declustering potential.

The samples were analyzed on an 8890 gas chromatograph with a 7693A autosampler coupled to a 5977B mass selective detector (Agilent, Basel, Switzerland). Data were acquired with MassHunter Workstation GC/MS Data Acquisition (Version 10.1.49) and analyzed with Enhanced ChemStation (F.01.03.2357) (Agilent). Chromatographic separation was performed on a 5% phenylmethylsiloxane column (HP-5ms Ultra Inert, 30 m, 250 µm i.d., 0.25-µm film thickness; Agilent J&W). Helium with a constant flow of 1 mL/min was used as a carrier gas. Chromatography occurred in pulsed splitless mode; injection volume was 1 µL. The oven temperature was set to 80°C at the beginning and was ramped with 10°C/min to 300°C and held for 1 min, resulting in a total separation time of 23 min. The quadrupole temperature was set to 150°C, and the source temperature to 230°C. The mass spectra (electron impact) were obtained with an ionization energy of 70 eV. The scan range was from *m/z* 40 to 650 with a scan speed of 1.562 s^{-1}.

1.5 | Fragmentation Behavior of HHCP and Metabolites

The product ion spectrum of HHCP shows fragment ions, which are characteristic for cannabinoids. Figure 1 shows the MS/MS spectrum of (9*R*)-HHCP. The epimer (9*S*)-HHCP shows the same spectrum (spectrum found in Figure S2).

The fragments can be divided into those that originate from the alicyclic part or from the aromatic part of the molecule. Hydroxylated HHCP show similar fragment ions to HHCP, which are shifted by +16 Da. Often only the dehydrated fragment ion is visible in the spectrum (shifted by −2 Da). Occurrence of the shifted fragments allows the determination of the hydroxylation position.

1.5.1 | Fragment Ions From the Alicyclic Part

The fragment ions *m/z* 137, *m/z* 95, and *m/z* 81 originate from the alicyclic moiety as shown in Figure 1. Hydroxylation on this part leads to the fragment ions *m/z* 153 and *m/z* 135.

1.5.2 | Fragment Ions From the Aromatic Part

The fragment ion *m/z* 289 is formed after elimination of *iso*-butene, it is barely visible. The dihydrochromenylium ion *m/z* 261 is low abundant as well. An ion with the same *m/z* (*m/z* 261) might also result from the McLafferty rearrangement on the side chain. The fragment *m/z* 221 is the main fragment ion of HHCP. The resulting benzylium/tropylium ion is very stable. Occurrence of the ion *m/z* 219 in similar abundance is an indicator for side-chain substitution, especially when its hydrate, the ion *m/z* 237, is still visible. Absence of the ion *m/z* 123 and the simultaneous presence of *m/z* 139 allows determining hydroxylations on the aromatic positions.

2 | Results

Urine samples of a volunteer who orally ingested 4 mg of HHCP were negative in immunoassays for THC and metabolites. This could be explained by poor cross-reactivity for longer alkyl chain dibenzopyran cannabinoids and their metabolites in immunoassays designed for THC and THC metabolites.

LC-QqTOF, LC-QqLIT, and GC–MS were used for metabolite identification. For the rapid in-house LC-QqTOF screening method, the urine samples were measured after and prior deglucuronidation for the identification of Phase I and Phase II metabolites. Phase I metabolites were bishydroxylated metabolites of HHCP (M1–M4) and monohydroxylated metabolites (M5 and M6). Phase II metabolites consisted of HHCP glucuronide, the glucuronides of bishydroxylated HHCP (M7–M10), and the glucuronides of bishydroxylated HHCP (M11–M13). Fragmentation

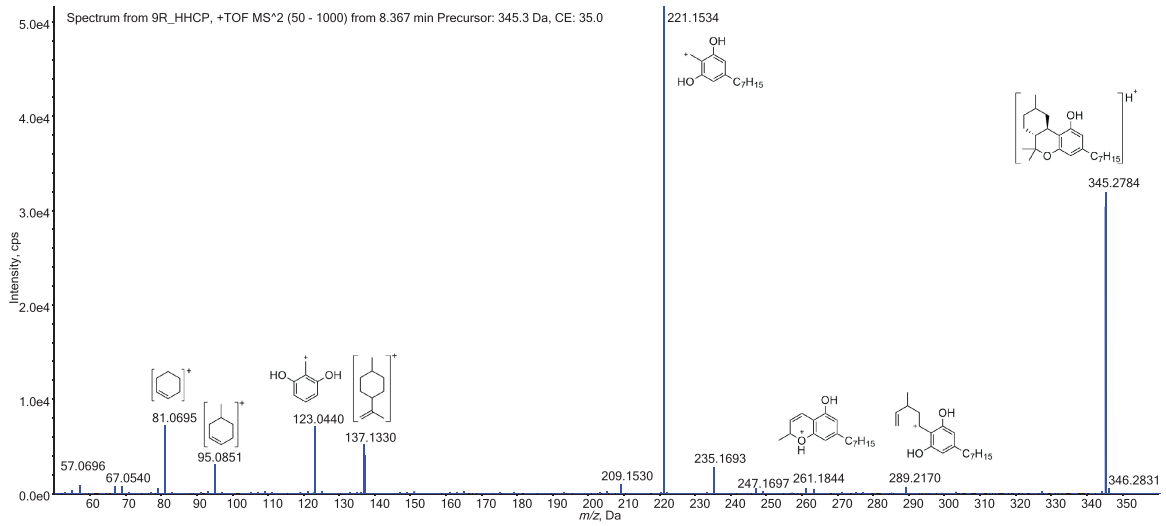

FIGURE 1 | Product ion spectrum of (9*R*)-HHCP.

patterns were elucidated from the exact masses of the molecular ions and fragments. They are similar to the patterns found in HHC and its respective metabolites. Metabolite coelution was an issue with this rapid screening method and therefore a LC-QqLIT method with a slower gradient was developed to separate Phase I metabolites.

In the LC-QqLIT method, bishydroxylated metabolites (M14–M17), monohydroxylated metabolites (M18–M21), and slight amounts of HHCP were detected. No carboxylated metabolites were found. Product ion spectra were acquired in EPI mode, and an MRM method was used for sensitive detection.

Additionally, a GC–MS method after derivatization of the metabolites was developed. The fragmentation mechanisms of dibenzopyran cannabinoids and their trimethylsilyl ethers with a similar structure to HHCP have been investigated thoroughly. HHCP and carboxylated metabolites were not detected. A monohydroxylated metabolite of HHCP was detected, which was tentatively identified as (9*R*)-11-OH-HHCP. Additionally, two bishydroxylated metabolites were detected.

The monohydroxylated metabolites were either hydroxylated on the alicyclic part or on the heptyl chain of HHCP. The bishydroxylated metabolites were hydroxylated once on the alicyclic part and once on the heptyl chain of HHCP, the minor metabolite M9 was an exception, and this bishydroxylated metabolite had two hydroxylation positions on the alicyclic moiety of HHCP. Their fragmentational behavior is explained later in the text.

2.1 | LC-QqTOF: Phase I Metabolites

After deglucuronidation of the urine samples, monohydroxylated and bishydroxylated metabolites of HHCP were found. HHCP was detected as well, but only in small quantities, which indicates a strong metabolization of HHCP. The chromatogram of a deglucuronidated urine sample is shown in Figure 2. A chromatogram of a deglucuronidated urine sample before the ingestion of HHCP is found in Figure S3. Bishydroxylated HHCP (M1–M4) and hydroxylated HHCP (M5 and M6) were found in the sample but no carboxylated metabolites. The spectra of the metabolites M1–M6 are found in Figures S4–S8.

Three bishydroxylated metabolites of HHCP were identified with LC-QqTOF. The mass spectrum of metabolite M1 shows the protonated molecular ion $[M+H^+]^+$ at *m/z* 377.2686 ($C_{23}H_{37}O_4^+$, −13.3 ppm). The base peak is formed after loss of H_2O at *m/z* 359.2581 ($C_{23}H_{35}O_3^+$, −1.4 ppm), a second loss of H_2O can be observed at *m/z* 341.2475 ($C_{23}H_{33}O_2^+$, −0.3 ppm). The phenolic hydroxy group remains intact. The hydroxylated tropylium ion at *m/z* 237.1485 ($C_{14}H_{21}O_3^+$, 1.7 ppm) is present and so is the ion after dehydratization at *m/z* 219.1380 ($C_{14}H_{19}O_2^+$, 2.7 ppm). The presence of these tropylium ions show that this metabolite is monohydroxylated at the side chain, the fragment ions are shown in Figure S37.

An ion with *m/z* 285.1849 ($C_{19}H_{25}O_2^+$, −2.8 ppm) is present which forms after the loss of *iso*-butene and two H_2O, the respective hydrates (*m/z* 303.1955 $[C_{19}H_{27}O_3^+]$ and *m/z* 321.2060 $[C_{19}H_{29}O_4^+]$) are not observed. The chromenylium ion *m/z* 257.1536 ($C_{17}H_{21}O_2^+$, 7.0 ppm) and its hydrate *m/z* 275.1642 ($C_{17}H_{23}O_3^+$, −7.3 ppm) are characteristic ions. The presence of the ions *m/z* 135.1168 ($C_{10}H_{15}^+$, −11.8 ppm) and its hydrate *m/z* 153.1274 ($C_{10}H_{17}O^+$, −12.4 ppm), which originate from the alicyclic part, indicates a hydroxylation on that part. The ion *m/z* 93.0699 ($C_7H_9^+$, −12.9 ppm), which originates from the alicyclic part, supports this. However, its hydrate (*m/z* 111.0804 $[C_7H_{11}O^+]$) was not detected.

Mass spectrum of metabolite M2 shows the same fragment ions but with different relative intensities, indicating that M2 is hydroxylated on the alicyclic part and on the heptyl group. The same is true for metabolite M3, which shows a similar mass spectrum. The bishydroxylated HHCP are all hydroxylated on the chain and the alicyclic moiety of the molecule. A mass spectrum for the metabolite M4 was only obtained from the SWATH

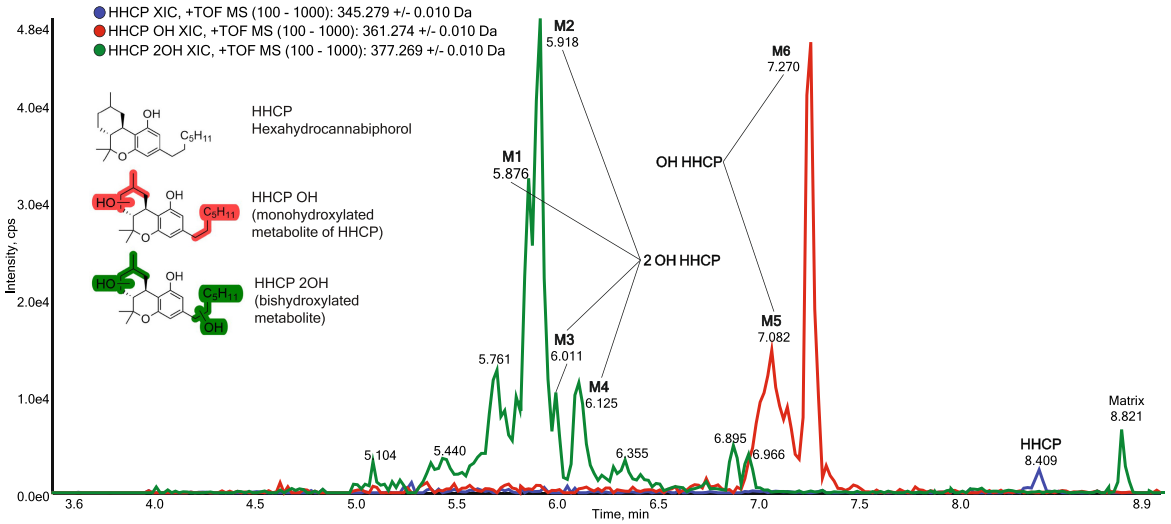

FIGURE 2 | Extracted ion chromatograms of a deglucuronidated urine sample, 10 h after oral ingestion of 4-mg HHCP. HHCP (blue), monohydroxylated HHCP (red), and bishydroxylated HHCP (green).

acquisition, the spectrum shows the same fragment ions as described for M1.

In the mass spectrum of the metabolite M5 a protonated molecular ion of *m/z* 361.2737 ($C_{23}H_{37}O_3^+$, −5.0 ppm) can be observed. Loss of H_2O forms the base peak of this spectrum *m/z* 343.2632 ($C_{23}H_{35}O_2^+$, 1.2 ppm). An ion of *m/z* 287.2006 ($C_{19}H_{27}O_2^+$, 4.5 ppm) is present which is formed after the loss of *iso*-butene and H_2O. The ion at *m/z* 259.1693 ($C_{17}H_{23}O_2^+$, −15.0 ppm) might be a dihydrochromenylium ion with an unsaturated side chain or the product after McLafferty rearrangement and loss of H_2O. The respective hydrates (*m/z* 277.1789 [$C_{17}H_{25}O_3^+$]) are not observed. The ion *m/z* 123.0441 ($C_7H_7O_2^+$, −8.1 ppm) is also seen for HHCP. The ions *m/z* 221.1536 ($C_{14}H_{21}O_2^+$, −21.3 ppm), *m/z* 135.1168 ($C_{10}H_{15}^+$, −21.5 ppm), and *m/z* 93.0699 ($C_7H_9^+$, −24.7 ppm) are observed which might be the fragments of a metabolite which is hydroxylated on the alicyclic moiety. In addition, the ions *m/z* 219.1380 ($C_{14}H_{19}O_2^+$, −5.9 ppm), *m/z* 137.1325 ($C_{10}H_{17}^+$, 1.5 ppm), and *m/z* 95.0855 (C_7H_{11}+, 0.0 ppm) can be observed in the mass spectrum. These are likely fragments of a metabolite, which is hydroxylated on the side chain. The characteristic fragment ions are shown in Figure S38. Coelution of side-chain hydroxylated and alicyclic hydroxylated metabolites would explain the presence of all the ions observed in this mass spectrum. The chromatogram shown in Figure 2 does not show well-separated peaks, and coelution of several monohydroxylated and bishydroxylated metabolites is assumed.

The mass spectrum of M6 shows the protonated molecular ion of *m/z* 361.2737 ($C_{23}H_{37}O_3^+$, −1.1 ppm). Loss of H_2O leads to an ion of *m/z* 343.2632 ($C_{23}H_{35}O_2^+$, 0.6 ppm). An ion of *m/z* 287.2006 ($C_{19}H_{27}O_2^+$, −3.5 ppm) is observed which forms after fragmentation of *iso*-butene and H_2O. The dihydrochromenylium ion of *m/z* 261.1849 ($C_{17}H_{25}O_2^+$, −13.4 ppm) is observable. Base peak of this spectrum is the tropylium ion *m/z* 221.1536 ($C_{14}H_{21}O_2^+$, −3.2 ppm). It indicates that this molecule has no hydroxyl group on the side chain. This can also be seen from the fragments resulting from the fragmentation of the alicyclic part *m/z* 93.0699 ($C_7H_9^+$, 0.0 ppm) and *m/z* 135.1168 ($C_{10}H_{15}^+$, −9.6 ppm); the respective hydrates (*m/z* 111.0804 [$C_7H_{11}O^+$] and *m/z* 153.1274 [$C_{10}H_{17}O_2^+$]) are not observed. The dihydrochromenylium ion of *m/z* 261.1849 ($C_{17}H_{25}O_2^+$) allows determining the hydroxylation position of this molecule even narrower at positions C6a, C7, or C8. Positions C7 and C8 seem more likely. The characteristic ions are shown in Figure S39. Metabolic hydroxylation at the *gem*-dimethyl carbons (C12 or C13) of similar cannabinoids. Brown and Harvey found hydroxylation at these positions in mouse liver after application of *abn*-Δ^8-THC-C1 [19].

2.2 | LC-QqTOF: Phase II Metabolites

Extracted ion chromatograms of a urine sample 10 h after the ingestion of 4-mg HHCP, which was not treated with β-glucuronidase shows HHCP, four bishydroxylated HHCP (M7–M10), and three hydroxylated HHCP (M11-M13) as their glucuronides as seen in Figure 3. A chromatogram with the same traces from a urine sample before the self-experiment is found in Figure S9.

Protonated HHCP glucuronide *m/z* 521.3109 ($C_{29}H_{45}O_8^+$, −5.0 ppm) is detected at 7.05 min. The elimination of two H_2O molecules can be observed (*m/z* 485.2898 [$C_{29}H_{41}O_6^+$], 7.6 ppm), which is probably due to the dehydration of the glucuronide moiety. Base peak of this spectrum is the protonated HHCP of *m/z* 345.2788 ($C_{23}H_{37}O_2^+$, −3.5 ppm), which forms after loss of dehydrated glucuronide. The same fragments with low *m/z* values as in HHCP are present but of lower abundancy. These are the tropylium ion of *m/z* 221.1536 ($C_{14}H_{21}O_2^+$, −14.5 ppm), the methyl-isopropenyl disubstituted cyclohexylium ion (*m/z* 137.1325 [$C_{10}H_{17}^+$], −11.7 ppm), and the methylcyclohexenylium ion (*m/z* 95.0855 [$C_7H_{11}^+$], −12.6 ppm). The corresponding spectrum is found in Figure S10.

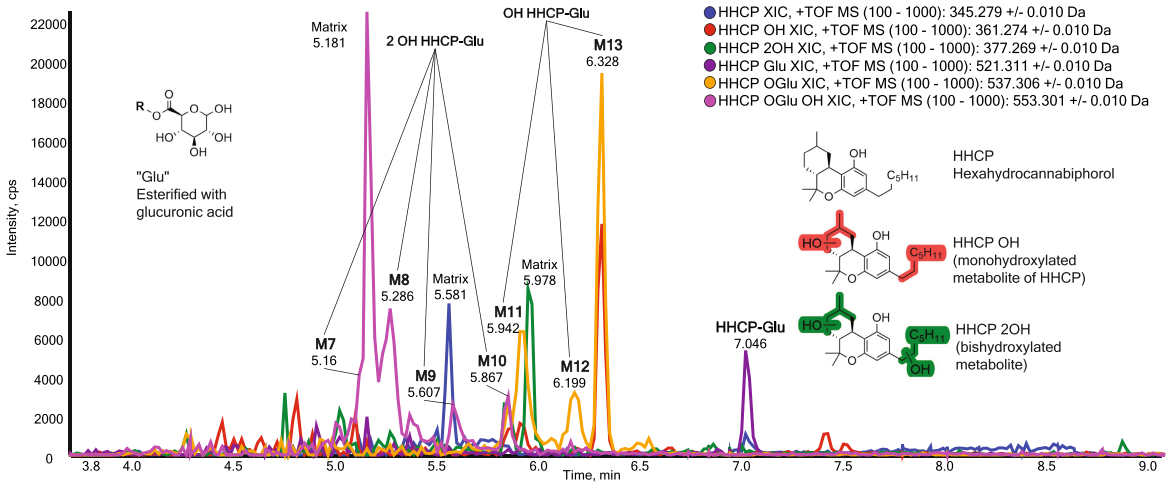

FIGURE 3 | Extracted ion chromatograms in an untreated urine sample, 10 h after oral consumption of 4-mg HHCP. HHCP (blue), HHCP glucuronide (purple, HHCP Glu), monohydroxylated HHCP (red, HHCP OH), monohydroxylated HHCP glucuronide (yellow, HHCP OGlu), bishydroxylated HHCP (green, HHCP 2OH), and bishydroxylated HHCP glucuronide (pink, HHCP OGlu OH). Peaks at 5.18 (purple), 5.58 (blue), and 5.98 min (green) also appear in a urine sample before the ingestion of HHCP.

Four metabolites (M7–M10) were detected that are likely bishydroxylated HHCP glucuronides (spectra found in Figures S11–S14). The mass spectrum of M7 shows a very abundant molecular ion as base peak (*m/z* 553.3007 [$C_{29}H_{45}O_{10}^+$], −9.4 ppm). After loss of the glucuronide moiety, a protonated bishydroxylated HHCP (*m/z* 377.2686 [$C_{23}H_{37}O_4^+$], −51.4 ppm) remains. Its anhydrate *m/z* 359.2581 ($C_{23}H_{35}O_3^+$, −24.2 ppm) is also present, resulting from the loss of H_2O. The tropylium ion *m/z* 219.1380 ($C_{14}H_{19}O_2^+$, 18.7 ppm) is the only indicator that this metabolite is hydroxylated on the side chain and the alicyclic part.

A mass spectrum of the metabolite M8 was only obtained by SWATH acquisition mode. The characteristic ions are the molecular ion *m/z* 553.3007 ($C_{29}H_{45}O_{10}^+$, 11.4 ppm), loss of glucuronide *m/z* 377.2686 ($C_{23}H_{37}O_4^+$, 4.2 ppm), loss of glucuronide and H_2O *m/z* 359.2581 ($C_{23}H_{35}O_3^+$, −7.5 ppm), and the tropylium ion *m/z* 219.1380 ($C_{14}H_{19}O_2^+$, −11.9 ppm), indicating that this metabolite is hydroxylated on the side chain and the alicyclic part.

The mass spectrum of the minor metabolite M9 shows the molecular ion *m/z* 553.3007 ($C_{23}H_{37}O_4^+$, 58.4 ppm), loss of glucuronide *m/z* 377.2686 ($C_{23}H_{37}O_4^+$, 0.0 ppm), loss of glucuronide and H_2O *m/z* 359.2581 ($C_{23}H_{35}O_3^+$, −14.2 ppm), further loss of H_2O *m/z* 341.2475 ($C_{23}H_{33}O_2^+$, 48.6 ppm), and the tropylium ion *m/z* 221.1536 ($C_{14}H_{21}O_2^+$, −1.8 ppm). This metabolite is bishydroxylated on the alicyclic part.

The mass spectrum of the minor metabolite M10 shows the molecular ion *m/z* 553.3007 ($C_{23}H_{37}O_4^+$, −19.5 ppm). Base peak of the spectrum is a protonated bishydroxy-HHCP of *m/z* 377.2686 ($C_{23}H_{37}O_4^+$, 2.9 ppm). Dehydration of the base peak might be present, an ion of *m/z* 359.2581 ($C_{23}H_{35}O_3^+$, −26.7 ppm) is observed. The tropylium ion with a hydroxyl group on the side chain is observable (*m/z* 237.1485 [$C_{14}H_{21}O_3^+$], −10.1 ppm). Interestingly, the dehydrated tropylium ion *m/z* 219.1380 ($C_{14}H_{19}O_2^+$) was not observed. This metabolite possesses a hydroxy group on the side chain and another one on the alicyclic moiety of the molecule.

The hydroxylated HHCP glucuronides are found at retention times of 5.94 (M11), 6.20 (M12), and 6.33 min (M13) (spectra are found in Figures S15–S18). Mass spectrum of the metabolite M12 shows a quite intensive protonated molecular ion of *m/z* 537.3058 ($C_{29}H_{45}O_9^+$, −6.7 ppm). Three losses of H_2O are observed (*m/z* 519.2952 [$C_{29}H_{43}O_8^+$], 3.5 ppm; *m/z* 501.2831 [$C_{29}H_{41}O_7^+$], −3.2 ppm; and *m/z* 483.2774 [$C_{29}H_{39}O_6^+$], 6.8 ppm). Protonated monohydroxy HHCP (*m/z* 361.2737 [$C_{23}H_{37}O_3^+$], −6.6 ppm) and its anhydrate (*m/z* 343.2632 [$C_{23}H_{35}O_2^+$], −0.9 ppm) are present, the latter forms the base peak of the spectrum. The ions *m/z* 287.2006 ($C_{19}H_{27}O_2^+$, 0.0 ppm), *m/z* 259.1693 ($C_{17}H_{23}O_2^+$, −7.3 ppm), *m/z* 221.1536 ($C_{14}H_{21}O_2^+$, −5.0 ppm), and *m/z* 135.1168 ($C_{10}H_{15}^+$, −3.7 ppm) indicate a metabolite with hydroxylation on the alicyclic moiety. But the ions *m/z* 261.1849 ($C_{17}H_{25}O_2^+$, 16.5 ppm), *m/z* 219.1380 ($C_{14}H_{19}O_2^+$, −4.6 ppm), and *m/z* 137.1325 ($C_{10}H_{17}^+$, 4.4 ppm), which indicate a side-chain hydroxylated metabolite, are also present. Coelution of metabolites would explain this finding.

Mass spectrum of the metabolite M13 shows the protonated molecular ion of *m/z* 537.3058 ($C_{29}H_{45}O_9^+$, 11.9 ppm). Protonated monohydroxy HHCP (*m/z* 361.2737 [$C_{23}H_{37}O_3^+$], −6.4 ppm) forms the base peak of this spectrum. The tropylium ion (*m/z* 221.1536 [$C_{14}H_{21}O_2^+$], 8.1 ppm), the hydroxycyclohexylium ion (*m/z* 153.1274 [$C_{10}H_{17}O^+$], −4.6 ppm), and its anhydrate (*m/z* 135.1168 [$C_{10}H_{15}^+$], 14.1 ppm) indicate that this metabolite is hydroxylated on the alicyclic part of the molecule. The ion *m/z* 287.2006 ($C_{19}H_{27}O_2^+$, 2.8 ppm), which forms after the elimination of *iso*-butene and H_2O, is of quite high intensity compared to the similar ion *m/z* 289.2162 ($C_{19}H_{29}O_2^+$) from the fragmentation of HHCP which indicates high stability due to conjugation of the ion.

The mass spectrum of the metabolite M10 also consists of coelution of side-chain hydroxylated and alicyclic hydroxylated HHCPs.

2.3 | LC-QqLIT Analysis

A chromatogram from the deglucuronidated urine sample 15 h after oral ingestion of 4-mg HHCP is shown in Figure 4. The chromatograms of the urine sample before and 10 h after the ingestion of HHCP are found in Figures S19 and S20. HHCP was barely detected after deglucuronidation (30.2 min). An intense metabolite with the transitions *m/z* 361.3 → *m/z* 343.3 and *m/z* 361.3 → *m/z* 221.2 is detected at 20.4 min. This compound is a monohydroxylated HHCP, which is hydroxylated at the alicyclic part. Several compounds with the transitions *m/z* 361.3 → *m/z* 343.3 and either *m/z* 361.3 → *m/z* 221.2 or *m/z* 361.3 → *m/z* 219.1 are detected between 16.5 and 19.0 min, which are not baseline separated, indicating that several monohydroxylated species are formed during metabolism. Two intense metabolites with characteristic mass transitions of *m/z* 377.3 → *m/z* 359.3 and *m/z* 377.3 → *m/z* 219.1 are seen at 6.4 and 6.7 min, respectively. These correspond to bishydroxylated species. EPI spectra of the precursor *m/z* 377.3 show the same ions as described in the LC-QqTOF analysis part.

2.4 | LC-QqLIT Bishydroxylated Metabolites

Four bishydroxylated metabolites (M14–M17) are found in the chromatogram at 4.9, 5.2, 6.4, and 6.8 min (mass spectra are included in Figures S21–S24). In addition, several minor metabolites are present, which might result from isomeric impurities of the ingested HHCP sample. The peak at 9.0 min results from the matrix, as it is also present in the urine sample collected before the self-administration of HHCP.

The product ion spectrum of M14 shows fragment ions, which seem to be not characteristic for bishydroxylated HHCP, this might be a bishydroxylated metabolite of an HHCP isomer which are present in the ingested HHCP sample. M15 shows a few characteristic ions but might also result from an isomer, the tropylium ion (*m/z* 219) is also of a quite low abundance. The product ion spectra of the major metabolite M16 shows the molecular ion (*m/z* 377.13) as base peak. Two losses of H_2O can be observed (*m/z* 359.22 and 341.25) which are the introduced hydroxyl groups. A very abundant tropylium ion with an unsaturated side chain is seen at *m/z* 219.09. In addition, the chromenylium ion with an unsaturated side chain (*m/z* 257.14) and its hydrate (*m/z* 275.11) are present, confirming that a hydroxylation position is present on the side chain and another one on the alicyclic moiety of the metabolite. A product ion spectrum of M16 is depicted on Figure 5.

The product ion spectrum of M17 shows the molecular ion (*m/z* 377.17). The tropylium ion (*m/z* 219.19) indicates a hydroxylation position on the side chain and the fragment ion (*m/z* 134.98) indicates a hydroxylation position on the alicyclic part of the molecule.

2.5 | LC-QqLIT Monohydroxylated Metabolites

The product ion spectrum of the metabolite M18 shows the ion *m/z* 219 indicating a side-chain hydroxylated HHCP. In the product ion spectra of M19 and M20, no characteristic ions were identified; instead, other ions are found. These compounds are not found in the blank urine chromatogram and are therefore likely metabolites of HHCP isomers, which were present in the ingested sample. The product ion spectrum of M21 (Figure 6) shows a very abundant ion of *m/z* 221. The metabolite M21 is likely (9*RS*)-11-OH-HHCP, as it shows a similar chromatographic behavior to the homologs (9*RS*)-11-OH-HHC [10]. It elutes after side-chain hydroxylated metabolites in similar chromatographic conditions. The major fragment ion is the tropylium ion *m/z* 221 (*m/z* 193 for the homolog (9*RS*)-11-OH-HHC), and the fragment ion after loss of water *m/z* 343 (*m/z* 315 for the homolog) is barely visible. The product ion spectrum is similar to the homolog (9*R*)-11-OH-HHC; the molecular ion (*m/z* 361) and main fragment ions (*m/z* 287, *m/z* 235 and *m/z* 221) are shifted by the mass of ethylene (C_2H_4, +28 Da). The product ion spectra of the metabolites M18–M21 are included in Figures S25–S28.

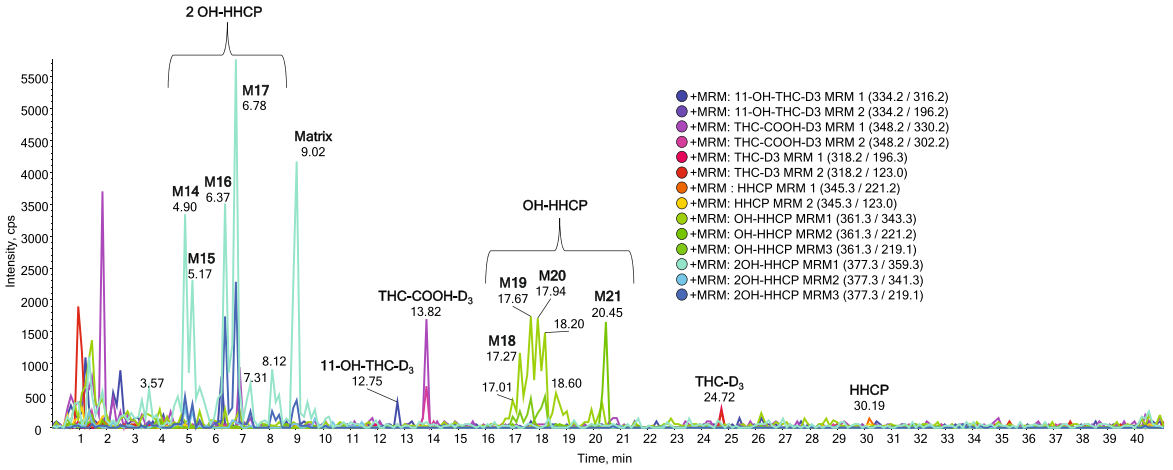

FIGURE 4 | Extracted ion chromatograms for characteristic mass transitions of HHCP (yellow, orange), monohydroxylated HHCP (green shades) and dihydroxylated HHCP (cyan, blue). Chromatogram shows a deglucuronidated urine sample collected 15 h after oral ingestion of 4-mg HHCP.

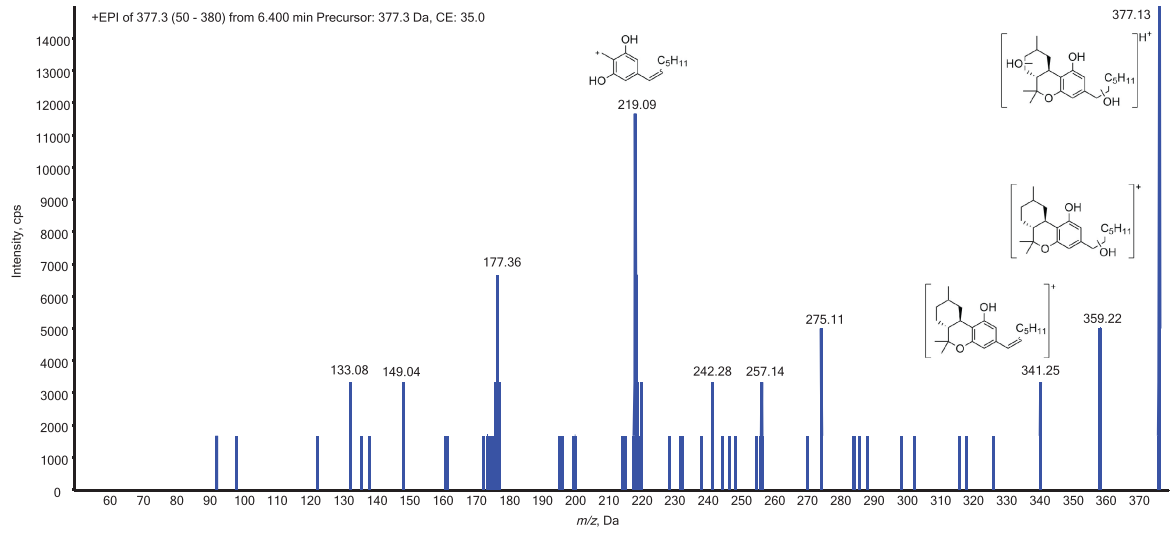

FIGURE 5 | Product ion spectrum of the metabolite M16. A bishydroxylated metabolite of HHCP.

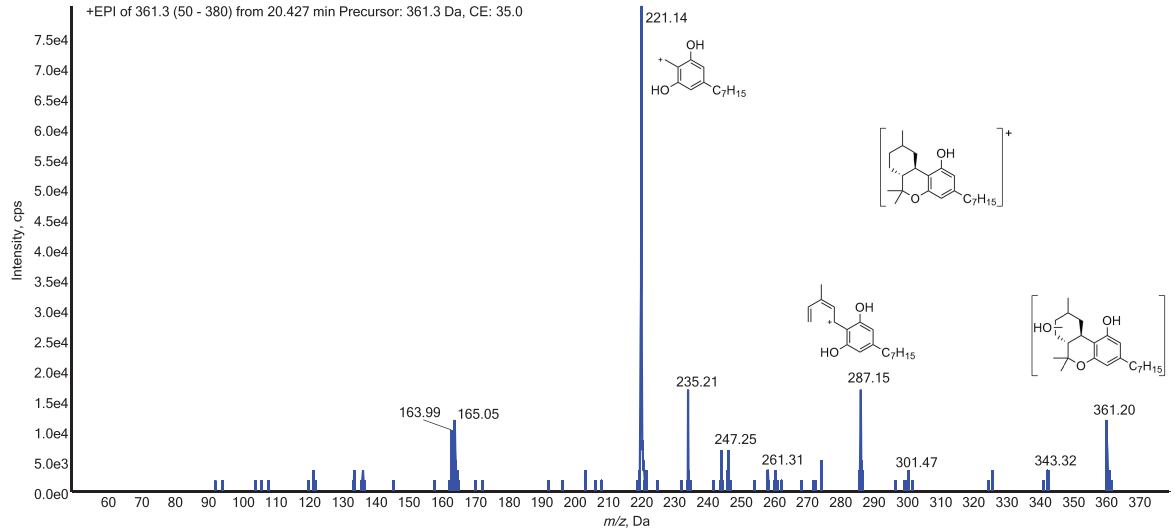

FIGURE 6 | Product ion spectrum of the metabolite M21. Tentatively identified as (9*R*)-11-OH-HHCP.

2.6 | GC–MS of HHCP-TMS

The mass spectra of (9*R*)-HHCP and (9*S*)-HHCP are identical. Formation of the relevant ions were discussed previously [9]. Major ions are the molecular ion ($[M]^{+\cdot}$, *m/z* 344), loss of a propyl radical ($[M\text{-}C_3H_7^{\cdot}]^+$, *m/z* 301), and the tropylium ion ($[M\text{-}123^{\cdot}]^+$, *m/z* 221). Loss of *n*-hexene from a McLafferty rearrangement ($[M\text{-}C_6H_{12}]^{+\cdot}$, *m/z* 260) is the base peak of their spectra. The unnatural diastereomer *cis*-HHCP ((6a*S*,9*R*,10a*R*)-configuration) shows the same mass spectrum [9].

Mass spectra of the trimethylsilylated (9*R*)- and (9*S*)-HHCP are indistinguishable. They show similar fragments with similar intensities as the underivatized samples but shifted by 72 Da (−H, +Si(CH_3)$_3$). The base peak is a radical cation with *m/z* 332, which results from the loss of *n*-hexene after McLafferty rearrangement. Loss of the methyl radical ($[M\text{-}CH_3^{\cdot}]^+$, *m/z* 401) is more prominent than in the fragmentation of underivatized HHCP. The same fragmentation pathways are suggested as for underivatized HHCP and other well-characterized cannabinoids and their trimethylsilyl ethers [9, 20–23]. Figure 7 shows an EI mass spectrum of trimethylsilylated (9*S*)-HHCP. Spectra and XIC (*m/z* 416) of (9*R*)- and (9*S*)-HHCP-TMS are included in Figures S29 and S30.

No HHCP-TMS was detected in the urine samples using this GC–MS method, indicating excessive metabolization of the parent compounds. Figure 8 shows that the derivatized urine sample, which was taken 10 h after oral ingestion of 4-mg HHCP, has no detectable amount of HHCP.

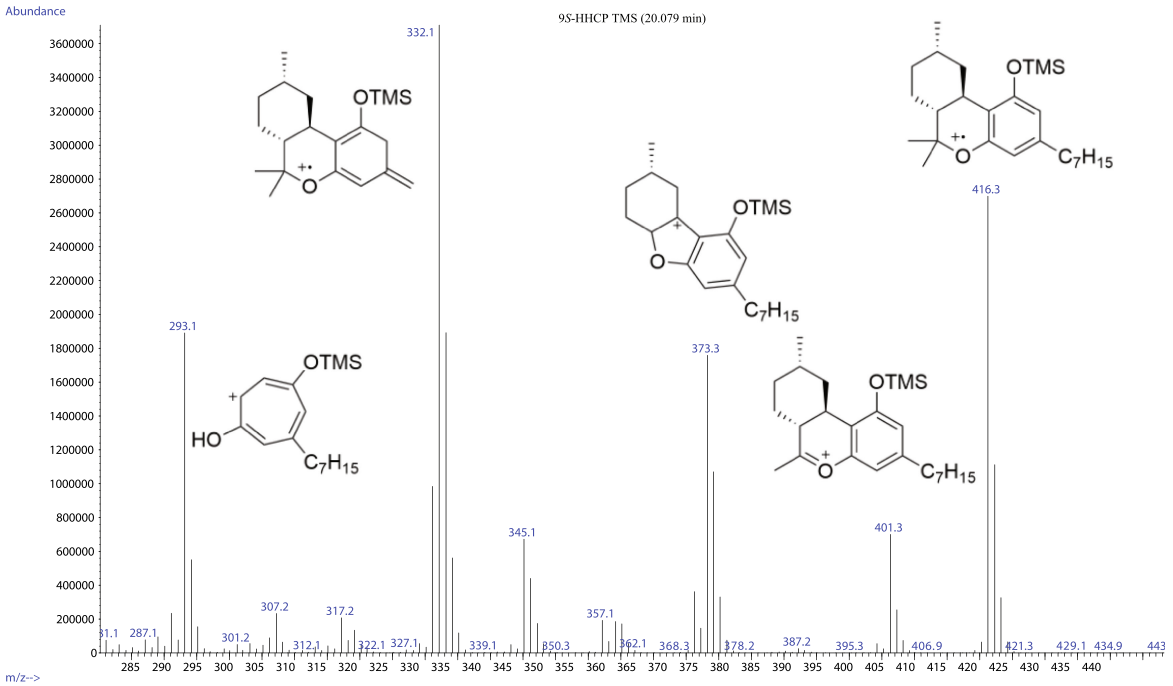

FIGURE 7 | EI mass spectrum of (9*S*)-HHCP-TMS with the structures of the most abundant ions. The same fragmentation patterns as in underivatized HHCP are suggested.

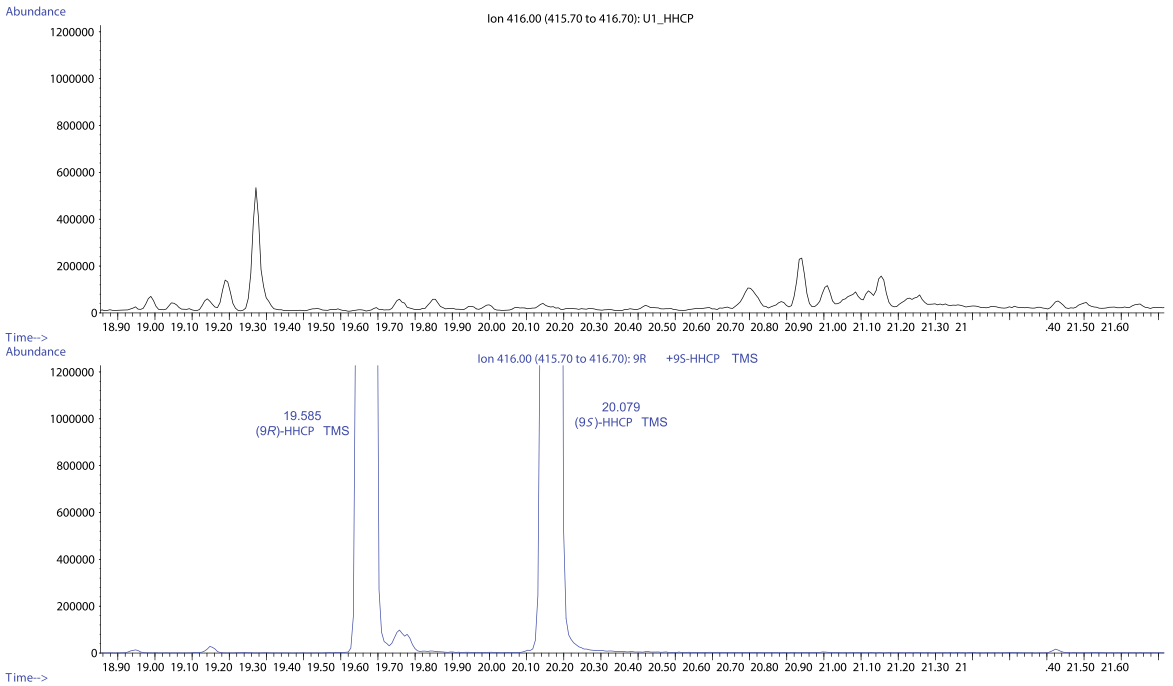

FIGURE 8 | Stacked XICs (*m/z* 416) of a reference solution containing (9*R*)- and (9*S*)-HHCP-TMS (bottom) and a trimethylsilylated urine sample 10 h after oral ingestion of 4-mg HHCP (top). No HHCP-TMS is seen in the urine sample.

2.7 | GC–MS of Monohydroxylated Metabolites

Extracted ion chromatogram of *m/z* 504 showed an intense peak at 21.83 min (see Figure S31). The corresponding spectrum is found in Figure S32. This molecule is presumably a hydroxylated HHCP (2xTMS). The mass spectrum shows characteristic fragments, which are shown in Figure S40. The molecular ion (*m/z* 504) forms the base peak. Elimination of a methyl radical (*m/z* 489) is present but of low intensity. The ion resulting from the McLafferty rearrangement is of a quite high abundance (*m/z* 420). A chromenylium ion (*m/z* 371) and a tropylium ion (*m/z* 293) with high intensity are present. The tropylium ion shows that the molecule had no hydroxyl group at the side chain. These fragments can be tentatively assigned to a structure using the spectra of monohydroxylated HHC TMS derivatives [21]. The ions and their relative abundances are similar to the respective ions of the TMS derivative of (9*R*)-11-OH-HHC. The ion from the McLafferty rearrangement remains the same (*m/z* 420). The other ions are shifted by *m/z* 28 due to a longer alkyl chain. This metabolite is therefore tentatively identified as (9*R*)-11-OH-HHCP.

2.8 | GC–MS of Bishydroxylated Metabolites

In contrast to HHC, a significant amount of HHCP is bishydroxylated. Two metabolites were identified that are likely bishydroxylated HHCP as shown in Figure S33 (their spectra are found in Figures S34 and S35). These two compounds show the ions *m/z* 420 from the McLafferty rearrangement indicating that the alicyclic moiety is monohydroxylated. In addition, the tropylium ions *m/z* 381 and its fragment ion *m/z* 291, which forms after the loss of TMSOH, are present. This indicates that there is a hydroxylation position on the side chain as well. The formation of the ions *m/z* 449 and *m/z* 562 is unknown. Extracted ion chromatograms of the appearing ions show that these ions coelute with the characteristic ions. The characteristic ions of the trimethylsilyl ethers of bishydroxylated HHCP are shown in Figure S41.

Retention times, Kováts indices, and the relevant ions of the trimethylsilyl ethers of HHCP and their detected metabolites are summarized in Table 2. A chromatogram of the *n*-alkane standard (C7–C40) used for the calculation of the Kováts indices is found in Figure S36.

TABLE 2 | Chromatographic data and relevant ions of the TMS derivatives of HHCP and their metabolites.

Name	RT (min)	RRI	Relevant ions (Da)
(9*R*)-HHCP-TMS	19.58	2546	416, 401, 373, 332, 293
(9*S*)-HHCP-TMS	20.08	2610	416, 401, 373, 332, 293
HHCP-OH 2xTMS	21.82	2850	504, 420, 371, 293
HHCP-2xOH 3xTMS	23.15	3029	592, 562, 420, 291
HHCP-2xOH 3xTMS	23.51	3072	592, 449, 420, 381, 291

Abbreviations: RRI: relative retention index (Kováts index), RT: retention time.

3 | Discussion

No cross-reactivities were observed from the urinary metabolites in the immunoassay for Δ^9-THC-COOH. This is in contrast to the human metabolites of HHC which show positive results in urine [10–15], whole blood [24], serum [11], and saliva [11]. (9*S*)-HHCP and (9*R*)-HHCP were only found in small amounts in urine after consumption, which indicates a strong metabolic degradation. It is however unlikely that the small amount of HHCP epimers are responsible for the negative immunoassay results. Their cross-reactivity in THC immunoassays is rather weak [13, 16, 25].

The HHCP sample, which was consumed in this study, was previously characterized, and it was found that in addition to (9*R*)-HHCP and (9*S*)-HHCP, other regioisomers and stereoisomers were present [9]. These isomeric compounds are probably metabolized in a similar way. It is therefore not clear whether any of the metabolites described originate from the metabolism of an impurity in the recreational HHCP product. However, most of the impurities in the HHCP product are present in very small quantities.

No carboxylic metabolites were found in urine after a single consumption of 4-mg HHCP. This is in accordance with the very low amount of 11-nor-9-carboxy-HHC in urine found after a single oral dose of 20-mg HHC [10]. This is also consistent with a study in which the hepatic metabolites of Δ^9-tetrahydrocannabiphorol (Δ^9-THCP) were analyzed in mice. The study showed that hepatic metabolites of Δ^9-THCP in mice were mainly hydroxylated compounds containing one to four hydroxyl groups. In contrast to Δ^9-THC, carboxy metabolites of Δ^9-THCP were present only in small amounts, although THCP has allylic positions that can be easily hydroxylated in vivo [26].

Polyhydroxylated metabolites of Δ^9-THC in human are known, but they are only found in small amounts [27, 28]. Only recently, Lindbom et al. reported on bishydroxylated metabolites of HHC in urine samples and in incubation experiments with HHCP using human hepatocytes [17].

The excessive metabolism of HHCP makes it difficult to prove consumption as the parent drug might not be present in urine samples. It is assumed that HHCP (LC-QqTOF and LC-QqLIT) and HHCP-TMS (GC–MS) have a low sensitivity under the measurement conditions used. The same observation was made in a similar experiment in which HHC was consumed. HHC glucuronide was easily detectable using LC–MS, but after deglucuronidation of the urine sample, HHC was barely detected [10]. No forensic markers for HHCP are established yet. Side-chain hydroxylated metabolites seem to be important forensic markers for saturated semisynthetic cannabinoids like HHC and HHCP [10, 14, 17].

In comparison to the recent study on the metabolites of (9*R*)-HHCP from incubation experiments with human hepatocytes, only monohydroxylated and bishydroxylated metabolites or their glucuronides were observed in the urine samples [17]. Differences

between in vitro and in vivo experiments are to be expected. A single small dose of HHCP would also lead to a different metabolic profile than a regular intake of HHCP. This was seen in a similar experiment with HHC where the respective carboxylic acids were only detected at a small level in urine [10]. Whereas urine samples of regular users from other studies have shown positive results for 11-nor-(9*R*)-carboxy-HHC or 11-nor-(9*S*)-carboxy-HHC [29, 30]. The carboxy metabolites of HHC were also found in human blood [24, 31]. It was recently shown that the carboxy metabolites of HHC are minor metabolites of Δ^9-tetrahydrocannabinol [32].

4 | Conclusions

At this stage, it is unclear which of the identified metabolites originate from (9*R*)-HHCP and (9*S*)-HHCP. The isomers and unreacted intermediates, which are present in the synthetic sample, are also excreted from the body after metabolism. One can expect that the metabolites of *cis*-HHCP are similar to the metabolites of (9*R*)-HHCP and (9*S*)-HHCP. Some of the identified metabolites might also originate from *cis*-HHCP. Composition of isomeric substance are highly dependent on the synthetic route, measures for stereochemical control, and for purification of the HHCP before sale. In order to maximize profit in an unregulated market, it can be expected that these control measures are rather low.

Monohydroxylated and bishydroxylated HHCP and their glucuronides are recommended as forensic markers for HHCP consumption. (9*R*)-11-OH-HHCP was the only tentatively identified metabolite but not the most abundant. The same metabolites were recommended as forensic markers for HHCP consumption after incubation experiments with human hepatocytes [17]. In addition, it should be noted that due to low cross-reactivity, samples from real cases might show negative results for cannabinoids when tested with immunoassays.

Acknowledgments

The team of the Forensic Toxicology and Chemistry from the Institute of Forensic Medicine is highly acknowledged for their help, especially to Isabelle Mösch for the quantification of the HHCP product and Dr. Stefan König for the measurements of the LC-QqTOF samples.

Conflicts of Interest

The authors declare no conflicts of interest.

Data Availability Statement

The data that support the findings of this study are available in the Supporting Information of this article.

References

1. I. Ujváry, "Hexahydrocannabinol and Closely Related Semi-Synthetic Cannabinoids: A Comprehensive Review," *Drug Testing and Analysis* 16 (2023): 127–161, https://doi.org/10.1002/dta.3519.

2. C. Caprari, E. Ferri, M. A. Vandelli, C. Citti, and G. Cannazza, "An Emerging Trend in Novel Psychoactive Substances (NPSs): Designer THC," *Journal of Cannabis Research* 6 (2024): 21, https://doi.org/10.1186/s42238-024-00226-y.

3. Schweizerische Eidgenossenschaft, "Verzeichnisse der Betäubungsmittel, Psychotropen Stoffe, Vorläuferstoffe und Hilfschemikalien (Betäubungsmittelverzeichnisverordnung, BetmVV-EDI) vom 30. Mai 2011 (Stand am 9. Oktober 2023)," https://www.fedlex.admin.ch/eli/cc/2011/363/de.

4. N. Reiter, K. Linnet, N. Østermark Andersen, et al., "Svær Forgiftning med Semisyntetiske Cannabinoider," *Ugeskrift for Laeger* 186 (2024): V04240241, https://doi.org/10.61409/V04240241.

5. Y. Iketani, S. Morita, T. Tsuji, et al., "A Case of Acute Intoxication From Sublingually Administering a Liquid Inhalation Product Containing a Marijuana Analoge," *Tokai Journal of Experimental and Clinical Medicine* 49 (2024): 128–132.

6. L. K. Janssens, K. Van Uytfanghe, J. B. Williams, et al., "Investigation of the Intrinsic Cannabinoid Activity of Hemp-Derived and Semisynthetic Cannabinoids With β-arrestin2 Recruitment Assays—And How This Matters for the Harm Potential of Seized Drugs," *Archives of Toxicology* 98 (2024): 2619–2630, https://doi.org/10.1007/s00204-024-03769-4.

7. M. Persson, R. Kronstrand, M. Evans-Brown, et al., "In Vitro Activation of the CB1 Receptor by the Semi-Synthetic Cannabinoids Hexahydrocannabinol (HHC), Hexahydrocannabinol Acetate (HHC-O) and Hexahydrocannabiphorol (HHC-P)," *Drug Testing and Analysis* (2024), https://doi.org/10.1002/dta.3750.

8. Drogeninformationszentrum Zürich (DIZ), "Haschisch mit HHCP, HHCP-O, Δ^8-THCP und Syntheseverunreinigungen," (2023), https://www.saferparty.ch/warnungen/haschisch-mit-synthetischem-cannabinoid-231023.

9. W. Schirmer, I. Gjuroski, M. Vermathen, et al., "Isolation and Characterization of Synthesis Intermediates and Side Products in Hexahydrocannabiphorol," *Drug Testing and Analysis* (2024), https://doi.org/10.1002/dta.3759.

10. W. Schirmer, V. Auwärter, J. Kaudewitz, et al., "Identification of Human Hexahydrocannabinol Metabolites in Urine," *European Journal of Mass Spectrometry* 29, no. 5–6 (2023): 326–337, https://doi.org/10.1177/14690667231200139.

11. L. Höfert, S. Becker, J. Dreßler, and S. Baumann, "Quantification of (9*R*)- and (9*S*)-Hexahydrocannabinol (HHC) via GC–MS in Serum/Plasma Samples From Drivers Suspected of Cannabis Consumption and Immunological Detection of HHC and Related Substances in Serum, Urine, and Saliva," *Drug Testing and Analysis* 16 (2024): 489–497, https://doi.org/10.1002/dta.3570.

12. P. Pettersson-Pablo and J. Oxelbark, "LC-MS/MS Analysis of 11-Nor-9-Carboxy-Hexahydrocannabinol (HHC-COOH) and 11-Hydroxy-Hexahydrocannabinol (HHC-OH) for Verification of Hexahydrocannabinol (HHC) Intake," *Scandinavian Journal of Clinical and Laboratory Investigation* 84 (2024): 109–114, https://doi.org/10.1080/00365513.2024.2333023.

13. A. Helander, M. Johansson, T. Villén, and A. Andersson, "Appearance of Hexahydrocannabinols as Recreational Drugs and Implications for cannabis Drug Testing—Focus on HHC, HHC-P, HHC-O and HHC-H," *Scandinavian Journal of Clinical and Laboratory Investigation* 84 (2024): 125–132, https://doi.org/10.1080/00365513.2024.2340039.

14. F. Pitterl, M. Pavlic, J. Liu, and H. Oberacher, "Insights Into the Human Metabolism of Hexahydrocannabinol by Non-Targeted Liquid Chromatography–High-Resolution Tandem Mass Spectrometry," *Journal of Analytical Toxicology* 48 (2024): 350–358, https://doi.org/10.1093/jat/bkae022.

15. J. Guyon, C. Paradis, K. Titier, et al., "Letter to the Editor: The Cannabinoid Consumed Is Not Necessarily the One Expected: Recent Experience With Hexahydrocannabinol," *Cannabis and Cannabinoid Research* 9, no. 5 (2024): e1459–e1461, https://doi.org/10.1089/can.2023.0154.

16. A. L. Patton, I. C. Pacheco, J. Z. Seither, et al., "Cross-Reactivity of 24 Cannabinoids and Metabolites in Blood Using the Immunalysis

Cannabinoids Direct Enzyme-Linked Immunosorbent Assay," *Journal of Analytical Toxicology* 48, no. 6 (2024): 439–446, https://doi.org/10.1093/jat/bkae036.

17. K. Lindbom, C. Norman, S. Baginski, et al., "Human Metabolism of the Semi-Synthetic Cannabinoids Hexahydrocannabinol, Hexahydrocannabiphorol and Their Acetates Using Hepatocytes and Urine Samples," *Drug Testing and Analysis* (2024), https://doi.org/10.1002/dta.3740.

18. W. Schirmer, S. Schürch, and W. Weinmann, "The Identification of Synthetic Impurities in a Vape pen Containing Δ^9-Tetrahydrocannabiphorol Using Gas Chromatography Coupled With Mass Spectrometry," *Psychoactives* 3, no. 4 (2024): 491–500.

19. N. K. Brown and D. J. Harvey, "*In Vivo* Metabolism of the Methyl Homologues of Delta-8-Tetrahydrocannabinol, Delta-9-Tetrahydrocannabinol and *abn*-Delta-8-Tetrahydrocannabinol in the Mouse," *Biomedical & Environmental Mass Spectrometry* 15 (1988): 389–398, https://doi.org/10.1002/bms.1200150706.

20. T. B. Vree, "Mass Spectrometry of Cannabinoids," *Journal of Pharmaceutical Sciences* 66 (1977): 1444–1450, https://doi.org/10.1002/jps.2600661025.

21. D. J. Harvey and N. K. Brown, "Electron Impact-Induced Fragmentation of the Trimethylsilyl Derivatives of Monohydroxy-Hexahydrocannabinols," *Biological Mass Spectrometry* 20 (1991): 292–302, https://doi.org/10.1002/bms.1200200510.

22. H. Budzikiewicz, R. T. Alpin, D. A. Lightner, et al., "Massenspektroskopie und Ihre Anwendung auf Strukturelle und Stereochemische Probleme—LXVIII: Massenspektroskopische Untersuchung der Inhaltstoffe von Haschisch," *Tetrahedron* 21 (1965): 1881–1888, https://doi.org/10.1016/S0040-4020(01)98657-0.

23. D. J. Harvey, "Mass Spectrometry of the Cannabinoids and Their Metabolites," *Mass Spectrometry Reviews* 6 (1987): 135–229, https://doi.org/10.1002/mas.1280060104.

24. R. Kronstrand, M. Roman, H. Green, and M. T. Truver, "Quantitation of Hexahydrocannabinol (HHC) and Metabolites in Blood From DUID Cases," *Journal of Analytical Toxicology* 48 (2024): 235–241, https://doi.org/10.1093/jat/bkae030.

25. A.-S. Derne, E. Pape, J.-Y. Jouzeau, A. Kolodziej, N. Gambier, and J. Scala-Bertola, "Immunological Detection of Hexahydrocannabinol (HHC) in Oral Fluid," *Drug Testing and Analysis* 16 (2024): 638–640, https://doi.org/10.1002/dta.3595.

26. D. J. Harvey, "Identification of Hepatic Metabolites of n-Heptyl-Delta-1-Tetrahydrocannabinol in the Mouse," *Xenobiotica* 15 (1985): 187–197, https://doi.org/10.3109/00498258509045349.

27. S. Agurell, M. Halldin, J. E. Lindgren, et al., "Pharmacokinetics and Metabolism of Delta 1-Tetrahydrocannabinol and Other Cannabinoids With Emphasis on Man," *Pharmacological Reviews* 38 (1986): 21–43.

28. R. J. Dinis-Oliveira, "Metabolomics of Δ9-Tetrahydrocannabinol: Implications in Toxicity," *Drug Metabolism Reviews* 48 (2016): 80–87, https://doi.org/10.3109/03602532.2015.1137307.

29. G. Kobidze, G. Sprega, E. Montanari, et al., "The First LC-MS/MS Stereoselective Bioanalytical Methods to Quantitatively Detect 9*R*- and 9*S*-Hexahydrocannabinols and Their Metabolites in Human Blood, Oral Fluid and Urine," *Journal of Pharmaceutical and Biomedical Analysis* 240 (2024): 115918, https://doi.org/10.1016/j.jpba.2023.115918.

30. A. Di Trana, A. Di Giorgi, G. Sprega, et al., "Disposition of Hexahydrocannabinol Epimers and Their Metabolites in Biological Matrices Following a Single Administration of Smoked Hexahydrocannabinol: A Preliminary Study," *Pharmaceuticals* 17, no. 2 (2024): 249.

31. S. K. Manier, J. A. Valdiviezo, A. C. Vollmer, N. Eckstein, and M. R. Meyer, "Analytical Toxicology of the Semi-Synthetic Cannabinoid Hexahydrocannabinol Studied in Human Samples, Pooled Human Liver S9 Fraction, Rat Samples and Drug Products Using HPLC–HRMS-MS," *Journal of Analytical Toxicology* 47 (2023): 818–825, https://doi.org/10.1093/jat/bkad079.

32. C. Falck Jørgensen, B. Schou Rasmussen, K. Linnet, and R. Thomsen, "Evidence of 11-Hydroxy-Hexahydrocannabinol and 11-Nor-9-Carboxy-Hexahydrocannabinol as Novel Human Metabolites of Δ9-Tetrahydrocannabinol," *Metabolites* 13, no. 12 (2023): 1169.

Supporting Information

Additional supporting information can be found online in the Supporting Information section.

2.5 Publication V

Identification of Tetrahydrocannabidiol Metabolites in Human Urine

Schirmer W., Mösch I., Schürch S., Weinmann W.
Drug Testing and Analysis, **2025**, *17*(12), 2333-2346
DOI: 10.1002/dta.3945

Description of own contribution

The initiation and conceptualization of this study was carried out by myself. Isabelle Mösch and I performed the sample preparation and instrumental analysis (LC-QqLIT, LC-QqTOF and GC-MS). I interpreted the mass spectra and proposed the metabolite structures. The manuscript was written by me and finalized by the help of Prof. Dr. Stefan Schürch and Prof. Dr. Wolfgang Weinmann.

Description of novelty

This work describes the discovery of Phase I and Phase II metabolites of H4CBD after oral consumption of 25 mg H4CBD and is currently the only publication covering the human *in vivo* metabolism of H4CBD. The metabolites were identified by GC-MS after trimethylsilylation and LC-QqTOF. Furthermore, a MRM method using a LC-QqLIT instrument was developed, which would allow quantification when reference standards will become available. In analogy to HHC, oxidation of the methyl group at the alicyclic moiety was not the main metabolic pathway, but it was observed. Two carboxy metabolites were observed, namely 7-COOH-H4CBD and 5"COOH-H4CBD. Several hydroxylated metabolites were discovered in high abundance that were hydroxylated on the alicyclic moiety or on the pentyl side chain of the molecule. Bishydroxylated metabolites were only present in small amounts.

Reprint permission

Drug Testing and Analysis

WILEY

RESEARCH ARTICLE OPEN ACCESS

Identification of Tetrahydrocannabidiol Metabolites in Human Urine

Willi Schirmer[1,2] | Isabelle Mösch[1] | Stefan Schürch[2] | Wolfgang Weinmann[1]

[1]Institute of Forensic Medicine, Forensic Toxicology and Chemistry, University of Bern, Bern, Switzerland | [2]Department of Chemistry, Biochemistry and Pharmaceutical Sciences, University of Bern, Bern, Switzerland

Correspondence: Willi Schirmer (willi.schirmer@irm.unibe.ch)

Received: 30 July 2025 | **Revised:** 20 August 2025 | **Accepted:** 22 August 2025

ABSTRACT

Tetrahydrocannabidiol (H4CBD) is an emerging semisynthetic cannabinoid, which has been known since 1940. Like hexahydrocannabinol (HHC), it is easily obtained by hydrogenation of available phytocannabinoids, in the case of H4CBD by hydrogenation of cannabidiol (CBD). H4CBD shows a weak affinity for the CB_1 receptor, but it is unclear if H4CBD shows psychoactive properties, as reports from users are divided. Only a few countries have placed H4CBD under their narcotic substance law, for example, France and Switzerland. The aim of this study was to identify human Phase I and II metabolites in urine as potential forensic targets. The H4CBD used for this study was bought from an online store and analyzed beforehand using GC–MS. The Phase I and II metabolites were identified using LC-HR-MS/MS and GC–MS after trimethylsilylation. The found H4CBD metabolites were carboxylated, hydroxylated, and bishydroxylated species and their glucuronides with hydroxylation and carboxylation positions on the alicyclic moiety and on the side chain. The tentatively identified metabolites were the carboxylic acids 5″-COOH-H4CBD and 7-COOH-H4CBD, the hydroxylated metabolites (1*R*,6*R*)-OH-H4CBD, (1*R*,6*S*)-OH-H4CBD, two epimers of 2″-OH-H4CBD, and both epimers of 7-OH-H4CBD. The identified bishydroxylated metabolites were side-chain hydroxylated derivatives of 7-OH-H4CBD. Various other hydroxylated metabolites were found, but their exact hydroxylation positions could not be determined. Some ESI+ spectra of the metabolites showed very unusual fragmentation patterns, like the loss of both oxygens from the resorcinol moiety with subsequent ring contraction and the appearance of radical cations for Phase II metabolites. These unusual patterns were noticed for H4CBD and its side-chain-altered metabolites.

1 | Introduction

Tetrahydrocannabidiol (H4CBD, also named H4-CBD or THD) is a fully hydrogenated derivative of cannabidiol (CBD) and was first described in 1940. Jacob and Todd isolated CBD from Egyptian hashish and observed that CBD reacts with two equivalents of hydrogen, indicating the two nonaromatic double bonds of CBD [1]. With the rise and fall of hexahydrocannabinol (HHC) in Europe, other semisynthetic cannabinoids emerged to replace the widely banned HHC. H4CBD is one of these successors, which is easily obtained by hydrogenation of CBD. From CBD, it is known that it acts as a negative allosteric modulator at the CB_1 receptor, acting antagonistically [2]. In contrast to CBD, H4CBD (epimeric mixture of (*R*)- and (*S*)-H4CBD) has a weak affinity of 145 nM at the CB_1 receptor [3]. Δ^9-Tetrahydrocannabinol (Δ^9-THC), the main psychoactive phytocannabinoid, in comparison, has an affinity of 40.7 nM at CB_1 [4]. It is therefore assumed that H4CBD might have cannabimimetic effects in higher doses. However, a recent study showed that neither of the H4CBD epimers showed significant CB_1 activation in comparison to Δ^9-THC. (*S*)-H4CBD showed the strongest CB_2 activation of the screened semisynthetic cannabinoids, whereas (*R*)-H4CBD showed no significant CB_2 activation in comparison with CP55,940 [5]. User reports from drug forums are inconsistent. Some users noted mild psychoactive effects, whereas others reported no effects at all after consumption. It is

not clear if the users who noticed psychoactive effects consumed solely H4CBD, as these products are often wrongly declared [6, 7]. In a recent study in Germany in which 79 confiscated samples were analyzed, H4CBD was the most frequently detected semisynthetic cannabinoid apart from HHC [8], probably because, like HHC, it can easily be produced from CBD, whereas other semisynthetic cannabinoids are not obtained from phytocannabinoids [9–11]. Products containing H4CBD were also reported in Japan and Denmark [7, 12]. Switzerland scheduled H4CBD under its narcotic substance law directory on October 9, 2023 [13].

In analogy to the metabolism of Δ^9-THC, CBD undergoes hydroxylation on the allylic methyl group at C7 to form the metabolite 7-OH-CBD, which is further oxidized to the corresponding acid 7-COOH-CBD. These metabolites were found in rat liver after in vitro metabolism and after in vivo experiments in mice liver after application of a CBD suspension [14, 15]. The same metabolites were later found in the urine of a dystonic patient who received treatment with CBD [16]. 7-OH-CBD and 7-COOH-CBD are commonly used as analytical targets after the consumption of CBD [17–19]. The aim of this study was to identify urinary Phase I and II metabolites of H4CBD and provide analytical targets for the proof of consumption.

2 | Materials and Methods

H4CBD was bought from a Swiss online shop before the substance was banned. The product was declared as pure H4CBD and was a reddish resin. It contained 34% (*R*)-H4CBD and 23% (*S*)-H4CBD, quantified by GC–MS using a single five-point calibration (see Figure S1). Deionized water (18.2 MΩ·cm) was produced from a Millipore Milli-Q IQ 7000 system (Billerica, MA, United States). *N*-methyl-*N*-trimethylsilyltrifluoracetamide (MSTFA) (≥ 98.5%), *n*-butyl acetate (*n*-BuOAc) (≥ 99.7%), the *n*-alkane standard (C7-C40, 1000 μg/mL), and ammonium formate (≥ 99.0%) were purchased from Sigma-Aldrich (Buchs, Switzerland). Ethyl acetate (EtOAc) (for liquid chromatography) and methanol (MeOH) (≥ 99.9%) were purchased from Carl Roth (Karlsruhe, Germany). Formic acid (50%, in water) and acetic acid (AcOH) were purchased from Grogg Chemie (Stettlen, Switzerland). Acetonitrile (MeCN) (≥ 99.9%) was purchased from Thermo Fisher Scientific (Reinach, Switzerland). Chromabond C18 SPE cartridges (3 mL, 500 mg) were purchased from Macherey-Nagel (Önsingen, Switzerland). (*R*)-Tetrahydrocannabidiol ((*R*)-H4CBD) and (*S*)-tetrahydrocannabidiol ((*S*)-H4CBD) were purchased from Cayman Chemical (Ann Arbor, MI, United States). The internal standard (−)-Δ^9-*trans*-tetrahydrocannabinol-D_3 (THC-D_3) was purchased from Cerilliant (Round Rock, TX, United States). Instant buffer I and *β*-glucuronidase (BGTurbo) from Finden KURA were used, which were purchased from Specialty Diagnostix (Passau, Germany). An aqueous solution of MeCN (60 V%) and formic acid (0.1 V%) was used for the reconstitution of LC–MS samples.

2.1 | Self-Administration Experiment

In a self-experiment, a cannabis-abstinent volunteer (60-year-old male) orally ingested 25 mg of a well-characterized H4CBD product after dissolving it in olive oil. Urine samples were collected for 3 days after ingestion, and the first sample was collected 1 h after ingestion. Further samples were collected 3, 13, 17, 27, and 48 h after oral ingestion. The described metabolites were detected in the urine sample 3 h after consumption. No cannabimimetic effects were noticed.

2.2 | LC-QqTOF

Urine sample preparation was performed according to Schirmer et al. [20]. For the analysis of Phase I metabolites, 800-μL urine, 100-μL instant buffer I, and 5-μL *β*-glucuronidase were incubated for 15 min at 50°C. The solution was extracted with 1-mL *n*-BuOAc by shaking it for 10 min, centrifuging for 10 min (13,000 rpm [17,190 *g*], 8°C), and separating the organic layer. The organic phase was evaporated to dryness at 50°C under a stream of nitrogen and reconstituted in a 100-μL reconstitution solution. For the analysis of Phase II metabolites, 800-μL urine was mixed with 100 μL of an ammonium formate (10 M) solution and extracted with 1-mL cold MeCN. The organic layer was evaporated to dryness and dissolved with 200-μL reconstitution solution. Samples were analyzed on a Dionex Ultimate 3000 HPLC system (Thermo Fisher Scientific, Reinach, Switzerland), which was coupled to a TripleTOF 5600 mass spectrometer (Sciex, Toronto, Canada). For the data acquisition, Analyst TF software (Version 1.7) was used, and data processing was performed with Peak View (Version 1.2.0.3) and Sciex OS (Version 2.0.0.45330). Mass spectra were acquired in positive ionization mode (ESI+) using an IonDrive Turbo V ion source with a TurboIonSpray probe. The curtain gas and the ion source gases 1 and 2 were set to 55.0 psi, the ion spray voltage floating was 5500 V, and the source temperature was 650°C. Chromatography was performed on a Kinetex C8 column, 50 × 2.1 mm, 2.6 μm, 100 Å. For the analysis of Phase I metabolites after deglucuronidation, a gradient method consisting of mobile phase A (0.1% aqueous formic acid [%V]) and mobile phase B (MeCN with 0.1% formic acid [%V]) with the following gradient was used: 0–5 min, 45%–62% B; 5–14.5 min, 62% B; 14.5–14.6 min, 62%–45% B; and 14.6–15 min, 45% B. The flow rate was 0.3 mL/min, the injection volume was 2.5 μL, and the column oven was set to 25.0°C. For the analysis of Phase II metabolites, the gradient was changed to the following: 0–5 min, 30%–40% B; 5–14.5 min, 40% B; 14.5–14.6 min, 40%–30% B; and 14.6–15 min, 30% B. The instrument was operated in IDA (information-dependent data acquisition) and in SWATH mode (sequential window acquisition of all theoretical mass spectra). A survey scan from *m/z* 100 to 950 was applied for IDA, which triggered the acquisition of product ion mass spectra from *m/z* 50 to 950. For SWATH mode, a mass range was scanned from *m/z* 100 to 950, acquiring product ion spectra in windows of 35 Da from *m/z* 50 to 950. A collision energy with a collision energy spread of 35 ± 15 V was used for IDA and SWATH mode [21].

3 | LC-QqLIT

The sample solutions after deglucuronidation as described above were analyzed using a Dionex Ultimate 3000 HPLC system (Thermo Fisher Scientific, Reinach, Switzerland) coupled to a QTRAP 4500 mass spectrometer (Sciex, Toronto, Canada),

TABLE 1 | MRM transitions of the LC-QqLIT method. A dwell time of 20 ms and an entrance potential of 10 V for every transition were applied.

Q1/Da	Q3/Da	DP/V	CE/V	CXP/V	Name
318.2	196.3	88	32	7	THC-D_3 MRM 1
318.2	123.0	100	43	8	THC-D_3 MRM 2
319.2	83.0	60	24	16	H4CBD MRM 1
319.2	55.0	60	60	13	H4CBD MRM 2
319.2	181.0	60	20	9	H4CBD MRM 3
335.3	271.2	60	20	10	H4CBD-OH MRM 1
335.3	137.0	60	20	10	H4CBD-OH MRM 2
335.3	193.1	60	20	10	H4CBD-OH MRM 3
335.3	191.1	60	20	10	H4CBD-OH MRM 4
349.2	193.1	60	20	10	H4CBD-COOH MRM 1
349.2	211.1	60	20	10	H4CBD-COOH MRM 2
349.2	139.2	60	20	10	H4CBD-COOH MRM 3

Abbreviations: CE: collision energy, CXP: cell exit potential, DP: declustering potential.

which was equipped with an IonDrive Turbo V ion source with TurboIonSpray probe. The curtain gas and the ion source gases 1 and 2 were set to 35.0 psi, the source temperature was 600°C, and the ion spray voltage was 5500 V. The column, mobile phases, injection volume, column oven temperature, flow rate, and gradient are the same as described for the analysis of deglucuronidated samples (Phase I metabolites) in the LC-QqTOF section. Mass spectra were acquired in positive ionization mode (ESI+). A multiple reaction monitoring method was developed for the detection of H4CBD and its metabolites, and the relevant transitions with their corresponding potentials are shown in Table 1.

4 | GC–MS

Sample preparation and analysis were performed according to Schirmer et al. [20]. Reference solutions were prepared by evaporating 50 µL of a 10-µg/mL solution under a stream of nitrogen to dryness. To the residue, 25-µL MSTFA and 25-µL EtOAc were added. The solutions were incubated at 90°C for 40 min. The sample solutions were prepared by incubating 1-mL urine with 100-µL instant buffer I and 5-µL β-glucuronidase at 50°C for 15 min. The mixture was extracted twice with 500 µL *n*-BuOAc by shaking for 10 min and centrifuging for 10 min (13,000 rpm [17,190 *g*], 8°C). The organic phases were combined and evaporated to dryness under a stream of nitrogen. The residue was dissolved in 1-mL MeCN, diluted with 2-mL water, and purified by solid-phase extraction. The Chromabond C18 cartridges (3 mL, 500 mg) were conditioned with 2-mL MeOH and 2-mL AcOH (0.1 M). The sample solutions were loaded onto the cartridges, and they were washed with 1-mL AcOH (0.1 M), 1-mL aqueous MeCN (40 V%), and 1-mL aqueous MeCN (70 V%). For the elution, 1.5-mL MeCN was used, and the eluate was evaporated to dryness under a stream of nitrogen at 70°C. 25-µL MSTFA and 25-µL EtOAc were added, and the mixture was incubated at 90°C for 40 min. The extracts and reference solutions were analyzed using an 8890 gas chromatograph with a 7693A autosampler coupled to a 5977B mass selective detector (Agilent, Basel, Switzerland). MassHunter Workstation GCMS Data Acquisition (Version 10.1.49) was used for acquisition and Enhanced ChemStation (F.01.03.2357) (Agilent) for data analysis. A 5% phenylmethylsiloxane column (HP-5 ms Ultra Inert, 30 m, 250 µm i.d., 0.25-µm film thickness; Agilent J&W) was used. Helium with a constant flow of 1 mL/min was used as the carrier gas. The injection volume was 1 µL in pulsed splitless mode. The oven temperature started at 80°C and was ramped with 10°C/min to 300°C and held for 1 min, resulting in a total separation time of 23 min. The quadrupole temperature was 150°C, and the source temperature was 230°C. EI mass spectra were obtained with an ionization energy of 70 eV. The scan range was from *m/z* 40 to 650, with a scan speed of 1.562 s^{-1}.

5 | Investigated H4CBD Product

The investigated H4CBD resin "for recreational use" was analyzed by GC–MS: (*R*)-H4CBD and (*S*)-H4CBD were quantified using a single 5-point calibration, and a single determination was performed. THC-D_3 was used as an internal standard. The quantification was run on another GC–MS device using identical instruments (Agilent 8890 gas chromatograph coupled to a 5977B mass spectrometer). This sample contained stearic acid and palmitic acid, presumably from the extraction of CBD from CBD-rich *Cannabis* plants. In addition, not fully hydrogenated CBD was detected (H2CBD) in the product.

6 | Results and Discussion

An overview of the Phase I and II metabolites that were identified by LC-QqTOF can be found in Table 2. Table 2 shows the retention times and relevant ions of the metabolites. The trimethylsilyl derivatives of Phase I metabolites, which were identified by GC–MS, are found in Table 3. The Kováts indices [22], retention times, and relevant fragment ions are listed. The Kováts indices were calculated according to van Den Dool and Kratz [23].

6.1 | LC-QqTOF Phase I Metabolites

The chromatogram of an extract from a deglucuronidated urine sample 3 h after ingestion showed H4CBD (M1), carboxylated

TABLE 2 | Chromatographic data and relevant ions of the Phase I and II metabolites of H4CBD (LC-QqTOF). The ions are detected in ESI+ with a collision energy of 35 ± 15 V.

Metabolite	Glucuronide	R_t/min	Relevant ions/Da
M1, (*R*,*S*)-H4CBD		9.35	**319.2632**, 181.1223, 139.1481, 97.1012, 83.0855, 69.0699, 57.0699, 55.0542
M2, 7-COOH-H4CBD		3.12	349.2373, 331.2268, 313.2162, 303.2319, 285.2213, 227.1794, **137.1325**
M3, 5″-COOH-H4CBD		4.51	349.2373, 331.2268, 313.2162, 303.2319, 211.0965, 193.0859, 139.1481, **83.0855**
M4, OH-H4CBD[a]		7.74	**335.2573**, 271.2420, 197.1172, 179.1067, 137.1325, 83.0855, 81.0699
M5, OH-H4CBD[a]		7.13	335.2573, **271.2420**, 197.1172, 179.1067, 137.1325, 83.0855, 81.0699
M6, 2″OH-H4CBD		4.87	335.2573, 317.2475, 261.1849, 179.1067, 137.1325, **123.0441**, 83.0855
M7, 2″OH-H4CBD		4.56	335.2573, 317.2475, 261.1849, 179.1067, 137.1325, 123.0441, **83.0855**
M8, 7-OH-H4CBD		4.37	335.2573, 317.2475, **193.1223**, 181.1223, 137.1325, 123.0441, 95.0855, 81.0699
M9, 7-OH-H4CBD		3.64	335.2573, 317.2475, **193.1223**, 181.1223, 137.1325, 123.0441, 95.0855, 81.0699
M10, diOH-H4CBD[b]		1.96	351.2530, 333.2424, 315.2319, 287.2369, 269.2264, 193.1223, 137.1325, **81.0699**
M11, H4CBD	M1	11.34	495.2952, 459.2741, 384.2659•, **319.2632**
M12, H4CBD	M1	11.82	495.2952, 459.2741, 384.2659•, **319.2632**
M13, 5″-COOH-H4CBD	M3	10.04	525.2694, 414.2401•, **349.2373**, 331.2268, 211.0965, 193.0859, 139.1481, 83.0855
M14, 7-COOH-H4CBD	M2	9.39	525.2694, 457.1857, 349.2373, 331.2268, 303.2319, **281.1536**, 193.1223, 181.1223
M15, OH-H4CBD[a]	M6	5.07	511.2902, 400.2608•, 335.2573, **317.2475**, 261.1849, 179.1067
M16, OH-H4CBD		5.79	511.2902, **335.2573**, 317.2475, 193.1223, 181.1223
M17, OH-H4CBD		7.18	511.2902, **335.2573**, 317.2475, 193.1223, 137.1325
M18, 7-OH-H4CBD	M8, M9	8.59	511.2902, 443.2064, **335.2573**, 317.2475, 193.1223, 181.1223
M19, 7-OH-H4CBD	M8, M9	9.32	511.2902, 443.2064, **335.2573**, 317.2475, 193.1223, 181.1223
M20, OH-H4CBD[a]		12.41	511.2902, **335.2573**, 317.2475, 299.2369, 271.2420, 197.1172, 179.1067, 137.1325
M21, OH-H4CBD[a]		12.67	511.2902, **335.2573**, 317.2475, 299.2369, 271.2420, 197.1172, 179.1067, 137.1325
M22, OH-H4CBD[a]		14.43	511.2902, **335.2573**, 317.2475, 299.2369, 271.2420, 197.1172, 179.1067, 137.1325
M23, diOH-H4CBD[b]		3.51	527.2851, **351.2530**, 333.2424, 193.1223, 181.1223
M24, diOH-H4CBD[c]		5.25	527.2851, **351.2530**, 333.2424, 137.1325
M25, diOH-H4CBD[c]		5.67	527.2851, **351.2530**, 333.2424, 193.1223, 137.1325

Note: Base peak is written in bold. The corresponding ESI+ product ion spectra of the Phase I metabolites are found in Figures S3–S13, and the ESI+ product ion spectra of Phase II metabolites are shown in Figures S15–S29.
Abbreviation: R_t: retention time.
[a]Hydroxylation on side chain.
[b]Two hydroxylation positions on alicyclic moiety.
[c]One hydroxylation position on side chain and another on the alicyclic moiety.

metabolites (M2 and M3), hydroxylated metabolites (M4–M9), and bishydroxylated metabolites (M10) (see Figure 1). A chromatogram of an extract from a deglucuronidated urine sample prior to H4CBD ingestion is shown in Figure S2. The corresponding spectra of H4CBD and its Phase I metabolites are found in Figures S3–S13. Reference spectra of (*S*)- and (*R*)-H4CBD are shown in Figures S44 and S45.

Metabolite M1 is H4CBD, eluting as an unresolved double peak at 9.35 min. The ESI+ product ion spectra of (*R*)-H4CBD and

(*S*)-H4CBD are indistinguishable and show only a few characteristic ions; see Figures S3 and S4. The base peak of the spectrum is the molecular ion (*m/z* 319.2632). The fragment ion with the highest abundance is the cyclohexylium ion (*m/z* 83.0855), which derives from the alicyclic moiety of the molecule. The most abundant ions in the spectrum of H4CBD are smaller fragments from the alicyclic moiety, which are not very characteristic, such as a butenylium ion (*m/z* 55.0542), a butylium ion (*m/z* 57.0699), a pentenylium ion (*m/z* 69.0699), and a methylcyclohexylium ion (*m/z* 97.1012). The characteristic ions are a methyl-isopropyl-cyclohexylium ion (*m/z* 139.1481) and a protonated olivetol ion (*m/z* 181.1223). Some very characteristic ions for CBD are not found for H4CBD, probably due to the lack of an olefinic group, which can be protonated under ESI+ conditions and initiate characteristic fragmentation patterns. The tropylium ions (*m/z* 193.1223 and *m/z* 123.0441), the former being the base peak of the CBD product ion spectrum, are absent in the spectrum of H4CBD. The ions resulting from partial fragmentation of the terpene moiety (*m/z* 259.1693 and *m/z* 217.1223), presumably chromenylium ions, are also not found in the product ion spectrum of H4CBD.

TABLE 3 | Chromatographic data (GC–MS) and relevant ions of the TMS derivatives of H4CBD and their metabolites.

Metabolite (trimethylsilylated)	R_t/ min	RRI	Relevant ions/ Da (70 eV)
M26, (*R*)-H4CBD	17.03	2235	462, **377**, 337
M27, (*S*)-H4CBD	17.66	2307	462, **377**, 337
M28, 7-COOH-H4CBD	19.70	2560	564, **447**, 337, 317
M29, 5″-COOH-H4CBD	20.30	2640	564, 479, 439, 354, **214**
M30, (1*R*,6*S*)-OH-H4CBD	18.62	2424	550, 476, 392, **377**, 342
M31, OH-H4CBD[a]	19.01	2473	550, **465**, 425
M32, (1*R*,6*R*)-OH-H4CBD	19.03	2475	550, **377**, 350, 337, 173
M33, 7-OH-H4CBD	19.15	2491	550, **447**, 337
M34, 7-OH-H4CBD	19.55	2541	550, **447**, 337
M35, OH-H4CBD[a]	19.59	2547	550, **465**, 425
M36, diOH-H4CBD[b]	20.86	2716	638, 535, 465, 425, **372**, 357
M37, diOH-H4CBD[b]	21.37	2787	638, **535**, 499, 425

Note: Base peak is shown in bold. The corresponding EI mass spectra of the trimethylsilylated Phase I metabolites are found in Figures S30–S41.
Abbreviations: RT: retention time, RRI: relative retention index (Kováts index).
[a]Hydroxylation on side chain.
[b]Hydroxylation on C7 and on side chain.

6.1.1 | Carboxylated Metabolites

The chromatogram of an extract from a deglucuronidated urine sample, which was collected 3 h after oral ingestion, showed two carboxylated metabolites (see Figure 1). The metabolite M2 eluting at 3.12 min shows the $[M+H]^+$ ion at *m/z* 349.2373 ($C_{21}H_{33}O_4^+$, −0.9 ppm); see Figure S5. The ions after loss of two H_2O at *m/z* 331.2268 ($C_{21}H_{31}O_3^+$, −0.9 ppm) and *m/z* 313.2162 ($C_{21}H_{29}O_2^+$, −3.5 ppm) and the ions after further loss of CO at *m/z* 303.2319 ($C_{20}H_{31}O_2^+$, 1.0 ppm) and *m/z* 285.2213 ($C_{20}H_{29}O^+$, −3.5 ppm) can be observed. An ion with *m/z* 227.1794 ($C_{17}H_{23}^+$, −3.5 ppm) is observed in the mass spectrum, and its formation mechanism is unknown. The base peak of the spectrum is an ion with *m/z* 137.1325 ($C_{10}H_{17}^+$, −3.6 ppm). The ion at *m/z* 227.1794 seems to be characteristic because a similar ion (*m/z* 225.1) is found in the product ion spectrum of 7-COOH-CBD (see Figures S42 and S43). This metabolite was tentatively identified as 7-COOH-H4CBD.

The metabolite M3 eluting at 4.51 min shows the $[M+H]^+$ ion at *m/z* 349.2373 ($C_{21}H_{33}O_4^+$, 2.6 ppm); see Figure S6. The ions after the loss of H_2O at *m/z* 331.2268 ($C_{21}H_{31}O_3^+$, −0.9 ppm) and

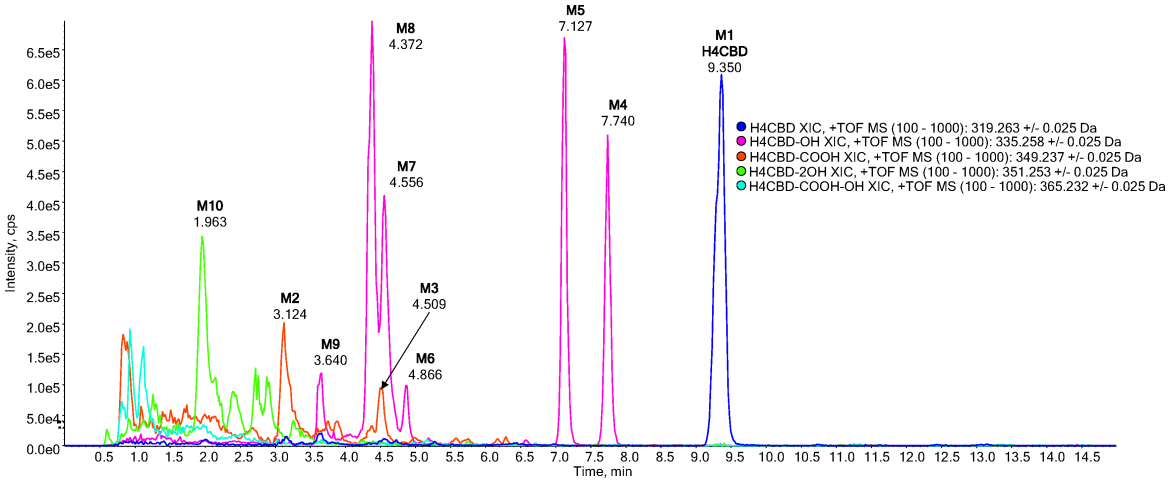

FIGURE 1 | Extracted ion chromatograms of an extract from a deglucuronidated urine sample, 3 h after oral ingestion of 25-mg H4CBD. H4CBD (blue, M1), carboxylated H4CBD (red, M2 and M3), monohydroxylated H4CBD (pink, M4–M9), and bishydroxylated H4CBD (green, M10).

subsequent loss of CO at *m/z* 303.2319 ($C_{20}H_{31}O_2^+$, 4.3 ppm) or the second loss of H_2O at *m/z* 313.2162 ($C_{21}H_{29}O_2^+$, −5.4 ppm) are found in the higher mass range of the spectrum. The characteristic ions are the protonated carboxy-olivetol at *m/z* 211.0965 ($C_{11}H_{15}O_4^+$, −1.4 ppm) and the oxonium ion after the loss of H_2O at *m/z* 193.0859 ($C_{11}H_{13}O_3^+$, −0.5 ppm). Ions resulting from the alicyclic moiety (*m/z* 139, *m/z* 97, *m/z* 83, *m/z* 69, *m/z* 57, and *m/z* 55) are identical to the ions from H4CBD, indicating as well that the side chain was metabolized. This metabolite was tentatively identified as 5″-COOH-H4CBD.

6.1.2 | Hydroxylated Metabolites

The metabolite M4 eluting at 7.74 min shows the $[M+H]^+$ ion at *m/z* 335.2581 ($C_{21}H_{35}O_3^+$, 5.7 ppm); see Figure S7. An ion after the loss of a H_2O molecule can be observed at *m/z* 317.2475 ($C_{21}H_{33}O_2^+$, 3.8 ppm), and an ion after a second loss of H_2O is present at *m/z* 299.2369 ($C_{21}H_{31}O^+$, 2.7 ppm). An ion can be observed at *m/z* 271.2420 ($C_{20}H_{31}^+$, 4.4 ppm), and this ion results from the formal loss of CH_4O_3, presumably from the loss of two H_2O and one CO. The loss of CO likely occurs from the phenol cation (*m/z* 299.2369), which tautomerizes to an oxocyclohexadienylium ion, stabilizing the positive charge on a sp^3-carbon. Elimination of CO from this ion leads to a ring contraction and to the formation of a cyclopentadienyl cation (*m/z* 271.2420). The ion at *m/z* 137.1325 ($C_{10}H_{17}^+$, 4.4 ppm) results from the alicyclic part of the molecule, and this ion might form after a 1,3-*H* shift of the cyclopentadienyl cation and subsequent elimination of the cyclopentadiene moiety. It is not an indicator for the hydroxylation position in this case. The ions at *m/z* 81.0699 ($C_6H_9^+$, 3.7 ppm) and *m/z* 83.0855 ($C_6H_{11}^+$, 2.4 ppm) result from two different processes, but their simultaneous presence is most likely indicative of a hydroxylation position on the side chain of the molecule. Two characteristic ions are found at *m/z* 197.1172 ($C_{11}H_{17}O_3^+$, 3.0 ppm) and its anhydrate at *m/z* 179.1067 ($C_{11}H_{15}O_2^+$, −1.1 ppm). These ions are a protonated olivetol with a hydroxylated side chain and its anhydrate. They are characteristic of side-chain hydroxylated metabolites. A suggested fragmentation pathway is shown in Figure 2.

The metabolite M5 eluting at 7.13 min shows the same ions as described for the metabolite M4, and the corresponding product ion spectrum is found in Figure S8. The presence of the ions *m/z* 179 and *m/z* 197 and the absence of the ion *m/z* 181 indicate that this metabolite is hydroxylated on the side chain. The base peak *m/z* 271 indicates that this ion emerged after the loss of CO from an oxocyclohexadienylium, a tautomer of the phenol cation.

The minor metabolite M6 eluting at 4.87 min shows the ion at *m/z* 179.1067 ($C_{11}H_{15}O_2^+$, 7.3 ppm), indicating that this metabolite is hydroxylated on the side chain; see Figure S9. The fragment ion at *m/z* 261.1849 ($C_{17}H_{25}O_2^+$, 7.3 ppm) might result from a tropylium ion, which is formed after degradation of the side chain, and a hydroxy group at C2 seems plausible. Further fragmentation of this ion leads to the tropylium ion with *m/z* 123.0441 ($C_7H_7O_2^+$, −2.4 ppm), which could also be formed from the ion with *m/z* 179 after elimination of *n*-butene from the side chain. The fragment ion *m/z* 137.0592 ($C_8H_9O_2^+$, 8.0 ppm) is from the aromatic part. The characteristic ion *m/z* 139.1481 ($C_{10}H_{19}^+$, −2.2 ppm) is present but very low in abundance, indicating that hydroxylation took place on the side chain. The metabolite M6 was tentatively identified as 2″OH-H4CBD, and a suggested fragmentation pathway is shown in Figure 3.

The metabolite M7 eluting at 4.56 min shows the same ions as M6, and it is therefore assumed that these two compounds are diastereomers, showing a different configuration at either C1, the hydroxylation position C2″, or at both positions. The corresponding product ion spectrum is shown in Figure S10.

The metabolite M8 (see Figure S11) eluting at 4.37 min shows the protonated olivetol ion at *m/z* 181.1223 ($C_{11}H_{17}O_2^+$, 0.6 ppm), indicating a hydroxylation position on the alicyclic moiety of the molecule. In addition, a tropylium ion at *m/z* 193.1223 ($C_{12}H_{17}O_2^+$, 0.0 ppm) is present, which fragments further by loss of the side chain, seen at *m/z* 123.0441 ($C_7H_7O_2^+$, −1.6 ppm). The presence of the ion at *m/z* 193.1223 is a further indicator of the hydroxylation on the alicyclic moiety. This tropylium ion has a saturated pentyl side chain, and it can only be formed if the hydroxylation position is found on the alicyclic moiety.

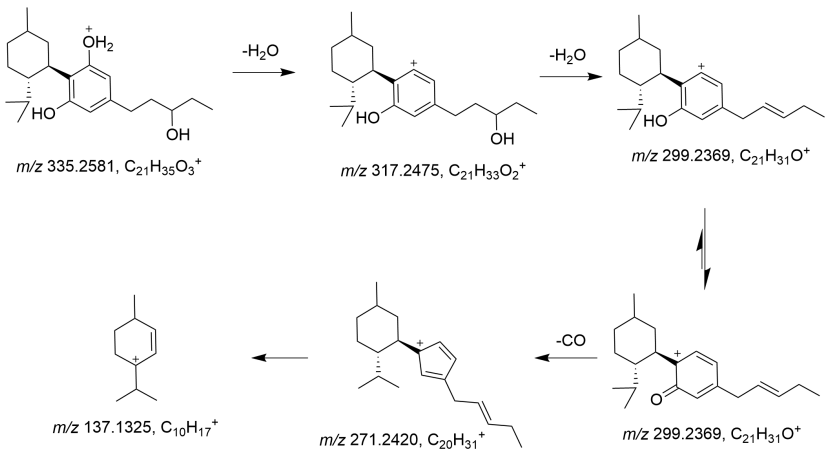

FIGURE 2 | Possible fragmentation pathway of the metabolite M4, an unusual carbenium ion (*m/z* 271) is seen in the spectrum. The position of the hydroxy group on the pentyl side chain is unknown.

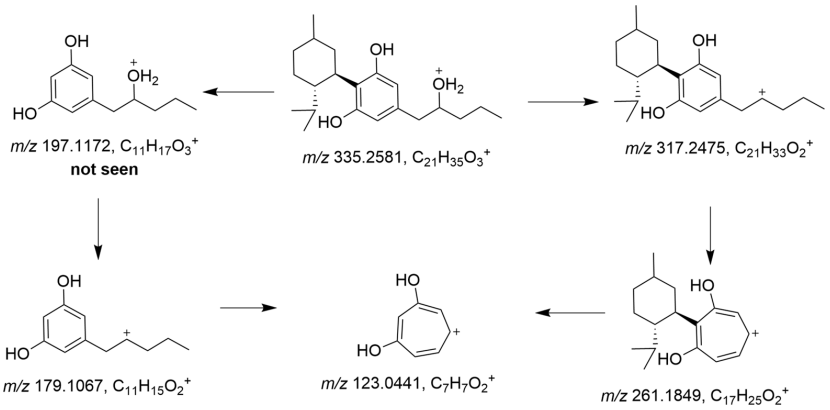

FIGURE 3 | Possible fragmentation pathway of 2″OH-H4CBD (metabolite M6).

A minor metabolite M9 can be seen at 3.64 min, which shows a very similar mass spectrum to the metabolite M8, probably a diastereomer. The product ion spectrum is shown in Figure S12.

6.1.3 | Bishydroxylated Metabolites

A bishydroxylated metabolite M10 eluting at 1.96 min shows a rather strong abundance. The presence of the ion at *m/z* 193.1223 ($C_{12}H_{17}O_2^+$, −1.6 ppm) indicates that this metabolite had two hydroxylation positions at the alicyclic moiety. A product spectrum is shown in Figure S13.

Some other coeluting bishydroxylated metabolites are present between 2.0 and 3.0 min, and most of them show the ions with *m/z* 193 or *m/z* 181, which are indicative ions for bishydroxylation on the alicyclic moiety.

6.2 | LC-QqTOF Phase II Metabolites

Several glucuronidated metabolites were found in an extract of the urine sample 3 h after the ingestion of H4CBD. The most abundant metabolites in urine after 3 h were the glucuronides of H4CBD (M11 and M12). The glucuronides of carboxylated (M13 and M14), hydroxylated (M15–M22), and bishydroxylated metabolites (M23–M25) of H4CBD are present as well. A chromatogram is shown in Figure 4, and a chromatogram prior to H4CBD ingestion can be found in Figure S14.

The epimers of H4CBD glucuronide eluted at 11.34 min (M11) and 11.82 min (M12). Their product ion spectra are shown in Figures S15 and S16. The $[M+H]^+$ ion can be found at *m/z* 495.2952 ($C_{27}H_{43}O_8^+$, −4.2 ppm), and the loss of two H_2O molecules is seen at *m/z* 459.2741 ($C_{27}H_{39}O_6^+$, −2.6 ppm). An odd-electron fragment is present at *m/z* 384.2659 ($C_{25}H_{36}O_3^{+\bullet}$, −4.4 ppm), which results from the fragmentation of the glucuronide moiety, and a H4CBD-furanyl radical cation seems to be a plausible structure for this fragment ion. A postulated fragmentation pathway is shown in Figure 5. The base peak of the spectrum is the protonated aglycone found at *m/z* 319.2632 ($C_{21}H_{35}O_2^+$, −3.1 ppm). The lower mass fragments, discussed earlier for the fragment ions of H4CBD, are of low abundance.

6.2.1 | Carboxylated Glucuronides

The metabolite M13 eluting at 10.04 min shows the $[M+H]^+$ ion at *m/z* 525.2694 ($C_{27}H_{41}O_{10}^+$, 24.7 ppm); see Figure S17. An odd-electron fragment ion can be seen at *m/z* 414.2401 ($C_{25}H_{34}O_5^{+\bullet}$, 0.5 ppm), which results from the fragmentation of the glucuronide moiety. The base peak of this spectrum is the protonated aglycone at *m/z* 349.2373 ($C_{27}H_{41}O_{10}^+$, −0.9 ppm). The same lower fragment ions can be seen as in the mass spectrum of the Phase I metabolite 5″-COOH-H4CBD (M3), namely, *m/z* 331.2268 ($C_{21}H_{31}O_3^+$, 1.5 ppm), *m/z* 211.0965 ($C_{11}H_{15}O_4^+$, 3.3 ppm), *m/z* 193.0859 ($C_{11}H_{13}O_3^+$, 3.6 ppm), *m/z* 139.1481 ($C_{10}H_{19}^+$, −6.5 ppm), and *m/z* 83.0855 ($C_6H_{11}^+$, −9.6 ppm). This metabolite was tentatively identified as 5″-COOH-H4CBD glucuronide.

Another glucuronidated carboxylic metabolite (M14) eluted at 9.39 min, and a product ion spectrum is shown in Figure S18. The $[M+H]^+$ ion is seen at *m/z* 525.2694 ($C_{27}H_{41}O_{10}^+$, 27.6 ppm). An ion at *m/z* 457.1857 ($C_{25}H_{29}O_8^+$, 0.2 ppm) and its deglucuronidated species at *m/z* 281.1536 ($C_{19}H_{21}O_2^+$, −8.9 ppm) are present, representing formal losses of $C_2H_{12}O_2$ (two H_2O and two CH_4) from the $[M+H]^+$ ion and the protonated aglycone, respectively. Their structures are unknown. Interestingly, the ion at *m/z* 281.1536 does only appear if the metabolite was priorly glucuronidated. The formation of the ion at *m/z* 169.1223 ($C_{10}H_{17}O_2^+$, −6.5 ppm) is unknown. It further decomposes by the loss of H_2O at *m/z* 151.1117 ($C_{10}H_{15}O^+$, 6.6 ppm) and the loss of CO at *m/z* 123.1168 ($C_9H_{15}^+$, −4.1 ppm). Additionally, the tropylium ion at *m/z* 193.1223 ($C_{12}H_{17}O_2^+$, −8.8 ppm) and the protonated olivetol ion at *m/z* 181.1223 ($C_{11}H_{17}O_2^+$, 4.4 ppm) appear in the mass spectrum, indicating that this metabolite is carboxylated at the alicyclic moiety. This metabolite was tentatively identified as the glucuronide of 7-COOH-H4CBD.

6.2.2 | Hydroxylated Glucuronides

The metabolite M15 eluting at 5.07 min shows the $[M+H]^+$ ion at *m/z* 511.2902 ($C_{27}H_{43}O_9^+$, −26.4 ppm); see Figure S19. Loss of three H_2O can be observed (*m/z* 493.2796, $C_{27}H_{41}O_8^+$, −13.8 ppm; *m/z* 475.2690, $C_{27}H_{39}O_7^+$, −3.4 ppm; *m/z* 457.2585, $C_{27}H_{37}O_6^+$, 10.5 ppm). The characteristic odd-electron fragment

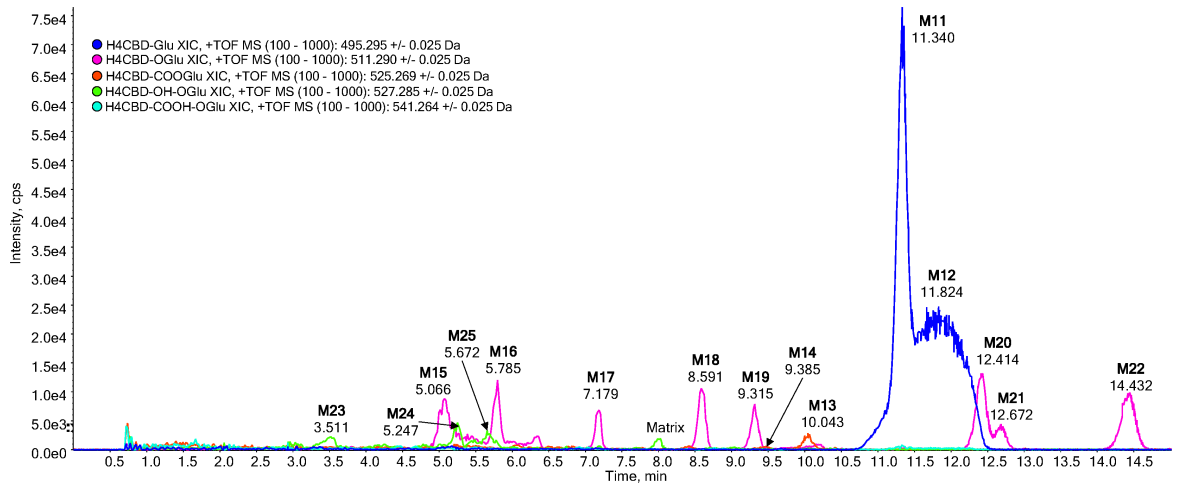

FIGURE 4 | Extracted ion chromatograms of an extract from a urine sample, 3 h after oral ingestion of 25-mg H4CBD. H4CBD glucuronide (blue, M11 and M12), carboxylated H4CBD glucuronide (red, M13 and M14), monohydroxylated H4CBD glucuronide (pink, M15–M22), and bishydroxylated H4CBD glucuronide (green, M23–M25). An extracted urine sample prior to H4CBD ingestion is shown in Figure S14.

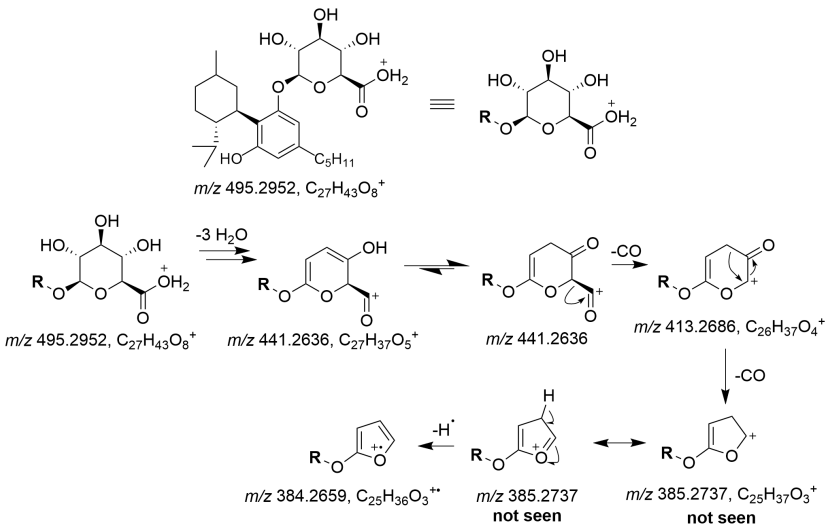

FIGURE 5 | Postulated fragmentation pathway of H4CBD glucuronide, explaining the formation of the radical cation *m/z* 384.

ion at *m/z* 400.2608 ($C_{25}H_{36}O_4^{+\bullet}$, −4.2 ppm) and its anhydrate at *m/z* 382.2502 ($C_{25}H_{34}O_3^{+\bullet}$, 4.4 ppm) can be found. The protonated aglycone is found at *m/z* 335.2581 ($C_{21}H_{35}O_3^+$, −1.2 ppm), and its anhydrate at *m/z* 317.2475 ($C_{21}H_{33}O_2^+$, −0.9 ppm) forms the base peak of this spectrum. The protonated and unsaturated olivetol ion at *m/z* 179.1067 ($C_{11}H_{15}O_2^+$, 1.1 ppm) is present, indicating that this metabolite was hydroxylated on the side chain. A very low-abundant ion with *m/z* 261.1849 ($C_{17}H_{25}O_2^+$, −10.0 ppm) is seen. This metabolite might be the glucuronide of the metabolite M6.

The metabolite eluting M16 at 5.79 min shows the $[M+H]^+$ ion at *m/z* 511.2902 ($C_{27}H_{43}O_9^+$, 4.7 ppm); see Figure S20. The base peak of this spectrum is the protonated aglycone at *m/z* 335.2581 ($C_{21}H_{35}O_3^+$, −2.4 ppm), and the anhydrate at *m/z* 317.2475 ($C_{21}H_{33}O_2^+$, 6.9 ppm) is also present. The tropylium ion at *m/z* 193.1223 ($C_{12}H_{17}O_2^+$, −3.6 ppm) and the protonated olivetol ion at *m/z* 181.1223 ($C_{11}H_{17}O_2^+$, 11.0 ppm) are characteristic ions for a hydroxylation position on the alicyclic moiety. The product ion spectrum is shown in Figure S20.

At 7.18 min, the metabolite M17 can be seen, and a product ion spectrum is found in Figure S21. It shows the $[M+H]^+$ ion at *m/z* 511.2902 ($C_{27}H_{43}O_9^+$, −5.1 ppm). The protonated aglycone at *m/z* 335.2581 ($C_{21}H_{35}O_3^+$, 0.6 ppm) and the anhydrate at *m/z* 317.2475 ($C_{21}H_{33}O_2^+$, −7.9 ppm) are present, and the latter forms the base peak of this spectrum. The tropylium ion at *m/z* 193.1223 ($C_{12}H_{17}O_2^+$, 9.3 ppm) and the ion at *m/z* 137.1325 ($C_{10}H_{17}^+$, −10.2 ppm) are indicative of a hydroxylation on the alicyclic moiety.

The metabolite M18, eluting at 8.59 min, shows the $[M+H]^+$ ion at *m/z* 511.2902 ($C_{27}H_{43}O_9^+$, −2.5 ppm) and its anhydrates at *m/z* 493.2796 ($C_{27}H_{41}O_8^+$, 8.7 ppm) and at *m/z* 475.2690 ($C_{27}H_{39}O_7^+$, 0.0 ppm); see Figure S22. An ion can be seen at *m/z* 443.2064 ($C_{25}H_{31}O_7^+$, −8.1 ppm) representing a formal loss of $C_2H_{12}O_2$, the same formal loss as observed for the glucuronidated carboxy metabolite M14. The base peak of the spectrum is the deglucuronidated molecule, seen at *m/z* 335.2581 ($C_{21}H_{35}O_3^+$, 2.7 ppm), and its anhydrate is seen at *m/z* 317.2475 ($C_{21}H_{33}O_2^+$, 5.0 ppm). The presence of the tropylium ion at *m/z* 193.1223 ($C_{12}H_{17}O_2^+$, −2.6 ppm), the protonated olivetol ion at *m/z* 181.1223 ($C_{11}H_{17}O_2^+$, −1.7 ppm), and the ion at *m/z* 137.1325 ($C_{10}H_{17}^+$, −2.9 ppm) are indicative of a metabolite that is hydroxylated on the alicyclic moiety. The same lower fragment ions appear as in the mass spectrum of the Phase I metabolites M8 and M9. This metabolite was tentatively identified as 7-OH-H4CBD glucuronide.

The metabolite M19 eluting at 9.32 min shows the same fragment ions as the metabolite M18, indicating that these two metabolites are diastereomers; see Figure S23. This metabolite was therefore tentatively identified as the other epimer of 7-OH-H4CBD glucuronide.

The metabolite M20 eluting at 12.41 min shows the $[M+H]^+$ ion at *m/z* 511.2902 ($C_{27}H_{43}O_9^+$, 1.6 ppm), shown in Figure S24. The protonated aglycone at *m/z* 335.2581 ($C_{21}H_{35}O_3^+$, 3.9 ppm) forms the base peak of the spectrum. Repetitive loss of two H_2O molecules resulting in the ions at *m/z* 317.2475 ($C_{21}H_{33}O_2^+$, −0.6 ppm) and at *m/z* 299.2369 ($C_{21}H_{31}O^+$, 4.3 ppm) is present. Further loss of CO at *m/z* 271.2420 ($C_{20}H_{31}^+$, 1.5 ppm) is also present. The ion at *m/z* 137.1325 ($C_{10}H_{17}^+$, −2.9 ppm) is not indicative of a hydroxylation on the alicyclic moiety in this case, as the ions at *m/z* 197.1178 ($C_{11}H_{17}O_3^+$, 5.1 ppm) and at *m/z* 179.1065 ($C_{11}H_{15}O_2^+$, −16.7 ppm) are present but not very abundant. The same lower fragment ions appear as in the mass spectrum of the Phase I metabolites M4 and M5, and the product ion spectrum of the metabolite M20 is found in Figure S24.

The mass spectrum of the metabolite M21 eluting at 12.67 min is very similar to the mass spectrum of the metabolite M20, and the same fragment ions appear in similar abundances. The product ion spectrum is found in Figure S25.

The mass spectrum of the metabolite M22 (see Figure S26) eluting at 14.43 min is similar to the mass spectra of the metabolites M20 and M21, but only the aglycone at *m/z* 335.2581 ($C_{21}H_{35}O_3^+$, 4.5 ppm) is of high abundance. The other fragment ions are even less abundant than in the spectra of the metabolites M20 and M21.

6.2.3 | Bishydroxylated Glucuronides

A glucuronidated bishydroxylated metabolite M23 eluted at 3.51 min; a product ion spectrum is found in Figure S27. The $[M+H]^+$ ion at *m/z* 527.2851 ($C_{27}H_{43}O_9^+$, 6.6 ppm) and loss of two H_2O molecules are seen at *m/z* 509.2745 ($C_{27}H_{41}O_8^+$, −4.1 ppm) and at *m/z* 491.2639 ($C_{27}H_{39}O_7^+$, −11.4 ppm). The protonated aglycone at *m/z* 351.2530 ($C_{21}H_{35}O_4^+$, 5.1 ppm) and loss of two H_2O molecules are seen at *m/z* 333.2424 ($C_{21}H_{33}O_3^+$, 4.8 ppm) and *m/z* 315.2319 ($C_{21}H_{31}O_2^+$, 14.6 ppm). The tropylium ion at *m/z* 193.1223 ($C_{12}H_{17}O_2^+$, 4.1 ppm) and the protonated olivetol ion at *m/z* 181.1223 ($C_{11}H_{17}O_2^+$, 2.8 ppm) can be observed. The ion at *m/z* 153.1274 ($C_{10}H_{17}O^+$, −3.3 ppm) and its anhydrate at *m/z* 135.1168 ($C_{10}H_{15}^+$, −20.7 ppm) are present, indicating two hydroxylation sites on the alicyclic moiety of the molecule. The ion at *m/z* 137.1325 ($C_{10}H_{17}^+$, 2.9 ppm) might result from a coeluting metabolite, as it is indicative of a metabolite that is hydroxylated on the alicyclic moiety and the side chain of the molecule.

Another glucuronidated bishydroxylated metabolite M24 eluted at 5.25 min; the product ion spectrum is found in Figure S28. The $[M+H]^+$ ion at *m/z* 527.2851 ($C_{27}H_{43}O_9^+$, 12.1 ppm) is seen. The deglucuronidated ion at *m/z* 351.2530 ($C_{21}H_{35}O_4^+$, −0.6 ppm) and the loss of two H_2O molecules are seen at *m/z* 333.2424 ($C_{21}H_{33}O_3^+$, 7.8 ppm) and *m/z* 315.2319 ($C_{21}H_{31}O_2^+$, 4.1 ppm). An ion from the alicyclic moiety can be seen at *m/z* 137.1325 ($C_{10}H_{17}^+$, −8.0 ppm), indicating that this metabolite is hydroxylated on the alicyclic moiety and on the side chain.

Another bishydroxylated glucuronide M25 eluted at 5.67 min; the product ion spectrum is seen in Figure S29. The $[M+H]^+$ ion at *m/z* 527.2851 ($C_{27}H_{43}O_9^+$, −2.8 ppm) and its anhydrate at *m/z* 509.2745 ($C_{27}H_{41}O_8^+$, −9.4 ppm) are observable. The base peak of the spectrum is the protonated aglycone at *m/z* 351.2530 ($C_{21}H_{35}O_4^+$, −3.7 ppm). Two losses of H_2O at *m/z* 333.2424 ($C_{21}H_{33}O_3^+$, 0.3 ppm) and at *m/z* 315.2319 ($C_{21}H_{31}O_2^+$, −5.7 ppm) are observed. The hydroxylated olivetol ion at *m/z* 197.1172 ($C_{11}H_{17}O_3^+$, 0.5 ppm) indicates that this metabolite had a hydroxylation site on the alicyclic moiety and on the side chain. The tropylium ion at *m/z* 193.1223 ($C_{12}H_{17}O_2^+$, 7.2 ppm) derives from a metabolite that bears two hydroxylation positions on the alicyclic moiety, which leads to the assumption that coelution of metabolites is likely in this case.

6.3 | GC–MS Phase I Metabolites (TMS Derivatives)

6.3.1 | Fragmentation Patterns of H4CBD and Its Trimethylsilylderivatives

The electron impact (EI) mass spectra of (*R*)-H4CBD and (*S*)-H4CBD are indistinguishable. They show the molecular ion at *m/z* 318. The main fragments are the dihydrochromenylium ion at *m/z* 233 and the tropylium ion at *m/z* 193. The dihydrochromenylium ion in hydrogenated cannabinoids like H4CBD or HHC is of high abundance. In their unsaturated analogs, CBD and the isomers of THC, the analogous chromenylium ion *m/z* 231 usually forms the base peak and is often the only highly abundant ion due to its simple formation and aromatic stability [24–26]. The tropylium ion forms the base peak of the H4CBD epimers as it does for the HHC epimers [24, 26–28].

The spectra of the trimethylsilylated H4CBD epimers are indistinguishable as well; see Figures S30 and S31. The most common fragments are the trimethylsilylated derivatives of the dihydrochromenylium ion *m/z* 377 and the trimethylsilylated tropylium ion *m/z* 337 discussed previously. The trimethylsilylated metabolites (*R*)-H4CBD TMS (M26) and (*S*)-H4CBD (M27) can be seen at 17.03 and 17.66 min, respectively (see Figure 6).

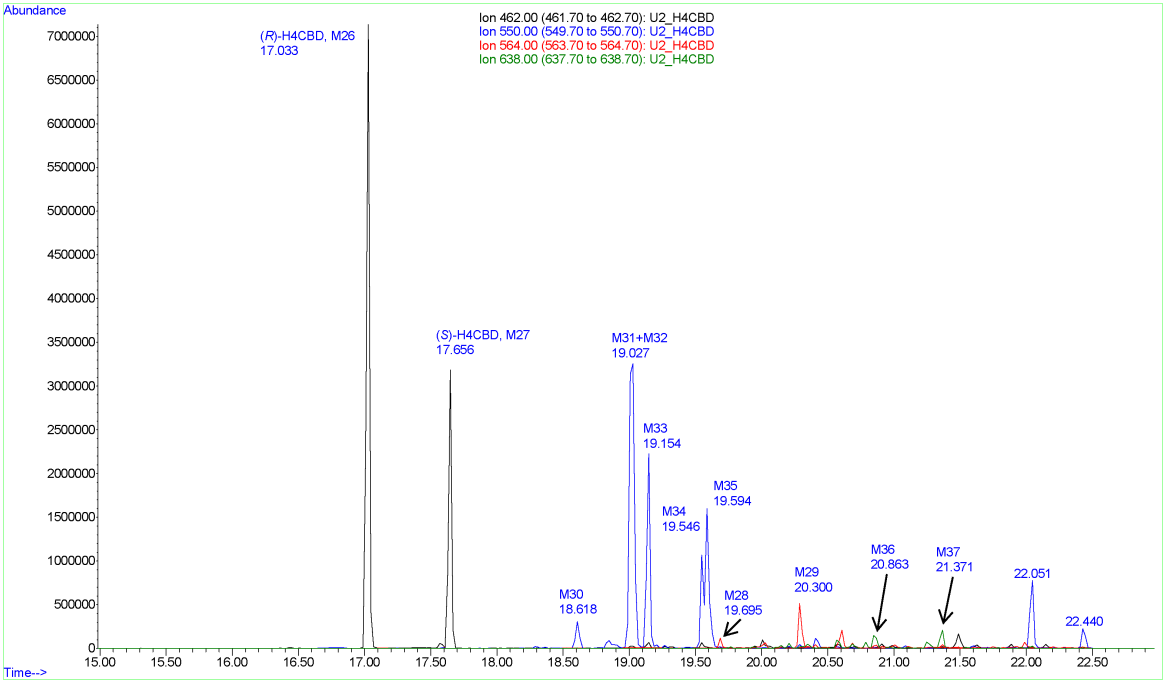

FIGURE 6 | Overlayed XIC of a trimethylsilylated extract from a deglucuronidated urine sample 3 h after oral ingestion of H4CBD. H4CBD (black, M26 and M27), carboxylated metabolites (red, M28 and M29), hydroxylated metabolites (blue, M30–M35), and bishydroxylated metabolites (green, M36 and M37).

6.3.2 | Carboxylated Metabolites, Trimethylsilylated

Two different carboxylated metabolites were detected. The metabolite M28 at 19.70 min shows the molecular ion at *m/z* 564 (see Figure S32). After loss of a trimethylsilyl radical and CO_2 from the trimethylsilylcarboxy group, the base peak of the spectrum at *m/z* 447 is formed. Additionally, the tropylium ion at *m/z* 337 is present, indicating that this metabolite was carboxylated on the alicyclic moiety. Trimethylsilylated 7-COOH-H4CBD fits with the observed fragments. The same fragmentation mechanisms as in 7-COOH-CBD occur, with the exception of the retro-Diels-Alder fragmentation of the cyclohexene ring due to a lacking double bond in the alicyclic ring [15].

Another carboxylated metabolite M29 is observed at 20.30 min (see Figure S33). This metabolite shows the fragment ion *m/z* 439 and *m/z* 479, which are trimethylsilylcarboxy derivatives of the dihydrochromenylium ion *m/z* 337 and the tropylium ion *m/z* 377, indicating that this metabolite is carboxylated on the side chain. This metabolite was therefore tentatively identified as 5″-COOH-H4CBD. The fragment ion *m/z* 439 can also be seen in the mass spectrum of trimethylsilylated 5″-COOH-CBD [15].

6.3.3 | Hydroxylated Metabolites, Trimethylsilylated

Metabolites that are hydroxylated on the side chain can be recognized by the presence of the ions with *m/z* 425 and *m/z* 465, whereas the ions with *m/z* 337 and *m/z* 377 are absent [29]. The former ions have an additional trimethylsilyloxy group on the side chain.

Five different hydroxylated metabolites of H4CBD are seen in the extracted ion chromatogram (XIC *m/z* 550). The minor metabolite M30 eluting at 18.62 min shows the dihydrochromenlyium ion *m/z* 377 as the base peak, indicating that this metabolite is hydroxylated on the alicyclic moiety (see Figure S34). The presence of the ion at *m/z* 392 might be indicative that this metabolite was hydroxylated on C6, synperiplanar to the methyl group at C1. Elimination of trimethylsilanol and subsequent retro-Diels-Alder reaction would lead to a fragment ion with *m/z* 392, a similar mechanism as shown in Figure 7. A plausible structure of this metabolite might be (1*R*,6*S*)-OH-H4CBD or (1*S*,6*R*)-OH-H4CBD, and the latter shows higher 1,3-diaxial strain in the conformation in which trimethylsilanol could be eliminated due to bulky axial groups. The EI mass spectrum is shown in Figure S34.

At 19.0 min, two different metabolites are almost coeluting; the first metabolite M31 at 19.01 min shows the ions *m/z* 465 and *m/z* 425, indicating that this metabolite is a side-chain hydroxylated metabolite. The hydroxylation position is unknown; a mass spectrum is shown in Figure S35.

The other metabolite M32 at 19.03 min shows the fragment ions *m/z* 377 and *m/z* 337, indicating a metabolite that is hydroxylated on the alicyclic part (see Figure S36). In addition, this metabolite shows a quite abundant fragment ion with *m/z* 350. This might be indicative that the hydroxylation position is either antiperiplanar to the methyl group or to the *iso*-propyl group.

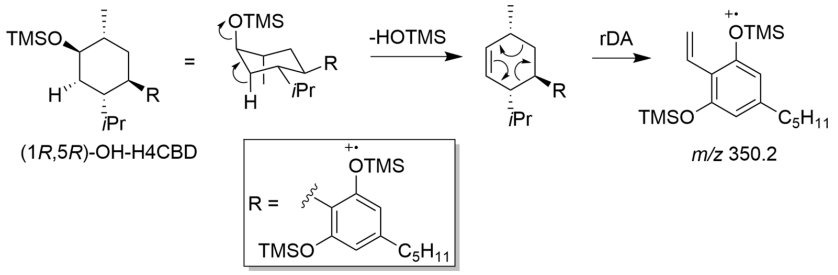

FIGURE 7 | Possible fragmentation pathway to the ion *m/z* 350 seen in the spectrum of (1*R*,5*R*)-OH-H4CBD (metabolite M32).

The tentative metabolite (1*R*,6*R*)-OH-H4CBD has a stable chair conformation in which the *iso*-propyl group and the aromatic moiety are equatorial substituents. In this conformation, the metabolite could eliminate trimethylsilanol, resulting in the formation of a 3,4,6-trisubstituted cyclohexene intermediate, which can fragment further to a styrene ion with *m/z* 350 after retro-Diels-Alder reaction. The potential metabolites (1*S*,5*S*)-OH-H4CBD, (1*R*,4*S*)-OH-H4CBD, and (1*S*,4*S*)-OH-H4CBD might undergo the same reaction cascade, but in these molecules, the conformation in which the elimination of trimethylsilanol could occur would have three bulky axial substituents, resulting in a high 1,3-diaxial strain. A possible fragmentation pathway is shown in Figure 7.

The mass spectra of the metabolites M33 and M34 eluting at 19.15 and 19.55 min are identical, showing the molecular ion at *m/z* 550 and two abundant ions at *m/z* 447 and *m/z* 337; see Figures S37 and S38. The ion with *m/z* 447 forms the base peak of their spectra and might form after the loss of a trimethylsilyl radical and formaldehyde. A primary alcohol is therefore suspected. The ion *m/z* 337 is the tropylium ion that is also present in the mass spectra of the H4CBD epimers, indicating that these metabolites were hydroxylated on the alicyclic moiety of the molecule. Hydroxylation position on C7 seems plausible; this would explain why the characteristic dihydrochromenylium ion *m/z* 377 is not present. These metabolites were therefore tentatively identified as 7-OH-(*R*)-H4CBD and 7-OH-(*S*)-H4CBD. The same fragmentation reactions occur in the TMS derivative of the analogue 7-OH-CBD, where the ion *m/z* 443 (unsaturated analogue of *m/z* 447) forms after the loss of a trimethylsilyl radical and formaldehyde; the ion *m/z* 337 is also present. An additional ion is formed in 7-OH-CBD with *m/z* 478, which cannot be formed from 7-OH-H4CBD, as this ion occurs from a retro-Diels-Alder pathway [14].

The metabolite M35 eluting at 19.59 min shows the ions *m/z* 465 and *m/z* 425 (see Figure S39). These are the discussed dihydrochromenylium ion (*m/z* 377) and tropylium ion (*m/z* 337) with an additional trimethylsilyloxy group, indicating that this metabolite is hydroxylated on the side chain.

6.3.4 | Bishydroxylated Metabolites, Trimethylsilylated

The metabolite M36 at 20.86 min shows the ion *m/z* 535, which is indicative of a hydroxylation position on C7 after the loss of a trimethylsilyl radical and formaldehyde (see Figure S40). The fragment ions at *m/z* 465 and *m/z* 425 are present, indicating a hydroxylation position on the side chain.

The metabolite M37 at 21.37 min shows two very abundant fragment ions (see Figure S41). The ion *m/z* 535 can be formed after the elimination of a trimethylsilyl radical and formaldehyde, the same fragmentation mechanism as in the tentatively identified 7-OH-H4CBD epimers and the metabolite M36. The other ion (*m/z* 425) is indicative of a hydroxylation position at the side chain. This metabolite was therefore tentatively identified as a side-chain hydroxylated derivative of 7-OH-H4CBD; an EI mass spectrum is shown in Figure S41. The analogous fragment ion *m/z* 531 and the same fragment ion *m/z* 425 are observed for the bishydroxylated metabolites of CBD 1″,7-DiOH-CBD, 3″,7-DiOH-CBD, 4″,7-DiOH-CBD, and 5″,7-DiOH-CBD [14, 15].

The Kováts indices, retention times, and relevant ions of the trimethylsilyl derivatives of H4CBD and the detected metabolites are summarized in Table 3. A chromatogram of the *n*-alkane standard that was used for the calculation of the Kováts indices can be found in Figure S46.

6.4 | Fragmentation Patterns of Phase I Metabolites

In ESI+, the fragmentation patterns of H4CBD are different from CBD. H4CBD does not fragment to the characteristic tropylium ion *m/z* 193.1223; instead, the aromatic moiety of the molecule can be seen as a protonated olivetol at *m/z* 181.1223 after fragmentation under ESI+ conditions. This is also true for their respective metabolites, side-chain hydroxylated metabolites of H4CBD fragment to a hydroxy-olivetol ion *m/z* 197.1178 and its anhydrate *m/z* 179.1065. H4CBD metabolites that are hydroxylated on the alicyclic moiety can undergo fragmentation to the characteristic tropylium ion *m/z* 193.1223. The presence of these ions in H4CBD metabolites is therefore indicative of the hydroxylation position.

Very unusual fragmentation patterns are found for several Phase I and Phase II metabolites. A Phase I metabolite (M2) that was tentatively identified as a carboxylic acid showed the fragment ion *m/z* 227.1794 that was identified as ($C_{17}H_{23}^+$). It is not clear how this ion is formed. A similar ion (*m/z* 225.1) is found in the mass spectrum of 7-COOH-CBD under ESI+ conditions.

The side-chain hydroxylated metabolites M4 and M5 showed loss of both oxygens from the phenol groups, presumably as H_2O and CO to form a cyclopentadienyl cation. The same fragmentation pattern to form a cyclopentadienyl ion can be seen in the ESI+ mass spectra of hydroquinone, pyrocatechol, and vanillin [30, 31].

The side-chain hydroxylated metabolites M6 and M7 form another tropylium ion (*m/z* 261.1849), which results from the fragmentation of the side chain, in contrast to the formation of the tropylium ion *m/z* 193.1223, which is formed from the fragmentation of the alicyclic moiety.

The fragmentation patterns of the trimethylsilylated derivatives of H4CBD and its Phase I metabolites under EI ionization are similar to those of the trimethylsilylated derivatives of CBD and its Phase I metabolites.

6.5 | Fragmentation Patterns of Phase II Metabolites

Several Phase II metabolites showed odd-electron fragment ions, which are presumably formed by the fragmentation of the glucuronide moiety to form a furanyl radical cation. This kind of fragmentation was seen for the glucuronides of H4CBD (M11, M12), the side-chain carboxylated metabolite 5″-COOH-H4CBD (M13), and the side-chain hydroxylated metabolite M15. The Phase II metabolites with functional groups on the alicyclic moiety did not show this fragmentation pattern. It is therefore assumed that side-chain oxidized metabolites of H4CBD can easily be protonated on the glucuronide, which is prone to fragmentation.

The tentatively identified metabolites 7-OH-H4CBD glucuronide and 7-COOH-H4CBD glucuronide (M14) showed a formal loss of $C_2H_{12}O_2$ (two H_2O and two CH_4) by an unknown process. The glucuronide moiety seems not to be fragmented in this fragmentation pathway because, in the case of the carboxy metabolite M14, the deglucuronidated species was found as well.

7 | Conclusions

The epimers of H4CBD and their respective glucuronides can be used as analytical targets, but might not be present because of metabolization, depending on the time between consumption and urine sampling. In this case, the side-chain hydroxylated metabolites M4 and M5, and the metabolite M8, which is presumably an epimer of 7-OH-H4CBD, might be better targets as they were very abundant in the chromatogram. Further investigations are needed to elucidate the structures of the very abundant side-chain hydroxylated metabolites M4 and M5. A method for the determination of H4CBD and its metabolites should also include the carboxylic acids 7-COOH-H4CBD and 5″-COOH-H4CBD, and it is assumed that they accumulate after frequent H4CBD consumption. The same metabolites can be analyzed as TMS derivatives by GC–MS. Glucuronides of the discussed metabolites would also suit as forensic markers. Currently, no analytical standards for the proof of H4CBD consumption are available besides (*R*)-H4CBD and (*S*)-H4CBD.

Acknowledgments

PD Dr. Urs Duthaler and Dr. Vanessa Hofmann from the Institute of Forensic Medicine Basel are acknowledged for providing product ion spectra of 7-COOH-CBD, which are shown in Figures S42 and S43. Open access publishing facilitated by Universitat Bern, as part of the Wiley - Universitat Bern agreement via the Consortium Of Swiss Academic Libraries.

Conflicts of Interest

The authors declare no conflicts of interest.

Data Availability Statement

The data that support the findings of this study are available from the corresponding author upon reasonable request.

References

1. A. Jacob and A. R. Todd, "119. *Cannabis indica*. Part II. Isolation of Cannabidiol From Egyptian Hashish. Observations on the Structure of Cannabinol," *Journal of the Chemical Society (Resumed)* (1940): 649–653, https://doi.org/10.1039/JR9400000649.

2. R. B. Laprairie, A. M. Bagher, M. E. M. Kelly, and E. M. Denovan-Wright, "Cannabidiol Is a Negative Allosteric Modulator of the Cannabinoid CB1 Receptor," *British Journal of Pharmacology* 172 (2015): 4790–4805, https://doi.org/10.1111/bph.13250.

3. S. Ben-Shabat, L. O. Hanuš, G. Katzavian, and R. Gallily, "New Cannabidiol Derivatives: Synthesis, Binding to Cannabinoid Receptor, and Evaluation of Their Antiinflammatory Activity," *Journal of Medicinal Chemistry* 49 (2006): 1113–1117, https://doi.org/10.1021/jm050709m.

4. E. W. Bow and J. M. Rimoldi, "The Structure–Function Relationships of Classical Cannabinoids: CB1/CB2 Modulation," *Perspectives in Medicinal Chemistry* 8 (2016): PMC.S32171, https://doi.org/10.4137/PMC.S32171.

5. L. K. Janssens, K. Van Uytfanghe, J. B. Williams, K. W. Hering, D. M. Iula, and C. P. Stove, "Investigation of the Intrinsic Cannabinoid Activity of Hemp-Derived and Semisynthetic Cannabinoids With β-Arrestin2 Recruitment Assays—and How This Matters for the Harm Potential of Seized Drugs," *Archives of Toxicology* 98 (2024): 2619–2630, https://doi.org/10.1007/s00204-024-03769-4.

6. B. Pulver, B. Schmitz, S. D. Brandt, et al., Chemical Analysis of Recreational Products Containing Semi-Synthetic Cannabinoids in Germany. Presented at the TIAFT2024 conference, St. Gallen, Switzerland, September 2024.

7. S. Watanabe, T. Murakami, S. Muratsu, H. Fujiwara, T. Nakanishi, and Y. Seto, "Discrepancies Between the Stated Contents and Analytical Findings for Electronic Cigarette Liquid Products: Identification of the New Cannabinoid, Δ9-Tetrahydrocannabihexol Acetate," *Drug Testing and Analysis* 17 (2024): 694–700, https://doi.org/10.1002/dta.3777.

8. M. Hundertmark, L. Besch, J. Röhrich, T. Germerott, and C. Wunder, "Characterising a New Cannabis Trend: Extensive Analysis of Semi-Synthetic Cannabinoid-Containing Seizures From Germany," *Drug Testing and Analysis* (2025): n/a, https://doi.org/10.1002/dta.3886.

9. W. Schirmer, I. Gjuroski, M. Vermathen, J. Furrer, S. Schürch, and W. Weinmann, "Isolation and Characterization of Synthesis Intermediates and Side Products in Hexahydrocannabiphorol," *Drug Testing and Analysis* 17 (2024): 531–543, https://doi.org/10.1002/dta.3759.

10. W. Schirmer, S. Schürch, and W. Weinmann, "The Identification of Synthetic Impurities in a Vape Pen Containing Δ^9-Tetrahydrocannabiphorol Using Gas Chromatography Coupled With

Mass Spectrometry," *Psychoactives* 3 (2024): 491–500, https://doi.org/10.3390/psychoactives3040030.

11. C. Caprari, E. Ferri, M. A. Vandelli, C. Citti, and G. Cannazza, "An Emerging Trend in Novel Psychoactive Substances (NPSs): Designer THC," *Journal of Cannabis Research* 6 (2024): 21, https://doi.org/10.1186/s42238-024-00226-y.

12. C. F. Jørgensen, B. S. Rasmussen, K. Linnet, and R. Thomsen, "Emergence of Semi-Synthetic Cannabinoids in Cannabis Products Seized in Eastern Denmark Over a 6-Year Period," *Journal of Forensic Sciences* 69 (2024): 2009–2017, https://doi.org/10.1111/1556-4029.15631.

13. Schweizerische Eidgenossenschaft. Verordnung des EDI Über die Verzeichnisse der Betäubungsmittel, Psychotropen Stoffe, Vorläuferstoffe und Hilfschemikalien (Betäubungsmittelverzeichnisverordnung, BetmVV-EDI) vom 30. Mai 2011 (Stand am 9. Oktober 2023), https://www.fedlex.admin.ch/eli/cc/2011/363/de.

14. B. Martin, M. Nordqvist, S. Agurell, J. E. Lindgren, K. Leander, and M. Binder, "Identification of Monohydroxylated Metabolites of Cannabidiol Formed by Rat Liver," *Journal of Pharmacy and Pharmacology* 28 (1976): 275–279, https://doi.org/10.1111/j.2042-7158.1976.tb04152.x.

15. B. R. Martin, D. J. Harvey, and W. D. Paton, "Biotransformation of Cannabidiol in Mice. Identification of New Acid Metabolites," *Drug Metabolism and Disposition* 5 (1977): 259–267, https://doi.org/10.1016/S0090-9556(25)05959-8.

16. D. J. Harvey and R. Mechoulam, "Metabolites of Cannabidiol Identified in Human Urine," *Xenobiotica* 20 (1990): 303–320, https://doi.org/10.3109/00498259009046849.

17. S. Malaca, M. Gottardi, F. Pigliasco, et al., "UHPLC-MS/MS Analysis of Cannabidiol and Its Metabolites in Serum of Patients With Resistant Epilepsy Treated With CBD Formulations," *Pharmaceuticals* 14, no. 7 (2021).

18. F. Pigliasco, S. Malaca, A. F. Lo Faro, et al., "Cannabidiol, Δ9-Tetrahydrocannabinol, and Metabolites in Human Blood by Volumetric Absorptive Microsampling and LC-MS/MS Following Controlled Administration in Epilepsy Patients," *Frontiers in Pharmacology* 13–2022 (2022).

19. S. Pichini, S. Malaca, M. Gottardi, et al., "UHPLC-MS/MS Analysis of Cannabidiol Metabolites in Serum and Urine Samples. Application to an Individual Treated With Medical Cannabis," *Talanta* 223 (2021): 121772, https://doi.org/10.1016/j.talanta.2020.121772.

20. W. Schirmer, S. Schürch, and W. Weinmann, "Identification of Hexahydrocannabiphorol Metabolites in Human Urine," *Drug Testing and Analysis* (2025): n/a, https://doi.org/10.1002/dta.3871.

21. S. Dresen, M. Gergov, L. Politi, C. Halter, and W. Weinmann, "ESI-MS/MS Library of 1,253 Compounds for Application in Forensic and Clinical Toxicology," *Analytical and Bioanalytical Chemistry* 395 (2009): 2521–2526, https://doi.org/10.1007/s00216-009-3084-2.

22. E. Kováts, "Gas-Chromatographische Charakterisierung Organischer Verbindungen. Teil 1: Retentionsindices Aliphatischer Halogenide, Alkohole, Aldehyde und Ketone," *Helvetica Chimica Acta* 41 (1958): 1915–1932, https://doi.org/10.1002/hlca.19580410703.

23. H. van Den Dool and P. D. Kratz, "A Generalization of the Retention Index System Including Linear Temperature Programmed Gas—Liquid Partition Chromatography," *Journal of Chromatography A* 11 (1963): 463–471, https://doi.org/10.1016/S0021-9673(01)80947-X.

24. H. Budzikiewicz, R. T. Alpin, D. A. Lightner, C. Djerassi, R. Mechoulam, and Y. Gaoni, "Massenspektroskopie und Ihre Anwendung auf Strukturelle und Stereochemische Probleme—LXVIII: Massenspektroskopische Untersuchung der Inhaltstoffe von Haschisch," *Tetrahedron* 21 (1965): 1881–1888, https://doi.org/10.1016/S0040-4020(01)98657-0.

25. T. B. Vree, "Mass Spectrometry of Cannabinoids," *Journal of Pharmaceutical Sciences* 66 (1977): 1444–1450, https://doi.org/10.1002/jps.2600661025.

26. D. J. Harvey, "Mass Spectrometry of the Cannabinoids and Their Metabolites," *Mass Spectrometry Reviews* 6 (1987): 135–229, https://doi.org/10.1002/mas.1280060104.

27. W. Schirmer, V. Auwärter, J. Kaudewitz, S. Schürch, and W. Weinmann, "Identification of Human Hexahydrocannabinol Metabolites in Urine," *European Journal of Mass Spectrometry* 29 (2023): 14690667231200139, https://doi.org/10.1177/14690667231200139.

28. P. Seccamani, C. Franco, S. Protti, et al., "Photochemistry of Cannabidiol (CBD) Revised. A Combined Preparative and Spectrometric Investigation," *Journal of Natural Products* 84 (2021): 2858–2865, https://doi.org/10.1021/acs.jnatprod.1c00567.

29. B. Martin, S. Agurell, M. Nordqvist, and A. J. E. Lindgren, "Dioxygenated Metabolites of Cannabidiol Formed by Rat Liver," *Journal of Pharmacy and Pharmacology* 28 (1976): 603–608, https://doi.org/10.1111/j.2042-7158.1976.tb02809.x.

30. H. Horai, M. Arita, S. Kanaya, et al., "MassBank: A Public Repository for Sharing Mass Spectral Data for Life Sciences," *Journal of Mass Spectrometry* 45 (2010): 703–714, https://doi.org/10.1002/jms.1777.

31. J. Hertzog, V. Carré, A. Dufour, and F. Aubriet, "Semi-Targeted Analysis of Complex Matrices by ESI FT-ICR MS or How an Experimental Bias May be Used as an Analytical Tool," *Journal of the American Society for Mass Spectrometry* 29 (2018): 543–557, https://doi.org/10.1007/s13361-017-1865-y.

Supporting Information

Additional supporting information can be found online in the Supporting Information section. **Figure S1:** Quantification of (*R*)- and (*S*)-H4CBD in the H4CBD product for recreational use with GC–MS. **Figure S2:** Chromatogram of deglucuronidated urine before ingestion of H4CBD, measured on a LC-QqTOF. **Figure S3:** LC-QqTOF spectrum of (*S*)-H4CBD (Metabolite M1). **Figure S4:** LC-QqTOF spectrum of (*R*)-H4CBD (Metabolite M1). **Figure S5:** Mass spectrum of metabolite M2, a carboxylated metabolite of H4CBD (from a deglucuronidated urine sample 3 h after ingestion of 25-mg H4CBD). **Figure S6:** Mass spectrum of metabolite M3, a carboxylated metabolite of H4CBD (from a deglucuronidated urine sample 3 h after ingestion of 25-mg H4CBD). **Figure S7:** Mass spectrum of metabolite M4, a side-chain hydroxylated metabolite of H4CBD (from a deglucuronidated urine sample 3 h after ingestion of 25-mg H4CBD). *The position of the hydroxy group is unknown. **Figure S8:** Mass spectrum of metabolite M5, a side-chain hydroxylated metabolite of H4CBD (from a deglucuronidated urine sample 3 h after ingestion of 25-mg H4CBD). *The position of the hydroxy group is unknown. **Figure S9:** Mass spectrum of metabolite M6, a hydroxylated metabolite of H4CBD (from a deglucuronidated urine sample 3 h after ingestion of 25-mg H4CBD). Tentatively identified as an epimer of 2″OH-H4CBD. **Figure S10:** Mass spectrum of metabolite M7, a hydroxylated metabolite of H4CBD (from a deglucuronidated urine sample 3 h after ingestion of 25-mg H4CBD). Tentatively identified as an epimer of 2″OH-H4CBD. **Figure S11:** Mass spectrum of metabolite M8, a hydroxylated metabolite of H4CBD (from a deglucuronidated urine sample 3 h after ingestion of 25-mg H4CBD). Tentatively identified as an epimer of 7-OH-H4CBD. **Figure S12:** Mass spectrum of metabolite M9, a hydroxylated metabolite of H4CBD (from a deglucuronidated urine sample 3 h after ingestion of 25-mg H4CBD). Tentatively identified as an epimer of 7-OH-H4CBD. **Figure S13:** Mass spectrum of metabolite M10, a bishydroxylated metabolite of H4CBD (from a deglucuronidated urine sample 3 h after ingestion of 25-mg H4CBD). The position of the hydroxy groups is unknown. **Figure S14:** Chromatogram of a urine sample before ingestion of H4CBD, measured on a LC-QqTOF. **Figure S15:** Mass spectrum of metabolite M11, a glucuronidated metabolite of H4CBD (from a urine sample 3 h after ingestion of 25-mg H4CBD). **Figure S16:** Mass spectrum of metabolite M12, a glucuronidated metabolite of H4CBD (from a urine sample 3 h after ingestion of 25-mg H4CBD). Acquired in SWATH mode. **Figure S17:** Mass spectrum of metabolite M13, a carboxylated and glucuronidated metabolite of H4CBD (from a urine sample 3 h after ingestion of 25-mg H4CBD). The position of the

glucuronide moiety is unknown. **Figure S18:** Mass spectrum of metabolite M14, a carboxylated and glucuronidated metabolite of H4CBD (from a urine sample 3 h after ingestion of 25-mg H4CBD). The position of the glucuronide moiety is unknown. **Figure S19:** Mass spectrum of metabolite M15, a hydroxylated and glucuronidated metabolite of H4CBD (from a urine sample 3 h after ingestion of 25-mg H4CBD). The position of the glucuronide moiety is unknown. **Figure S20:** Mass spectrum of metabolite M16, a hydroxylated and glucuronidated metabolite of H4CBD (from a urine sample 3 h after ingestion of 25-mg H4CBD). The position of the glucuronide moiety and the hydroxy group is unknown. **Figure S21:** Mass spectrum of metabolite M17, a hydroxylated and glucuronidated metabolite of H4CBD (from a urine sample 3 h after ingestion of 25-mg H4CBD). The position of the glucuronide moiety and the hydroxy group is unknown. **Figure S22:** Mass spectrum of metabolite M18, a hydroxylated and glucuronidated metabolite of H4CBD (from a urine sample 3 h after ingestion of 25-mg H4CBD). The position of the glucuronide moiety is unknown. **Figure S23:** Mass spectrum of metabolite M19, a hydroxylated and glucuronidated metabolite of H4CBD (from a urine sample 3 h after ingestion of 25-mg H4CBD). The position of the glucuronide moiety is unknown. **Figure S24:** Mass spectrum of metabolite M20, a hydroxylated and glucuronidated metabolite of H4CBD (from a urine sample 3 h after ingestion of 25-mg H4CBD). The position of the hydroxy group and the glucuronide is unknown. **Figure S25:** Mass spectrum of metabolite M21, a hydroxylated and glucuronidated metabolite of H4CBD (from a urine sample 3 h after ingestion of 25-mg H4CBD). The position of the hydroxy group and the glucuronide is unknown. **Figure S26:** Mass spectrum of metabolite M22, a hydroxylated and glucuronidated metabolite of H4CBD (from a urine sample 3 h after ingestion of 25-mg H4CBD). The position of the hydroxy group and the glucuronide is unknown. **Figure S27:** Mass spectrum of metabolite M23, a bishydroxylated and glucuronidated metabolite of H4CBD (from a urine sample 3 h after ingestion of 25-mg H4CBD). Both hydroxylation positions are found on the alicyclic moiety, and their position and the position of the glucuronide are not clear. **Figure S28:** Mass spectrum of metabolite M24, a bishydroxylated and glucuronidated metabolite of H4CBD (from a urine sample 3 h after ingestion of 25-mg H4CBD). One hydroxylation position is found on the alicyclic moiety, the other hydroxylation position is on the side-chain, and their position and the position of the glucuronide are not clear. **Figure S29:** Mass spectrum of metabolite M25, a bishydroxylated and glucuronidated metabolite of H4CBD (from a urine sample 3 h after ingestion of 25-mg H4CBD). Both hydroxylation positions are found on the alicyclic moiety, and their position and the position of the glucuronide are not clear. The ion *m/z* 197.1173 could result from a coeluting metabolite with a hydroxylation position on the side-chain. **Figure S30:** EI mass spectrum of the metabolite M26 (*R*)-H4CBD TMS. **Figure S31:** EI mass spectrum of the metabolite M27 (*S*)-H4CBD TMS, the same ions are formed as for (*R*)-H4CBD TMS. **Figure S32:** EI mass spectrum of the carboxylated metabolite M28 7-COOH-H4CBD TMS. **Figure S33:** EI mass spectrum of the carboxylated metabolite M29 5″-COOH-H4CBD TMS. **Figure S34:** EI mass spectrum of the hydroxylated metabolite M30, hydroxylated on the alicyclic moiety. **Figure S35:** EI mass spectrum of the hydroxylated metabolite M31, hydroxylated on the side-chain. Hydroxylation position unknown. **Figure S36:** EI mass spectrum of the hydroxylated metabolite M32, hydroxylated on the alicyclic moiety. **Figure S37:** EI mass spectrum of the hydroxylated metabolite M33, hydroxylated on the alicyclic moiety. Presumably 7-OH-(*R*)-H4CBD. **Figure S38:** EI mass spectrum of the hydroxylated metabolite M34, hydroxylated on the alicyclic moiety. Presumably 7-OH-(*S*)-H4CBD. **Figure S39:** EI mass spectrum of the hydroxylated metabolite M35, hydroxylated on the side-chain. Hydroxylation position unknown. **Figure S40:** EI mass spectrum of the bishydroxylated metabolite M36, hydroxylated on C7 of the alicyclic moiety and on the side-chain. Position of the side-chain hydroxylation is unknown. **Figure S41:** EI mass spectrum of the bishydroxylated metabolite M37, hydroxylated on C7 of the alicyclic moiety and on the side-chain. Position of the side-chain hydroxylation is unknown. **Figure S42:** Product ion spectrum of 7-COOH-CBD at a collision energy of +46 V. **Figure S43:** Product ion spectrum of 7-COOH-CBD at a collision energy of +73 V. **Figure S44:** Product ion spectrum of (*S*)-H4CBD (reference standard). **Figure S45:** Product ion spectrum of (*R*)-H4CBD (reference standard). **Figure S46:** Chromatogram of an *n*-alkane standard (C7–C40) used for the determination of Kováts indices.

2.6 Publication VI

Rapid LC-QTOF-MS screening method for semi-synthetic cannabinoids in whole blood

Schirmer W., Walton S. E., Schürch S., Weinmann W., Logan B. K., Krotulski A. J.
Journal of Analytical Toxicology, **2025** (Ahead of print)
DOI: 10.1093/jat/bkaf095

Description of own contribution

This work was initialized by Dr. Alex Krotulski, Dr. Barry Logan, Prof. Dr. Wolfgang Weinmann and myself. The chromatographic method was developed by Dr. Alex Krotulski and other people working at the Center of Forensic Research and Education (CFSRE). I have modified the method, performed the LC-QqTOF analysis and validated the method. Dr. Alex Krotulski and Sara Walton supervised me during my stay at CFSRE and helped me with the operation of the instruments. I have written the manuscript and Sara Walton, Prof. Dr. Stefan Schürch, Prof. Dr. Wolfgang Weinmann, Dr. Barry Logan and Dr. Alex Krotulski proof read it and helped to finalize the manuscript.

Description of novelty

This publication describes a screening method for semi-synthetic cannabinoids in whole blood and is currently one of two published methods for screening semi-synthetic cannabinoids in physiological samples. Due to the emergence of these compounds, a method that can safely identify these in biological samples is needed to verify if a suspect was under the influence of these drugs. Methods like the described one are especially important if people are suspected to be driving under the influence of semi-synthetic cannabinoids.

Reprint permission

Rapid LC-QTOF-MS screening method for semi-synthetic cannabinoids in whole blood

Willi Schirmer[1, 2], Sara E. Walton[3], Wolfgang Weinmann[1], Stefan Schürch[2], Barry K. Logan[3, 4], Alex J. Krotulski[3]

[1]Institute of Forensic Medicine, Forensic Toxicology and Chemistry, University of Bern, Murtenstrasse 26, 3008 Bern, Switzerland

[2]Department of Chemistry, Biochemistry and Pharmaceutical Sciences, University of Bern, Freiestrasse 3, 3012 Bern, Switzerland

[3]Center for Forensic Science Research and Education, Fredric Rieders Family Foundation, Horsham, PA, 19044, United States

[4]NMS Labs, Horsham, PA, 19044, United States

Corresponding author:
Willi Schirmer, Institute of Forensic Medicine, Forensic Toxicology and Chemistry, University of Bern, Murtenstrasse 26, 3008 Bern, Switzerland
e-mail address: willi.schirmer@irm.unibe.ch

ORCID:
1st author orcid: 0009-0004-5579-2217
2nd author orcid: -
3rd author orcid: 0000-0001-8659-1304
4th author orcid: 0000-0001-5109-4623
5th author orcid: 0000-0003-2400-4711
Last author orcid: 0000-0003-1775-1882

Abstract

Semi-synthetic cannabinoids are a class of new psychoactive substances (NPSs) with structural similarities to the main psychoactive phytocannabinoid Δ^9-tetrahydrocannabinol (Δ^9-THC) found in *Cannabis sativa* L. The first semi-synthetic cannabinoids, which were used as legal substitutes for marijuana were Δ^8-tetrahydrocannabinol (Δ^8-THC) and hexahydrocannabinol (HHC). Δ^8-THC emerged around 2019 on the recreational drug market in the United States after it became legal due to an ambiguity in the Agricultural Improvement Act 2018 (Farm Bill 2018). It was never legal outside the United States as the isomers of THC are regulated in the United Single Convention on Narcotic Drugs from 1971. HHC, a hydrogenated derivative of THC, followed as a legal substitute on the European recreational drug market. Many countries already placed HHC in their narcotic substance law, which lead to the emergence of other structurally related derivatives of THC. An existing rapid screening method for the qualitative analysis of various new psychoactive substances was expanded for semi-synthetic cannabinoids in whole blood using a LC-QTOF-MS system. This method was validated for 24 different phytocannabinoids and semi-synthetic cannabinoids in blood. Recovery rates of the analytes from a liquid-liquid-extraction ranged from 87-118%, matrix effects ranged from 24-93%, and limits of detection (LOD) ranged from 0.8-16 ng/mL.

Keywords: Semi-synthetic cannabinoids, LC-QTOF-MS, SSC, THC, HHC, screening

Introduction

The emergence of Δ^8-tetrahydrocannabinol (Δ^8-THC) and hexahydrocannabinol (HHC) on the recreational cannabinoid market has led to a new class of new psychoactive substances (NPSs) with cannabimimetic effects, commonly referred to as semi-synthetic cannabinoids [1]. Semi-synthetic cannabinoids are structurally related to Δ^9-tetrahydrocannabinol (Δ^9-THC), the main psychoactive substance in *Cannabis sativa* L. (marijuana). Currently, the most prevalent semi-synthetic cannabinoids worldwide are HHC and Δ^8-THC [1]. They both occur naturally in small amounts in the cannabis plant [2,3]. However, it is unclear if HHC is naturally formed or only as a degradation product from the disproportionation of Δ^9-THC to cannabinol (CBN) and HHC [4]. The first description of HHC was in 1940 after the hydrogenation of cannabis extracts [5]. Even though their natural occurrence in cannabis, the low content of Δ^8-THC and HHC in the cannabis plant makes it cost prohibited for extraction. Both can be synthesized from cannabidiol (CBD), which is legal in many countries, including the United States through the enactment of the 2018 "Farm Bill" [6], and are then sprayed on hemp, or used as an ingredient in vaping liquids or edibles [1]. Acidic catalyzed ring-closure of CBD yields Δ^9-THC and Δ^8-*iso*-THC, respectively. Further acid catalyzed isomerization converts the products to the thermodynamically more stable Δ^8-THC and $\Delta^{4(8)}$-*iso*-THC, respectively (see Figure 1). The product composition depends on the reaction conditions (e.g., choice of acid, solvent, temperature and time) [7]. After hydrogenation of the THC mixture, HHC is obtained as a mixture of two epimers: (9*R*)-HHC and (9*S*)-HHC [8,9]. While hydrogenation of Δ^9-THC delivers an excess of (9*S*)-HHC, the hydrogenation of Δ^8-THC yields an excess of (9*R*)-HHC [9]. The *iso*-THCs are undesired side-products commonly found in recreational products containing Δ^8-THC and have not been identified in *Cannabis sativa* L. [10-12]. Their hydrogenation delivers *iso*-HHC, which is a synthetic impurity in recreational HHC

products [13]. Like Δ^9-THC, Δ^8-THC is a partial agonist on the CB_1 cannabinoid receptor but it is commonly accepted to be less potent than Δ^9-THC [14]. Of the two HHC epimers, (9*R*)-HHC shows a greater cannabimimetic potency [9,15] and a greater binding affinity towards CB_1 [16-18]. The *iso*-THCs potentially lack any cannabimimetic properties, and their pharmacology has not been studied yet due to suggested lower significance and importance.

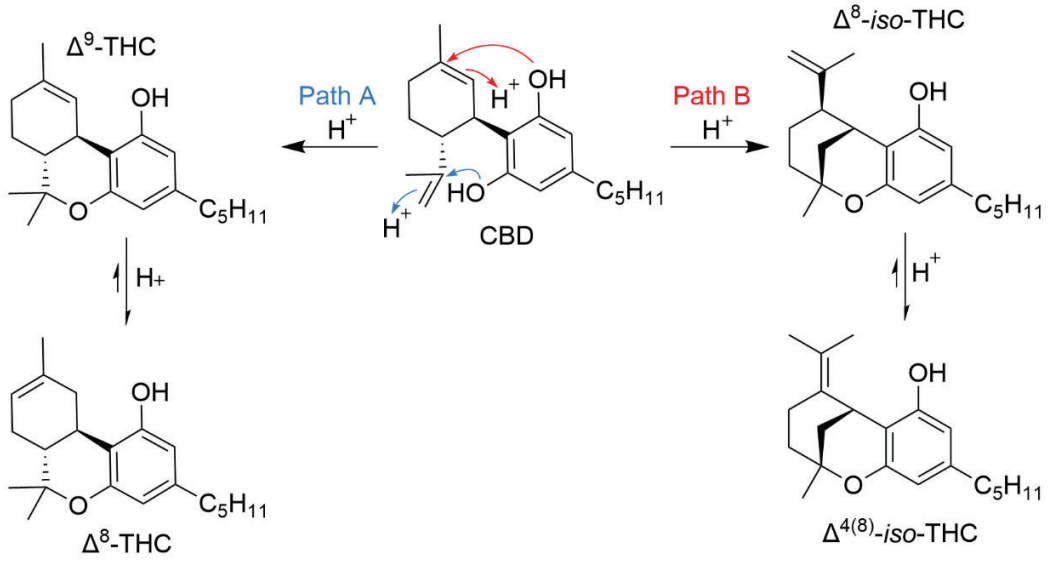

Figure 1: Acid catalyzed synthesis of Δ^9-THC and Δ^8-THC from CBD (Path A). Acid catalyzed synthesis of Δ^8-*iso*-THC and $\Delta^{4(8)}$-*iso*-THC from CBD (Path B).

Even though Δ^9-THC and all its double-bonded isomers are listed in Schedule I of the United Nations (UN) Convention on Psychotropic Substances of 1971 [19], Δ^8-THC is not legally regulated in the United States due to an ambiguity in the Agriculture Improvement Act of 2018 ("Farm Bill"). Hemp derived products are in a legal gray area in the United States as long as the product does not contain more than 0.3% Δ^9-THC by dry weight [20]. In 2021, HHC entered the recreational drug market and spread rapidly as a legal substitute for *Cannabis* [1]. The regulation of HHC in many European countries has led to other unregulated semi-synthetic cannabinoids being available on the recreational drug market [21,22]. Some semi-synthetic cannabinoids on the

recreational market, like 11-OH-Δ^9-THC and 8-OH-Δ^9-THC, are known active metabolites of Δ^9-THC [23-25]. Their synthesis is not as simple as for Δ^8-THC or HHC [26,27]. Other semi-synthetic cannabinoids like Δ^9-THCP or Δ^9-tetrahydrocannabihexol (Δ^9-THCH) have been previously discovered as natural trace compounds in *Cannabis sativa* L. A content of 29 µg/g was reported for Δ^9-THCP and 7 µg/g for Δ^9-THCH, respectively [28,29], indicating that they cannot be cost efficiently be extracted from the cannabis plant. Instead, these semi-synthetic cannabinoids that do not share the pentyl moiety of Δ^8-THC or HHC are synthesized from 5-alkylresorcinols or 5-alkylcyclohexane-1,3-diones [30-32]. Suppliers claim that these semi-synthetic cannabinoids are made from CBD; however, this seems unlikely because of the alteration of the cannabinoid pentyl substituent. A general structure for semi-synthetic cannabinoids is depicted in Figure 2. Semi-synthetic cannabinoids are derivatives of Δ^9-THC and share the dibenzopyran moiety with it. The differences to Δ^9-THC are the position or presence of the double bond. Acylation or alkylation of the phenolic hydroxy group, or homologation of the pentyl group are encountered as well. Other derivatives are hydroxylated at the positions C8, C10, or C11. Recently, three novel THC analogs were identified bearing an allyl or a propen-2-yl group at position C2. These derivatives are likely products after a Claisen rearrangement of THC allyl ethers [33]. The herein presented method expands an already existing screening method to include semi-synthetic cannabinoids [34]. Recently, a targeted method for the determination of THC isomers, analogs, homologs, and metabolites in blood and urine was published [35].

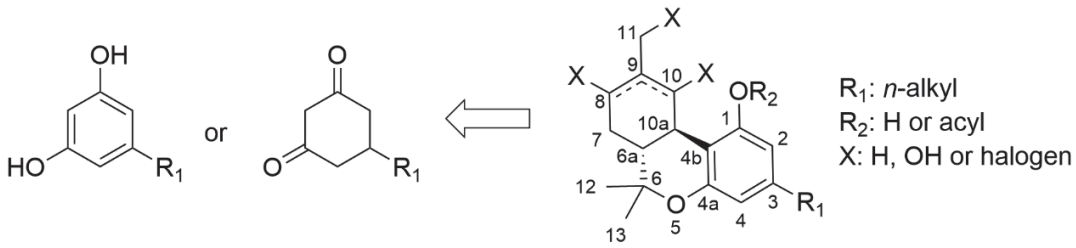

Figure 2: Retrosynthesis of semi-synthetic cannabinoids. Common precursors are depicted on the left (5-alkylresorcinols and 5-alkylcyclohexane-1,3-diones). A general structure for semi-synthetic cannabinoids is shown on the right side. The differences to Δ^9-THC are the position or presence of the double bond, acylation or alkylation of the phenolic hydroxy group or the chain length of R_1.

Adsorption of Δ^9-THC on different surfaces is a well-known phenomenon [36]. Compounds with a large octanol-water partition coefficient (log P_{ow}), like semi-synthetic cannabinoids, may adsorb to hydrophobic surfaces, such as polymers or siloxane groups of glass [37]. For THC analogues, it is known that their lipophilicity (log P_{ow}) increases by a factor of approximatively three for each methylene group added to the side chain [38]. This might lead to preanalytical challenges when such hydrophobic compounds are analyzed. Storage and workup of samples might lead to analyte loss due to non-specific binding of the highly hydrophobic substances on storage containers, test tubes or vials prior analysis. Adsorption of Δ^9-THC has been described on polystyrene, glass and polypropylene [36,39,40].

Materials and methods

Chemicals and reagents

Δ^9-Tetrahydrocannabiorcol (Δ^9-THCO), Δ^9-THC-ethyl (Δ^9-THCE), Δ^9-THC-butyl (Δ^9-THCB), Δ^9-tetrahydrocannabinol (Δ^9-THC), Δ^9-tetrahydrocannabihexol (Δ^9-THCH), Δ^9-tetrahydrocannabiphorol (Δ^9-THCP), Δ^9-THC-octyl (Δ^9-THC-C8), Δ^9-tetrahydrocannabinol methyl ether (Δ^9-THC-OMe), Δ^9-tetrahydrocannabinol acetate (Δ^9-THC-O), cannabinol (CBN), cannabidiol (CBD), cannabigerol (CBG), (9*R*)-hexahydrocannabinol ((9*R*)-HHC), (9*S*)-hexahydrocannabinol ((9*S*)-HHC), (9*R*)-hexahydrocannabihexol ((9*R*)-HHCH), (9*R*)-hexahydrocannabiphorol ((9*R*)-HHCP), (9*R*)-hexahydrocannabinol acetate ((9*R*)-HHC-O), Δ^8-tetrahydrocannabinol (Δ^8-THC), (±)-9α-hydroxy hexahydrocannabinol (9α-OH-HHC), (±)-9β-hydroxy hexahydrocannabinol (9β-OH-HHC), (−)-11-hydroxy-Δ^8-tetrahydrocannabinol (11-OH-Δ^8-THC), (±)-hydroxy-Δ^9-tetrahydrocannabinol (11-OH-Δ^9-THC), (±)-11-nor-9-carboxy-Δ^9-tetrahydrocannabinol (11-COOH-Δ^9-THC) and 11-nor-(9*R*)-carboxy-hexahydrocannabinol (11-COOH-(9*R*)-HHC) at concentrations of 1.0 mg/mL were purchased from Cayman Chemical (Ann Arbor, MI, United States). Cannabidiol-D_3 (CBD-D_3) and Δ^9-tetrahydrocannabinol-D_3 (THC-D_3) at concentrations of 100 µg/mL were purchased from Cerilliant (Round Rock, TX, United States). Bond Elut C18 Solid Phase Extraction cartridges (500 mg, 3 mL) were purchased from Agilent (Santa Clara, CA, United States). Hexanes (95% *n*-hexane), ethyl acetate (EtOAc), *tert*-butyl methyl ether (TBME), and LC-MS grade solvents (e.g., methanol (MeOH), acetonitrile (MeCN), and water) were purchased from Honeywell Chemicals (Charlotte, NC, United States), formic acid ampules (1 mL) were purchased from Thermo Fisher Scientific (Waltham, MA, United States), ammonium formate was purchased from Millipore Sigma (St. Louis, MO, United States), phosphoric acid was purchased from VWR (Radnor, PA, United States). A solution of MeOH in

water (90%, V%) with formic acid (0.1%, V%) was used to reconstitute samples prior to analysis. The internal standard (ISTD) solution consisted of CBD-D_3 and THC-D_3 (γ = 500 ng/mL) in reconstitution solution. A solution of *n*-hexane, TBME and EtOAc (8/1/1; V/V/V) was used for the liquid extraction from blood. Drug-free human blood preserved with sodium fluoride and potassium oxalate was purchased from BioIVT (Westbury, NY, United States). Drug-free status was determined through comprehensive toxicology screening onsite after basic and acidic liquid-liquid-extraction described previously [34,41].

Library semi-synthetic cannabinoids

Reference mass spectra from the cannabinoid standards were implemented in the library by measuring diluted cannabinoid standards (40 ng injected from each analyte). Standard solutions (2 µL, γ = 1 mg/mL) were diluted with 1.0 mL mobile phase B (γ = 2 µg/mL). From these solutions, 20 µL were injected on a Sciex Exion liquid chromatograph coupled to a Sciex X500R quadrupole time-of-flight mass spectrometer (LC-QTOF-MS) using SWATH-acquisition.

Reference mixtures 1 and 2

For the determination of limits of detection (LOD), recovery rates and matrix effects, two different mixtures were prepared. Reference mixture 1 was prepared by mixing 2 µL of 13 different standards (γ = 1 mg/mL) and diluting the mixture with 974 µL of mobile phase B (γ = 2 µg/mL). The standards were Δ^9-THCO, 9α-OH-HHC, 11-OH-Δ^9-THC, Δ^9-THCE, 11-COOH-Δ^9-THC, Δ^8-THC, CBG, Δ^9-THCB, CBN, Δ^9-THCH, Δ^9-THCP, (9*S*)-HHC and Δ^9-THC-C8.

Reference mixture 2 was prepared by mixing 2 µL of 11 different standards (γ = 1 mg/mL) and diluting the mixture with 978 µL of mobile phase B (γ = 2 µg/mL). The standards were 11-OH-Δ^8-

164 THC, 11-COOH-(9*R*)-HHC, 9β-OH-HHC, CBD, Δ^9-THC, (9*R*)-HHCH, Δ^9-THC-O, (9*R*)-HHCP,
165 (9*R*)-HHC, (9*R*)-HHC-O and Δ^9-THC-OMe.

166 Blood samples were fortified with the Reference mixtures 1 and 2 prior extraction for the
167 determination of the recovery rates and LOD, and after the extraction for the determination for the
168 matrix effects.

169 **LC-QTOF-MS method**

170 A previously published method with adjustments to the electrospray voltage was used for the
171 measurements [34]. Five-hundred µL of blood was mixed with 8 µL ISTD working solution in a
172 test tube. To this solution, 1 mL H_3PO_4 (5%, m%) and 3 mL extraction mixture were added. The
173 mixture was rotated for 15 min and then centrifuged for 5 min (3398 *g*). To facilitate the phase
174 separation, the test tubes were put in the freezer for 15 min at -80 °C. The organic phase was
175 decanted into a clean test tube and evaporated to dryness. The residue was dissolved in 200 µL
176 reconstitution solution. Instrumental analysis was performed as described above using an Exion
177 LC coupled to a X500R mass spectrometer (Sciex, Framingham, MA, United States) equipped
178 with an ESI twinspray electrode assembly. The mass spectra were measured in positive ionization
179 mode utilizing SWATH acquisition. The mobile phase A was an aqueous ammonium formate
180 solution (10 mM, pH 3) containing formic acid, and mobile phase B was a solution of MeOH and
181 MeCN (1/1, V/V) containing formic acid (0.1 %, V%). The injection volume was 20 µL.
182 Chromatography was performed at 30 °C on a Kinetex C18 column, 50 × 3 mm, 2.6 µm, 100 Å
183 (Phenomenex, Torrance, CA, United States). A gradient method was used for chromatographic
184 separation with the following conditions: 0-1 min: 5% B, 1-10 min: 5-95% B, 10-13 min: 95% B,
185 13-13.1 min: 95-5% B, 13.1-15.5 min: 5%. The curtain gas was set to 45 psi, ion source gas 1 to
186 40 psi, ion source gas 2 to 75 psi, the electrospray voltage was set to 4000 V and the source

temperature was 600 °C. Precursor ions from 100 – 510 Da were selected. Fragmentation was induced by using a collision energy spread of 35 ± 15 V [42]. The fragment scan range was 40 – 510 Da. The declustering potential was 80 V. Data were acquired on SciexOS (version 3.3.143) and processed with Peak View (version 2.2.0.11391) and MasterView (version 1.1.1944.0).

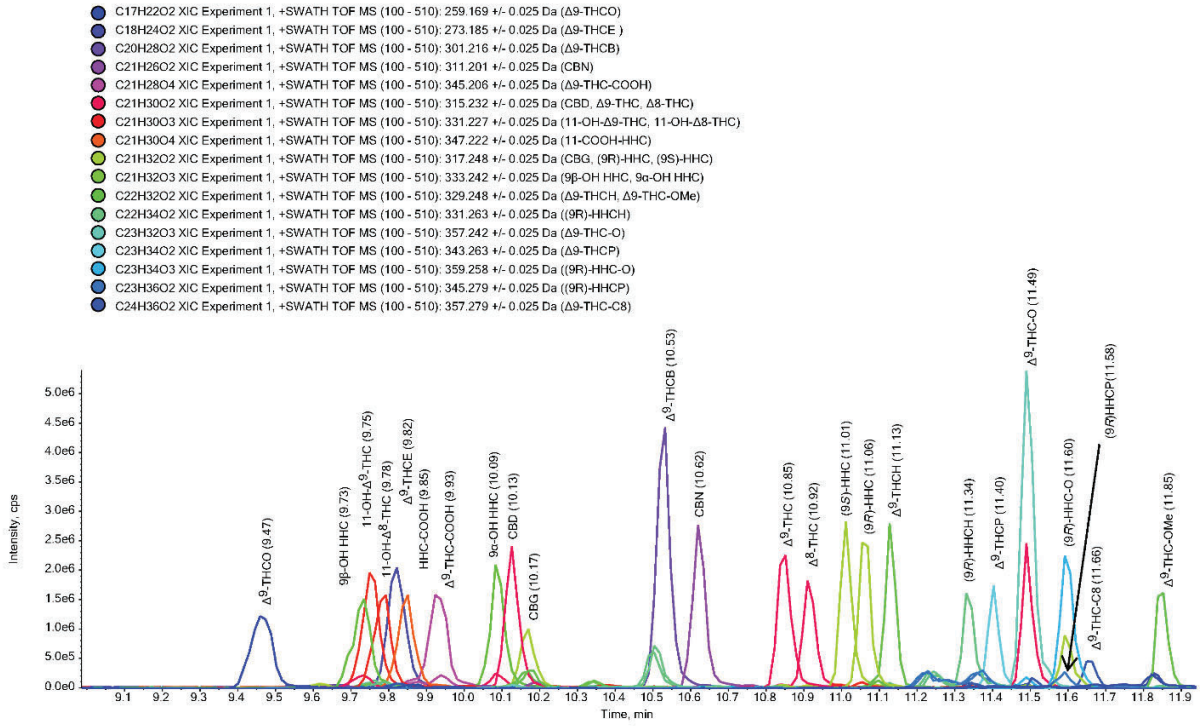

Figure 3: Overlay of two blank blood samples fortified to a concentration of γ = 500 ng/mL with reference mixture 1 and 2, respectively.

Method validation

A laboratory validation plan was developed and evaluated according to a previous screening validation performed by Krotulski et al. [34]. Validation experiments included recovery, matrix effects, limit of detection, carryover and inter- and intra-day reproducibility (mass-accuracy,

retention times and analyte area ratio to CBD-D_3). The validation was evaluated for suitability for the method's intended use: qualitative broad-based semi-synthetic cannabinoid identification.

For the inter-day reproducibility, the blood samples were fortified on each day with the reference mixtures 1 and 2, respectively. A five-fold determination was performed on three different days. Intra-day reproducibility was calculated by comparing the retention times, mass accuracy, and area ratios of the analyte to CBD-D_3 over a five-fold determination.

Recovery and Matrix effects

Analyte recovery rates and matrix effects were evaluated for a liquid-liquid extraction (LLE) and a solid-phase extraction (SPE) protocol. The method was validated using the LLE protocol described below, however; both extraction protocols were evaluated for optimal recovery and matrix effects. Recovery rates and matrix effects rates were determined in triplicate.

Liquid-liquid extraction

In a test tube 0.5 mL blood, 1 mL H_3PO_4 (5%, m%), and 8 µL of the ISTD solution (γ = 20 ng/mL) were added. For the determination of the recovery rates, 2.5 µL reference mixture 1 or mixture 2 (γ = 25 ng/mL) were added, additionally. The solution was mixed, and 3 mL of the extraction solvent mixture was added. The test tubes were rotated for 15 min and centrifuged for 5 min (3398 *g*). Afterwards, the test tubes were put in the freezer at -80 °C for 15 min, the organic phase was transferred to a new test tube and the solvent was evaporated in a TurboVap at 40 °C for 30 min. The residue was dissolved in 200 µL reconstitution solution, transferred to a vial and analyzed on the X500R QTOF-MS.

For the determination of the matrix effects 0.5 mL blood, 1 mL H_3PO_4 (5%, m%) and 8 µL of the ISTD solution (γ = 20 ng/mL) were added into a test tube. The mixture was extracted and

separated as mentioned for the determination of the recovery rates. After separation of the organic phase, 2.5 µL reference mixture 1 or mixture 2 (γ = 25 ng/mL) was added and the solvent was evaporated. The residue was dissolved in 200 µL reconstitution solution, transferred to a vial and analyzed on the X500R QTOF-MS.

Solid phase extraction

A validated method for the extraction of Δ^9-THC and its metabolites from serum was used with the slight modification that the cartridges were additionally eluted with EtOAc [43]. C18 Bond Elut cartridges were conditioned with 2 mL MeOH and 2 mL AcOH (0.1 M). Five-hundred µL blood was mixed with 8 µL ISTD (γ = 20 ng/mL). For the determination of the recovery rates, 2.5 µL reference mixture 1 or mixture 2 (γ = 25 ng/mL) were added. The samples were briefly vortexed and loaded on the cartridges. After loading, the cartridges were washed with 1 mL AcOH (0.1 M) and 1 mL MeCN (40 %, V%). The samples were eluted using 1.5 mL MeCN and then with 1.5 mL EtOAc. The solutions were evaporated to dryness, dissolved in 200 µL reconstitution solution, transferred to a PP vial and analyzed on the X500R QTOF-MS.

The determination of the matrix effects were determined similar with the difference that the 2.5 µL reference mixture 1 or mixture 2 (γ = 25 ng/mL) were added to the organic phase after the extraction step. The eluted solutions were evaporated to dryness and dissolved in 200 µL reconstitution solution, transferred to a PP vial and analyzed on the X500R QTOF-MS.

Limit of detection

Limits of detection (LOD) were determined from fortified blood samples at different concentrations (γ = 0.8 ng/mL, 2 ng/mL, 4 ng/mL, 8 ng/mL and 16 ng/mL) after LLE. The given LOD show a signal-to-noise ratio greater than 3 (S/N > 3). The noise near the analyte signal was used for the determination of the S/N. The LOD were determined from one measurement per level.

Inter-day and intra-day reproducibility

For investigation of the reproducibility inter-day and intra-day measurements were performed, and mass accuracy, relative standard deviation of retention time (RSD(R_t)) and signal area (RSD(A)) were calculated. For inter-day and intra-day reproducibility blank blood was fortified to a concentration of γ = 10 ng/mL with reference mixture 1 and 2, respectively. For the inter-day reproducibility a five-fold determination on three different days were prepared. The intra-day reproducibility was determined from a five-fold determination.

Carryover

For the investigation of carryover effects, blank solutions were injected after reference solutions (γ = 2000 ng/mL).

Results

Validation

Validation of the LC-QTOF-MS screening method was performed successfully. The method was validated for the liquid-liquid-extraction protocol using polypropylene (PP) vials. The recovery rates ranged from 87-118% and the matrix effects ranged from 24-93% (see Table 1 and

Supplementary Material S2). LOD ranged from 0.8 ng/mL to 16 ng/mL, they are summarized in Table 1. For the inter-day reproducibility the mass errors of the analytes ranged from -2.1 to 1.3 ppm. The relative standard deviations of the retention times were RSD(R_t) ≤ 0.32%, and the relative standard deviations of the peak area were RSD(A) ≤ 48.2%. The values are summarized in Table 1. For the intra-day reproducibility, the mass errors of the analytes ranged from -3.7 to 0.2 ppm. The relative standard deviations of the retention times were RSD(R_t) ≤ 0.11%, and the relative standard deviations of the peak area were RSD(A) ≤ 22.5%. The values are summarized in Table 1. No carryover was observed.

The recovery rates from the liquid-liquid-extraction using non-silanized glass vials ranged from 0-113% (see Supplementary Material S1 and S3). The matrix effects ranged from 11-76% (see Supplementary Material S1). For the SPE protocol the recovery rates ranged from 28-90% (see Supplementary Material S1 and S4), and the matrix effects ranged from 33-171% (see Supplementary Material S1).

Table 1: Validation parameters for the analytes. LOD: Limit of detection, RSD: relative standard deviation, M.E.: Matrix effect, R_t: retention time. Recoveries and matrix effects are from the LLE protocol measured in PP vials.

Analyte	Mass $[M+H^+]^+$	LOD / ng*mL^{-1}	Recovery / %	M.E. / %	R_t / min	Interday reproducibility			Intraday reproducibility		
						Area RSD / %	Mass accuracy RSD / ppm	R_t RSD / %	Area RSD / %	Mass accuracy RSD / ppm	R_t RSD / %
Δ^9-THCO	259.1693	2	108 ± 6.9	70	9.47	29.2	0.2	0.30	12.9	-0.1	0.09
9β-OH-HHC	333.2424	4	97 ± 5.7	43	9.73	17.9	-0.1	0.31	5.9	-0.2	0.07
11-OH-Δ^9-THC	331.2268	2	104 ± 9.9	32	9.75	33.1	-0.5	0.29	13.2	-1.4	0.08
11-OH-Δ^8-THC	331.2268	4	95 ± 5.2	46	9.78	15.3	0.1	0.32	9.0	-0.5	0.09
Δ^9-THCE	273.1849	0.8	100 ± 8.1	30	9.82	18.5	-0.4	0.30	5.3	-0.5	0.05
11-COOH-(9*R*)-HHC	347.2217	8	88 ± 12.4	63	9.85	11.8	-0.9	0.31	5.1	-1.0	0.11
11-COOH-Δ^9-THC	345.2060	0.8	100 ± 6.2	59	9.93	14.9	-2.0	0.28	6.4	-3.1	0.05
9α-OH-HHC	333.2424	2	101 ± 6.4	41	10.09	26.7	-0.9	0.28	4.8	-1.9	0.10
CBD	315.2319	2	101 ± 4.8	66	10.13	13.6	0.1	0.27	10.8	-0.6	0.11
CBG	317.2475	2	99 ± 9.6	61	10.17	20.2	-0.2	0.23	6.3	-0.6	0.05
Δ^9-THCB	301.2162	2	102 ± 8.2	62	10.53	20.3	-2.1	0.27	5.0	-3.0	0.08
CBN	311.2006	2	106 ± 8.2	50	10.62	19.8	-1.9	0.27	9.5	-2.6	0.05
Δ^9-THC	315.2319	2	100 ± 5.2	24	10.85	19.6	-0.8	0.26	10.8	-1.6	0.07
Δ^8-THC	315.2319	2	111 ± 8.1	24	10.92	20.9	-1.0	0.26	6.7	-1.9	0.09
(9*S*)-HHC	317.2475	2	101 ± 10.2	67	11.01	32.9	-1.5	0.25	10.4	-2.1	0.09
(9*R*)-HHC	317.2475	2	102 ± 5.6	44	11.06	25.9	-0.8	0.26	10.5	-1.7	0.08
Δ^9-THCH	329.2475	8	106 ± 4.6	93	11.13	18.8	-0.1	0.25	6.1	-0.7	0.05
(9*R*)-HHCH	331.2632	4	118 ± 4.4	24	11.34	21.3	1.3	0.16	22.5	0.5	0.06
Δ^9-THCP	343.2632	4	97 ± 5.4	53	11.40	17.0	-0.8	0.24	11.0	-1.8	0.10
Δ^9-THC-O	357.2424	2	92 ± 10.7	80	11.49	48.2	-2.4	0.25	19.6	-3.7	0.06
(9*R*)-HHCP	345.2788	16	87 ± 10.0	25	11.58	16.7	0.5	0.25	11.0	-0.1	0.07
(9*R*)-HHC-O	359.2581	2	94 ± 11.6	42	11.60	16.9	-0.1	0.22	18.4	-0.6	0.08
Δ^9-THC-C8	357.2788	8	90 ± 7.0	35	11.66	22.8	0.0	0.24	2.6	-0.6	0.06
Δ^9-THC-OMe	329.2475	4	91 ± 3.0	71	11.85	25.5	0.5	0.24	17.6	0.2	0.04

Application to authentic samples

The validated LC-QTOF-MS method described above was applied to authentic driving under the influence of drugs (DUID) samples where the consumption of cannabinoids other than or in addition to Δ^9-THC was suspected. Twenty-three deidentified human blood specimens collected between December 2023 and February 2024 were provided by NMS Labs (Horsham, PA, United States) and were subjected to the optimized workflow described in this manuscript. The semi-synthetic cannabinoid HHC and its metabolite HHC-COOH were identified in one blood specimen (1 of 23). THC and THC-COOH were identified in eighteen samples (18 of 23). Four samples (4 of 23) did not contain any cannabinoids described in the method above the listed LOD (Table 1).

For the confirmation of the results of the qualitative QTOF screening method on THC isomers, the described samples were re-analyzed using an in-house research method (LC-QqQ). This method enables the chromatographic separation of the THC isomers: Δ^8-THC and Δ^9-THC were both qualitatively identified in the majority of the samples (18 of 23), three were tested positive for only Δ^9-THC (3 of 23), one sample was only positive for Δ^8-THC (1 of 23) and one sample did not contain any THC isomers (1 of 23).

Discussion

Adsorption

During the recovery experiments, it was found that the larger semi-synthetic cannabinoids (by mass) showed a low recovery rate. (9*R*)-HHCH, Δ^9-THCP, Δ^9-THCP-O, Δ^9-THC-C8 and Δ^9-THC-OMe were initially not detected after extraction. It was found that this problem occurred when analysis was performed from non-silanized glass vials with inserts. Vials made from polypropylene did not show this behavior and were therefore used for validation and further

analyses, even though adsorption of phytocannabinoids has been described on glass and on polypropylene [39,40]. It is assumed that the adsorption of the more hydrophobic analytes emerged from the interactions with the hydrophobic siloxane groups on the glass surface. These groups would not be affected through silanization, only the hydrophilic silanol groups would be desactivated.

The analyte recovery rates from the tested solid-phase extraction protocol dropped noticeably with the lipophilicity of the analytes. It is assumed that the more lipophilic analytes experienced such a strong retention that elution did not occur completely, even additional elution with EtOAc showed no improved recovery rates. The solid-phase extraction protocol, which was tested for this method was from a validated method for the determination of Δ^9-THC and its metabolites from serum [43]. For the extraction of semi-synthetic cannabinoids from blood another SPE protocol should be developed.

Limitations

Missing forensic markers and sensitivity

For most analytes described in this method, no established forensic markers (e.g., metabolites) are known due to scarce research on the metabolism of semi-synthetic cannabinoids. It is unclear to what extent the analytes are metabolized and if the consumption of such substances leads to a detectable concentration of the unmetabolized consumed drug in blood, particularly if the consumption was days prior. Work on HHCP has shown that semi-synthetic cannabinoids with a longer side-chain might metabolize excessive to mono- and bishydroxylated phase-I metabolites [44,45]. Semi-synthetic cannabinoids with a longer side-chain are more potent than Δ^9-THC, lower LODs should therefore be achieved for these compounds [17,18]. This might however not be possible due to their poor ionizability. Currently unknown phase-I or phase-II

metabolites are better targets and should be included after their respective discovery and availability as reference standard.

Resolution of THC isomers

Initially, the panel included more THC isomers, which could be synthesized from CBD, namely Δ^8-THC, Δ^9-THC, Δ^8-*iso*-THC, Δ^8-THC, (9*S*)-$\Delta^{6a,10a}$-THC, (9*S*)-Δ^7-THC, exo-THC and (6a*R*,9*R*)-Δ^{10}-THC. Only Δ^8- and Δ^9-THC were then included due to poor separation of the THC isomers using the method described. From the possible isomers with natural configuration, only Δ^8-THC has a significant prevalence besides the main cannabinoid Δ^9-THC. The isomers (6a*R*, 9*S*)-Δ^{10}-THC, (9*R*, 10a*R*)-Δ^{6a}-THC, (9*S*, 10a*R*)-Δ^{6a}-THC, (9*R*)-Δ^7-THC and the enantiomer of the initially included cannabinoid (9*R*)-$\Delta^{6a,10a}$-THC were not measured. These THC isomers could also be prepared from CBD. To the authors' knowledge no method exists which separates all THC isomers in a single chromatographic method, which is somewhat inhibited by the introduction of new isomers to the recreational market yearly. Our LC-QTOF-MS qualitative screening method did not fully resolve Δ^9-THC from Δ^8-THC and 11-OH-Δ^9-THC from 11-OH-Δ^8-THC. The HHC epimers (9*S*)-HHC and (9*R*)-HHC are coeluting within this screening method (see Supplementary Material S5-S8).

Interferences from regio- and stereo-chemical synthetic impurities

Previous work on HHCP and THCP has shown that these substances possess isomeric impurities such as abnormal cannabinoids or *cis*-cannabinoids [31,32]. These unnatural regio- and stereo-isomers show similar chromatographic properties and very similar fragmentation patterns which might interfere with the detection of the semi-synthetic cannabinoids. These impurities were not included in this screening method and might interfere with the detection of semi-synthetic cannabinoids in authentic specimens.

Conclusion

Due to the emergence of semi-synthetic cannabinoids on the recreational market and their potent cannabimimetic effects, existing screening methods should be updated to include these novel substances in their screening panel. There is limited information in the literature about comprehensive screening for semi-synthetic cannabinoids and our LC-QTOF-MS demonstrates the feasibility for application to authentic forensic biological specimens. The lipophilicity of these cannabinoid substances might lead to adsorption on material used for sample preparation or storage and should be taken into account if an analytical method should cover these analytes.

Data availability statement

The data underlying this article will be shared on reasonable request to the corresponding author.

Acknowledgments & Funding

The University of Bern is acknowledged for funding the research stay of W.S. at the CFSRE through their funding program "UniBE Short Travel Grants for (Post)Docs". The Center for Forensic Research and Education (CFSRE) is funded by the National Institute of Justice, Office of Justice Programs, U.S. Department of Justice (Award Number 15PNIJ-22-GG-04434-MUMU, “Implementation of NPS Discovery – An Early Warning System for Novel Drug Intelligence, Surveillance, Monitoring, Response, and Forecasting using Drug Materials and Toxicology Populations in the United States”). The authors would like to acknowledge the staff and scientists at the CFSRE for their assistance. Ayako Chan-Hosokawa from NMS Labs is acknowledged for providing insights and the DUID samples.

References

1. Ujváry I. Hexahydrocannabinol and closely related semi-synthetic cannabinoids: A comprehensive review. *Drug Testing and Analysis*. 2023;16(2):127-161. doi:https://doi.org/10.1002/dta.3519
2. Hively RL, Mosher WA, Hoffmann FW. Isolation of *trans*-Δ^6-Tetrahydrocannabinol from Marijuana. *Journal of the American Chemical Society*. 1966/04/01 1966;88(8):1832-1833. doi:https://doi.org/10.1021/ja00960a056
3. Basas-Jaumandreu J, de las Heras FXC. GC-MS Metabolite Profile and Identification of Unusual Homologous Cannabinoids in High Potency Cannabis sativa. *Planta Med*. 2020/03/23 2020;86(05):338-347. doi:https://doi.org/10.1055/a-1110-1045
4. Garrett ER, Gouyette AJ, Roseboom H. Stability of Tetrahydrocannabinols II. *Journal of Pharmaceutical Sciences*. 1978/01/01/ 1978;67(1):27-32. doi:https://doi.org/10.1002/jps.2600670108
5. Adams R, Pease DC, Cain CK, Clark JH. Structure of Cannabidiol. VI. Isomerization of Cannabidiol to Tetrahydrocannabinol, a Physiologically Active Product. Conversion of Cannabidiol to Cannabinol. *Journal of the American Chemical Society*. 1940/09/01 1940;62(9):2402-2405. doi:https://doi.org/10.1021/ja01866a040
6. United States Department of Agriculture (USDA), Agricultural Marketing Service, https://www.ams.usda.gov/rules-regulations/hemp/enforcement
7. Marzullo P, Foschi F, Coppini DA, et al. Cannabidiol as the Substrate in Acid-Catalyzed Intramolecular Cyclization. *Journal of Natural Products*. 2020/10/23 2020;83(10):2894-2901. doi:https://doi.org/10.1021/acs.jnatprod.0c00436
8. Collins A, Ramirez G, Tesfatsion T, Ray KP, Caudill S, Cruces W. Synthesis and Characterization of the Diastereomers of HHC and H4CBD. *Natural Product Communications*. 2023/03/01 2023;18(3):1934578X231158910. doi:10.1177/1934578X231158910
9. Russo F, Vandelli MA, Biagini G, et al. Synthesis and pharmacological activity of the epimers of hexahydrocannabinol (HHC). *Scientific Reports*. 2023/07/08 2023;13(1):11061. doi:https://doi.org/10.1038/s41598-023-38188-5
10. Radwan MM, Wanas AS, Gul W, Ibrahim EA, ElSohly MA. Isolation and Characterization of Impurities in Commercially Marketed Δ^8-THC Products. *Journal of Natural Products*. 2023/04/28 2023;86(4):822-829. doi:https://doi.org/10.1021/acs.jnatprod.2c01008
11. Gul W, Shahzadi I, Sarma N, Kim N-C, ElSohly MA. Development and Validation of a GC-FID Method for the Quantitation of Δ^8-Tetrahydrocannabinol and Impurities Found in Synthetic Δ^8-Tetrahydrocannabinol and Vaping Products. *Planta Med*. 2024/02/22 2024;90(04):316-332. doi:https://doi.org/10.1055/a-2249-7824
12. Geci M, Scialdone MA-O, Tishler J. The Dark Side of Cannabidiol: The Unanticipated Social and Clinical Implications of Synthetic Δ^8-THC. *Cannabis and Cannabinoid Research*. 2023;8(2):270-282. doi:http://doi.org/10.1089/can.2022.0126
13. Tanaka R, Kikura-Hanajiri R. Identification of hexahydrocannabinol (HHC), dihydro-*iso*-tetrahydrocannabinol (dihydro-*iso*-THC) and hexahydrocannabiphorol (HHCP) in electronic cigarette cartridge products. *Forensic Toxicology*. 2023/06/26 2023;doi:https://doi.org/10.1007/s11419-023-00667-9
14. Hollister LE, Gillespie HK. Delta-8- and delta-9-tetrahydrocannabinol; Comparison in man by oral and intravenous administration. *Clinical Pharmacology & Therapeutics*. 1973/05/01 1973;14(3):353-357. doi:https://doi.org/10.1002/cpt1973143353

15. Reggio PH, Greer KV, Cox SM. The importance of the orientation of the C9 substituent to cannabinoid activity. *Journal of Medicinal Chemistry*. 1989/07/01 1989;32(7):1630-1635. doi:https://doi.org/10.1021/jm00127a038
16. Nasrallah DJ, Garg NK. Studies Pertaining to the Emerging Cannabinoid Hexahydrocannabinol (HHC). *ACS Chemical Biology*. 2023/09/15 2023;18(9):2023-2029. doi:10.1021/acschembio.3c00254
17. Janssens LK, Van Uytfanghe K, Williams JB, Hering KW, Iula DM, Stove CP. Investigation of the intrinsic cannabinoid activity of hemp-derived and semisynthetic cannabinoids with β-arrestin2 recruitment assays—and how this matters for the harm potential of seized drugs. *Archives of Toxicology*. 2024/05/12 2024;doi:https://doi.org/10.1007/s00204-024-03769-4
18. Persson M, Kronstrand R, Evans-Brown M, Green H. In vitro activation of the CB1 receptor by the semi-synthetic cannabinoids hexahydrocannabinol (HHC), hexahydrocannabinol acetate (HHC-O) and hexahydrocannabiphorol (HHC-P). *Drug Testing and Analysis*. 2024/06/19 2024;n/a(n/a)doi:https://doi.org/10.1002/dta.3750
19. United Nations Convention on Psychotropic Substances 1971, https://www.unodc.org/pdf/convention_1971_en.pdf
20. Congress. Agriculture Improvement Act of 2018, Government. U.S. Government Publishing Office, November 17, 2023. https://www.govinfo.gov/app/details/COMPS-15214/
21. European Union Drugs Agency EUDA, EU Drug Market: New psychoactive substances - Distribution and supply in Europe: Semi-synthetic cannabinoids, June 2024
22. United Nations Office on Drugs and Crime UNODC, SMART Forensics Update, Beyond plants: semi-synthetic diversify the cannabis market, Vol. 01, May 2024
23. Gasse A, Pfeiffer H, Köhler H, Schürenkamp J. 8β-OH-THC and 8β,11-diOH-THC—minor metabolites with major informative value? *International Journal of Legal Medicine*. 2018/01/01 2018;132(1):157-164. doi:10.1007/s00414-017-1692-5
24. Radwan MM, ElSohly MA, El-Alfy AT, et al. Isolation and Pharmacological Evaluation of Minor Cannabinoids from High-Potency Cannabis sativa. *Journal of Natural Products*. 2015/06/26 2015;78(6):1271-1276. doi:10.1021/acs.jnatprod.5b00065
25. Huestis MA. Pharmacokinetics and Metabolism of the Plant Cannabinoids, Δ9-Tetrahydrocannibinol, Cannabidiol and Cannabinol. In: Pertwee RG, ed. *Cannabinoids*. Springer Berlin Heidelberg; 2005:657-690.
26. Pitt CG, Fowler MS, Sathe S, Srivastava SC, Williams DL. Synthesis of Metabolites of Δ^9-Tetrahydrocannabinol. *Journal of the American Chemical Society*. 1975/06/01 1975;97(13):3798-3802. doi:10.1021/ja00846a040
27. Pasquale Linciano, Cinzia Citti, Fabiana Russo, Livio Luongo, Monica Iannotta, Carmela Belardo, Sabatino Maione, Maria Angela Vandelli, Flavio Forni, Giuseppe Gigli, Aldo Laganá, Anna Laura Capriotti, Carmela Maria Montone, Giuseppe Cannazza. Cannabis extracts and uses thereof. US Patent US2022064090A1, filed 9 July 2021, and issued 3 March 2022.
28. Citti C, Linciano P, Russo F, et al. A novel phytocannabinoid isolated from *Cannabis sativa* L. with an *in vivo* cannabimimetic activity higher than Δ^9-tetrahydrocannabinol: Δ^9-Tetrahydrocannabiphorol. *Scientific Reports*. 2019/12/30 2019;9(1):20335. doi:https://doi.org/10.1038/s41598-019-56785-1
29. Linciano P, Citti C, Russo F, et al. Identification of a new cannabidiol *n*-hexyl homolog in a medicinal cannabis variety with an antinociceptive activity in mice: cannabidihexol. *Scientific Reports*. 2020/12/16 2020;10(1):22019. doi:10.1038/s41598-020-79042-2
30. Caprari C, Ferri E, Vandelli MA, Citti C, Cannazza G. An emerging trend in Novel Psychoactive Substances (NPSs): designer THC. *Journal of Cannabis Research*. 2024/05/03 2024;6(1):21. doi:https://doi.org/10.1186/s42238-024-00226-y

31. Schirmer W, Gjuroski I, Vermathen M, Furrer J, Schürch S, Weinmann W. Isolation and characterization of synthesis intermediates and side products in hexahydrocannabiphorol. *Drug Testing and Analysis*. 2024/07/01 2024;n/a(n/a)doi:https://doi.org/10.1002/dta.3759
32. Schirmer W, Schürch S, Weinmann W. The Identification of Synthetic Impurities in a Vape Pen Containing Δ^9-Tetrahydrocannabiphorol Using Gas Chromatography Coupled with Mass Spectrometry. *Psychoactives*. 2024;3(4):491-500. doi:https://doi.org/10.3390/psychoactives3040030
33. Dadiotis E, Mpakaoukas S, Mitsis V, Melliou E, Magiatis P. Identification of Three Novel Tetrahydrocannabinol Analogs in the European Market. *Drug Testing and Analysis*. 2025/02/06 2025;n/a(n/a)doi:https://doi.org/10.1002/dta.3866
34. Krotulski AJ, Varnum SJ, Logan BK. Sample Mining and Data Mining: Combined Real-Time and Retrospective Approaches for the Identification of Emerging Novel Psychoactive Substances. *Journal of Forensic Sciences*. 2020/03/01 2020;65(2):550-562. doi:https://doi.org/10.1111/1556-4029.14184
35. Muir LS, Doumit SE, Seither JZ, Knittel JL, Walterscheid JP, Karschner EL. Comprehensive LC-MS/MS analysis of THC isomers, analogs, homologs and metabolites in blood and urine. *Journal of Analytical Toxicology*. 2025:bkaf023. doi:10.1093/jat/bkaf023
36. Christophersen AS. Tetrahydrocannabinol Stability in Whole Blood: Plastic Versus Glass Containers. *Journal of Analytical Toxicology*. 1986;10(4):129-131. doi:10.1093/jat/10.4.129
37. Murakoshi M, Fukuzawa K, Sato Y, Asakawa N. Adsorption Phenomenon and Development of Low Adsorption Vials for LC and LC/MS. *Shimadzu Poster*. 2017;
38. Thomas BF, Compton DR, Martin BR. Characterization of the lipophilicity of natural and synthetic analogs of delta 9-tetrahydrocannabinol and its relationship to pharmacological potency. *The Journal of Pharmacology and Experimental Therapeutics*. 1990/11/01/ 1990;255(2):624-630. doi:https://doi.org/10.1016/S0022-3565(25)23000-2
39. Stephenson JB, Carter DN, Richardson M. Surface adsorption of cannabinoids in LC–MS/MS applications. *Forensic Toxicology*. 2020/01/01 2020;38(1):292-296. doi:10.1007/s11419-019-00505-x
40. Molnar A, Lewis J, Fu S. Recovery of spiked Δ9-tetrahydrocannabinol in oral fluid from polypropylene containers. *Forensic Science International*. 2013/04/10/ 2013;227(1):69-73. doi:https://doi.org/10.1016/j.forsciint.2012.11.006
41. Krotulski AJ, Mohr ALA, Friscia M, Logan BK. Field Detection of Drugs of Abuse in Oral Fluid Using the Alere™ DDS®2 Mobile Test System with Confirmation by Liquid Chromatography Tandem Mass Spectrometry (LC–MS/MS). *Journal of Analytical Toxicology*. 2018;42(3):170-176. doi:10.1093/jat/bkx105
42. Dresen S, Gergov M, Politi L, Halter C, Weinmann W. ESI-MS/MS library of 1,253 compounds for application in forensic and clinical toxicology. *Analytical and Bioanalytical Chemistry*. 2009/12/01 2009;395(8):2521-2526. doi:10.1007/s00216-009-3084-2
43. Stumptner D, Kempf J, Weinmann W. *Increase of extraction efficiency for THC in serum by larger SPE cartridges*. XIII. GTFCh-Symposium, Ausgewählte Aspekte der Forensischen Toxikologie: Verlag Dr. Dieter Helm, Heppenheim 2004; 2003:374-378.
44. Lindbom K, Norman C, Baginski S, et al. Human metabolism of the semi-synthetic cannabinoids hexahydrocannabinol, hexahydrocannabiphorol and their acetates using hepatocytes and urine samples. *Drug Testing and Analysis*. 2024/05/28 2024;n/a(n/a)doi:https://doi.org/10.1002/dta.3740
45. Schirmer W, Schürch S, Weinmann W. Identification of Hexahydrocannabiphorol Metabolites in Human Urine. *Drug Testing and Analysis*. 2025/02/21 2025;n/a(n/a)doi:https://doi.org/10.1002/dta.3871

3 Discussion

After the regulation of HHC in many European countries, other semi-synthetic cannabinoids emerged, which are homologs of HHC and THC with a longer side chain like HHCP or Δ^9-THCP. Manufacturers of these products claim that the homologs have a natural origin, which is CBD or are derived from CBD. This marketing strategy intends to present their products as a natural product and not a synthetic drug, which is more appealing for potential customers and might be considered as hemp-derived according the Agricultural Improvement Act of 2018. The manufacturers claim that these compounds are made by prolongation of the alkyl side chain of HHC or a THC isomer, which are obtainable from CBD. However, homologation reactions for alkanes are unknown. In order to homologize an alkane, one would have to selectively oxidize the terminal carbon to an aldehyde or a carboxylic acid, which seems too challenging, if not impossible. Aldehydes can be prolonged to alkynes via either a Seyferth-Gilbert or a Corey-Fuchs reaction. The resulting alkyne is then hydrogenated to obtain a alkane, which is a single CH_2 unit longer than the starting alkane. If further prolongation would be required, the alkyne is hydroborated to an aldehyde and the homologation reaction would be repeated. Carboxylic acids can be homologized using the Arndt-Eistert reaction. These reactions all occur via carbenes, which are highly reactive intermediates. Controlling the conditions to avoid side reactions seems too challenging. Additionally, these reactions use diazo compounds or *n*-butyl lithium in order to work, which are either explosive or pyrophoric. High safety measurements would have to be taken into account. A homologation strategy of converting Δ^9-THC to Δ^9-THCP is shown in Figure 28.

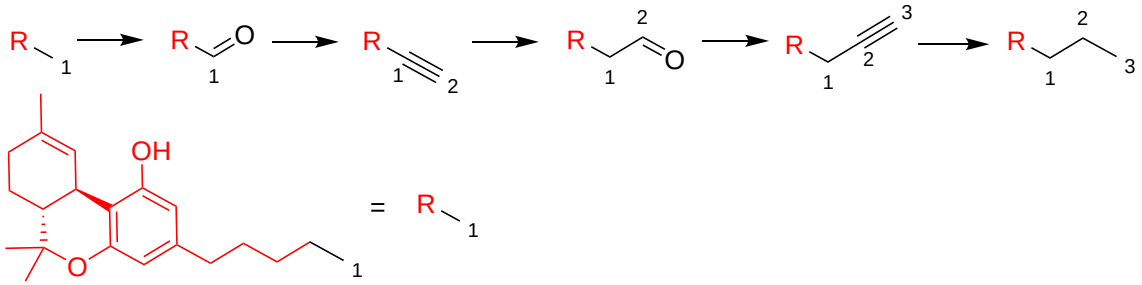

Figure 28: Hypothetical homologation strategy of converting Δ^9-THC to Δ^9-THCP.

In order to gain an insight into the procedures used for the synthesis of HHCP (**Publication I**) and Δ^9-THCP (**Publication II**), recreational products were investigated. It was found that the distributors claims do not withstand a critical proof. Typical undesired side products from a carbene driven reaction like dimeric alkenes and cyclopropanes, or the intermediates have not been found. Instead, the identified intermediates and side products are compounds, which are similar to these described in the literature for the total synthesis of HHC and Δ^9-THC, respectively (see subsection 1.2.4). Briefly: abnormal cannabinoids, unnatural stereoisomers and bisalkylated cannabinoids. These side products cannot be explained if one would assume that a homologation protocol has been used. The appearance of the isolated α,β-unsaturated ketones is a strong hint that the HHCP

sample in (**Publication I**) was synthesized by a route adapted from Tietze et al.[123] However, the suspected starting material 5-heptylcyclohexa-1,3-dione was not identified in the HHCP sample. After further consideration, more attempts should have been made to isolate the (9*S*)-HHCP from the recreational sample, it was later suspected that the (9*S*)-HHCP in this sample was its unnatural enantiomer (6a*S*,9*R*,10a*S*)-HHCP. Verification of this assumption would support the hypothesis that the Tietze route has been used, as this route uses *R*-citronellal which could only lead to a HHCP isomer with (9*R*)-configuration of which the psychoactive (9*R*)-HHCP is the desired product.

During the investigation of a vape pen containing Δ^9-THCP (**Publication II**), it was attempted to isolate some of the compounds from the vape pen liquid for the structural elucidation by NMR and stereoanalysis after derivatization with Moshers acid chloride. Only Δ^9-THCP and 5-heptylresorcinol could succesfully be isolated. The interpretation of the side products relied solely on mass spectrometric comparison with literature data of similar derivatives and the compounds were identified as oxidation products of Δ^9-THCP, and a *cis*-isomer of Δ^9-THCP. Additionally, cannabiphorol (CBP), another oxidation product, and cannabidiphorol (CBDP) were identified by comparison with analytical reference standards. The absolute configuration of these identified side products is unknown. Further side products were the bisalkylated cannabinoids, which were also found in **Publication I**. Their presence and the occurence of the isolated precursor 5-heptylresorcinol lead to the conclusion that this Δ^9-THCP was made by a total synthetic approach. It was not possible to identify the second starting material as this Δ^9-THCP sample contained a fraction of terpenes, of which several could have been used for the total synthesis. Many synthetic approaches for the synthesis of Δ^9-THC using olivetol and a terpene have been described in the literature.[117] These publications show that various synthetic routes are commonly used for the synthesis of semi-synthetic cannabinoids that do not share the pentyl side chain of THC isomers or CBD. These routes could also be used for the synthesis of pentyl substituted cannabinoids, but routes starting from THC isomers or CBD are less laborous. A strict regulation of the phytocannabinoid precursor would possibly lead to the total synthetic workarounds as they are currently used for the non-pentylic homologs.

After a single inhalative and after an oral consumption of HHC with two volunteers (**Publication III**), several metabolites were identified that show similarities to the metabolites of Δ^9-THC. The positions C8 and C11 are affected by CYP isomers leading to hydroxylation on these positions. Contrary to Δ^9-THC, these positions are not allylic positions in saturated cannabinoids such as HHC, which is why they do not oxidize as easily. This is reflected in the metabolic profile: it seemed that the most abundant metabolites were side chain hydroxylated metabolites for both volunteers. The most abundant metabolite was tentatively identified as an epimer of 4'OH-HHC, the absolute configuration at the positions C9 and C4' is unknown. A limitation of this study is that some of the identified major metabolites could not be identified unambiguously as no reference substances are available. The only unambigously identified major metabolites were 11-OH-(9*S*)-HHC and 11-OH-(9*R*)-HHC. These

epimers were, however, not baseline separated. The most methods in the literature chose to quantify both epimers as a sum (11-OH-HHC). An approach, which is not flawless. Even though their mass spectra are indistinguishable, it is merely assumed that this also applies to signal sensitivity. Furthermore, it was found that 11-OH-HHC and 11-COOH-HHC are also metabolites of Δ^9-THC, which might lead to incorrect interpretation in case of polysubstance abuse. Various publications recommended different main metabolites of HHC and therefore suggested different analytical targets to prove the consumption of HHC. There are some reasons why this is the case, first of all not every research group investigated side chain hydroxylated metabolites. This can be seen in their methodology as the main transition for side chain hydroxylated HHC metabolites (m/z 333 → m/z 191) was not included. Secondly, the number of volunteers is very limited, it is expected that interindividual differences are reflected in the metabolic profile. Finally, the signal sensitivity of the isomeric metabolites for the selected potentials for ionization and product formation is not optimal for all metabolites.

Another issue which applies generally to metabolism studies of saturated cannabinoids is that the different epimers will undergo different metabolic pathways. This can be somewhat mitigated as the study can be designed in such a way that the metabolisms of the epimers are investigated separately, as it has been realized in current *in vitro* metabolism studies. However, semi-synthetic cannabinoids on the recreational market are always available as a mixture of epimers. For a proper investigation in real cases, at least one characteristic metabolite for each epimer should be investigated.

It was expected that the *in vivo* metabolism of HHCP (**Publication IV**) would be similar to the metabolism of HHC (**Publication III**). Similarities have been found as side chain hydroxylated metabolites were quite abundant. In contrast to HHC, however, bishydroxylation was very common. It is assumed that this would facilitate the excretion because the lipophilicity of the homologs increases with the chain length. For Δ^9-THC homologs, it is known that their lipophilicity (K_{ow}) increases by a factor of approximately 3 for each CH_2 group added to the side chain.[217] An *in vitro* metabolism study of HHC and HHCP using human hepatocytes came to the same conclusions regarding the tendency of bishydroxylation on HHCP.[37] However, the opposite observation has been made in *in vitro* studies with pooled human liver microsomes. The tendency of bishydroxylation decreased with increasing chain length.[38] For the investigation of the metabolism of HHCP (**Publication IV**) a well characterized, but impure HHCP product (see **Publication I**) was orally ingested. It is therefore likely that some of the detected metabolites are not metabolites of the epimers (9*R*)- or (9*S*)-HHCP but metabolites of the intermediates and side products that have been identified in the recreational HHCP product. As for HHC, the major metabolites could only be identified tentatively, and further analysis with certified reference material will be needed for unambiguous metabolite identification. Side products or their metabolites found in biological samples might serve as indicators for the utilized synthetic route like detection of 1-(cyclohexa-1,4-dien-1-yl)-*N*-methylpropan-2-amine (CMP) in biological samples, which is indicative for the consumption of

methamphetamine synthesized by the Birch reduction.[218]

The work on the *in vivo* metabolsim of H4CBD (**Publication V**) has shown that the mass spectrometrical interpretation of new psychoactive substances (NPS) can be challenging, even if the NPS is a simple derivative of a known compound like CBD in this case. While the EI mass spectra of trimethylsilylated derivatives of H4CBD metabolites and the CBD analogs are similar, this is not the case for the ESI+ mass spectra of H4CBD metabolites and the corresponding CBD analogs. The metabolism of H4CBD is somewhat similar to CBD. It was observed that hydroxylation on the methyl group at C7 is not the preferred metabolic pathway of H4CBD. This is in accordance to the observations made for the *in vivo* metabolism of HHC and HHCP, (**Publication III** and **IV**). Similar to the metabolism studies on HHC and HHCP, a limitation in this work is the lack of stereochemical knowledge of the metabolites. It is not clear which metabolite is formed from which H4CBD epimer, as no certified reference material is available. Further studies should include them.

The developed screening method for semi-synthetic cannabinoids in human blood (**Publication VI**) is one of two comprehensive screening methods covering a wide range of semi-synthetic cannabinoids.[33] Due to scarce information on the metabolism of semi-synthetic cannabinoids, both methods lack good analytical targets. The metabolism study on HHCP (**Publication IV**) indicates that more lipophilic cannabinoids might undergo strong metabolism, the unmetabolized drug might not be detectable in real case samples. It is recommended that sample storage containers and vials are tested for unspecific adsorption to these extremely lipophilic compounds when setting up an analytical workflow. During the validation of this method, it was found that the glass vials adsorbed the more lipophilic compounds to such a degree that no analytical signal was detected. A change to polypropylene vials did resolve this issue. From early Δ^9-THC analysis is known that analyte loss can be observed by storing the physiological samples in inadequate containers.[219]

4 Outlook

Cannabis is the most consumed recreational drug worldwide and this will remain. This is also reflected in the approximately 950 monitored NPS by the EUDA. Roughly 30% of these NPS are either synthetic or semi-synthetic cannabinoids. In countries that prohibit the consumption of cannabis, one might expect that the consumers are taking replacement drugs, sometimes unknowingly. Since the emergence of HHC in 2022, new semi-synthetic cannabinoids entered the market and it has to be expected that this market will evolve in order to circumvent the latest regulations. After the regulation of HHC, stronger and longer lasting compounds like Δ^9-THCP, HHCP and HHC-C8 emerged. Consumption of these compounds has lead to severe intoxications in the past. To this date, no fatalities have been reported, but this might change as soon as newly emerging compounds are becoming more potent. The newest compounds in the recreational market show that the synthesis strategies have evolved. The compounds, available prior 2023 were simple derivatives of Δ^9-THC that were obtained after esterification or hydrogenation. Today, after the regulation of HHC, more complex compounds have emerged that are obtained from total synthetic routes, or after more complex derivatization of Δ^9-THC like aromatic allylation or aromatic halogenation. These newly introduced functions would enable further derivatization, and it is to be expected that these new cannabinoids will appear on the recreational drug market, particularly in countries where recreational cannabis use is prohibited. The most recent formal notifications on NPS from EUDA already show this trend. The latest semi-synthetic cannabinoids show branched side chains. One can also expect that other cannabimimetic scaffolds will be used, which only vaguely resemble phytocannabinoids. Such a scaffold might be the hydroxycyclohexylphenol scaffold, which is found in the synthetic cannabinoids CP 55,940, CP 47,497, and cannabicyclohexanol, the C8 homolog of CP 47,497. Some of these compounds are already listed in the Swiss Narcotics Schedule Ordinance (BetmVV-EDI).[8] Cannabicyclohexanol was among the first synthetic cannabinoids detected in the herbal smoking blend 'Spice' in 2009.[197] It can be expected that the newly emerging drugs are either simple derivatives of existing NPS or, as before, will be hijacked from basic research or patents.[220–223]

It is therefore necessary that the synthetic origin can be traced back to the manufacturers and this is only possible if we as forensic investigators understand how these compounds are synthesized. This is achievable by analyzing recreational products and identifying side products and intermediates, as they are characteristic for a given route. Frequently identified precursor compounds such as the olivetol homologs could then ultimately be scheduled. In order to prove the use and abuse of these compounds, we further need to develop detection methods. The work on HHCP has shown that physiological samples, which are positive on cannabinoids, might be unnoticed as they are not detected by immunoassays and would not be detected in a routine screening method. Screening methods have to be updated to identify the presence of emerging NPS. Understanding the metabolism of these emerging compounds is the basis of developing such methods.

5 References

[1] Clarke, R. C.; Merlin, M. D. Natural Origins and Early Evolution of Cannabis. In *Cannabis: Evolution and Ethnobotany*, 1 ed.; University of California Press: **2013**.

[2] Pisanti, S.; Bifulco, M. *Journal of Cellular Physiology* **2019,** *234,* 8342-8351.

[3] Clarke, R. C.; Merlin, M. D. Ethnobotanical Origins, Early Cultivation, and Evolution through Human Selection. In *Cannabis: Evolution and Ethnobotany*, 1 ed.; University of California Press: **2013**.

[4] Russo, E. *Chemistry & Biodiversity* **2007,** *4,* 1614-1648.

[5] "World Drug Report 2025, United Nations Office on Drugs and Crime (UNODC)", `https://www.unodc.org/unodc/data-and-analysis/world-drug-report-2025.html`, **2025**.

[6] "European Drug Report 2025: Trends and developments, European Union Drug Agency (EUDA)", `https://www.euda.europa.eu/publications/european-drug-report/2025_en`, **2025**.

[7] "Prävalenz des Cannabiskonsums, Bundesamt für Gesundheit (BAG)", `https://ind.obsan.admin.ch/indicator/monam/cannabiskonsum-alter-15-64`, **2024**.

[8] "Verordnung des EDI über die Verzeichnisse der Betäubungsmittel, psychotropen Stoffe, Vorläuferstoffe und Hilfschemikalien", `https://www.fedlex.admin.ch/eli/cc/2011/363/de`, Accessed: 2025-08-05.

[9] "Bundesgesetz über die Betäubungsmittel und die psychotropen Stoffe, Betäubungsmittelgesetz (BetmG), Art. 19b, Abs. 2", `https://www.fedlex.admin.ch/eli/cc/2011/363/de`, Accessed: 2025-08-05.

[10] Bondolfi, S. "Leiturteil des Bundesgerichts - Cannabis: bis 10 Gramm Eigenkonsum keine Beschlagnahmung möglich", `https://www.srf.ch/news/schweiz/leiturteil-des-bundesgerichts-cannabis-bis-10-gramm-eigenkonsum-keine-beschlagnahmung-moeglich`, **2023** Accessed: 2025-08-21.

[11] Rock, E. M.; Parker, L. A. Constituents of Cannabis Sativa. In *Cannabinoids and Neuropsychiatric Disorders*; Murillo-Rodriguez, E.; Pandi-Perumal, S. R.; Monti, J. M., Eds.; Springer International Publishing: Cham, **2021**.

[12] Radwan, M. M.; Chandra, S.; Gul, S.; ElSohly, M. A. *Molecules* **2021,** *26,* 2774.

[13] Adams, R.; Pease, D. C.; Cain, C. K.; Clark, J. H. *Journal of the American Chemical Society* **1940,** *62,* 2402–2405.

[14] Appendino, G. *Rendiconti Lincei - Scienze Fisiche e Naturali* **2020,** *31,* 919–929.

[15] Gaoni, Y.; Mechoulam, R. *Journal of the American Chemical Society* **1964,** *86,* 1646–1647.

[16] Grunfeld, Y.; Edery, H. *Psychopharmacologia* **1969,** *14,* 200–210.

[17] Mechoulam, R.; Shani, A.; Edery, H.; Grunfeld, Y. *Science* **1970,** *169,* 611-612.

[18] Edery, H.; Grunfeld, Y.; Ben-Zvi, Z.; Mechoulam, R. *Annals of the New York Academy of Sciences* **1971,** *191,* 40-53.

[19] ElSohly, M. A.; Mehmedic, Z.; Foster, S.; Gon, C.; Chandra, S.; Church, J. C. *Biological Psychiatry* **2016,** *79,* 613–619.

[20] ElSohly, M. A.; Majumdar, C. G.; Chandra, S.; Radwan, M. M. *Frontiers in Public Health* **2024,** *Volume 12 - 2024,.*

[21] Brenneisen, R. Chemistry and Analysis of Phytocannabinoids and Other Cannabis Constituents. In *Marijuana and the Cannabinoids*; ElSohly, M. A., Ed.; Humana Press: Totowa, NJ, **2007**.

[22] König, S.; Schläpfer, M. "SGRM Fachgruppe Forensische Chemie, Statistiken THC", `https://sgrm.ch/de/forensische-chemie-und-toxikologie/fachgruppe-forensische-chemie/statistiken-thc`, **2004-2023** Accessed: 2025-10-06.

[23] Madras, B. K. *Neuropsychopharmacology* **2019,** *44,* 215–216.

[24] Englund, A.; Oliver, D.; Chesney, E.; Chester, L.; Wilson, J.; Sovi, S.; De Micheli, A.; Hodsoll, J.; Fusar-Poli, P.; Strang, J.; Murray, R. M.; Freeman, T. P.; McGuire, P. *Neuropsychopharmacology* **2023,** *48,* 869–876.

[25] Schoeler, T.; Ferris, J.; Winstock, A. R. *Translational Psychiatry* **2022,** *12,* 369.

[26] Adams, R.; Pease, D. C.; Clark, J. H. *Journal of the American Chemical Society* **1940,** *62,* 2194–2196.

[27] Jacob, A.; Todd, A. R. *Nature* **1940,** *145,* 350–350.

[28] Adams, R.; Hunt, M.; Clark, J. H. *Journal of the American Chemical Society* **1940,** *62,* 196–200.

[29] Mechoulam, R.; Shvo, Y. *Tetrahedron* **1963,** *19,* 2073-2078.

[30] Ujváry, I. *Drug Testing and Analysis* **2024,** *16,* 127-161.

[31] Ujváry, I.; Evans-Brown, M.; Gallegos, A.; Planchuelo, G.; de Morais, J.; Christie, R.; Jorge, R.; Sedefov, R.; European Monitoring Centre for Drugs and Drug Addiction (EMCDDA), "Hexahydrocannabinol (HHC) and Related Substances.", **2023**.

[32] Monti, M. C.; Stoll, A.; Schlotterbeck, G.; Duthaler, U. *Journal of Chromatography A* **2025,** *1760,* 466276.

[33] Muir, L. S.; Doumit, S. E.; Seither, J. Z.; Knittel, J. L.; Walterscheid, J. P.; Karschner, E. L. *Journal of Analytical Toxicology* **2025,** *49,* 322-331.

[34] Patton, A. L.; Muir, L.; Seither, J. Z.; Walterscheid, J. P.; Karschner, E. L. *Journal of Analytical Toxicology* **2024,** *49,* 96-103.

[35] Hundertmark, M.; Besch, L.; Röhrich, J.; Germerott, T.; Wunder, C. *Drug Testing and Analysis* **2025,** Online ahead of print.

[36] Gameli, P. S.; Taoussi, O.; Trana, A. D.; Tronconi, L. P.; Pichini, S.; Carlier, J.; Huestis, M. A.; Busardò, F. P. *Clinica Chimica Acta* **2026,** *578,* 120480.

[37] Lindbom, K.; Norman, C.; Baginski, S.; Krebs, L.; Stalberga, D.; Rautio, T.; Wu, X.; Kronstrand, R.; Gréen, H. *Drug Testing and Analysis* **2025,** *17,* 372-386.

[38] Watanabe, S.; Murakami, T.; Muratsu, S.; Takeshi, S.; Seto, Y. *Clinical Chemistry* **2025,** hvaf087.

[39] Falck Jørgensen, C.; Schou Rasmussen, B.; Linnet, K.; Thomsen, R. *Metabolites* **2023,** *13,* 1169.

[40] Kobidze, G.; Sprega, G.; Montanari, E.; Taoussi, O.; Bambagiotti, G.; Fede, M. S.; Di Trana, A.; Pichini, S.; Busardò, F. P.; Tini, A.; Chankvetadze, B.; Faro, A. F. L. *Journal of Pharmaceutical and Biomedical Analysis* **2024,** *240,* 115918.

[41] Pettersson-Pablo, P.; Oxelbark, J. *Scandinavian Journal of Clinical and Laboratory Investigation* **2024,** *84,* 109–114.

[42] Helander, A.; Johansson, M.; Villén, T.; Andersson, A. *Scandinavian Journal of Clinical and Laboratory Investigation* **2024,** *84,* 125–132.

[43] Derne, A.-S.; Jouzeau, J.-Y.; Pape, E.; Kolodziej, A.; Gibaja, V.; Marchand, E.; Gambier, N.; Scala-Bertola, J. *European Addiction Research* **2024,** *30,* 402-407.

[44] Kronstrand, R.; Roman, M.; Green, H.; Truver, M. T. *Journal of Analytical Toxicology* **2024,** *48,* 235-241.

[45] Höfert, L.; Franz, B.; Groß, C.; Kuntze, D.; Jurásek, B.; Kuchař, M.; Dreßler, J.; Becker, S.; Baumann, S. *Scientific Reports* **2025,** *15,* 10086.

[46] Zhang, S.; Alam, M. M.; Chandler, B. D.; Lanorio, J. P.; Deskins, C.; Song, L. *Molecules* **2025,** *30,* 2597.

[47] Casati, S.; Rota, P.; Bergamaschi, R. F.; Palmisano, E.; La Rocca, P.; Ravelli, A.; Angeli, I.; Minoli, M.; Roda, G.; Orioli, M. *Cannabis and Cannabinoid Research* **2024,** *9,* 622-628.

[48] Bottinelli, C.; Baradian, P.; Poly, A.; Hoizey, G.; Chatenay, C. *Rapid Communications in Mass Spectrometry* **2024,** *38,* e9711.

[49] Pitterl, F.; Pavlic, M.; Liu, J.; Oberacher, H. *Journal of Analytical Toxicology* **2024,** *48,* 350-358.

[50] Manier, S. K.; Valdiviezo, J. A.; Vollmer, A. C.; Eckstein, N.; Meyer, M. R. *Journal of Analytical Toxicology* **2023,** *47,* 818-825.

[51] Grapp, M.; Kaufmann, C.; Peschel, A.; Potzscher, M.; Dziadosz, M.; Marquenie, L.; Teske, J. *Journal of Pharmaceutical and Biomedical Analysis* **2025,** *261,* 116833.

[52] Tanaka, R.; Kikura-Hanajiri, R. *Forensic Toxicology* **2024,** *42,* 71–81.

[53] Tanaka, R.; Ito, M.; Kikura-Hanajiri, R. *Drug Testing and Analysis* **2025,** *17,* 1795-1802.

[54] Tanaka, R.; Kawamura, M.; Ito, M.; Kikura-Hanajiri, R. *Drug Testing and Analysis* **2025,** Online ahead of print.

[55] Dadiotis, E.; Mpakaoukas, S.; Mitsis, V.; Melliou, E.; Magiatis, P. *Drug Testing and Analysis* **2025,** *17,* 1594-1600.

[56] Höfert, L.; Becker, S.; Dreßler, J.; Baumann, S. *Drug Testing and Analysis* **2024,** *16,* 489-497.

[57] Di Trana, A.; Sprega, G.; Kobidze, G.; Taoussi, O.; Lo Faro, A. F.; Bambagiotti, G.; Montanari, E.; Fede, M. S.; Carlier, J.; Tini, A.; Busardò, F. P.; Di Giorgi, A.; Pichini, S. *Molecules* **2024,** *29,* 3440.

[58] Lucuta, L.; Schwarz, L.; Liut, J.; Hose, J.; Nauroth, L.; Juebner, M.; Andresen-Streichert, H. *Forensic Science International* **2025,** *370,* 112437.

[59] Jørgensen, C. F.; Rasmussen, B. S.; Linnet, K.; Thomsen, R. *Journal of Forensic Sciences* **2024,** *69,* 2009-2017.

[60] Watanabe, S.; Murakami, T.; Muratsu, S.; Fujiwara, H.; Nakanishi, T.; Seto, Y. *Drug Testing and Analysis* **2025,** *17,* 694-700.

[61] Collins, A.; Ramirez, G.; Tesfatsion, T.; Ray, K. P.; Caudill, S.; Cruces, W. *Natural Product Communications* **2023,** *18,* 1934578X231158910.

[62] Belbasi, Z.; Petr, J.; Hrbac, J.; Jirovsky, D. *Journal of Pharmaceutical and Biomedical Analysis* **2025,** *262,* 116875.

[63] Derne, A.-S.; Pape, E.; Jouzeau, J.-Y.; Kolodziej, A.; Gambier, N.; Scala-Bertola, J. *Drug Testing and Analysis* **2024,** *16,* 638-640.

[64] Patton, A. L.; Pacheco, I. C.; Seither, J. Z.; Brown, J. T.; Walterscheid, J. P.; Karschner, E. L. *Journal of Analytical Toxicology* **2024,** *48,* 439-446.

[65] Thomsen, R.; Axelsen, T. M.; Løkken, N.; Krogh, L. M. G.; Reiter, N.; Rasmussen, B. S.; Laursen, E. L. *Toxicology Reports* **2025,** *14,* 101912.

[66] Tsujikawa, K.; Okada, Y.; Segawa, H.; Yamamuro, T.; Kuwayama, K.; Kanamori, T.; Iwata, Y. T. *Forensic Toxicology* **2025,** *43,* 365–369.

[67] Yates, T. L.; Poklis, J. L.; Holt, A. K.; Fleming, J. H.; Bayard, C.; Raso, S. A.; Peace, M. R. *Journal of Analytical Toxicology* **2025,** bkaf055.

[68] "Convention on Psychotropic Substances (1971), United Nations", `https://www.unodc.org/pdf/convention_1971_en.pdf`, Accessed: 2025-08-21.

[69] "Agriculture Improvement Act of 2018, Pub. L. No. 115-334, 132 Stat. 4982 (2018)", `https://www.govinfo.gov/app/details/PLAW-115publ334`, Accessed: 2025-08-21.

[70] Zawatsky, C. N.; Mills-Huffnagle, S.; Augusto, C. M.; Vrana, K. E.; Nyland, J. E. *Medical Cannabis and Cannabinoids* **2024,** *7,* 10-18.

[71] O'Mahony, B.; O'Malley, A.; Kerrigan, O.; McDonald, C. *Irish Journal of Psychological Medicine* **2024,** *41,* 405–408.

[72] O'Mahony, B.; Lanigan, S.; Lally, N.; O'Malley, A.; Smyth, B.; McDonald, C.; Hallahan, B. *BJPsych Bulletin* **2025,** 1–6.

[73] Naughton, S.; Clarke, M. *Irish Journal of Psychological Medicine* **2024,** *41,* 505–505.

[74] Labadie, M.; Nardon, A.; Castaing, N.; Bragança, C.; Daveluy, A.; Gaulier, J.-M.; Balkhi, S. E.; Grenouillet, M.; and, *Clinical Toxicology* **2024,** *62,* 112–119.

[75] Čečrle, M.; Běhounková, M.; Kotíková, K.; Zacharov, S. *Pharmacology Research & Perspectives* **2025,** *13,* e70162 e70162 PRP2-2025-02-0056.R1.

[76] Szapanyos, A. "Kábító gumicukor ütött ki 31 külföldit: öntudatlanul feküdt a kórházban több fogyasztó is", `https://www.blikk.hu/aktualis/belfold/gumicukor-kannabisz-korhaz/nnd7d0d?fx_ps=d_2`, **2024** Accessed: 2025-08-05.

[77] Sárosi, P. "The Challenge of the Emerging Semi-Synthetic Cannabinoid Market in Europe", `https://drogriporter.hu/en/the-challenge-of-the-emerging-semi-synthetic-cannabinoid-market-in-europe/`, **2024** Accessed: 2025-08-05.

[78] Iketani, Y.; Morita, S.; Tsuji, T.; Noguchi, W.; Maki, Y.; Inoue, K.; Nakagawa, Y. *Tokai Journal of Experimental and Clinical Medicine* **2024,** *49,* 128-132.

[79] Reiter, N.; Linnet, K.; Østermark Andersen, N.; Rasmussen, B. S.; Klose Nielsen, M.; Reenberg Eriksen, K.; Palmqvist, D. F. *Ugeskrift for Læger* **2024,** *186,*.

[80] Munger, K. R.; Jensen, R. P.; Strongin, R. M. *Chemical Research in Toxicology* **2022,** *35,* 1202–1205.

[81] Wu, D.; O'Shea, D. F. *Proceedings of the National Academy of Sciences* **2020,** *117,* 6349-6355.

[82] Strongin, R. M. *Proceedings of the National Academy of Sciences* **2020,** *117,* 7553-7554.

[83] Marrocco, A.; Singh, D.; Christiani, D. C.; Demokritou, P. *Critical Reviews in Toxicology* **2022,** *52,* 188–220.

[84] Boudi, F. B.; Patel, S.; Boudi, A.; Chan, C. *Cureus* **2019,** *11,* e6350.

[85] The Alpha-Tocopherol, Beta Carotene Cancer Prevention Study Group, *New England Journal of Medicine* **1994,** *330,* 1029-1035.

[86] Slatore, C. G.; Littman, A. J.; Au, D. H.; Satia, J. A.; White, E. *American Journal of Respiratory and Critical Care Medicine* **2008,** *177,* 524-530.

[87] Caprari, C.; Ferri, E.; Schmid, M. G.; Del Mercato, L. L.; Citti, C.; Cannazza, G. *Forensic Chemistry* **2024,** *40,* 100595.

[88] Kaczor, E. E.; Greene, K.; Babu, K. M.; Berthold, E. C.; Sharma, A.; Carreiro, S. P. *Journal of Medical Toxicology* **2024,** *20,* 31–38.

[89] Pulver, B.; Schmitz, B.; Brandt, S. D.; Auwärter, V. *Chemical analysis of recreational products containing semi-synthetic cannabinoids in Germany*, presented at The International Association of Forensic Toxicologists (TIAFT) 61^{st} annual meeting, St. Gallen, Switzerland, **2024**.

[90] Pulver, B.; Schmitz, B.; Evans-Brown, M.; Brandt, S. D.; Auwärter, V. *Chemical analysis of recreational products containing semi-synthetic cannabinoids in Germany*, presented at XXIV. GTFCh-Symposium, Mosbach, Germany, **2025**.

[91] Giorgetti, A.; Busardò, F. P.; Tittarelli, R.; Auwärter, V.; Giorgetti, R. *Frontiers in Psychiatry* **2020,** *Volume 11 - 2020,*.

[92] Yoganathan, P.; Claridge, H.; Chester, L.; Englund, A.; Kalk, N. J.; Copeland, C. S. *Cannabis and Cannabinoid Research* **2022,** *7,* 516-525.

[93] Tai, S.; Fantegrossi, W. E. *Current Addiction Reports* **2014,** *1,* 129–136.

[94] Reekie, T. A.; Kassiou, M. Chapter 38 - Synthetic cannabinoid receptor agonists: An overview. In *Neurobiology and Physiology of the Endocannabinoid System*; Patel, V. B.; Preedy, V. R.; Martin, C. R., Eds.; Academic Press: **2023**.

[95] Pulver, B.; Fischmann, S.; Gallegos, A.; Christie, R. *Drug Testing and Analysis* **2023,** *15,* 255-276.

[96] Booth, V. "What Is THCP? The New Cannabinoid on the Block", `https://www.vice.com/en/article/what-is-thcp/`, **2025** Accessed: 2025-08-25.

[97] Radwan, M. M.; Wanas, A. S.; Gul, W.; Ibrahim, E. A.; ElSohly, M. A. *Journal of Natural Products* **2023,** *86,* 822–829.

[98] Huang, S.; van Beek, T. A.; Claassen, F. W.; Janssen, H.-G.; Ma, M.; Chen, B.; Zuilhof, H.; Salentijn, G. *Food Chemistry* **2024,** *440,* 138187.

[99] Gaoni, Y.; Mechoulam, R. *Israel Journal of Chemistry* **1968,** *6,* 679-690.

[100] Hale, R. L.; Solas, D. W.; Simis, K.; Lu, A. T.; Lloyd, P. M. "Heat-Labile Prodrugs, WO 2008/134668 A2", **2008**.

[101] Edery, H.; Grunfeld, Y.; Porath, G.; Ben-Zvi, Z.; Shani, A.; Mechoulam, R. *Arzneimittelforschung* **1972,** *22,* 1995–2003.

[102] Razdan, R. K. *Pharmacological Reviews* **1986,** *38,* 75-149.

[103] Compton, D. R.; Prescott, Jr, W. R.; Martin, B. R.; Siegel, C.; Gordon, P. M.; Razdan, R. K. *Journal of Medicinal Chemistry* **1991,** *34,* 3310–3316.

[104] Rehman, A.-u.; Ali Javed, S.; Athar Abbasi, M.; Irshad, M.; Gul, S.; Hussain, G.; Nafeesa, K.; Rubab, K.; Ahmad, I. *Asian Journal of Chemistry* **2013,** 8522–8526.

[105] Wang, N.-Y.; Dubler, R. E.; Schneider-Ungemach, F.; Walters, R. L.; Thacker, S. A. "Fluorescence polarization immunoassay for tetrahydrocannabinoids. EP 0279308 A2", **1988**.

[106] Hamer, S.; Westphal, F.; Pütz, M. *Identification of recently emerging (semi-)synthetic cannabinoids and related products sold in shops and vending machines*, presented at XXIV. GTFCh-Symposium, Mosbach, Germany, **2025**.

[107] Fahrenholtz, K. E.; Lurie, M.; Kierstead, R. W. *Journal of the American Chemical Society* **1966,** *88,* 2079–2080.

[108] Srebnik, M.; Mechoulam, R.; Yona, I. *Journal of the Chemical Society, Perkin Transactions 1* **1987,** 1423-1427.

[109] Usami, N.; Kobana, K.; Yoshida, H.; Kimura, T.; Watanabe, K.; Yoshimura, H.; Yamamoto, I. *Chemical & Pharmaceutical Bulletin* **1998,** *46,* 1462-1467.

[110] Umemoto, T.; Kawada, K.; Tomita, K. *Tetrahedron Letters* **1986,** *27,* 4465-4468.

[111] Martin, B. R.; Compton, D. R.; Semus, S. F.; Lin, S.; Marciniak, G.; Grzybowska, J.; Charalambous, A.; Makriyannis, A. *Pharmacology Biochemistry and Behavior* **1993,** *46,* 295-301.

[112] Russo, F.; Vandelli, M. A.; Biagini, G.; Schmid, M.; Luongo, L.; Perrone, M.; Ricciardi, F.; Maione, S.; Laganà, A.; Capriotti, A. L.; Gallo, A.; Carbone, L.; Perrone, E.; Gigli, G.; Cannazza, G.; Citti, C. *Scientific Reports* **2023,** *13,* 11061.

[113] Nasrallah, D. J.; Garg, N. K. *ACS Chemical Biology* **2023,** *18,* 2023–2029.

[114] Mechoulam, R.; Braun, P.; Gaoni, Y. *Journal of the American Chemical Society* **1967,** *89,* 4552–4554.

[115] Petrzilka, T.; Sikemeier, C. *Helvetica Chimica Acta* **1967,** *50,* 1416-1419.

[116] Razdan, R. K.; Dalzell, H. C.; Handrick, G. R. *Journal of the American Chemical Society* **1974,** *96,* 5860–5865.

[117] Bloemendal, V. R. L. J.; van Hest, J. C. M.; Rutjes, F. P. J. T. *Organic & Biomolecular Chemistry* **2020,** *18,* 3203-3215.

[118] Docampo-Palacios, M. L.; Ramirez, G. A.; Tesfatsion, T. T.; Okhovat, A.; Pittiglio, M.; Ray, K. P.; Cruces, W. *Molecules* **2023,** *28,* 6434.

[119] Petrzilka, T.; Haefliger, W.; Sikemeier, C. *Helvetica Chimica Acta* **1969,** *52,* 1102-1134.

[120] Janssens, L. K.; Van Uytfanghe, K.; Williams, J. B.; Hering, K. W.; Iula, D. M.; Stove, C. P. *Archives of Toxicology* **2024,** *98,* 2619–2630.

[121] Adams, R.; Loewe, S.; Jelinek, C.; Wolff, H. *Journal of the American Chemical Society* **1941,** *63,* 1971–1973.

[122] Adams, R.; Loewe, S.; Smith, C. M.; McPhee, W. D. *Journal of the American Chemical Society* **1942,** *64,* 694–697.

[123] Tietze, L.-F.; von Kiedrowski, G.; Berger, B. *Angewandte Chemie International Edition in English* **1982,** *21,* 221-222.

[124] Lee, Y. R.; Xia, L. *Tetrahedron Letters* **2008,** *49,* 3283-3287.

[125] Uliss, D. B.; Dalzell, H. C.; Handrick, G. R.; Howes, J. F.; Razdan, R. K. *Journal of Medicinal Chemistry* **1975,** *18,* 213–215.

[126] Houry, S.; Mechoulam, R.; Fowler, P. J.; Macko, E.; Loev, B. *Journal of Medicinal Chemistry* **1974,** *17,* 287–293.

[127] Millimaci, A. M.; Trilles, R. V.; McNeely, J. H.; Brown, L. E.; Beeler, A. B.; Porco, Jr, J. A. *The Journal of Organic Chemistry* **2023,** *88,* 13135–13141.

[128] Dinis-Oliveira, R. J. *Drug Metabolism Reviews* **2016,** *48,* 80–87.

[129] Chayasirisobhon, S. *The Permanente Journal* **2021,** *25,* 1-3.

[130] Huestis, M. A. Pharmacokinetics and Metabolism of the Plant Cannabinoids, Δ^9-Tetrahydrocannabinol, Cannabidiol and Cannabinol. In *Cannabinoids*; Pertwee, R. G., Ed.; Springer Berlin Heidelberg: Berlin, Heidelberg, **2005**.

[131] Ujváry, I.; Hanuš, L. *Cannabis and Cannabinoid Research* **2016,** *1,* 90-101.

[132] Harvey, D. J.; Mechoulam, R. *Xenobiotica* **1990,** *20,* 303–320.

[133] Jiang, R.; Yamaori, S.; Takeda, S.; Yamamoto, I.; Watanabe, K. *Life Sciences* **2011,** *89,* 165-170.

[134] Harvey, D. J. Metabolism and pharmacokinetics of the cannabinoids. In *Biochemistry and Physiology of substance abuse*, 1 ed.; CRC Press: **1991**.

[135] Harvey, D. J.; Brown, N. K. *Drug Metabolism and Disposition* **1991,** *19,* 714–716.

[136] Harvey, D. J.; Brown, N. K. *Pharmacology Biochemistry and Behavior* **1991,** *40,* 533-540.

[137] Ortiz de Montellano, P. R. *Chemical Reviews* **2010,** *110,* 932–948.

[138] Di Trana, A.; Di Giorgi, A.; Sprega, G.; Carlier, J.; Kobidze, G.; Montanari, E.; Taoussi, O.; Bambagiotti, G.; Fede, M. S.; Lo Faro, A. F.; Tini, A.; Busardò, F. P.; Pichini, S. *Pharmaceuticals* **2024,** *17,*.

[139] Šíchová, K.; Mallarino, B.; Janečková, L.; Palivec, P.; Vágnerová, M.; Vejmola, Č.; Nikolič, M.; Ladislavová, L.; Mazochová, K.; Ryšánek, P.; Šíma, M.; Šafanda, A.; Hiep, B. Q.; Koutrouli, I. R. A.; Kuchař, M.; Páleníček, T. *International Journal of Neuropsychopharmacology* **2025,** *28,* pyaf041.

[140] Budzikiewicz, H.; Alpin, R.; Lightner, D.; Djerassi, C.; Mechoulam, R.; Gaoni, Y. *Tetrahedron* **1965,** *21,* 1881-1888.

[141] Vree, T. *Journal of Pharmaceutical Sciences* **1977,** *66,* 1444-1450.

[142] Harvey, D. J. *Mass Spectrometry Reviews* **1987,** *6,* 135-229.

[143] Harvey, D. J. Cannabinoids. In *Mass Spectrometry: Clinical and Biomedical Applications*; Desiderio, D. M., Ed.; Springer US: Boston, MA, **1992**.

[144] Bijlsma, L.; Sancho, J. V.; Hernández, F.; Niessen, W. M. *Journal of Mass Spectrometry* **2011,** *46,* 865-875.

[145] Harvey, D. J. *Biomedical Mass Spectrometry* **1981,** *8,* 575-578.

[146] Terlouw, J.; Heerma, W.; Burgers, P.; Dijkstra, G.; Boon, A.; Kramer, H.; Salemink, C. *Tetrahedron* **1974,** *30,* 4243-4248.

[147] Boeren, E. G.; Heerma, W.; Terlouw, J. K. *Organic Mass Spectrometry* **1976,** *11,* 659-663.

[148] Driessen, R. A. *Deuterium labeled cannabinoids,* Dissertation Rijksuniversiteit Utrecht (Netherlands), **1979**, available at `https://inis.iaea.org/records/nrmhn-grn30`.

[149] Cha, H. J.; Song, Y. J.; Lee, D. E.; Kim, Y.-H.; Shin, J.; Jang, C.-G.; Suh, S. K.; Kim, S. J.; Yun, J. *Toxicological Research* **2019,** *35,* 37–44.

[150] Mackie, K. *PLOS Biology* **2007,** *5,* 1-3.

[151] Lichtman, A. H.; Wiley, J. L.; LaVecchia, K. L.; Neviaser, S. T.; Arthur, D. B.; Wilson, D. M.; Martin, B. R. *European Journal of Pharmacology* **1998,** *357,* 139-148.

[152] Huestis, M. A.; Boyd, S. J.; Heishman, S. J.; Preston, K. L.; Bonnet, D.; Le Fur, G.; Gorelick, D. A. *Psychopharmacology* **2007,** *194,* 505–515.

[153] Wiley, J. L.; Martin, B. R. *European Journal of Pharmacology* **2003,** *471,* 185-193.

[154] Bow, E. W.; Rimoldi, J. M. *Perspectives in Medicinal Chemistry* **2016,** *8,* PMC.S32171.

[155] Adams, R. *Bulletin of the New York Academy of Medicine* **1942,** *18,* 705-730.

[156] Leaf, G.; Todd, A. R.; Wilkinson, S. *Journal of the Chemical Society* **1942,** 185-188.

[157] Mechoulam, R.; Feigenbaum, J. J.; Lander, N.; Segal, M.; Järbe, T. U. C.; Hiltunen, A. J.; Consroe, P. *Experientia* **1988,** *44,* 762–764.

[158] Devane, W. A.; Dysarz, F. A.; Johnson, M. R.; Melvin, L. S.; Howlett, A. C. *Molecular Pharmacology* **1988,** *34,* 605-613.

[159] Munro, S.; Thomas, K. L.; Abu-Shaar, M. *Nature* **1993,** *365,* 61–65.

[160] Luethi, D.; Liechti, M. E. *International Journal of Neuropsychopharmacology* **2018,** *21,* 926-931.

[161] Bächle, F.; Besch, L.; Danz, K.; Schallenberg, D.; Wirth, M. *Toxichem Krimtech* **2025,** *92,* 136–180.

[162] Howlett, A. C.; Barth, F.; Bonner, T. I.; Cabral, G.; Casellas, P.; Devane, W. A.; Felder, C. C.; Herkenham, M.; Mackie, K.; Martin, B. R.; Mechoulam, R.; Pertwee, R. G. *Pharmacological Reviews* **2002,** *54,* 161–202.

[163] Adams, R.; Chen, K. H.; Loewe, S. *Journal of the American Chemical Society* **1945,** *67,* 1534–1537.

[164] Huffman, J. W.; Lainton, J. A. H.; Kenneth Banner, W.; Duncan, S. G.; Jordan, R. D.; Yu, S.; Dai, D.; Martin, B. R.; Wiley, J. L.; Compton, D. R. *Tetrahedron* **1997,** *53,* 1557–1576.

[165] Huffman, J. W.; Duncan, S. G.; Wiley, J. L.; Martin, B. R. *Bioorganic & Medicinal Chemistry Letters* **1997,** *7,* 2799-2804.

[166] Huffman, J. W.; Liddle, J.; Duncan, S. G.; Yu, S.; Martin, B. R.; Wiley, J. L. *Bioorganic & Medicinal Chemistry* **1998,** *6,* 2383-2396.

[167] Russell, P. B.; Todd, A. R.; Wilkinson, S.; Macdonald, A. D.; Woolfe, G. *Journal of the Chemical Society* **1941,** 826-829.

[168] Papahatjis, D. P.; Nikas, S. P.; Andreou, T.; Makriyannis, A. *Bioorganic & Medicinal Chemistry Letters* **2002,** *12,* 3583-3586.

[169] Papahatjis, D. P.; Nikas, S. P.; Kourouli, T.; Chari, R.; Xu, W.; Pertwee, R. G.; Makriyannis, A. *Journal of Medicinal Chemistry* **2003,** *46,* 3221–3229.

[170] Papahatjis, D. P.; Nahmias, V. R.; Nikas, S. P.; Andreou, T.; Alapafuja, S. O.; Tsotinis, A.; Guo, J.; Fan, P.; Makriyannis, A. *Journal of Medicinal Chemistry* **2007,** *50,* 4048–4060.

[171] Papahatjis, D. P.; Kourouli, T.; Abadji, V.; Goutopoulos, A.; Makriyannis, A. *Journal of Medicinal Chemistry* **1998,** *41,* 1195–1200.

[172] Martin, B. R.; Jefferson, R.; Winckler, R.; Wiley, J. L.; Huffman, J. W.; Crocker, P. J.; Saha, B.; Razdan, R. K. *The Journal of Pharmacology and Experimental Therapeutics* **1999,** *290,* 1065–1079.

[173] Coutts, A. A.; Brewster, N.; Ingram, T.; Razdan, R. K.; Pertwee, R. G. *British Journal of Pharmacology* **2000,** *129,* 645-652.

[174] Lu, D.; Meng, Z.; Thakur, G. A.; Fan, P.; Steed, J.; Tartal, C. L.; Hurst, D. P.; Reggio, P. H.; Deschamps, J. R.; Parrish, D. A.; George, C.; Järbe, T. U. C.; Lamb, R. J.; Makriyannis, A. *Journal of Medicinal Chemistry* **2005,** *48,* 4576–4585.

[175] Lu, D.; Guo, J.; Duclos, Jr, R. I.; Bowman, A. L.; Makriyannis, A. *Journal of Medicinal Chemistry* **2008,** *51,* 6393–6399.

[176] Papahatjis, D. P.; Nahmias, V. R.; Andreou, T.; Fan, P.; Makriyannis, A. *Bioorganic & Medicinal Chemistry Letters* **2006,** *16,* 1616-1620.

[177] Huffman, J. W.; Yu, S. *Bioorganic & Medicinal Chemistry* **1998,** *6,* 2281-2288.

[178] Khanolkar, A. D.; Lu, D.; Fan, P.; Tian, X.; Makriyannis, A. *Bioorganic & Medicinal Chemistry Letters* **1999,** *9,* 2119-2124.

[179] Hua, T.; Vemuri, K.; Nikas, S. P.; Wu, Y.; Qu, L.; Pu, M.; Korde, A.; Jiang, S.; Ho, J.-H.; Han, G. W.; Ding, K.; Li, X.; Liu, H.; Hanson, M. A.; Zhao, S.; Bohn, L. M.; Makriyannis, A.; Stevens, R. C.; Liu, Z.-J. *Nature* **2025,** Online ahead of print.

[180] Bergel, F.; Morrison, A. L.; Rinderknecht, H.; Todd, A. R.; Macdonald, A. D.; Woolfe, G. *Journal of the Chemical Society* **1943,** 286-287.

[181] Sharma, R.; Nikas, S. P.; Paronis, C. A.; Wood, J. T.; Halikhedkar, A.; Guo, J. J.; Thakur, G. A.; Kulkarni, S.; Benchama, O.; Raghav, J. G.; Gifford, R. S.; Järbe, T. U. C.; Bergman, J.; Makriyannis, A. *Journal of Medicinal Chemistry* **2013,** *56,* 10142–10157.

[182] Griffin, G.; Williams, S.; Aung, M. M.; Razdan, R. K.; Martin, B. R.; Abood, M. E. *British Journal of Pharmacology* **2001,** *132,* 525-535.

[183] Singer, M.; Ryan, W. J.; Saha, B.; Martin, B. R.; Razdan, R. K. *Journal of Medicinal Chemistry* **1998,** *41,* 4400–4407.

[184] Charalambous, A.; Lin, S.; Marciniak, G.; Banijamali, A.; Friend, F.; Compton, D.; Martin, B.; Makriyannis, A. *Pharmacology Biochemistry and Behavior* **1991,** *40,* 509-512.

[185] Nikas, S. P.; Grzybowska, J.; Papahatjis, D. P.; Charalambous, A.; Banijamali, A. R.; Chari, R.; Fan, P.; Kourouli, T.; Lin, S.; Nitowski, A. J.; Marciniak, G.; Guo, Y.; Li, X.; Wang, C.-L. J.; Makriyannis, A. *The AAPS Journal* **2004,** *6,* 30.

[186] Griffin, G.; Wray, E. J.; Martin, B. R.; Abood, M. E. *British Journal of Pharmacology* **1999,** *128,* 684-688.

[187] Martin, B. R.; Wiley, J. L.; Beletskaya, I.; Sim-Selley, L. J.; Smith, F. L.; Dewey, W. L.; Cottney, J.; Adams, J.; Baker, J.; Hill, D.; Saha, B.; Zerkowski, J.; Mahadevan, A.; Razdan, R. K. *The Journal of Pharmacology and Experimental Therapeutics* **2006,** *318,* 1230-1239.

[188] Huffman, J. W.; Liddle, J.; Yu, S.; Aung, M. M.; Abood, M. E.; Wiley, J. L.; Martin, B. R. *Bioorganic & Medicinal Chemistry* **1999,** *7,* 2905-2914.

[189] Gareau, Y.; Dufresne, C.; Gallant, M.; Rochette, C.; Sawyer, N.; Slipetz, D. M.; Tremblay, N.; Weech, P. K.; Metters, K. M.; Labelle, M. *Bioorganic & Medicinal Chemistry Letters* **1996,** *6,* 189-194.

[190] Matsumoto, K.; Stark, P.; Meister, R. G. *Journal of Medicinal Chemistry* **1977,** *20,* 17–24.

[191] Adams, R.; Smith, C. M.; Loewe, S. *Journal of the American Chemical Society* **1941,** *63,* 1973–1976.

[192] Loev, B.; Bender, P. E.; Dowalo, F.; Macko, E.; Fowler, P. J. *Journal of Medicinal Chemistry* **1973,** *16,* 1200–1206.

[193] Matsumoto, K.; Stark, P.; Meister, R. G. *Journal of Medicinal Chemistry* **1977,** *20,* 25–30.

[194] Mechoulam, R.; Edery, H. Structure activity relationships in the cannabinoid series. In *Marijuana Chemistry, Pharmacology, Metabolism, and Clinical Effects*, 1 ed.; Academic Press: **1973**.

[195] Consroe, P.; Martin, A. R.; Fish, B. S. *Journal of Medicinal Chemistry* **1982,** *25,* 596–599.

[196] Weissman, A.; Milne, G. M.; Melvin, L. S. *The Journal of Pharmacology and Experimental Therapeutics* **1982,** *223,* 516-523.

[197] Auwärter, V.; Dresen, S.; Weinmann, W.; Müller, M.; Pütz, M.; Ferreirós, N. *Journal of Mass Spectrometry* **2009,** *44,* 832-837.

[198] Glass, M.; Faull, R.; Dragunow, M. *Neuroscience* **1997,** *77,* 299-318.

[199] Huffman, J. W.; Kenneth Banner, W.; Zoorob, G. K.; Howard Joyner, H.; Reggio, P. H.; Martin, B. R.; Compton, D. R. *Tetrahedron* **1995,** *51,* 1017-1032.

[200] Mechoulam, R.; Ben-Zvi, Z.; Varconi, H.; Samuelov, Y. *Tetrahedron* **1973,** *29,* 1615-1619.

[201] Rosati, O.; Messina, F.; Pelosi, A.; Curini, M.; Petrucci, V.; Gertsch, J.; Chicca, A. *European Journal of Medicinal Chemistry* **2014,** *85,* 77-86.

[202] Arnone, A.; Merlini, L.; Servi, S. *Tetrahedron* **1975,** *31,* 3093-3096.

[203] Srebnik, M.; Lander, N.; Breuer, A.; Mechoulam, R. *Journal of the Chemical Society, Perkin Transactions 1* **1984,** 2881-2886.

[204] Adams, R.; Cain, C. K.; Loewe, S. *Journal of the American Chemical Society* **1941,** *63,* 1977–1978.

[205] Mechoulam, R.; Lander, N.; Varkony, T. H.; Kimmel, I.; Becker, O.; Ben-Zvi, Z.; Edery, H.; Porath, G. *Journal of Medicinal Chemistry* **1980,** *23,* 1068–1072.

[206] Wilson, R. S.; May, E. L.; Martin, B. R.; Dewey, W. L. *Journal of Medicinal Chemistry* **1976,** *19,* 1165–1167.

[207] Lemberger, L.; Rowe, H. *Clinical Pharmacology & Therapeutics* **1975,** *18,* 720-726.

[208] Adams, R.; Loewe, S.; Theobald, C. W.; Smith, C. M. *Journal of the American Chemical Society* **1942,** *64,* 2653–2655.

[209] Russell, P. B.; Todd, A. R.; Wilkinson, S.; Macdonald, A. D.; Woolfe, G. *Journal of the Chemical Society* **1941,** 169-172.

[210] Razdan, R. K.; Handrick, G. R.; Dalzell, H. C.; Howes, J. F.; Winn, M.; Plotnikoff, N. P.; Dodge, P. W.; Dren, A. T. *Journal of Medicinal Chemistry* **1976,** *19,* 552–554.

[211] Razdan, R. K.; Zitko Terris, B.; Handrick, G. R.; Dalzell, H. C.; Pars, H. G.; Howes, J. F.; Plotnikoff, N. P.; Dodge, P. W.; Dren, A. T. *Journal of Medicinal Chemistry* **1976,** *19,* 549–551.

[212] Pars, H. G.; Granchelli, F. E.; Razdan, R. K.; Keller, J. K.; Teiger, D. G.; Rosenberg, F. J.; Harris, L. S. *Journal of Medicinal Chemistry* **1976,** *19,* 445–454.

[213] Martin, B. R.; Harris, L. S.; Dewey, W. L. Pharmacological Activity of Delta-9-THC Metabolites and Analogs of CBD, Delta-8-THC, and Delta-9-THC. In *The Cannabinoids: Chemical, Pharmacologic, and Therapeutic Aspects*, 1 ed.; Academic Press: **1984**.

[214] Appendino, G.; Minassi, A.; Taglialatela-Scafati, O. *Natural Product Reports* **2014,** *31,* 880-904.

[215] Cannaert, A.; Sparkes, E.; Pike, E.; Luo, J. L.; Fang, A.; Kevin, R. C.; Ellison, R.; Gerona, R.; Banister, S. D.; Stove, C. P. *ACS Chemical Neuroscience Journal* **2020,** *11,* 4434–4446.

[216] Razdan, R. K. Structure–Activity Relationships of Classical Cannabinoids. In *The Cannabinoid Receptors*; Reggio, P. H., Ed.; Humana Press: Totowa, NJ, **2009**.

[217] Thomas, B. F.; Compton, D. R.; Martin, B. R. *The Journal of Pharmacology and Experimental Therapeutics* **1990,** *255,* 624-630.

[218] Marshall, W. P.; Logan, B. K. *Journal of Analytical Toxicology* **2004,** *28,* 299.

[219] Christophersen, A. S. *Journal of Analytical Toxicology* **1986,** *10,* 129-131.

[220] Ujváry, I.; Christie, R.; Evans-Brown, M.; Gallegos, A.; Jorge, R.; de Morais, J.; Sedefov, R. *ACS Chemical Neuroscience* **2021,** *12,* 1072–1092.

[221] Westwell, A. D.; Caldicott, D. G. E.; Hutchings, A. *Future Medicinal Chemistry* **2012,** *4,* 129–132.

[222] Wiley, J. L.; Marusich, J. A.; Huffman, J. W.; Balster, R. L.; Thomas, B. F. *RTI International* **2011,** *2011,* 17971.

[223] Nichols, D. *Nature* **2011,** *469,* 7–7.

Supplementary Information

Isolation and characterization of synthesis intermediates and byproducts in hexahydrocannabiphorol (HHCP)

Willi Schirmer[1, 2], Ilche Gjuroski[2], Martina Vermathen[2], Julien Furrer[2], Stefan Schürch[2], Wolfgang Weinmann[1]

[1]Institute of Forensic Medicine, Forensic Toxicology and Chemistry, University of Bern, Murtenstrasse 26, 3008 Bern, Switzerland

[2]Department of Chemistry, Biochemistry and Pharmaceutical Sciences, University of Bern, Freiestrasse 3, 3012 Bern, Switzerland

Corresponding author:

Willi Schirmer, Institute of Forensic Medicine, Forensic Toxicology and Chemistry, University of Bern, Murtenstrasse 26, 3008 Bern, Switzerland

e-mail address: willi.schirmer@irm.unibe.ch

NMR (^{1}H-NMR, ^{1}H-^{1}H-COSY, ^{1}H-^{13}C-HSQC, ^{1}H-^{13}C-HMBC, ^{1}H-^{1}H-NOESY)

GC-MS

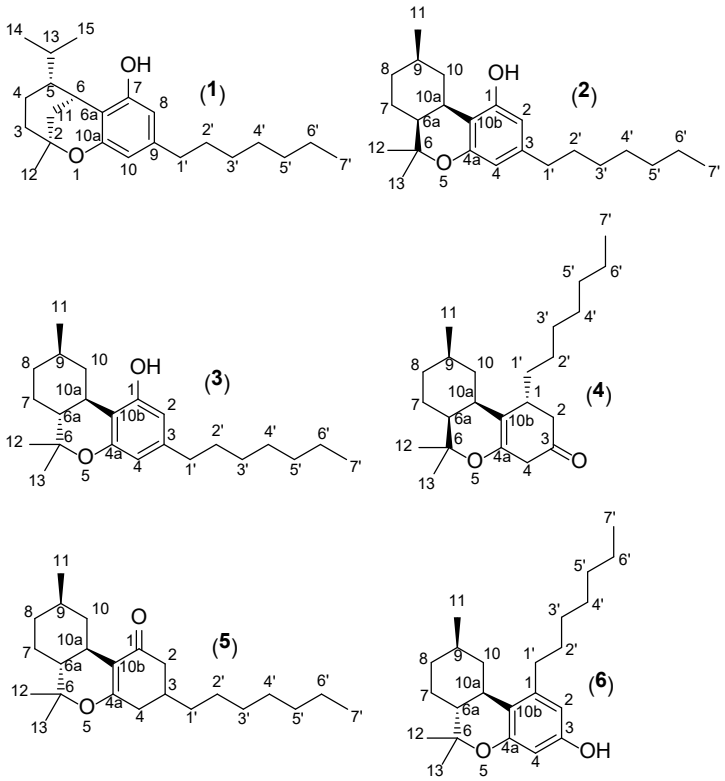

Compound **1**: *rel*-(2*S*,5*R*,6*S*)-9-heptyl-5-isopropyl-2-methyl-3,4,5,6-tetrahydro-2*H*-2,6-methanobenzo[*b*]oxocin-7-ol (*iso*-HHCP)

Compound **2**: *rel*-(6a*S*,9*R*,10a*R*)-3-heptyl-6,6,9-trimethyl-6a,7,8,9,10,10a-hexahydro-6H-benzo[*c*]chromen-1-ol (*cis*-HHCP)

Compound **3**: *rel*-(6a*R*, 9R, 10a*R*)-6,6,9-trimethyl-3-heptyl-6a,7,8,9,10,10a-hexahydrobenzo[*c*]chromen-1-ol ((9*R*)-HHCP)

Compound **4**: *rel*-(1*R*,6a*S*,9*R*,10a*R*)-1-heptyl-6,6,9-trimethyl-2,3,4,6,6a,7,8,9,10,10a-decahydro-1*H*-benzo[*c*]chromen-3-one (precursor to *cis-abn*-HHCP)

Compound **5**: *rel*-(6a*R*,9*R*,10a*R*)-3-heptyl-6,6,9-trimethyl-2,3,4,6,6a,7,8,9,10,10a-decahydro-1*H*-benzo[*c*]chromen-1-one (precursor to (9*R*)-HHCP)

Compound **6**: *rel*-(6a*S*,9*R*,10a*S*)-1-heptyl-6,6,9-trimethyl-6a,7,8,9,10,10a-hexahydro-6*H*-benzo[*c*]chromen-3-ol (precursor to *ortho*-HHCP)

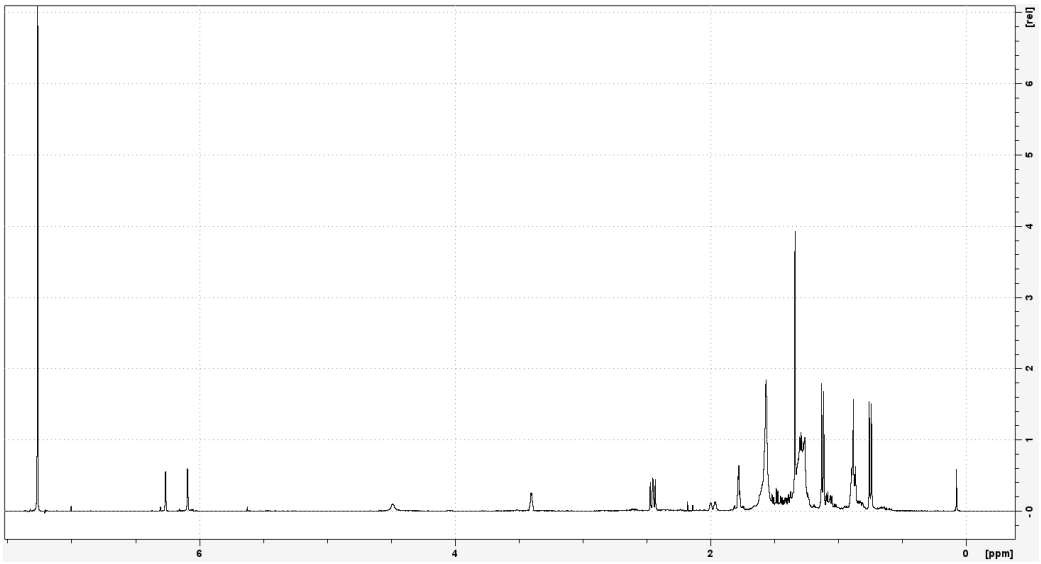

S1: ^{1}H-NMR of Compound **1**. Recorded at 400.33 MHz in $CDCl_3$.

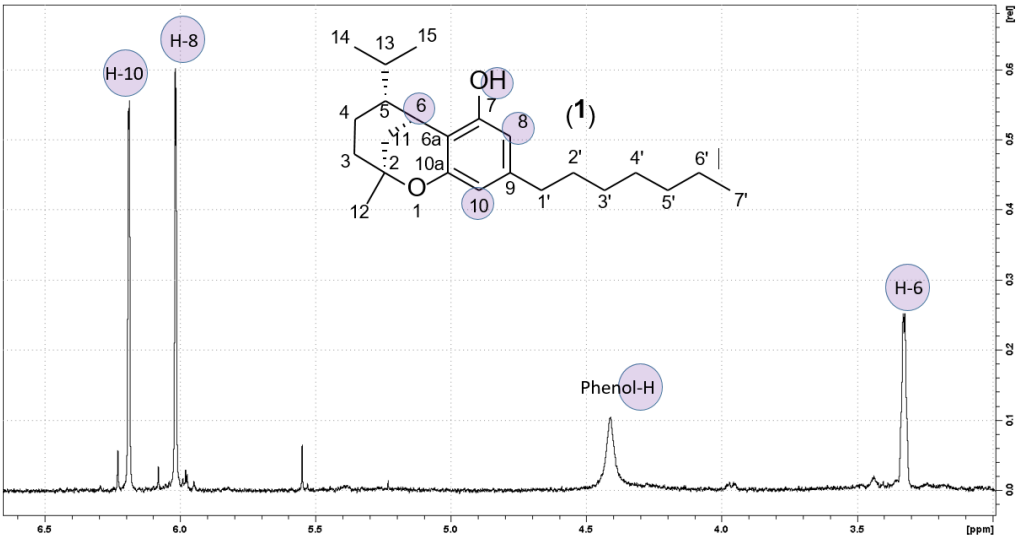

S2: ^{1}H-NMR of Compound **1**, detailed view. Recorded at 400.33 MHz in $CDCl_3$.

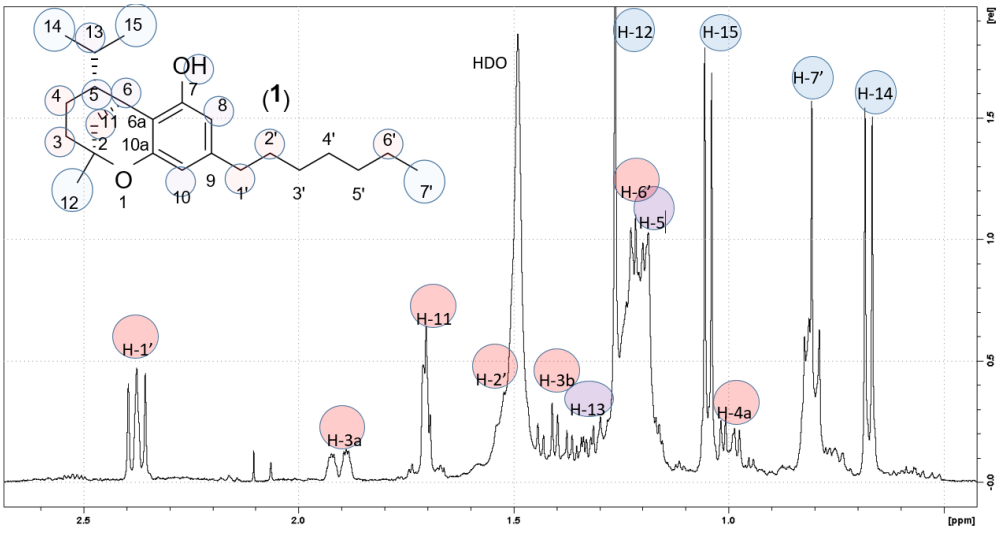

S3: ^{1}H-NMR of Compound **1**, detailed view. Recorded at 400.33 MHz in $CDCl_3$.

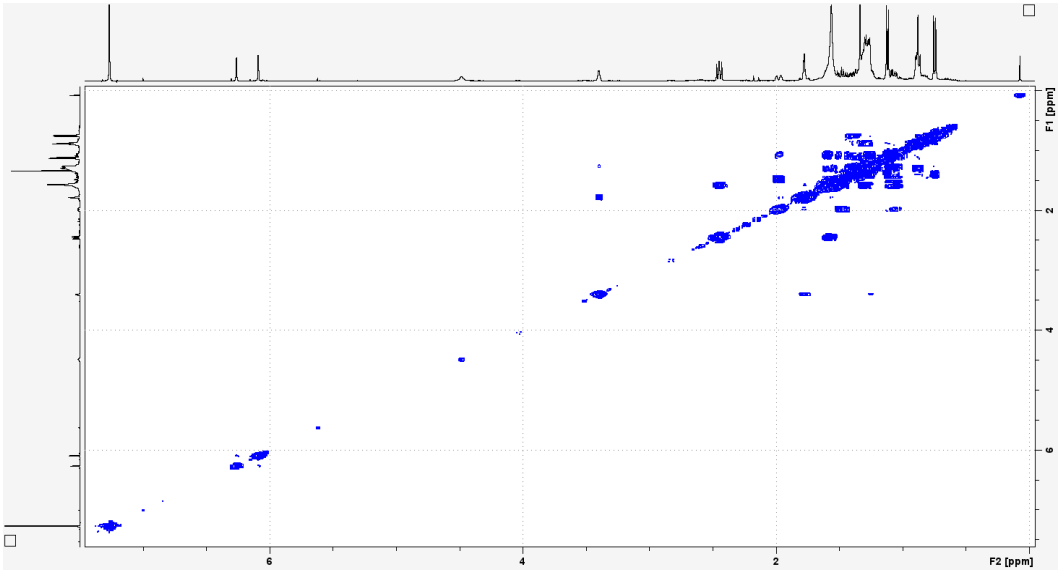

S4: ^{1}H-^{1}H-COSY of Compound **1**. Recorded at 400.33 MHz in $CDCl_3$.

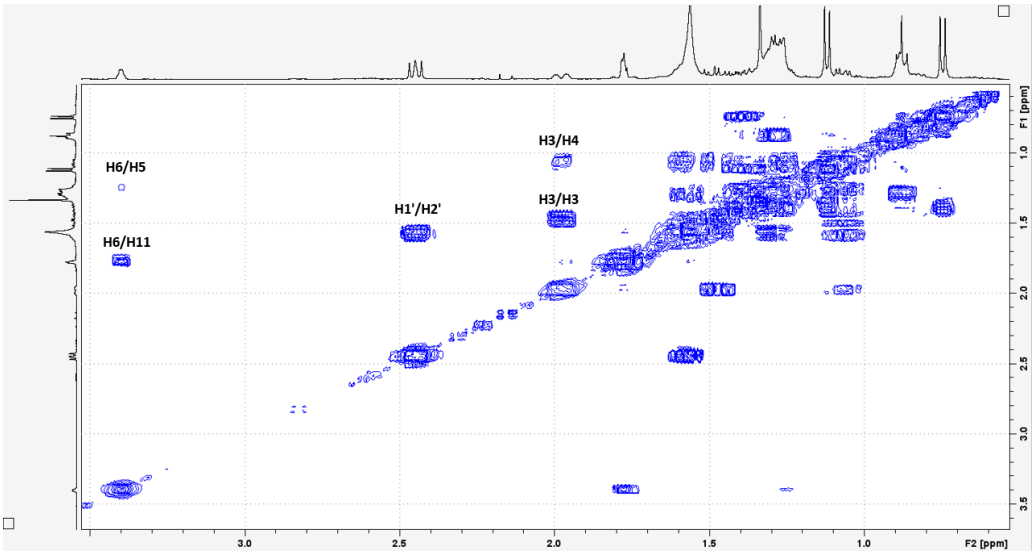

S5: ^{1}H-^{1}H-COSY of Compound **1**, detailed view. Recorded at 400.33 MHz in $CDCl_3$.

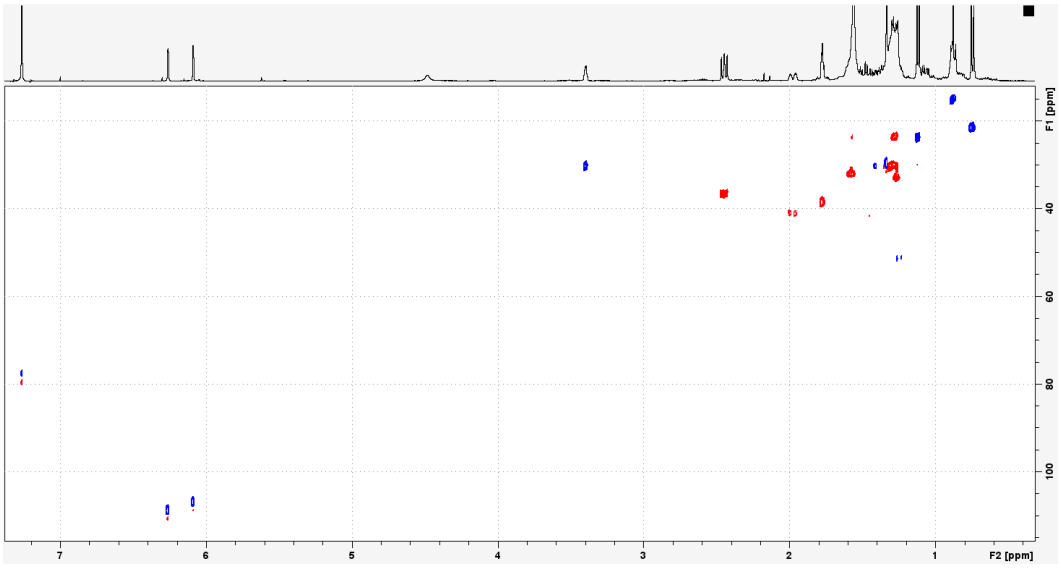

S6: ^{1}H-^{13}C-HSQC of Compound **1**. Recorded at 400.33 MHz in $CDCl_3$.

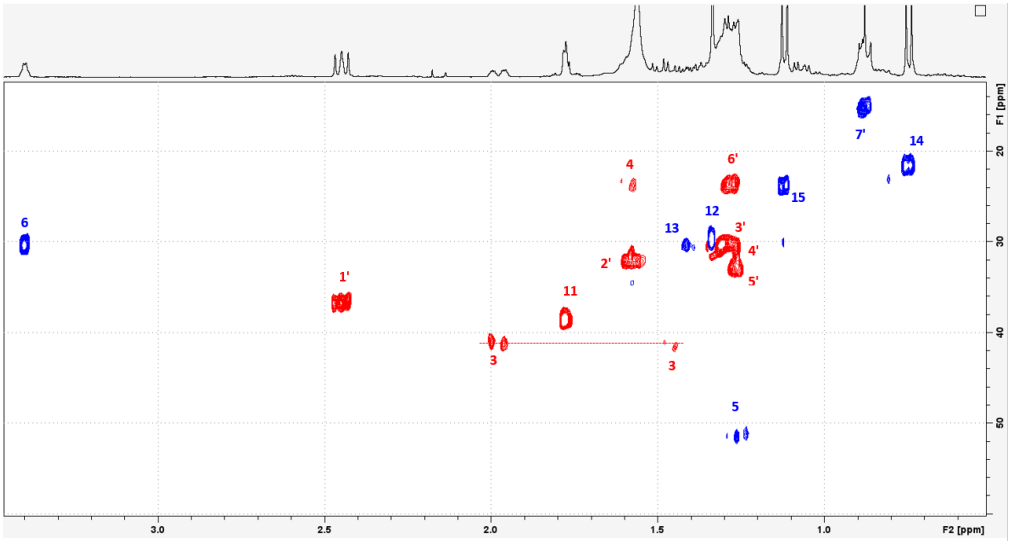

S7: ^{1}H-^{13}C-HSQC of Compound **1**, detailed view. Recorded at 400.33 MHz in $CDCl_3$.

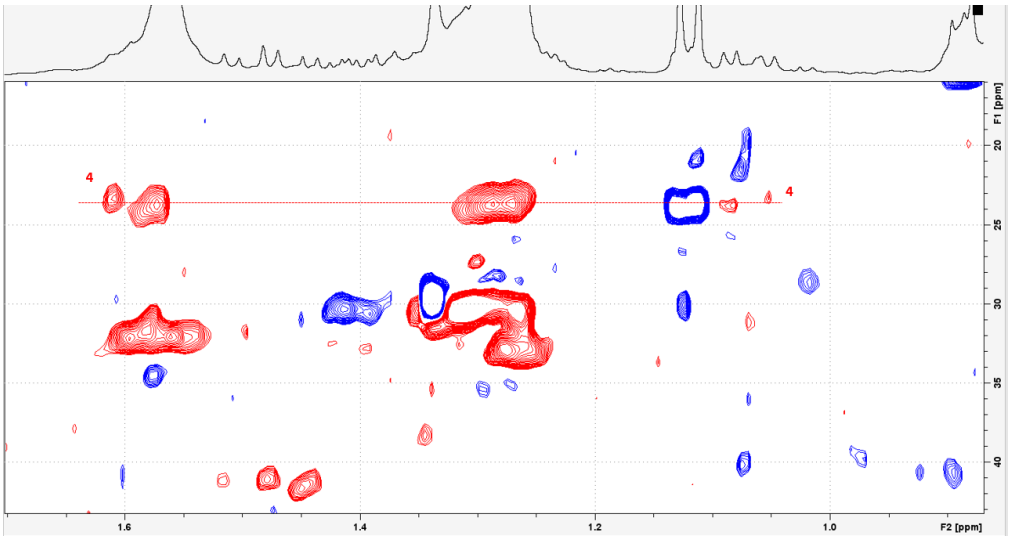

S8: ^{1}H-^{13}C-HSQC of Compound **1**, detailed view. Recorded at 400.33 MHz in $CDCl_3$.

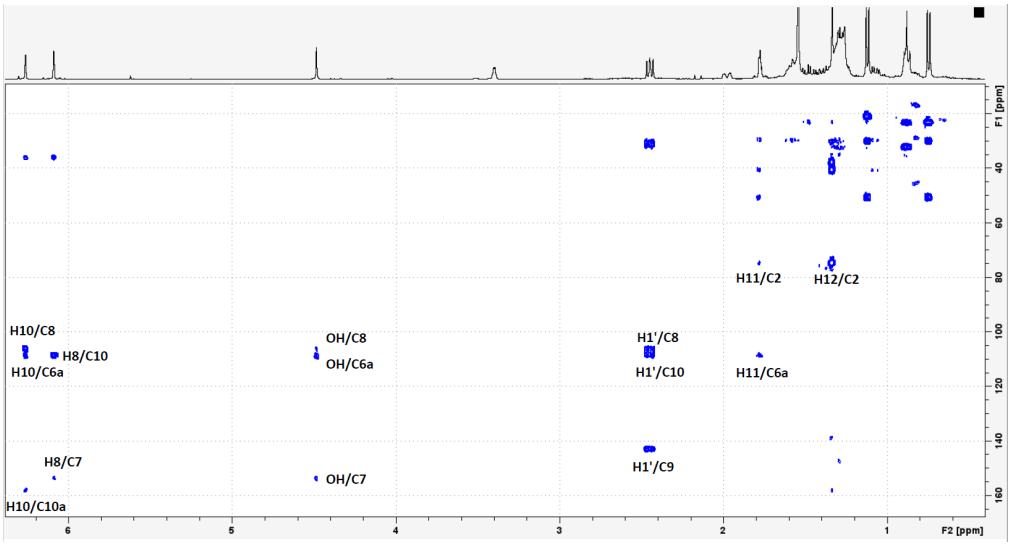

S9: ^{1}H-^{13}C-HMBC of Compound **1**. Recorded at 400.33 MHz in $CDCl_3$.

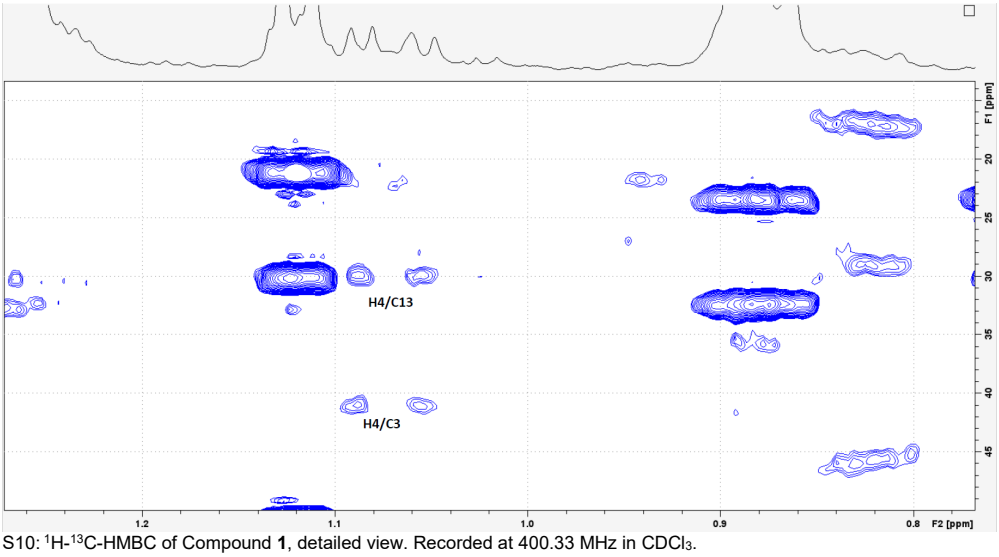

S10: ^{1}H-^{13}C-HMBC of Compound **1**, detailed view. Recorded at 400.33 MHz in $CDCl_3$.

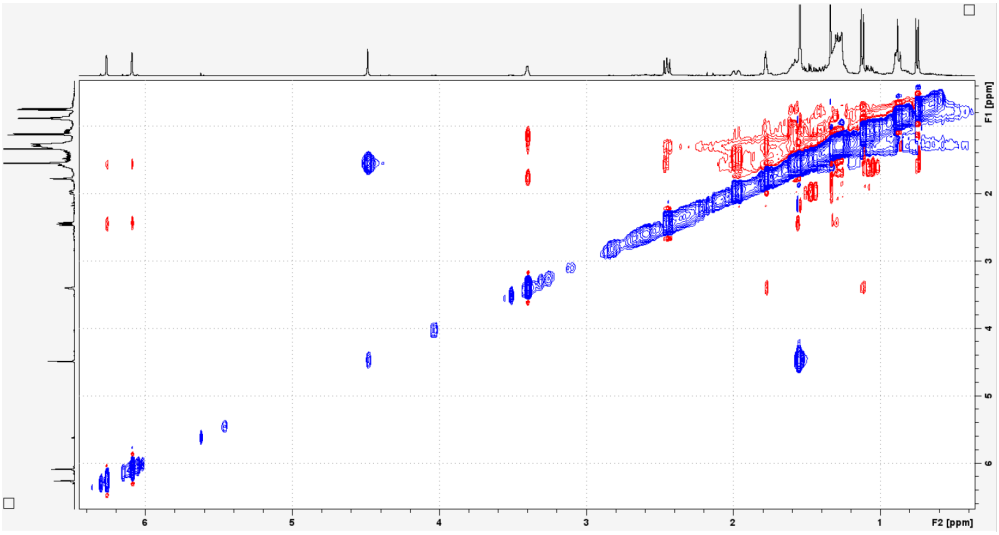

S11: NOESY of Compound **1**. Recorded at 400.33 MHz in $CDCl_3$.

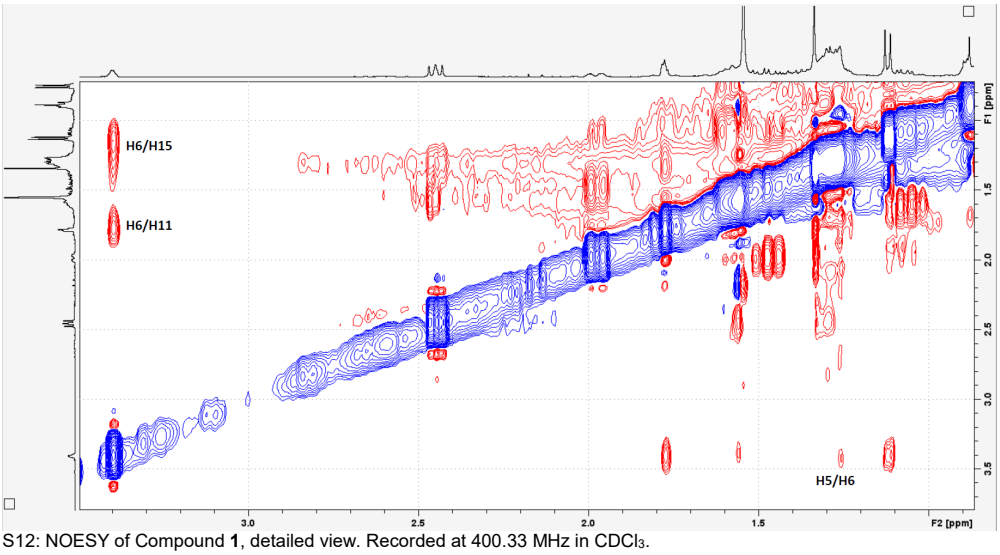

S12: NOESY of Compound **1**, detailed view. Recorded at 400.33 MHz in $CDCl_3$.

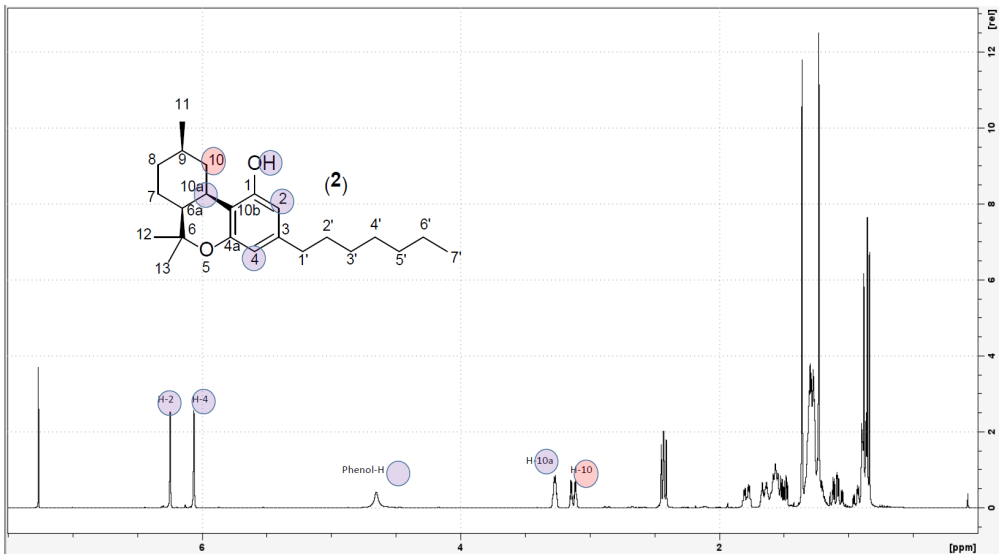

S13: ^{1}H-NMR of Compound **2**. Recorded at 400.33 MHz in $CDCl_3$.

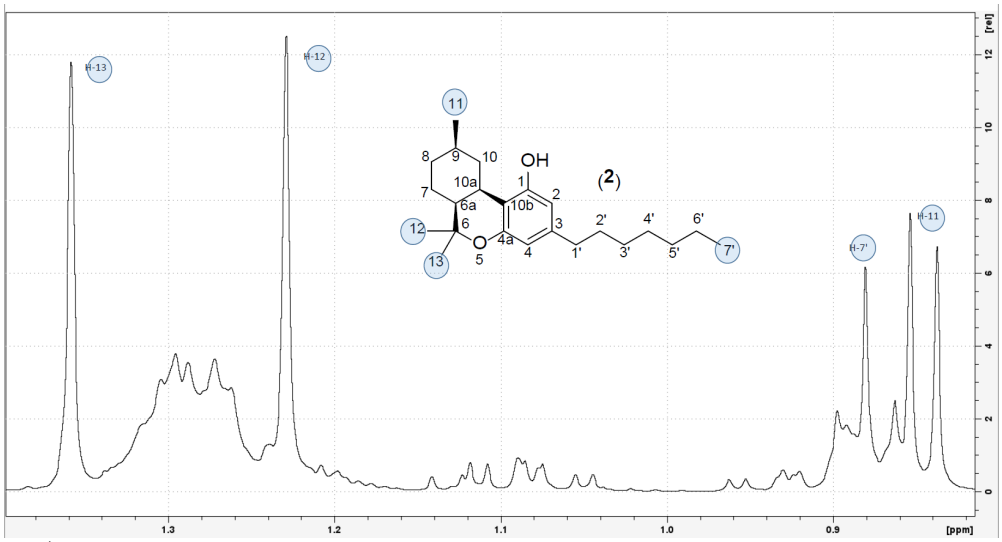

S14: ^{1}H-NMR of Compound **2**, detailed view. Recorded at 400.33 MHz in $CDCl_3$.

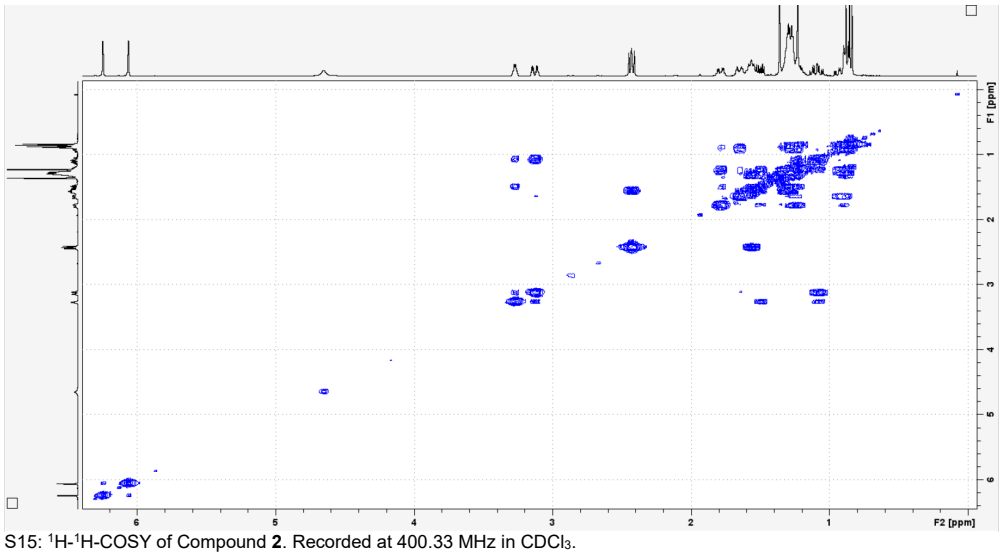

S15: ^{1}H-^{1}H-COSY of Compound **2**. Recorded at 400.33 MHz in $CDCl_3$.

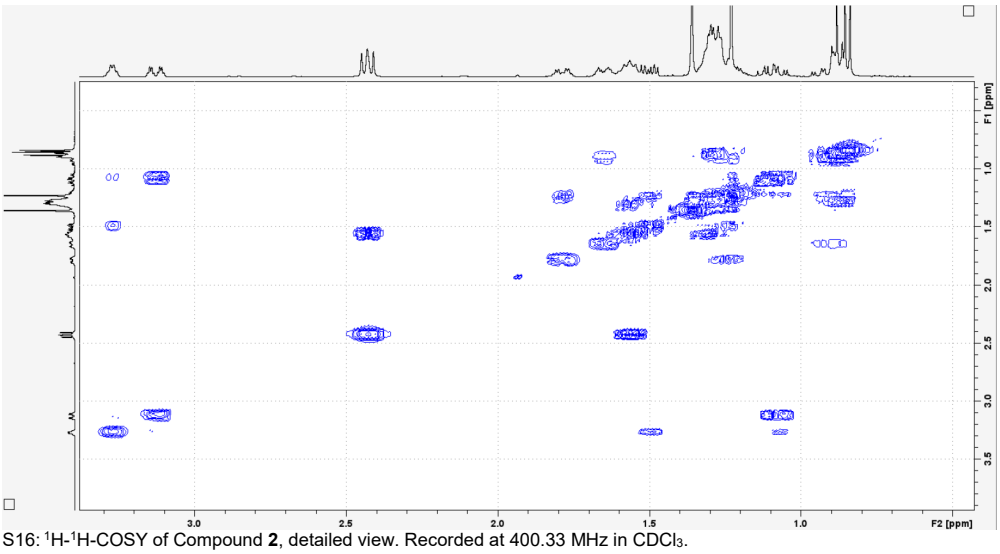

S16: ^{1}H-^{1}H-COSY of Compound **2**, detailed view. Recorded at 400.33 MHz in $CDCl_3$.

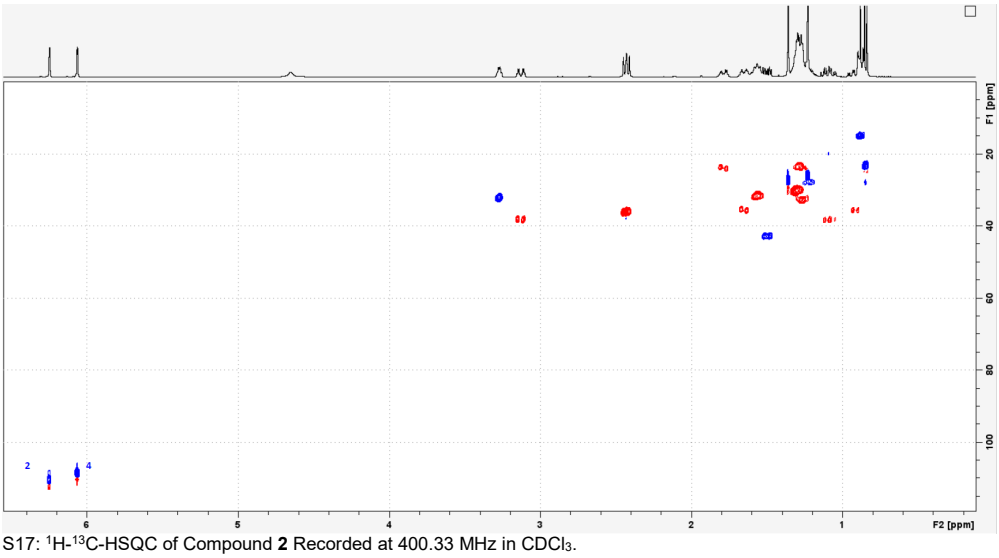

S17: ^{1}H-^{13}C-HSQC of Compound **2** Recorded at 400.33 MHz in $CDCl_3$.

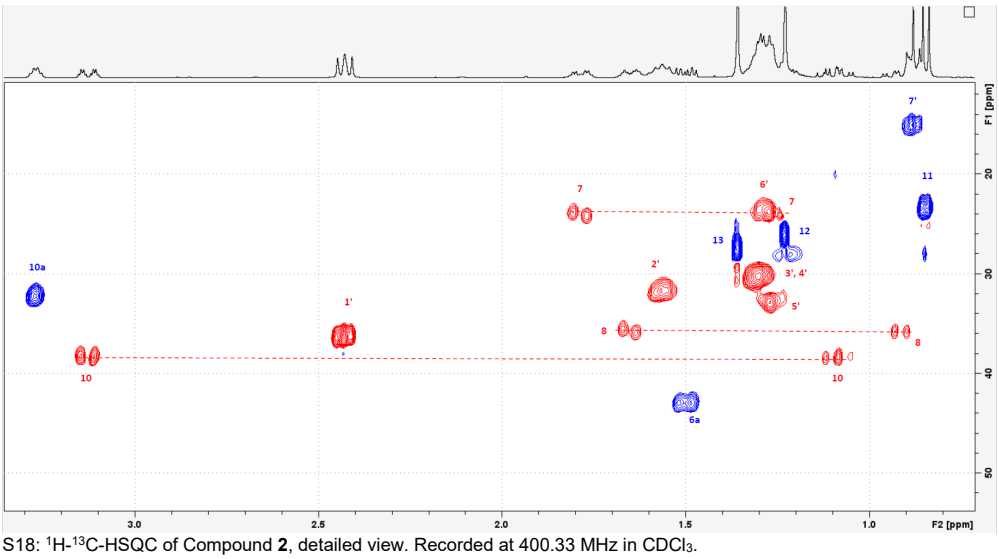

S18: ^{1}H-^{13}C-HSQC of Compound **2**, detailed view. Recorded at 400.33 MHz in $CDCl_3$.

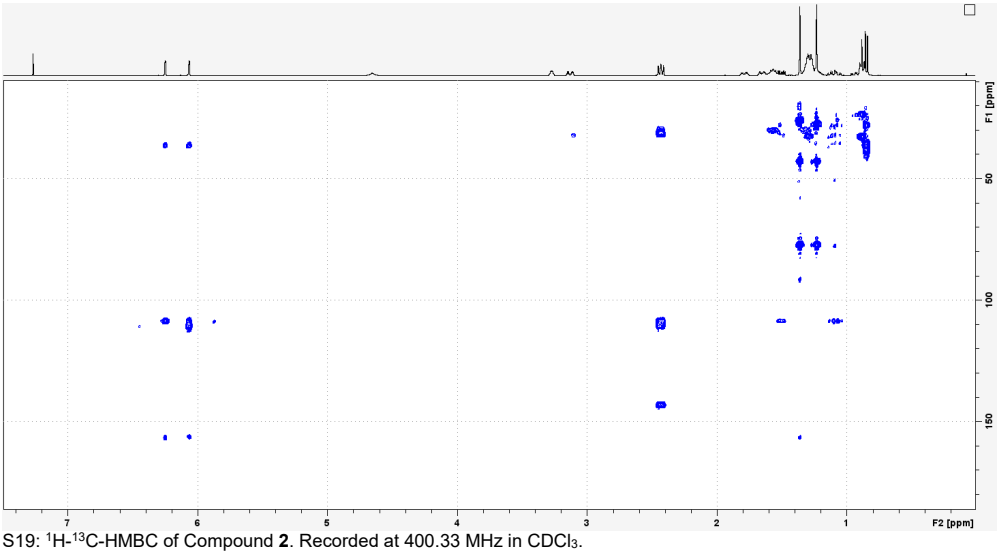

S19: ^{1}H-^{13}C-HMBC of Compound **2**. Recorded at 400.33 MHz in $CDCl_3$.

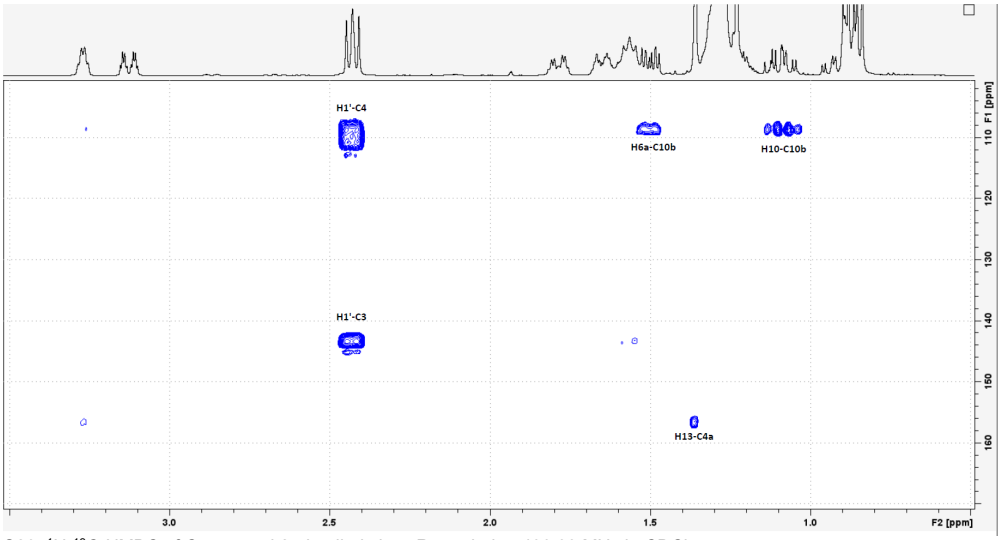

S20: ^{1}H-^{13}C-HMBC of Compound **2**, detailed view. Recorded at 400.33 MHz in $CDCl_3$.

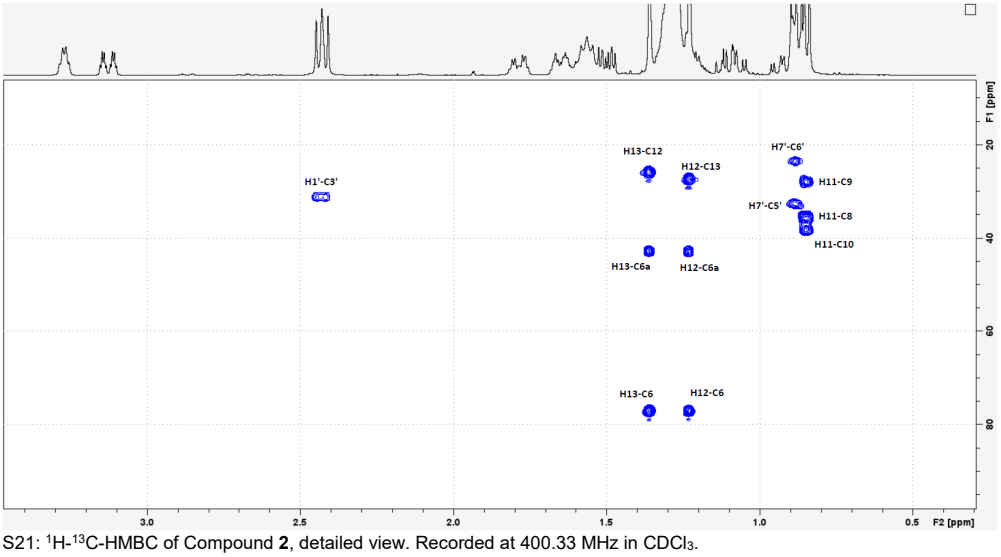

S21: ^{1}H-^{13}C-HMBC of Compound **2**, detailed view. Recorded at 400.33 MHz in $CDCl_3$.

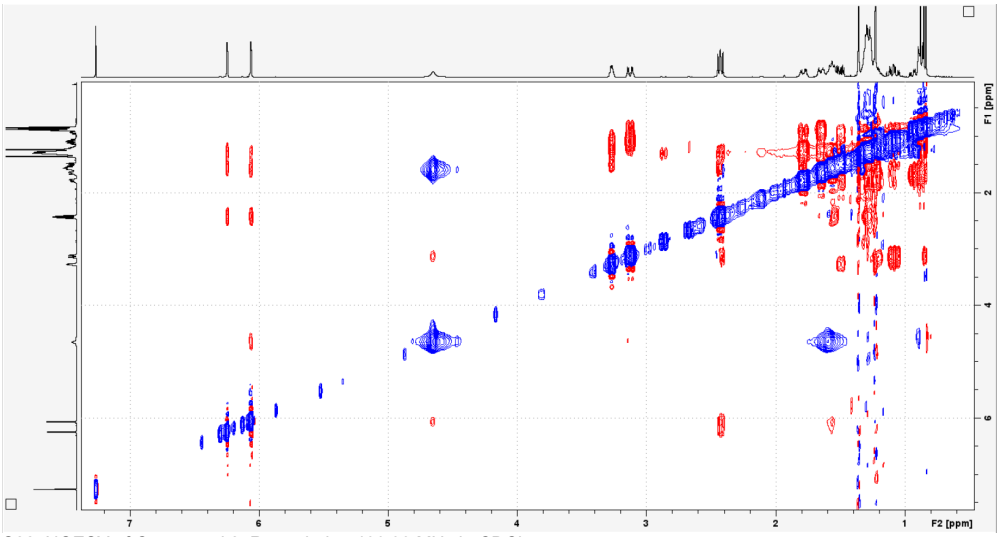

S22: NOESY of Compound **2**. Recorded at 400.33 MHz in $CDCl_3$.

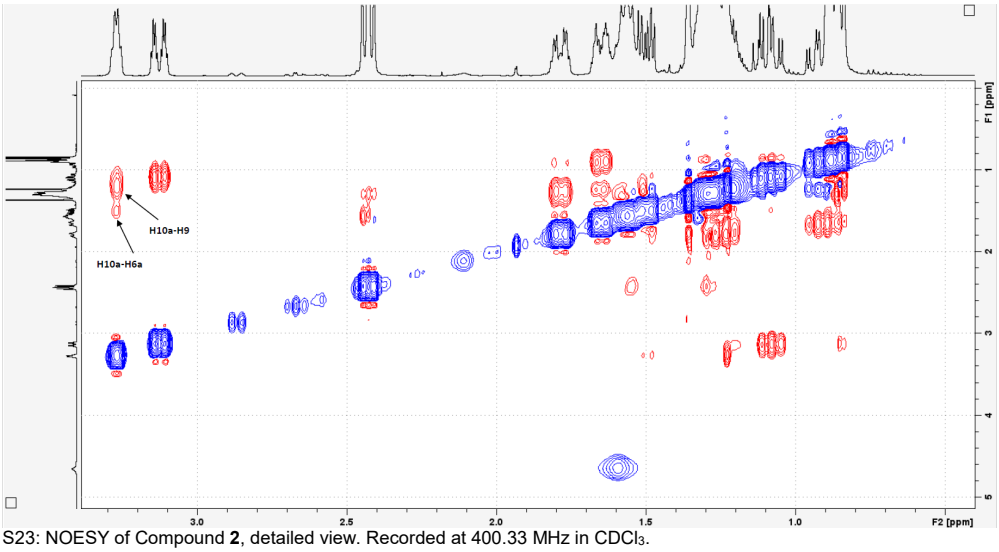

S23: NOESY of Compound **2**, detailed view. Recorded at 400.33 MHz in $CDCl_3$.

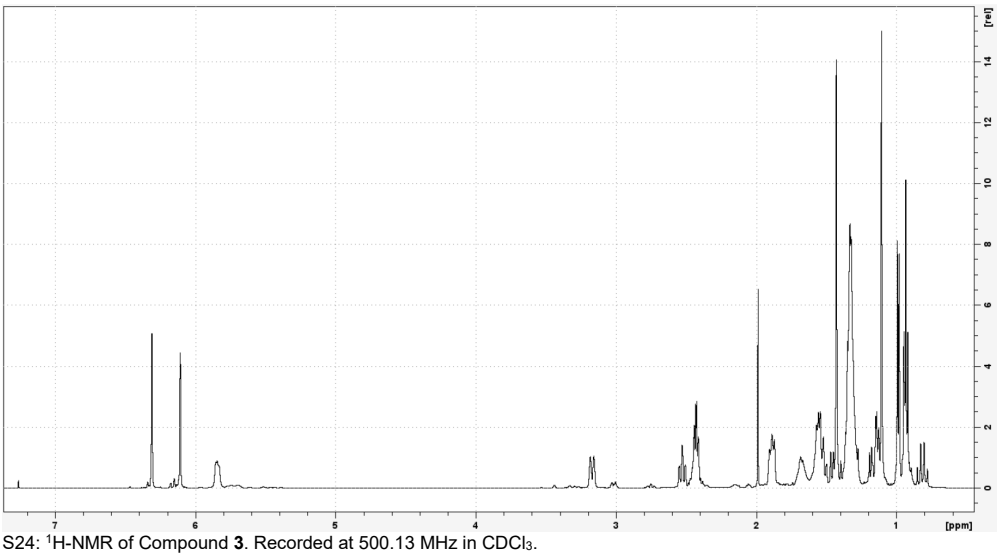

S24: ^{1}H-NMR of Compound **3**. Recorded at 500.13 MHz in $CDCl_3$.

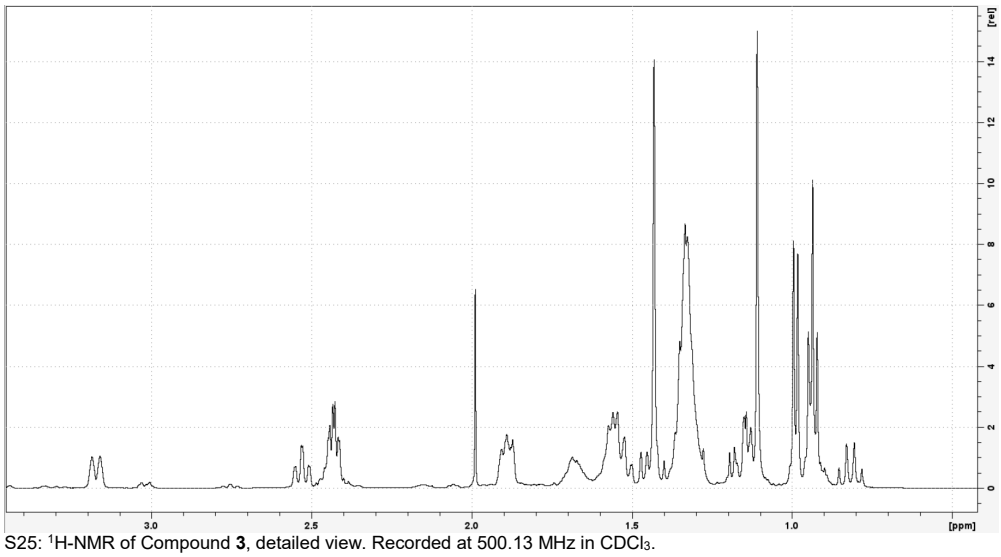

S25: ^{1}H-NMR of Compound **3**, detailed view. Recorded at 500.13 MHz in $CDCl_3$.

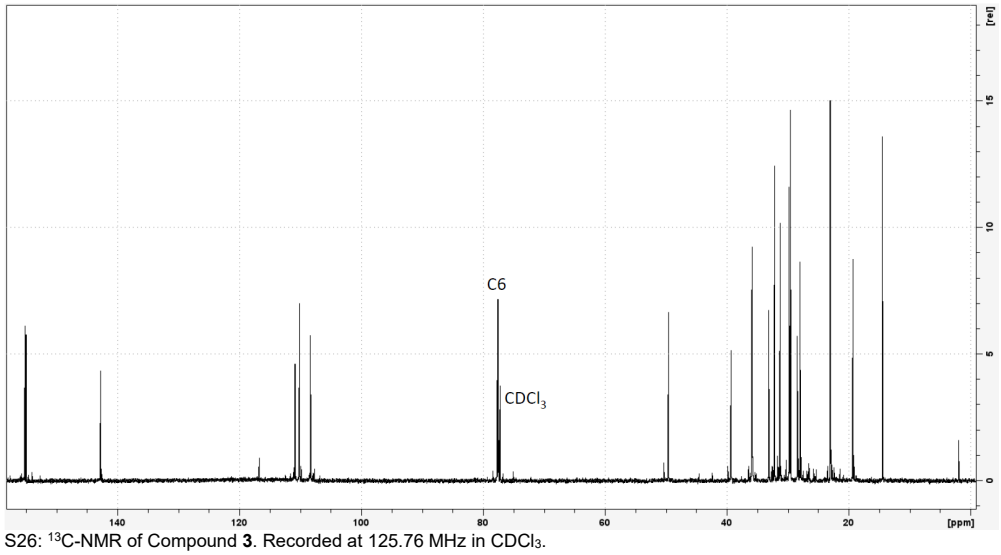

S26: ^{13}C-NMR of Compound **3**. Recorded at 125.76 MHz in $CDCl_3$.

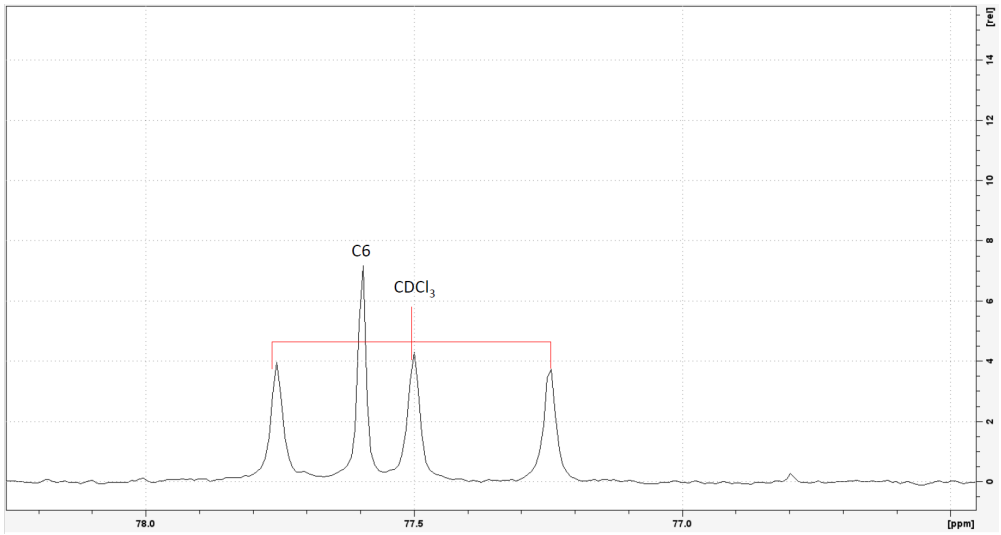

S27: ^{13}C-NMR of Compound **3**, detailed view. Recorded at 125.76 MHz in $CDCl_3$.

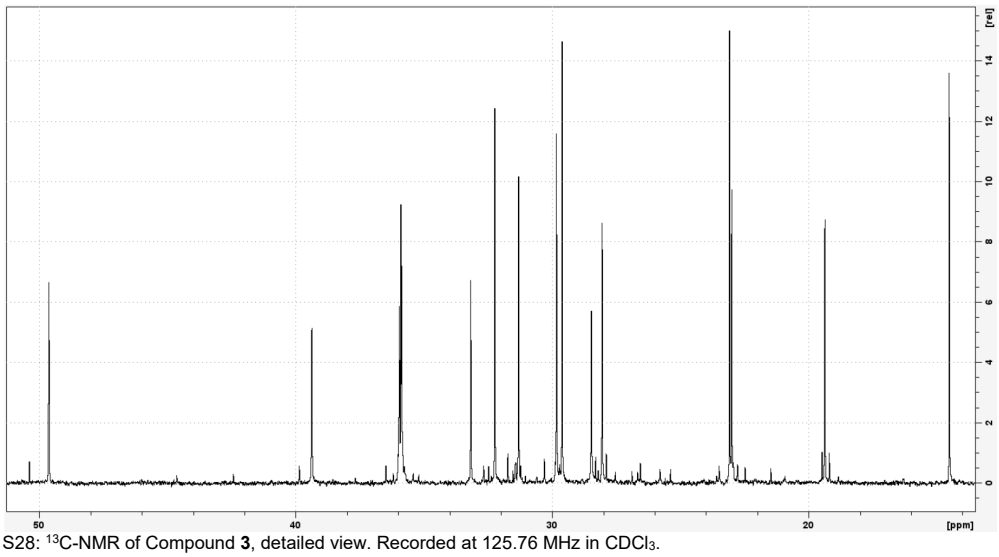

S28: ^{13}C-NMR of Compound **3**, detailed view. Recorded at 125.76 MHz in $CDCl_3$.

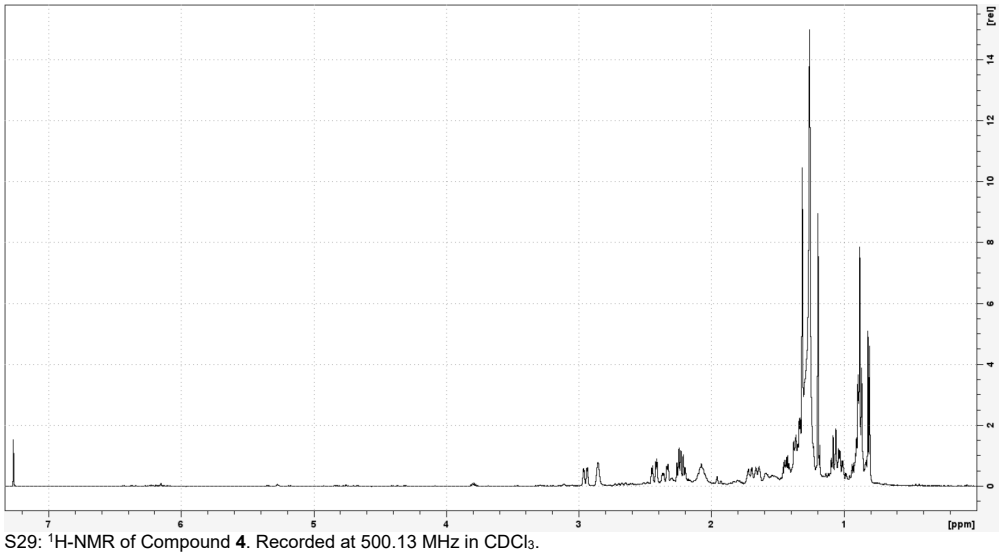

S29: ^{1}H-NMR of Compound **4**. Recorded at 500.13 MHz in $CDCl_3$.

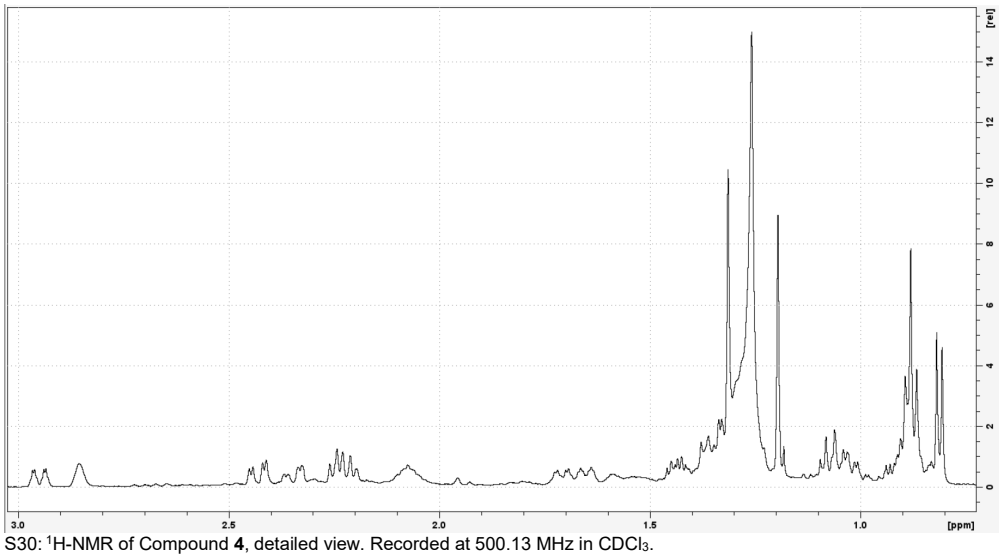

S30: ^{1}H-NMR of Compound **4**, detailed view. Recorded at 500.13 MHz in $CDCl_3$.

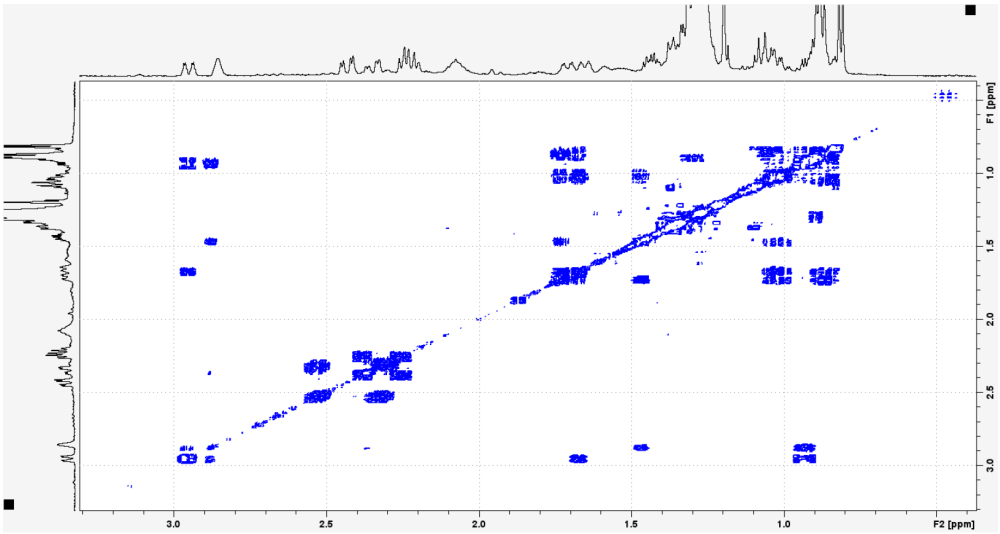

S31: ^{1}H-^{1}H-COSY of Compound **4**. Recorded at 500.13 MHz in $CDCl_3$.

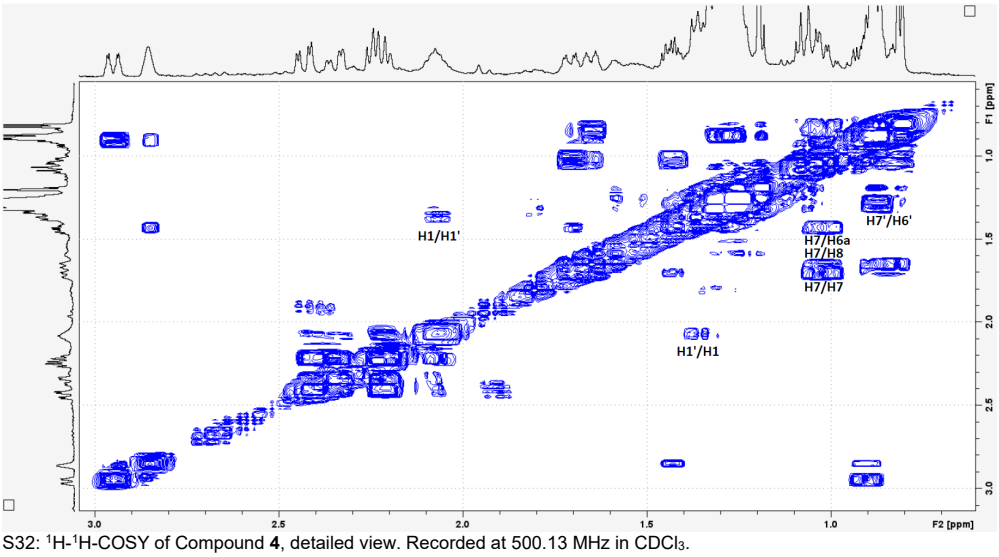

S32: ^{1}H-^{1}H-COSY of Compound **4**, detailed view. Recorded at 500.13 MHz in $CDCl_3$.

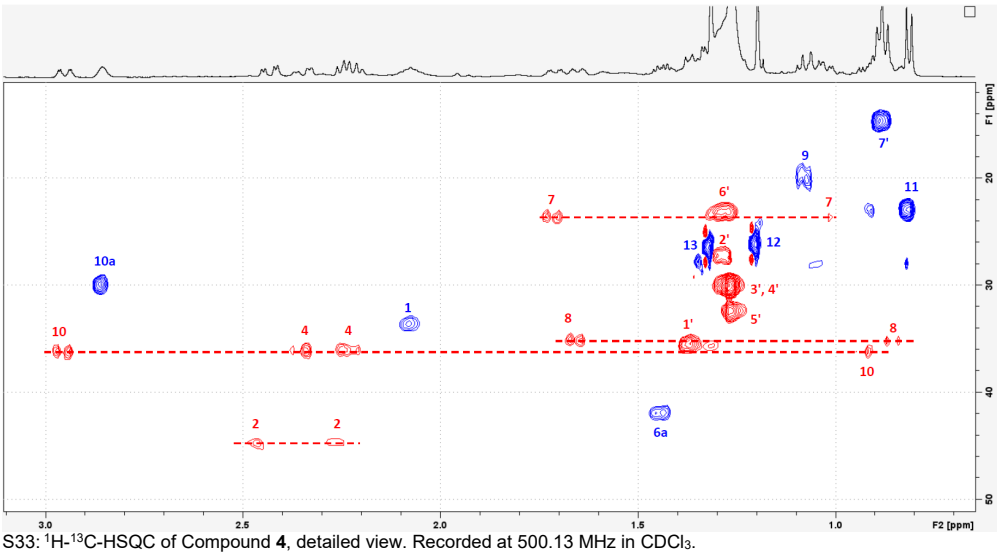

S33: ^{1}H-^{13}C-HSQC of Compound **4**, detailed view. Recorded at 500.13 MHz in $CDCl_3$.

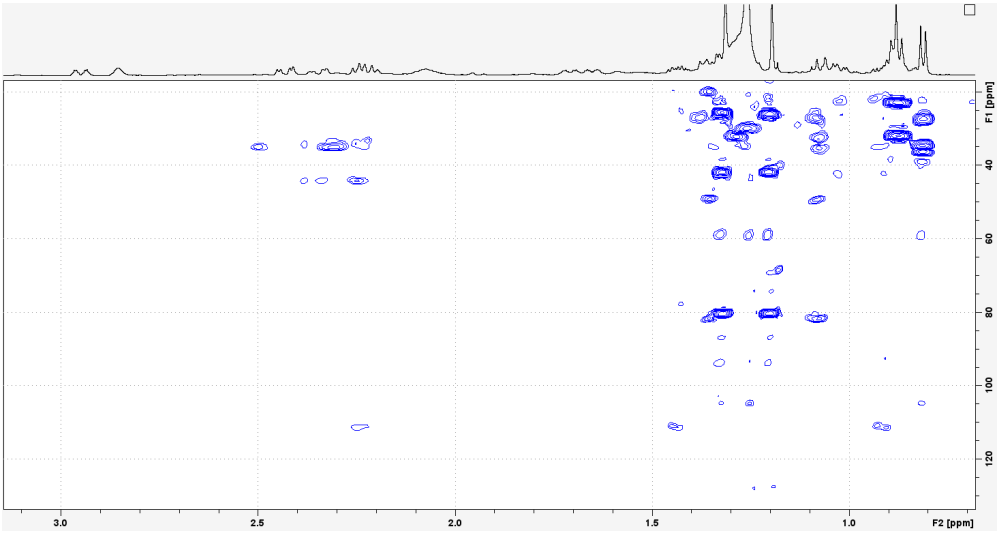

S34: ^{1}H-^{13}C-HMBC of Compound **4**. Recorded at 500.13 MHz in $CDCl_3$.

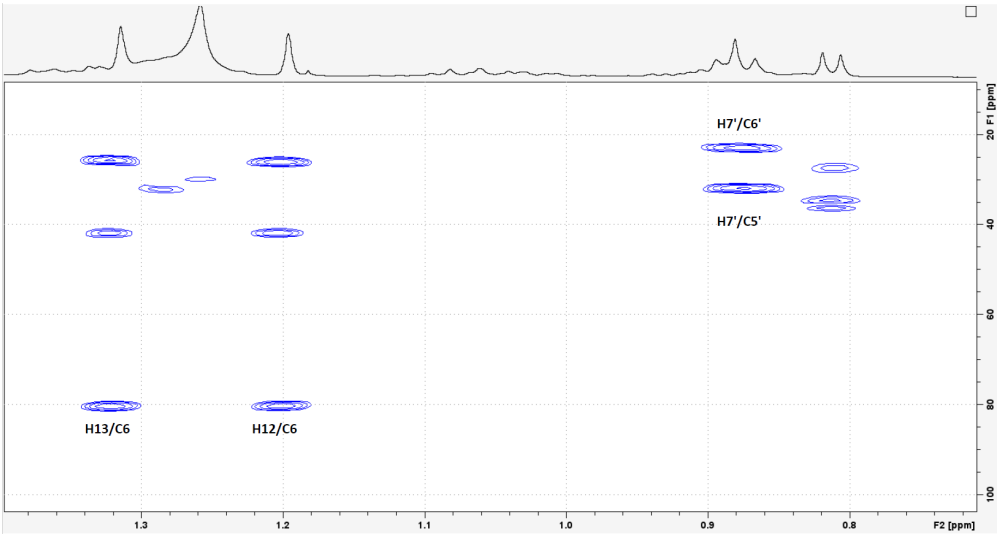

S35: ^{1}H-^{13}C-HMBC of Compound **4**, detailed view. Recorded at 500.13 MHz in $CDCl_3$.

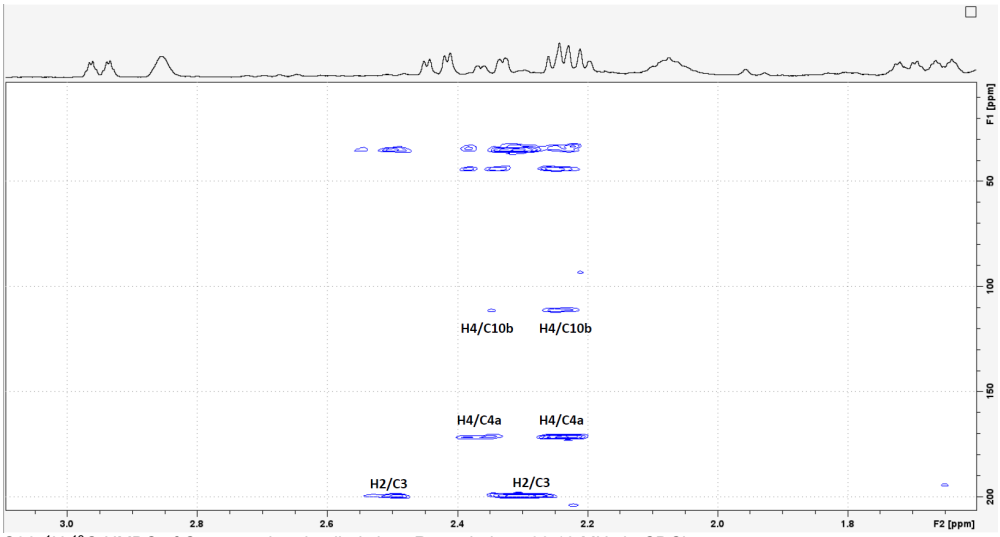

S36: ^{1}H-^{13}C-HMBC of Compound **4**, detailed view. Recorded at 500.13 MHz in $CDCl_3$.

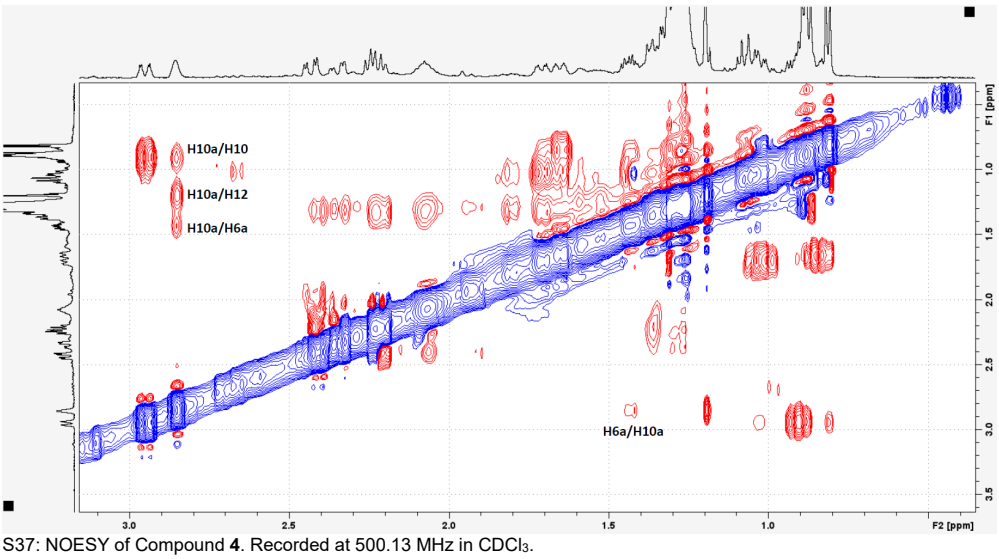

S37: NOESY of Compound **4**. Recorded at 500.13 MHz in $CDCl_3$.

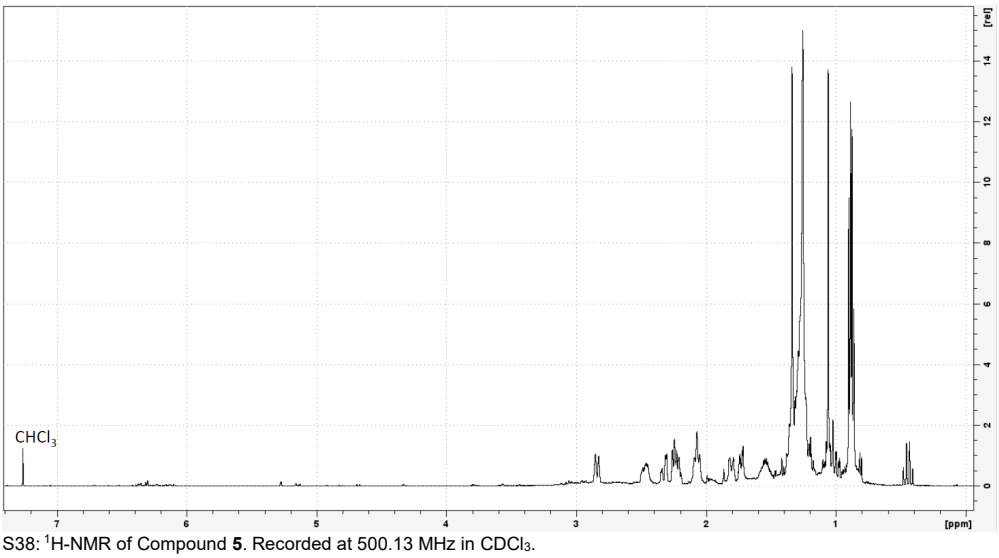

S38: ^{1}H-NMR of Compound **5**. Recorded at 500.13 MHz in $CDCl_3$.

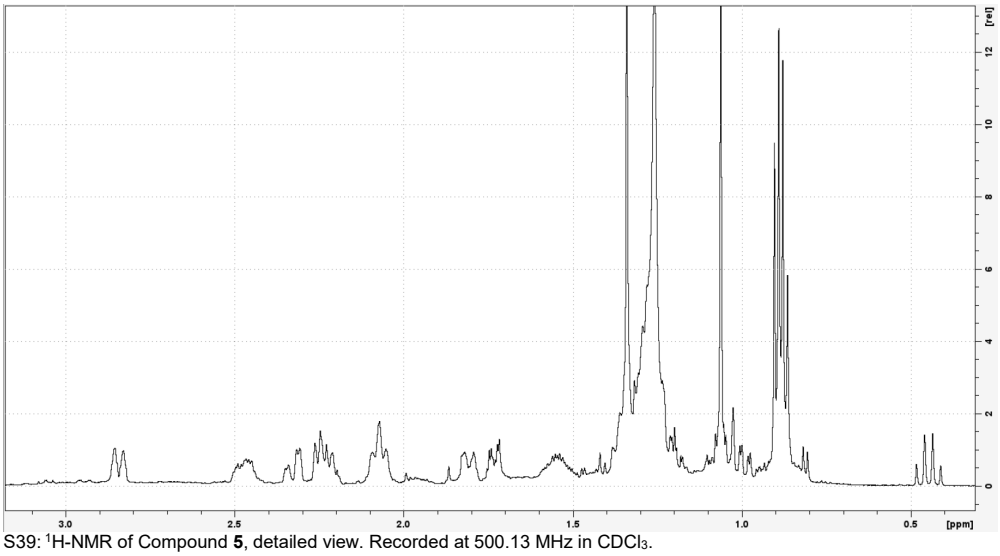

S39: ^{1}H-NMR of Compound **5**, detailed view. Recorded at 500.13 MHz in $CDCl_3$.

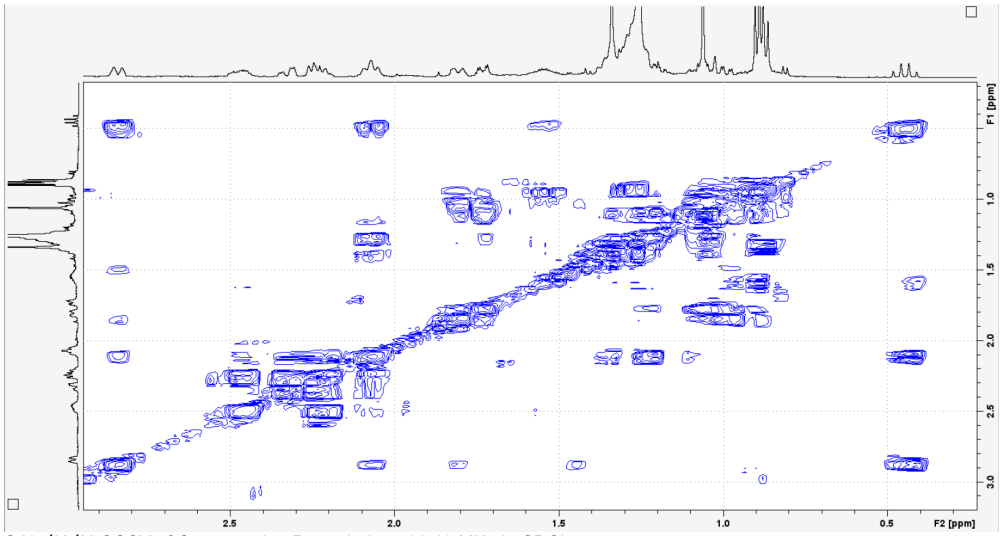

S40: ^{1}H-^{1}H-COSY of Compound **5**. Recorded at 500.13 MHz in $CDCl_3$.

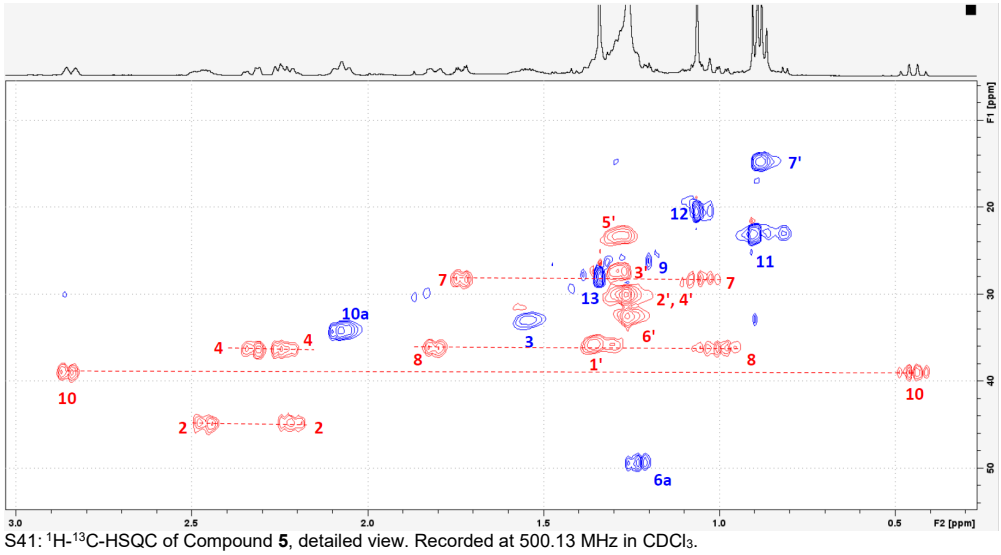

S41: ^{1}H-^{13}C-HSQC of Compound **5**, detailed view. Recorded at 500.13 MHz in $CDCl_3$.

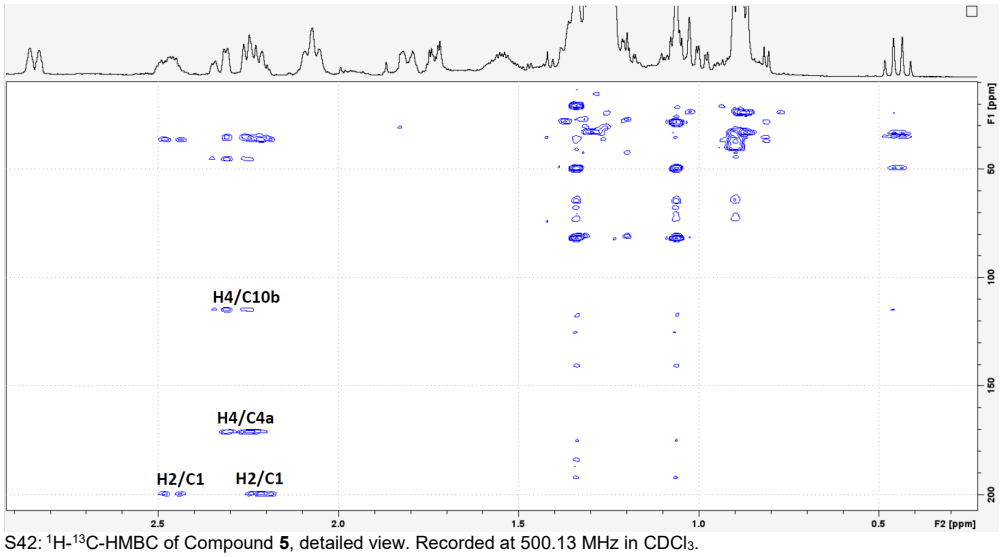

S42: ^{1}H-^{13}C-HMBC of Compound **5**, detailed view. Recorded at 500.13 MHz in $CDCl_3$.

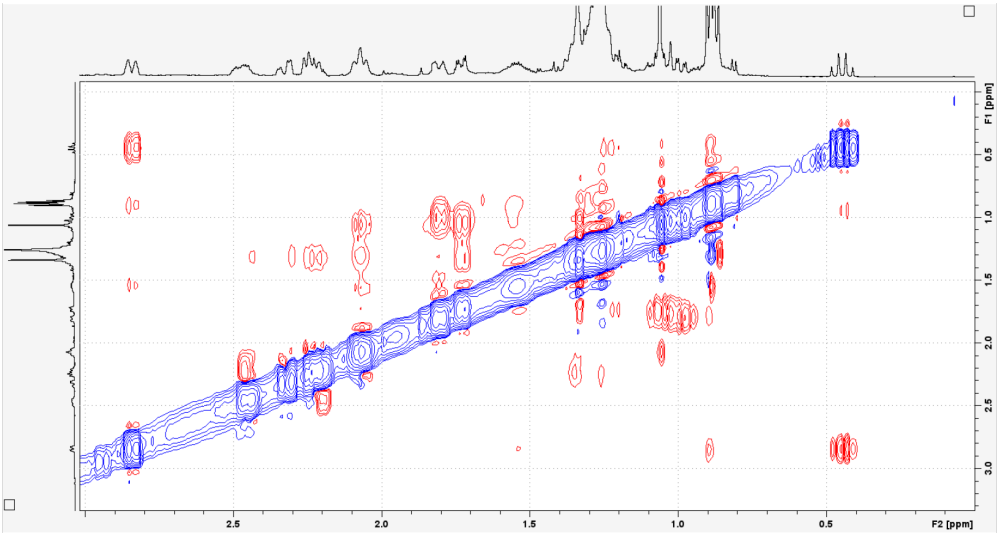

S43: NOESY of Compound **5**. Recorded at 500.13 MHz in $CDCl_3$.

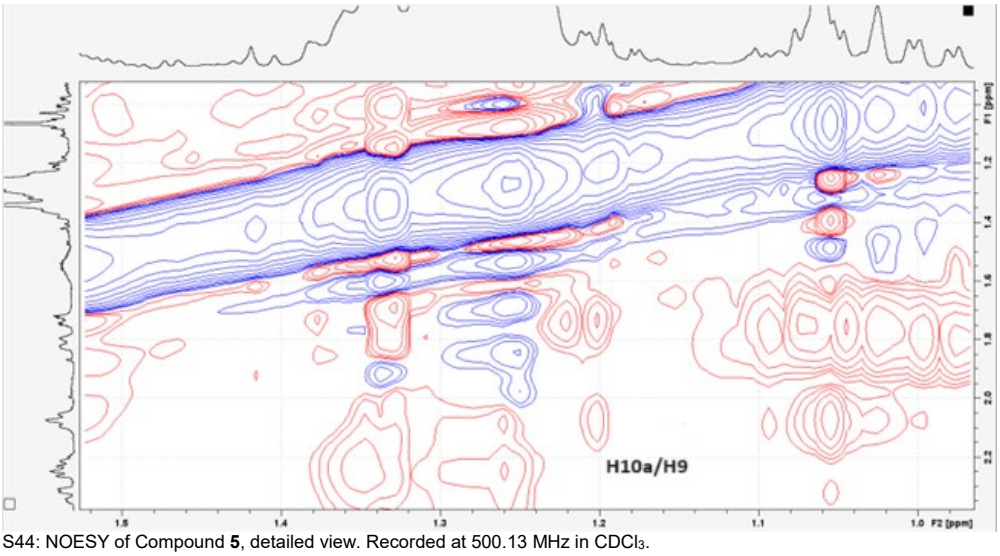

S44: NOESY of Compound **5**, detailed view. Recorded at 500.13 MHz in $CDCl_3$.

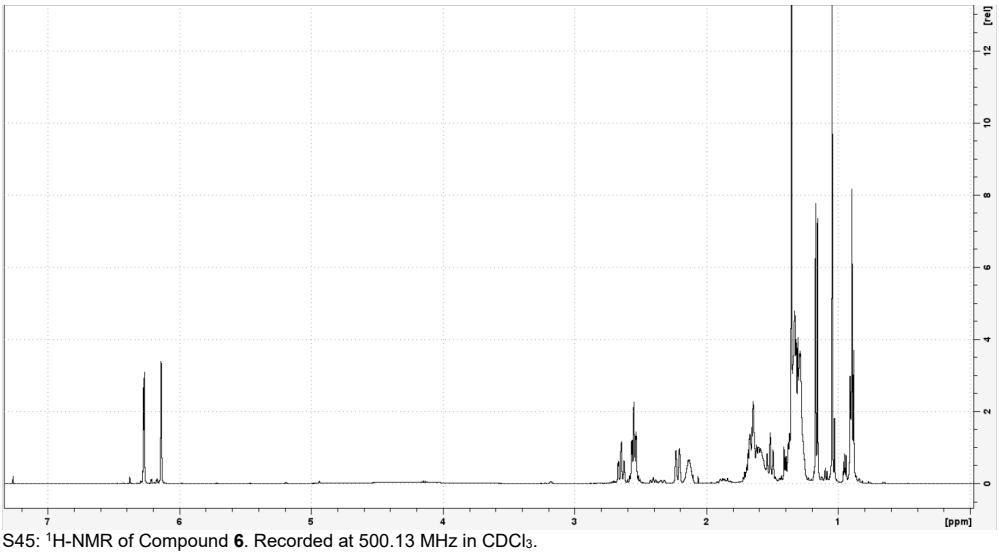

S45: ^{1}H-NMR of Compound **6**. Recorded at 500.13 MHz in $CDCl_3$.

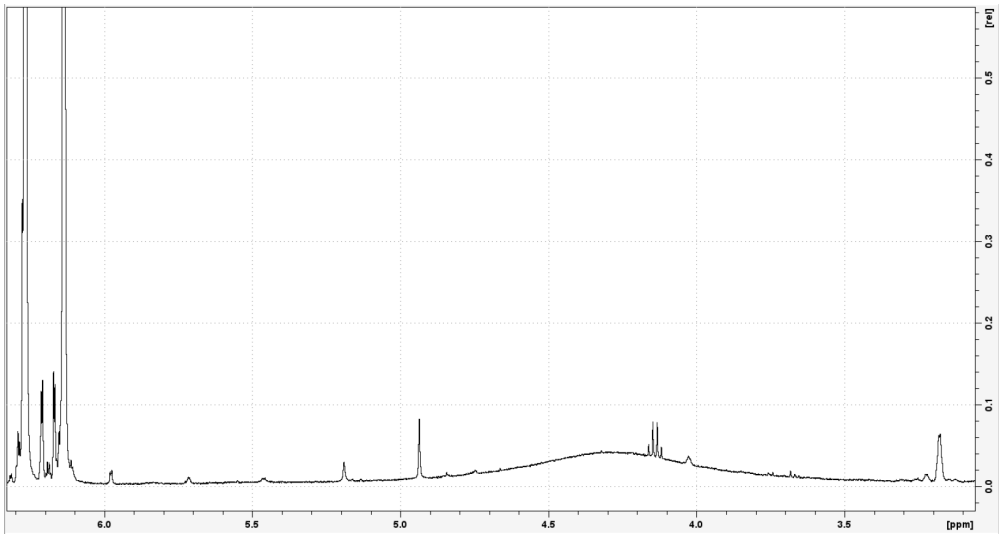

S46: ^{1}H-NMR of Compound **6**, detailed view. Recorded at 500.13 MHz in $CDCl_3$.

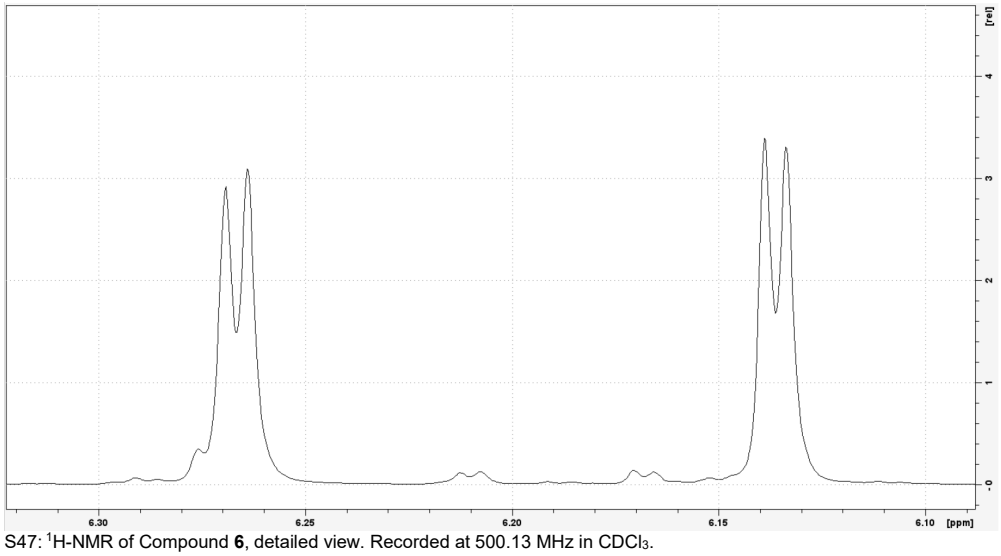

S47: ^{1}H-NMR of Compound **6**, detailed view. Recorded at 500.13 MHz in $CDCl_3$.

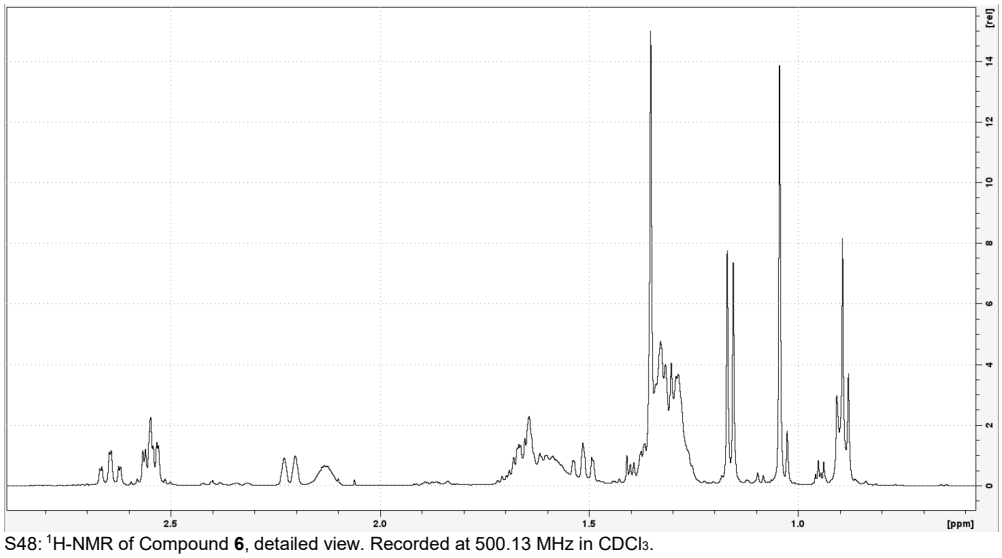

S48: ^{1}H-NMR of Compound **6**, detailed view. Recorded at 500.13 MHz in $CDCl_3$.

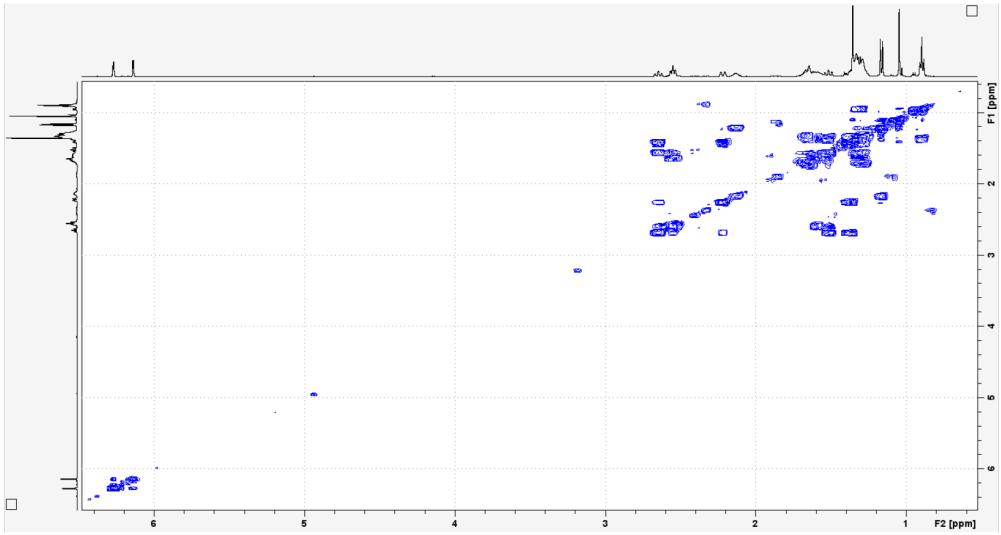

S49: ^{1}H-^{1}H-COSY of Compound **6**. Recorded at 500.13 MHz in $CDCl_3$

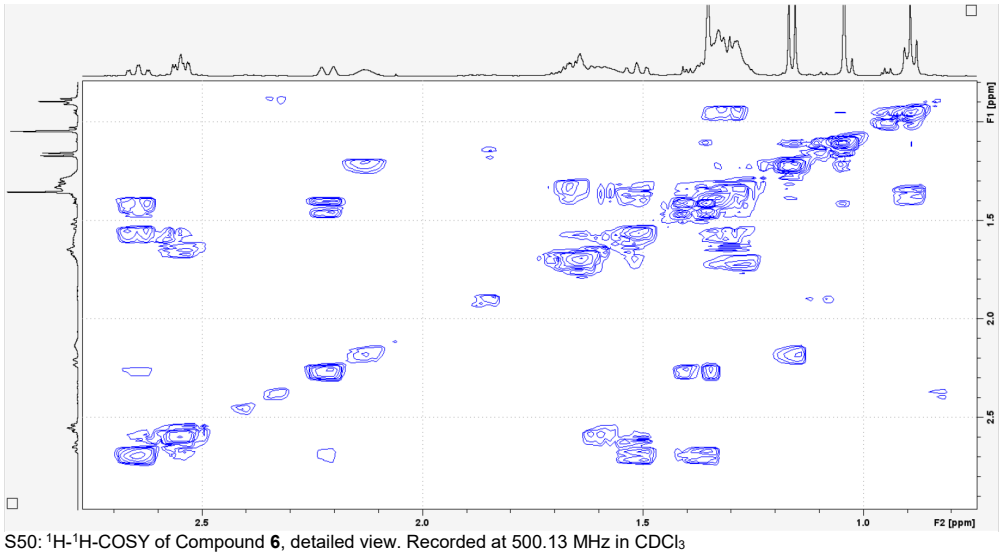

S50: ^{1}H-^{1}H-COSY of Compound **6**, detailed view. Recorded at 500.13 MHz in $CDCl_3$

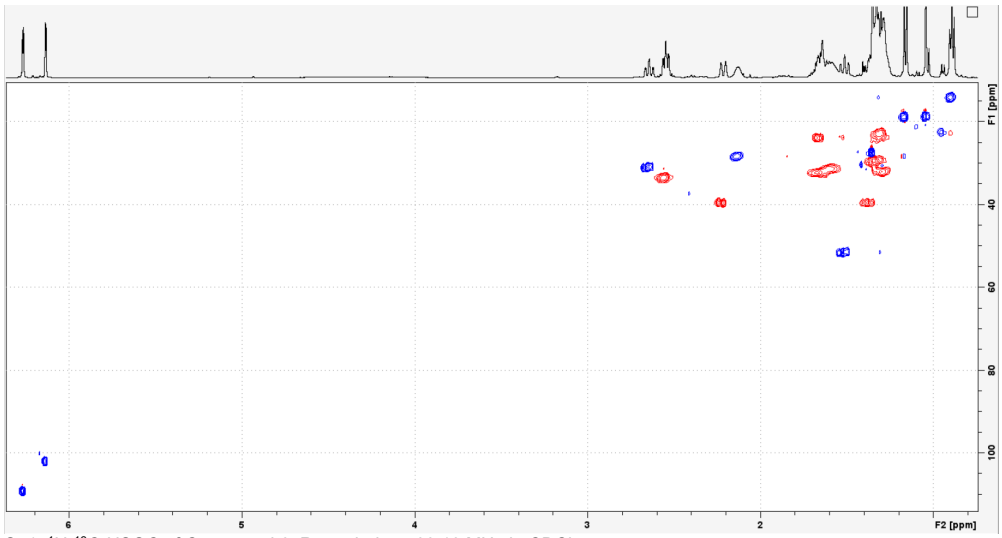

S51: ^{1}H-^{13}C-HSQC of Compound **6**. Recorded at 500.13 MHz in $CDCl_3$.

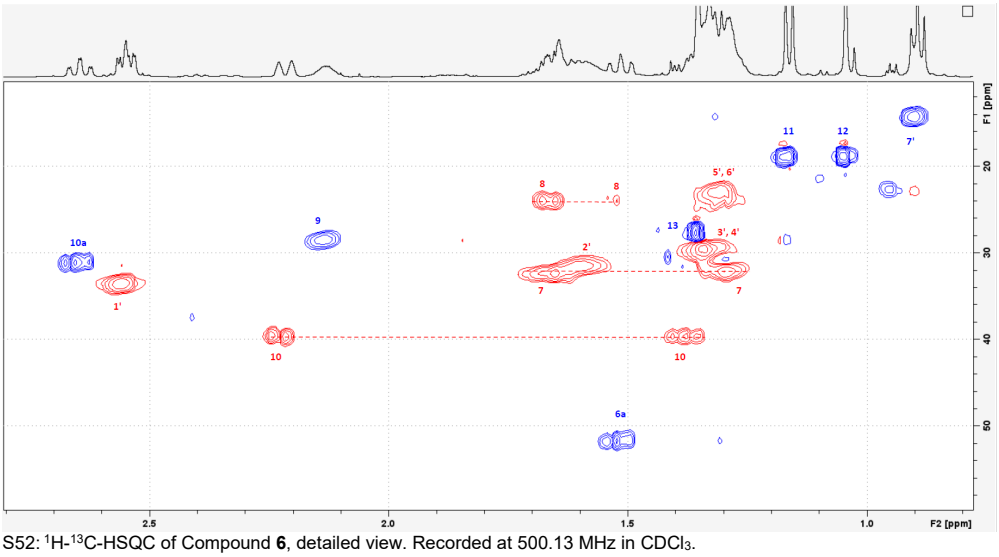

S52: ^{1}H-^{13}C-HSQC of Compound **6**, detailed view. Recorded at 500.13 MHz in $CDCl_3$.

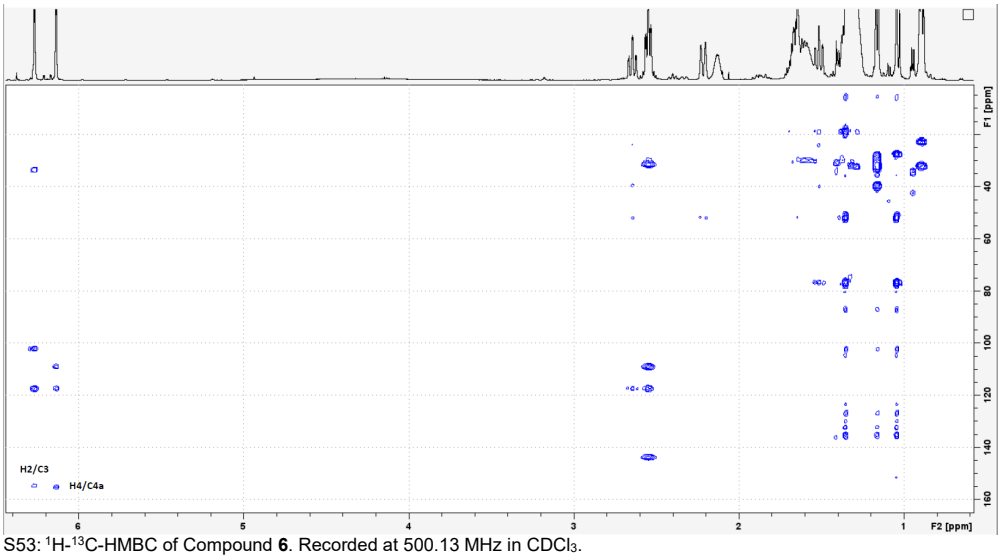

S53: ^{1}H-^{13}C-HMBC of Compound **6**. Recorded at 500.13 MHz in $CDCl_3$.

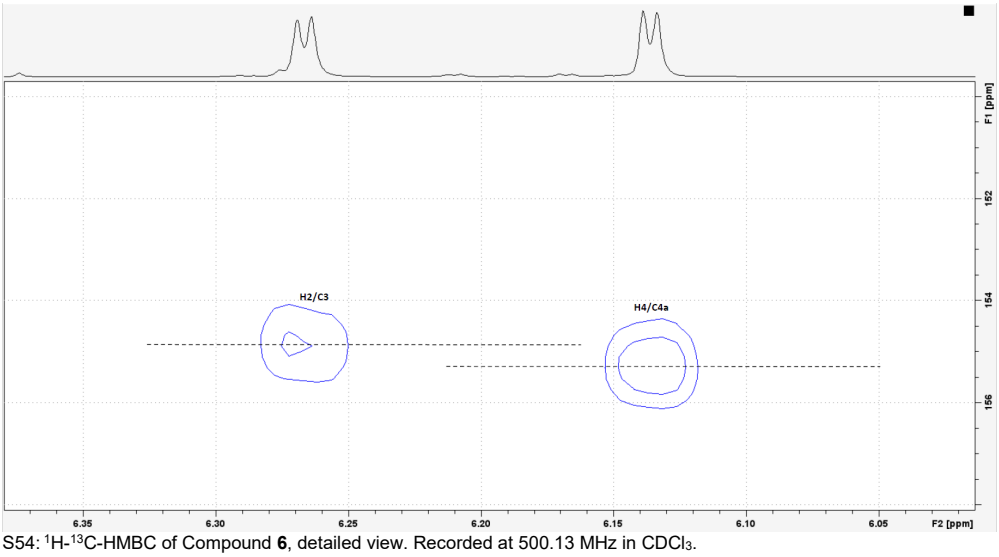

S54: ^{1}H-^{13}C-HMBC of Compound **6**, detailed view. Recorded at 500.13 MHz in $CDCl_3$.

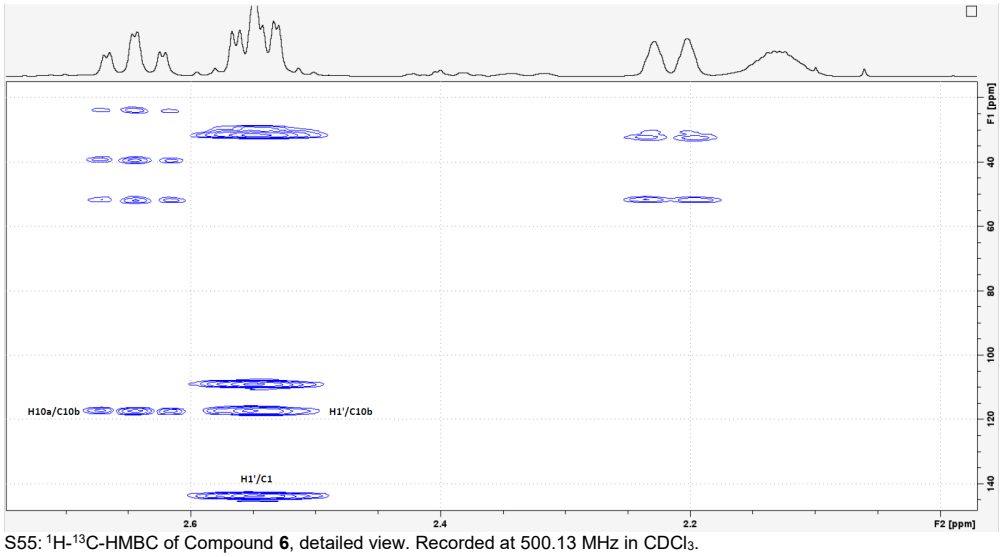

S55: ^{1}H-^{13}C-HMBC of Compound **6**, detailed view. Recorded at 500.13 MHz in $CDCl_3$.

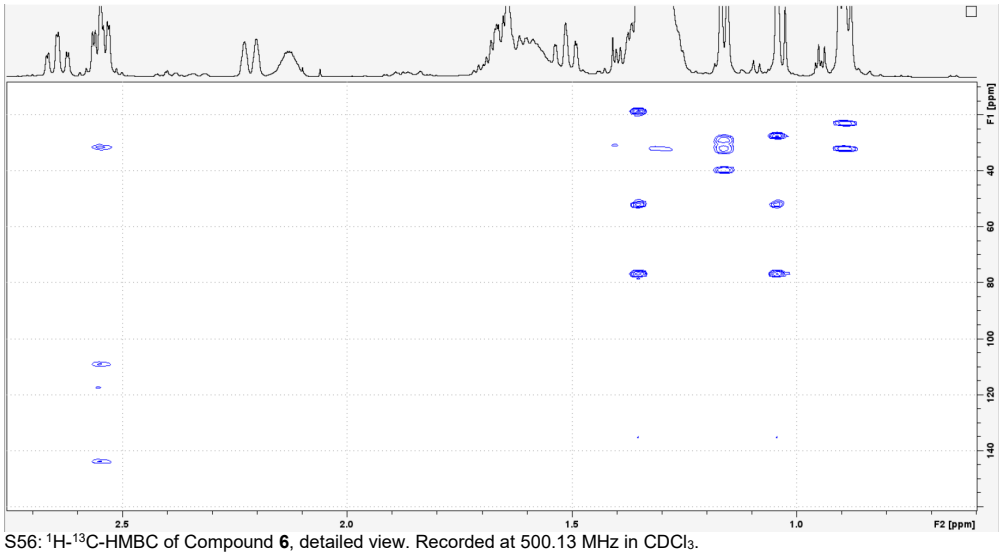

S56: ^{1}H-^{13}C-HMBC of Compound **6**, detailed view. Recorded at 500.13 MHz in $CDCl_3$.

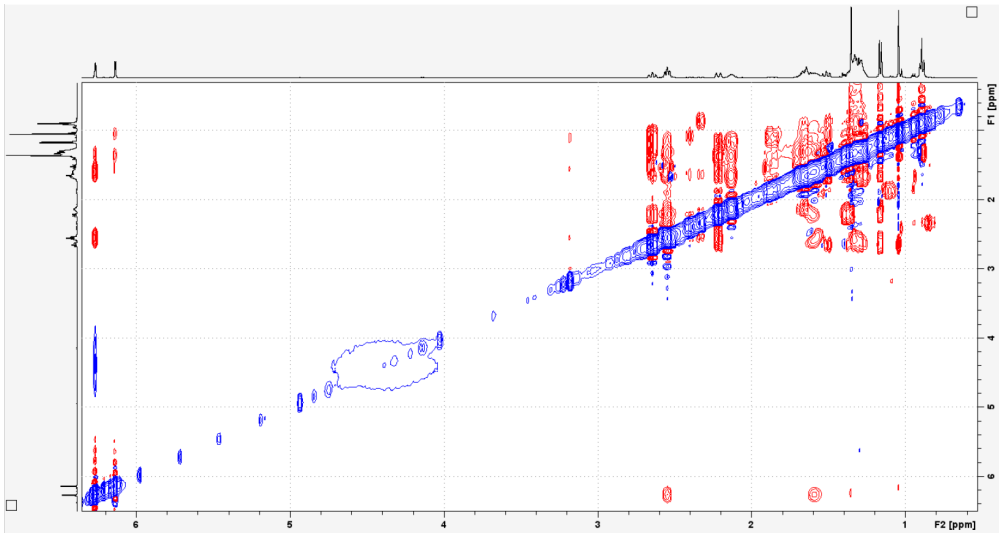

S57: NOESY of Compound **6**. Recorded at 500.13 MHz in $CDCl_3$.

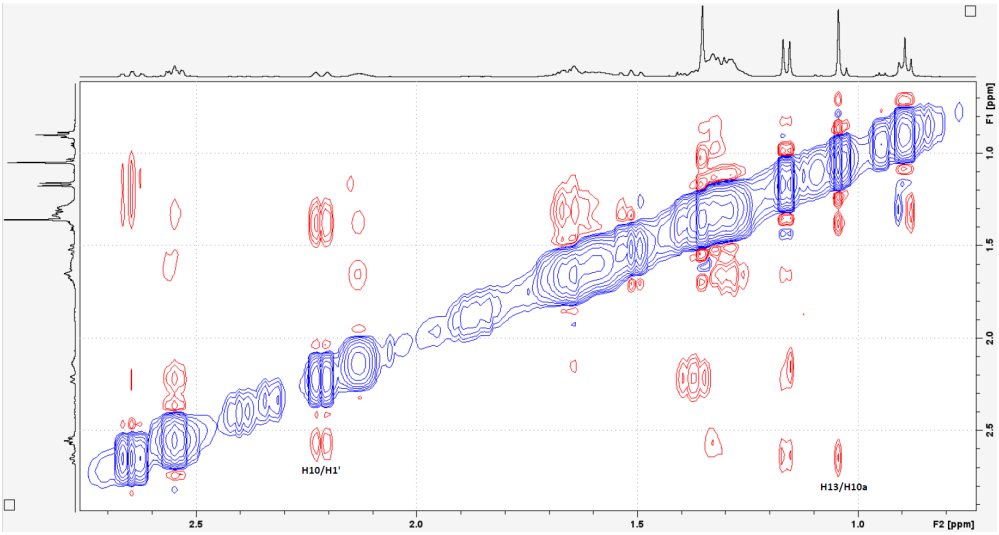

S58: NOESY of Compound **6**, detailed view. Recorded at 500.13 MHz in $CDCl_3$.

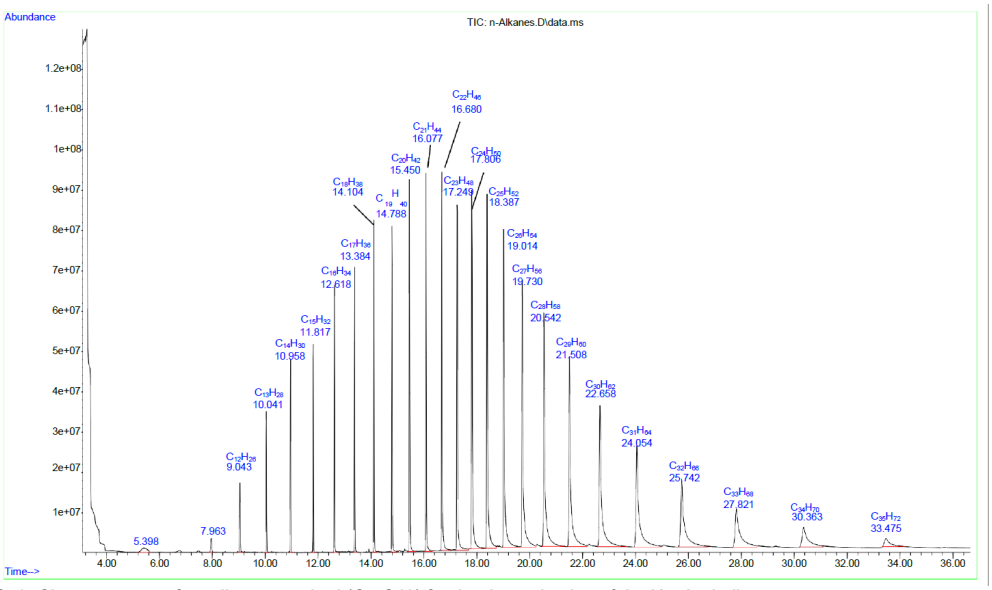

S59: Chromatogram of an alkane standard (C7-C40) for the determination of the Kováts indices.

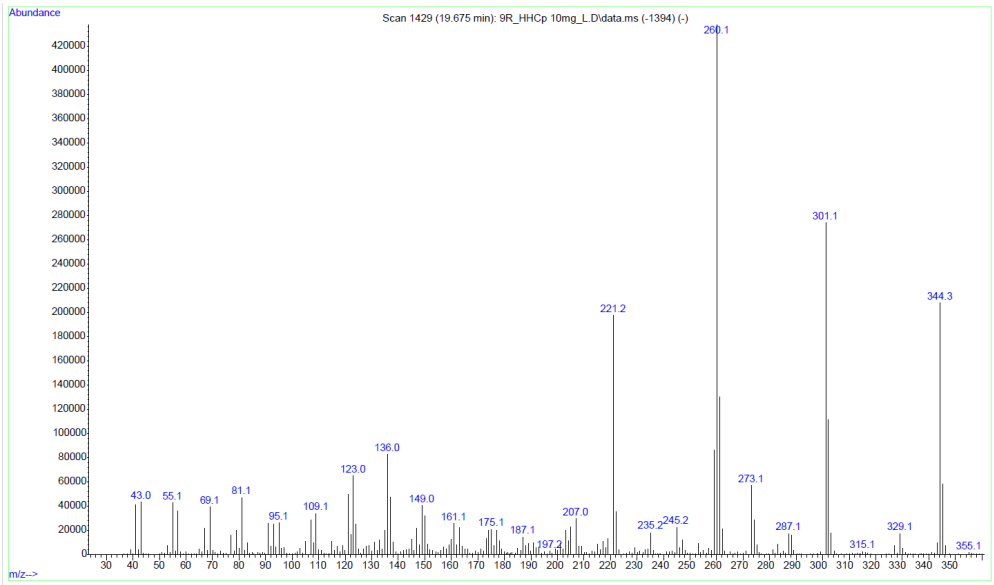

S60: GC-EI-MS of (9*R*)-HHCP.

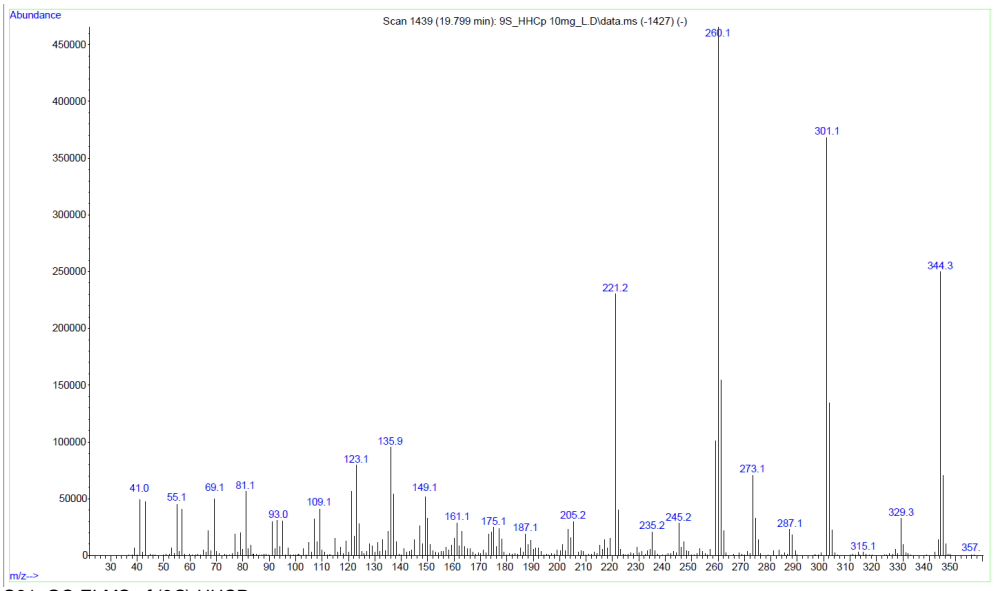

S61: GC-EI-MS of (9*S*)-HHCP.

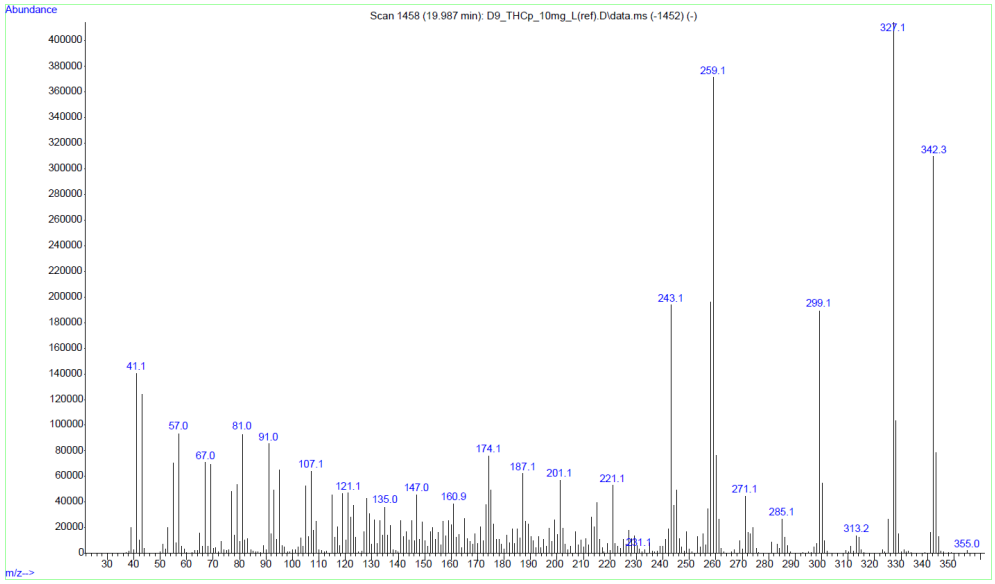

S62: GC-EI-MS of Δ^9-THCP.

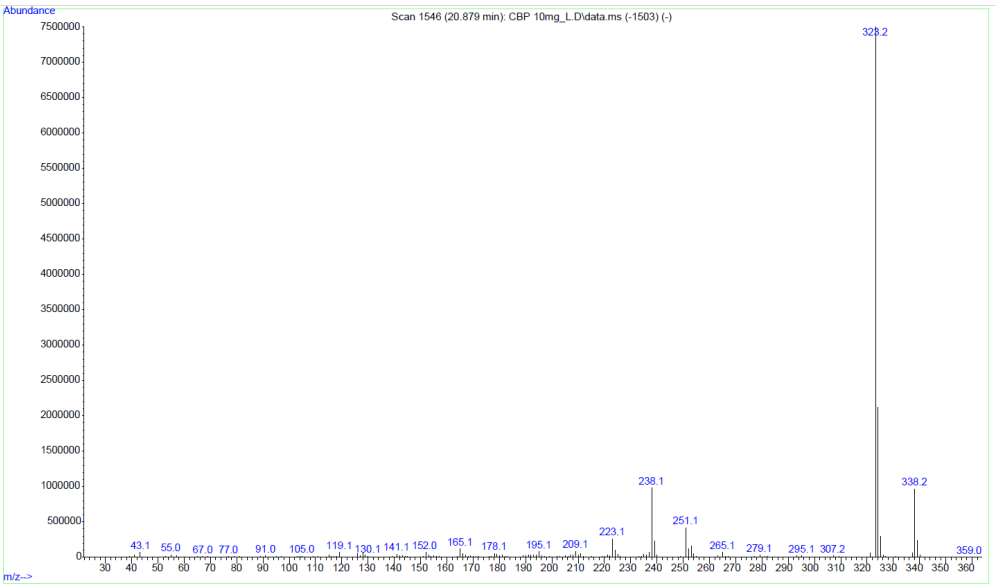

S63: GC-EI-MS of cannabiphorol (CBP).

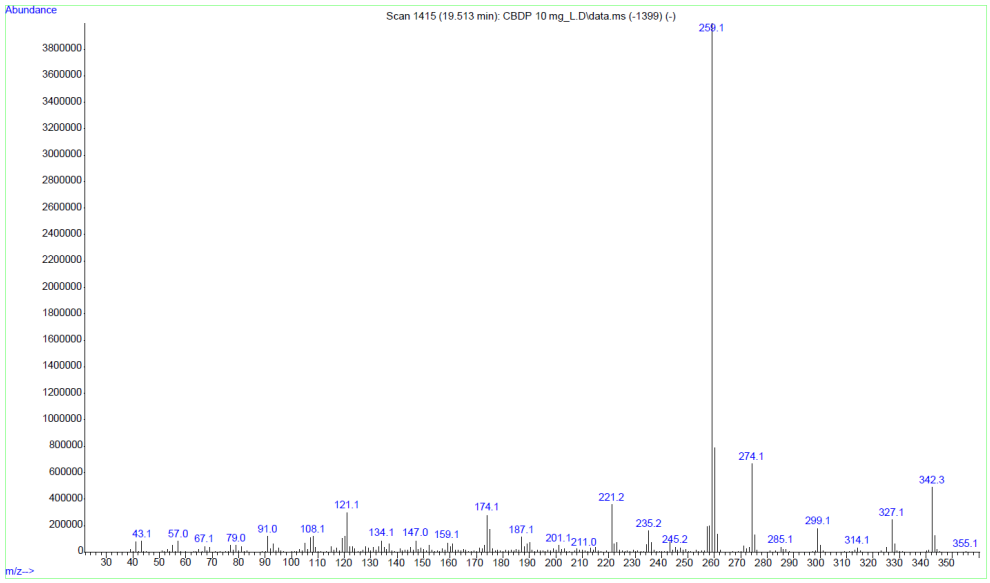

S64: GC-EI-MS of cannabidiphorol (CBDP).

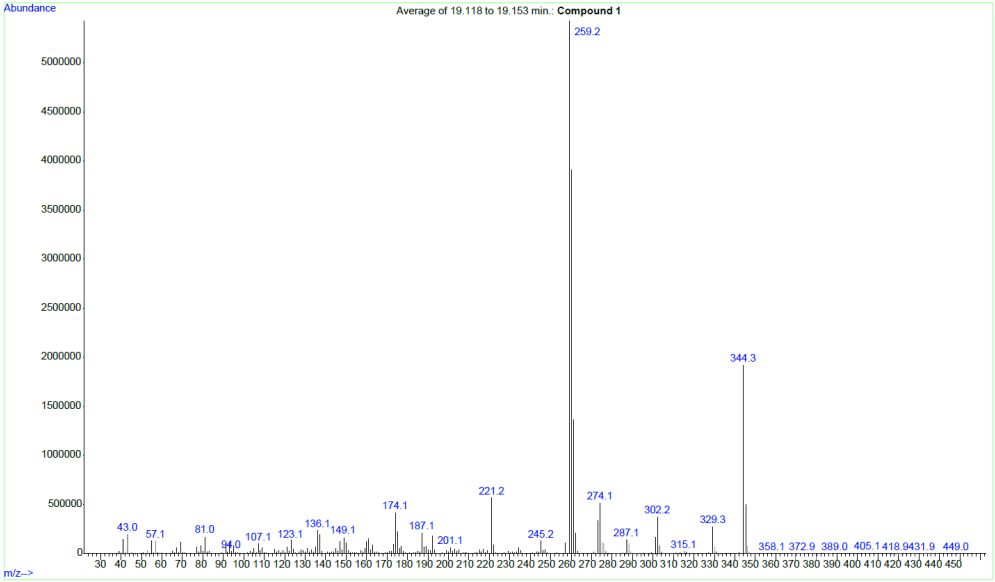

S65: GC-EI-MS of Compound **1**.

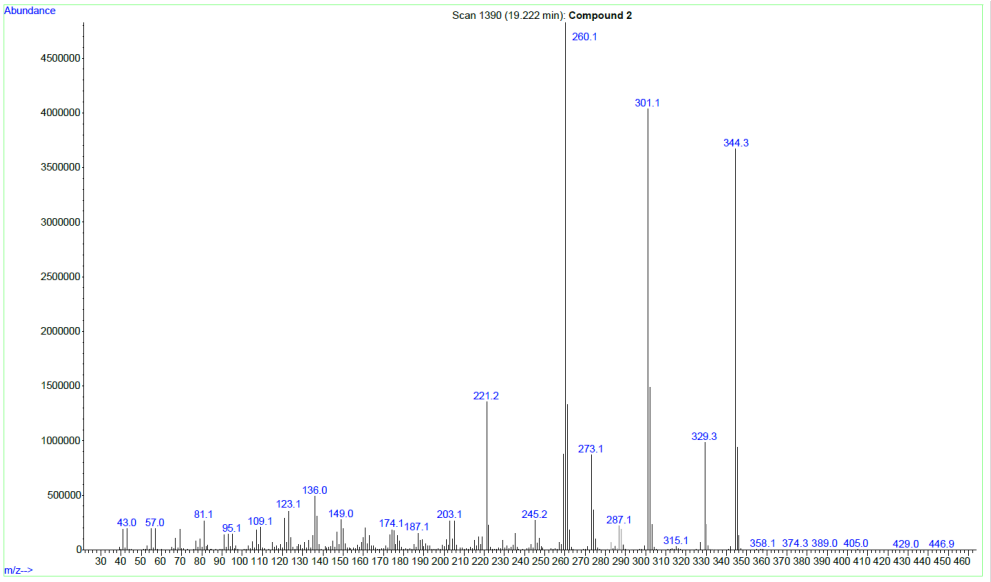

S66: GC-EI-MS of Compound **2**.

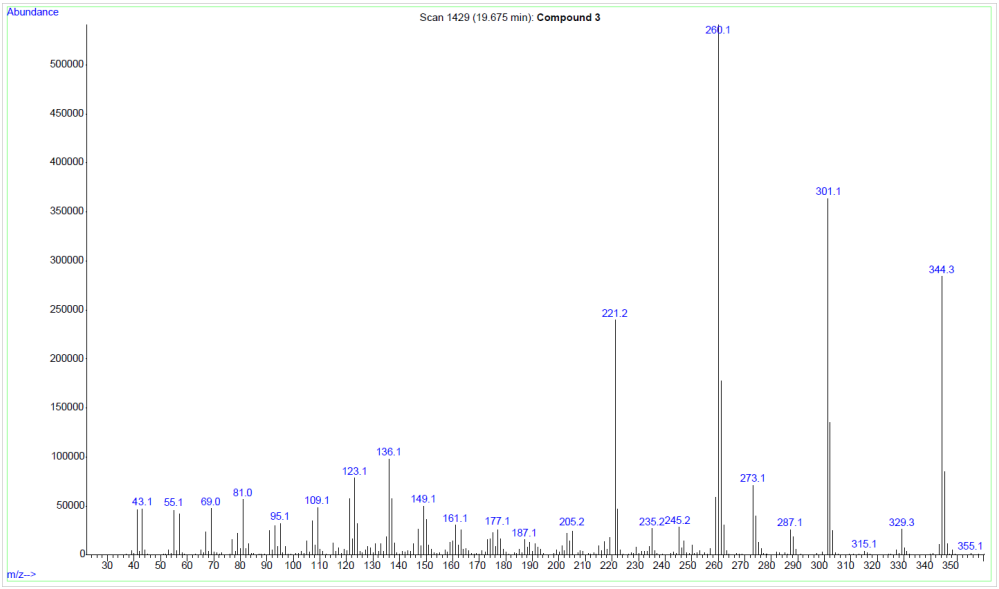

S67: GC-EI-MS of Compound **3**.

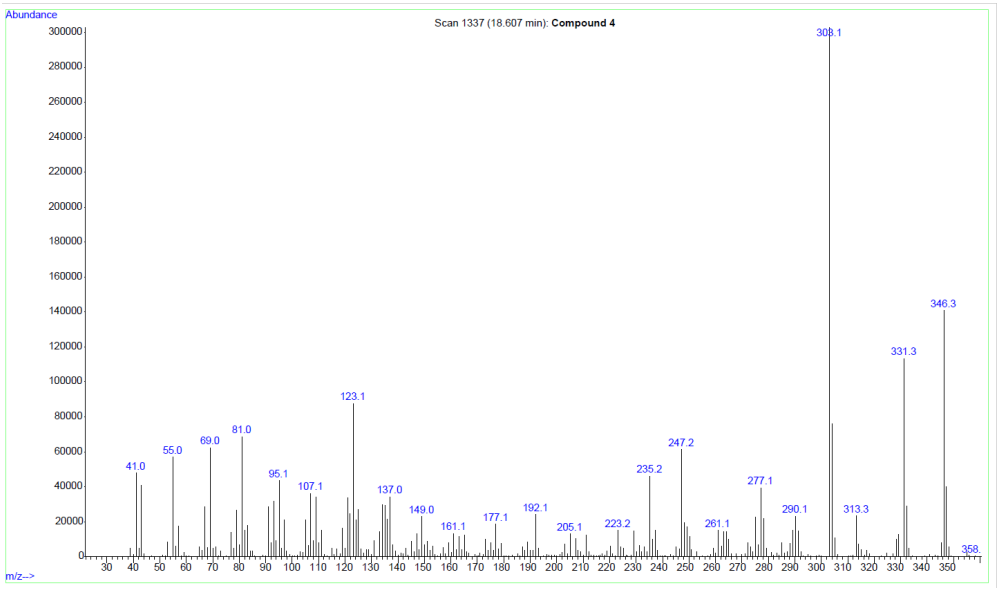

S68: GC-EI-MS of Compound **4**.

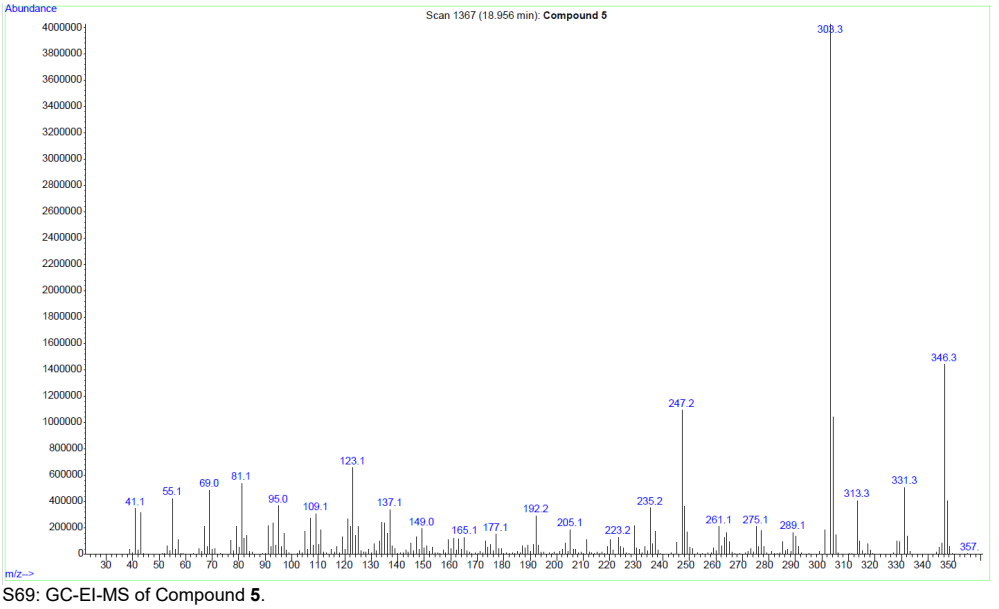

S69: GC-EI-MS of Compound **5**.

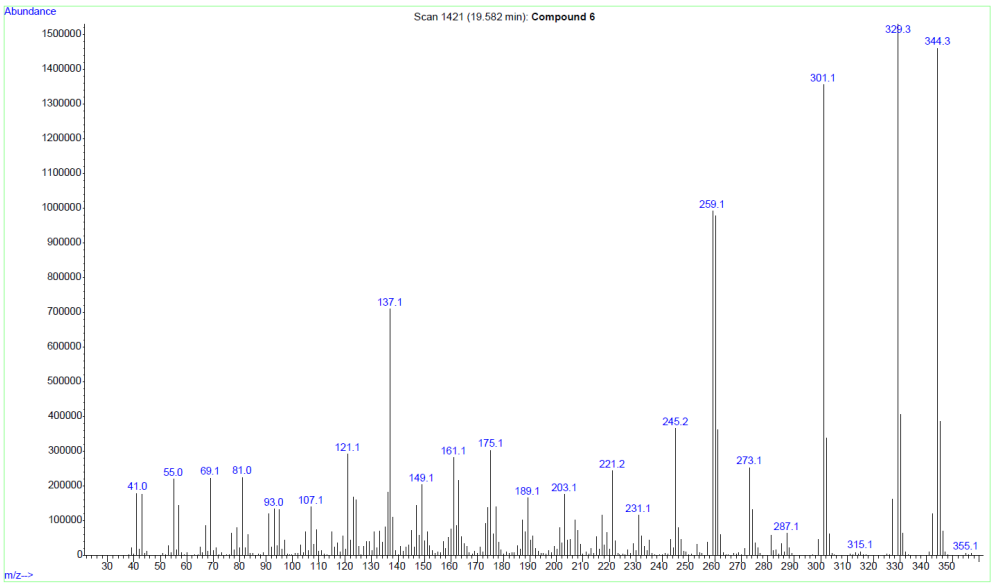

S70: GC-EI-MS of Compound **6**.

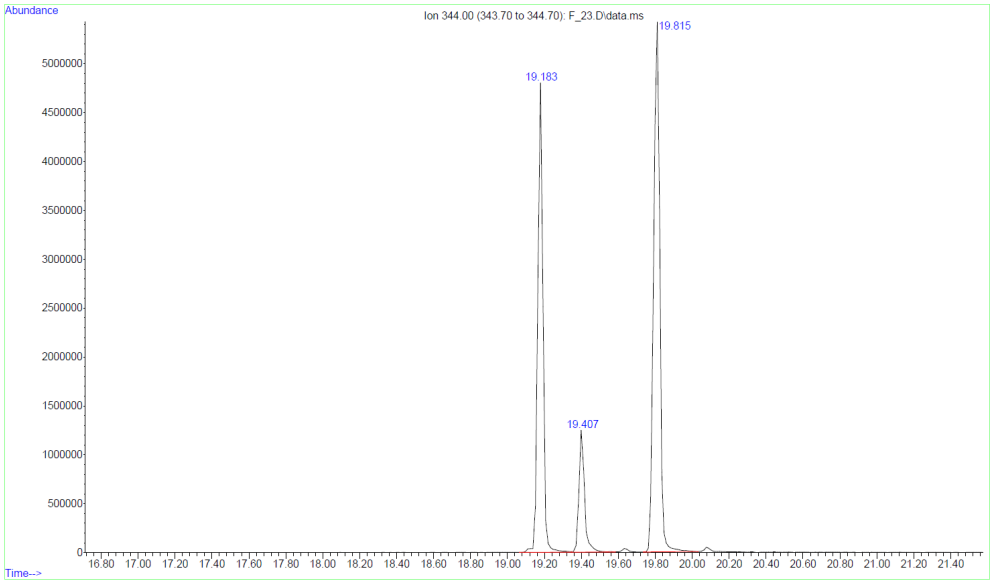

S71: Extracted ion chromatogram (*m/z* 344) of a fraction containing (9*S*)-HHCP

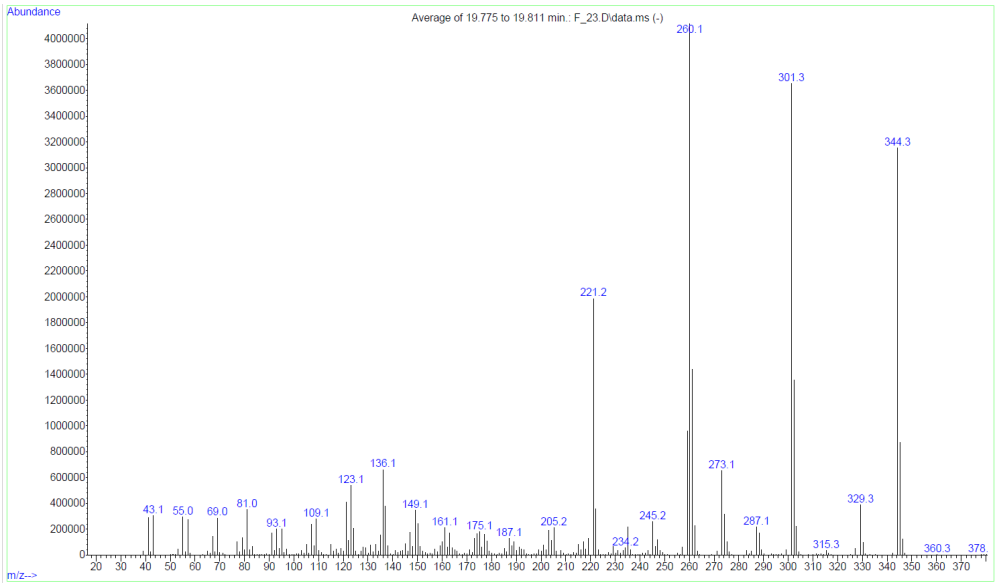

S72: GC-EI-MS of the compound eluting 19.82 min ((9*S*)-HHCP)

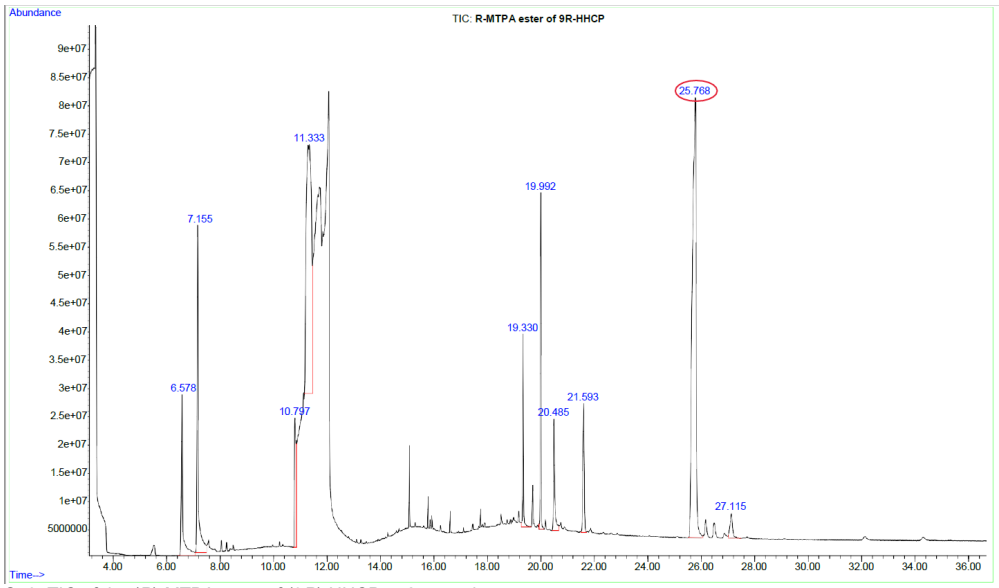

S73: TIC of the (*R*)-MTPA ester of (9*R*)-HHCP at 25.77 min.

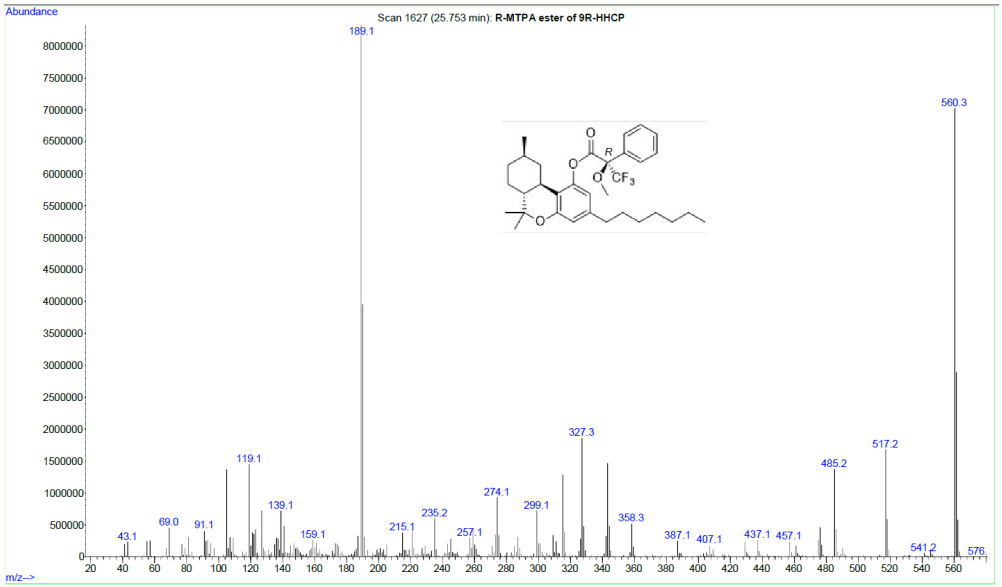

S74: GC-EI-MS of the (*R*)-MTPA ester of (9*R*)-HHCP.

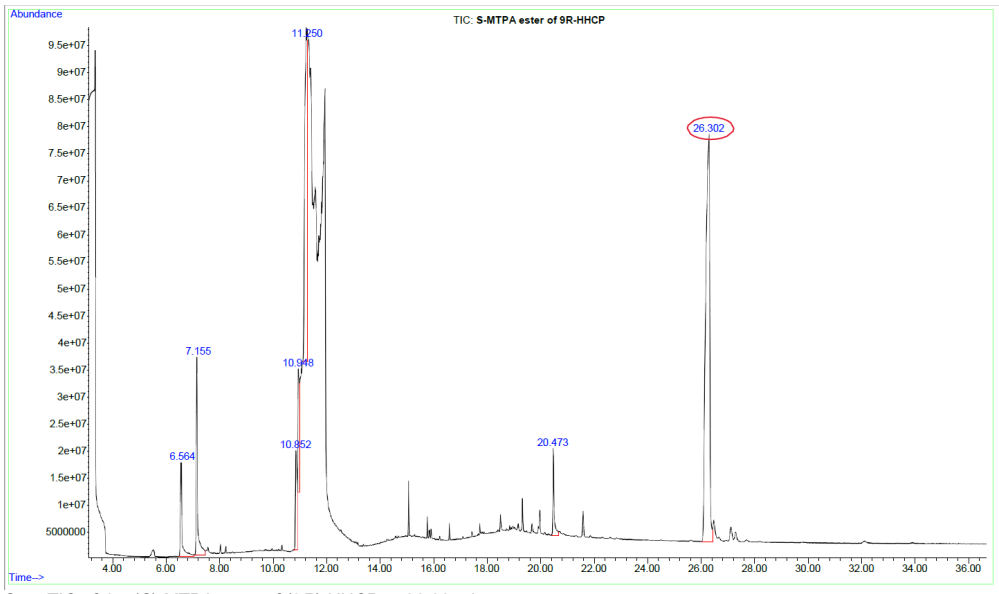

S75: TIC of the (*S*)-MTPA ester of (9*R*)-HHCP at 26.30 min.

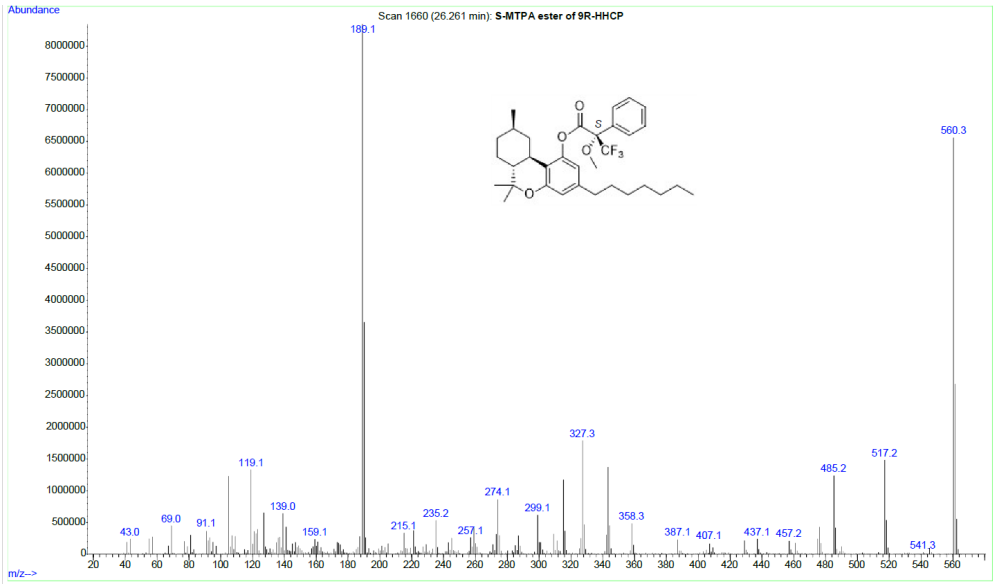

S76: GC-EI-MS of the (*S*)-MTPA ester of (9*R*)-HHCP.

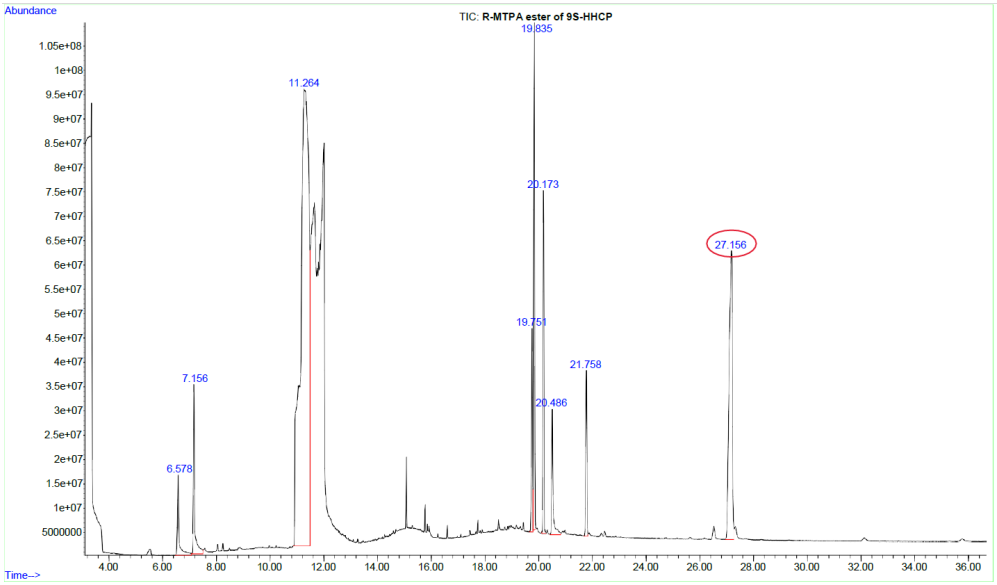

S77: TIC of the (*R*)-MTPA ester of (9*S*)-HHCP at 27.16 min.

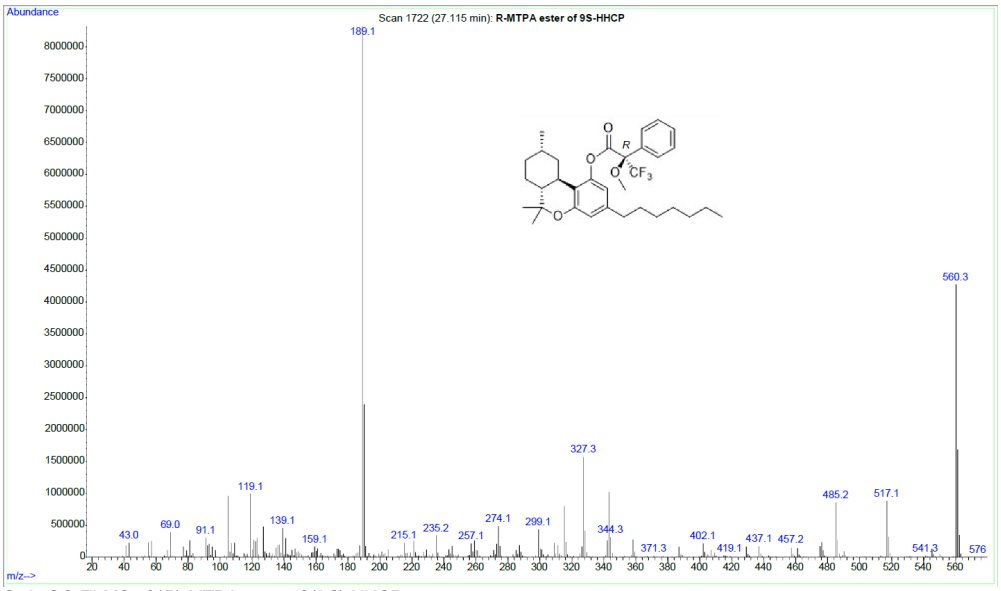

S78: GC-EI-MS of (*R*)-MTPA ester of (9*S*)-HHCP.

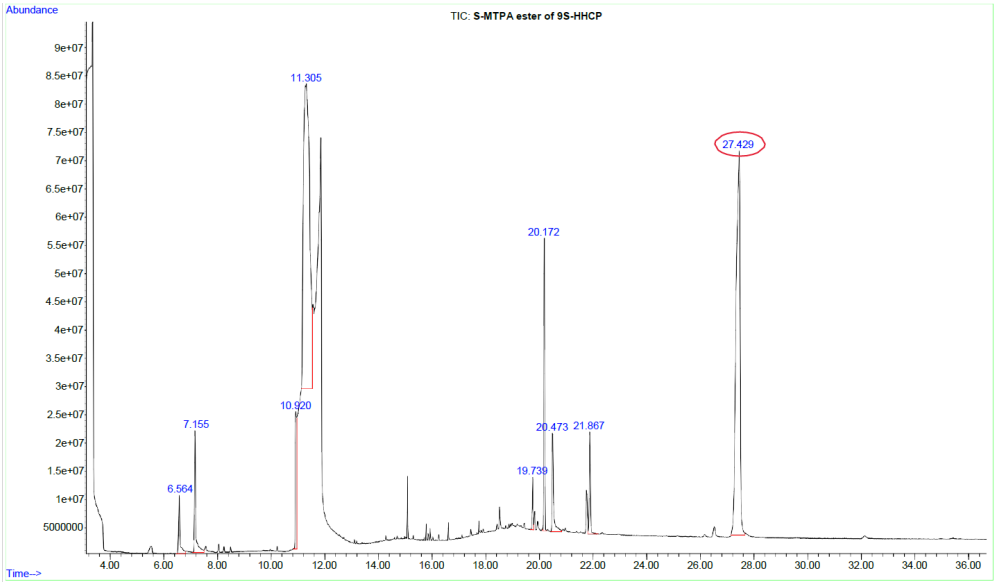

S79: TIC of the (*S*)-MTPA ester of (9*S*)-HHCP at 27.43 min.

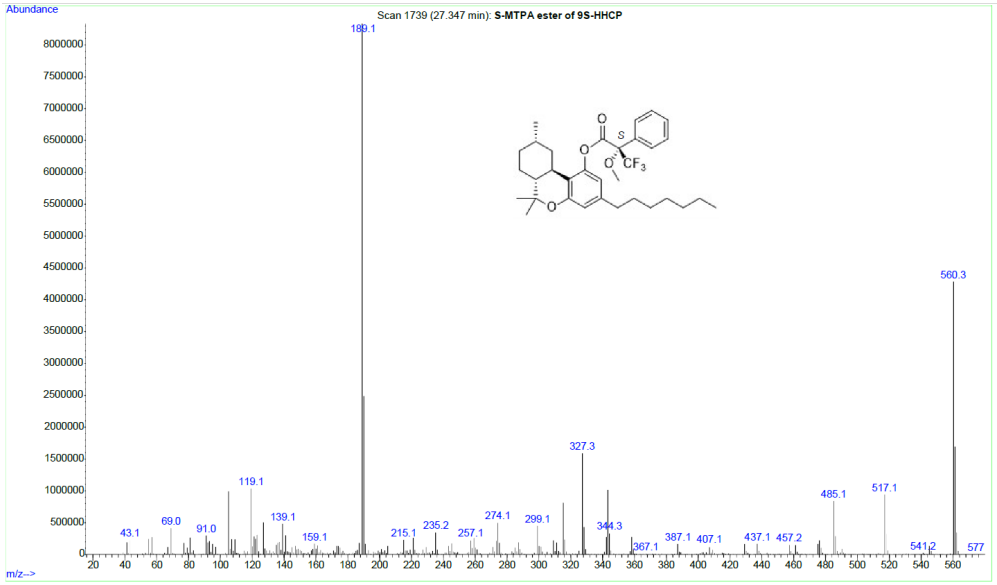

S80: GC-EI-MS of the (*S*)-MTPA ester of (9*S*)-HHCP.

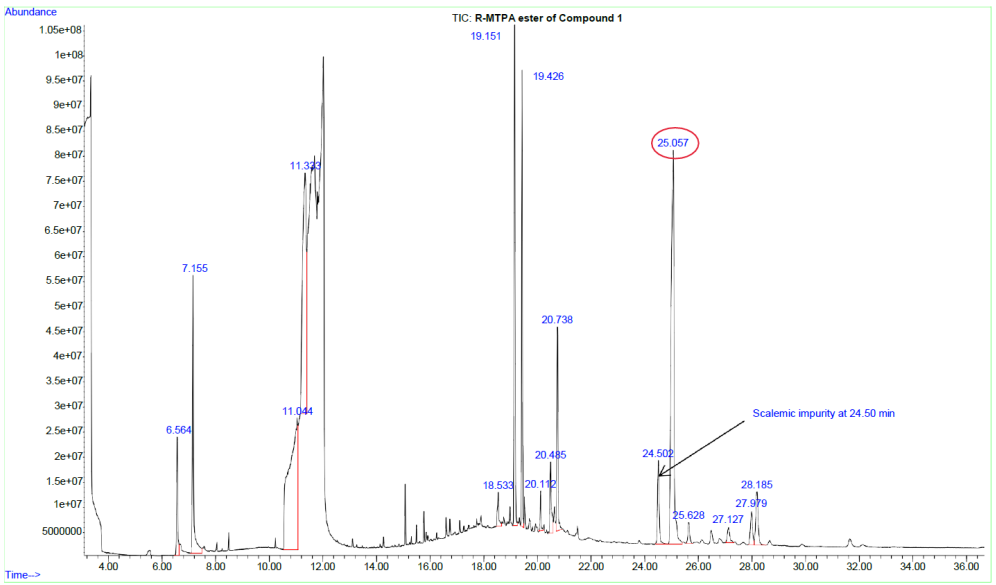

S81: TIC of the (*R*)-MTPA ester of Compound 1 at 25.06 min. A scalemic impurity is seen at 24.50 min (same retention time (S84) and mass spectrum (S85))

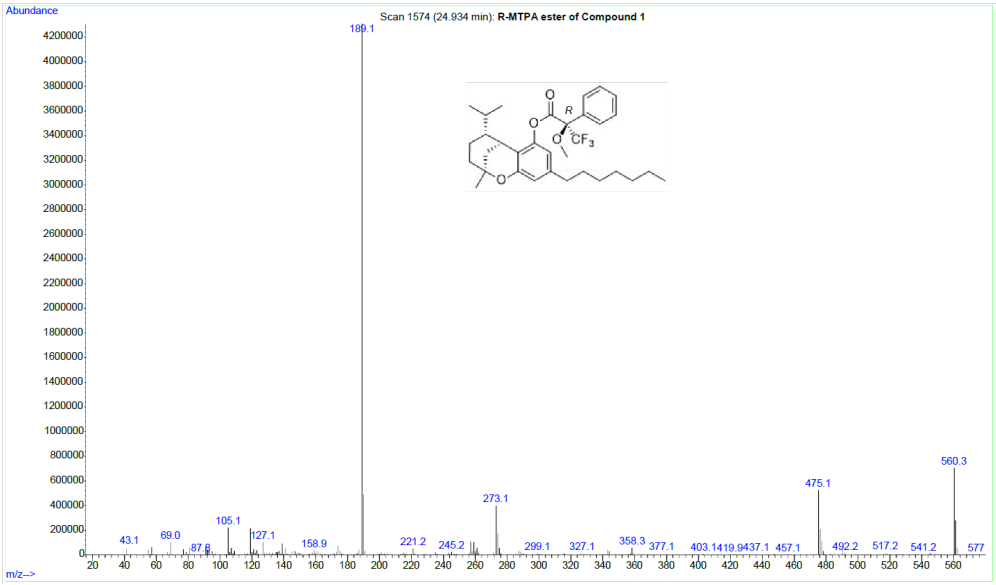

S82: GC-EI-MS of the (*R*)-MTPA ester of Compound **1**. (Enantiomer to S86)

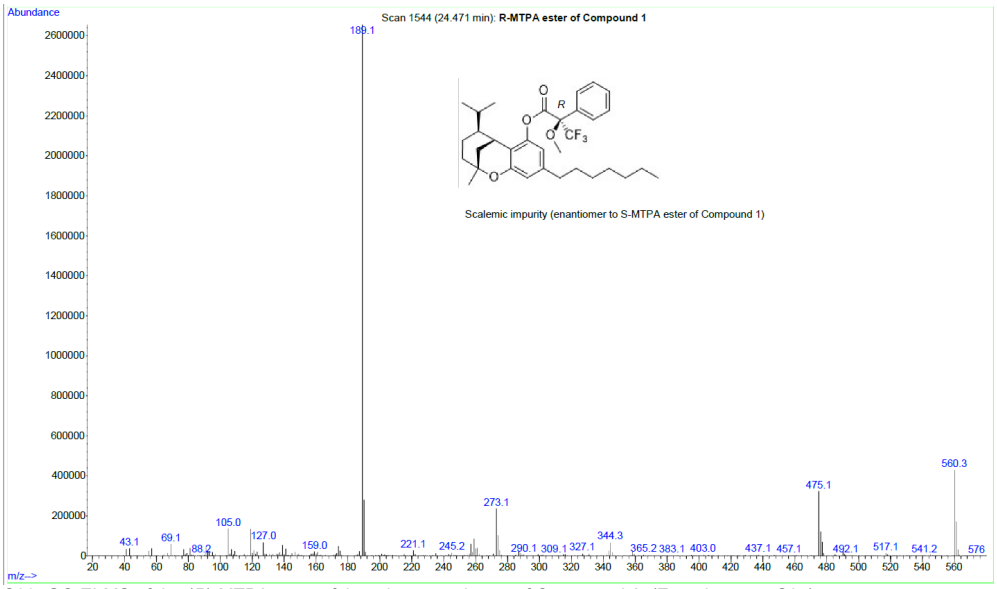

S83: GC-EI-MS of the (*R*)-MTPA ester of the other enantiomer of Compound **1**. (Enantiomer to S85)

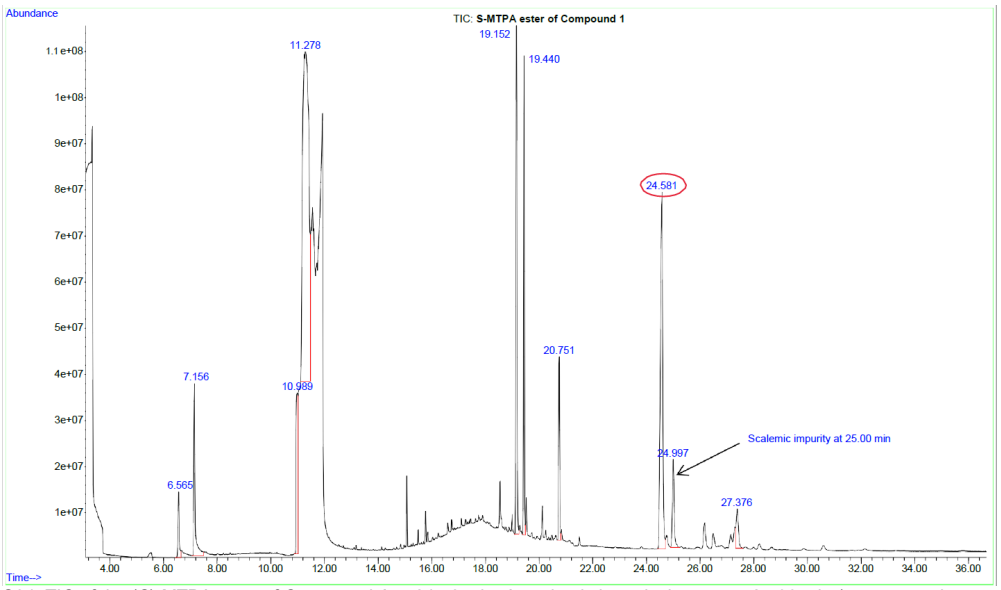

S84: TIC of the (*S*)-MTPA ester of Compound **1** at 24.58 min. A scalemic impurity is seen at 25.00 min (same retention time as S81.

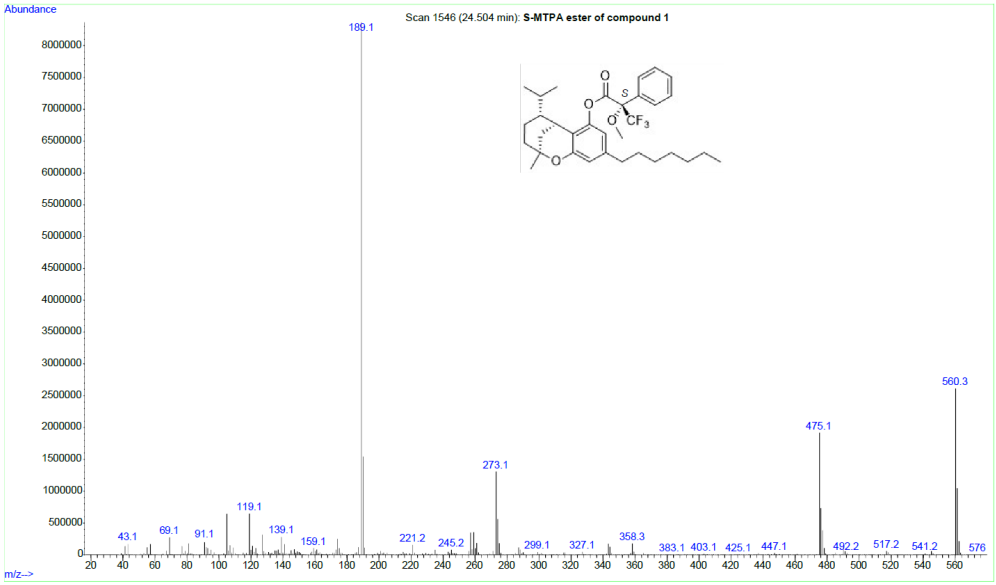

S85: GC-EI-MS of the (*S*)-MTPA ester of Compound **1**. (Enantiomer to S83)

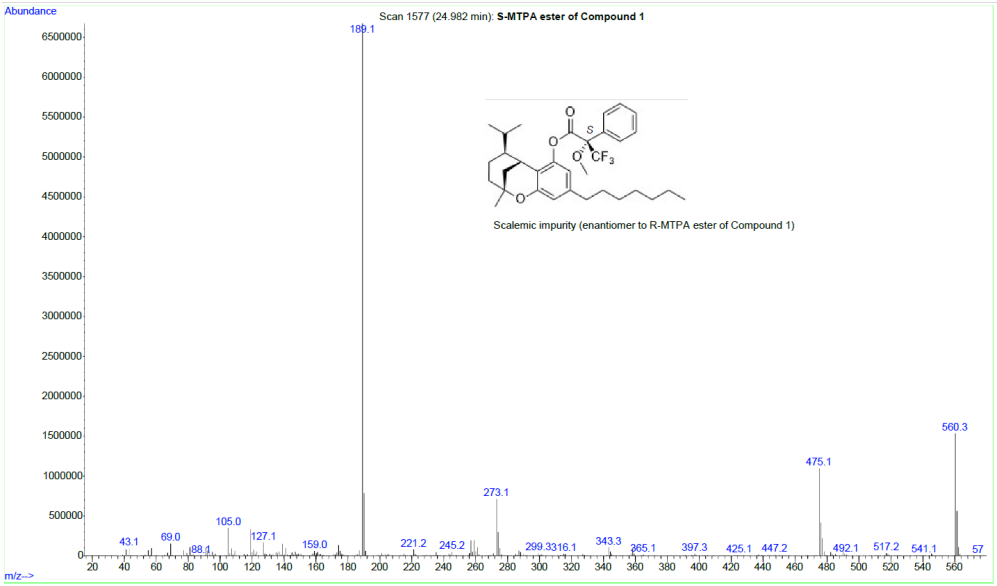

S86: GC-EI-MS of the (*S*)-MTPA ester of the enantiomer of Compound **1**. (Enantiomer to S82)

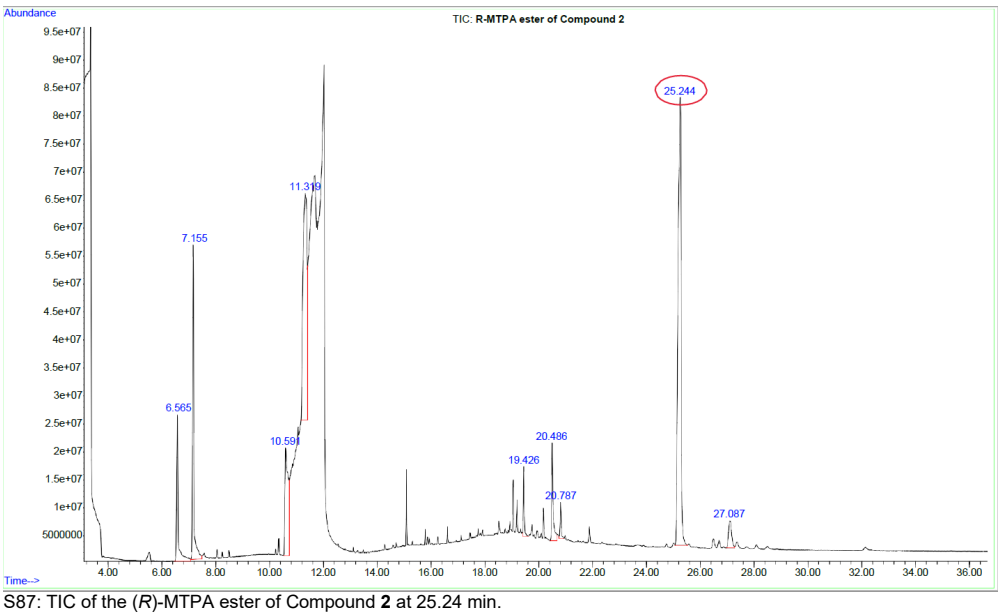

S87: TIC of the (*R*)-MTPA ester of Compound **2** at 25.24 min.

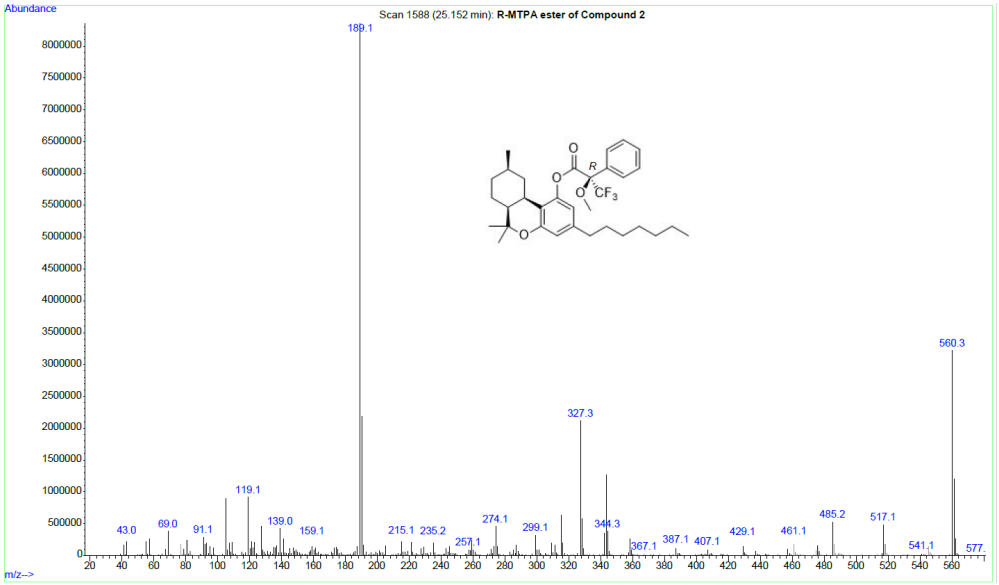

S88: GC-EI-MS of the (*R*)-MTPA ester of Compound **2**.

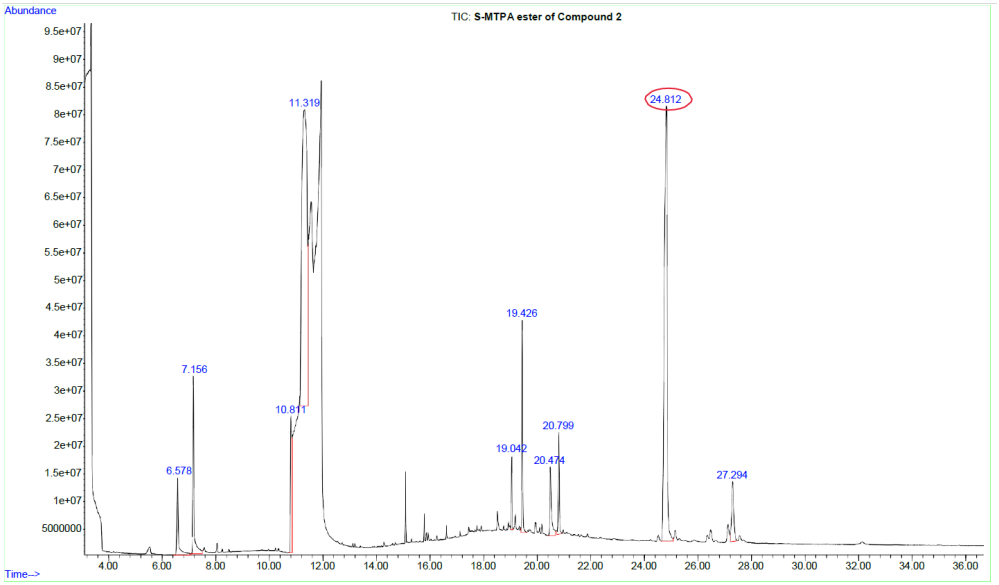

S89: TIC of the (*S*)-MTPA ester of Compound **2** at 24.81 min.

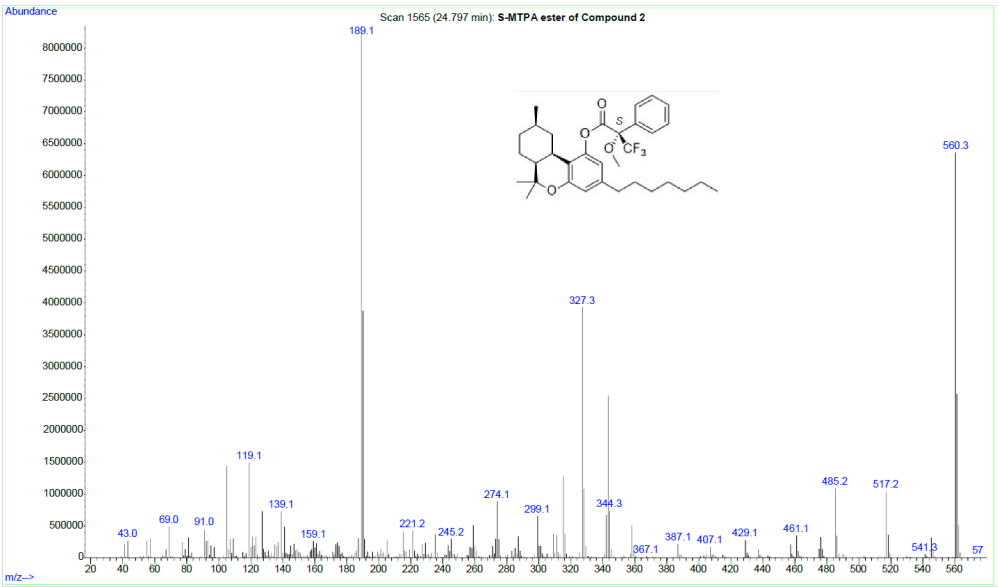

S90: GC-EI-MS of the (*S*)-MTPA ester of Compound **2**.

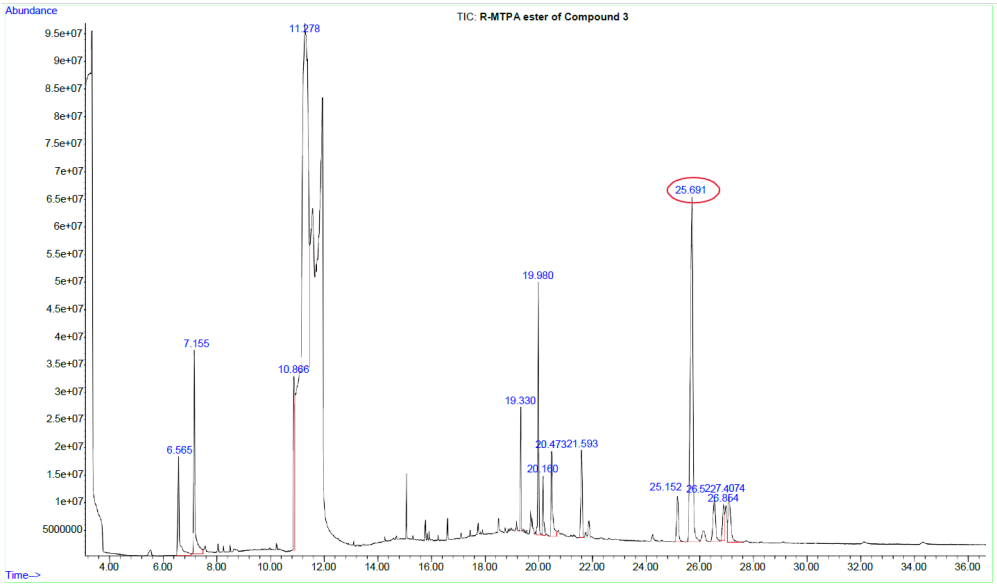

S91: TIC of the (*R*)-MTPA ester of Compound 3 at 25.69 min. (Identical to (9*R*)-HHCP)

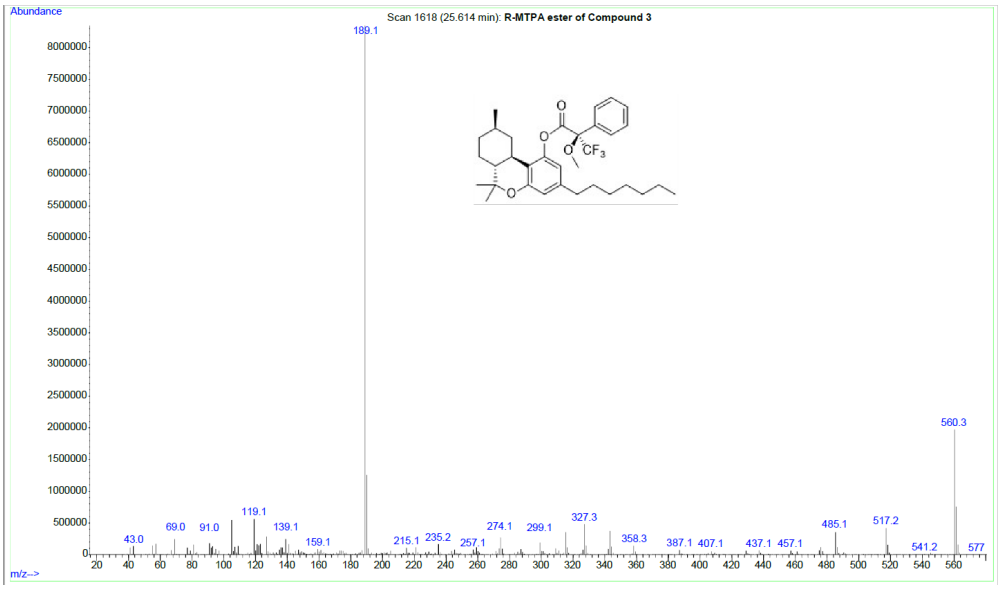

S92: GC-EI-MS of the (*R*)-MTPA ester of Compound **3**. (Identical to (9*R*)-HHCP)

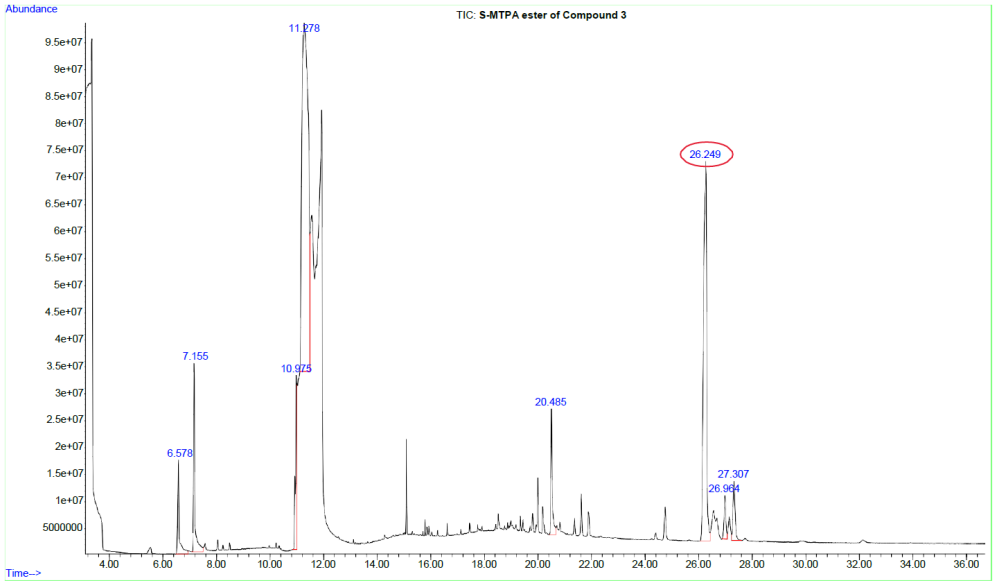

S93: TIC of the (*S*)-MTPA ester of Compound **3** at 26.25 min. (Identitcal to (9*R*)-HHCP)

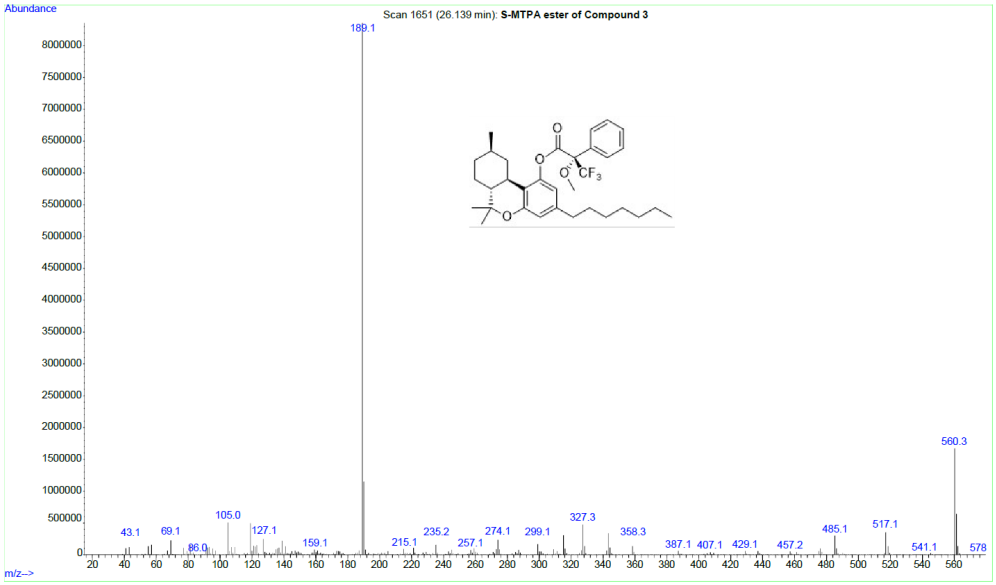

S94: GC-EI-MS of the (*S*)-MTPA ester of Compound **3**. (Identical to (9*R*)-HHCP)

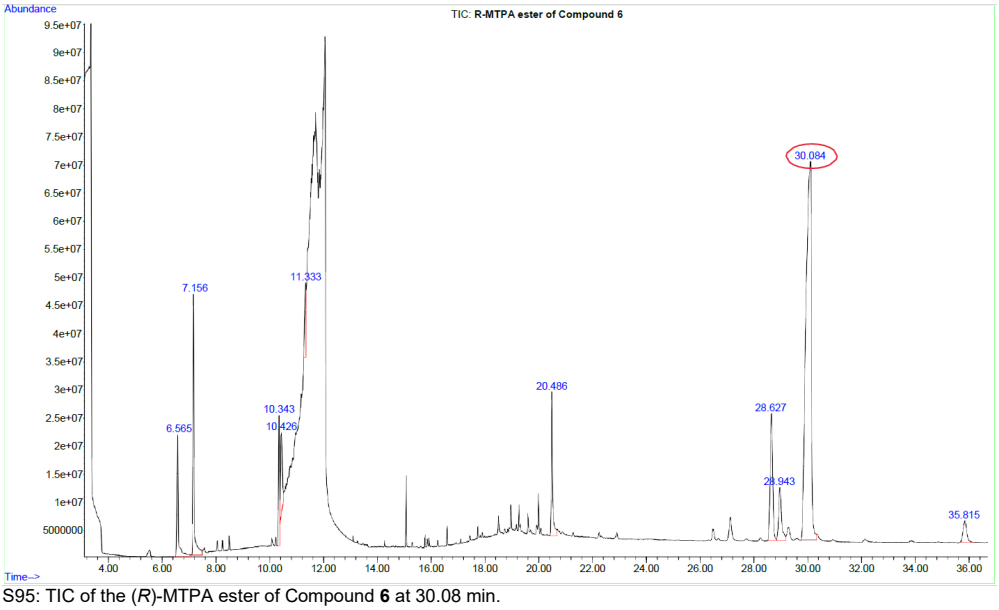

S95: TIC of the (*R*)-MTPA ester of Compound **6** at 30.08 min.

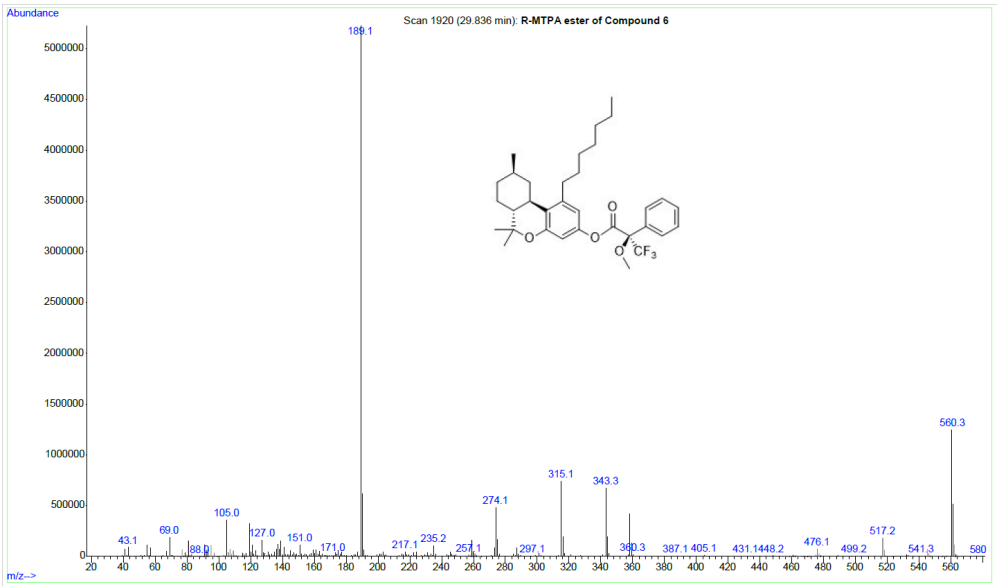

S96: GC-EI-MS of the (*R*)-MTPA ester of Compound **6**.

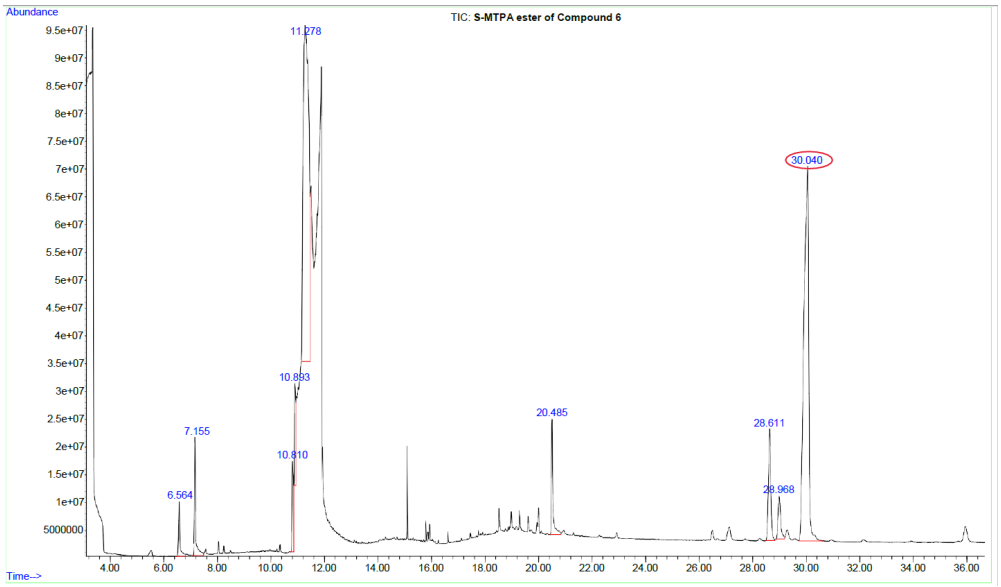

S97: TIC of the (*S*)-MTPA ester of Compound **6** at 30.04 min.

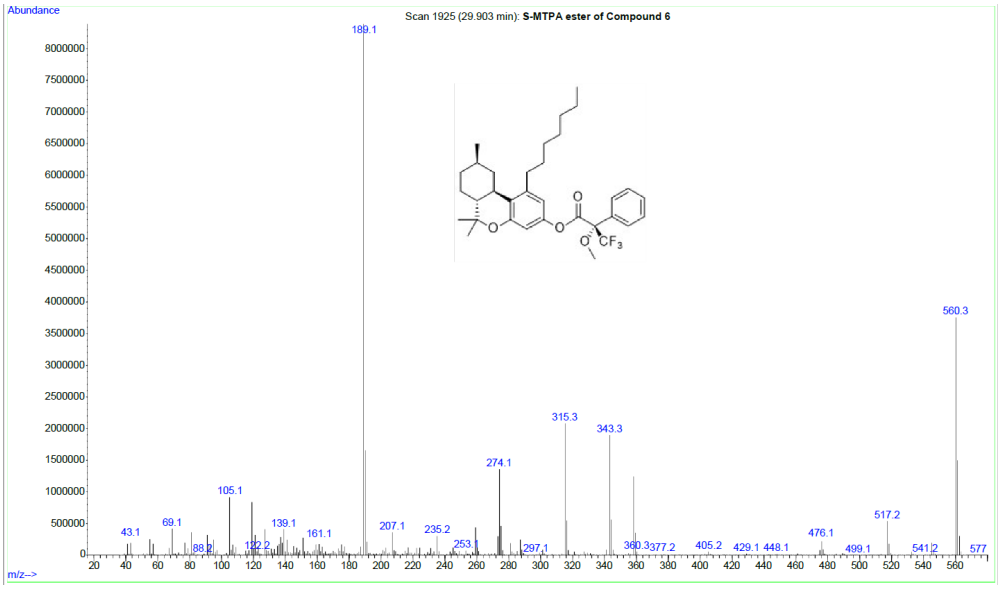

S98: GC-EI-MS of the (*S*)-MTPA ester of Compound **6**.

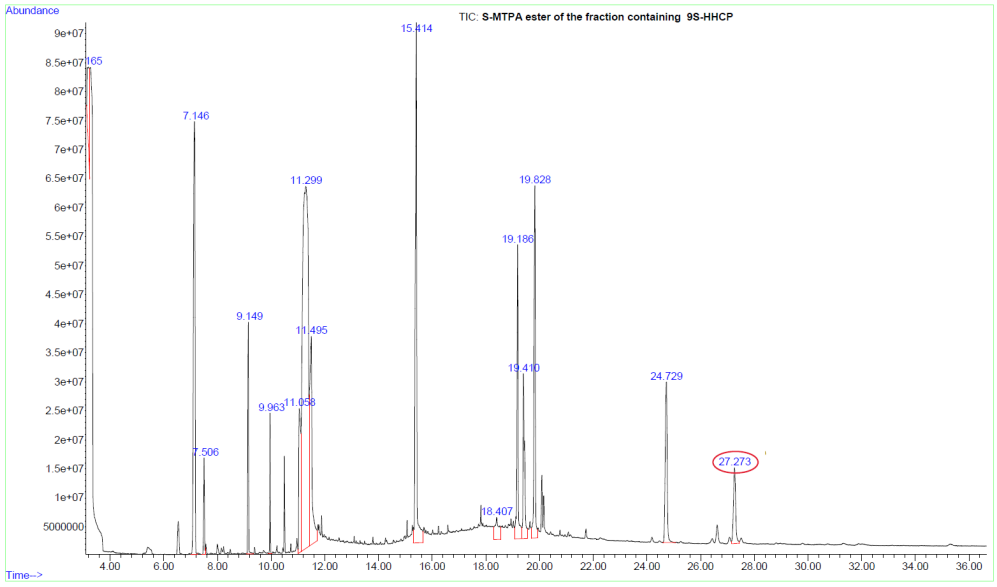

S99: TIC of the fraction containing (9*S*)-HHCP after derivatization with (*R*)-MTPA-Cl

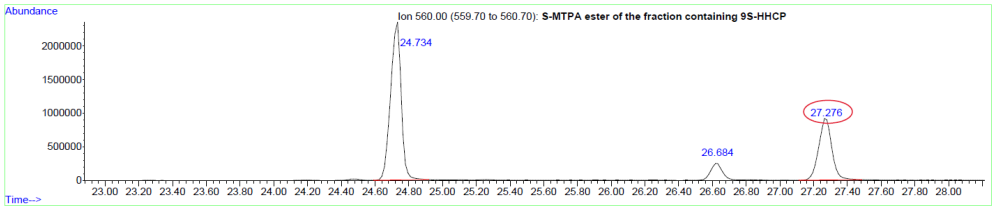

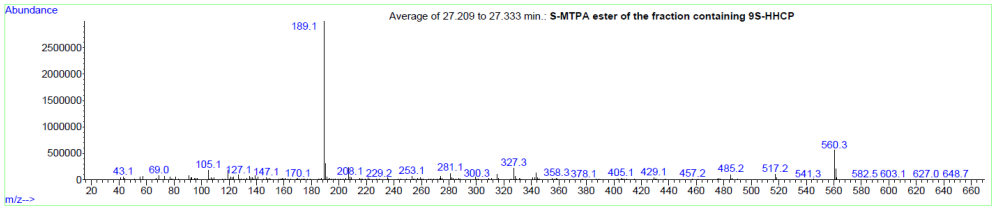

S100: top: XIC(560) of the fraction containing (9*S*)-HHCP, bottom: GC-EI-MS of (9*S*)-HHCP (*S*)-MTPA ester.

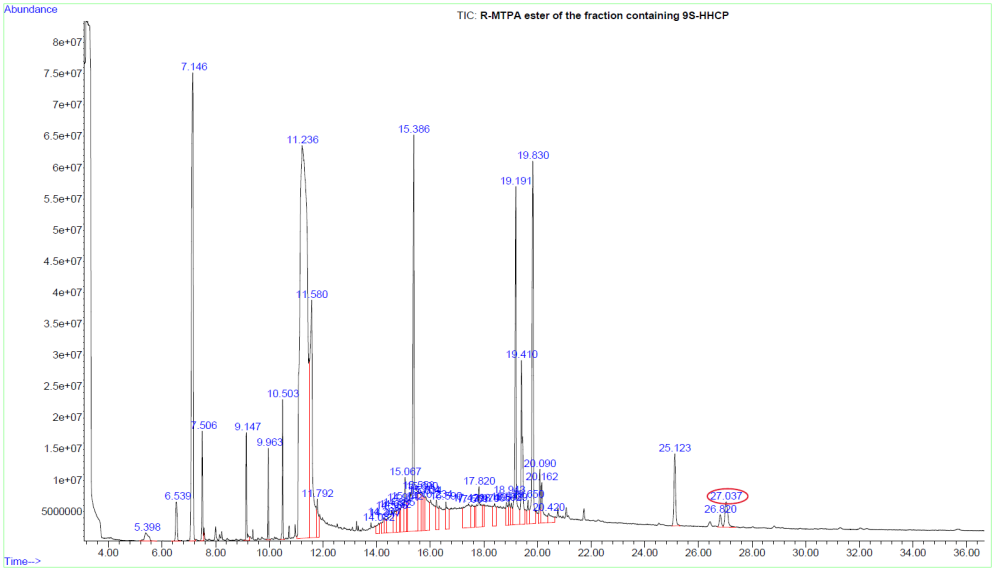

S101: TIC of the fraction containing (9*S*)-HHCP after derivatization with (*S*)-MTPA-Cl

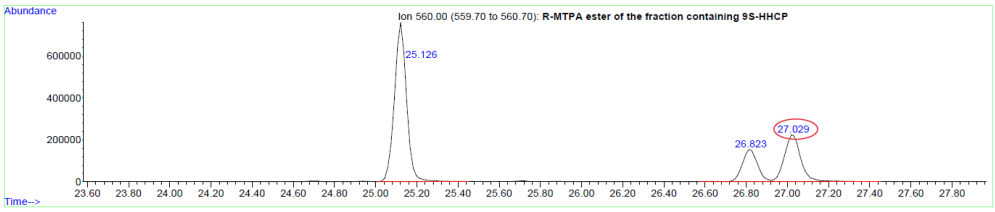

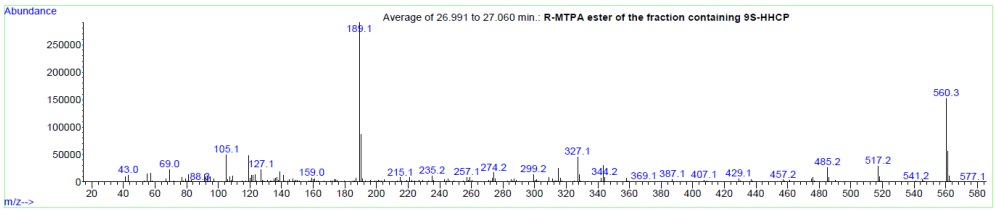

S102: top: XIC(560) of the fraction containing (9*S*)-HHCP, bottom: GC-EI-MS of (9*S*)-HHCP (*R*)-MTPA ester.

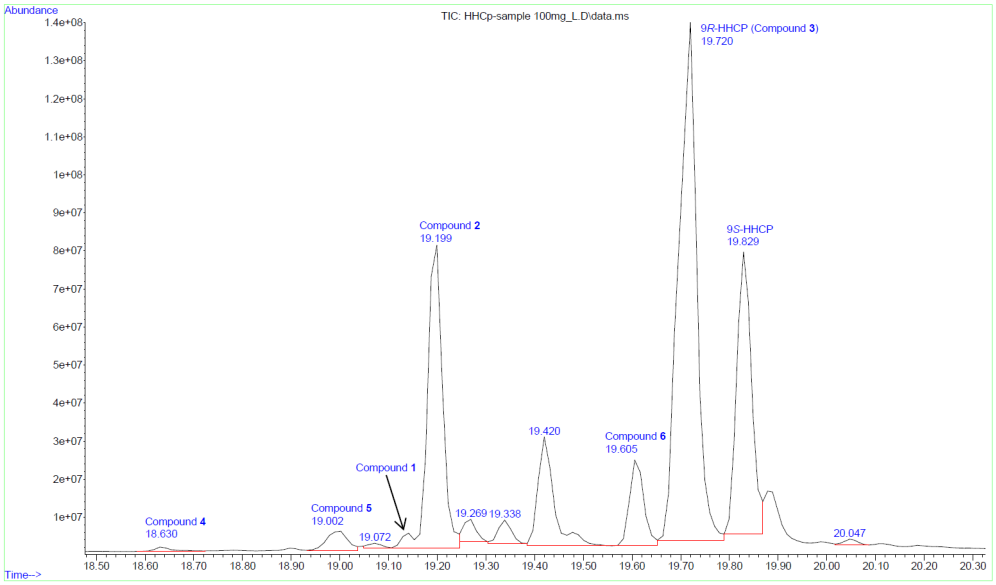

S103: TIC of the HHCP sample (γ = 100 mg/L). Other compounds besides the isolated compounds 1-6 are present.

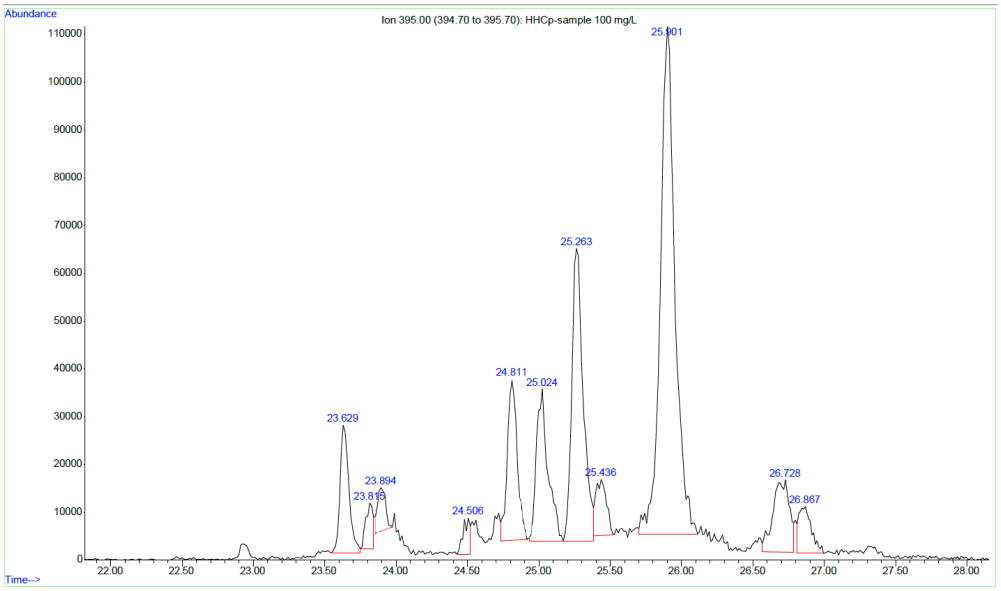

S104: XIC (395) of the HHCP sample (γ = 100 mg/L). High-molecular mass impurities, *m/z* 395 is a common fragment ion of them.

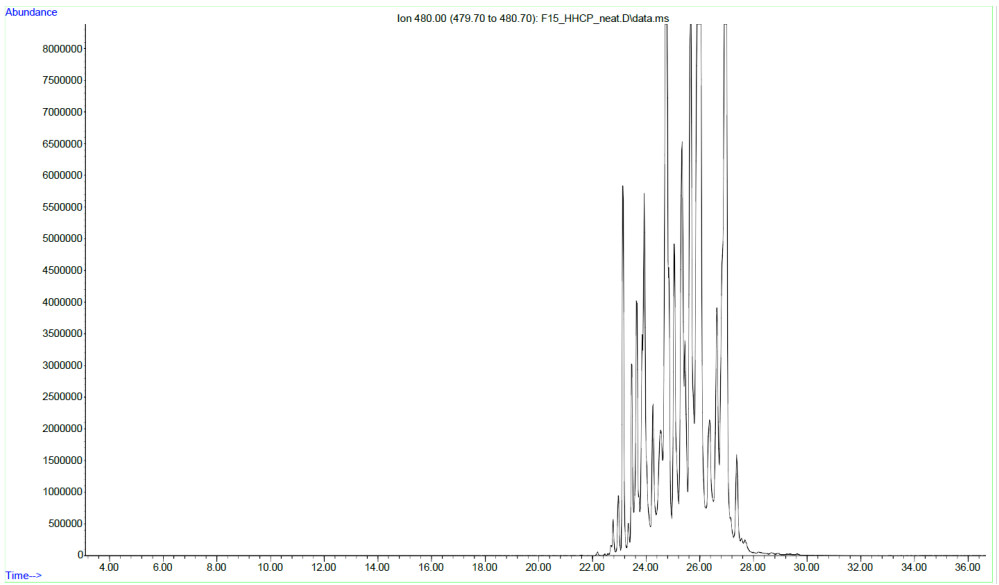

S105: XIC (480) of the underivatized fraction containing the impurities with a high molecular mass.

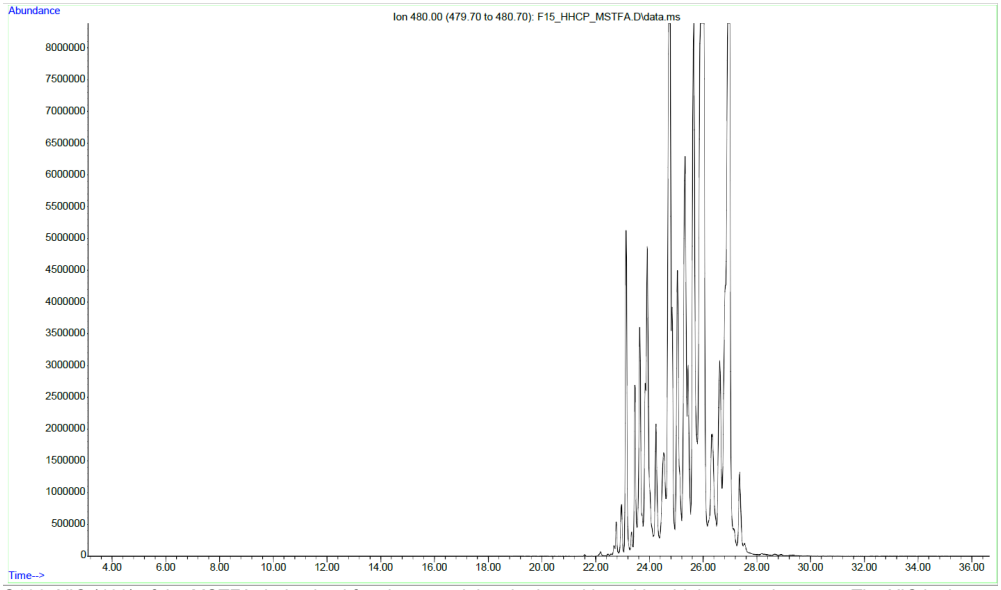

S106: XIC (480) of the MSTFA derivatized fraction containing the impurities with a high molecular mass. The XIC looks identical to S101 indicating that these compounds do not possess reactive groups (phenols, enols).

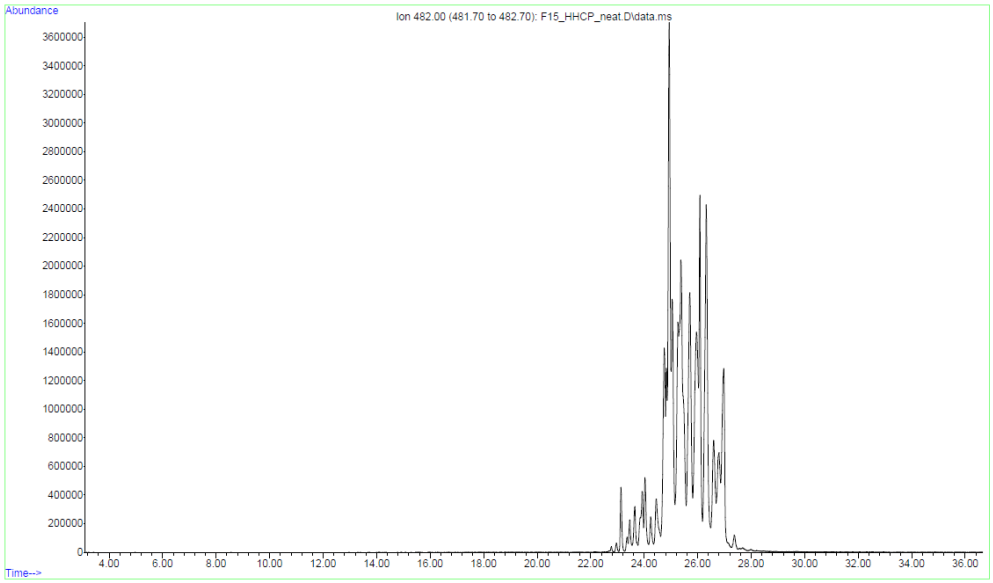

S107: XIC (482) of the underivatized fraction containing the impurities with a high molecular mass.

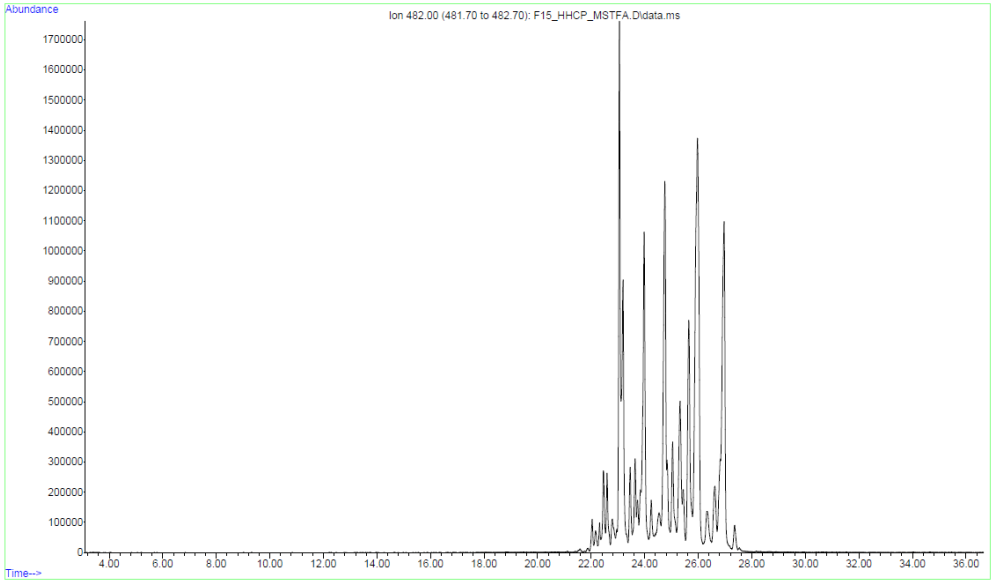

S108: XIC (482) of the MSTFA derivatized fraction containing the impurities with a high molecular mass. XIC looks very different to S103 and of lower abundances. Most compounds with a molecular mass of 482 were derivatized.

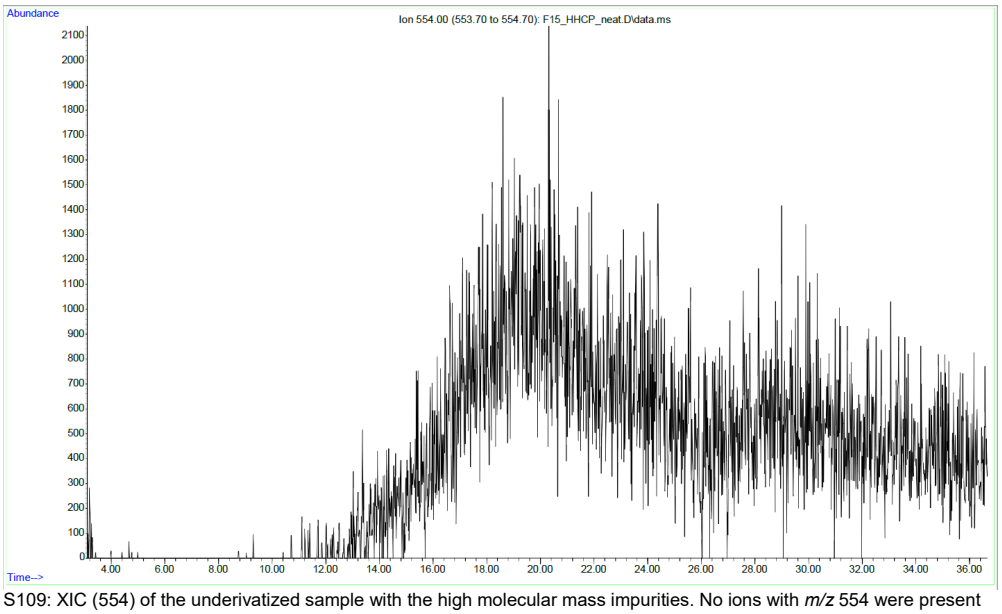

S109: XIC (554) of the underivatized sample with the high molecular mass impurities. No ions with *m/z* 554 were present prior derivatization.

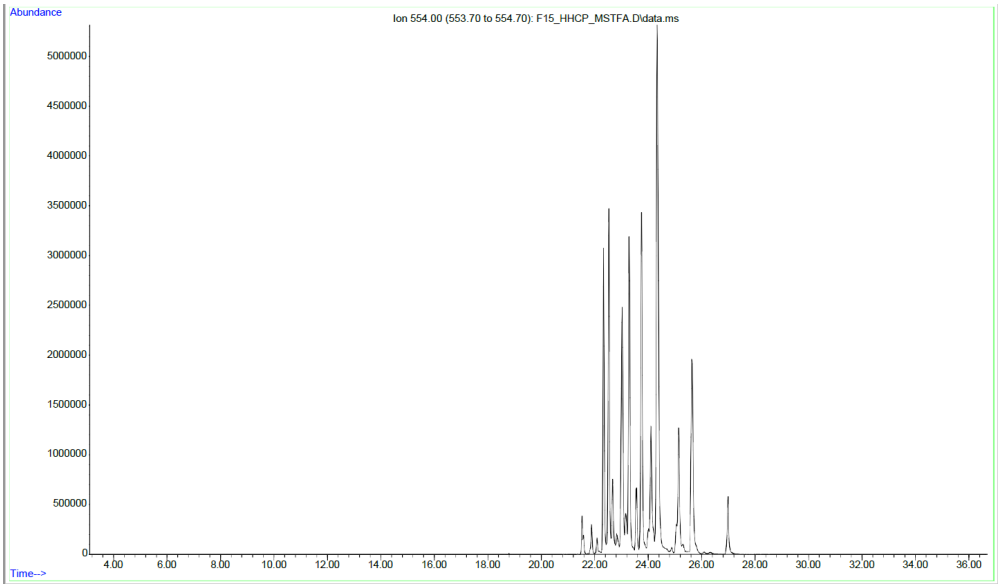

S110: XIC (554) of the MSTFA derivatized sample with the high molecular mass impurities. A lot of compounds with the molecular ion (or fragment ion) *m/z* 554 are present after trimethylsilylation (482+72).

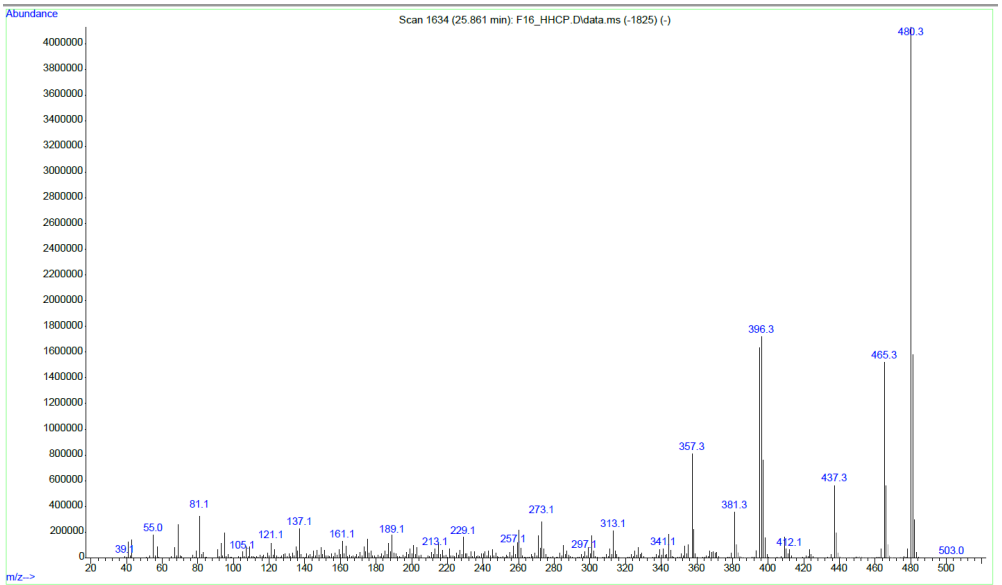

S111: GC-EI-MS of a byproduct with high molecular mass prior silylation. Characteristic fragmentation reactions for HHCP are observable.

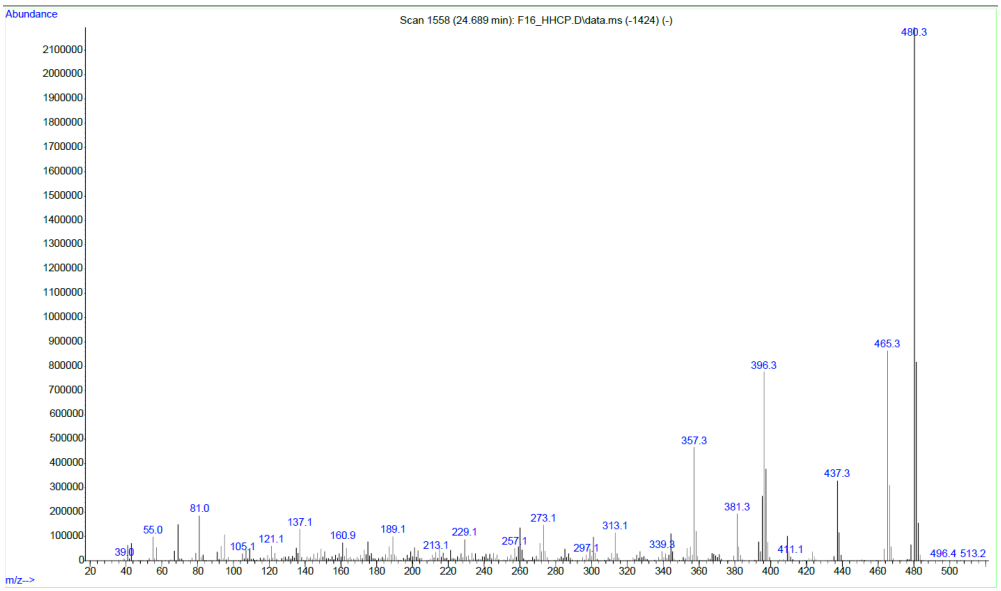

S112: GC-EI-MS of a byproduct with high molecular mass prior silylation. Characteristic fragmentation reactions for HHCP are observable.

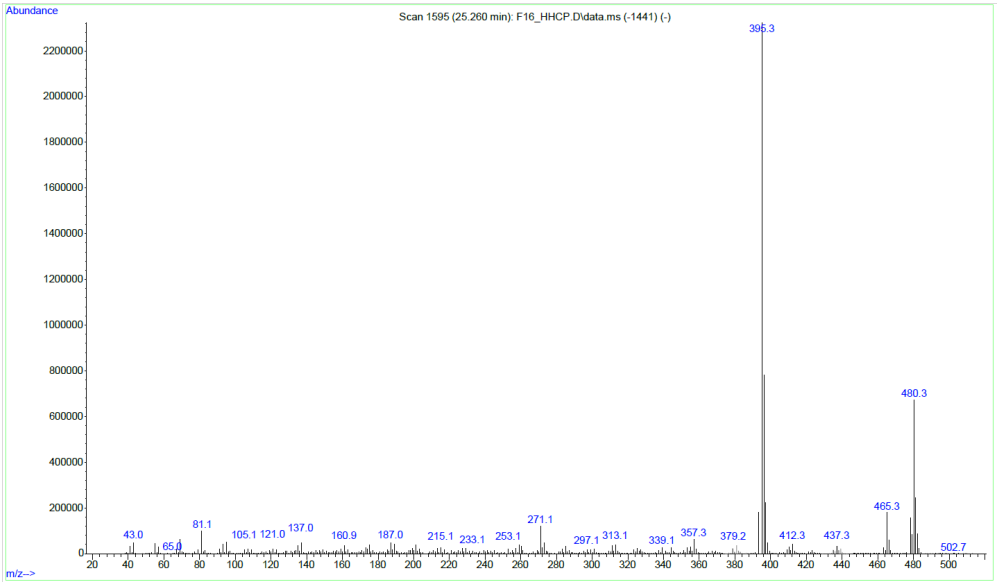

S113: GC-EI-MS of a byproduct with high molecular mass prior silylation. Characteristic fragmentation reactions for dibenzopyran cannabinoids are observable.

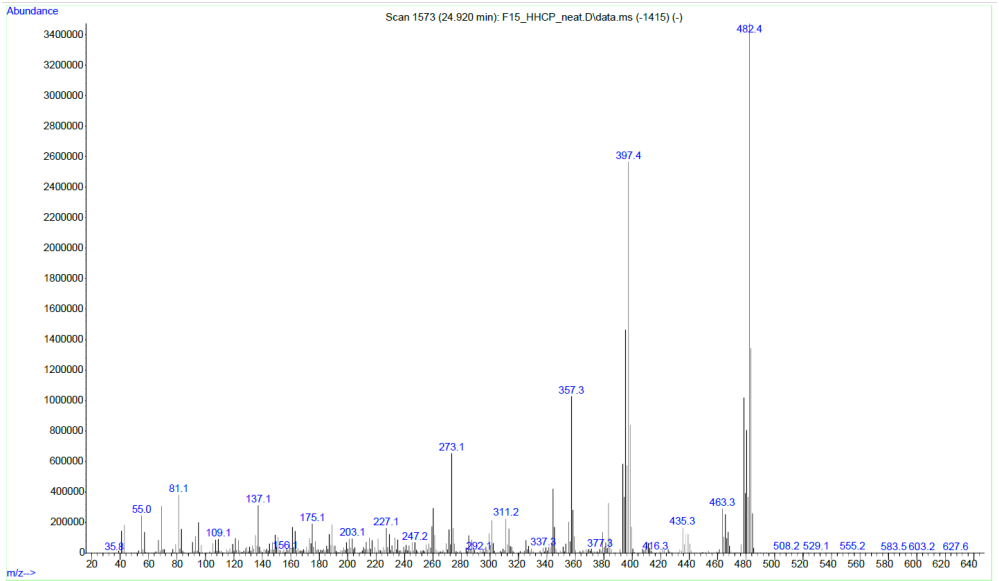

S114: GC-EI-MS of a byproduct with high molecular mass prior silylation. Similar fragmentation reactions as in the isolated ketones **4** and **5** appear.

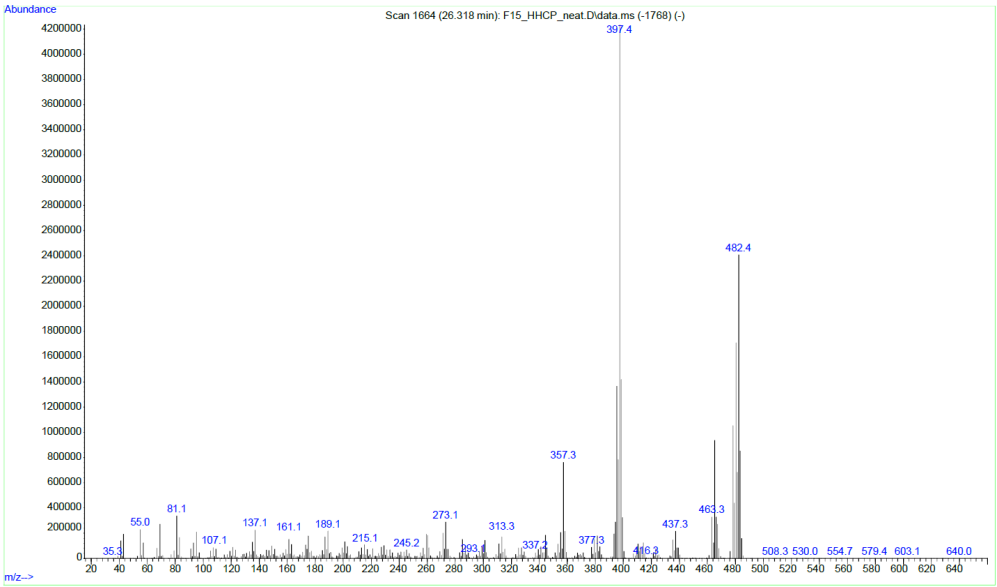

S115: GC-EI-MS of a byproduct with high molecular mass prior silylation. Similar fragmentation reactions as in the isolated ketones **4** and **5** appear.

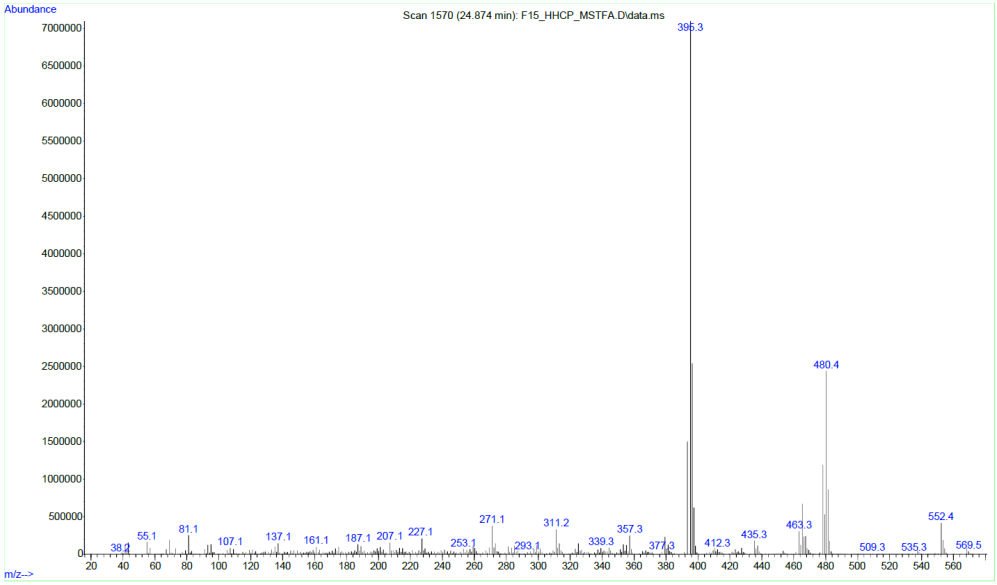

S116: GC-EI-MS of a byproduct with high molecular mass after mono-silylation. Similar fragmentation reactions appear as in dibenzopyran cannabinoids.

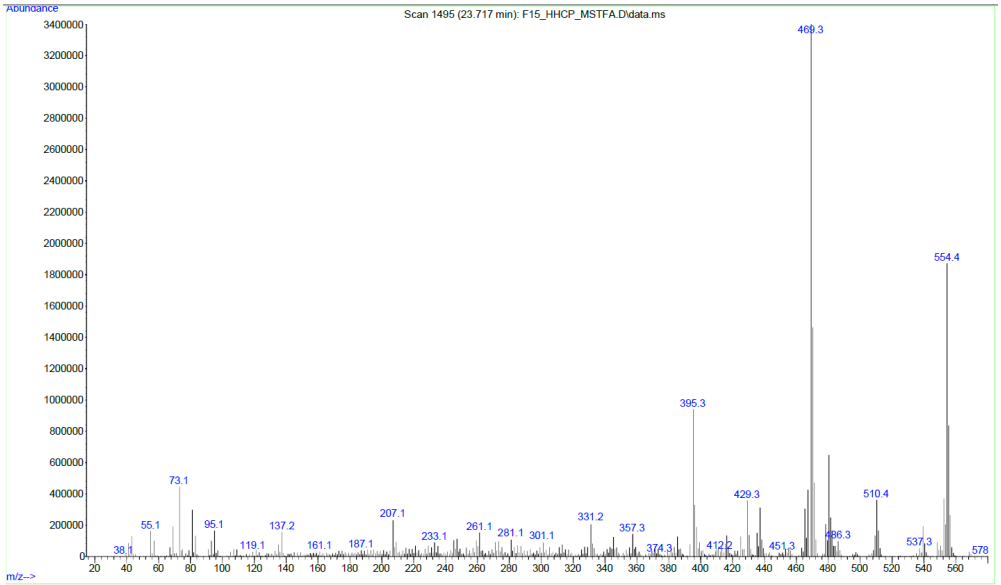

S117: GC-EI-MS of a byproduct with high molecular mass after mono-silylation. Similar fragmentation reactions appear as in dibenzopyran cannabinoids.

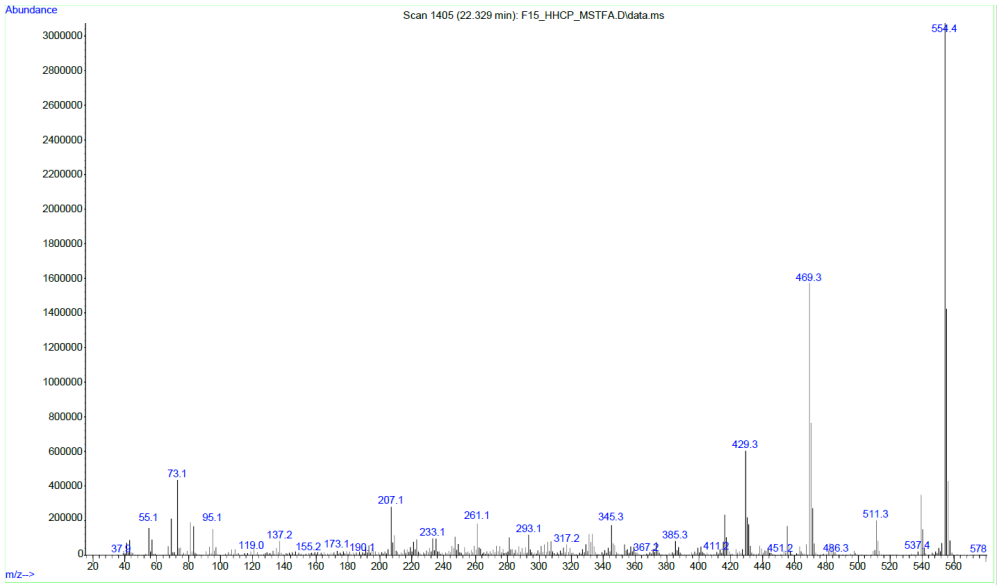

S118: GC-EI-MS of a byproduct with high molecular mass after mono-silylation. Similar fragmentation reactions appear as in dibenzopyran cannabinoids.

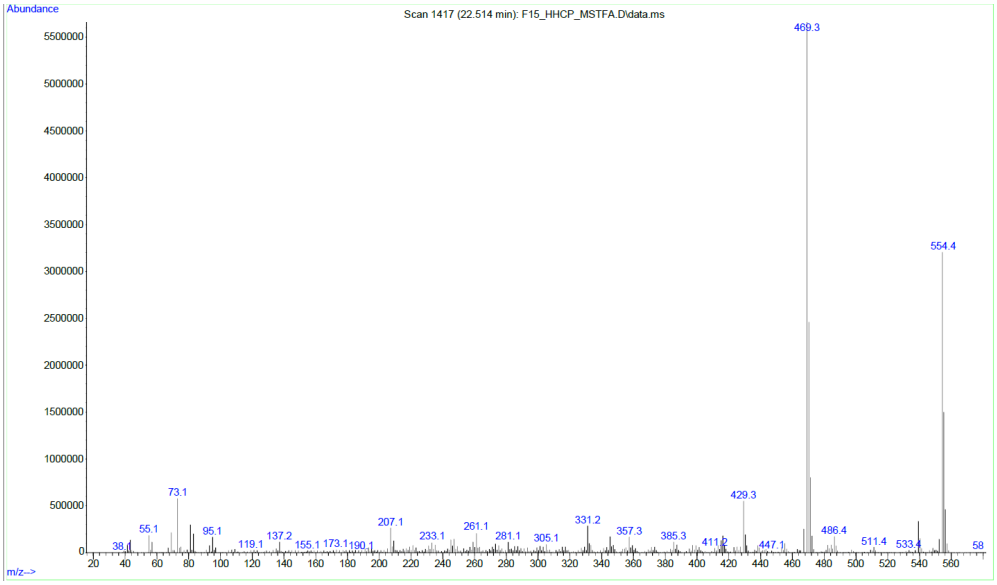

S119: GC-EI-MS of a byproduct with high molecular mass after mono-silylation. Similar fragmentation reactions as in the isolated ketones **4** and **5** appear.

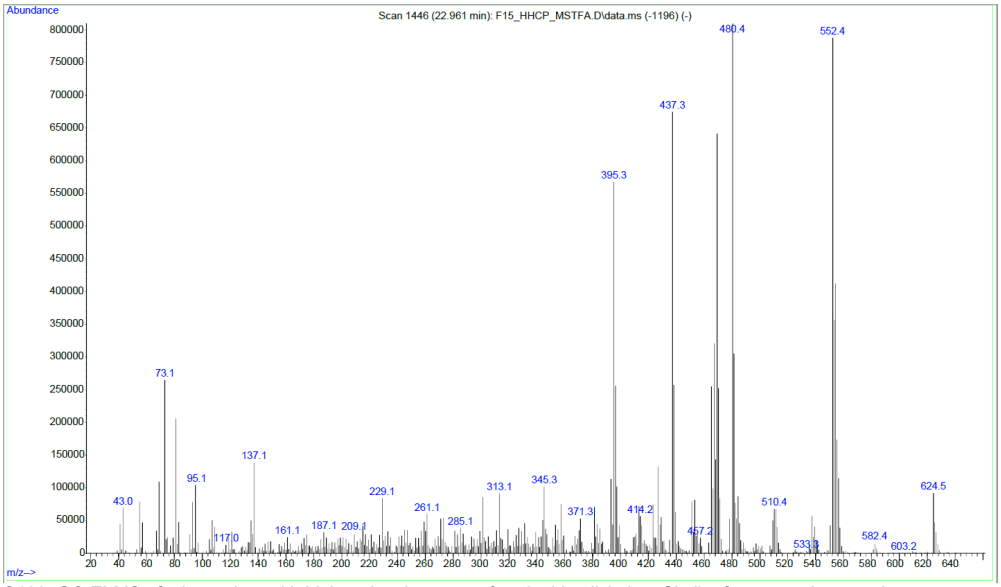

S120: GC-EI-MS of a byproduct with high molecular mass after double-silylation. Similar fragmentation reactions appear as in dibenzopyran cannabinoids.

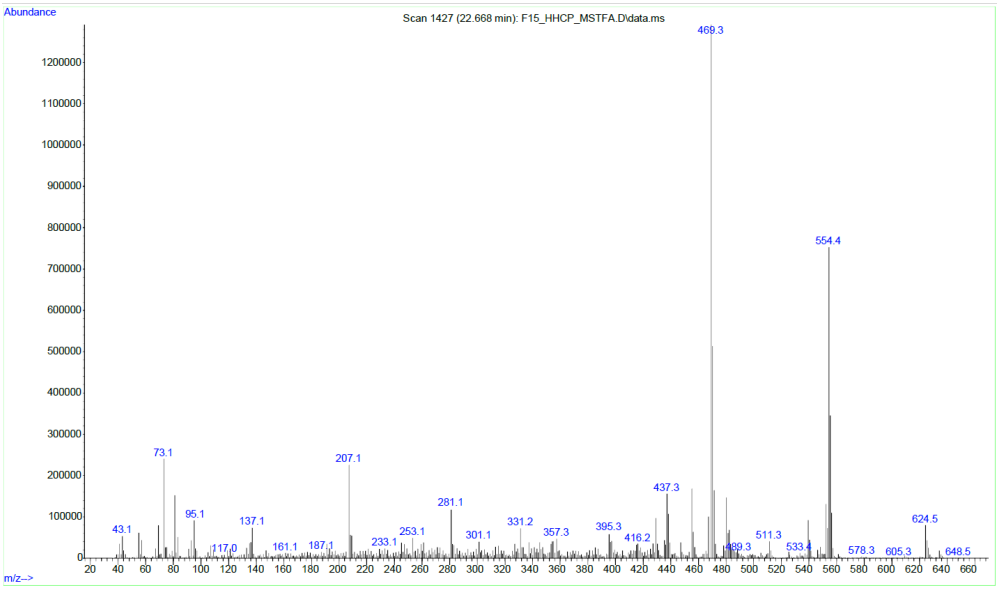

S121: GC-EI-MS of a byproduct with high molecular mass after double-silylation. Similar fragmentation reactions appear as in dibenzopyran cannabinoids.

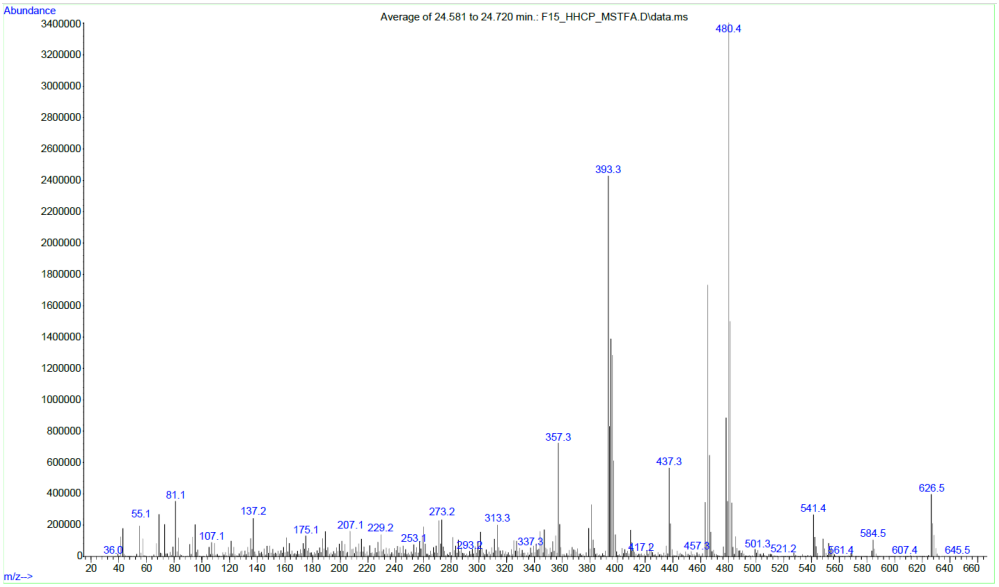

S122: GC-EI-MS of a byproduct with high molecular mass after double-silylation. Similar fragmentation reactions appear as in dibenzopyran cannabinoids.

Supplementary Information

Identification of synthetic impurities in a vape pen containing Δ⁹-tetrahydrocannabiphorol by GC-MS

Willi Schirmer[1, 2], Stefan Schürch[2], Wolfgang Weinmann[1]

[1]Institute of Forensic Medicine, Forensic Toxicology and Chemistry, University of Bern, Murtenstrasse 26, 3008 Bern, Switzerland

[2]Department of Chemistry, Biochemistry and Pharmaceutical Sciences, University of Bern, Freiestrasse 3, 3012 Bern, Switzerland

Corresponding author:

Willi Schirmer, Institute of Forensic Medicine, Forensic Toxicology and Chemistry, University of Bern, Murtenstrasse 26, 3008 Bern, Switzerland

e-mail address: willi.schirmer@irm.unibe.ch

Table of contents

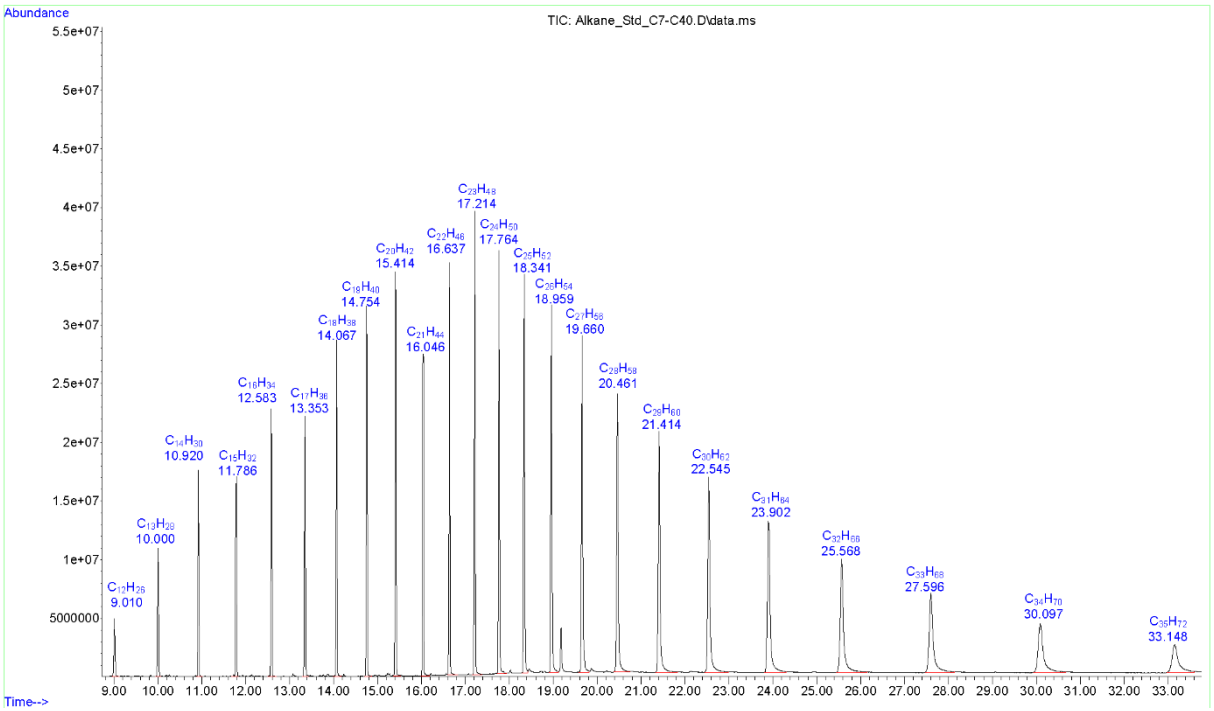

S1 TIC of an alkane standard (C7-C40) for the determination of Kováts indices.

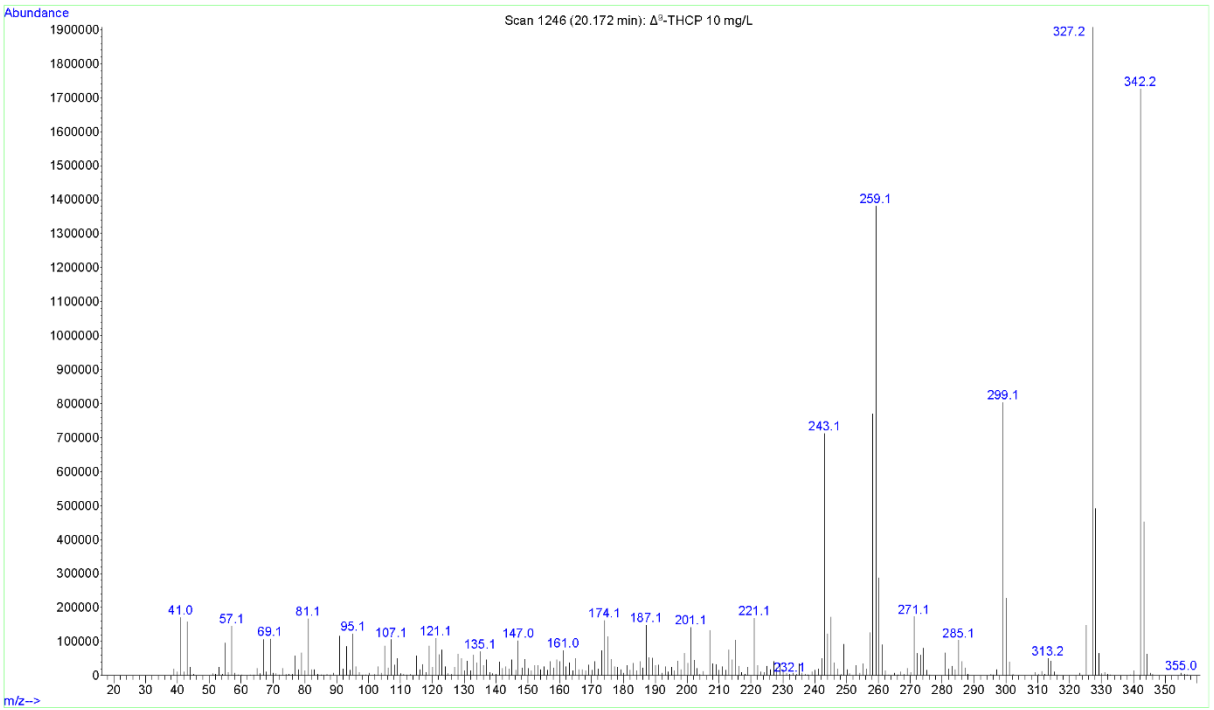

S2: EI mass spectrum of Δ^9-THCP (reference)

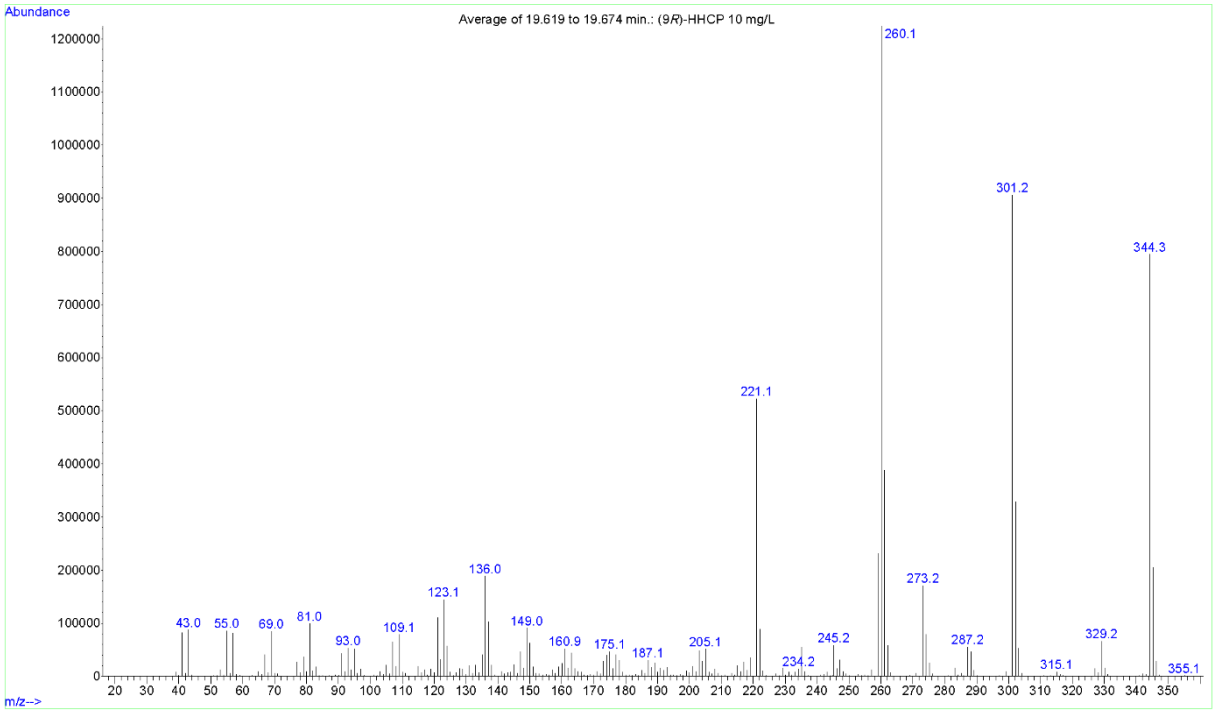

S3: EI mass spectrum of (9*R*)-HHCP (reference)

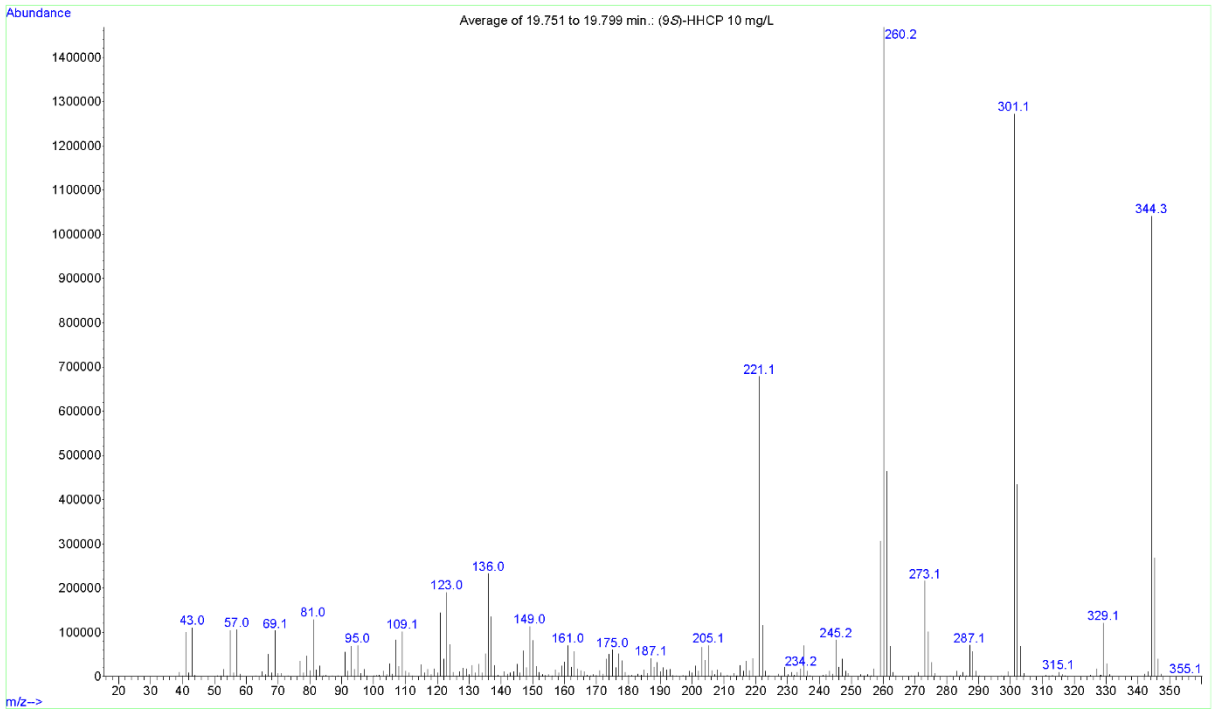

S4: EI mass spectrum of (9*S*)-HHCP (reference)

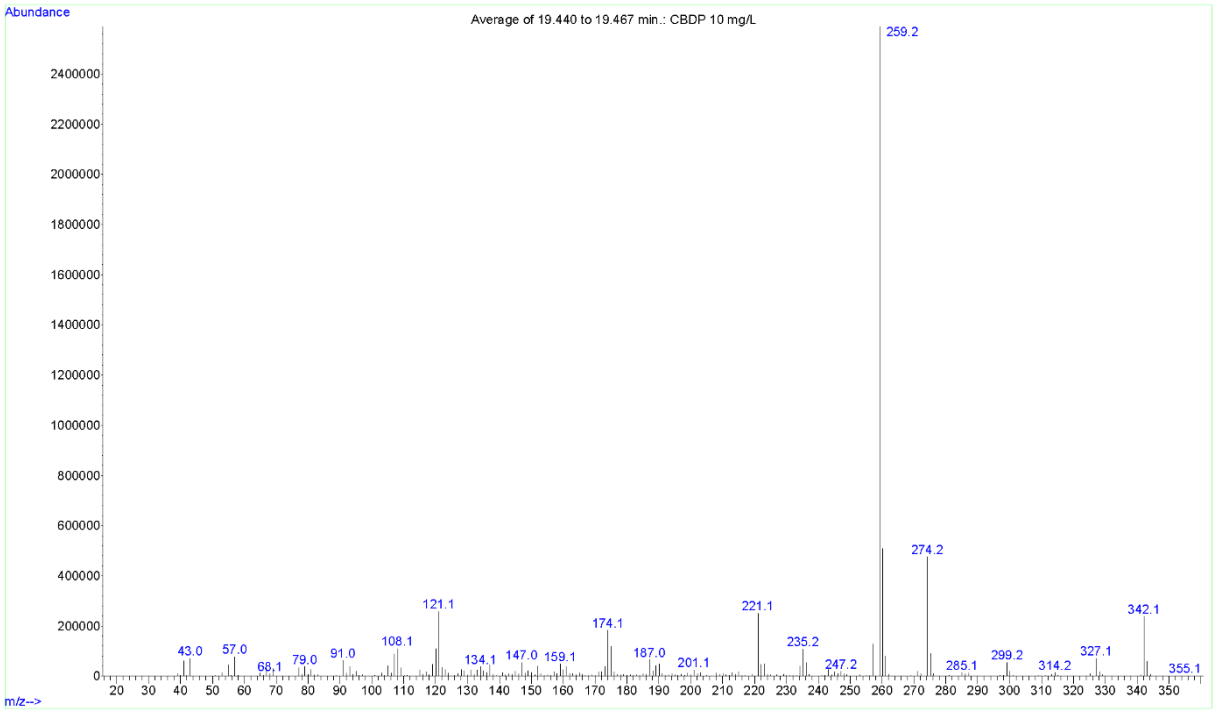

S5: EI mass spectrum of CBDP (reference)

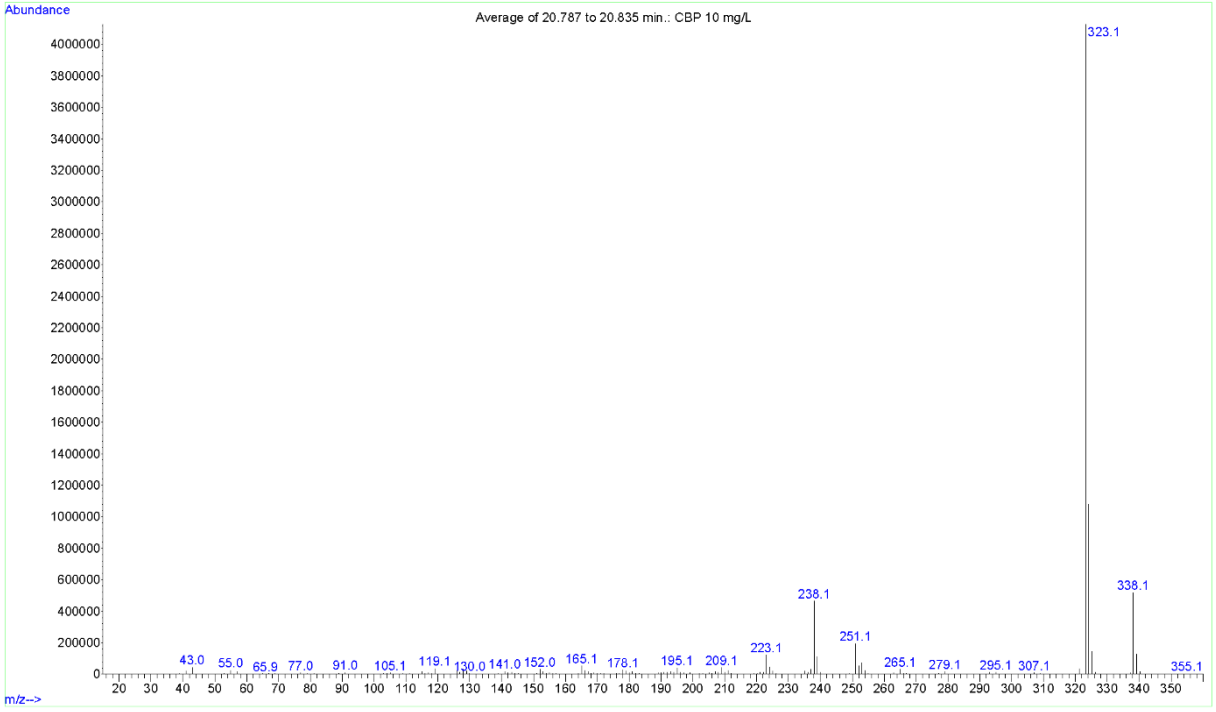

S6: EI mass spectrum of CBP (reference)

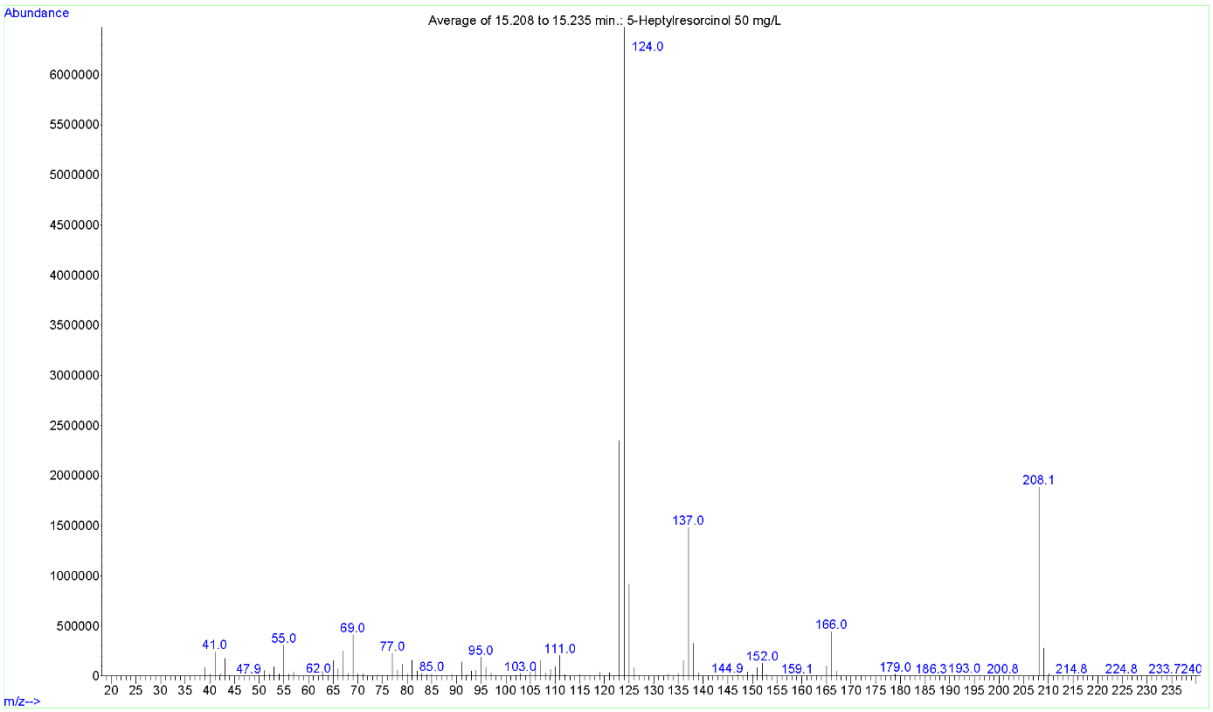

S7: EI mass spectrum of 5-heptylresorcinol (reference)

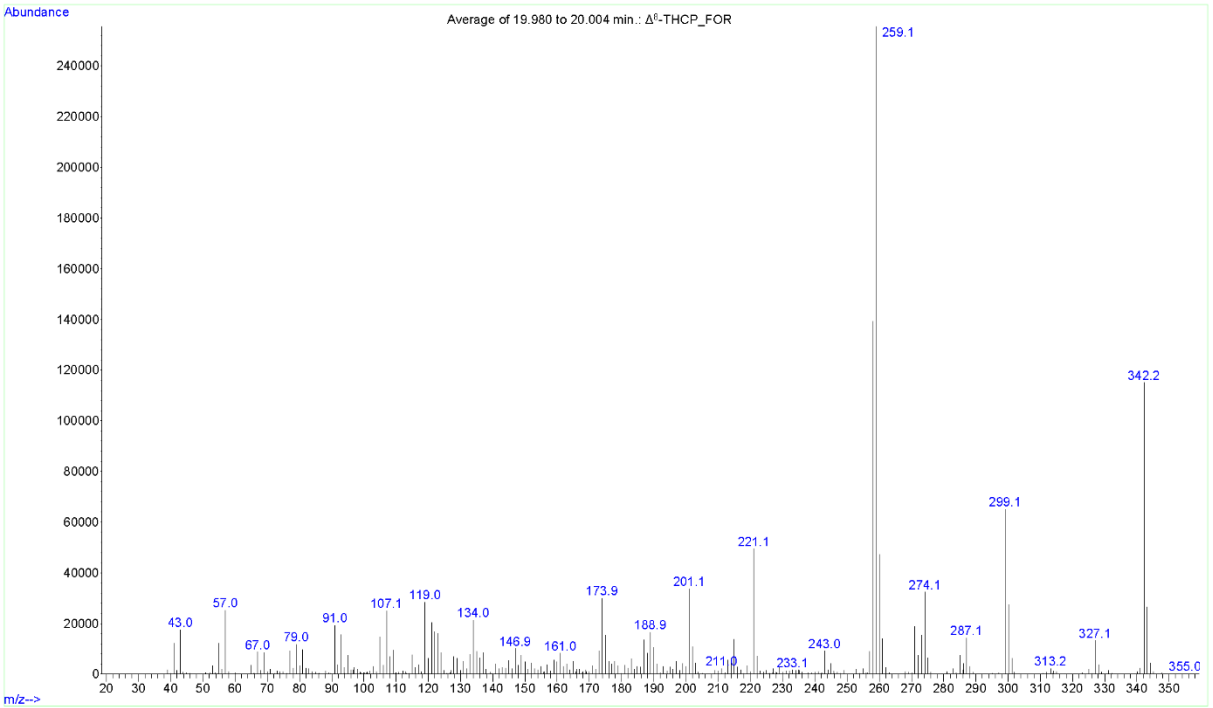

S8: EI mass spectrum of Δ^8-THCP (reference)

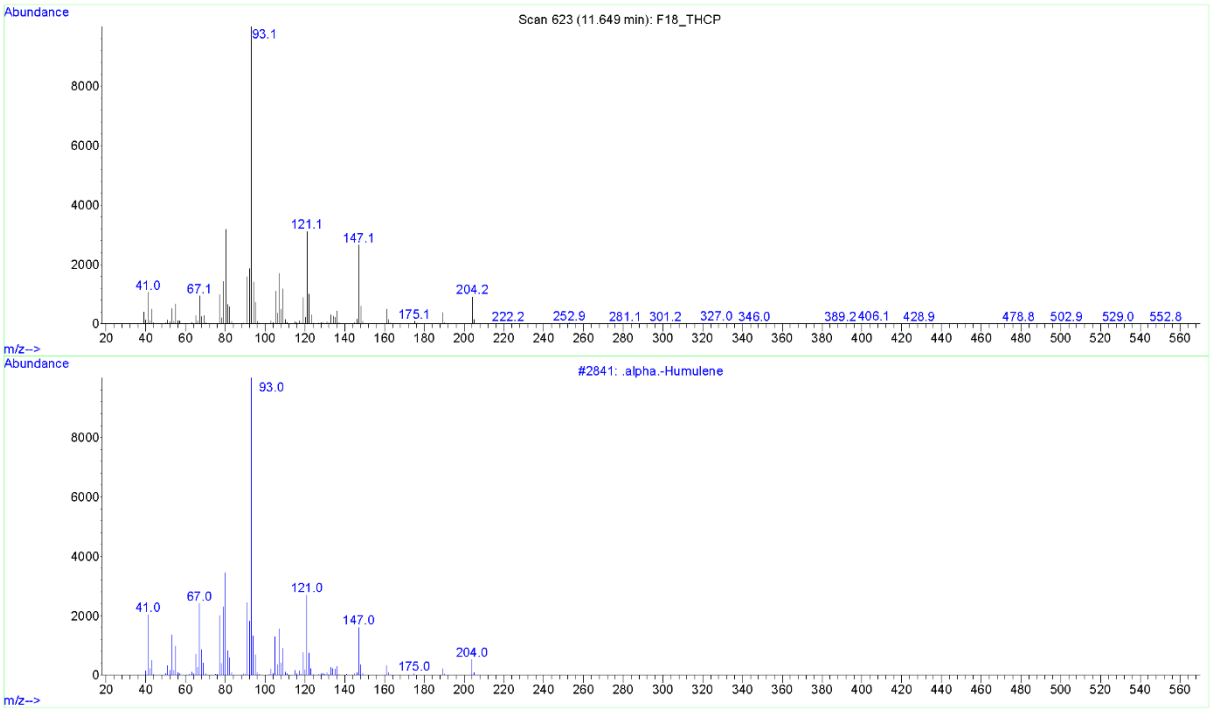

S9: α-Humulene found in a chromatographic fraction of the THCP vape pen liquid.

S10: β-Myrcene found in a chromatographic fraction of the THCP vape pen liquid.

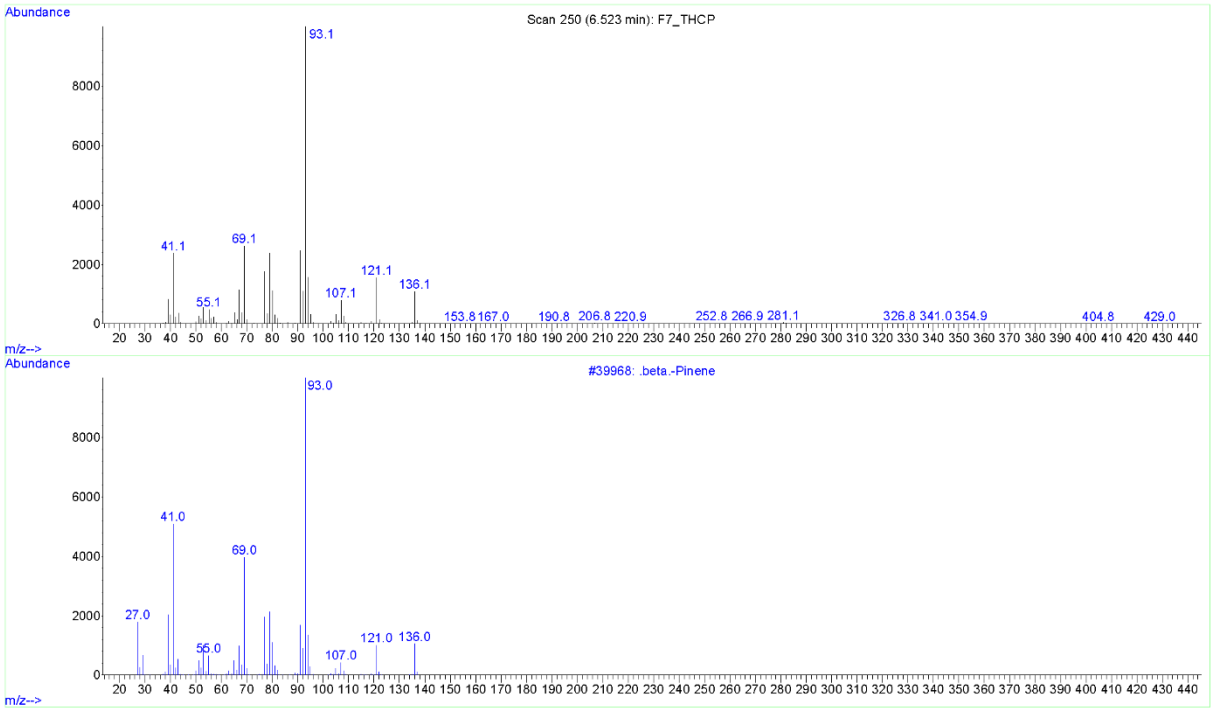

S11: β-Pinene found in a chromatographic fraction of the THCP vape pen liquid

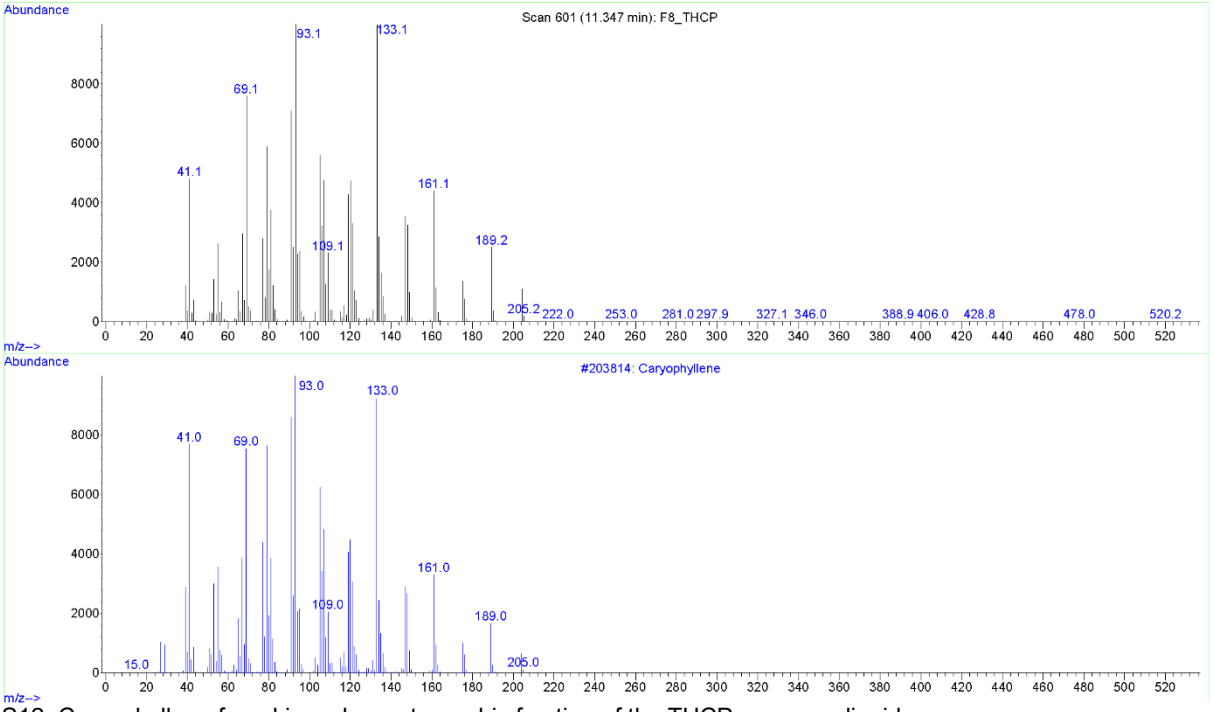

S12: Caryophyllene found in a chromatographic fraction of the THCP vape pen liquid

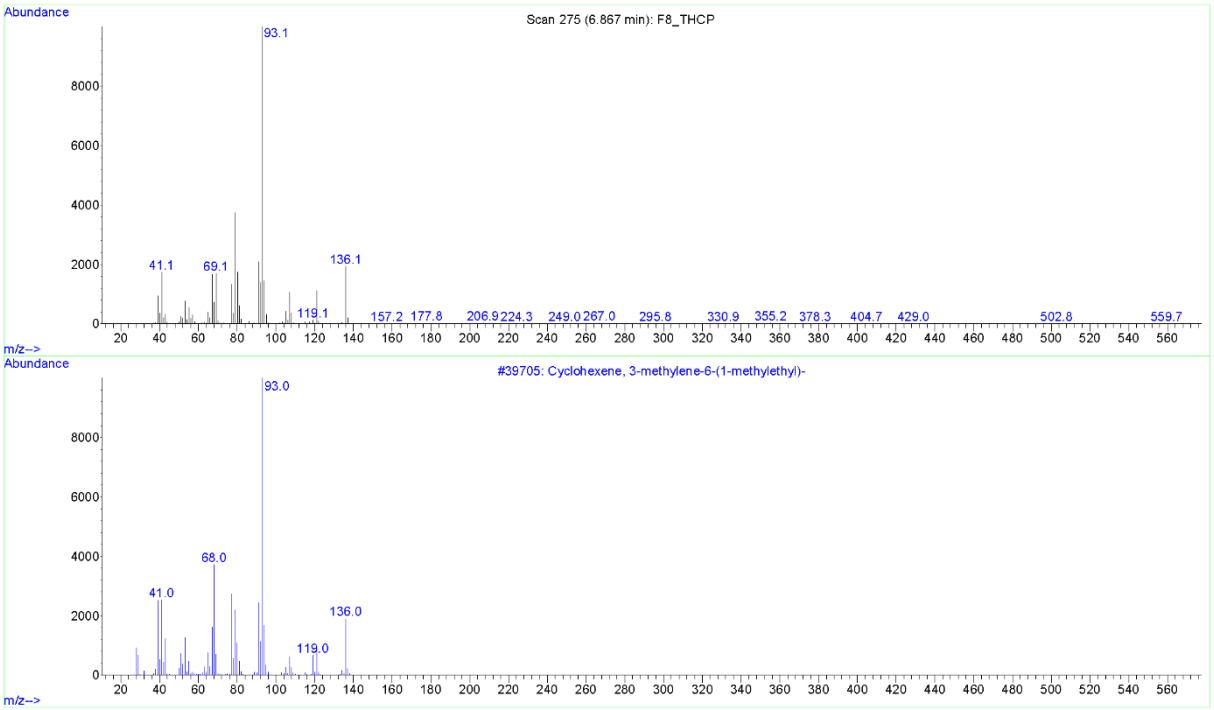

S13: β-Phellandrene found in a chromatographic fraction of the THCP vape pen liquid

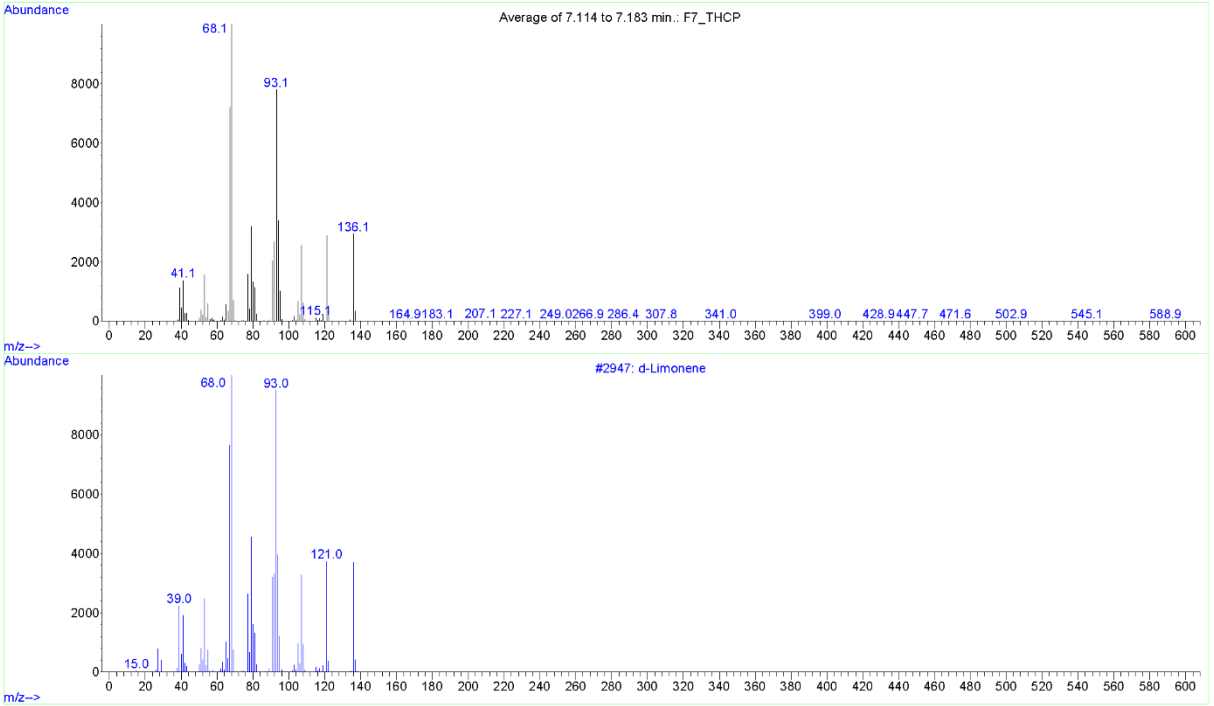

S14: (*R*)-Limonene found in a chromatographic fraction of the THCP vape pen liquid

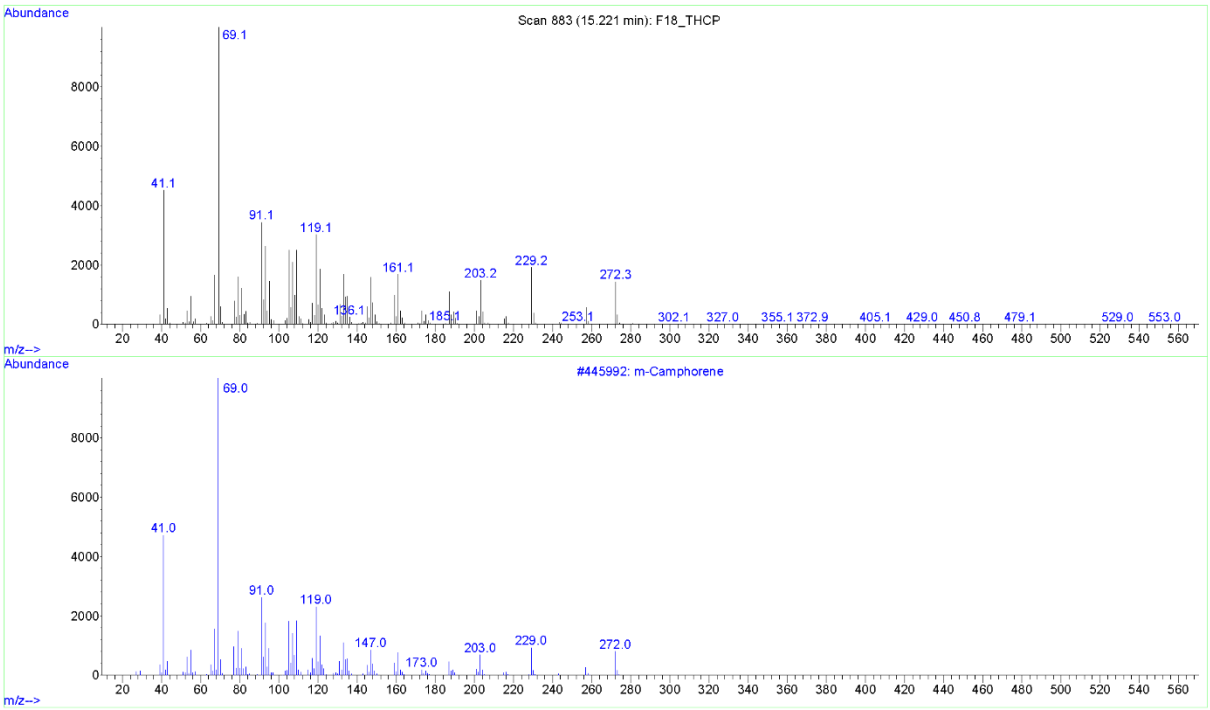

S15: *m*-Camphorene found in a chromatographic fraction of the THCP vape pen liquid

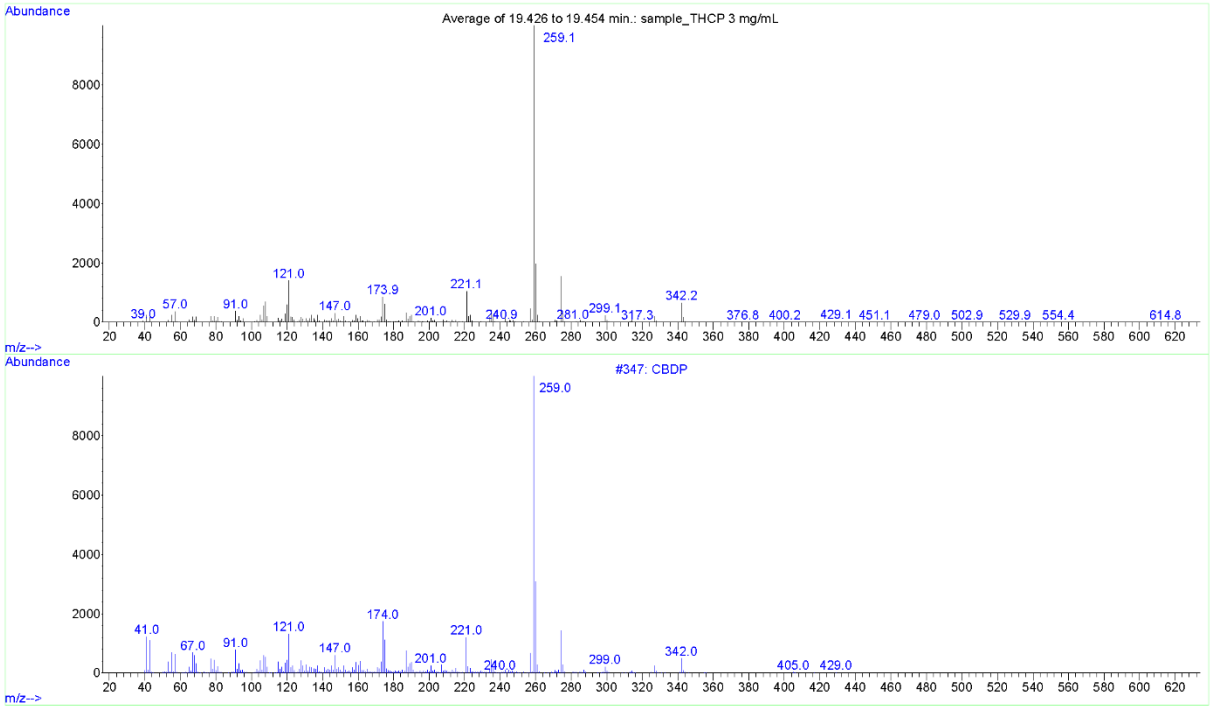

S16: CBDP found in the THCP vape pen liquid

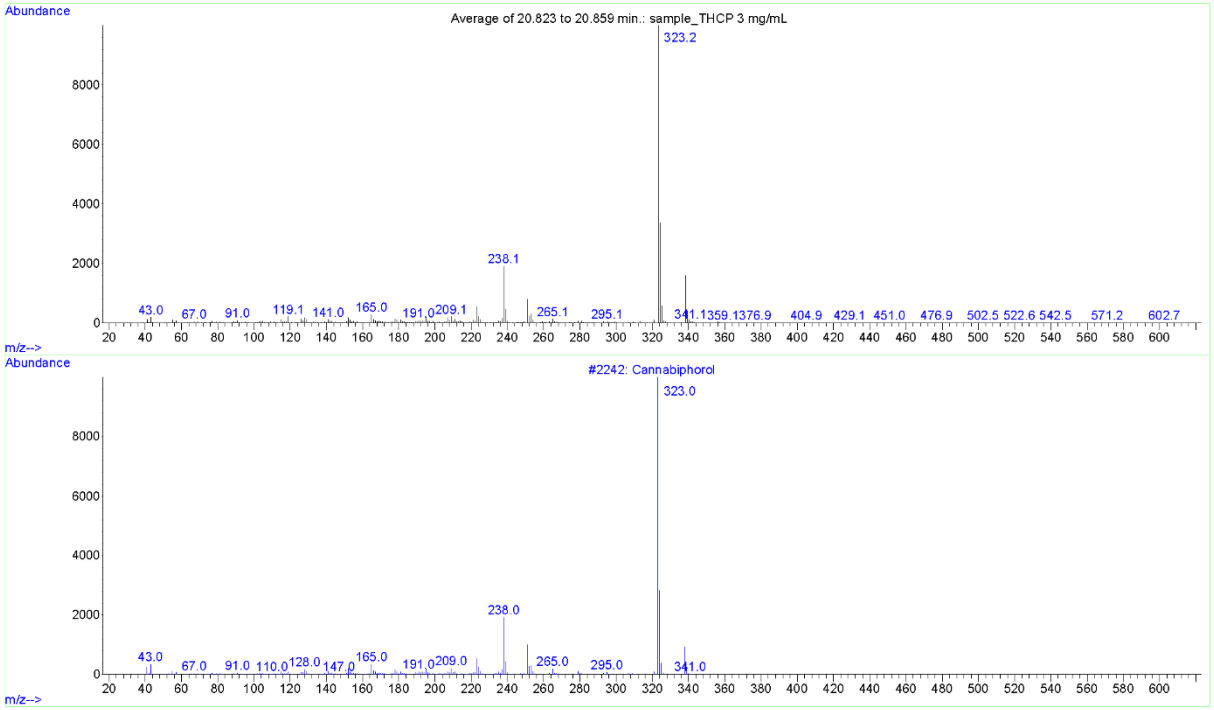

S17: CBP found in the THCP vape pen liquid

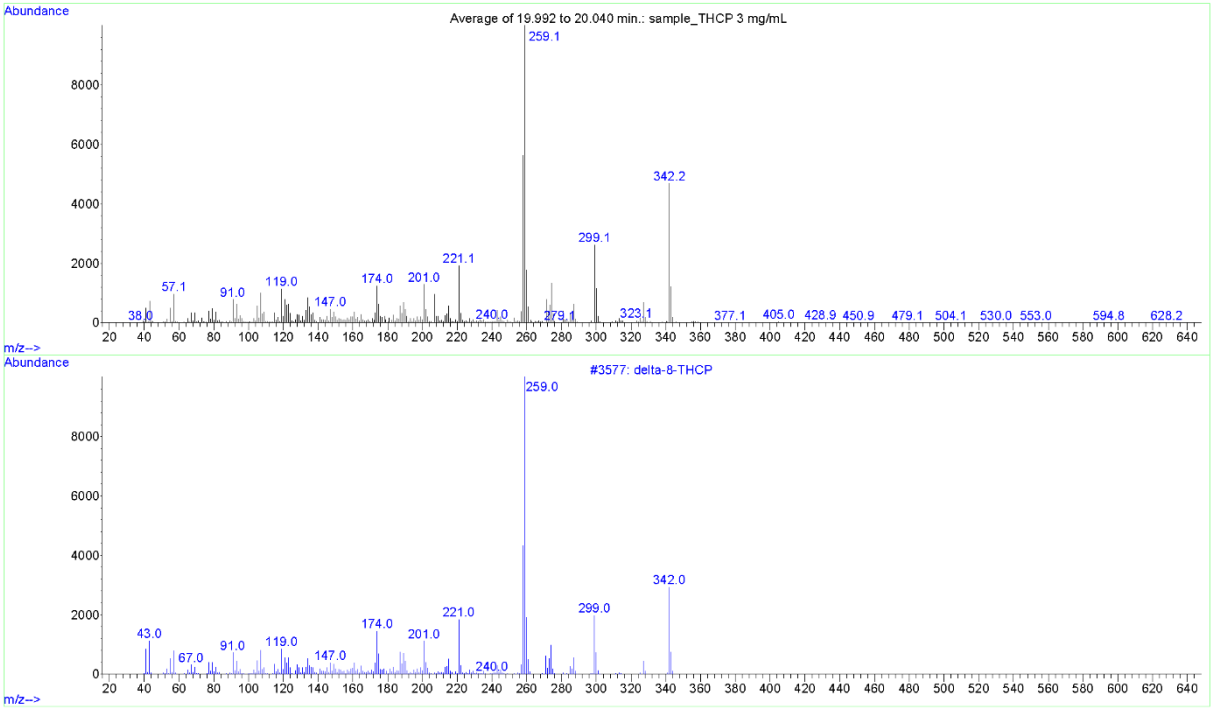

S18: Δ^8-THCP found in the THCP vape pen liquid

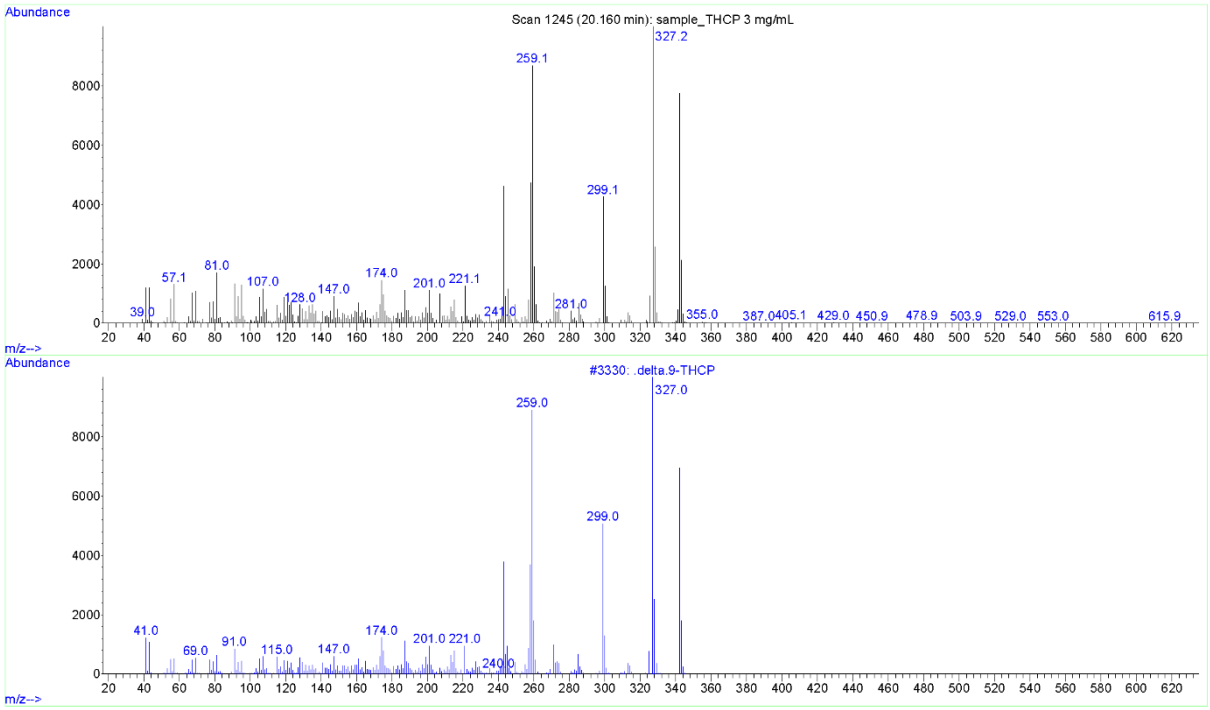

S19: Δ^9-THCP found in the THCP vape pen liquid

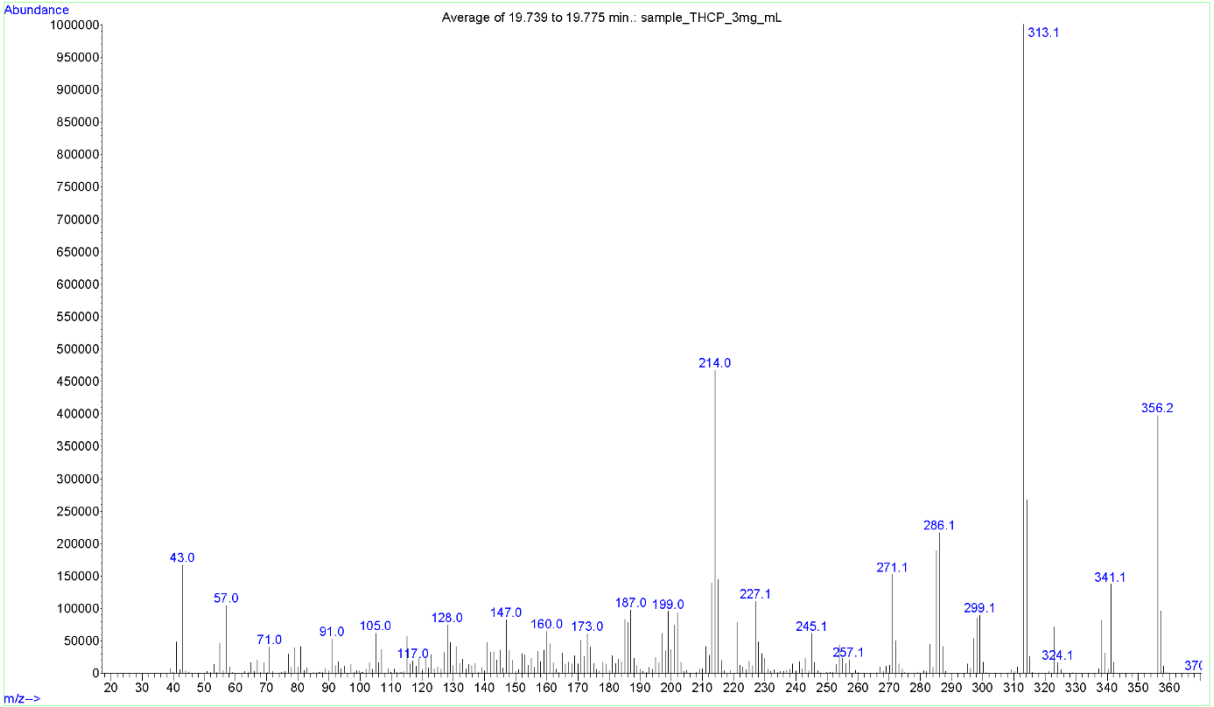

S20: Unknown THCP impurity found in the THCP vape pen liquid, potentially an oxo-THCP. (THCP impurity A)

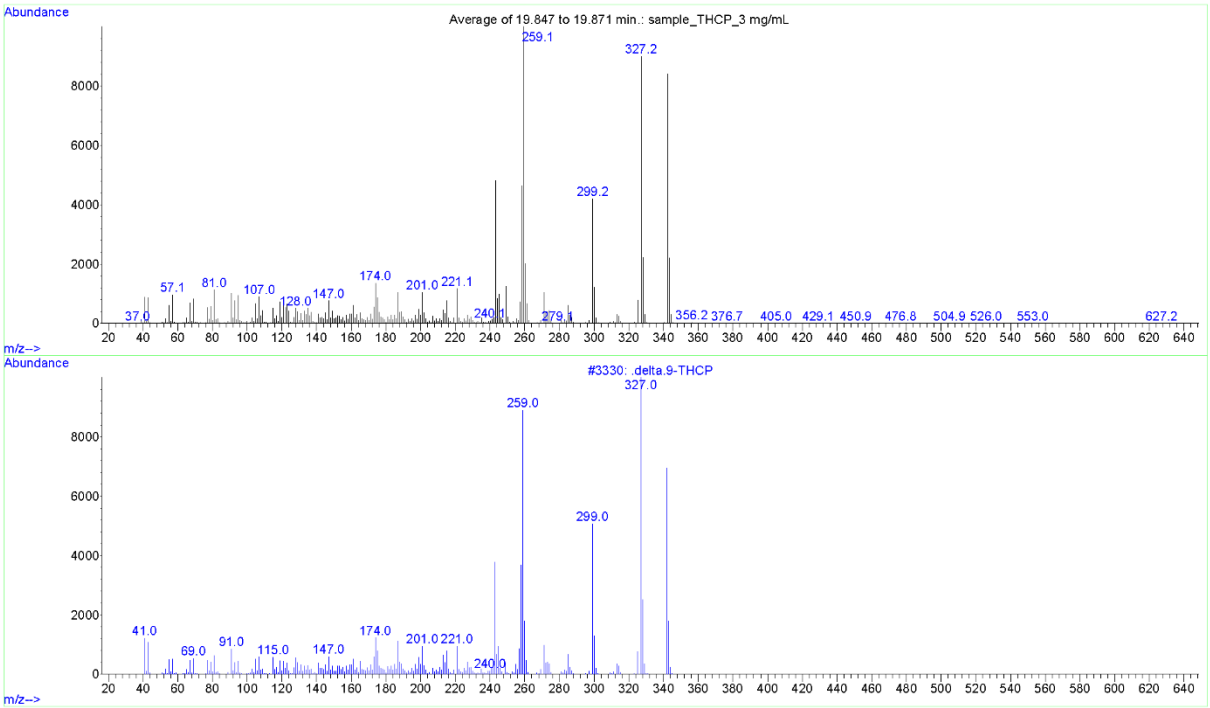

S21: THCP isomer found in the THCP vape pen liquid with a very similar fragmentation pattern as Δ^9-THCP, potentially the *cis*-isomer *cis*-Δ^9-THCP (THCP impurity B)

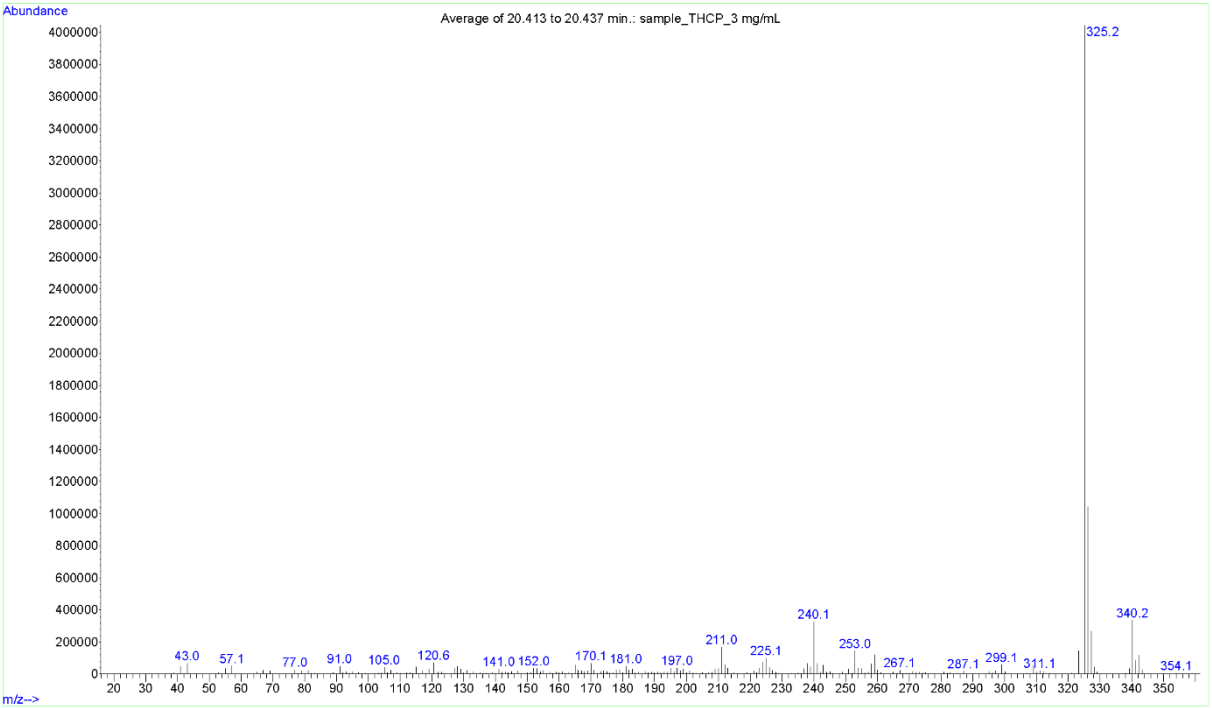

S22: Unknown impurity found in the THCP vape pen liquid, potentially a dihydrocannabiphorol (THCP impurity C)

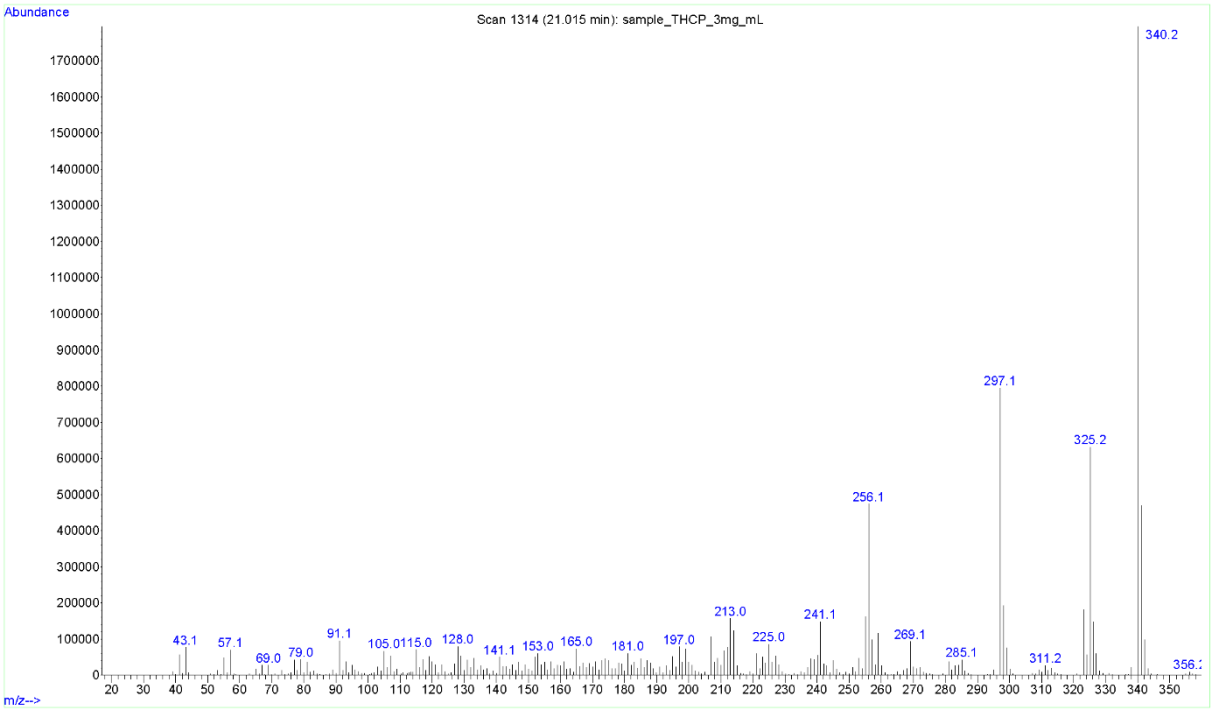

S23: Unknown impurity found in the THCP vape pen liquid, potentially a second dihydrocannabiphorol (THCP impurity D)

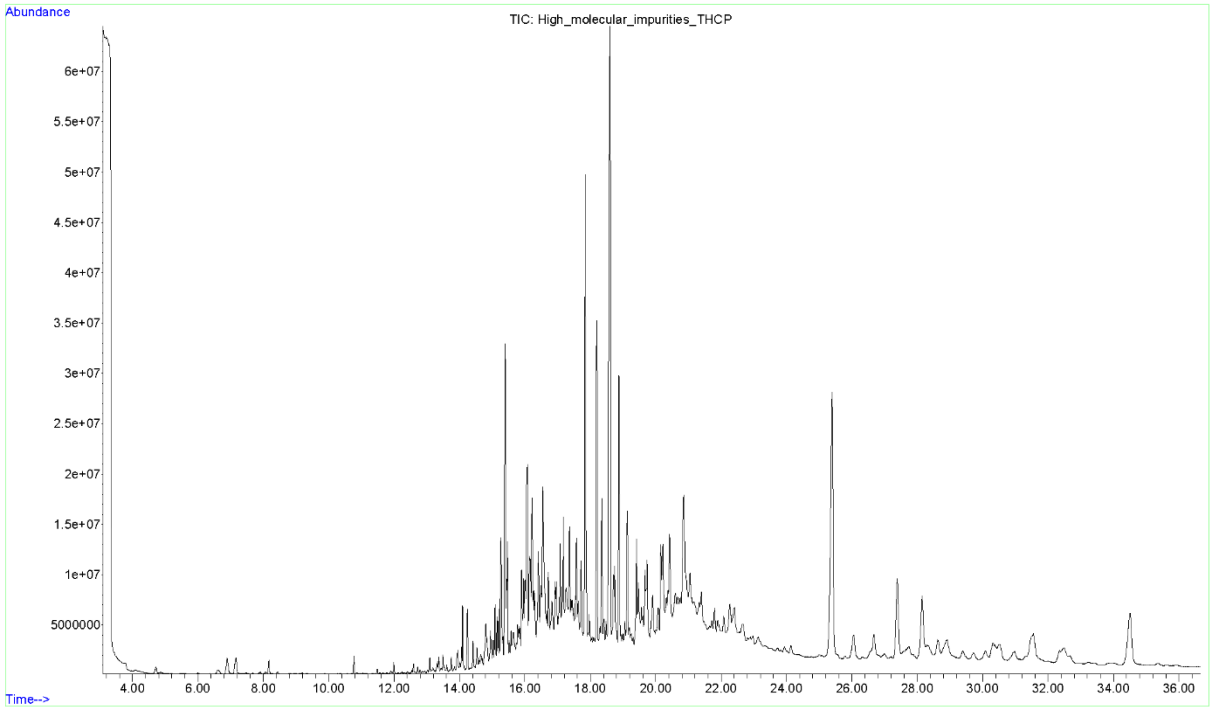

S24: TIC of a chromatographic fraction from the THCP vape pen liquid containing impurities with a high molecular mass. The impurities are found between 24 and 36 min.

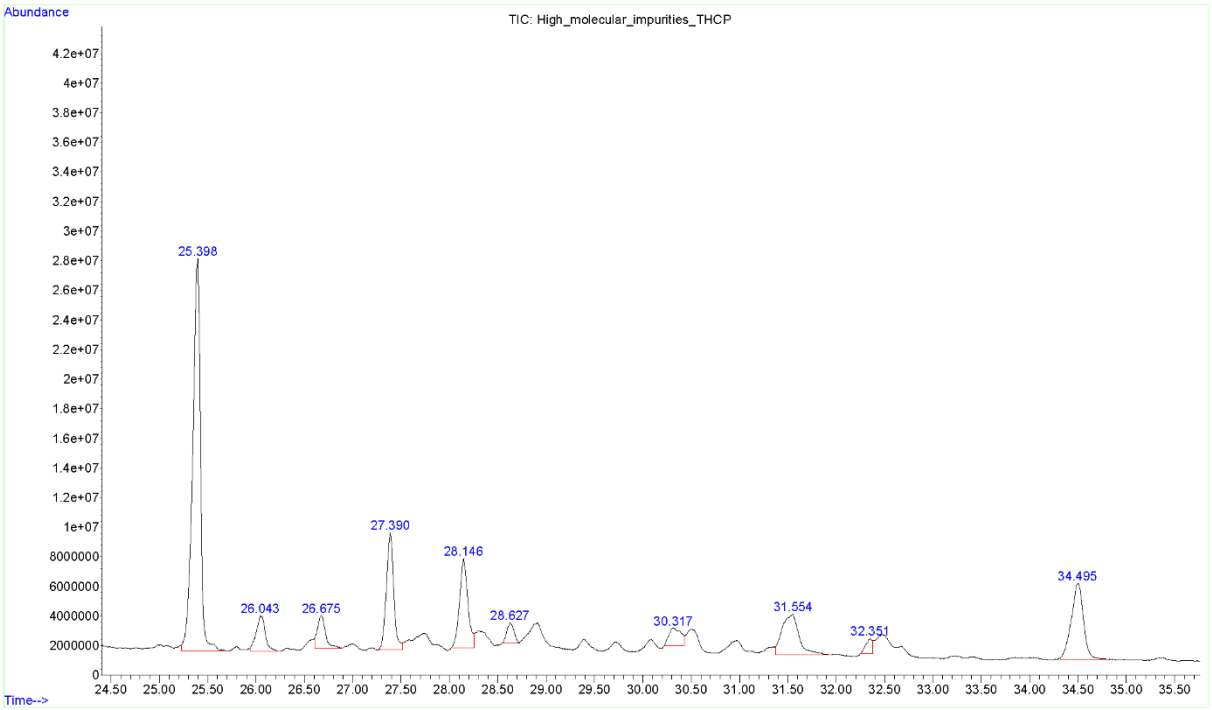

S25: TIC of a chromatographic fraction of the THCP vape pen liquid. Detail from S25.

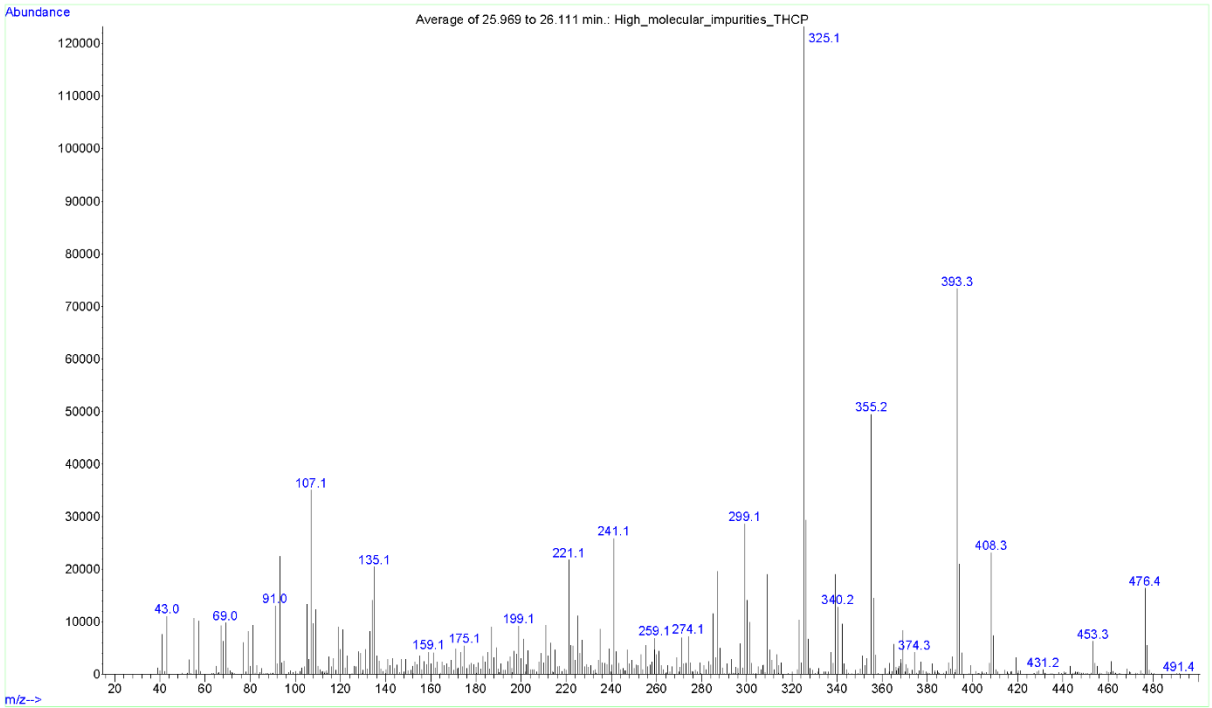

S26: EI mass spectrum of a bisalkylated cannabinoid

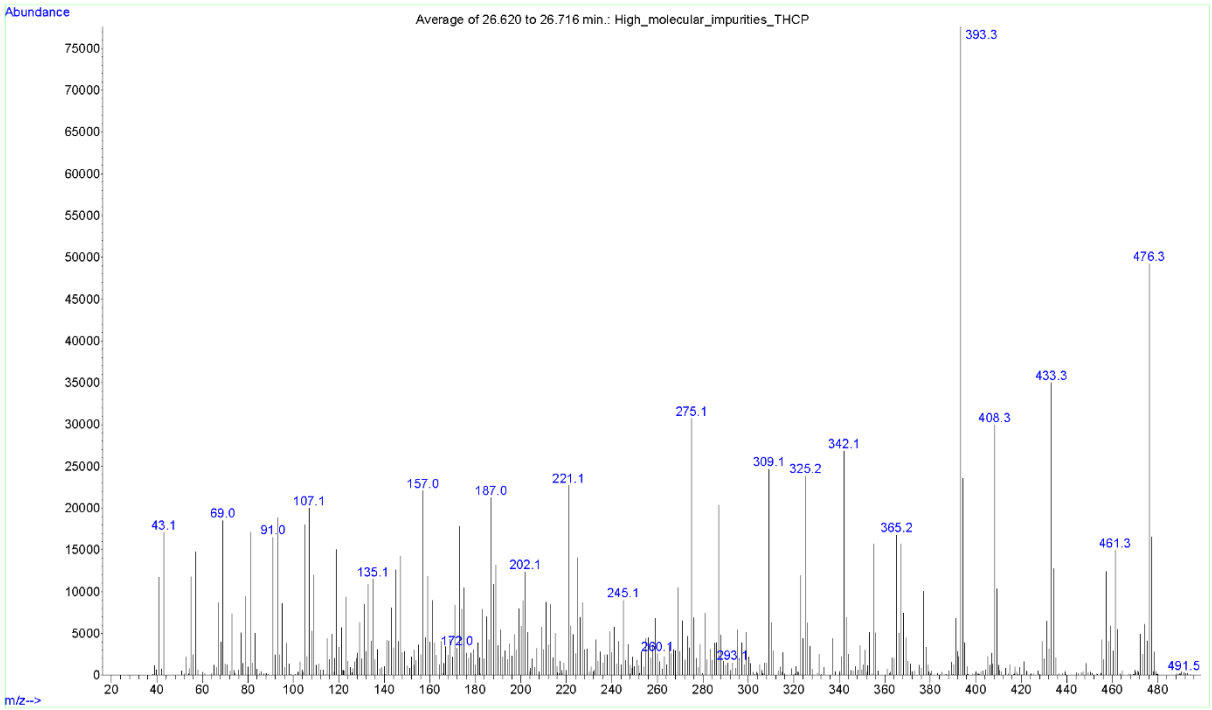

S27: EI mass spectrum of a bisalkylated cannabinoid

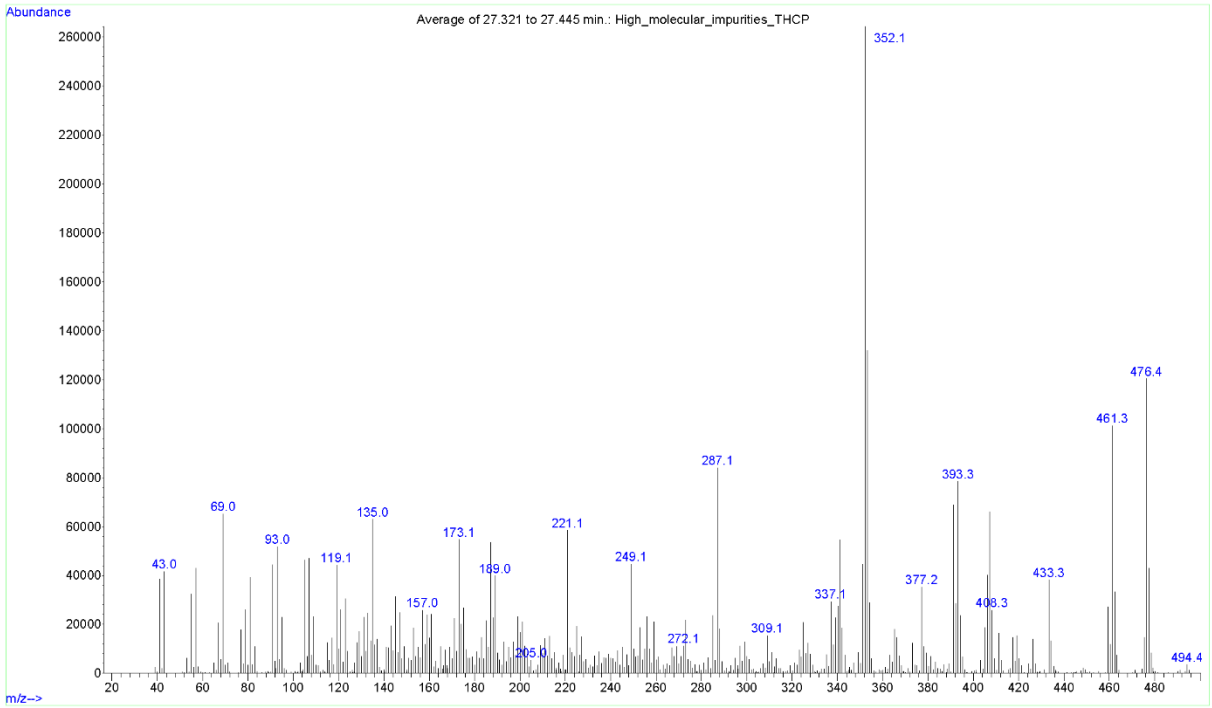

S28: EI mass spectrum of a bisalkylated cannabinoid

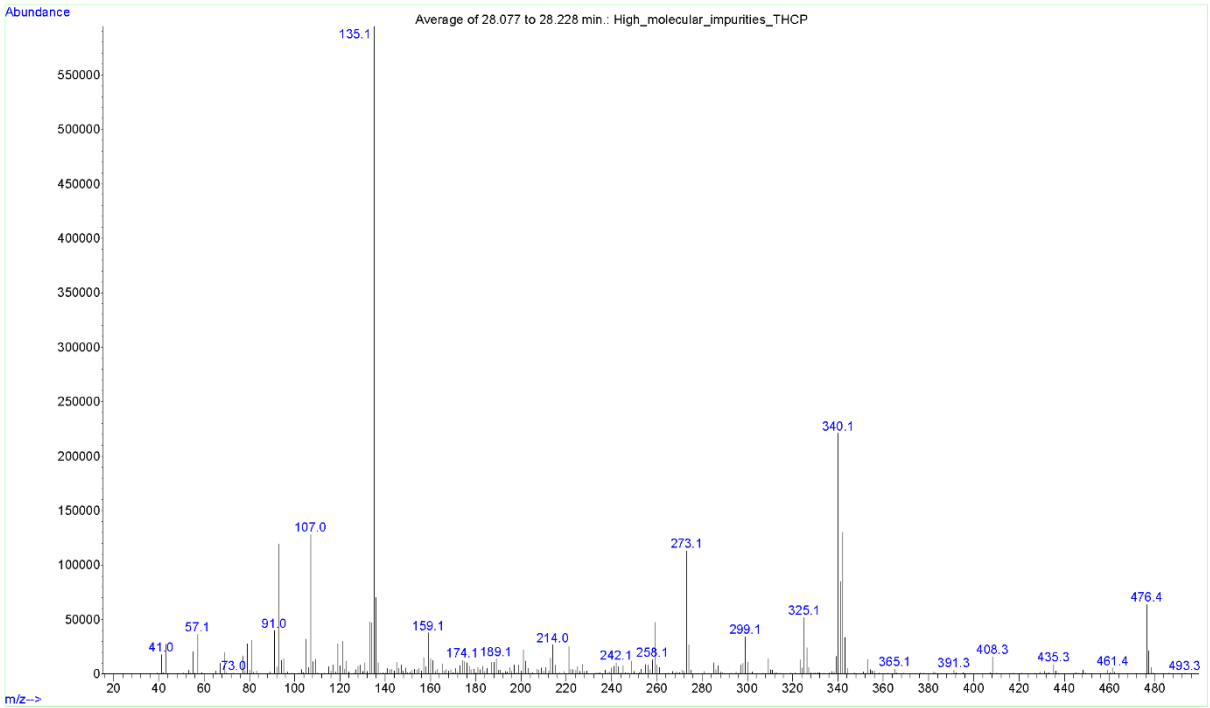

S29: EI mass spectrum of a bisalkylated cannabinoid

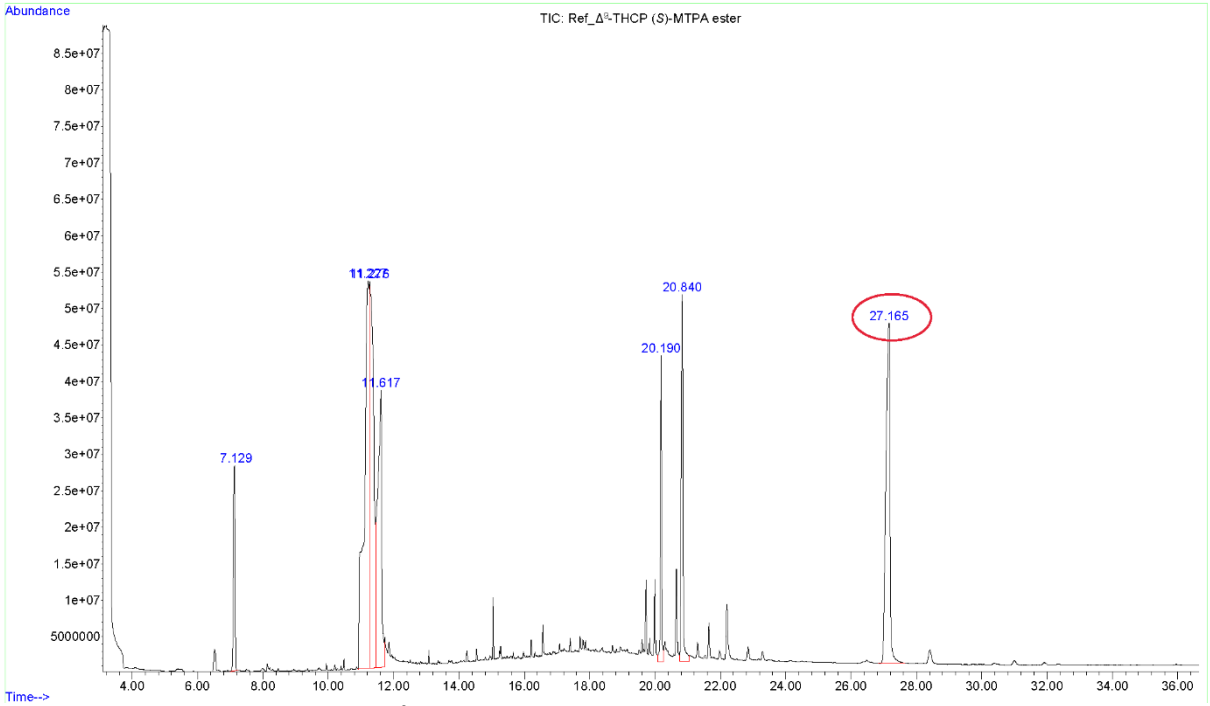

S30: TIC of the (*S*)-Mosher ester of Δ^9-THCP.

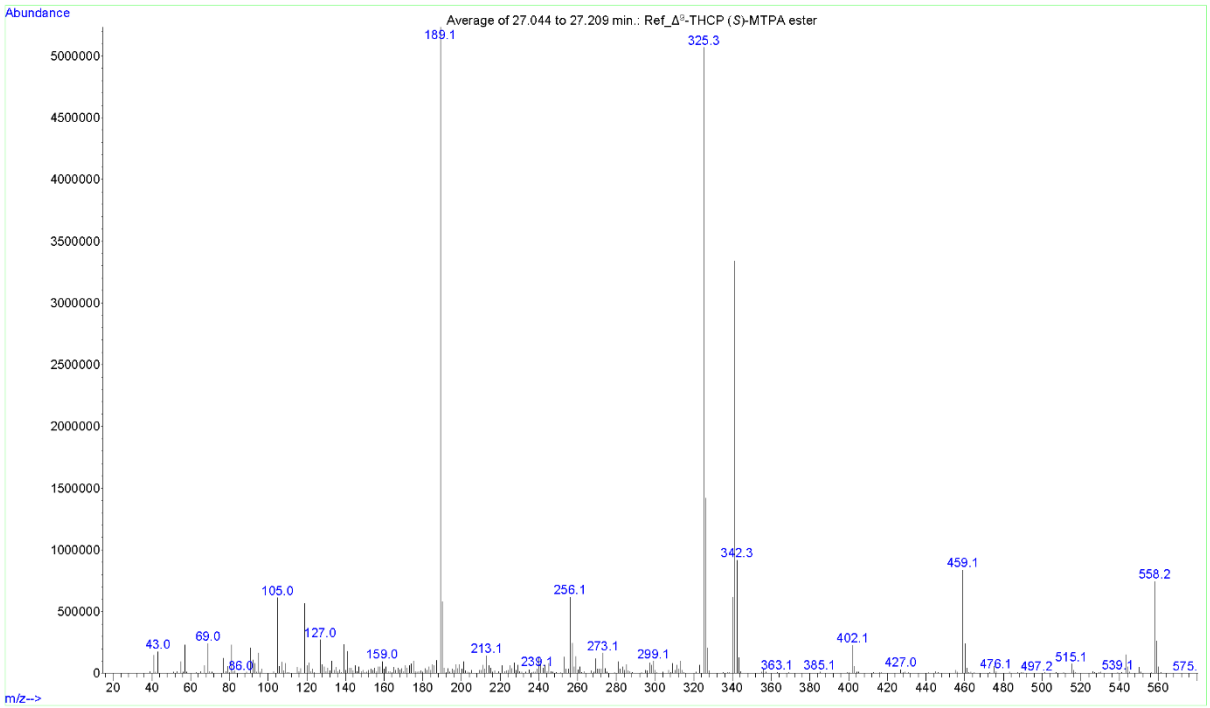

S31: EI mass spectrum of the (*S*)-Mosher ester of Δ^9-THCP.

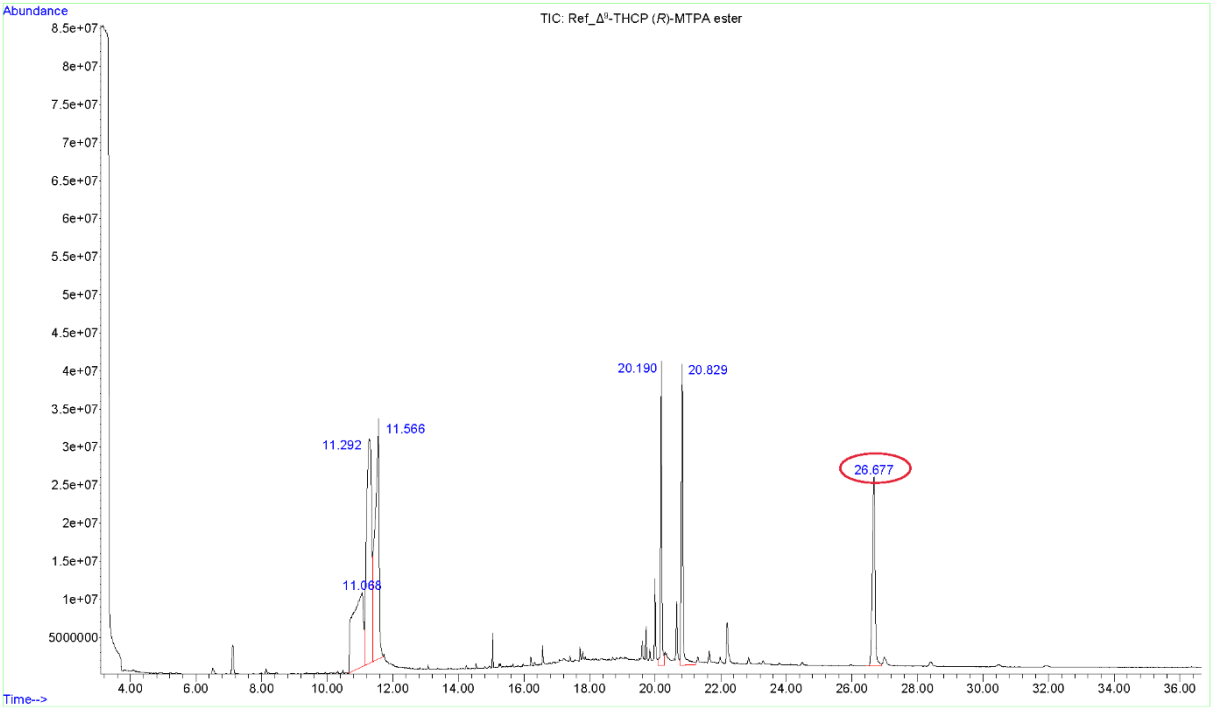

S32: TIC of the (*R*)-Mosher ester of Δ^9-THCP.

S33: EI mass spectrum of the (*R*)-Mosher ester of Δ^9-THCP.

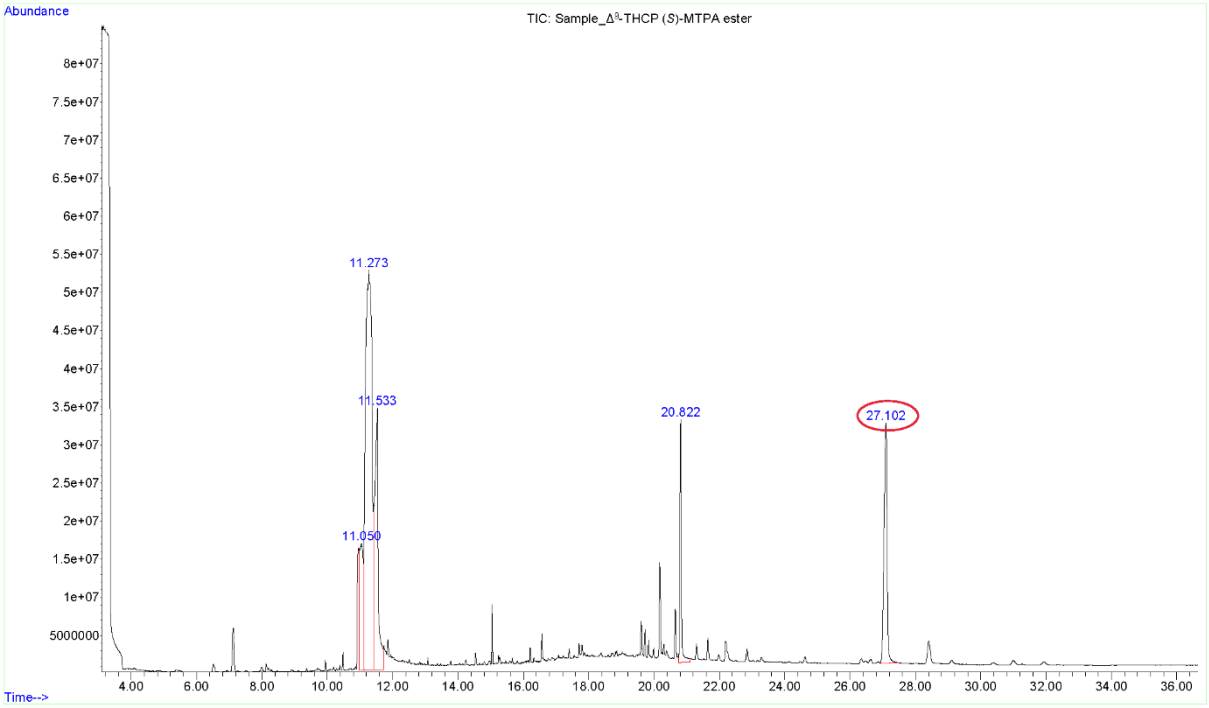

S34: TIC of the (*S*)-Mosher ester of the isolated Δ^9-THCP.

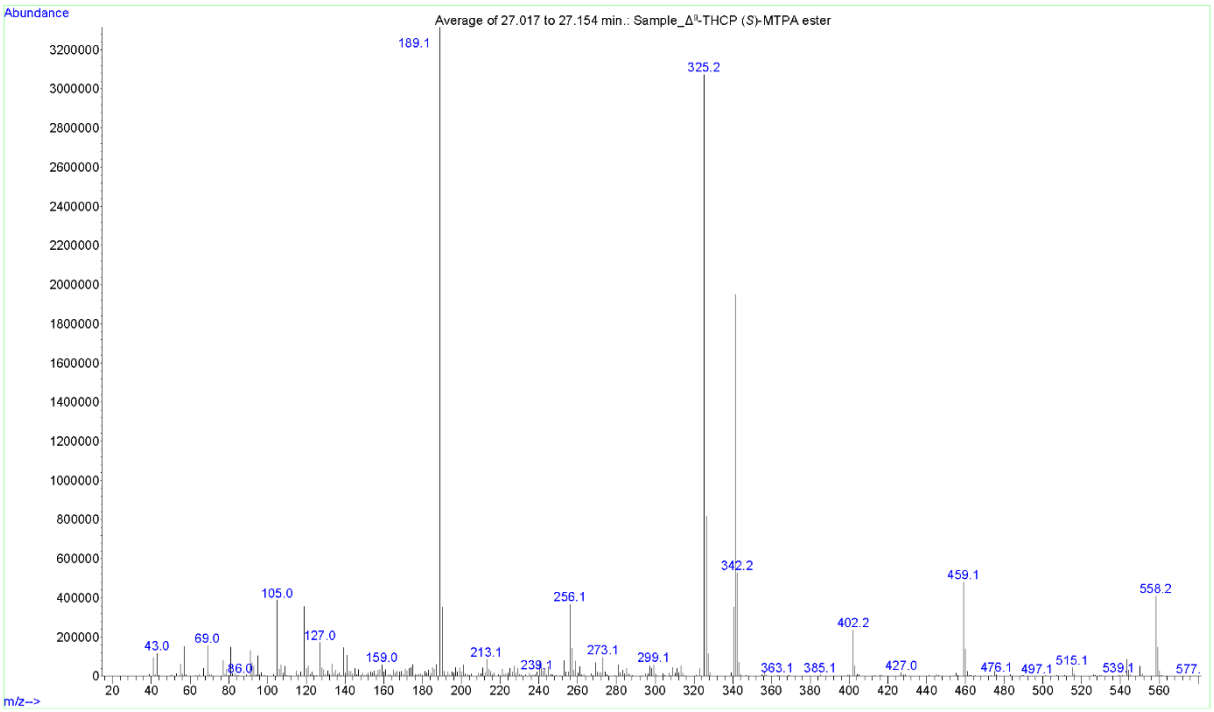

S35: EI mass spectrum of the (*S*)-Mosher ester of the isolated Δ^9-THCP.

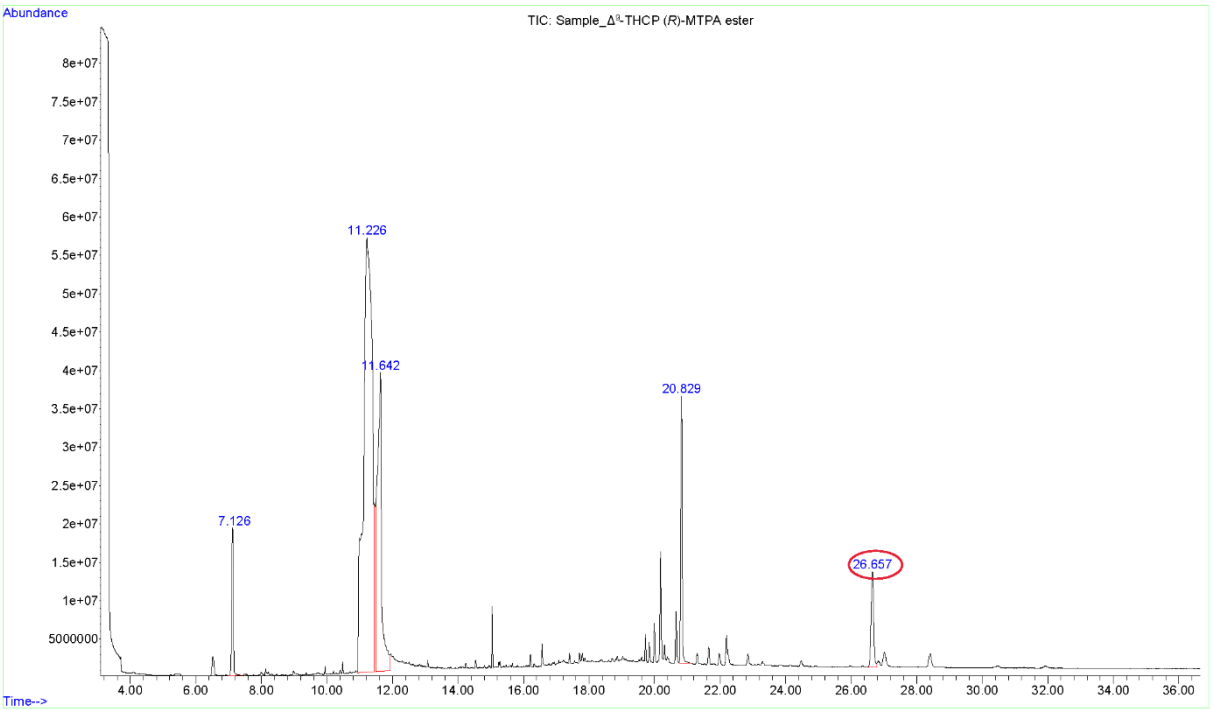

S36: TIC of the (*R*)-Mosher ester of the isolated Δ^9-THCP.

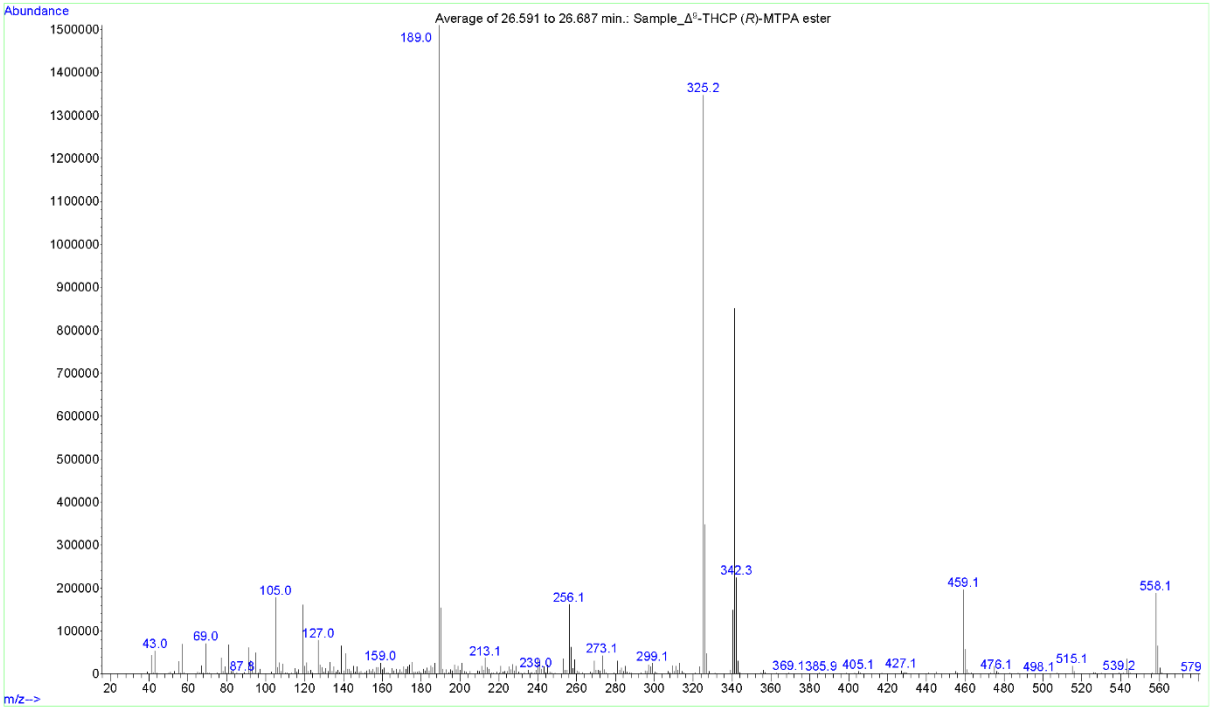

S37: EI mass spectrum of the (*R*)-Mosher ester of the isolated Δ^9-THCP.

Supplementary Information to "Identification of human hexahydrocannabinol metabolites in urine"

Willi Schirmer[1, 2], Volker Auwärter[3,4], Julia Kaudewitz[3,4], Stefan Schürch[2], Wolfgang Weinmann[1]

[1]Institute of Forensic Medicine, Forensic Toxicology and Chemistry, University of Bern, Murtenstrasse 26, 3008 Bern, Switzerland

[2]Department of Chemistry, Biochemistry and Pharmaceutical Sciences, University of Bern, Freiestrasse 3, 3012 Bern, Switzerland

[3]Forensic Toxicology, Institute of Forensic Medicine, , Medical Center – University of Freiburg, Freiburg, Germany

[4]Faculty of Medicine, University of Freiburg, Freiburg, Germany

Corresponding author:

Willi Schirmer, Institute of Forensic Medicine, Forensic Toxicology and Chemistry, University of Bern, Murtenstrasse 26, 3008 Bern, Switzerland

E-mail address: willi.schirmer@irm.unibe.ch

ORCID:

1st author orcid and e-mail address: 0009-0004-5579-2217

2nd author orcid: 0000-0002-1883-2804

3rd author orcid:

4th author orcid: 0000-0001-5109-4623

Last author orcid: 0000-0001-8659-1304

Table of contents

Dibenzopyran numbering of cannabinoids

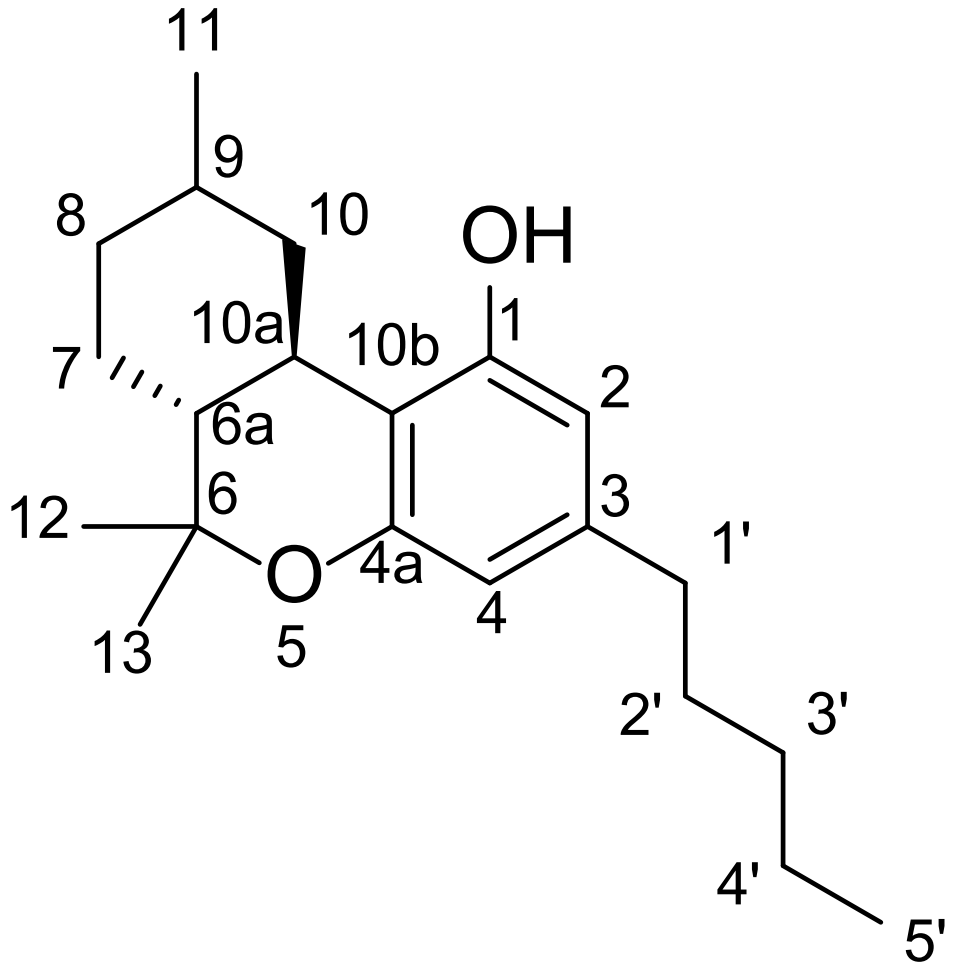

Numbering shown on HHC (no stereochemistry specified on C9)

LC-QqTOF chromatograms of deglucuronidated urine sample

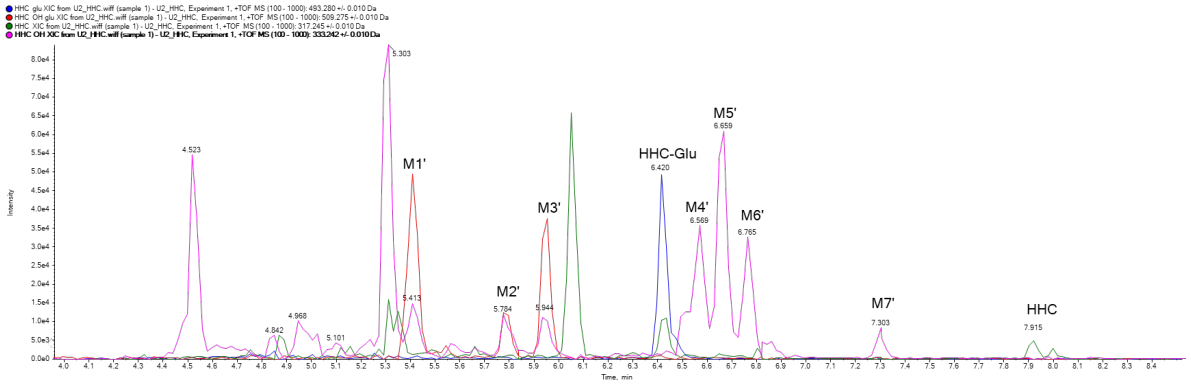

Extracted ion chromatograms of protonated HHC (green), HHC glucuronide (blue), HHC OH (pink) and HHC OH glucuronide (red) in a urine sample 2 h after oral ingestion of 20 mg HHC. The urine sample was treated with β-glucuronidase but the glucuronides were not fully hydrolysed (M1', M2', M3' and HHC glucuronide). The found metabolites are marked. The unmarked peaks can also be found in a urine sample treated in the same manner before the ingestion of HHC (see chromatogram below).

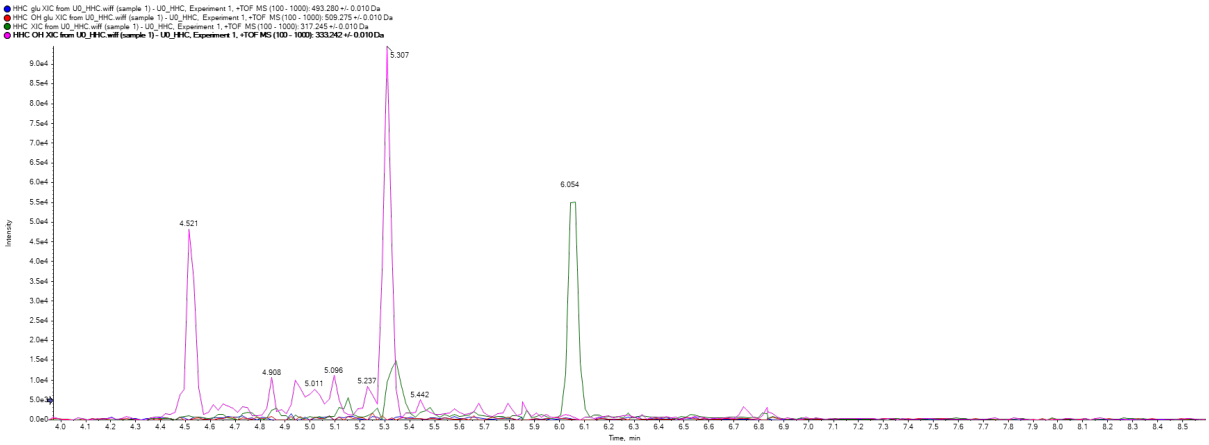

LC-QqTOF chromatograms of untreated urine sample

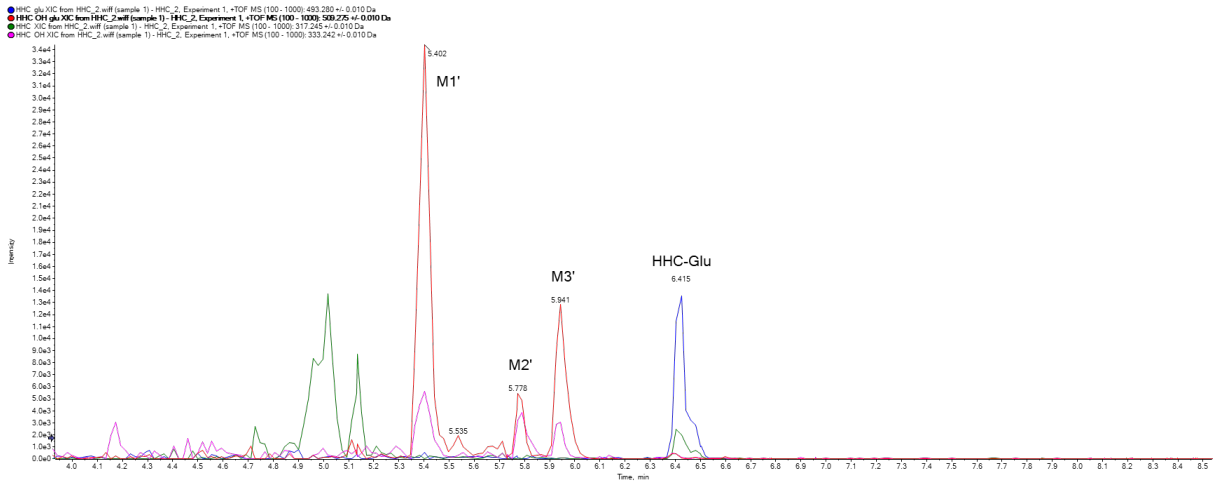

Extracted ion chromatograms of protonated HHC (green), HHC glucuronide (blue), HHC OH (pink) and HHC OH glucuronide (red) in a urine sample 2 h after oral ingestion of 20 mg HHC. The urine sample was extracted but not treated with β-glucuronidase. The deglucuronidated species can be seen at the same retention time as the glucuronides due to fragmentation. The unmarked peaks are also in a urine sample treated in the same manner prior ingestion of HHC (see below).

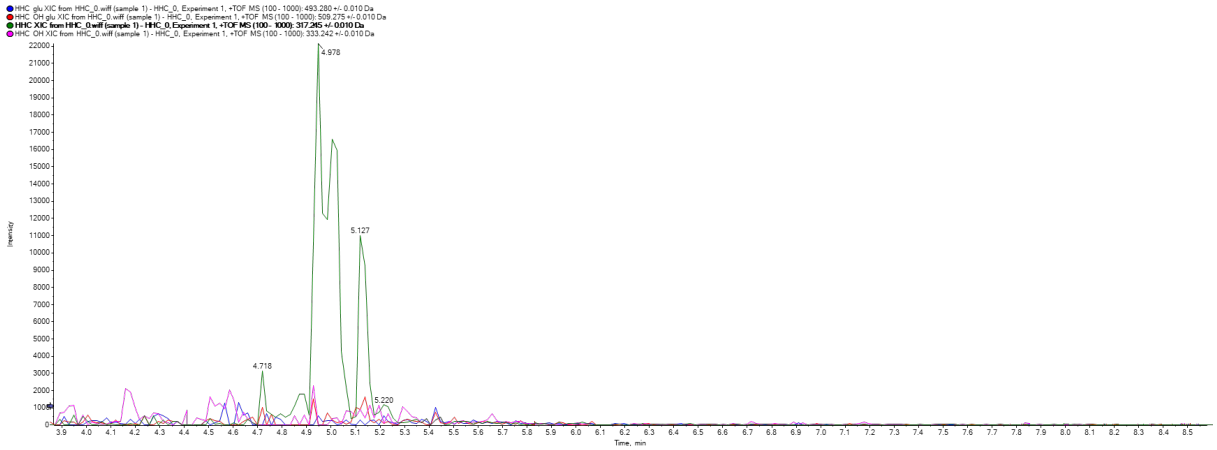

LC-QqTOF spectrum of M1

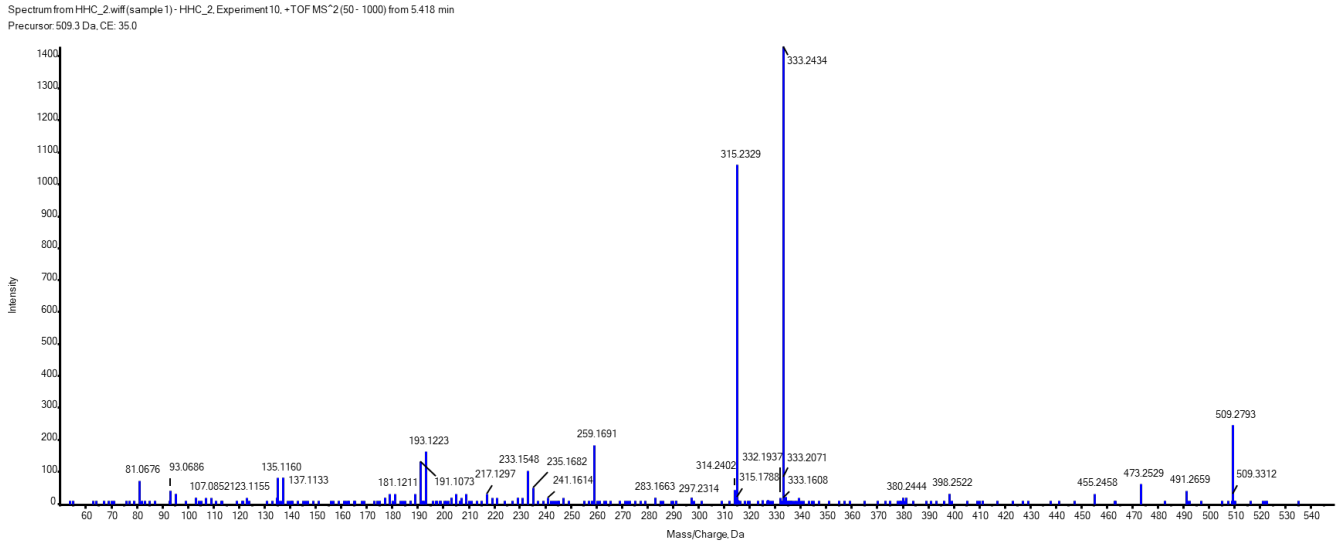

M1': $[M+H^+]^+$: 509.2793 Da (9.4 ppm)
$[M+H^+]^+$- H_2O: 491.2659 Da (4.1 ppm)
$[M+H^+]^+$- 2 H_2O: 473.2529 Da (-1.1 ppm)
$[M+H^+]^+$- 3 H_2O: 455.2458 Da (6.6 ppm)
$[M+H^+]^+$ - Glu: 333.2434 Da (3.0 ppm)
$[M+H^+]^+$- Glu - H_2O: 315.2329 Da (3.2 ppm)
259.1691 Da (-0.8 ppm)
193.1223 Da (0.0 ppm)
191.1073 Da (3.1 ppm)
137.1333 Da (5.8 ppm)
135.1160 Da (-5.9 ppm)

LC-QqTOF spectrum of M2

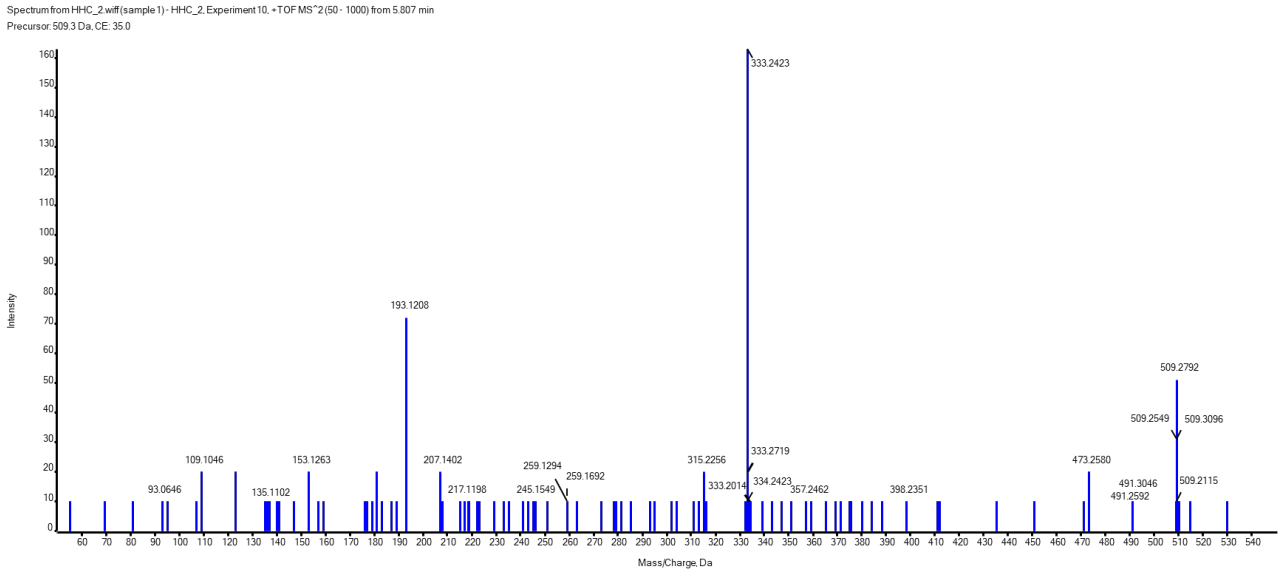

M2': $[M+H^+]^+$: 509.2792 Da (9.2 ppm)
$[M+H^+]^+$- H_2O > 491.2592 Da (-9.6 ppm)
$[M+H^+]^+$- 2 H_2O > 473.2580 Da (9.7 ppm)
$[M+H^+]^+$ - Glu > 333.2423 Da (-0.3 ppm)
$[M+H^+]^+$- Glu - H_2O > 315.2334 Da (4.8 ppm)
259.1692 Da (-0.4 ppm)
193.1208 Da (-7.8 ppm)
153.1263 Da (-7.2 ppm)
135.1102 Da (-48.8 ppm)

LC-QqTOF spectrum of M3

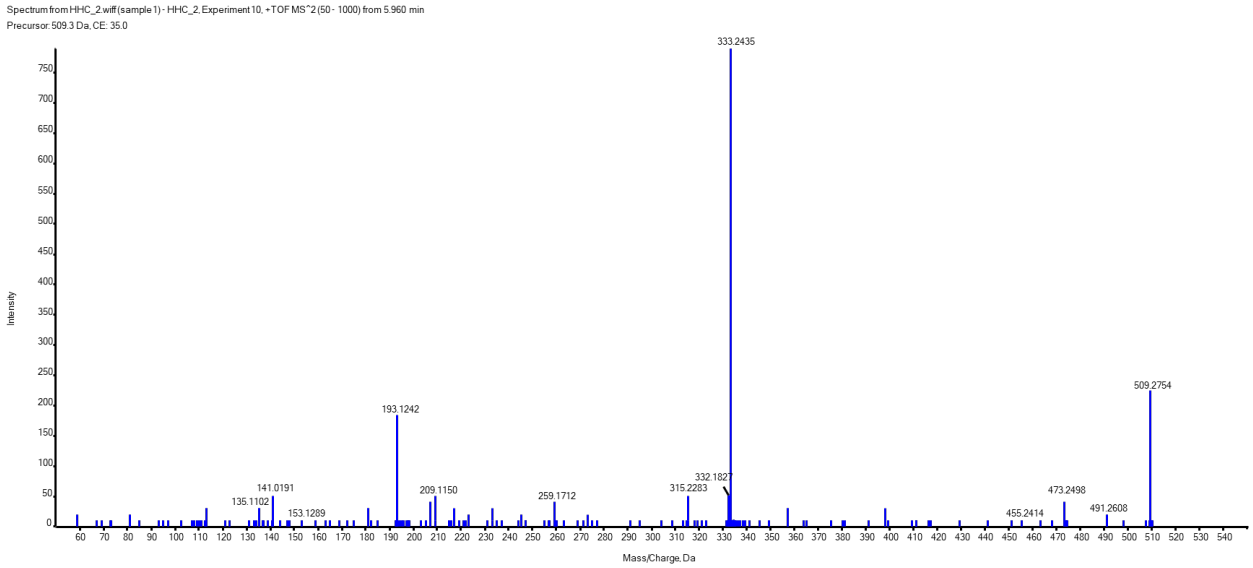

M3': $[M+H^+]^+$: 509.2754 Da (9.2 ppm)
$[M+H^+]^+$- H_2O: 491.2608 Da (-6.3 ppm)
$[M+H^+]^+$- 2 H_2O: 473.2498 Da (-7.6 ppm)
$[M+H^+]^+$- 3 H_2O: 455.2414 Da (-3.1)
$[M+H^+]^+$ - Glu: 333.2435 Da (3.3 ppm)
$[M+H^+]^+$- Glu - H_2O: 315.2283 Da (-11.4 ppm)
259.1712 Da (7.3 ppm)
193.1242 Da (9.8 ppm)
153.1289 Da (9.8 ppm)
135.1102 Da (-6.7 ppm)

LC-QqTOF spectrum of M4

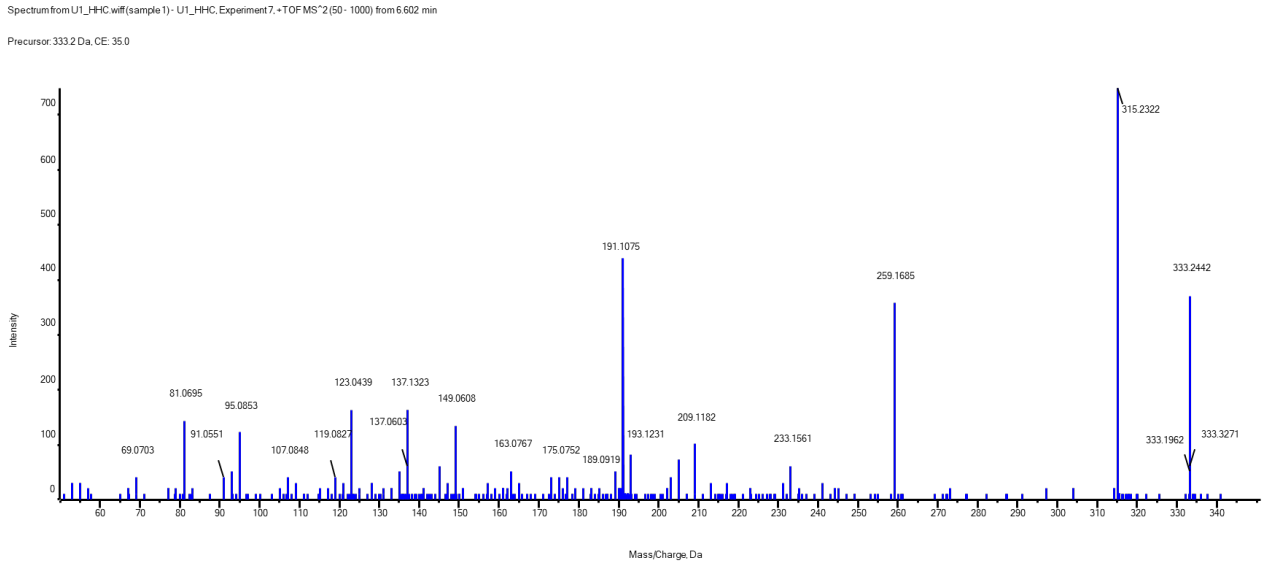

M4': $[M+H^+]^+$: 333.2442 Da (5.4 ppm)
$[M+H^+]^+$- H_2O: 315.2322 Da (1.0 ppm)
259.1685 Da (-3.1 ppm)
209.1182 Da (4.8 ppm)
191.1075 Da (4.2 ppm)
137.1323 Da (-1.5 ppm)

LC-QqTOF spectrum of M5

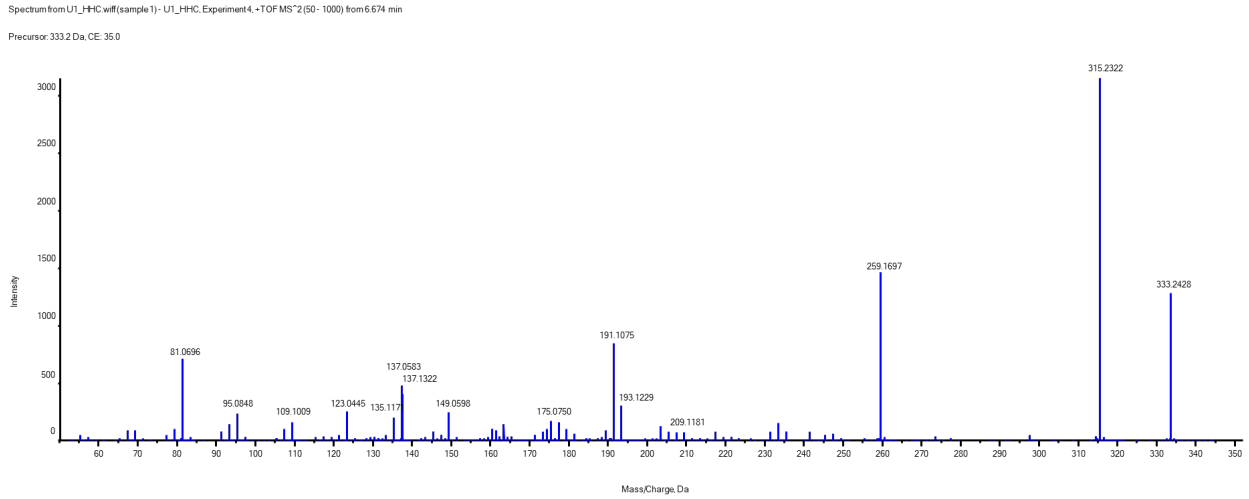

M5': $[M+H^+]^+$: 333.2428 Da (1.2 ppm)
$[M+H^+]^+$- H_2O: 315.2322 Da (1.0 ppm)
259.1697 Da (1.5 ppm)
209.1181 Da (4.3 ppm)
193.1229 Da (3.1 ppm)
191.1075 Da (4.2 ppm)
137.1322 Da (-2.2 ppm)
135.1171 Da (2.2 ppm)

LC-QqTOF spectrum of M6 (SWATH acquisition)

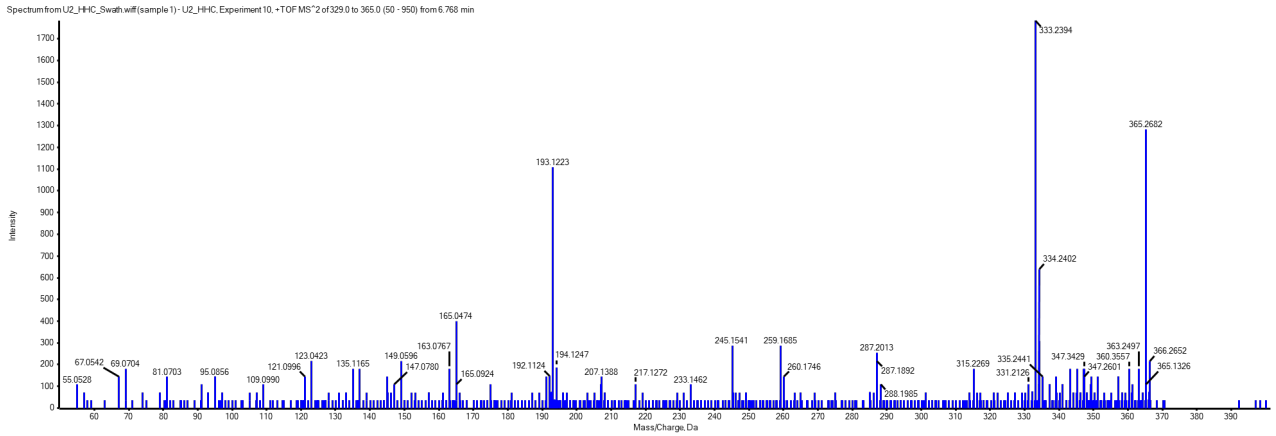

M6': $[M+H^+]^+$: 333.2394 Da (-9.0 ppm)
193.1223 Da (0.0 ppm)

LC-QqTOF spectrum of M7 (SWATH acquisition)

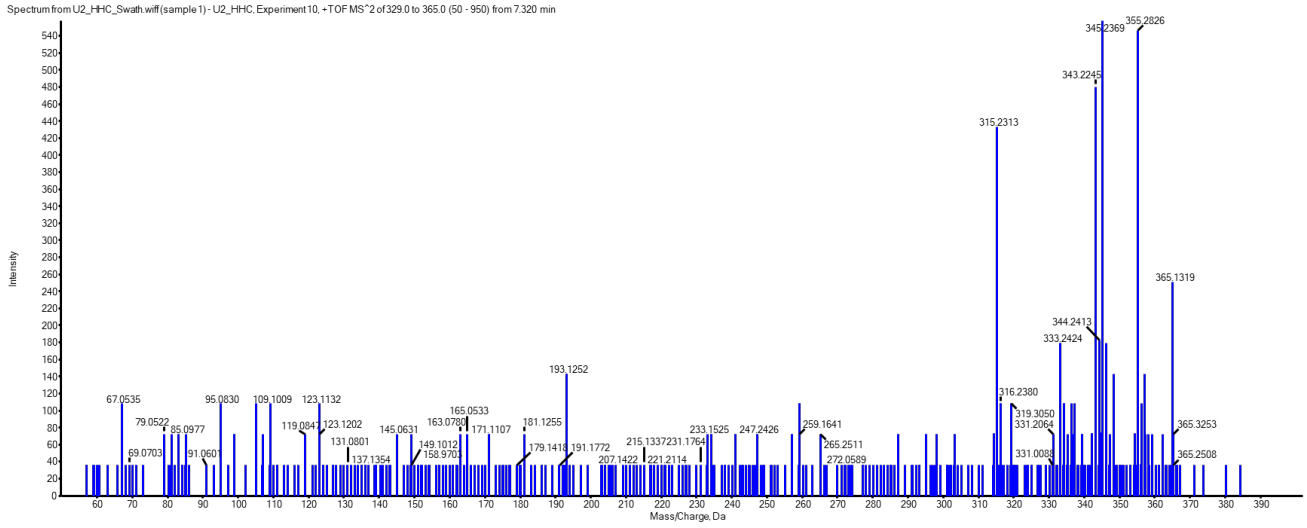

M7': $[M+H^+]^+$: 333.2424 Da (0.0 ppm)
315.2313 Da (-1.9 ppm)
193.1252 Da (15.0 ppm)

LC-QqTOF spectrum of HHC glucuronide

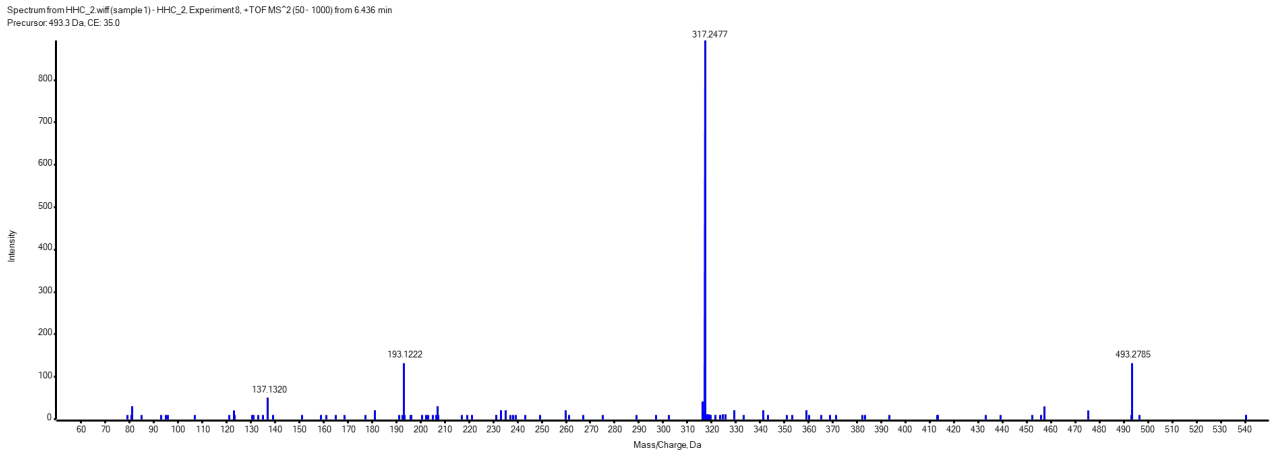

HHC-Glucuronide: $[M+H^+]^+$: 493.2785 Da (-2.2 ppm)
$[M+H^+]^+$- H_2O: 475.2683 Da (-1.5 ppm)
$[M+H^+]^+$- 2 H_2O: 457.2594 Da (2.0 ppm)
$[M+H^+]^+$- Glu: 317.2477 Da (0.6 ppm)
193.1222 Da (-0.5 ppm)
137.1320 Da (-3.6 ppm)

LC-QqTOF spectrum of HHC (metabolite after deglucuronidation) (SWATH acquisition)

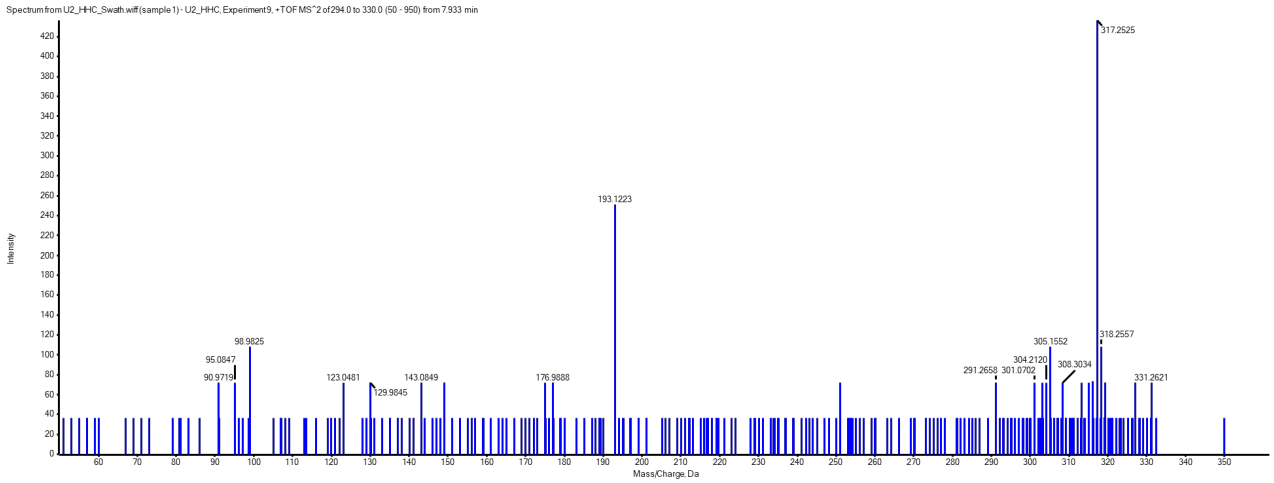

HHC SWATH: $[M+H^+]^+$: 317.2525 Da (15.8 ppm)
193.1223 Da (0.0 ppm)

LC-QqTOF spectrum of a HHC sample (diastereomeric mixture)

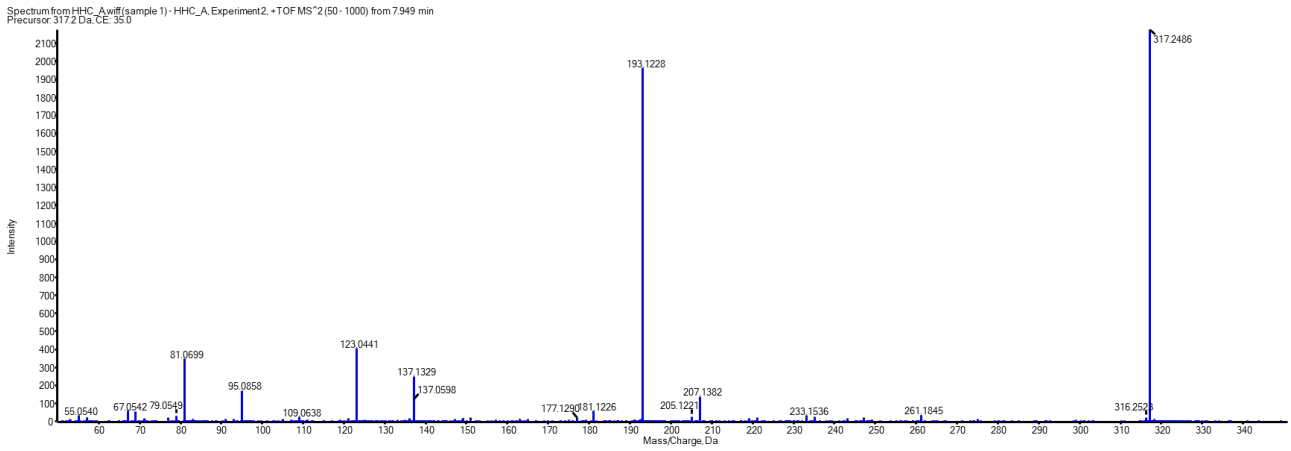

Product ion spectrum of an authentic HHC sample (Diastereomeric mixture)
$[M+H^+]^+$:317.2486 Da (3.5 ppm)
261.1845 Da (-1.5 ppm)
233.1536 (0.0 ppm)
193.1228 Da (2.6 ppm)
137.1329 Da (2.9 ppm)
123.0441 Da (0.0 ppm)
95.0858 Da (3.2 ppm)

Explanation of fragment ions

Origin of m/z 261

The ion with m/z 261 is formed by loss of isobutene from the terpene moiety. This pathway is less pronounced than the same mechanism in Δ9-THC where the resulting carbocation can be delocalized, one of this mesomeric states is also a tertiary carbocation increasing its stability. This ion might also cyclize to the cyclobutachromenylium ion proposed by Maralikova and Weinmann.1 A degradation from the pentyl chain is less likely.2 259 indicates a double bond in the terpene moiety, Δ8-THC also fragments to 259 under positive ESI conditions.[3]

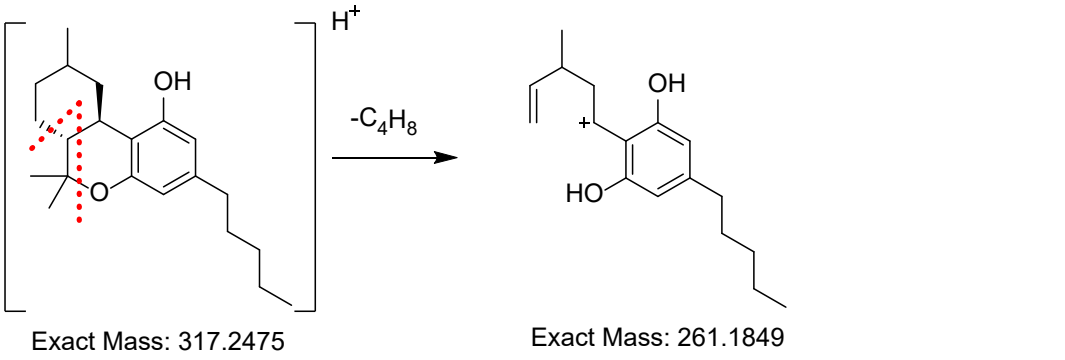

Exact Mass: 317.2475 Exact Mass: 261.1849

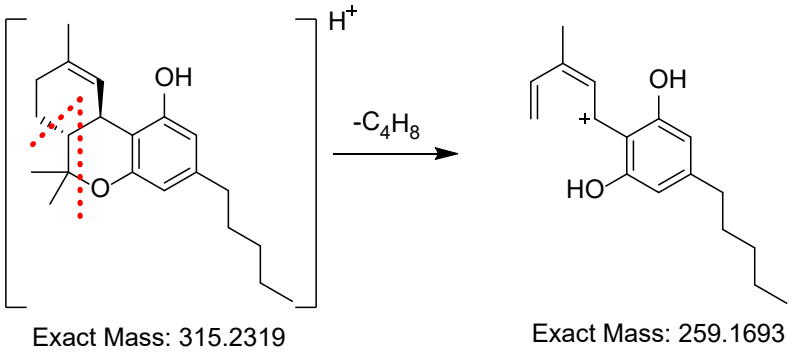

Exact Mass: 315.2319 Exact Mass: 259.1693

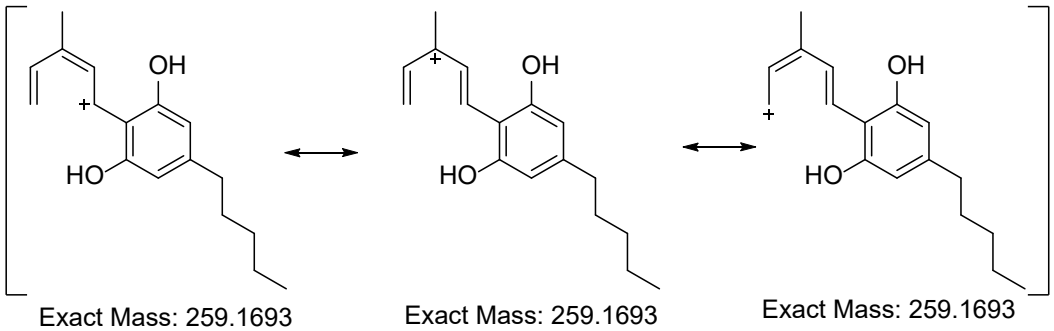

Exact Mass: 259.1693 Exact Mass: 259.1693 Exact Mass: 259.1693

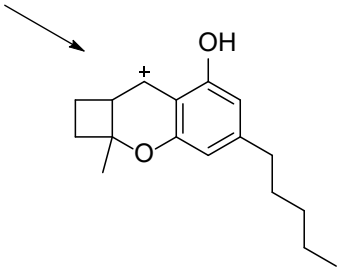

Exact Mass: 259.1693

Origin of m/z 233

The ion with m/z 233 is also barely visible, this fragmentation mechanism leads to a dihydrochromenylium ion, in the case of Δ^9-THC this mechanism leads to an aromatic chromenylium ion with m/z 231 with quite high abundance.[4]

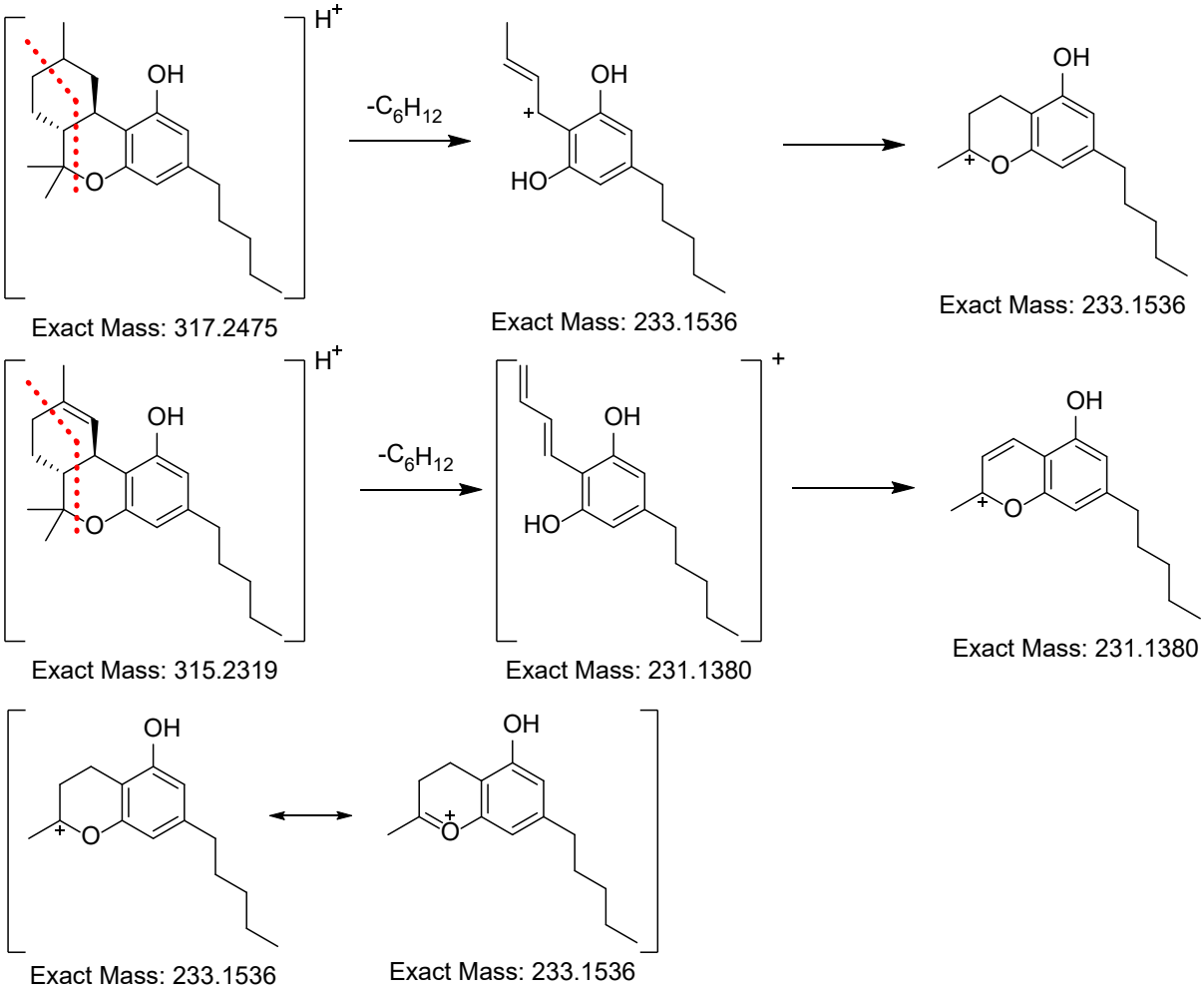

Origin of m/z 193

The ion with m/z 193 corresponds to 2,6-dihydroxy-4-pentylphenyl)methylium and is a widely encountered ion in phytocannabinoids. This benzylic cation is extremely stable due to rearrangement to a to a tropylium species, stabilizing the positive charge via aromaticity. This ion was discussed by Budzikiewicz et al.[4]

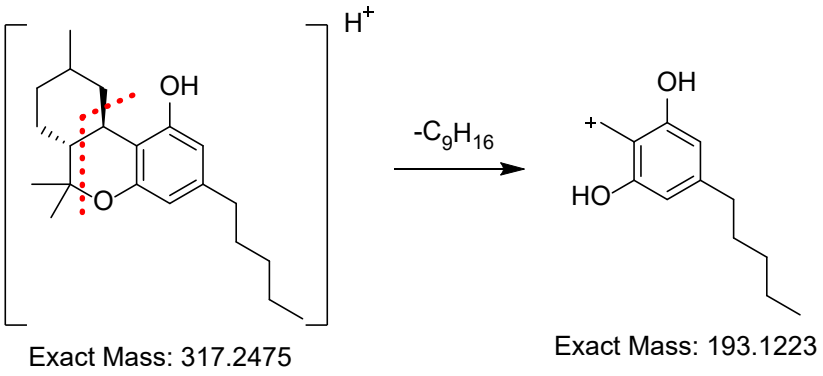

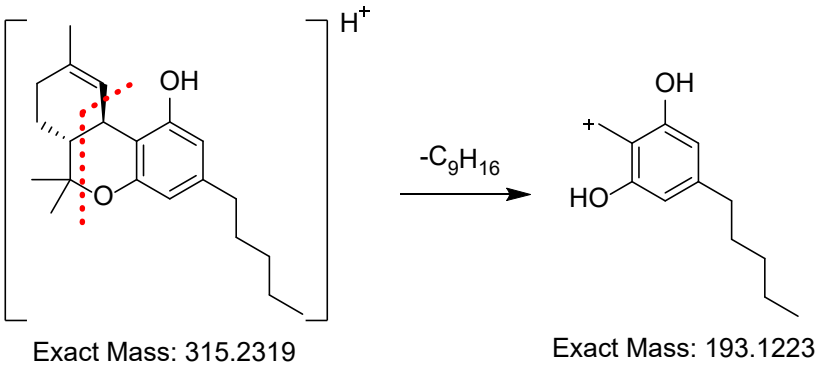

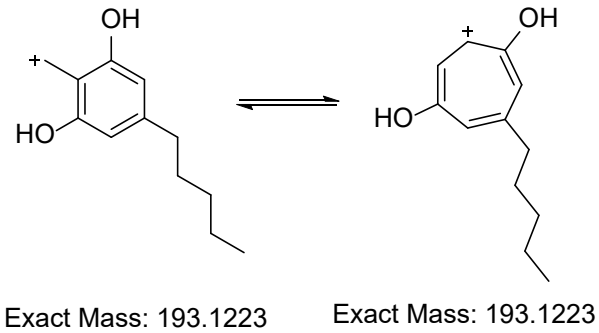

Origin of m/z 137 and 123

The ion with m/z 137 corresponds to an ion which corresponds to partially hydrogenated limonene. The analogue ion from the fragmentation of Δ^8- and Δ^9-THC leads to charged limonene with m/z 135.[2]

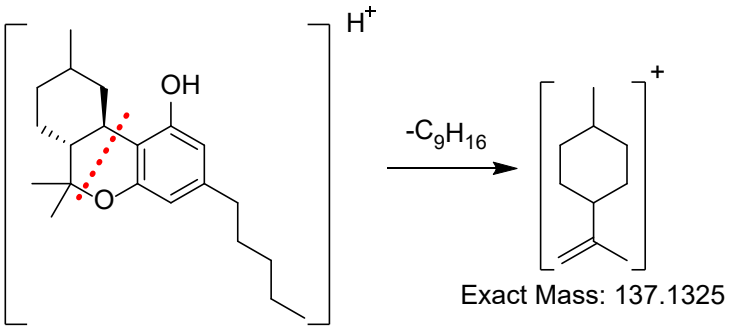

Exact Mass: 317.2475

Exact Mass: 137.1325

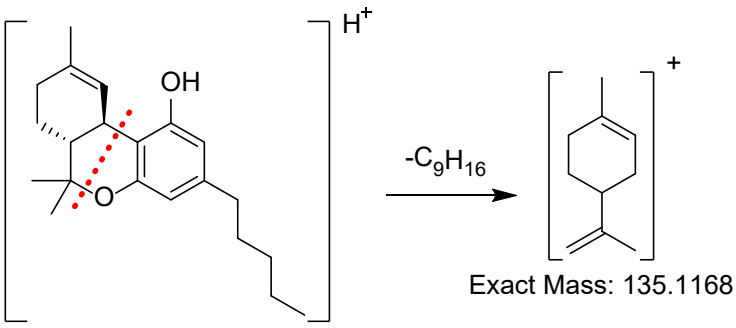

Exact Mass: 315.2319

Exact Mass: 135.1168

m/z 123 corresponds to (2,6-dihydroxyphenyl)methylium which is also stabilized via a tropylium species. The same ion is encountered in the product mass spectra of Δ^8- and Δ^9-THC and allows no distinction between the phytocannabinoids.[2]

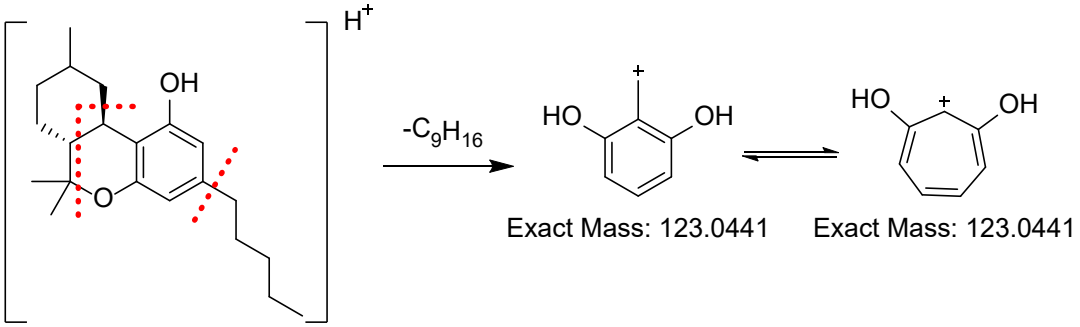

Exact Mass: 317.2475 Exact Mass: 123.0441 Exact Mass: 123.0441

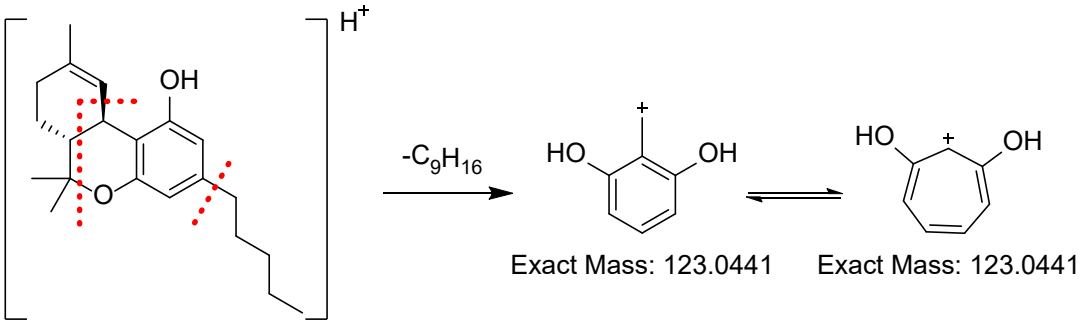

Exact Mass: 315.2319 Exact Mass: 123.0441 Exact Mass: 123.0441

Origin of m/z 95

m/z 95 corresponds to a 4-methylcyclohex-1-enium ion, the corresponding ion from the fragmentation of Δ^8- and Δ^9-THC possesses an additional double bound inside the ring with m/z 93. This ion can be used for the differentiation of THC and HHC.[2]

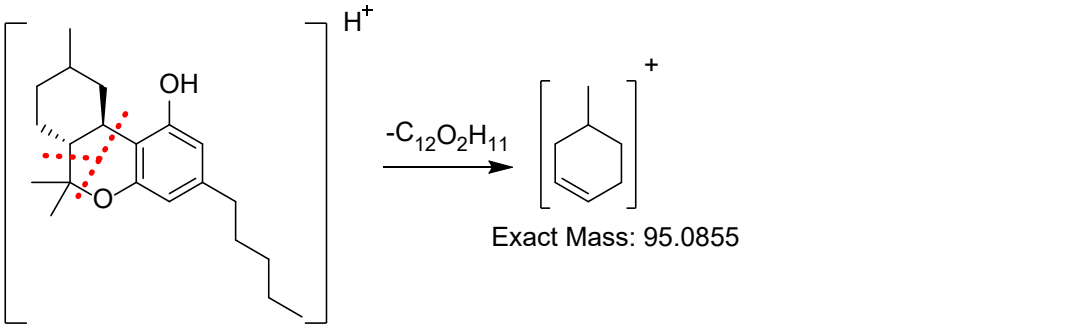

Exact Mass: 317.2475 Exact Mass: 95.0855

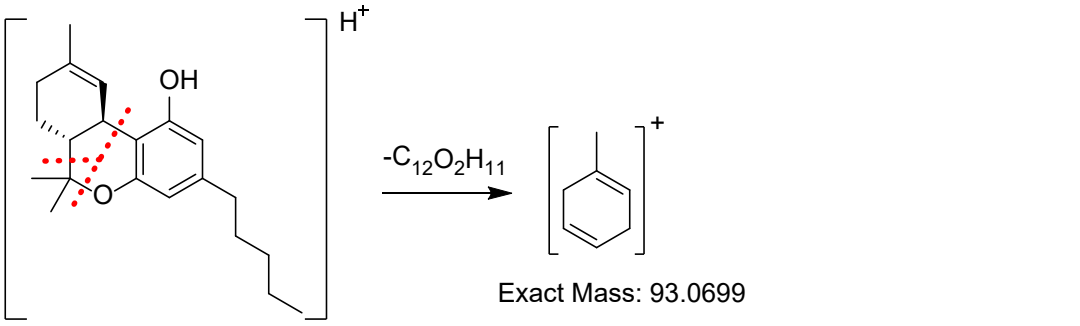

Exact Mass: 315.2319 Exact Mass: 93.0699

Differentiation of hydroxylation position on OH-HHCs

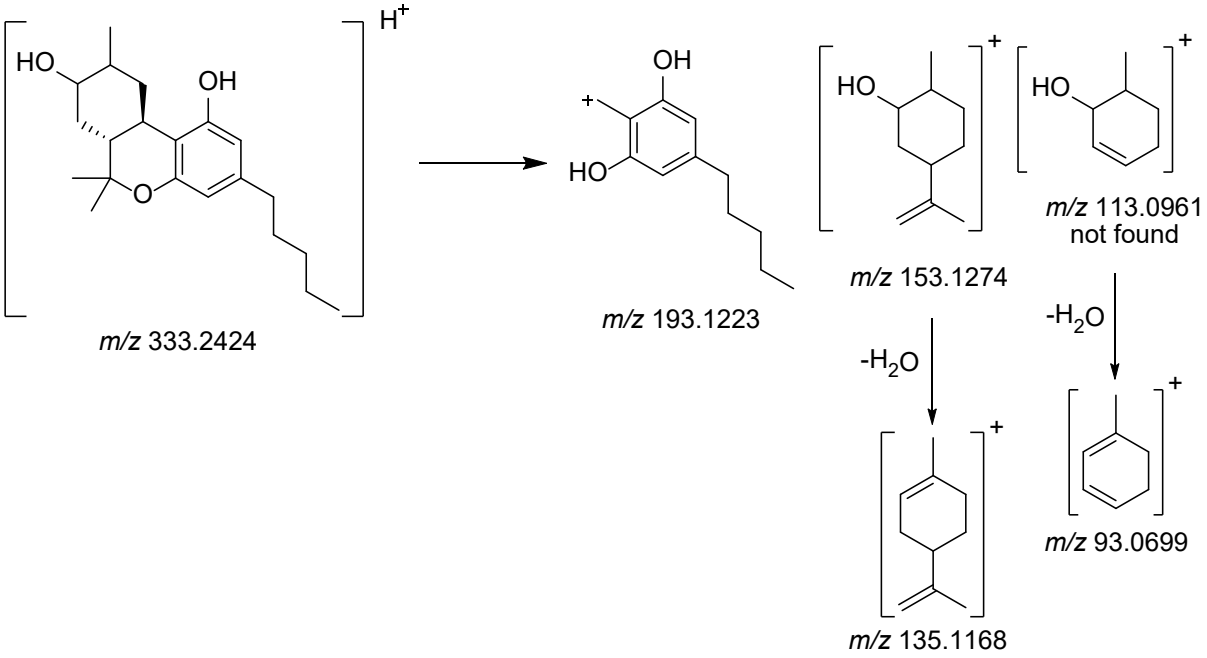

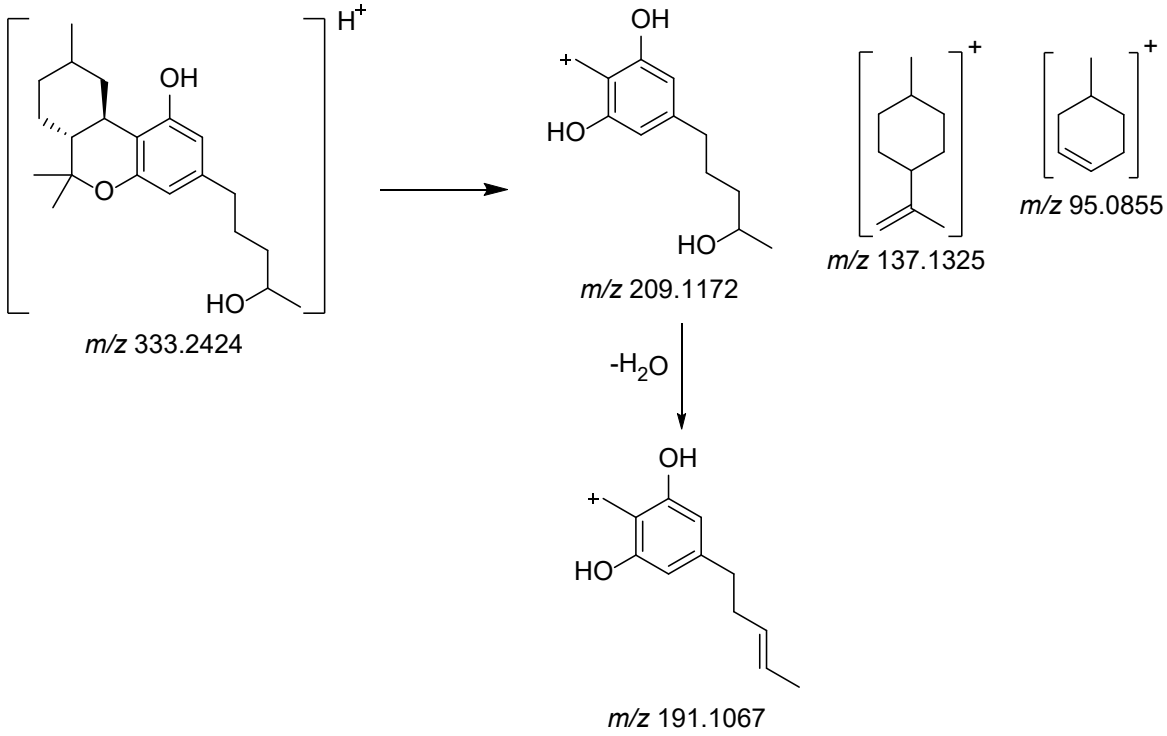

LC-QqLIT chromatograms and spectra

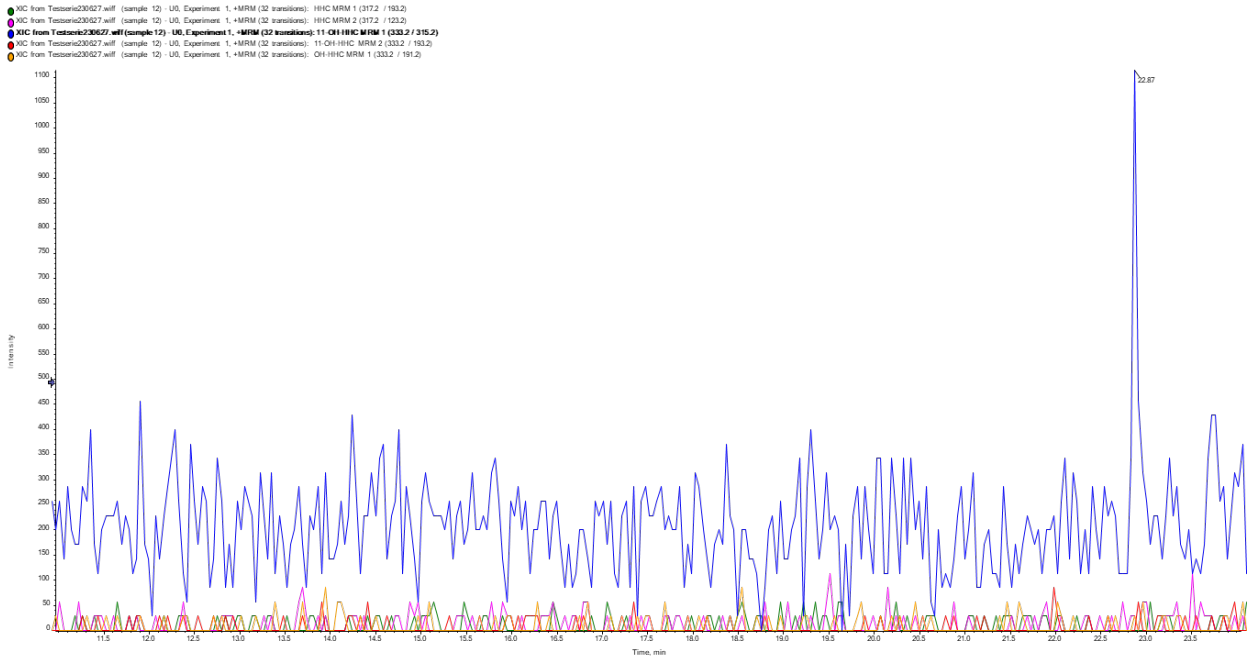

Spectrum of a urine sample treated with β-glucuronidase prior HHC consumption. The traces for mass reactions typical for OH HHC are shown. Matrix peak at 22.87 min can be seen.

(8*S*, 9*S*)-8-OH-HHC

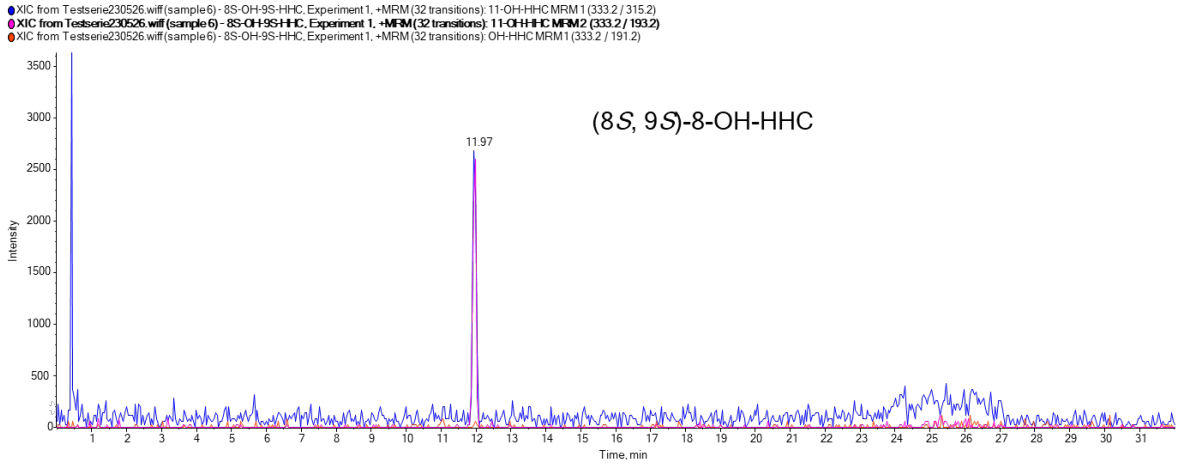

Spectrum from Testserie230526.wiff (sample 6) - 8S-OH-9S-HHC, Experiment 2, +MS^2 of 333.2 (50 - 350) from 11.963 min

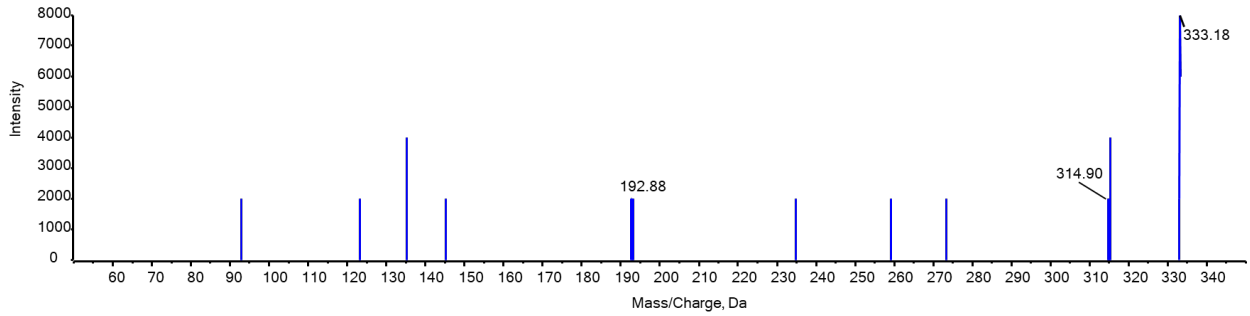

(8*R*, 9*S*)-8-OH-HHC

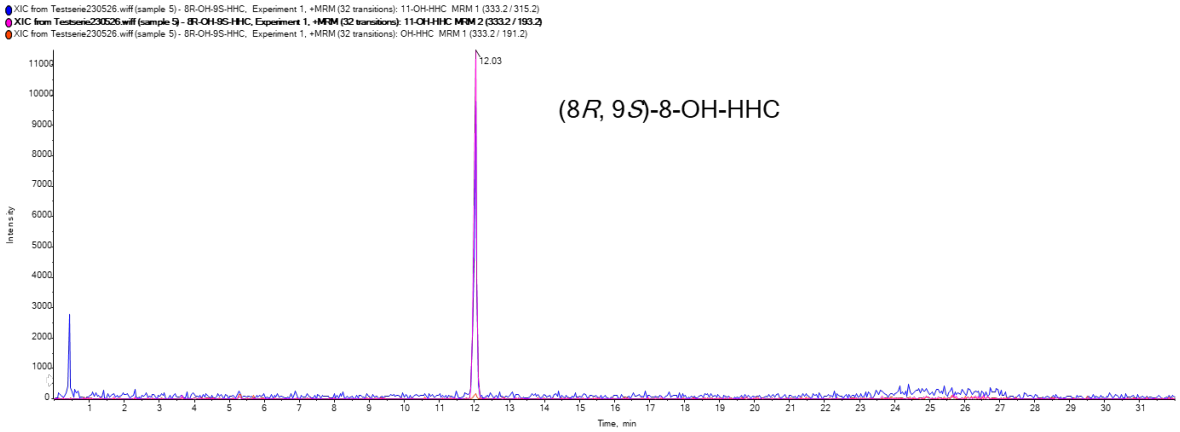

Spectrum from Testserie230526.wiff (sample 5) - 8R-OH-9S-HHC, Experiment 2, +MS^2 of 333.2 (50 - 350) from 12.048 min

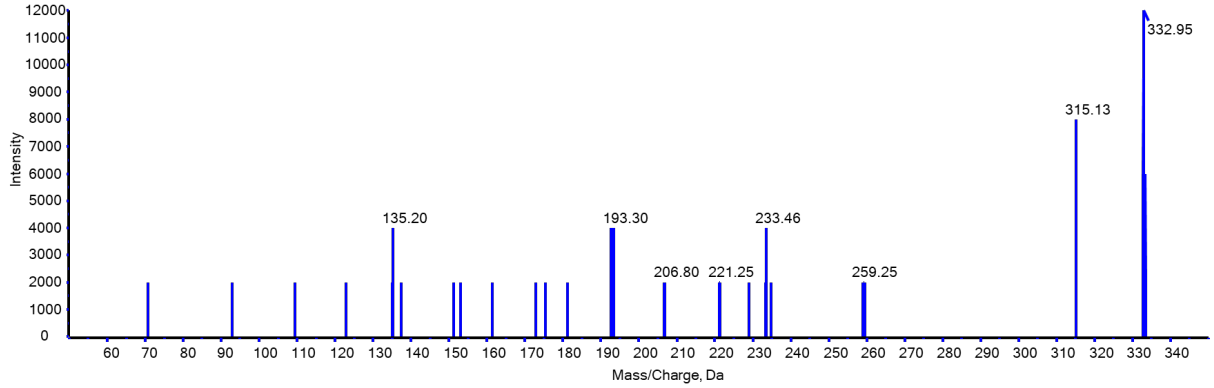

(8*R*, 9*R*)-8-OH-HHC

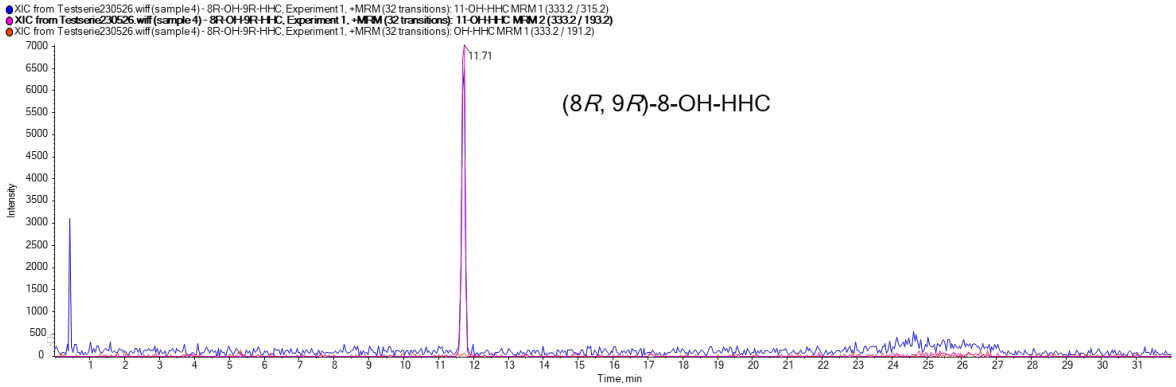

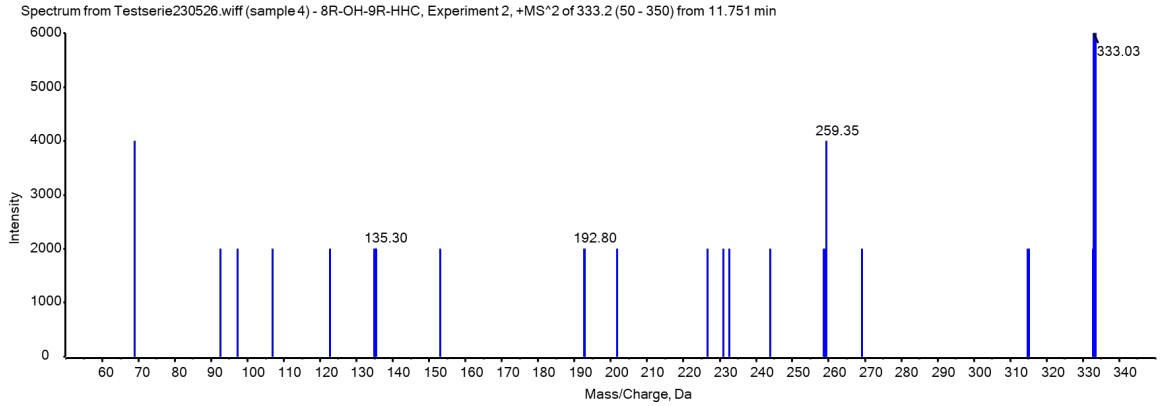

(9*S*)-11-OH-HHC

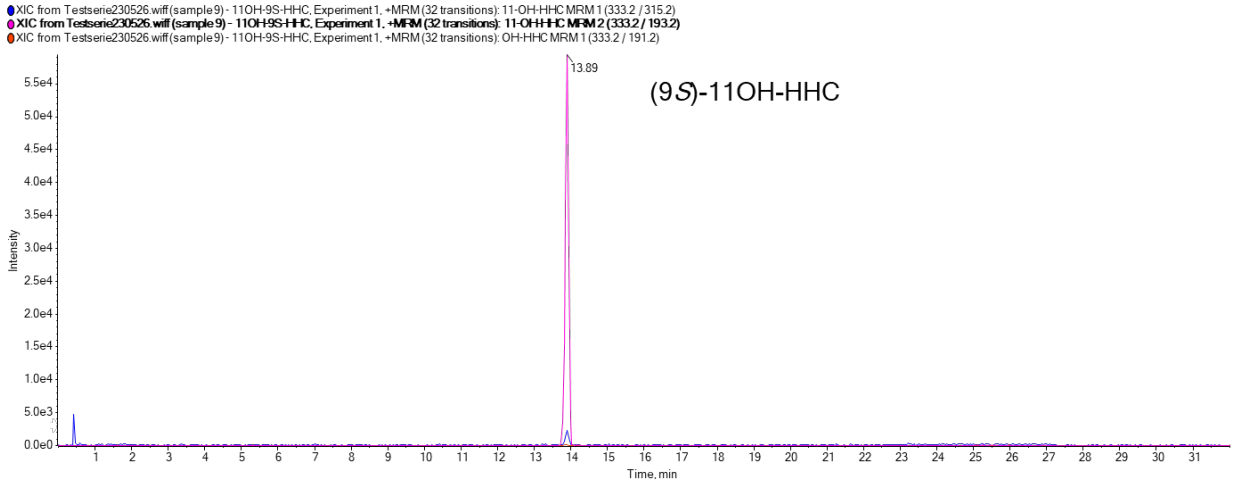

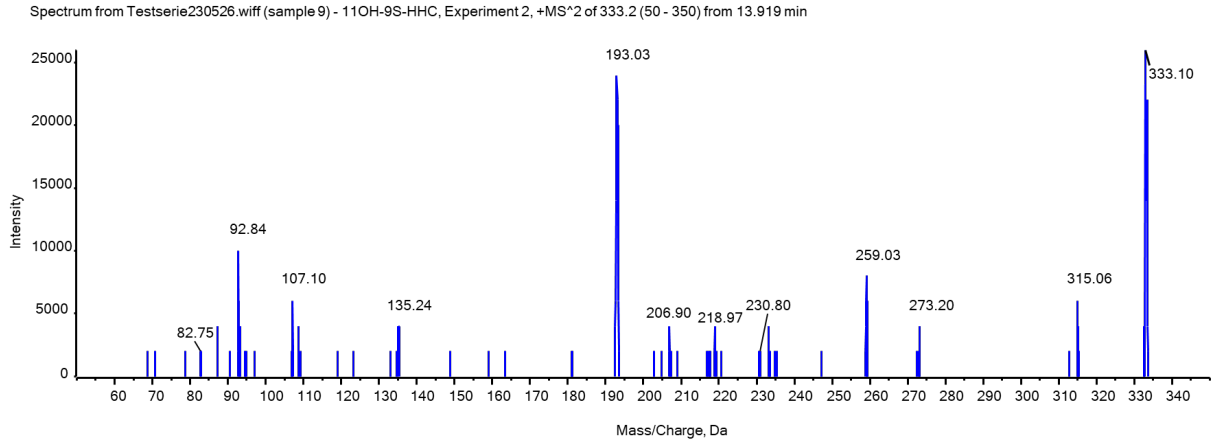

(9*R*)-11-OH-HHC

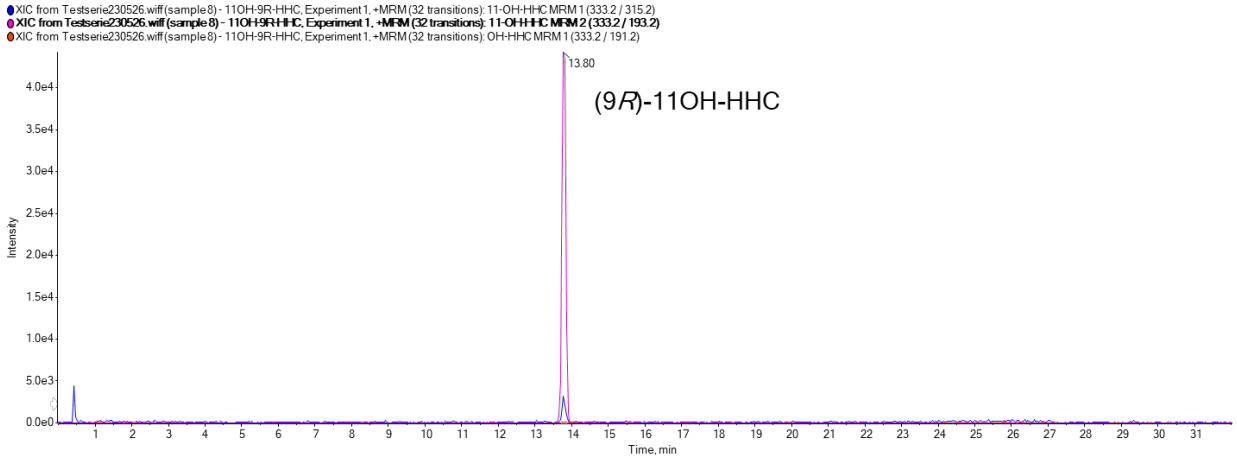

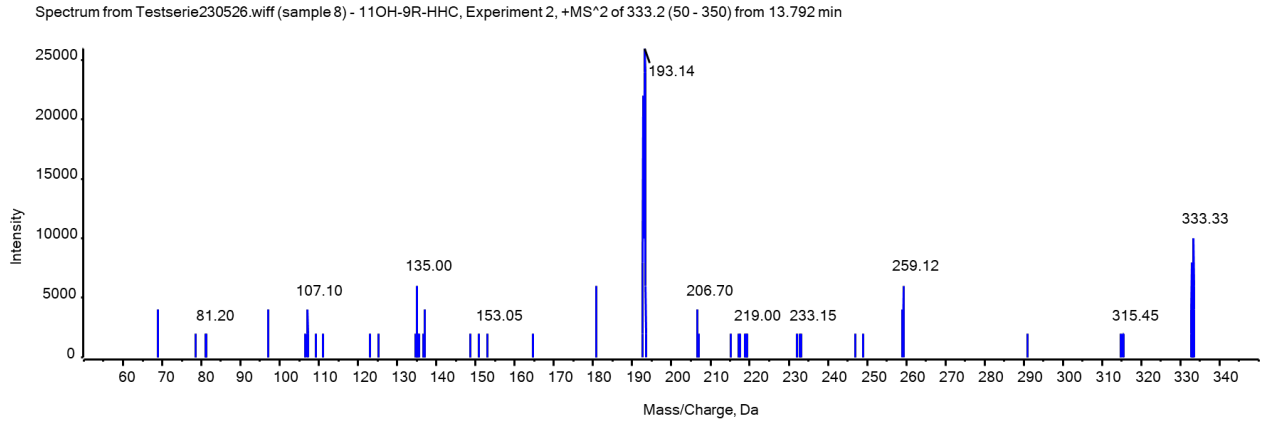

OH-HHC Mix

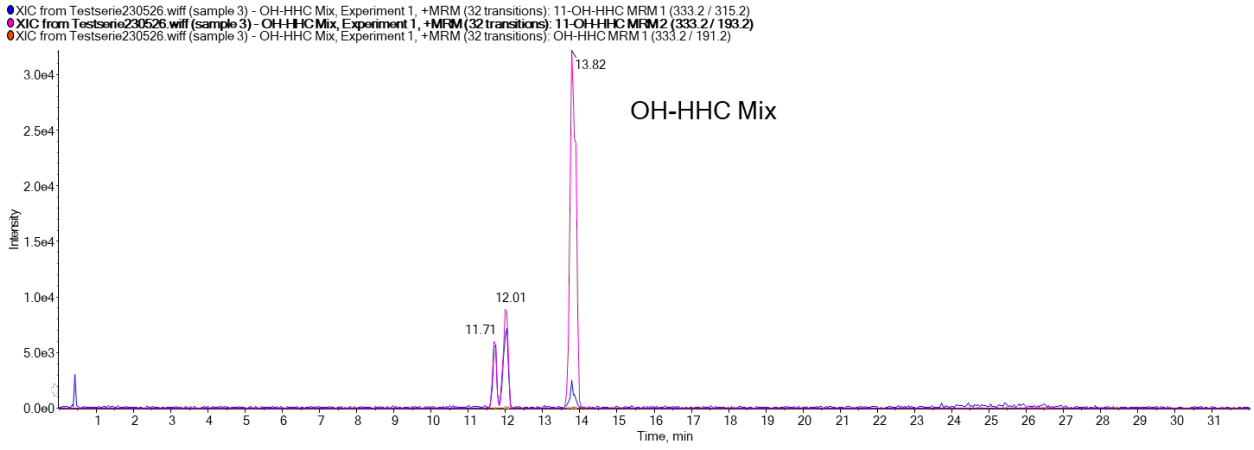

(9*S*)-11-nor-9-carboxy HHC

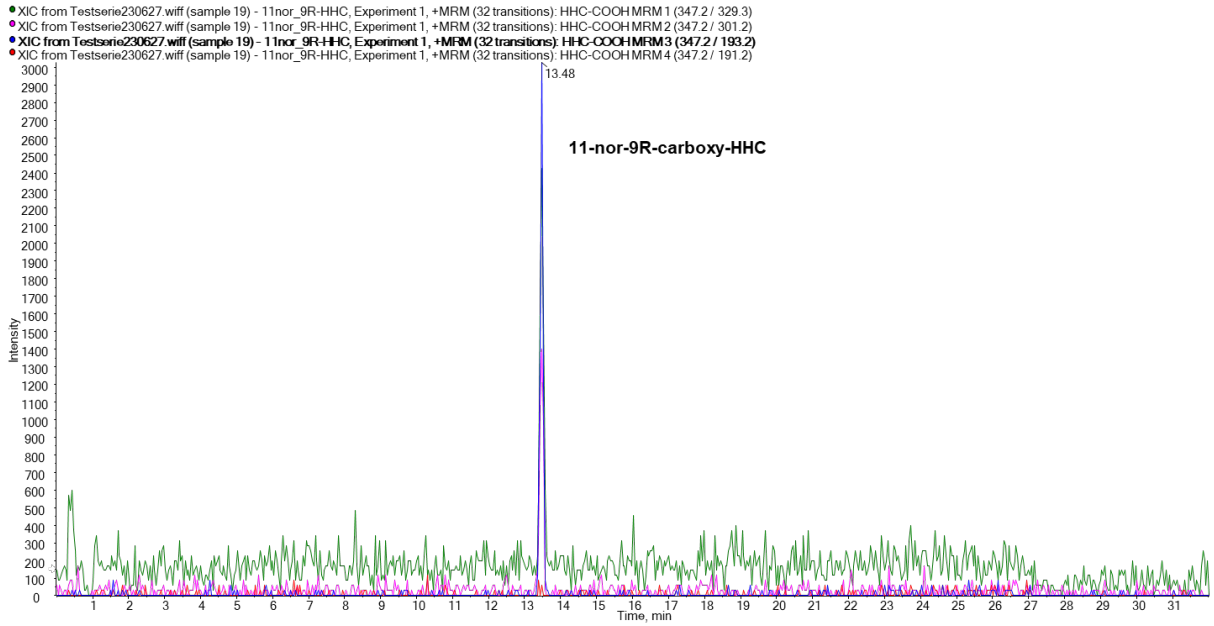

(9*R*)-11-nor-9-carboxy HHC

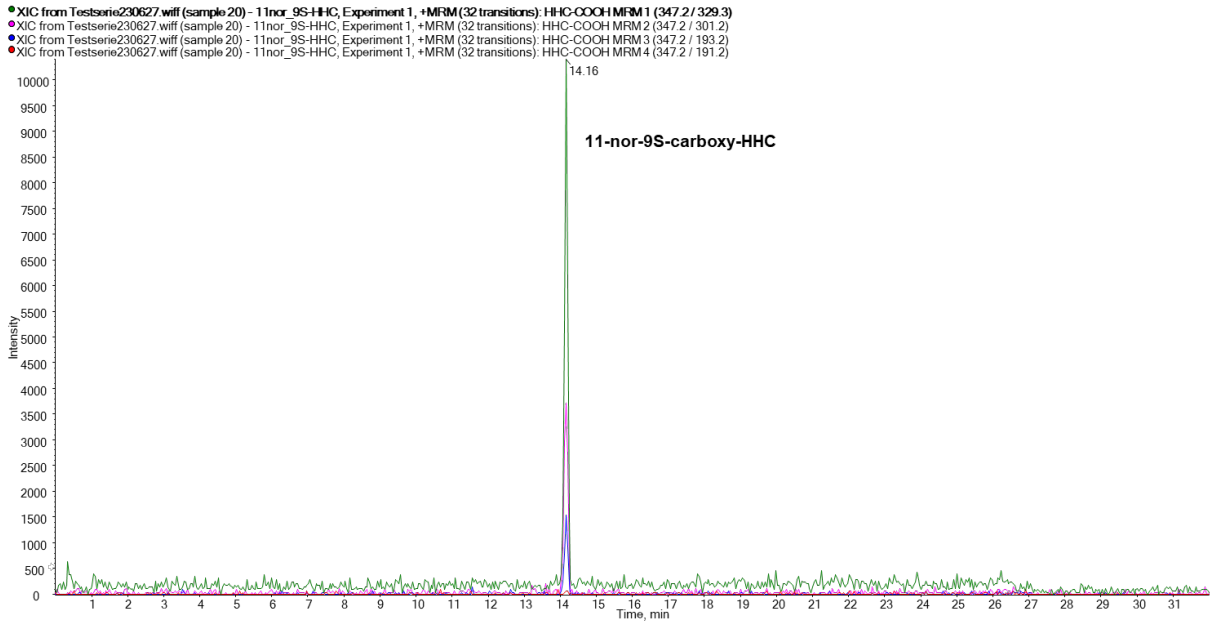

No product ion spectra measured for the epimers of 11-nor-9-carboxy-HHC

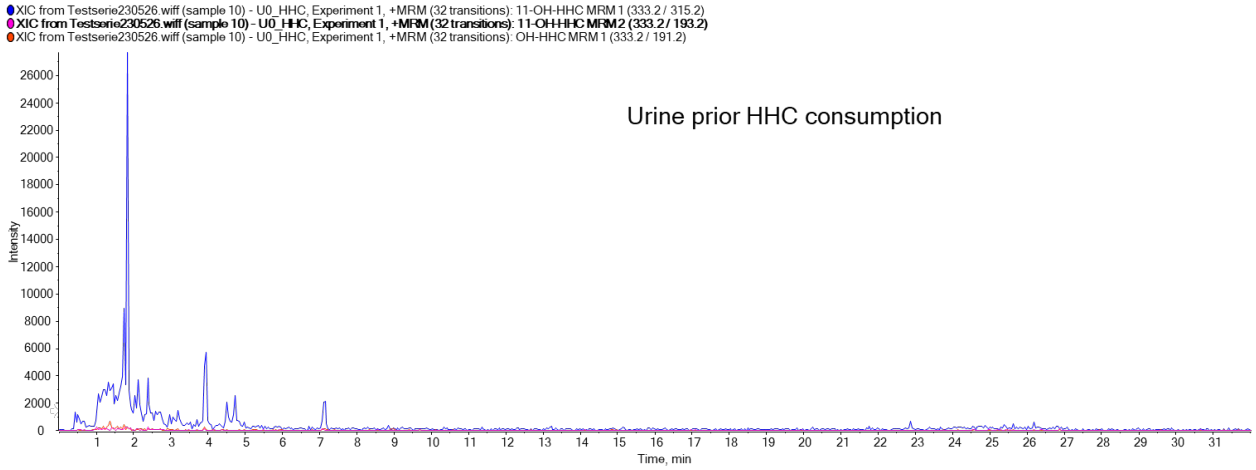

GC-MS chromatograms and spectra

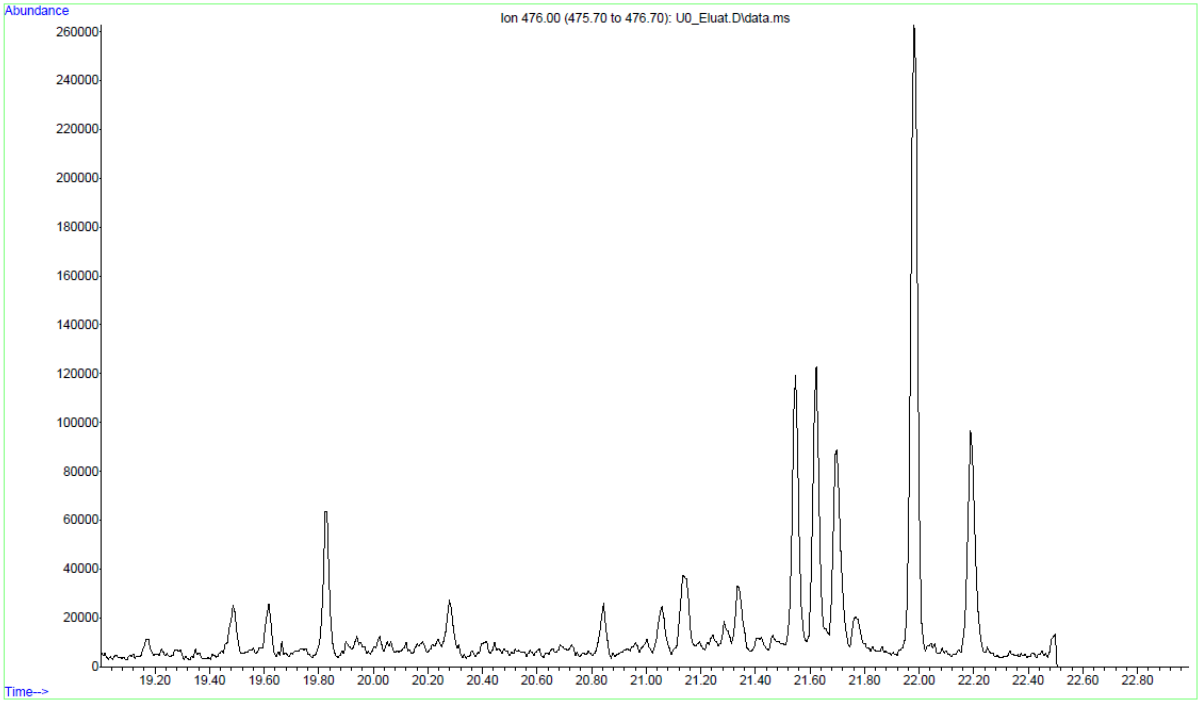

Extracted ion chromatogram of m/z 476 (OH-HHC 2xTMS) of a urine sample prior HHC ingestion.

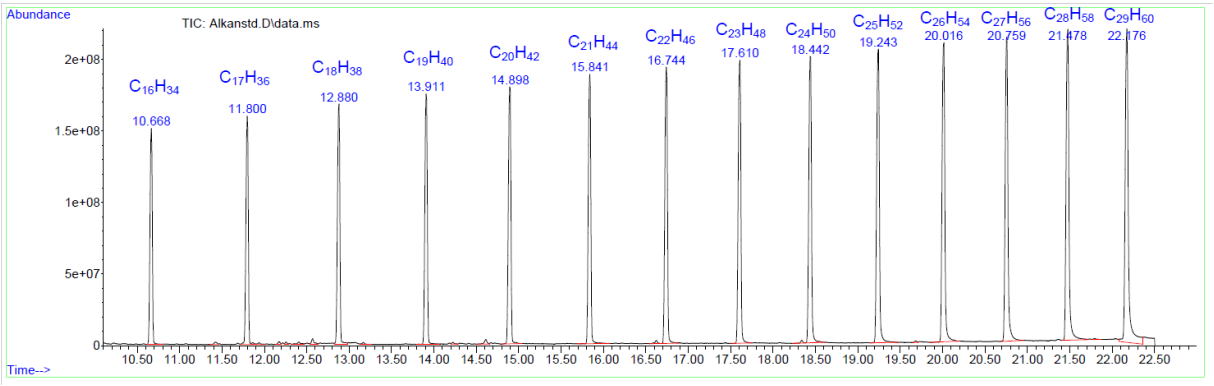

Alkane standard for determination of Kováts-indices

GC-MS reference spectra (TMS)

(9*R*)-HHC TMS

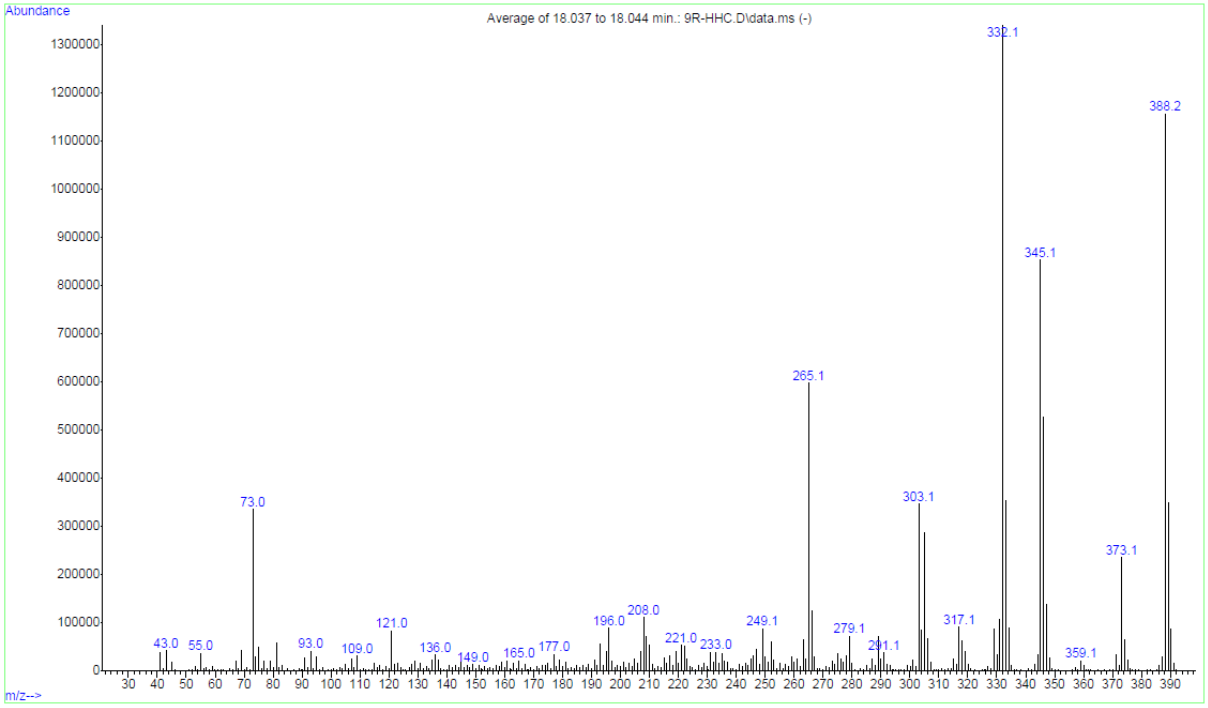

(9*S*)-HHC TMS

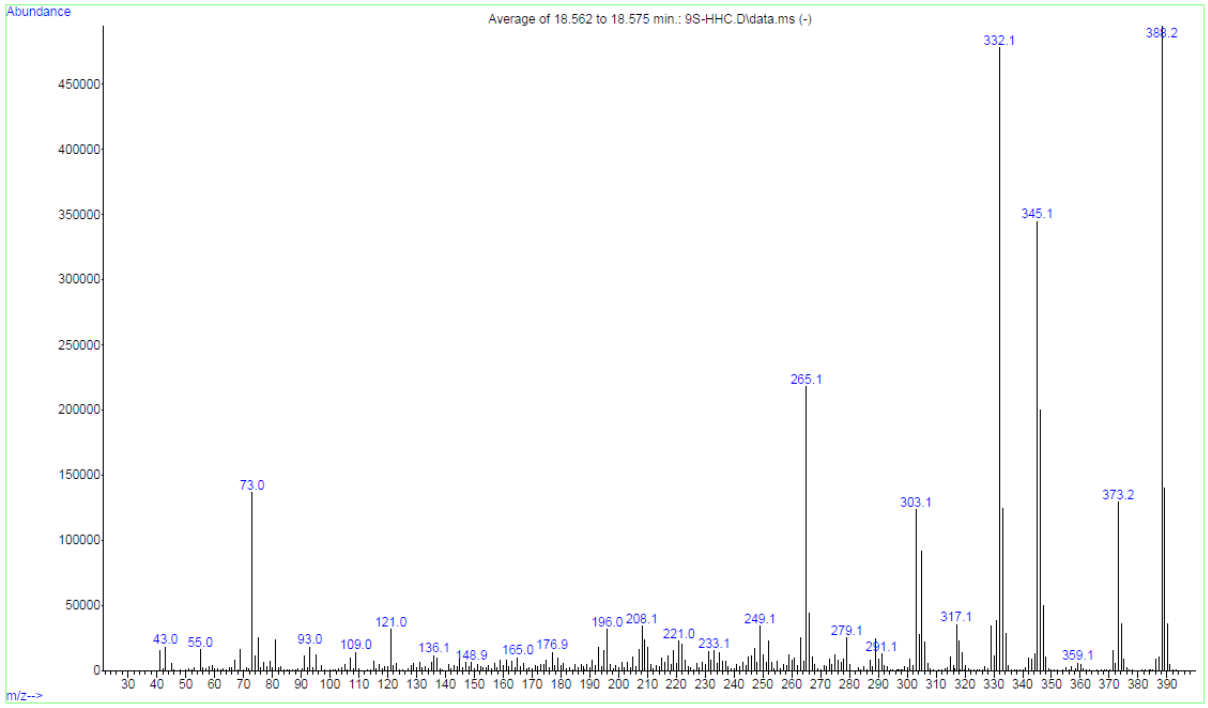

(8*R*, 9*R*)-8-OH-HHC 2xTMS

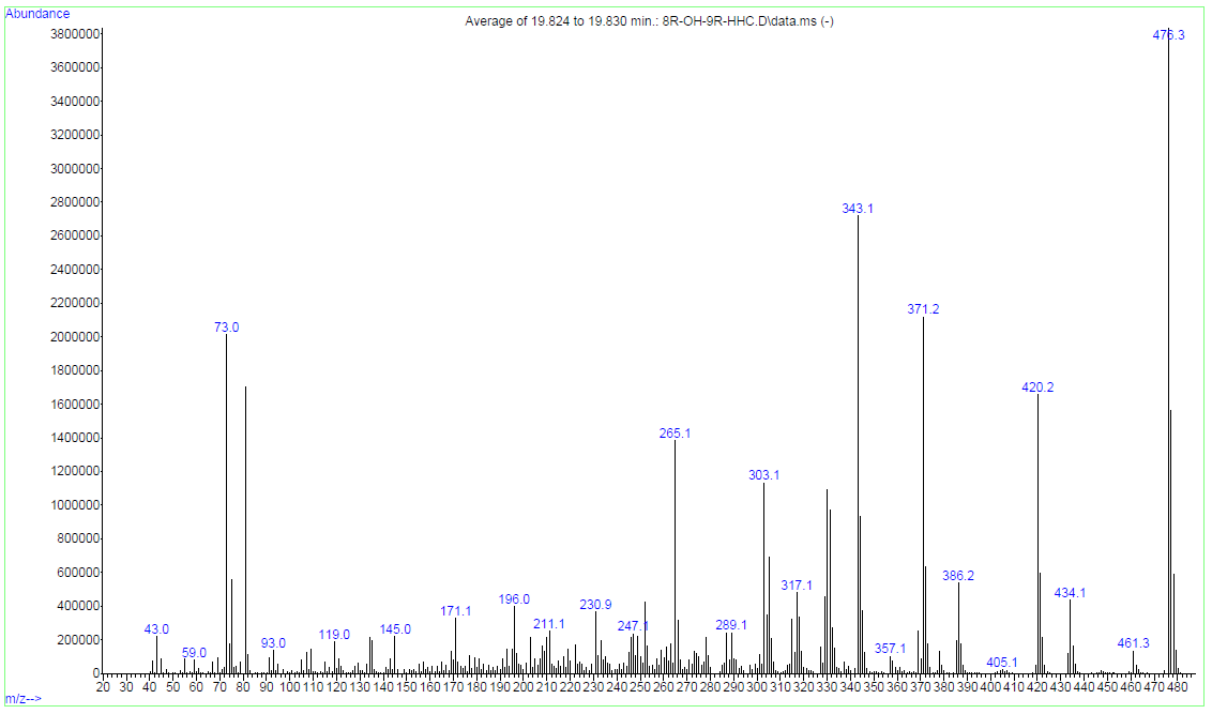

(8*R*, 9*S*)-8-OH-HHC 2xTMS

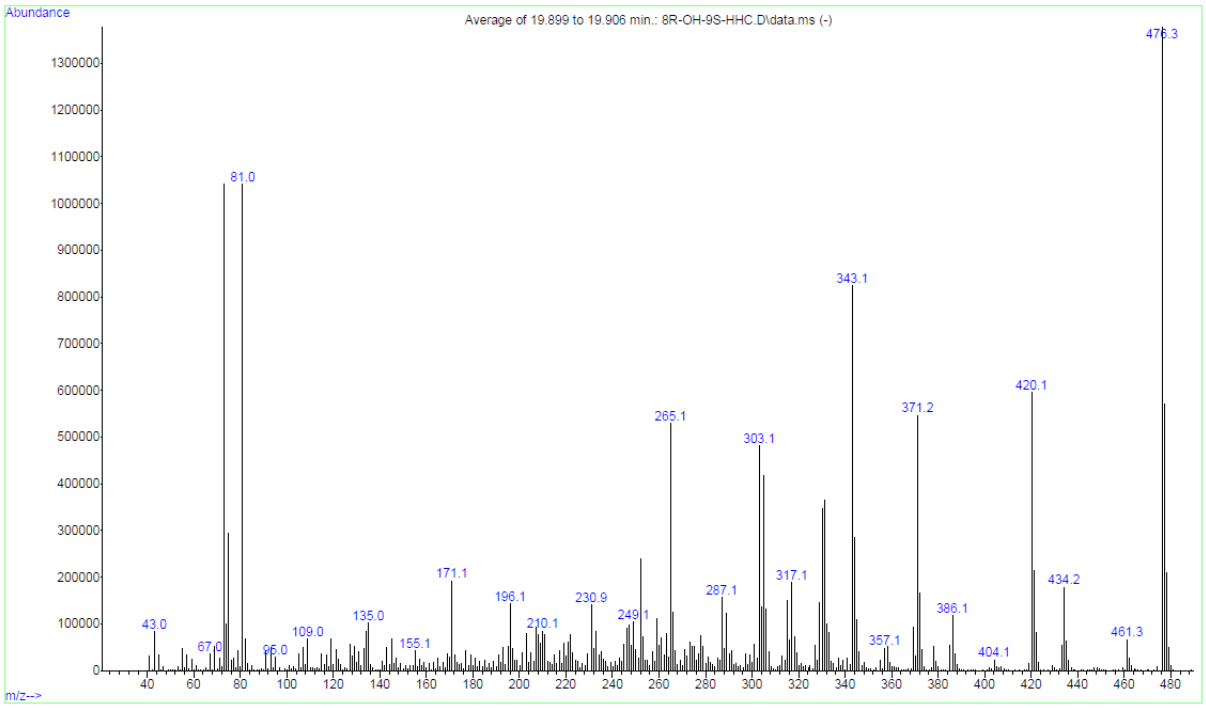

(8*S*, 9*S*)-8-OH-HHC 2xTMS

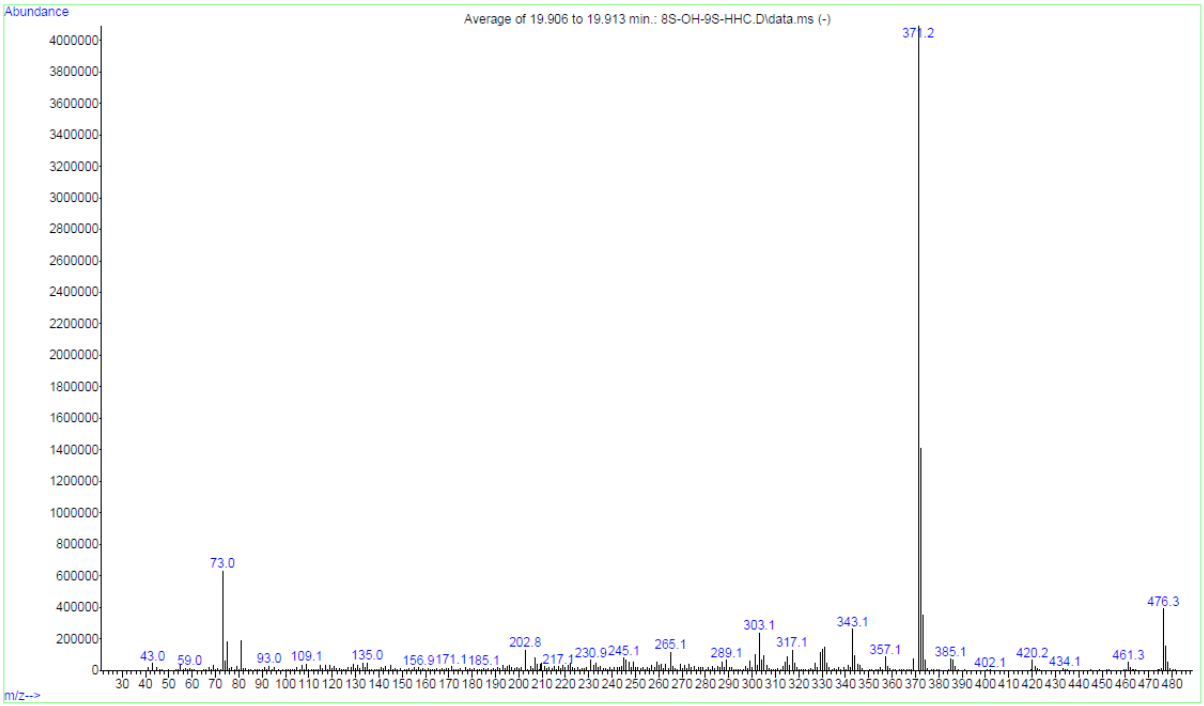

(9*R*)-11-OH-HHC 2xTMS

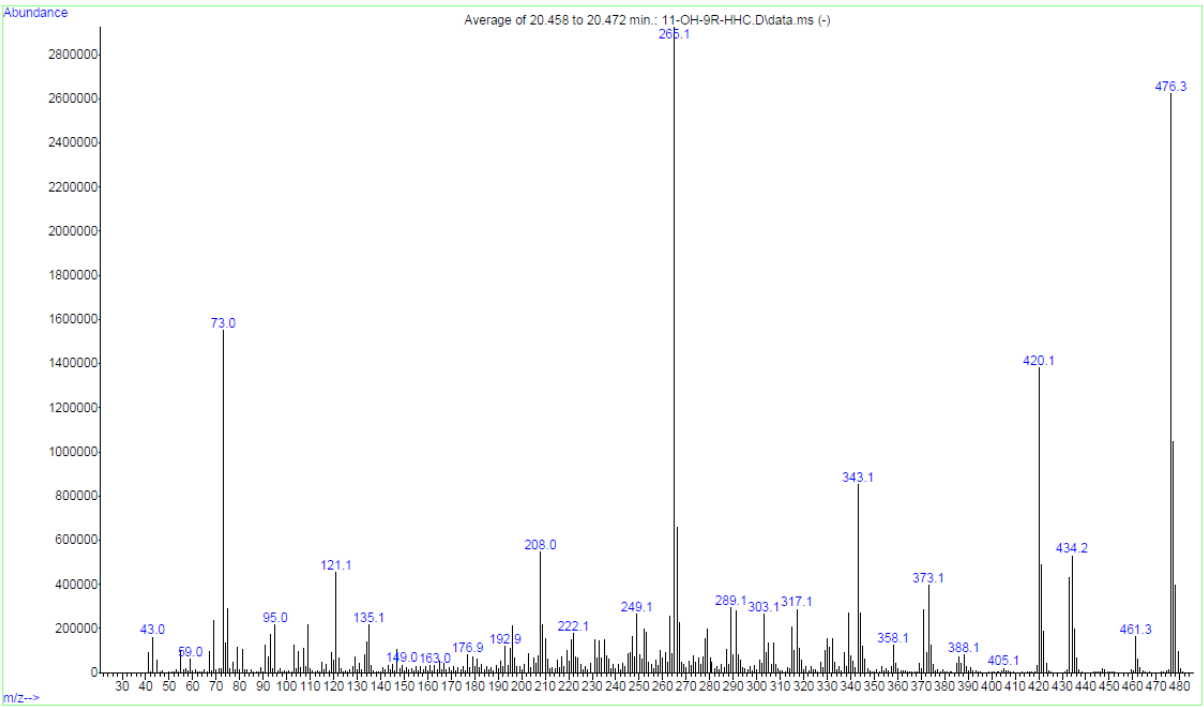

(9*S*)-11-OH-HHC 2xTMS

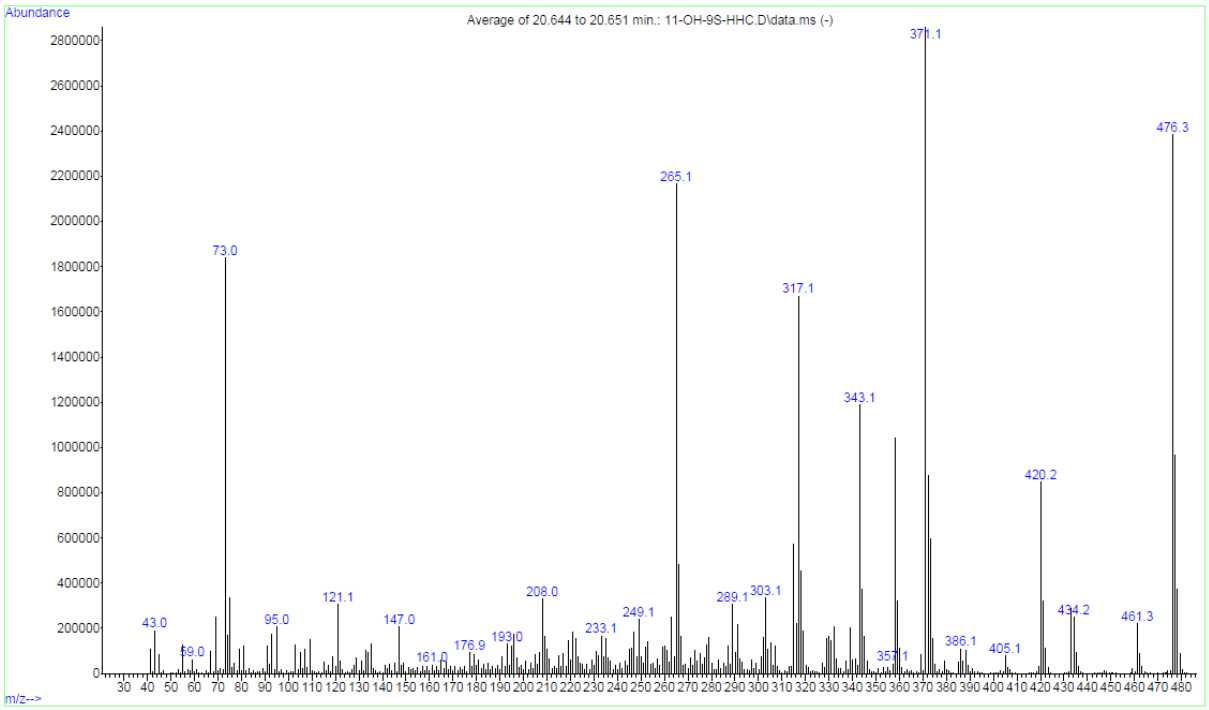

(9*R*)-11-nor-9-carboxy-HHC 2xTMS

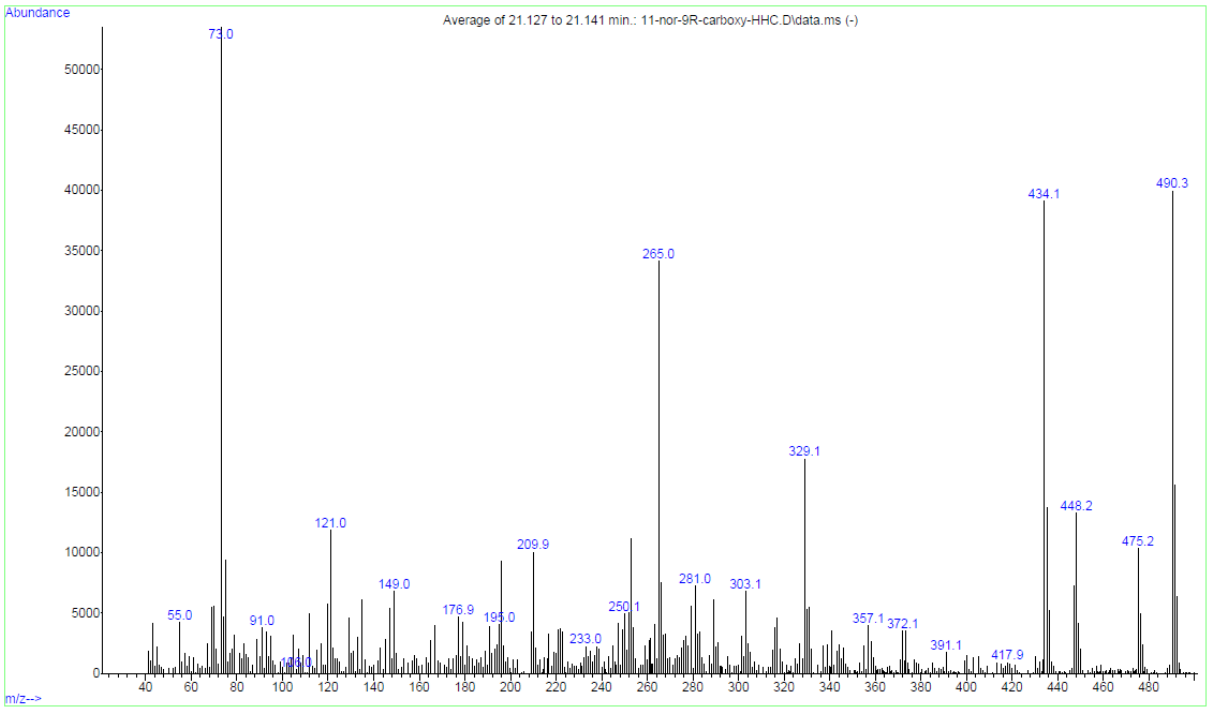

(9*S*)-11-nor-9-carboxy-HHC 2xTMS

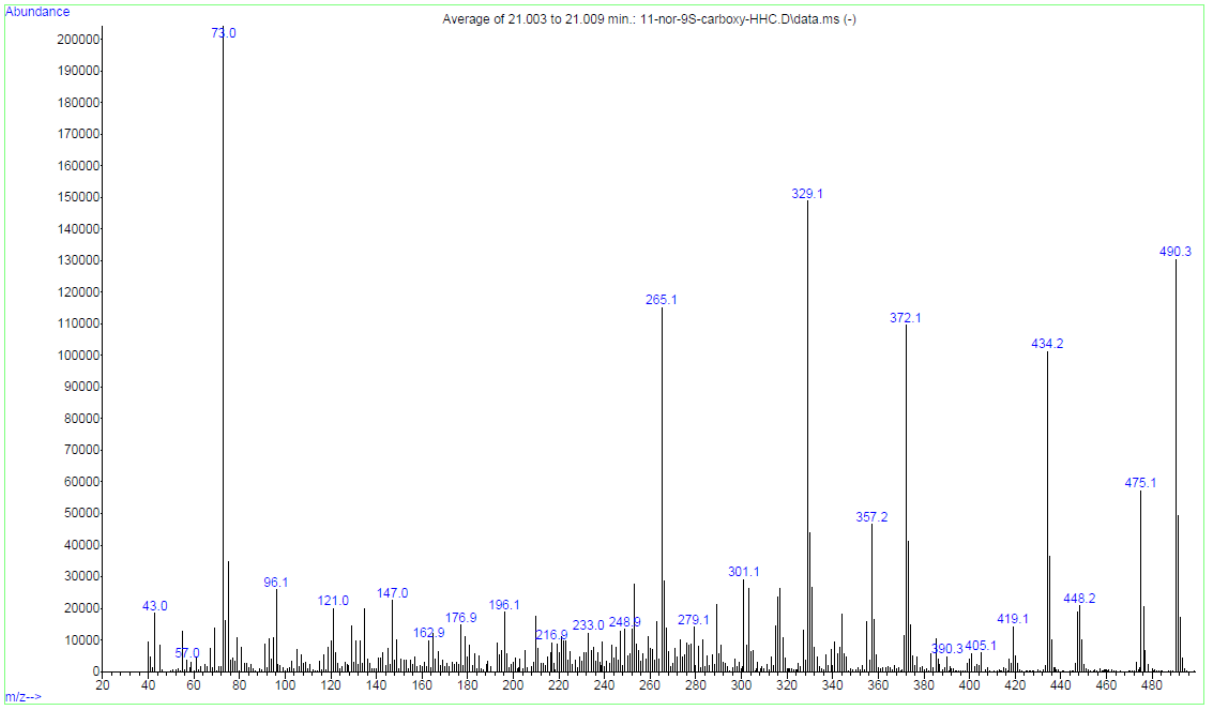

GC-MS/MS ion chromatogram

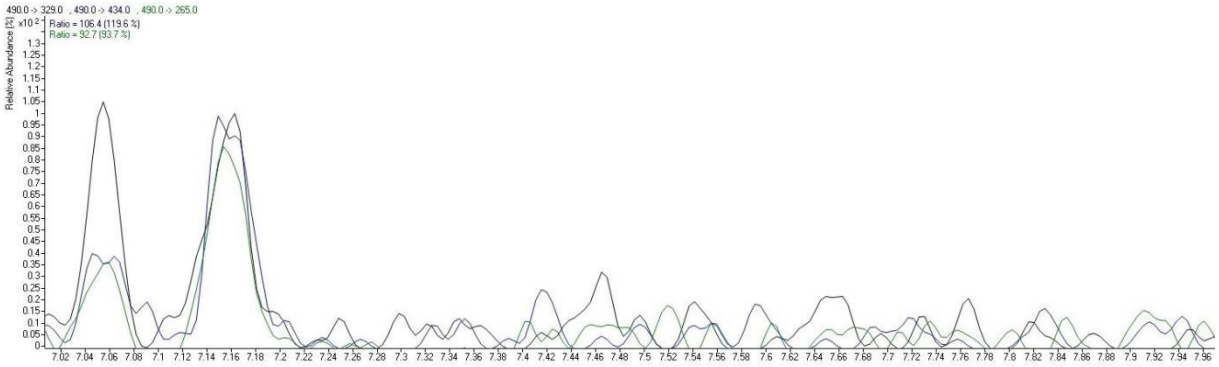

Extracted ion chromatogram for the three monitored ion transitions characteristic for 11-nor-9-carboxy-HHC of a urine sample of the volunteer who vaped 15 mg of HHC. The urine sample showing the highest response in immunochemical screening for cannabinoids (taken 2 hours post administration) was used.

References

1. Maralikova B and Weinmann W. Simultaneous determination of Δ9-tetrahydrocannabinol, 11-hydroxy-Δ9-tetrahydrocannabinol and 11-nor-9-carboxy- Δ9-tetrahydrocannabinol in human plasma by high-performance liquid chromatography/tandem mass spectrometry. *Journal of Mass Spectrometry* 2004; 39: 526-531. DOI: https://doi.org/10.1002/jms.616.

2. Ferrer I. Chapter Fourteen - Analyses of cannabinoids in hemp oils by LC/Q-TOF-MS. In: Ferrer I and Thurman EM (eds) *Comprehensive Analytical Chemistry*. Elsevier, 2020, pp.415-452.

3. Ray CL, Bylo MP, Pescaglia J, et al. Delta-8 Tetrahydrocannabinol Product Impurities. *Molecules* 2022; 27: 6924.
4. Budzikiewicz H, Alpin RT, Lightner DA, et al. Massenspektroskopie und ihre Anwendung auf strukturelle und stereochemische Probleme—LXVIII: Massenspektroskopische Untersuchung der Inhaltstoffe von Haschisch. *Tetrahedron* 1965; 21: 1881-1888. DOI: https://doi.org/10.1016/S0040-4020(01)98657-0.

Supplementary Information

Identification of hexahydrocannabiphorol metabolites in human urine

Willi Schirmer[1, 2], Stefan Schürch[2], Wolfgang Weinmann[1]

[1]Institute of Forensic Medicine, Forensic Toxicology and Chemistry, University of Bern, Murtenstrasse 26, 3008 Bern, Switzerland

[2]Department of Chemistry, Biochemistry and Pharmaceutical Sciences, University of Bern, Freiestrasse 3, 3012 Bern, Switzerland

Corresponding author:

Willi Schirmer, Institute of Forensic Medicine, Forensic Toxicology and Chemistry, University of Bern, Murtenstrasse 26, 3008 Bern, Switzerland

e-mail address: willi.schirmer@irm.unibe.ch

conc / mg/L	Area R-HHCP	Area S-HHCP	Area ISTD	Area Ratio R	Area Ratio S
1	13449020	24867414	8911424	1.509188655	2.79050575
2	39535290	64348226	9059341	4.364035971	7.102969852
3	70866537	112608487	10082468	7.028689503	11.16874232
4	84191177	131604340	7802717	10.78998213	16.86647613

Sample	Area R-HHCP	Area S-HHCP	Area ISTD	Area Ratio R	Area Ratio S	R-HHCP	S-HHCP	% R-HHCP	% S-HHCP
5 mg/L	54924786	16480167	10182202	5.394195283	1.618526818	2.326669881	0.801356	46.5	16.0
10 mg/L	201955250	60895701	13242896	15.25008201	4.598367381	5.445039514	1.542662	54.5	15.4

inside calibration

ISTD: THC-D3

S1: Quantification of (9*R*)- and (9*S*)-HHCP in the HHCP product for recreational use with GC-MS.

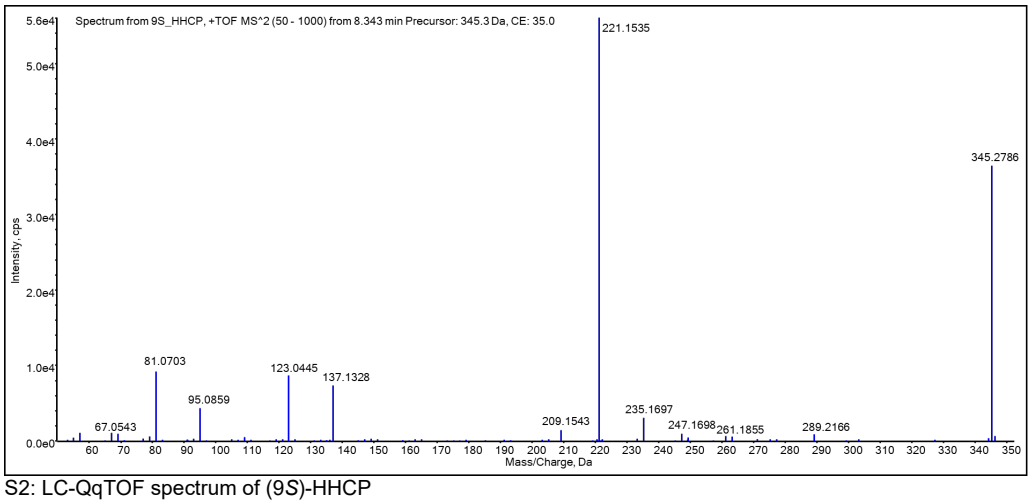

S2: LC-QqTOF spectrum of (9*S*)-HHCP

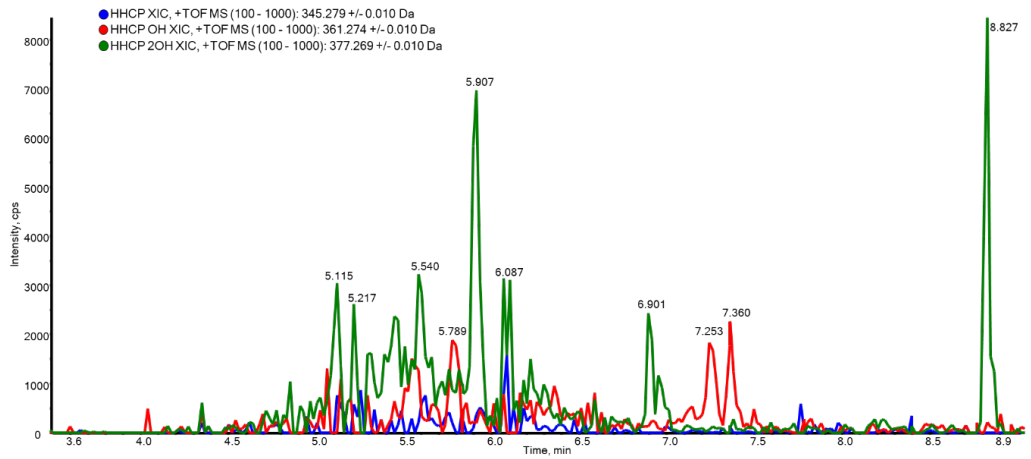

S3: Deglucuronidated urine before ingestion of HHCP (LC_QqTOF)

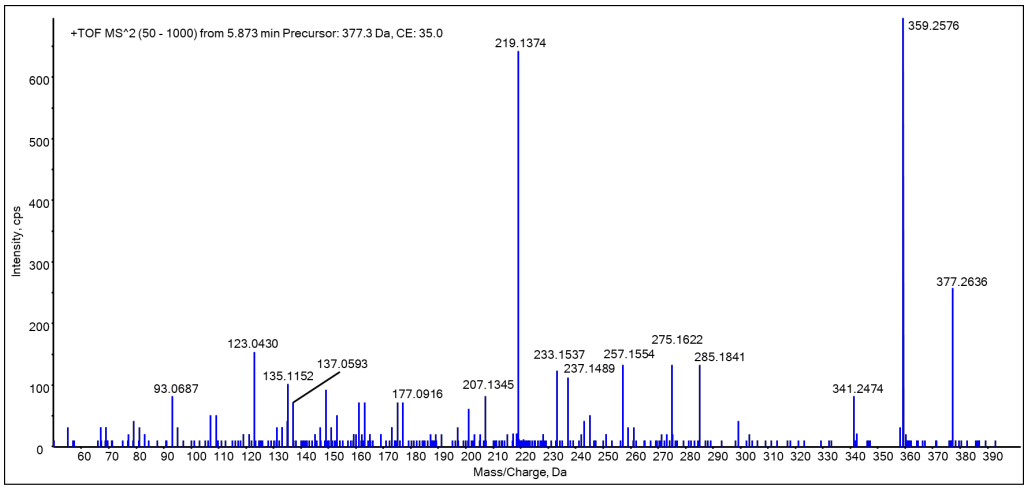

S4: Mass spectrum of metabolite M1, a bishydroxylated metabolite of HHCP (from a deglucuronidated urine sample 10 h after ingestion of 4 mg HHCP)

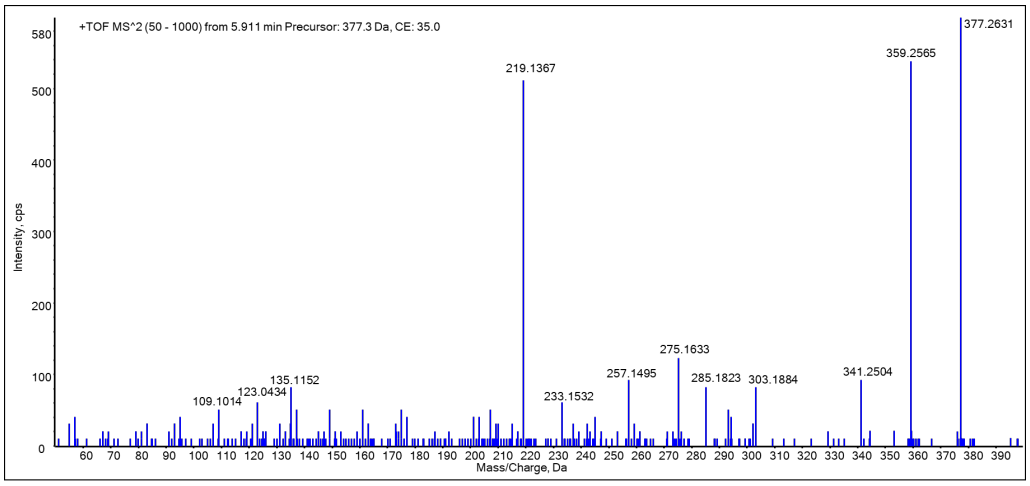

S5: Mass spectrum of metabolite M2, a bishydroxylated metabolite of HHCP (from a deglucuronidated urine sample 10 h after ingestion of 4 mg HHCP)

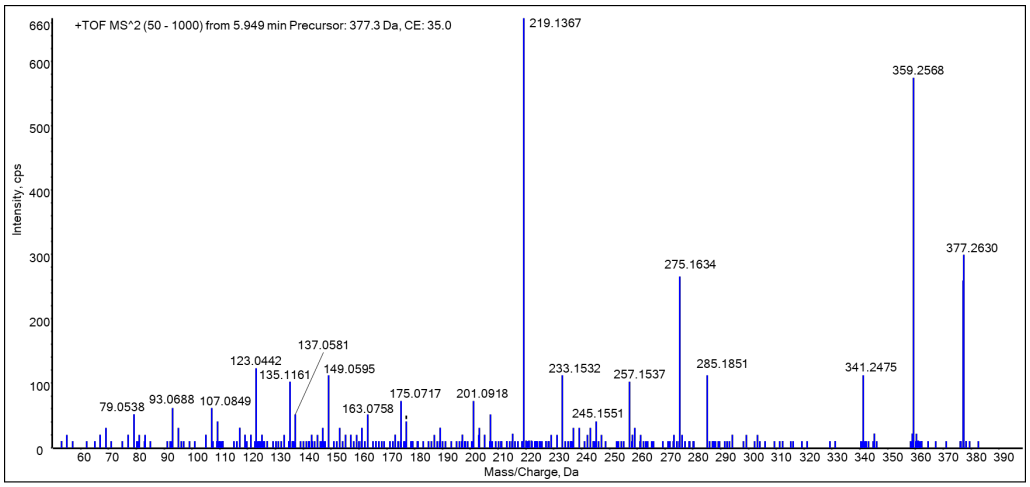

S6: Mass spectrum of metabolite M3, a bishydroxylated metabolite of HHCP (from a deglucuronidated urine sample 10 h after ingestion of 4 mg HHCP)

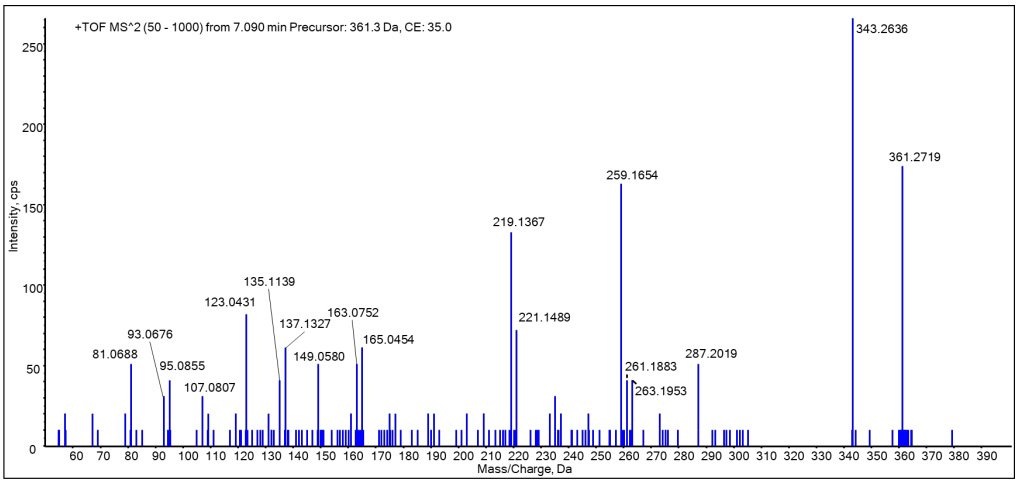

S7: Mass spectrum of metabolite M5, a hydroxylated metabolite of HHCP (from a deglucuronidated urine sample 10 h after ingestion of 4 mg HHCP)

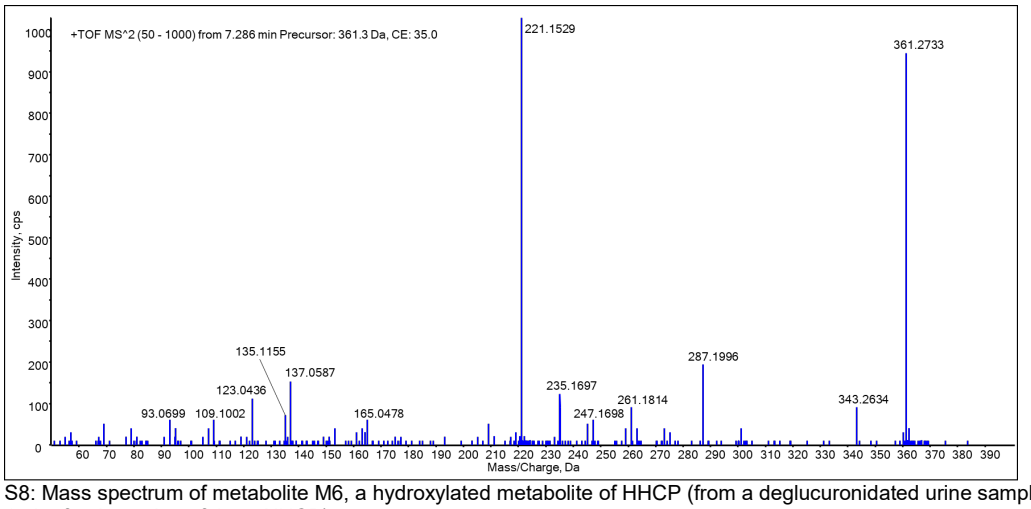

S8: Mass spectrum of metabolite M6, a hydroxylated metabolite of HHCP (from a deglucuronidated urine sample 10 h after ingestion of 4 mg HHCP)

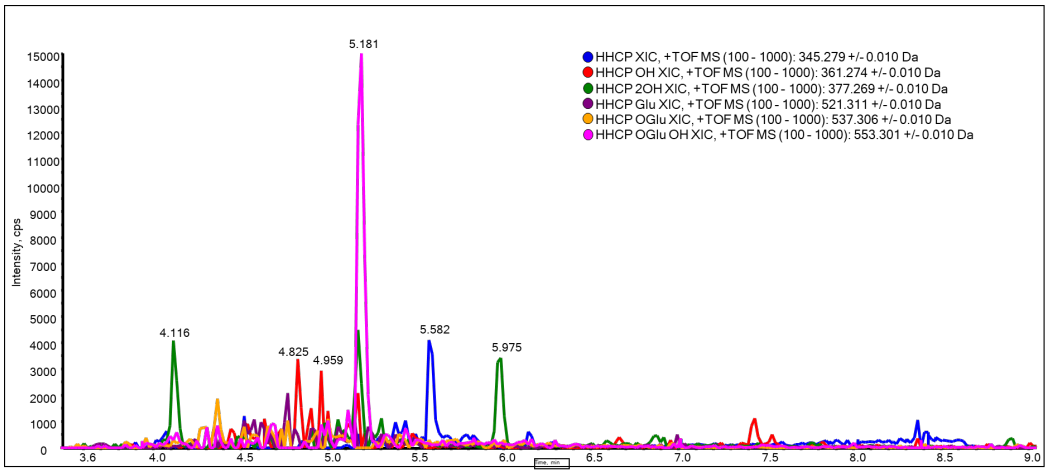

S9: Urine sample before ingestion of HHCP (LC_QqTOF)

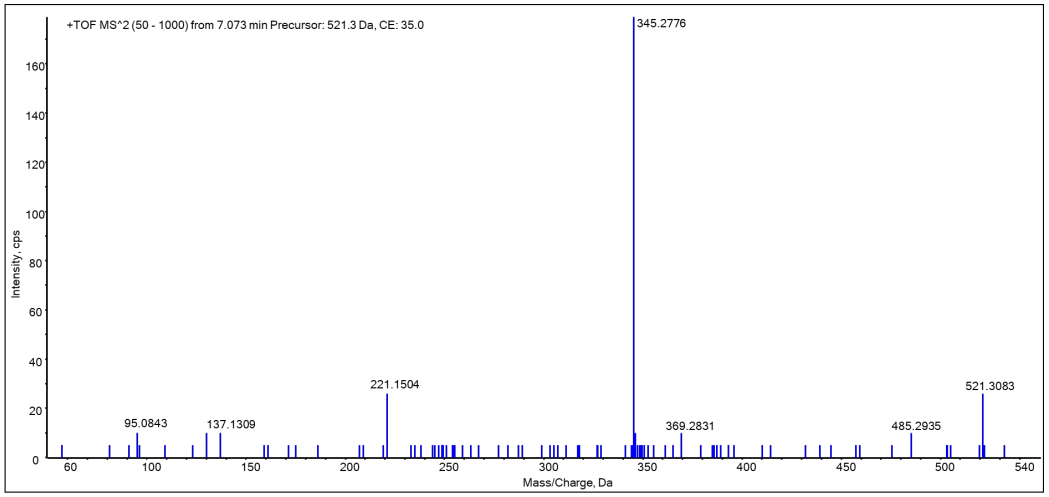

S10: Mass spectrum of HHCP glucuronide (from a urine sample 10 h after ingestion of 4 mg HHCP)

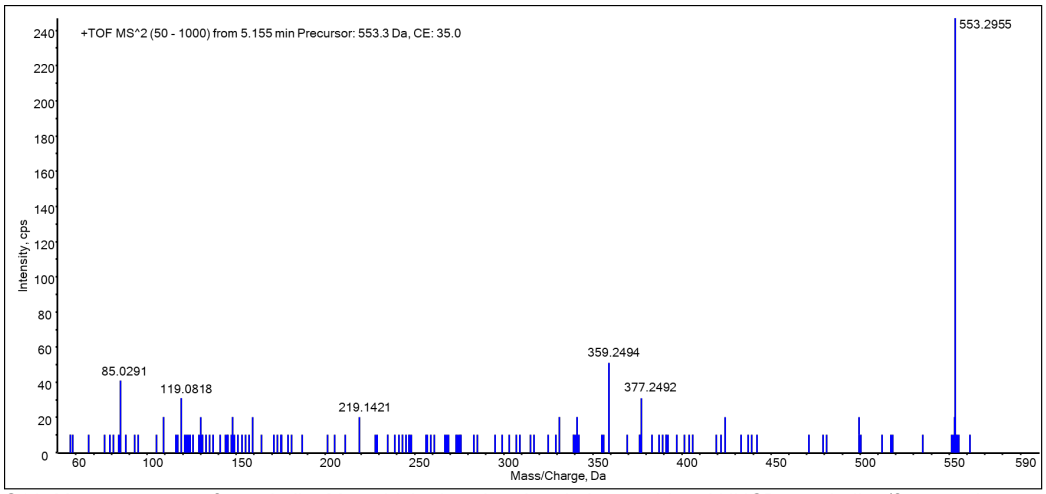

S11: Mass spectrum of metabolite M7, a bishydroxylated and glucuronidated HHCP metabolite (from a urine sample 10 h after ingestion of 4 mg HHCP)

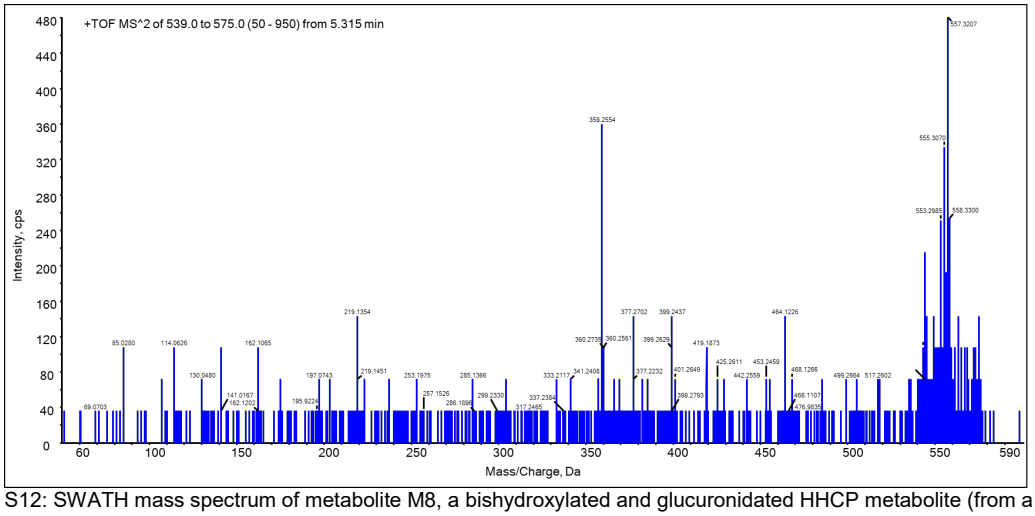

S12: SWATH mass spectrum of metabolite M8, a bishydroxylated and glucuronidated HHCP metabolite (from a urine sample 10 h after ingestion of 4 mg HHCP)

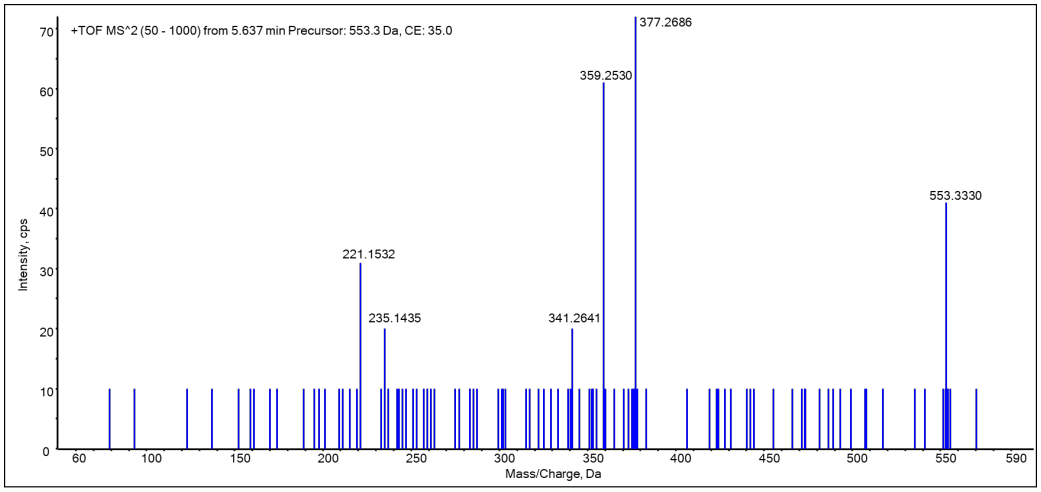

S13: Mass spectrum of metabolite M9, a bishydroxylated and glucuronidated HHCP metabolite (from a urine sample 10 h after ingestion of 4 mg HHCP)

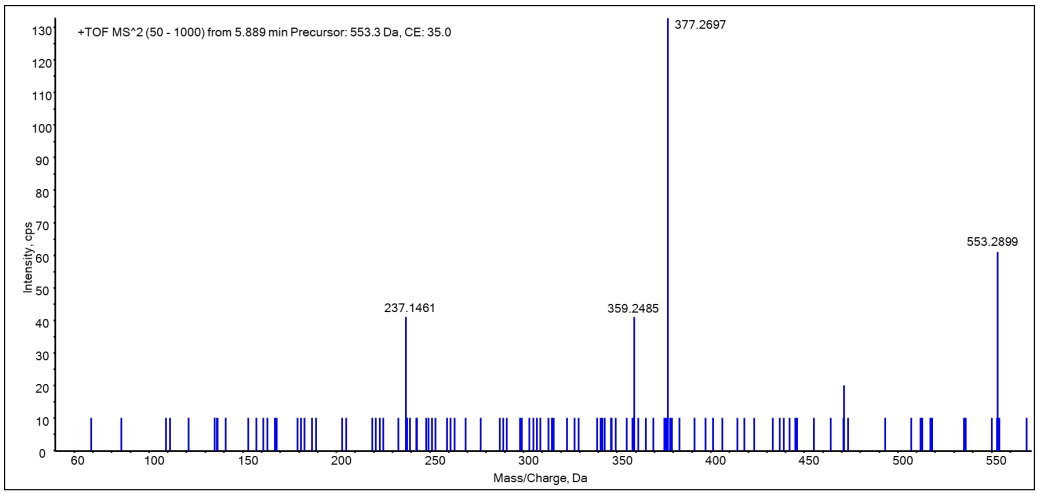

S14: Mass spectrum of metabolite M10, a bishydroxylated and glucuronidated HHCP metabolite (from a urine sample 10 h after ingestion of 4 mg HHCP) *m/z* 237 is likely a tropylium with a hydroxylated heptyl chain.

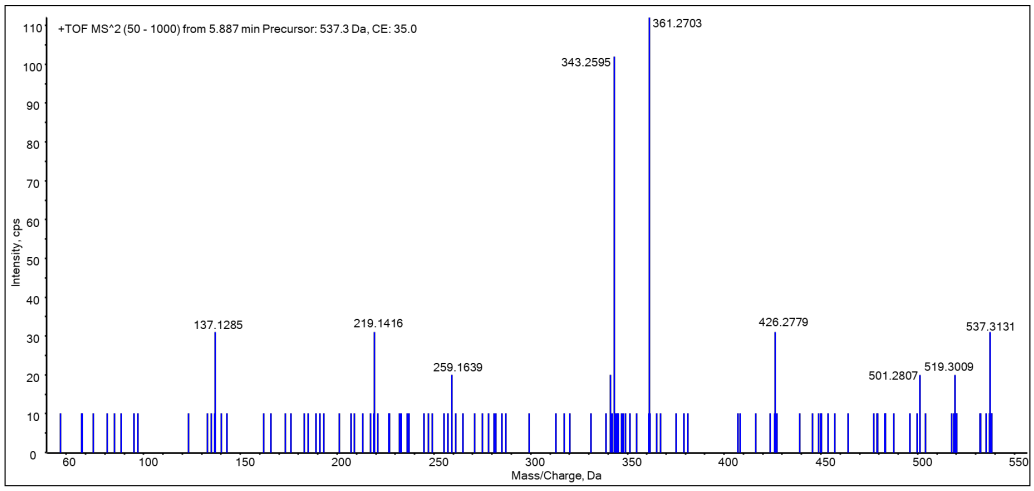

S15: Mass spectrum of metabolite M11, a hydroxylated and glucuronidated metabolite of HHCP (from a urine sample 10 h after ingestion of 4 mg HHCP)

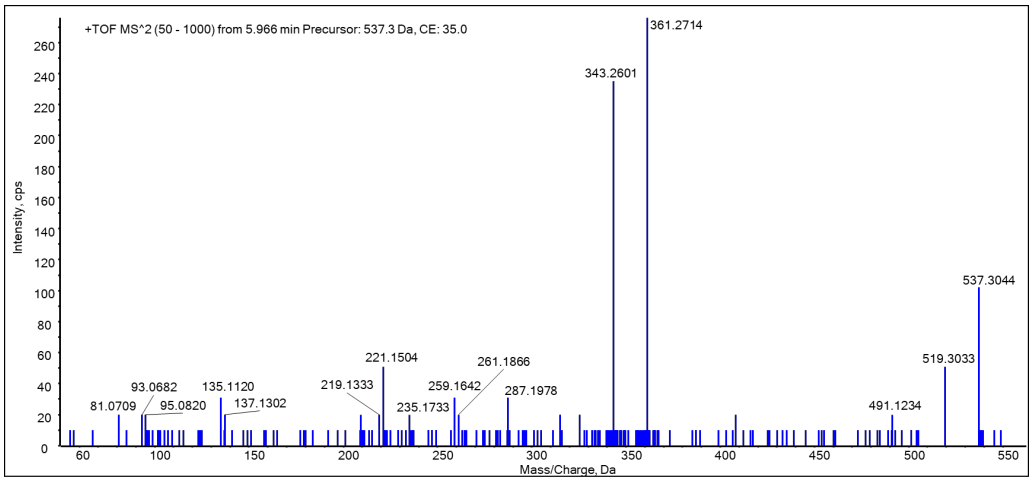

S16: Mass spectrum of a metabolite coeluting with metabolite M11, a hydroxylated and glucuronidated metabolite

of HHCP (from a urine sample 10 h after ingestion of 4 mg HHCP)

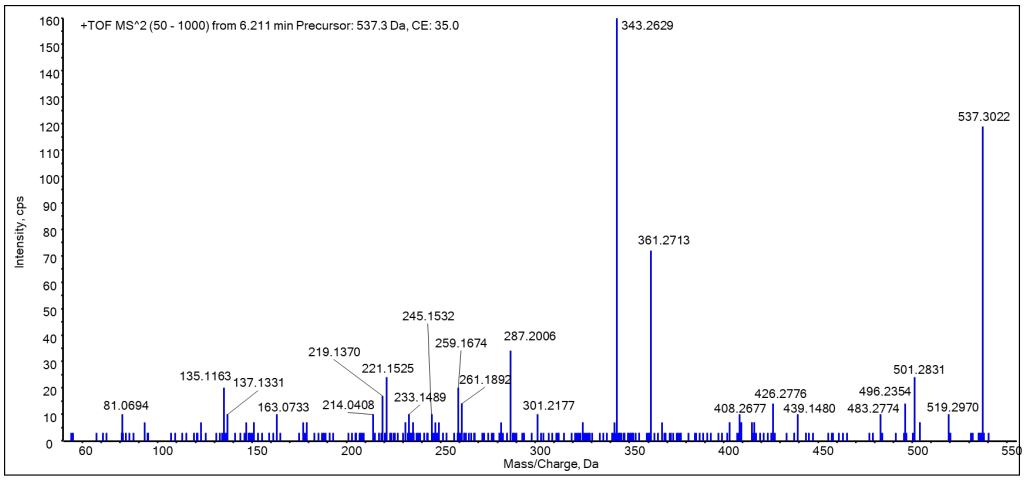

S17: Mas spectrum of coeluting metabolites (M12), hydroxylated and glucuronidated metabolites of HHCP (from a urine sample 10 h after ingestion of 4 mg HHCP)

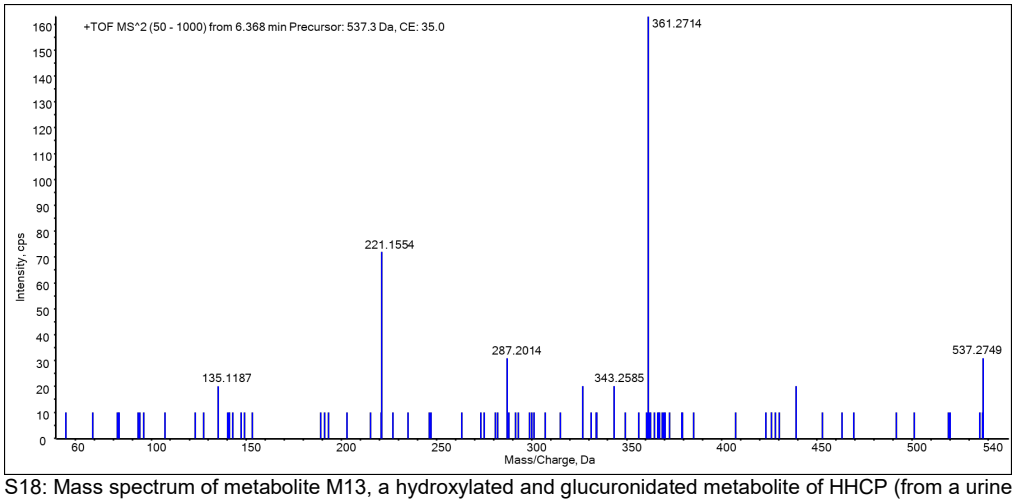

S18: Mass spectrum of metabolite M13, a hydroxylated and glucuronidated metabolite of HHCP (from a urine sample 10 h after ingestion of 4 mg HHCP)

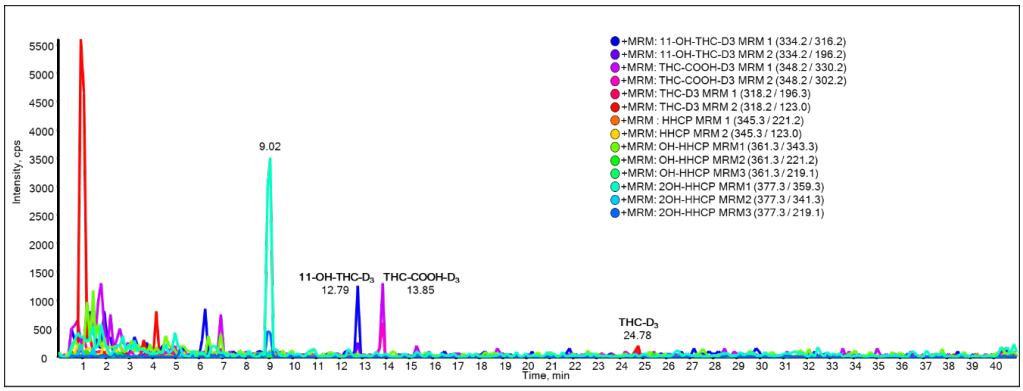

S19: Extracted ion chromatograms for characteristic mass transitions of a deglucuronidated urine sample prior ingestion of HHCP, Matrix peak is seen at 9.02 min

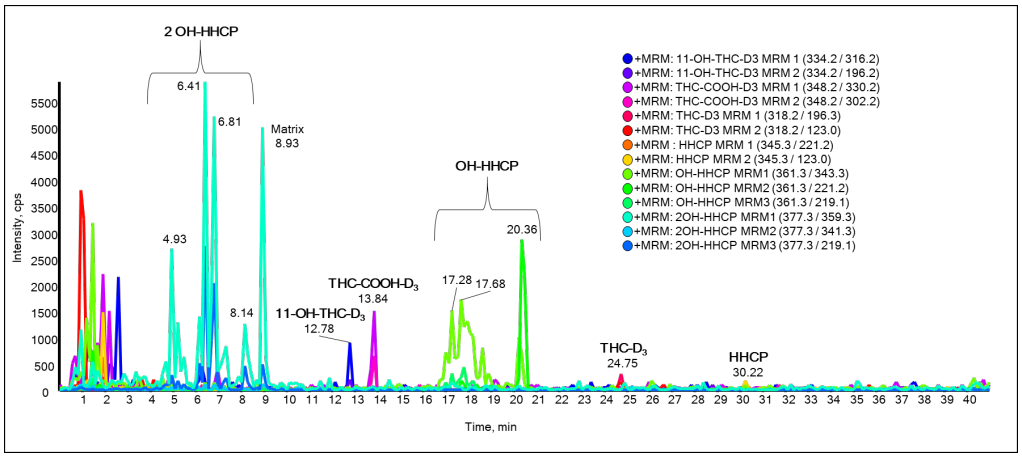

S20: Extracted ion chromatograms for characteristic mass transitions of a deglucuronidated urine sample (10 h after oral ingestion of 4 mg HHCP)

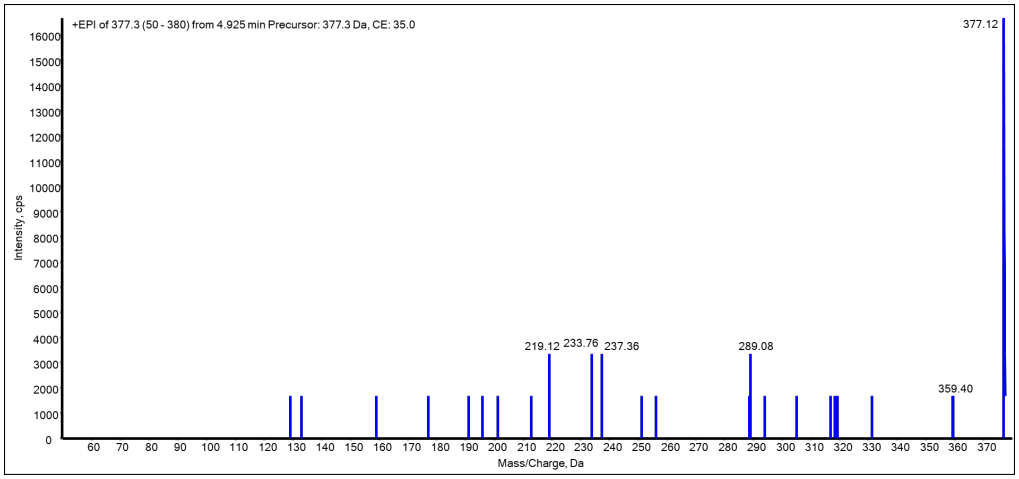

S21: Enhanced product ion spectrum of the bishydroxylated metabolite M14 (from a deglucuronidated urine sample 15 h after oral ingestion of 4 mg HHCP)

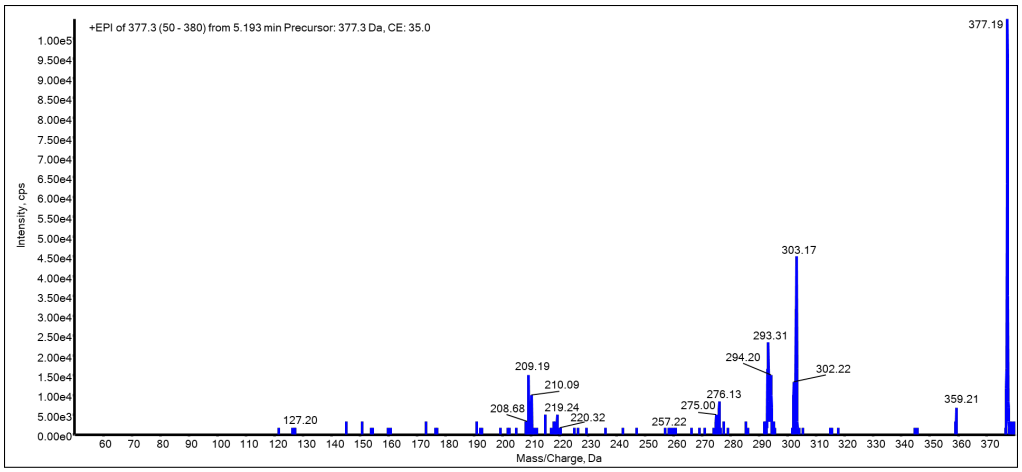

S22: Enhanced product ion spectrum of the bishydroxylated metabolite M15 (from a deglucuronidated urine sample 15 h after oral ingestion of 4 mg HHCP)

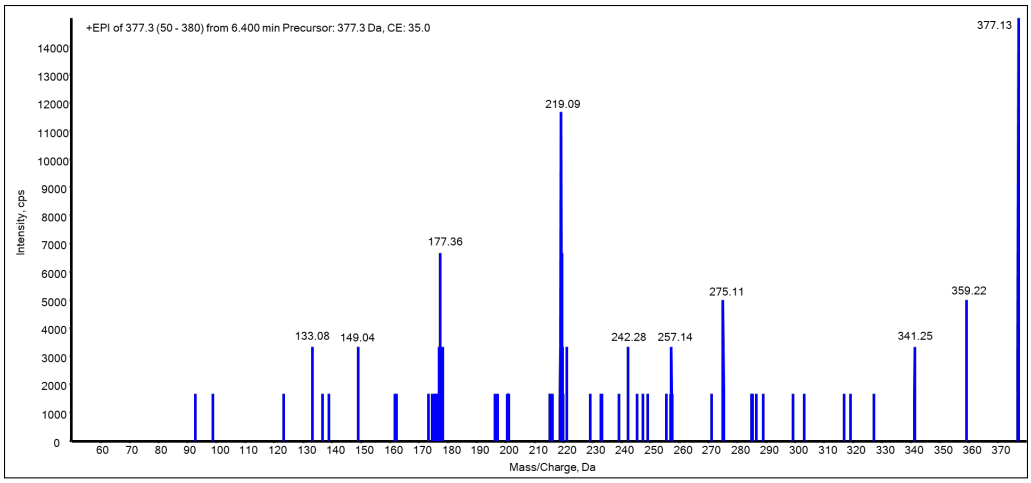

S23: Enhanced product ion spectrum of the bishydroxylated metabolite M16 (from a deglucuronidated urine sample 15 h after oral ingestion of 4 mg HHCP)

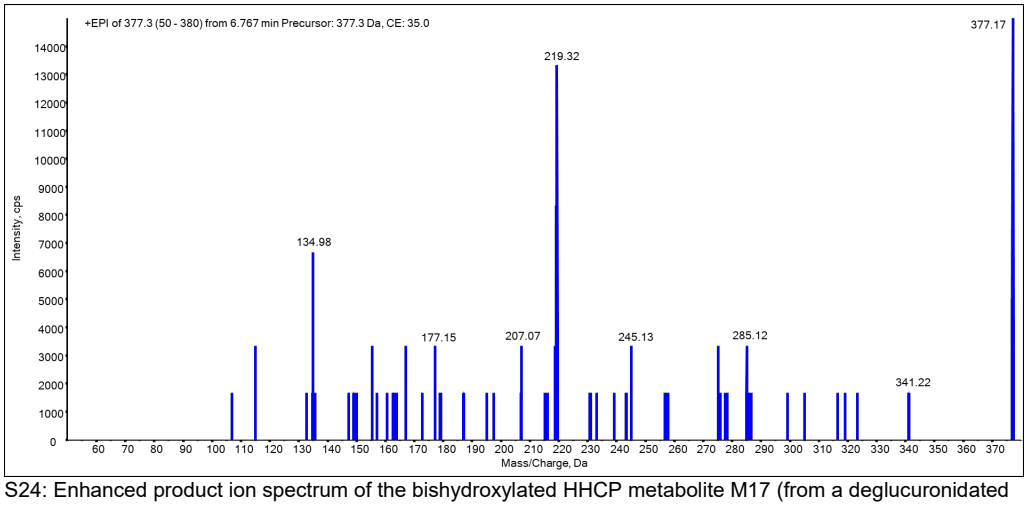

S24: Enhanced product ion spectrum of the bishydroxylated HHCP metabolite M17 (from a deglucuronidated urine sample 15 h after oral ingestion of 4 mg HHCP)

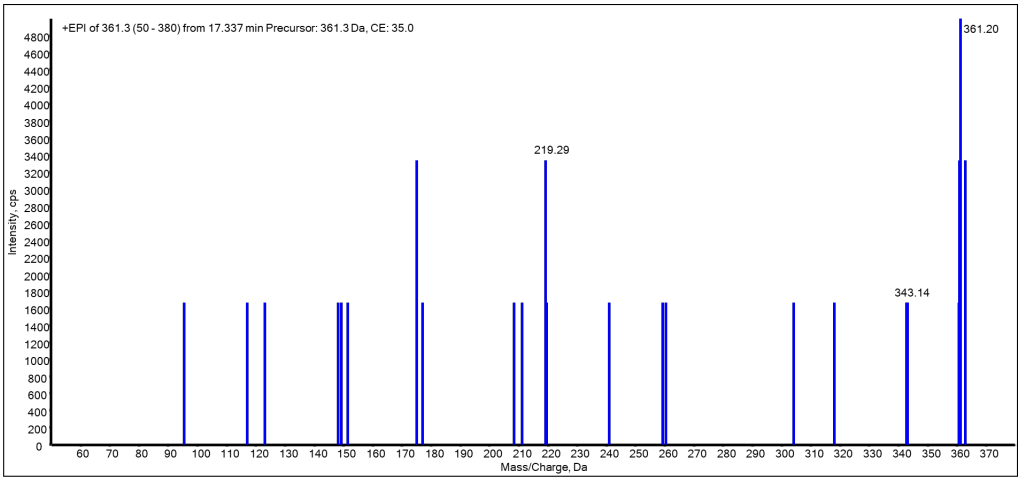

S25: Enhanced product ion spectrum of the hydroxylated HHCP metabolite M18 (from a deglucuronidated urine sample 15 h after oral ingestion of 4 mg HHCP)

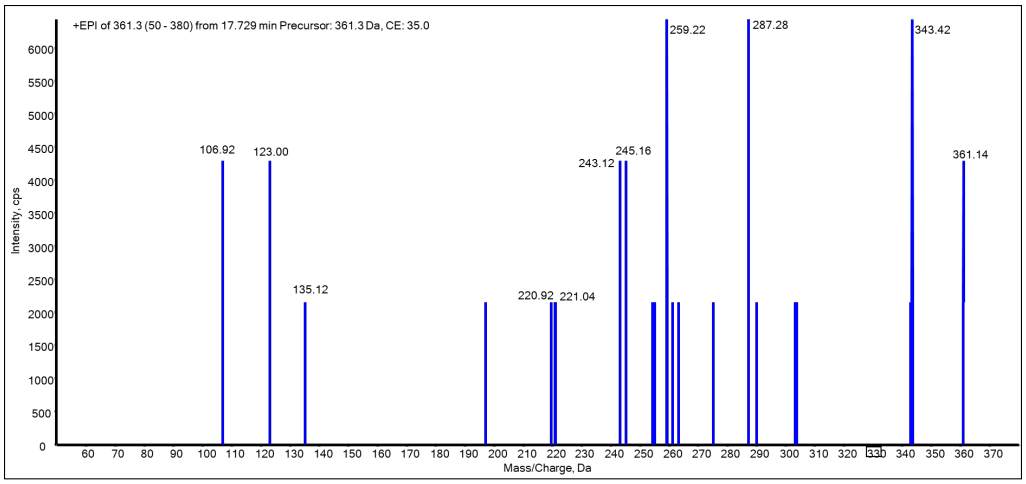

S26: Enhanced product ion spectrum of the hydroxylated HHCP metabolite M19 (from a deglucuronidated urine sample 15 h after oral ingestion of 4 mg HHCP)

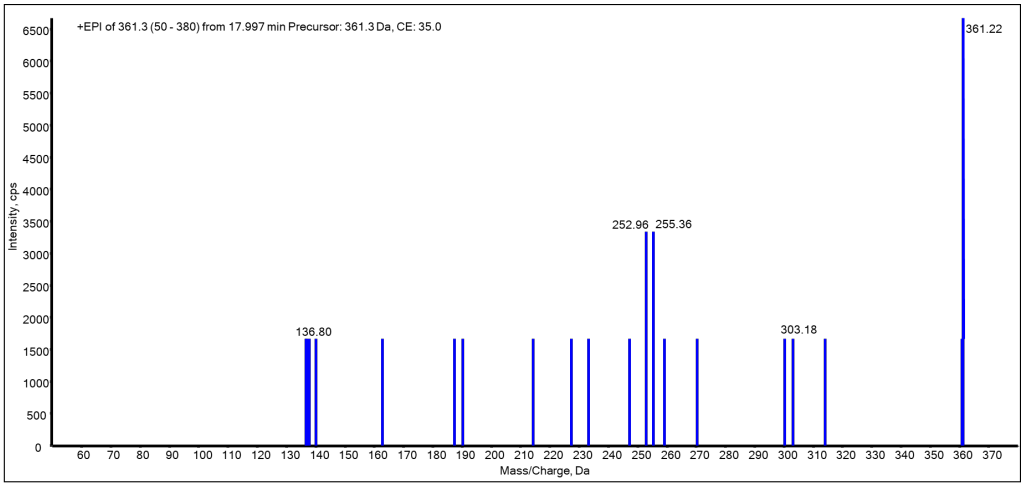

S27: Enhanced product ion spectrum of the hydroxylated HHCP metabolite M20 (from a deglucuronidated urine sample 15 h after oral ingestion of 4 mg HHCP)

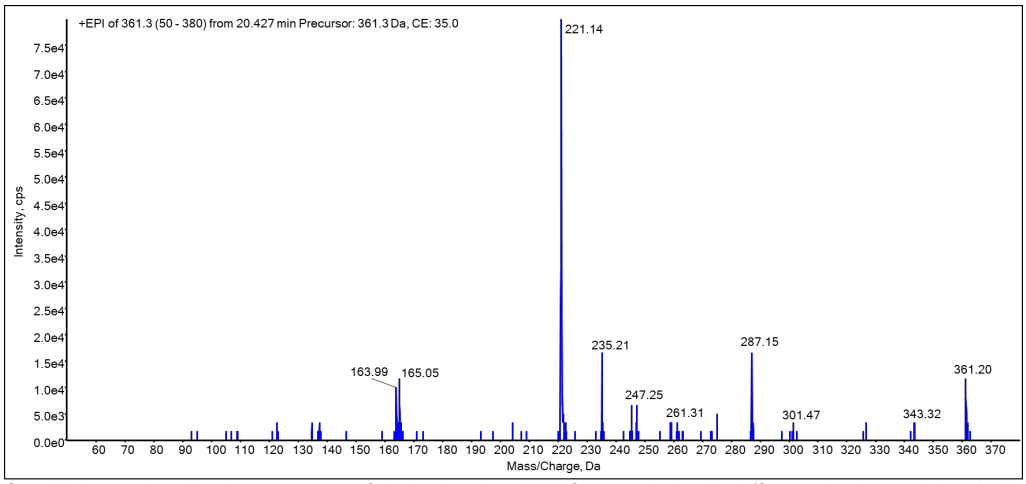

S28: Enhanced product ion spectrum of the hydroxylated HHCP metabolite M21 (from a deglucuronidated urine sample 15 h after oral ingestion of 4 mg HHCP)

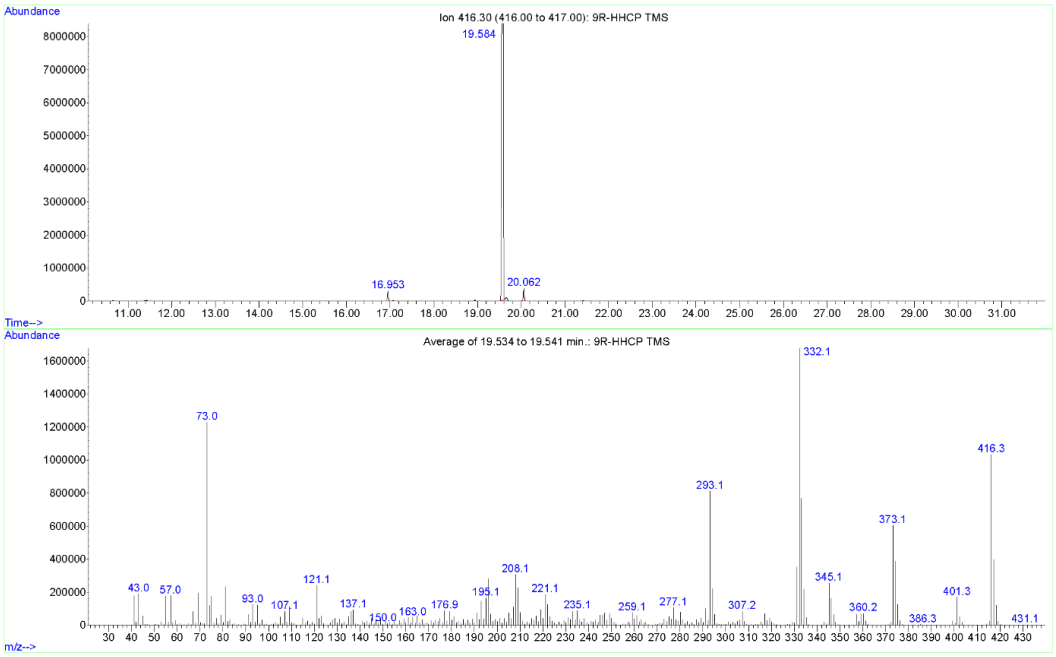

S29: EI mass spectrum of (9*R*)-HHCP TMS (derivatized reference)

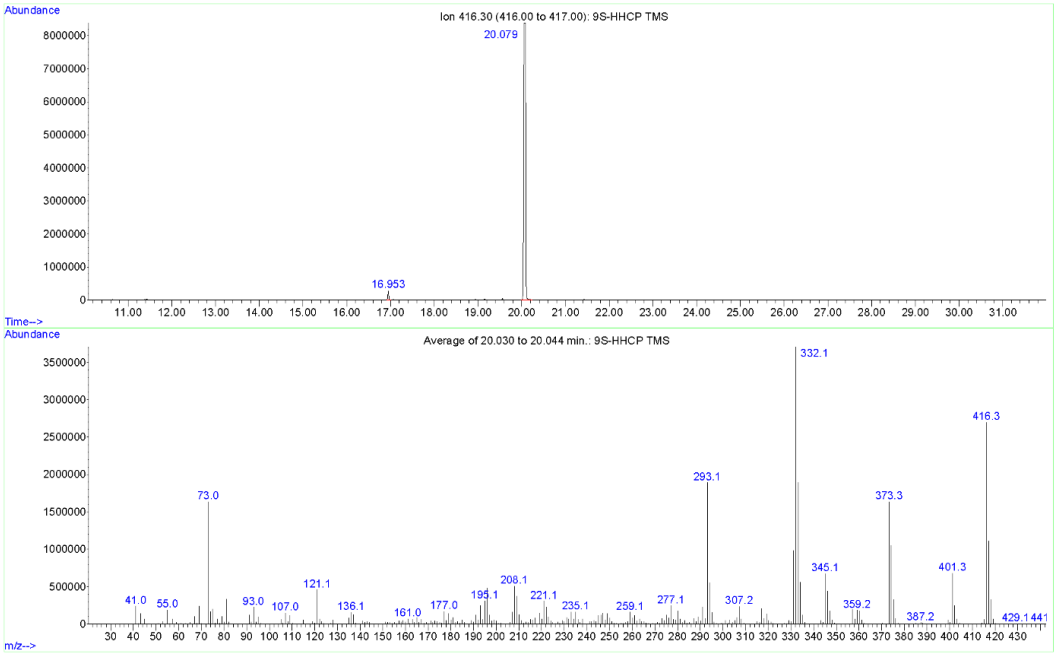

S30: EI mass spectrum of (9*S*)-HHCP TMS (derivatized reference)

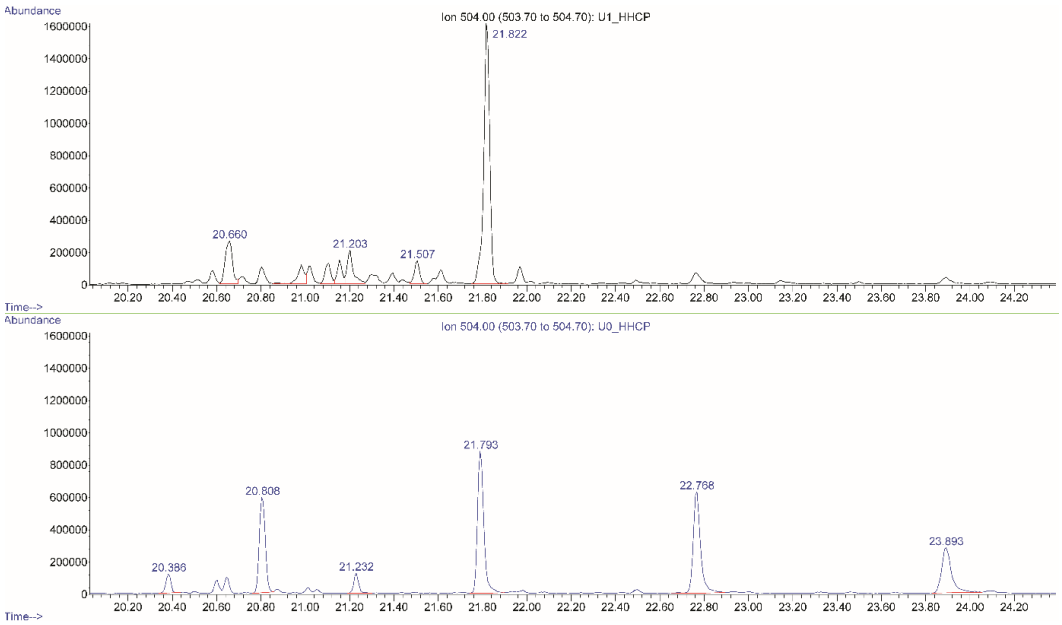

S31: Stacked XICs (*m/z* 504) of a trimethylsilylated urine sample collected before the oral ingestion of HHCP (top) and a trimethylsilyated urine sample from the same person 10 h after oral ingestion of 4 mg HHCP (bottom).

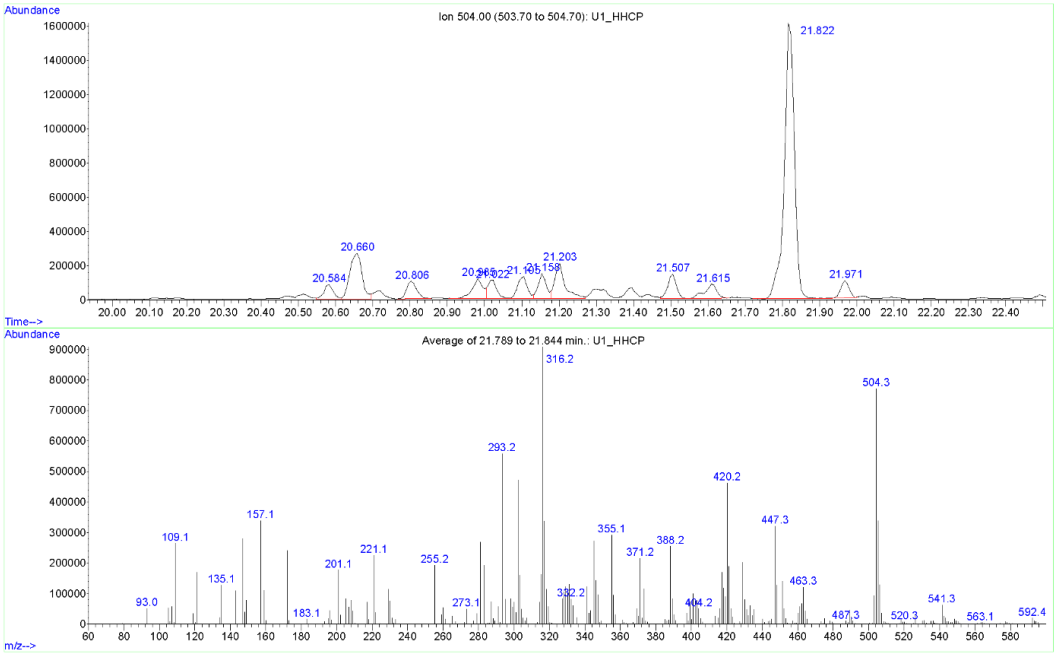

S32: Top: XIC (*m/z* 504) of a trimethylsilylated urine sample 10 h after oral ingestion of 4 mg HHCP. Bottom: EI mass spectrum of the compound eluting at 21.82 min.

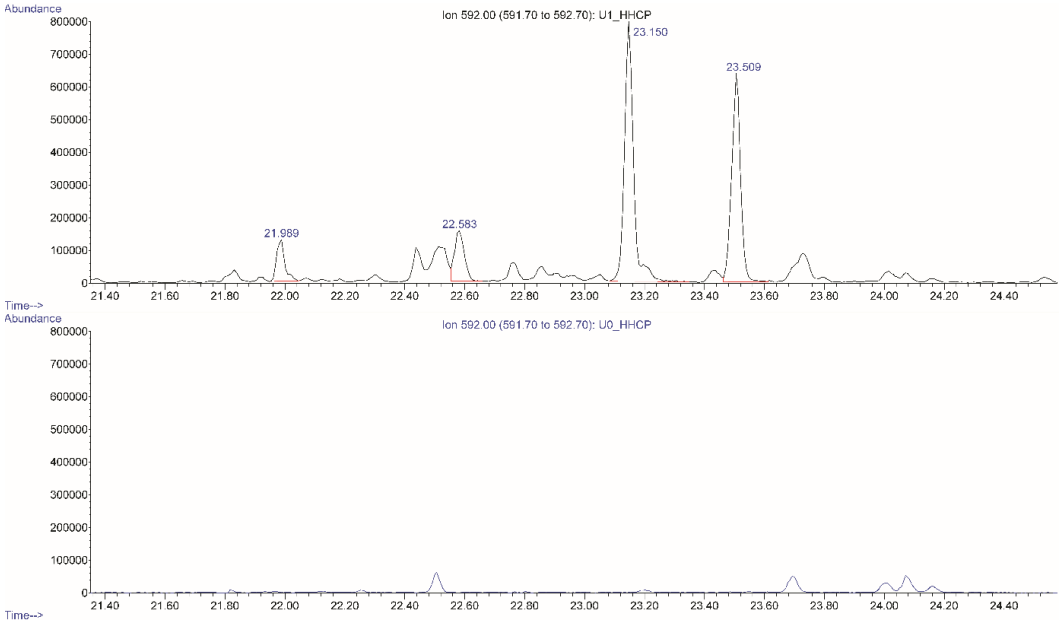

S33: Stacked XICs (*m/z* 592) of a trimethylsilylated urine sample collected before the oral ingestion of HHCP (top) and a trimethylsilyated urine sample from the same person 10 h after oral ingestion of 4 mg HHCP (bottom).

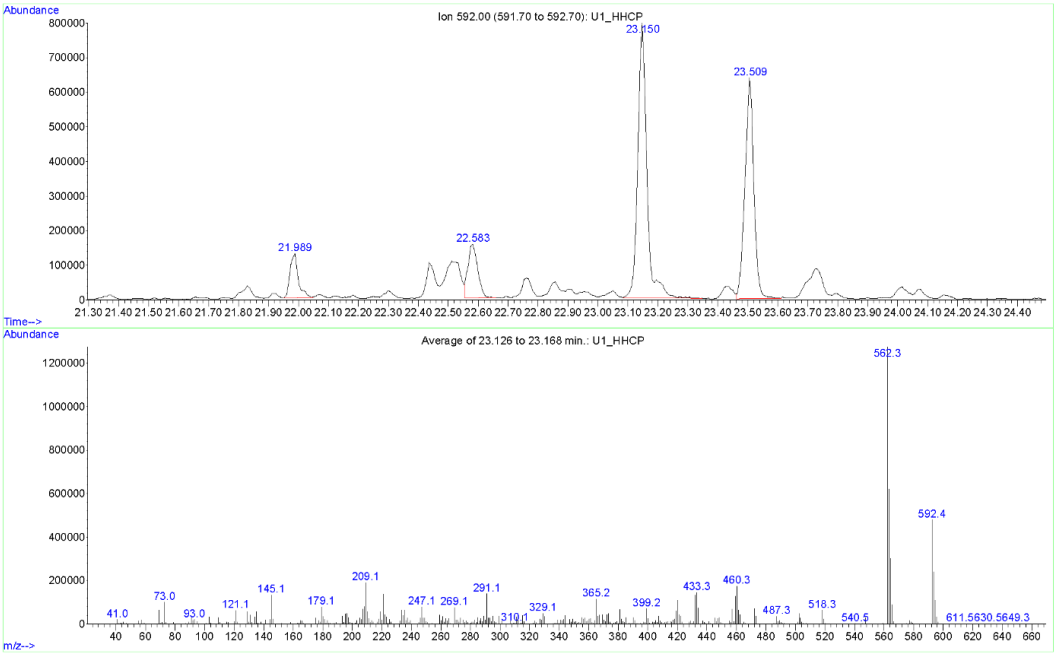

S34: Top: XIC (*m/z* 592) of a trimethylsilylated urine sample 10 h after oral ingestion of 4 mg HHCP. Bottom: EI mass spectrum of the compound eluting at 23.15 min.

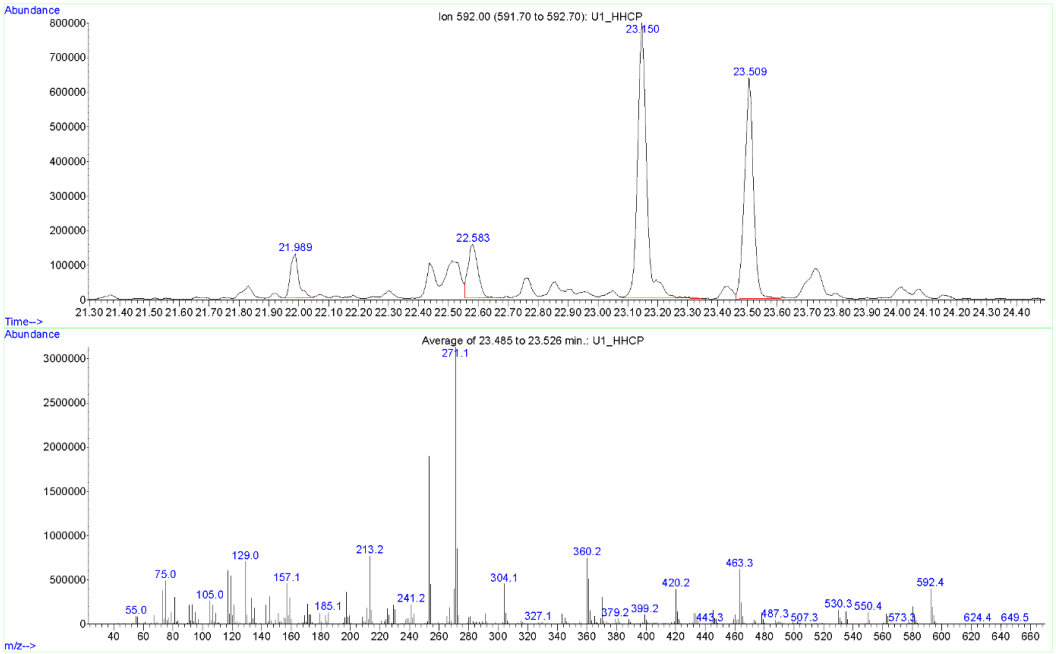

S35: Top: XIC (*m/z* 592) of a trimethylsilylated urine sample 10 h after oral ingestion of 4 mg HHCP. Bottom: EI mass spectrum of the compound eluting at 23.15 min.

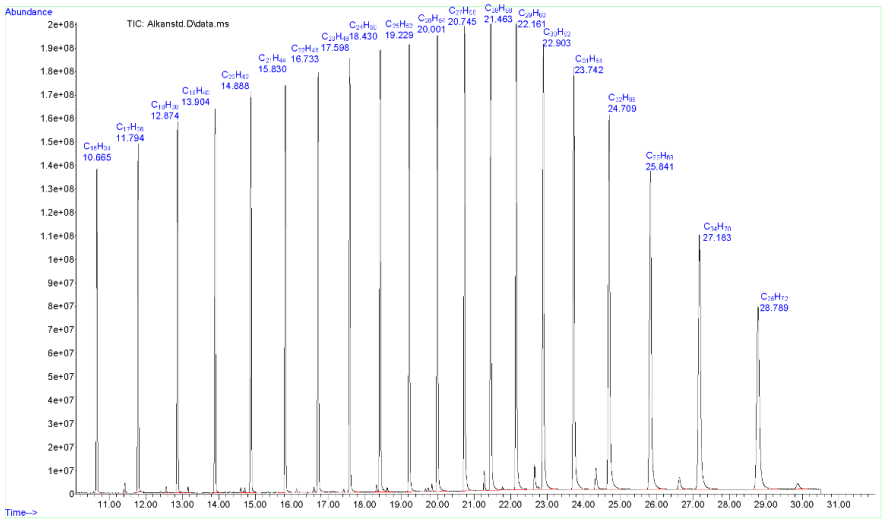

S36: TIC of an alkane standard (C7-C40) for the determination of Kováts indices.

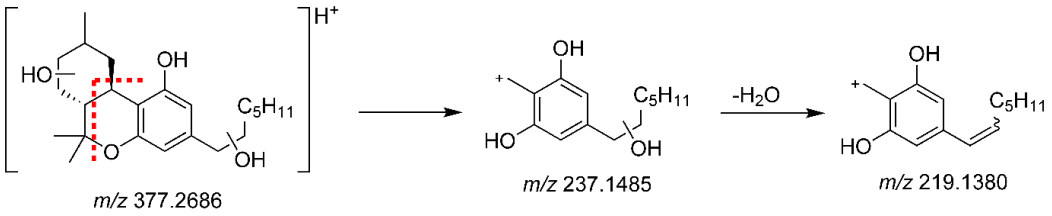

S37: Formation of the tropylium ions *m/z* 237 and *m/z* 219 which are characteristic ions for side chain hydroxylated HHCP. Position of the non-phenolic hydroxyl groups are not known, one is on the alicyclic moiety the other on the alkyl chain. Stereochemistry and position of the double bond on the alkyl chain of the ion *m/z* 219 is unknown.

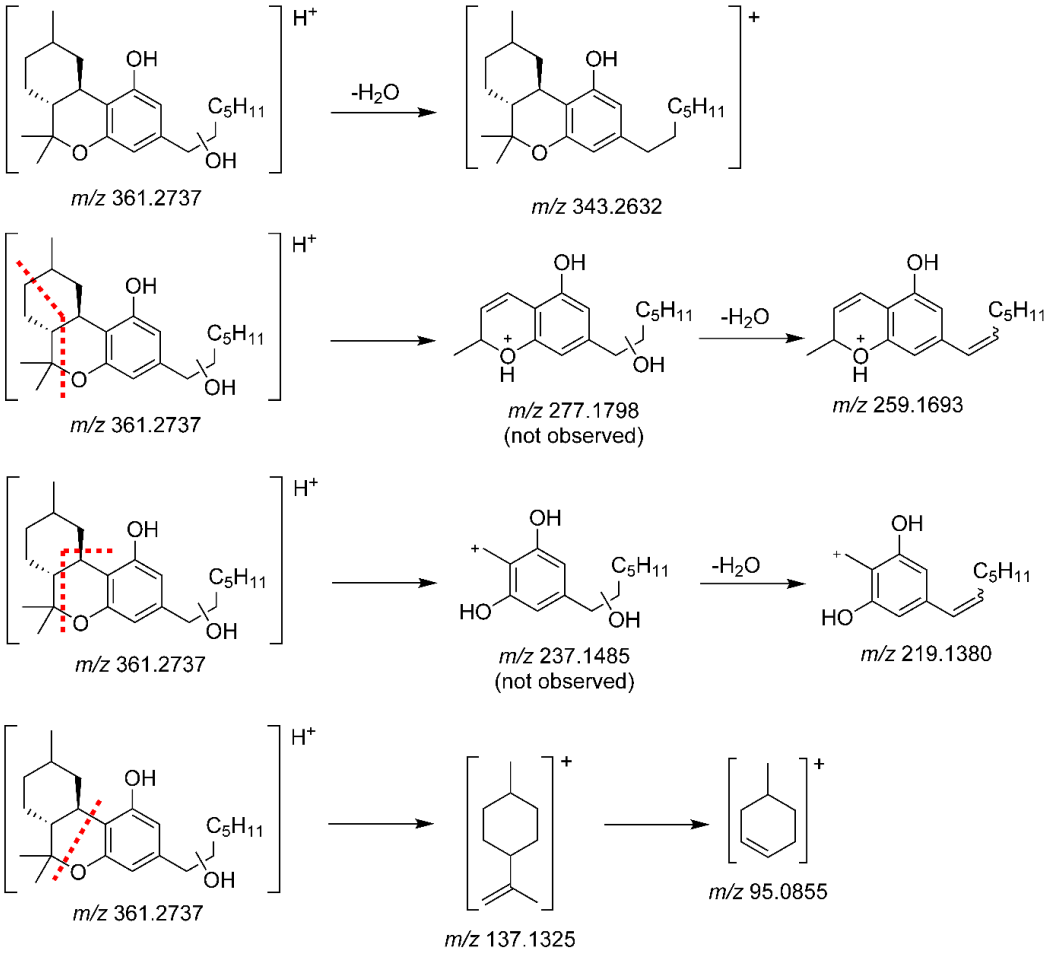

S38: LC-QqTOF ions of the monohydroxylated HHCP metabolite M5. Stereochemistry and position of the hydroxy group or double bond in the side chain is unknown.

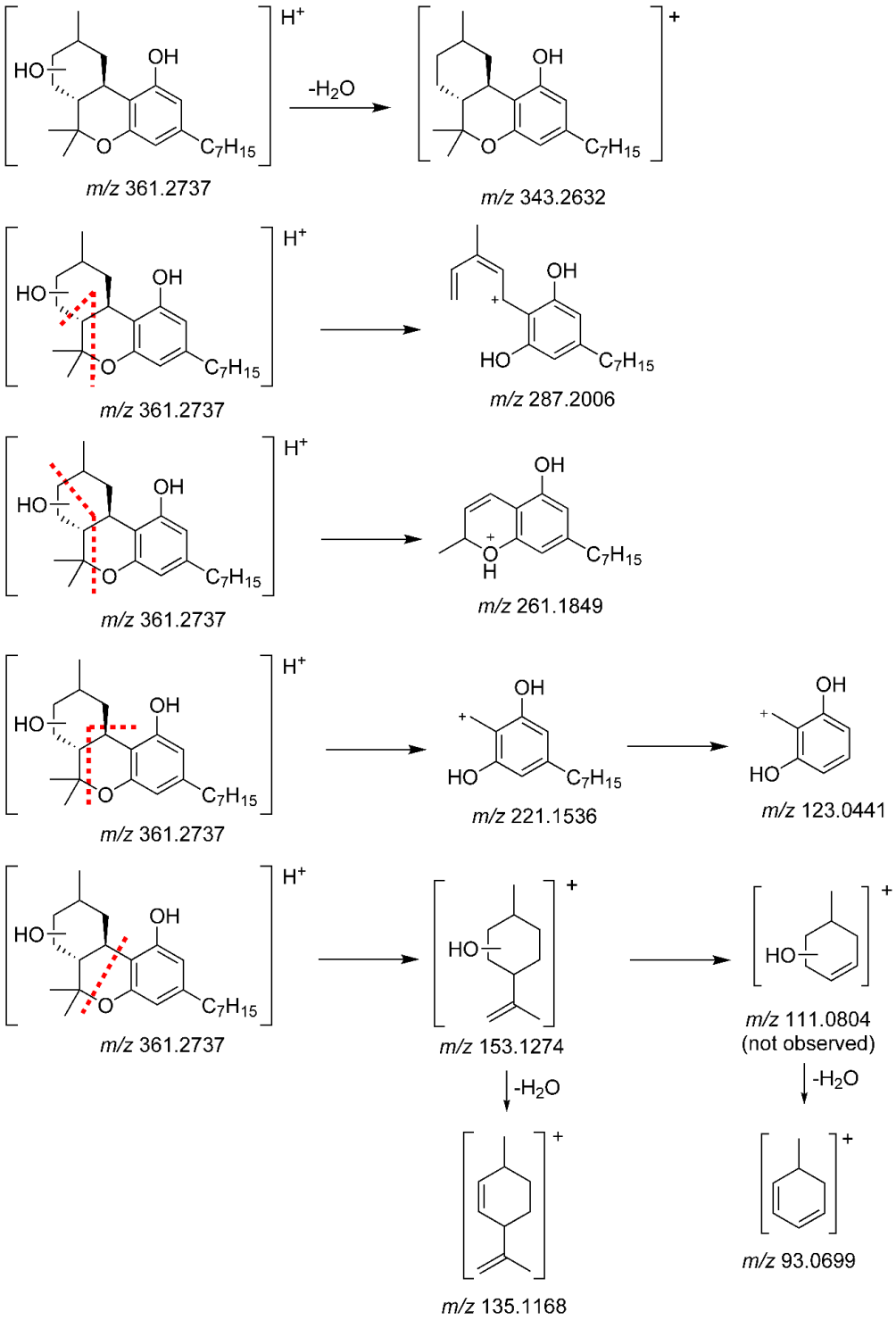

S 39: LC-QqTOF fragment ions of a monohydroxylated HHCP metabolite. The fragments are observed in the mass spectrum of M5 and in the mass spectrum of M6 besides fragment ions, which are characteristic for side-chain hydroxylation.

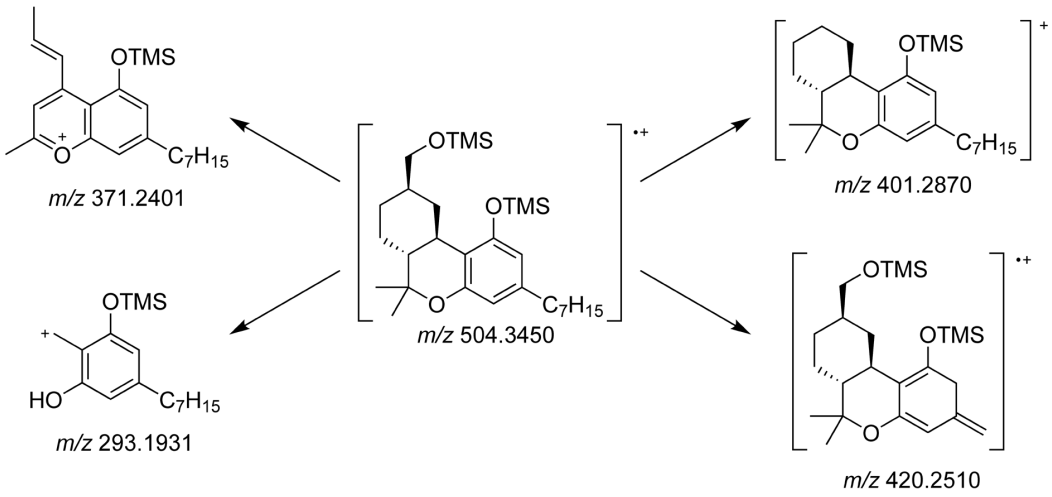

S40: Characteristic fragment ions of the only monohydroxylated HHCP metabolite found with GC-MS after derivatization with MSTFA. It is suspected that this metabolite is (9*R*)-11-OH-HHCP.

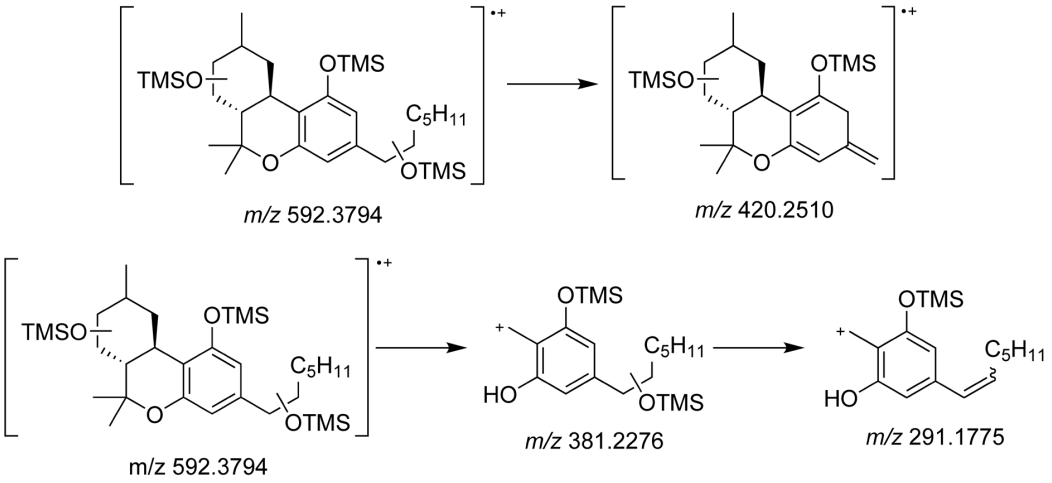

S41: Characteristic fragment ions of the dihydroxylated HHCP metabolites after derivatization with MSTFA. The exact positions of the additional trimethylsilyethers are unknown. The position of the double bond of the fragment ion *m/z* 291 is unknown.

Supplementary Information

Identification of of tetrahydrocannabidiol metabolites in human urine

Willi Schirmer[1, 2], Isabelle Mösch[1], Stefan Schürch[2], Wolfgang Weinmann[1]

[1]Institute of Forensic Medicine, Forensic Toxicology and Chemistry, University of Bern, Murtenstrasse 26, 3008 Bern, Switzerland

[2]Department of Chemistry, Biochemistry and Pharmaceutical Sciences, University of Bern, Freiestrasse 3, 3012 Bern, Switzerland

Corresponding author:

Willi Schirmer, Institute of Forensic Medicine, Forensic Toxicology and Chemistry, University of Bern, Murtenstrasse 26, 3008 Bern, Switzerland

e-mail address: willi.schirmer@irm.unibe.ch

Table of contents (Figures S1-S46)

conc / mg/L	Area R-H4CBD	Area S-H4CBD	Area ISTD	Area Ratio R	Area Ratio S
1	1238511	1744565	1040731	1.190039501	1.676288109
2	3385726	4461547	1185703	2.855458745	3.762786296
3	4387702	5784118	982003	4.46811466	5.890122535
4	7385986	9196394	1206435	6.12215826	7.622784485
5	12110670	14216076	1455767	8.319099142	9.765351186
Sample	2049708	1794724	901295	2.27418104	1.991272558
				1.677993166	1.127472462

ISTD: THC-D3

% R-H4CBD	% S-H4CBD
33.6	22.5

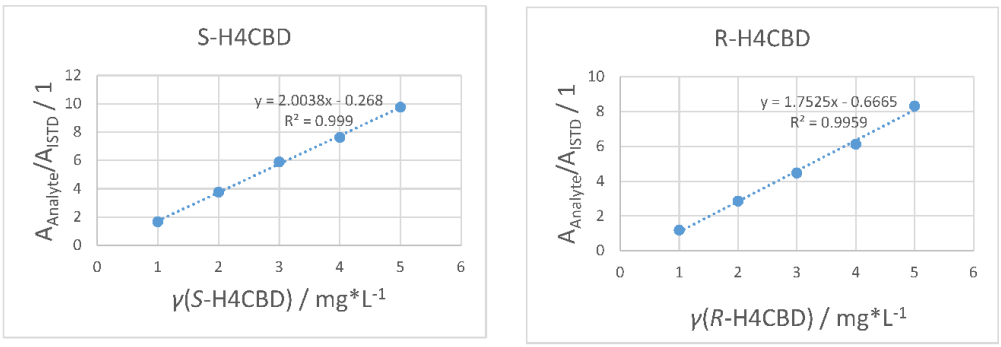

Figure S1: Quantification of (*R*)- and (*S*)-H4CBD in the H4CBD product for recreational use with GC-MS.

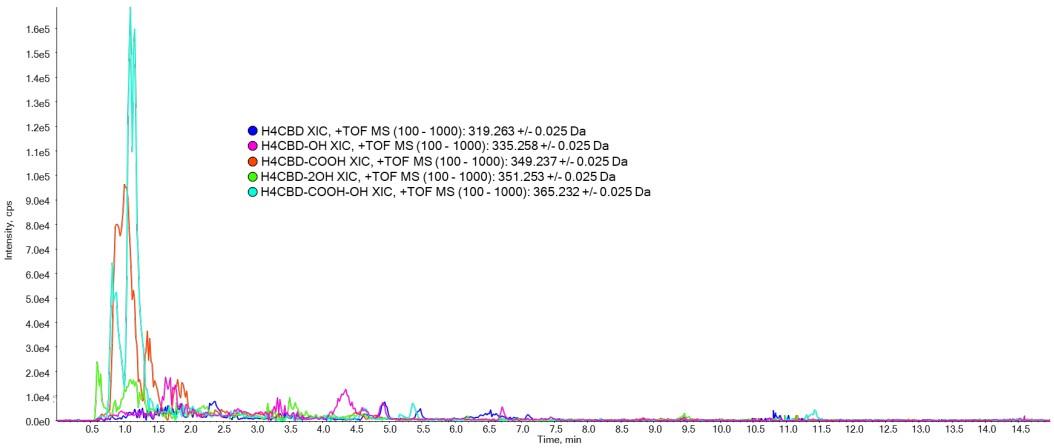

Figure S1: Chromatogram of deglucuronidated urine before ingestion of H4CBD, measured on a LC-QqTOF

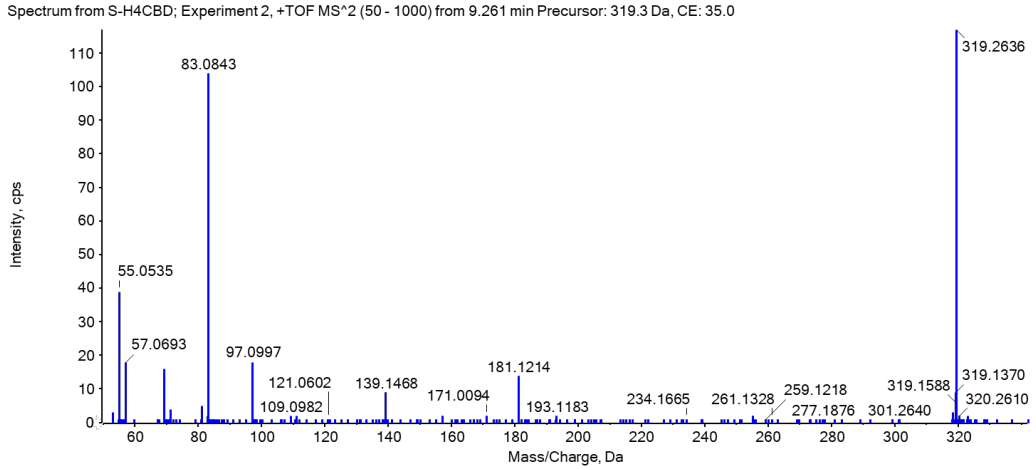

Figure S2: LC-QqTOF spectrum of (*S*)-H4CBD (Metabolite M1)

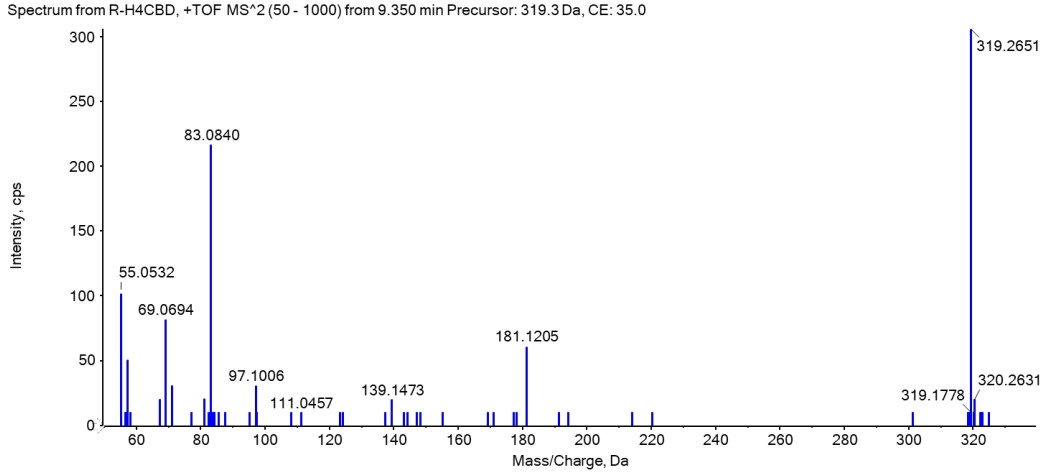

Figure S3: LC-QqTOF spectrum of (*R*)-H4CBD (Metabolite M1)

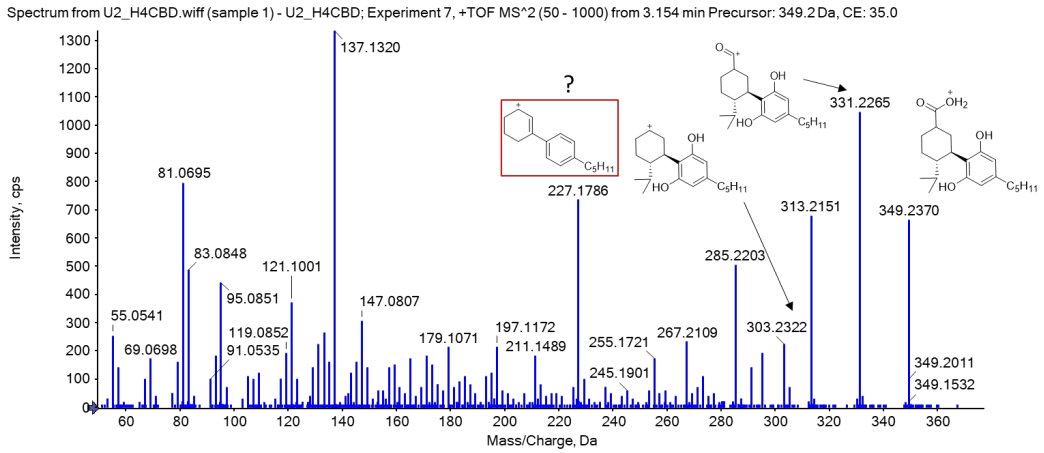

Figure S4: Mass spectrum of metabolite M2, a carboxylated metabolite of H4CBD (from a deglucuronidated urine sample 3 h after ingestion of 25 mg H4CBD)

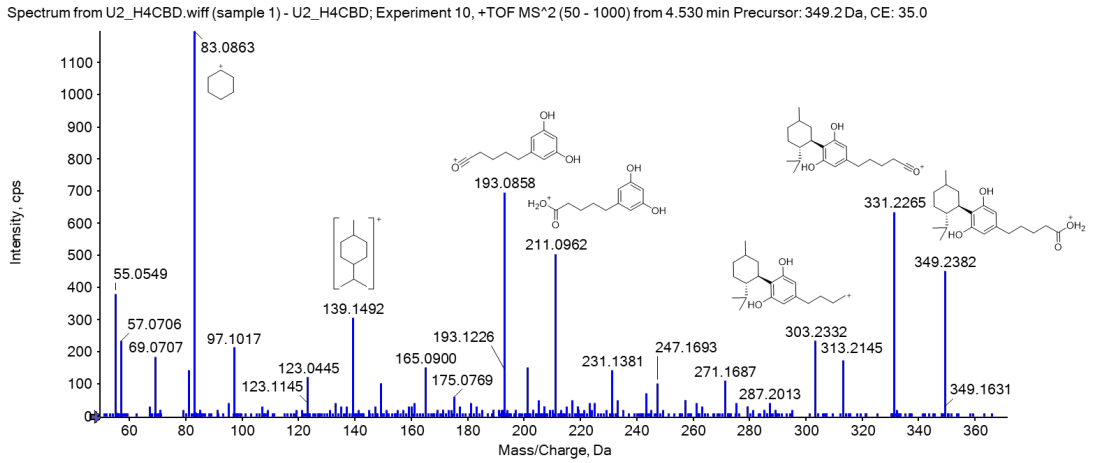

Figure S5: Mass spectrum of metabolite M3, a carboxylated metabolite of H4CBD (from a deglucuronidated urine sample 3 h after ingestion of 25 mg H4CBD)

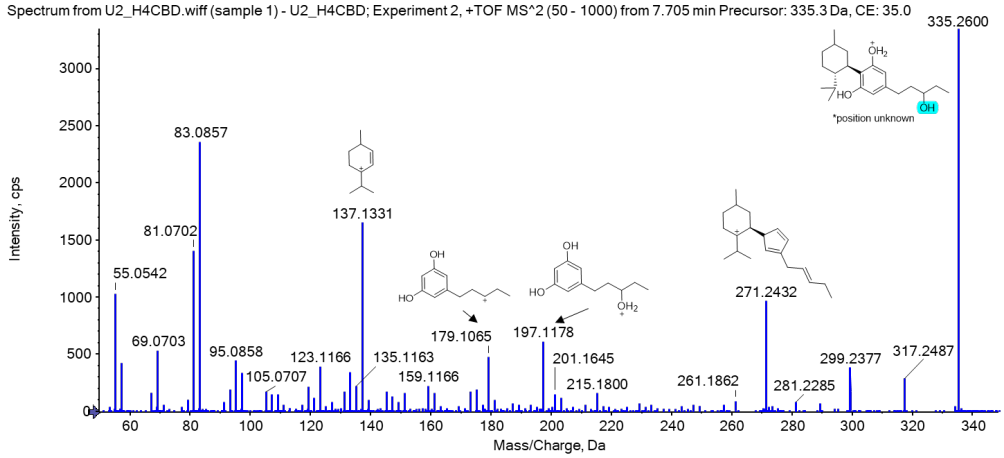

Figure S6: Mass spectrum of metabolite M4, a side chain hydroxylated metabolite of H4CBD (from a deglucuronidated urine sample 3 h after ingestion of 25 mg H4CBD). *The position of the hydroxy group is unknown.

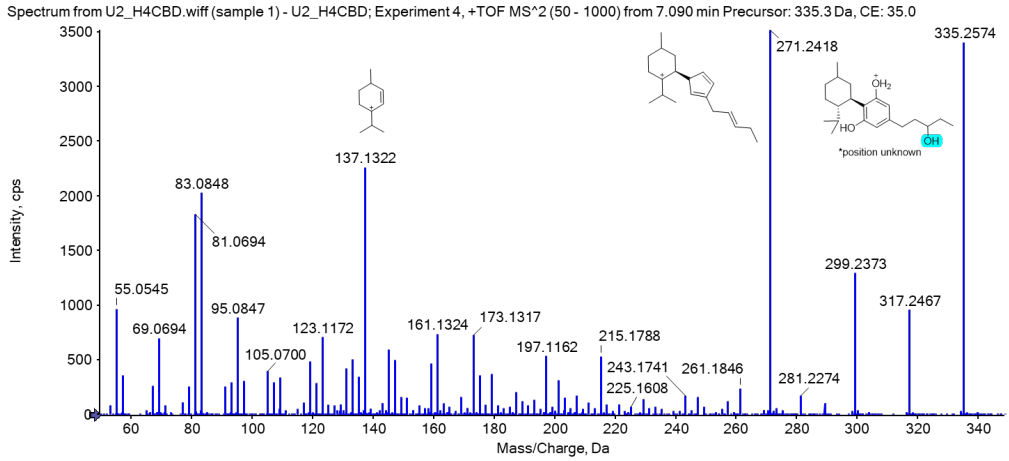

Figure S7: Mass spectrum of metabolite M5, a side chain hydroxylated metabolite of H4CBD (from a deglucuronidated urine sample 3 h after ingestion of 25 mg H4CBD). *The position of the hydroxy group is unknown.

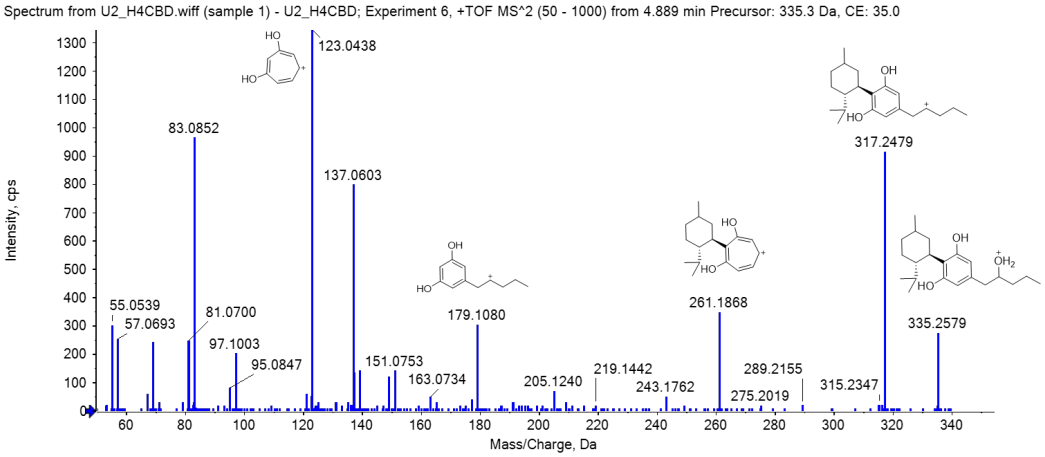

Figure S8: Mass spectrum of metabolite M6, a hydroxylated metabolite of H4CBD (from a deglucuronidated urine sample 3 h after ingestion of 25 mg H4CBD). Tentatively identified as an epimer of 2"OH-H4CBD.

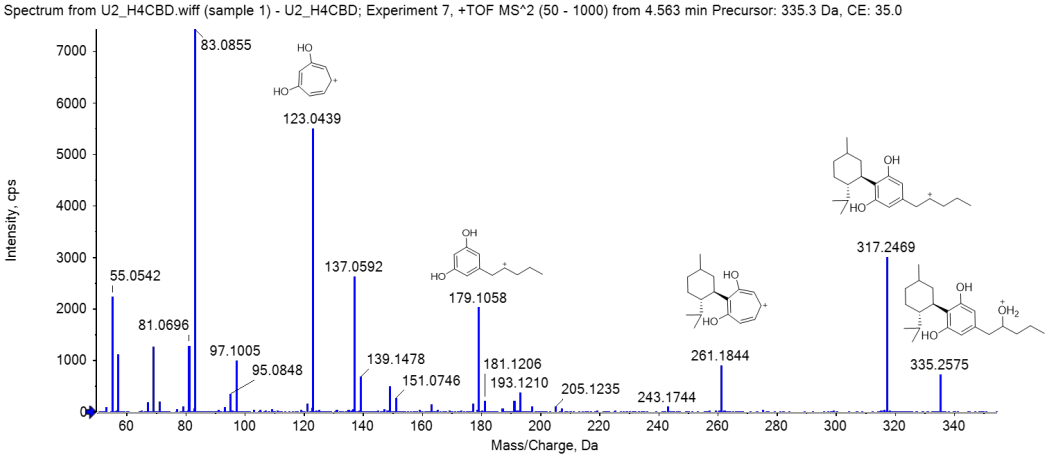

Figure S9: Mass spectrum of metabolite M7, a hydroxylated metabolite of H4CBD (from a deglucuronidated urine sample 3 h after ingestion of 25 mg H4CBD). Tentatively identified as an epimer of 2"OH-H4CBD.

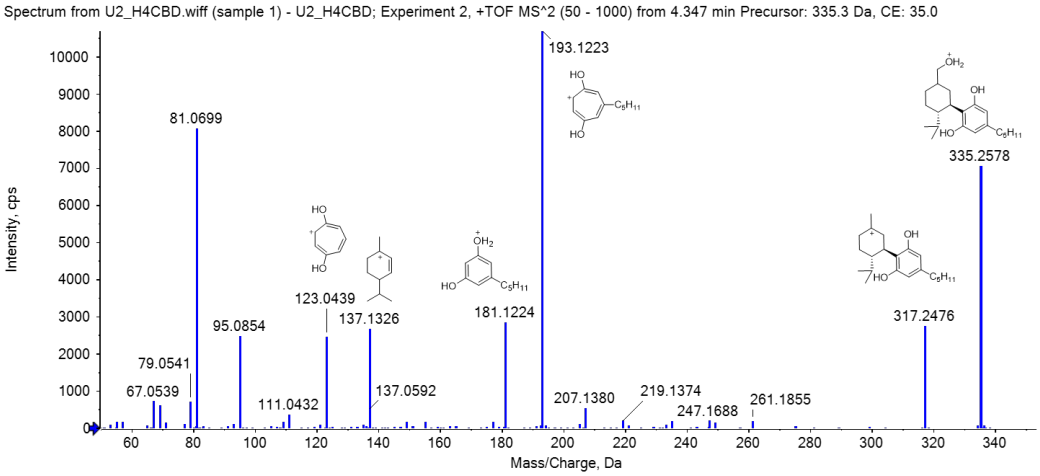

Figure S10: Mass spectrum of metabolite M8, a hydroxylated metabolite of H4CBD (from a deglucuronidated urine sample 3 h after ingestion of 25 mg H4CBD). Tentatively identified as an epimer of 7-OH-H4CBD.

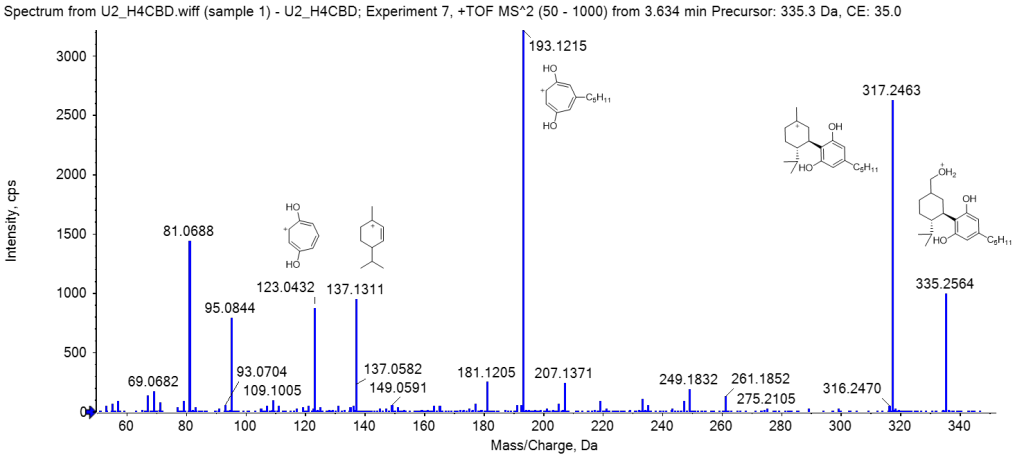

Figure S11: Mass spectrum of metabolite M9, a hydroxylated metabolite of H4CBD (from a deglucuronidated urine sample 3 h after ingestion of 25 mg H4CBD). Tentatively identified as an epimer of 7-OH-H4CBD.

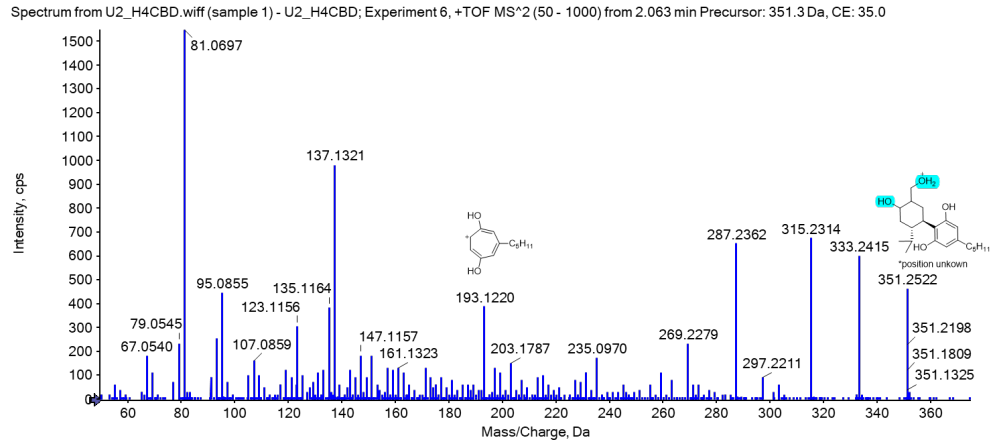

Figure S12: Mass spectrum of metabolite M10, a bishydroxylated metabolite of H4CBD (from a deglucuronidated urine sample 3 h after ingestion of 25 mg H4CBD). The position of the hydroxy groups are unknown.

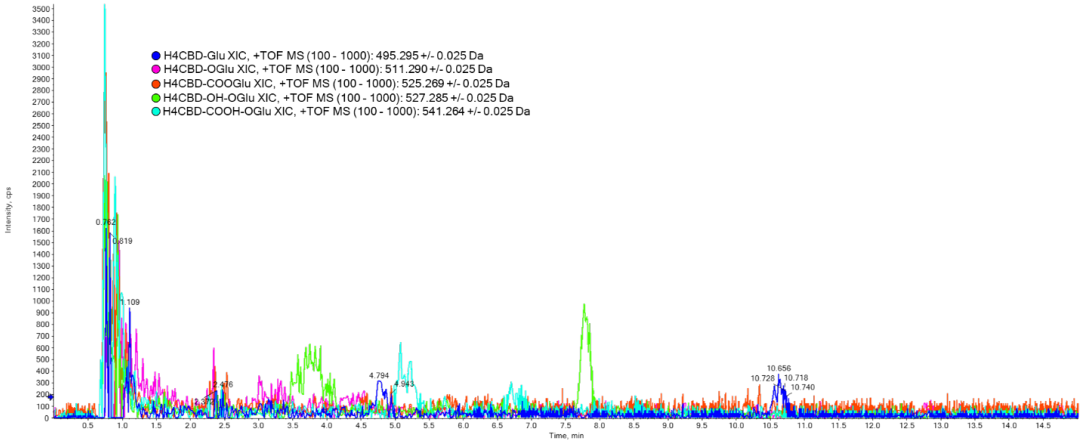

Figure S13: Chromatogram of a urine sample before ingestion of H4CBD, measured on a LC-QqTOF

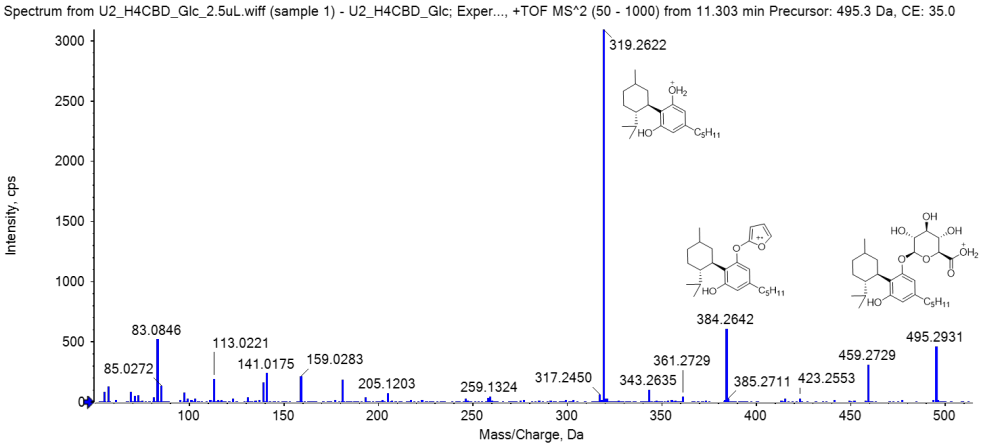

Figure S14: Mass spectrum of metabolite M11, a glucuronidated metabolite of H4CBD (from a urine sample 3 h after ingestion of 25 mg H4CBD).

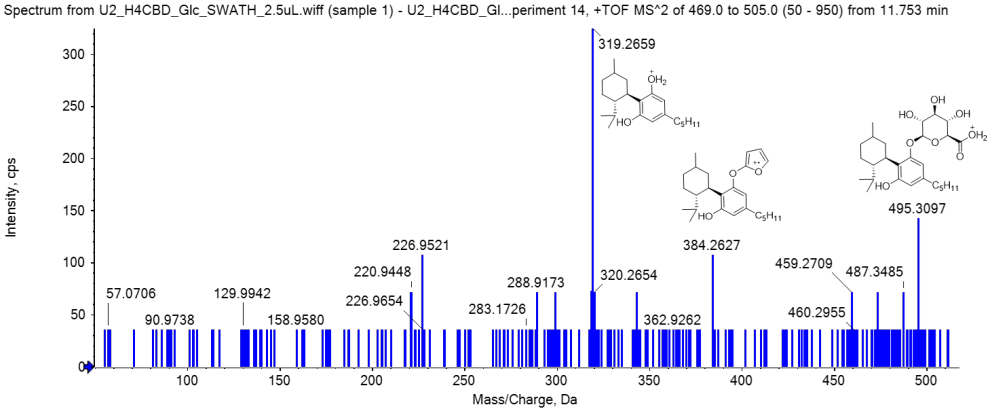

Figure S15: Mass spectrum of metabolite M12, a glucuronidated metabolite of H4CBD (from a urine sample 3 h after ingestion of 25 mg H4CBD). Acquired in SWATH mode.

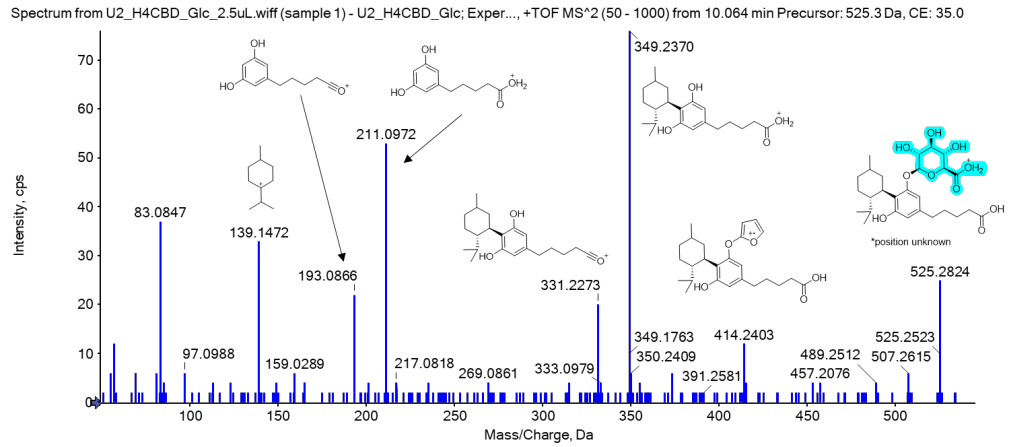

Figure S16: Mass spectrum of metabolite M13, a carboxylated and glucuronidated metabolite of H4CBD (from a urine sample 3 h after ingestion of 25 mg H4CBD). The position of the glucuronide moiety is unknown.

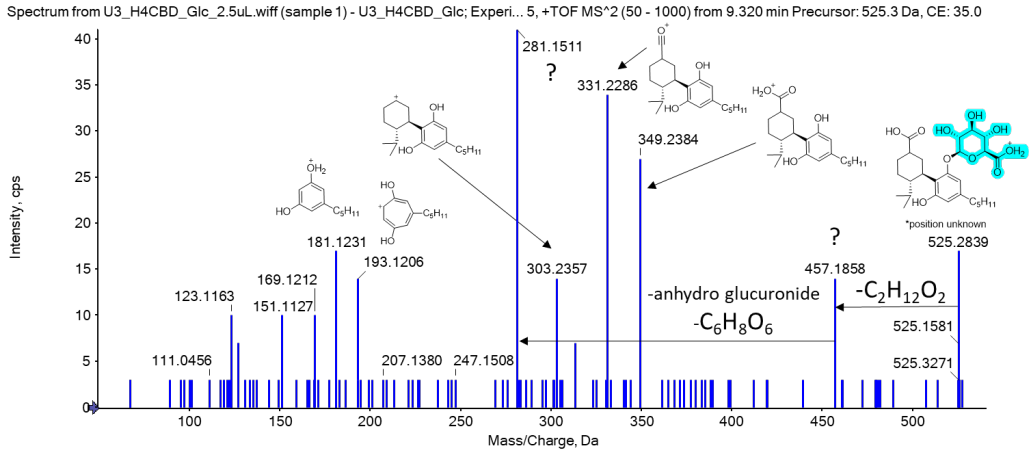

Figure S17: Mass spectrum of metabolite M14, a carboxylated and glucuronidated metabolite of H4CBD (from a urine sample 3 h after ingestion of 25 mg H4CBD). The position of the glucuronide moiety is unknown.

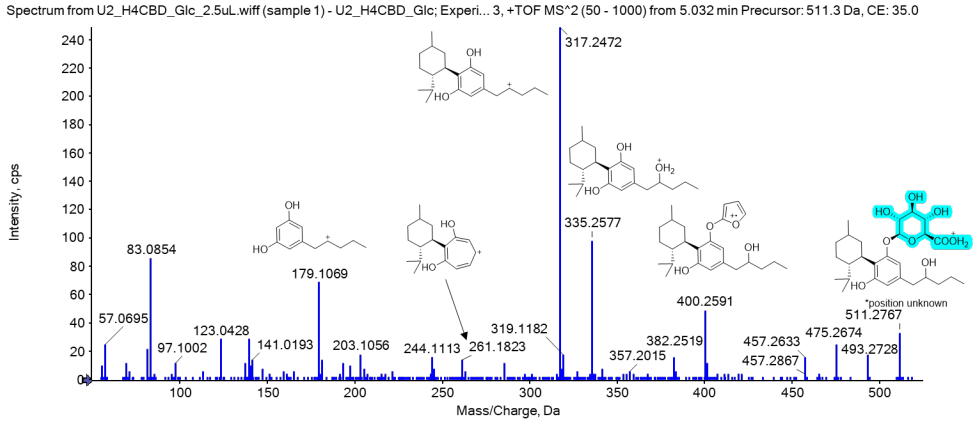

Figure S18: Mass spectrum of metabolite M15, a hydroxylated and glucuronidated metabolite of H4CBD (from a urine sample 3 h after ingestion of 25 mg H4CBD). The position of the glucuronide moiety is unknown.

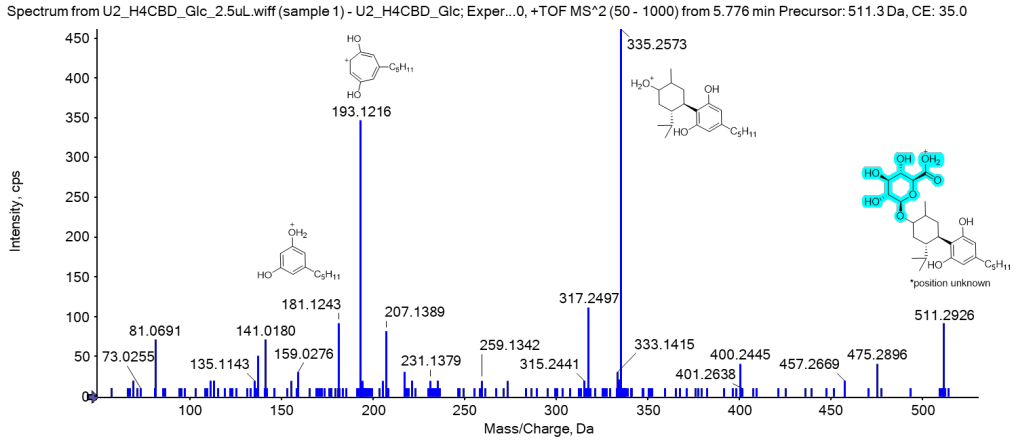

Figure S19: Mass spectrum of metabolite M16, a hydroxylated and glucuronidated metabolite of H4CBD (from a urine sample 3 h after ingestion of 25 mg H4CBD). The position of the glucuronide moiety and the hydroxy group are unknown.

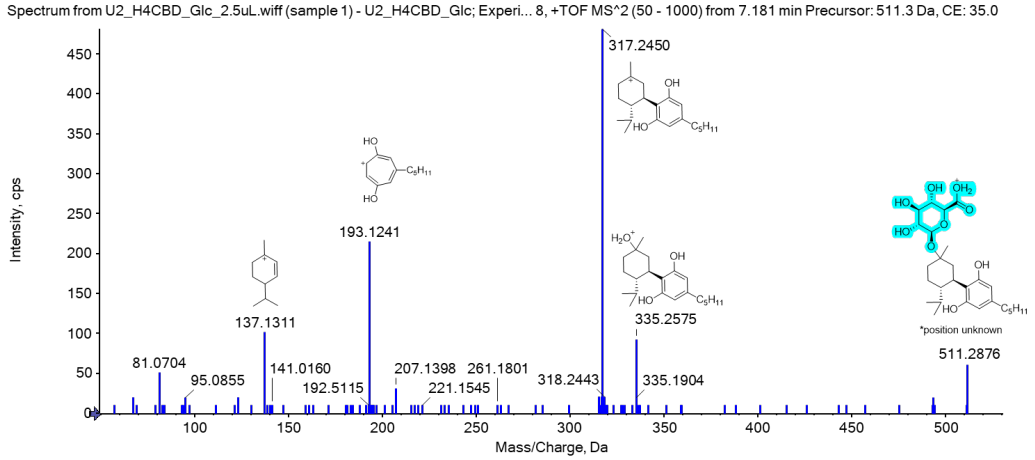

Figure S20: Mass spectrum of metabolite M17, a hydroxylated and glucuronidated metabolite of H4CBD (from a urine sample 3 h after ingestion of 25 mg H4CBD). The position of the glucuronide moiety and the hydroxy group is unknown.

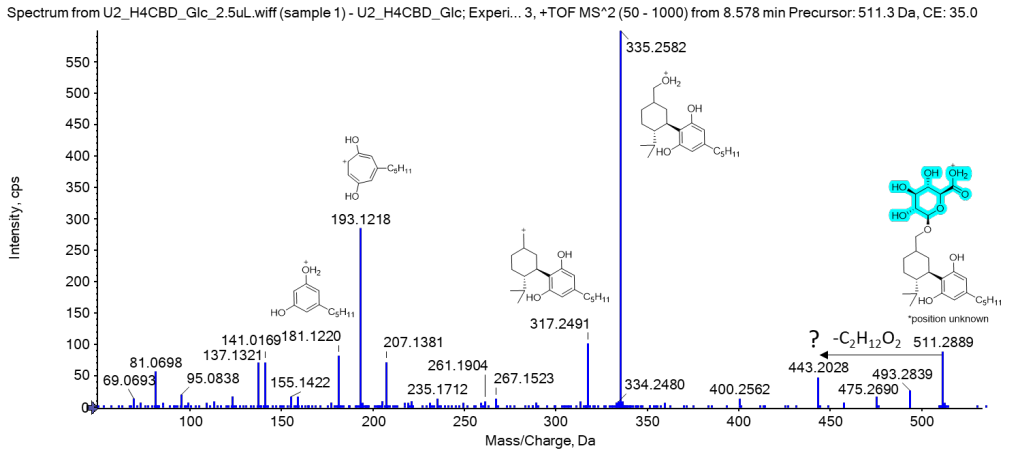

Figure S21: Mass spectrum of metabolite M18, a hydroxylated and glucuronidated metabolite of H4CBD (from a urine sample 3 h after ingestion of 25 mg H4CBD). The position of the glucuronide moiety is unknown.

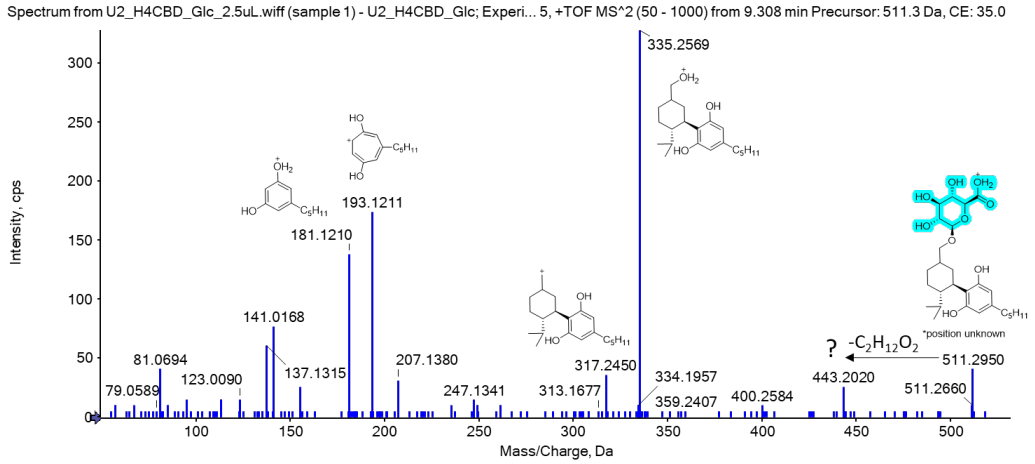

Figure S22: Mass spectrum of metabolite M19, a hydroxylated and glucuronidated metabolite of H4CBD (from a urine sample 3 h after ingestion of 25 mg H4CBD). The position of the glucuronide moiety is unknown.

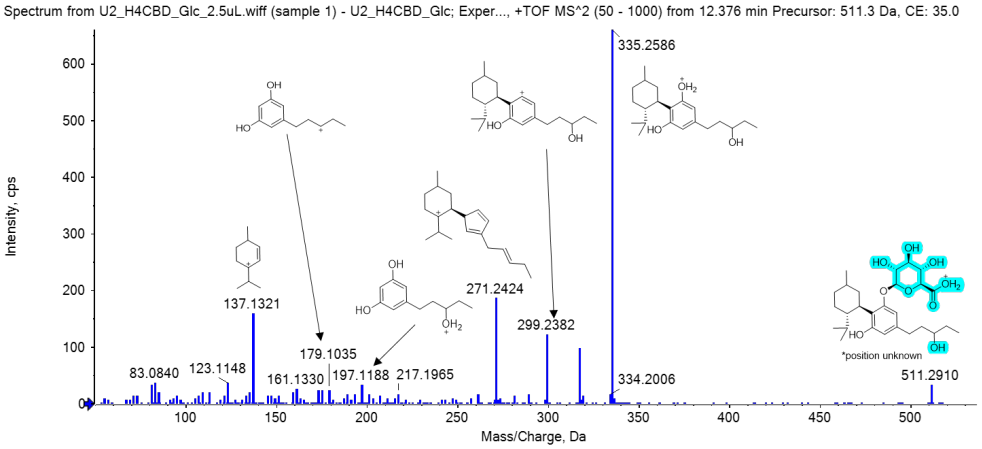

Figure S23: Mass spectrum of metabolite M20, a hydroxylated and glucuronidated metabolite of H4CBD (from a urine sample 3 h after ingestion of 25 mg H4CBD). The position of the hydroxy group and the glucuronide are unknown.

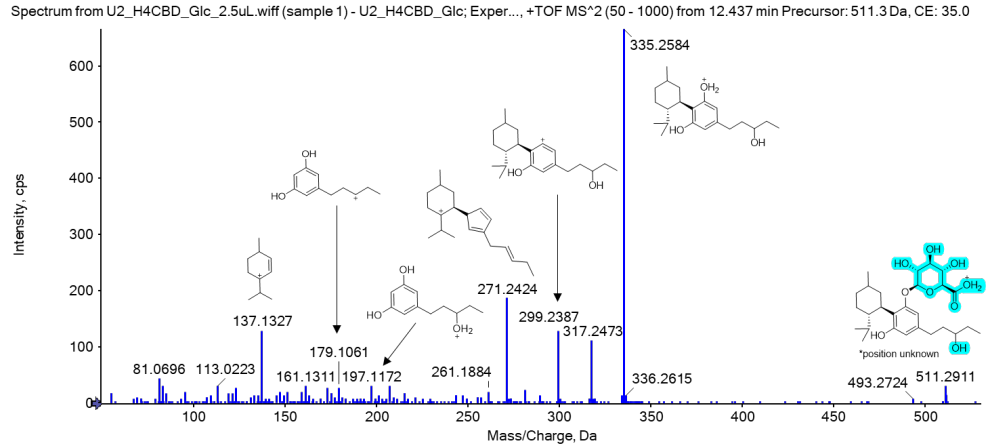

Figure S24: Mass spectrum of metabolite M21, a hydroxylated and glucuronidated metabolite of H4CBD (from a urine sample 3 h after ingestion of 25 mg H4CBD). The position of the hydroxy group and the glucuronide are unknown.

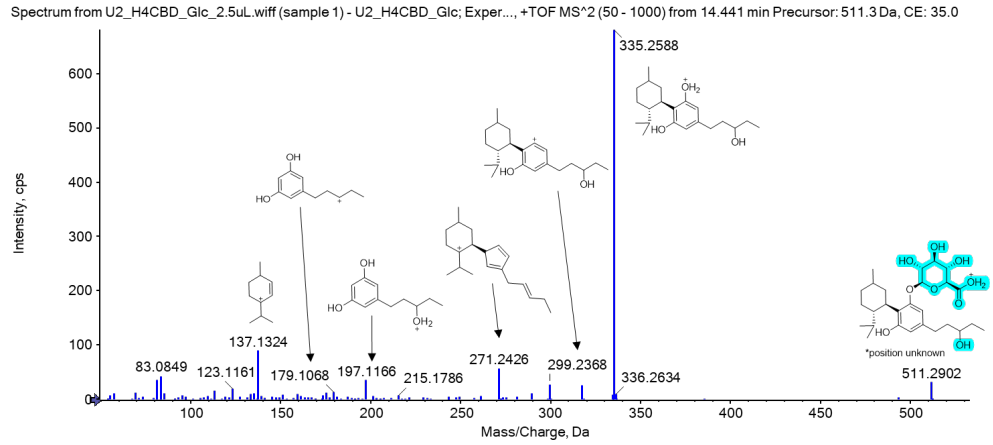

Figure S25: Mass spectrum of metabolite M22, a hydroxylated and glucuronidated metabolite of H4CBD (from a urine sample 3 h after ingestion of 25 mg H4CBD). The position of the hydroxy group and the glucuronide are unknown.

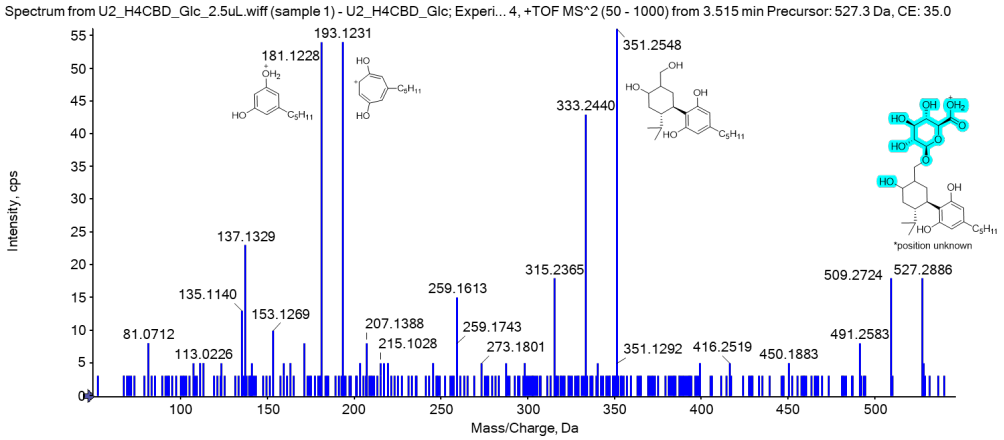

Figure S26: Mass spectrum of metabolite M23, a bishydroxylated and glucuronidated metabolite of H4CBD (from a urine sample 3 h after ingestion of 25 mg H4CBD). Both hydroxylation positions are found on the alicyclic moiety, their position and the position of the glucuronide are not clear.

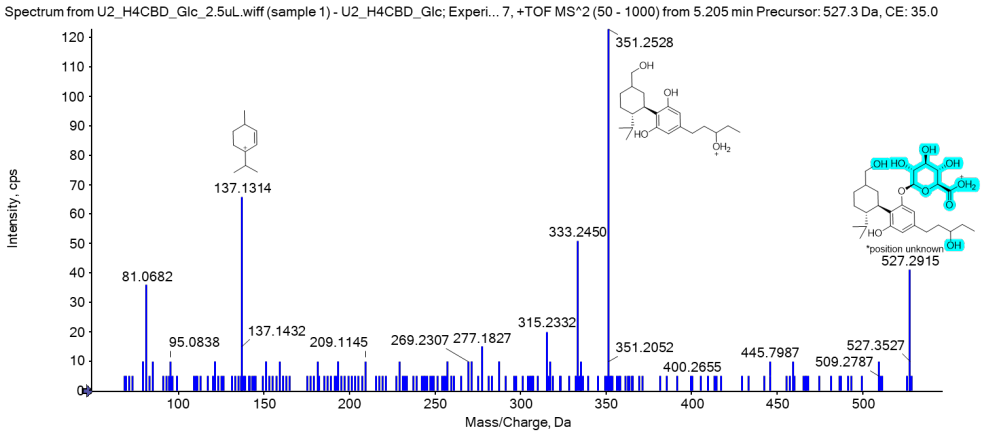

Figure S27: Mass spectrum of metabolite M24, a bishydroxylated and glucuronidated metabolite of H4CBD (from a urine sample 3 h after ingestion of 25 mg H4CBD). One hydroxylation positions is found on the alicyclic moiety, the other hydroxylation position is on the side-chain, their position and the position of the glucuronide are not clear.

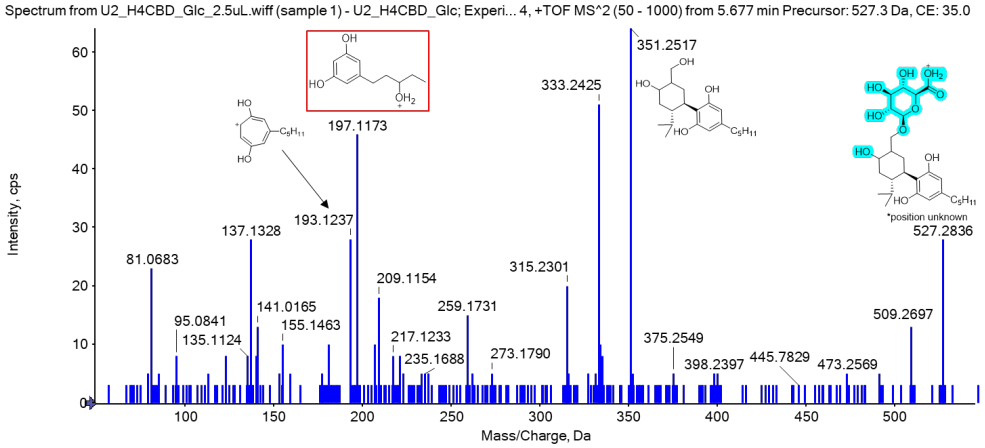

Figure S28: Mass spectrum of metabolite M25, a bishydroxylated and glucuronidated metabolite of H4CBD (from a urine sample 3 h after ingestion of 25 mg H4CBD). Both hydroxylation positions are found on the alicyclic moiety, their position and the position of the glucuronide are not clear. The ion *m/z* 197.1173 could result from a coeluting metabolite with a hydroxylation position on the side-chain.

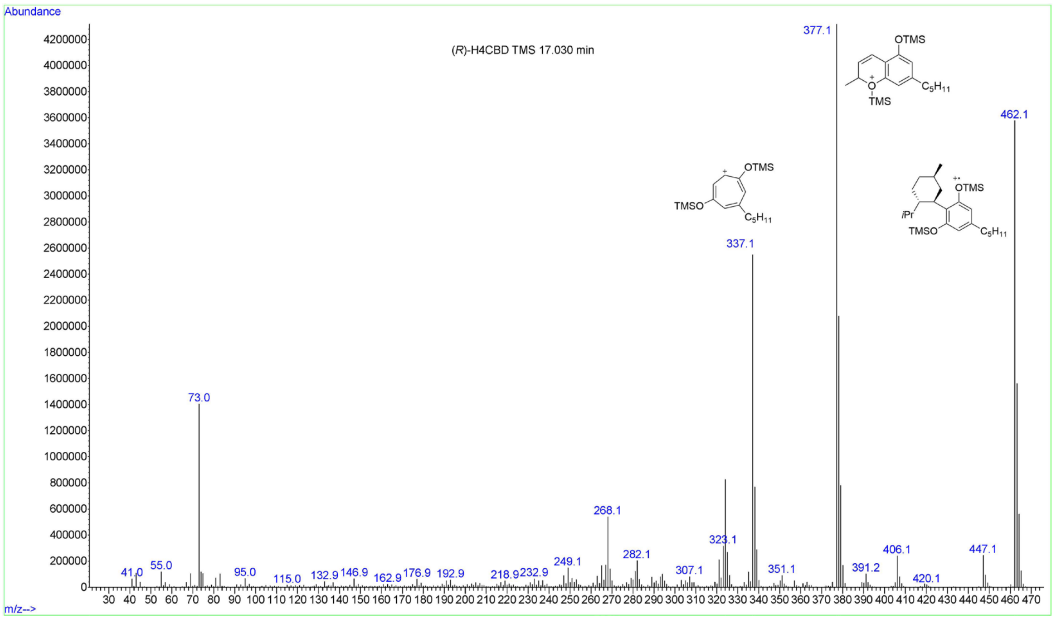

Figure S29: EI mass spectrum of the metabolite M26 (*R*)-H4CBD TMS

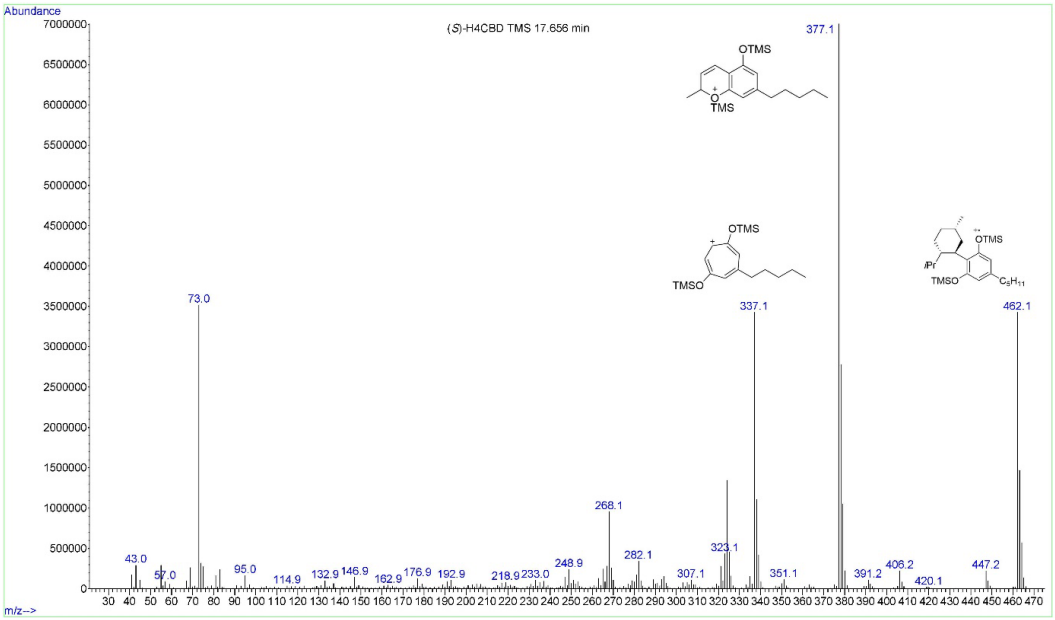

Figure S30: EI mass spectrum of the metabolite M27 (*S*)-H4CBD TMS, the same ions are formed as for (*R*)-H4CBD TMS.

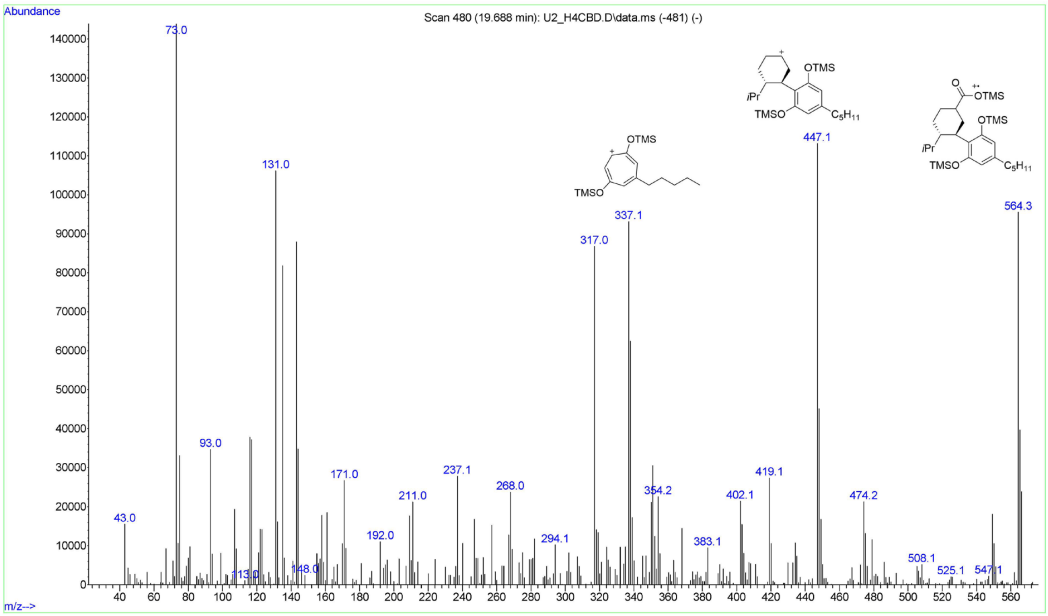

Figure S31: EI mass spectrum of the carboxylated metabolite M28 7-COOH-H4CBD TMS.

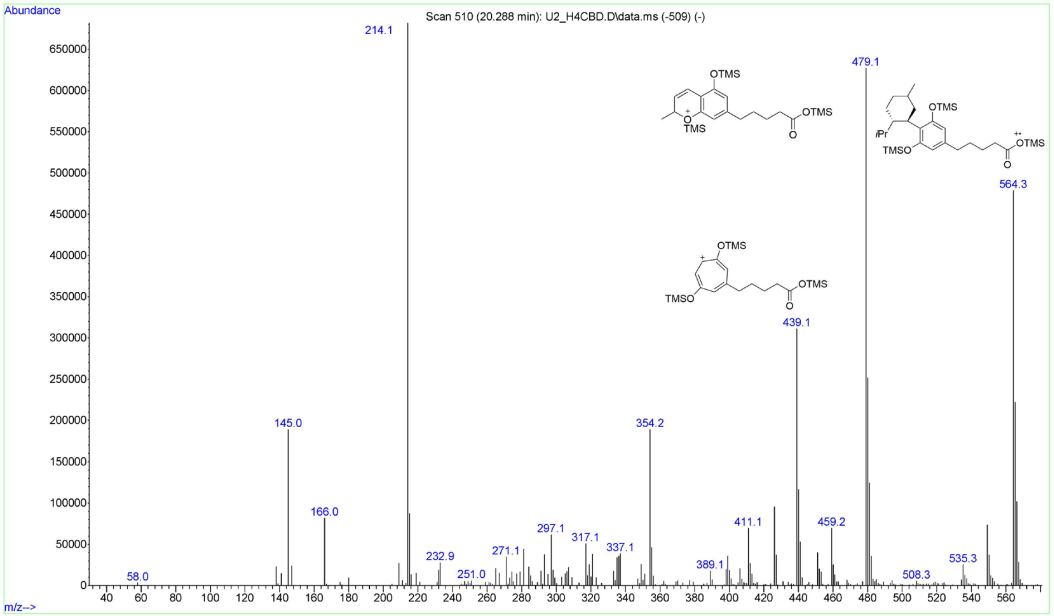

Figure S32: EI mass spectrum of the carboxylated metabolite M29 5''-COOH-H4CBD TMS.

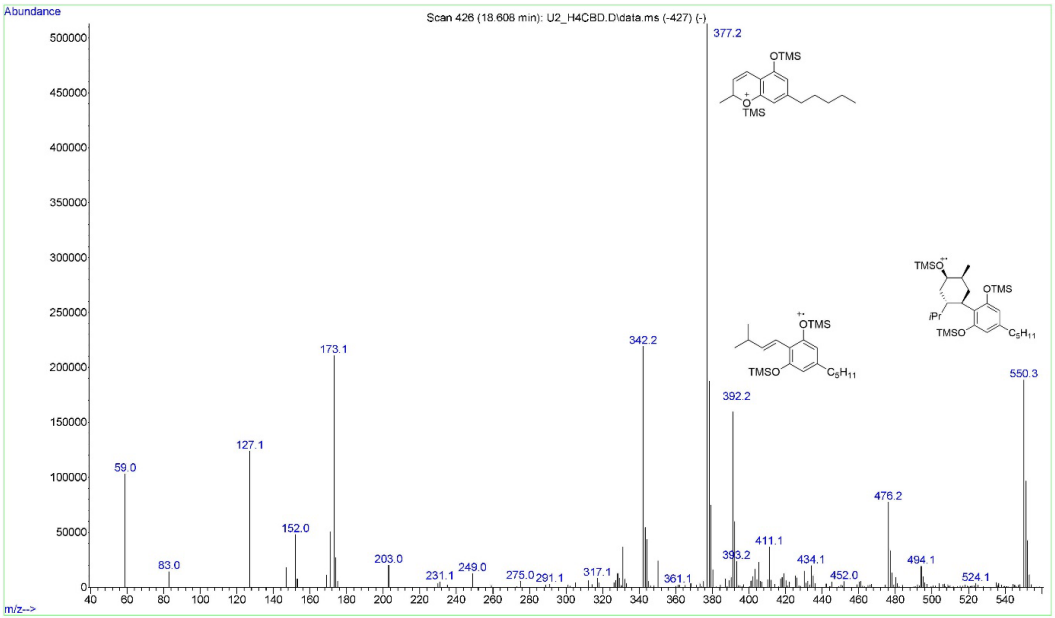

Figure S33: EI mass spectrum of the hydroxylated metabolite M30, hydroxylated on the alicyclic moiety.

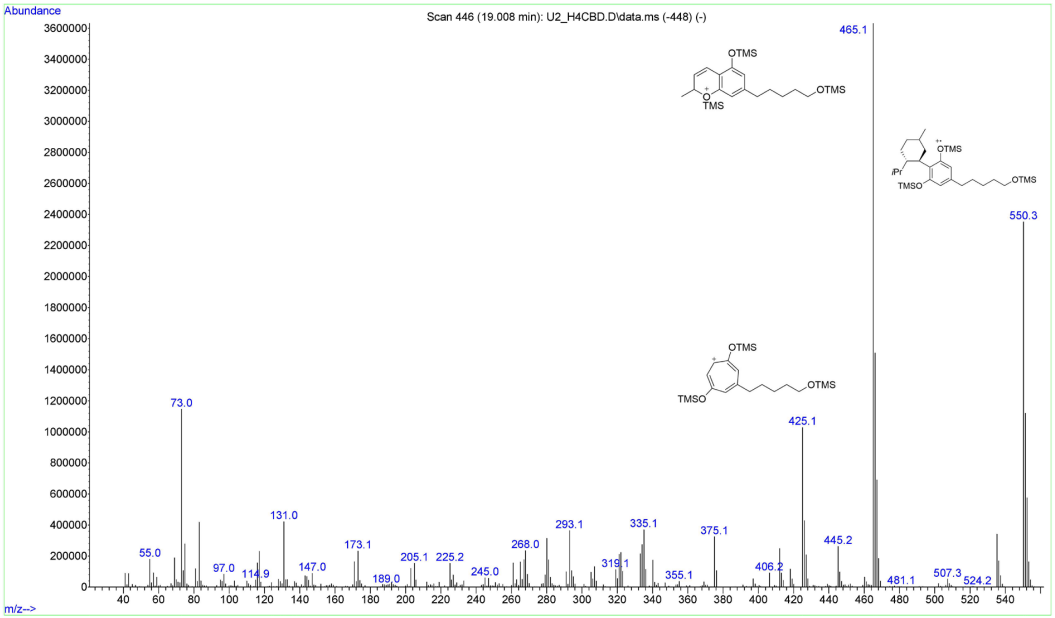

Figure S34: EI mass spectrum of the hydroxylated metabolite M31, hydroxylated on the side-chain. Hydroxylation position unknown.

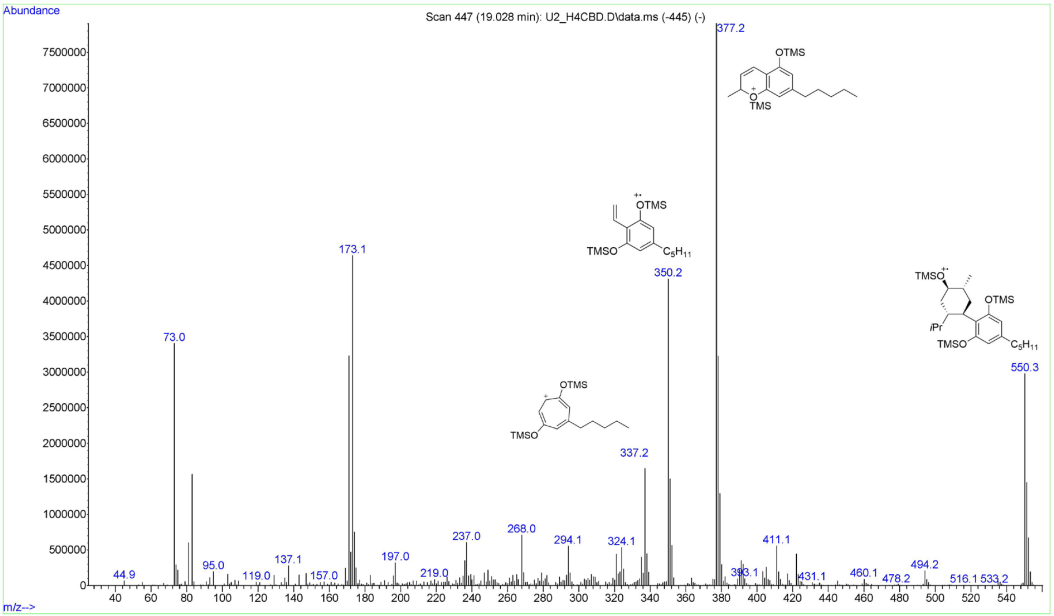

Figure S35: EI mass spectrum of the hydroxylated metabolite M32, hydroxylated on the alicyclic moiety.

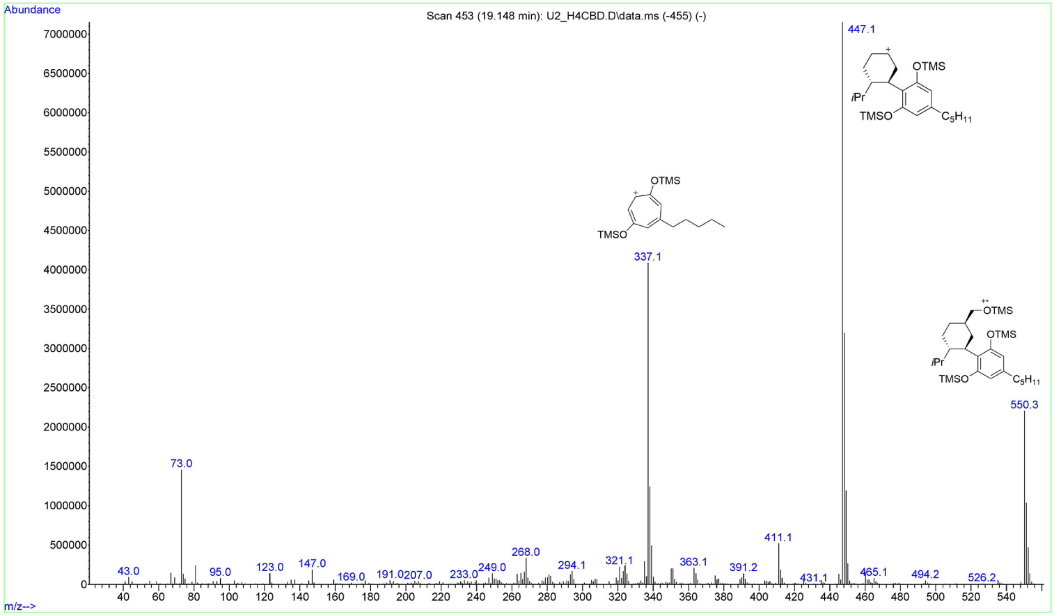

Figure S36: EI mass spectrum of the hydroxylated metabolite M33, hydroxylated on the alicyclic moiety. Presumably 7-OH-(*R*)-H4CBD

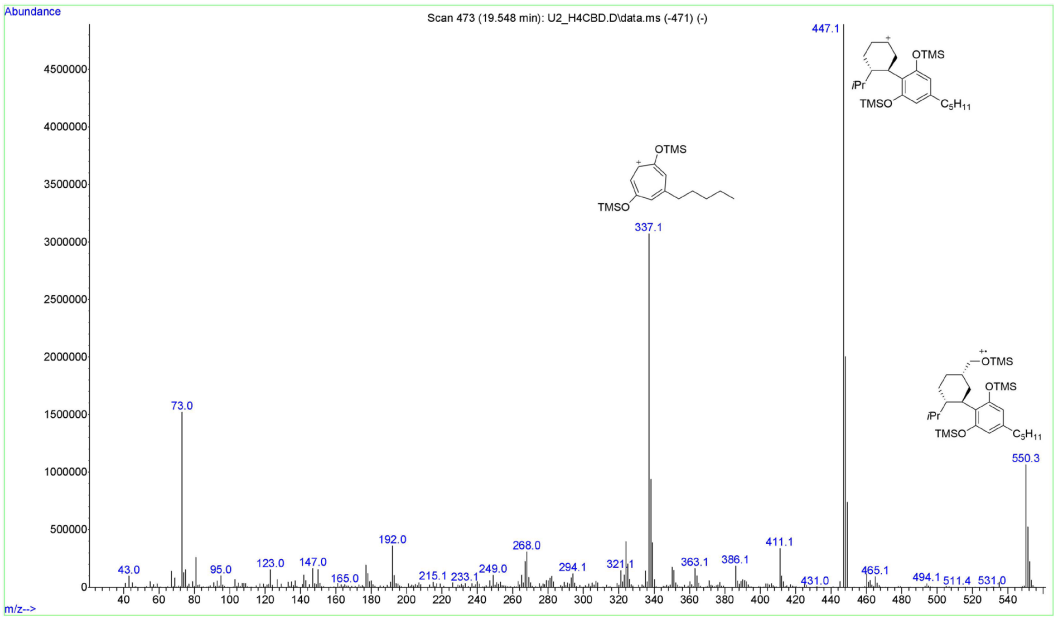

Figure S37: EI mass spectrum of the hydroxylated metabolite M34, hydroxylated on the alicyclic moiety. Presumably 7-OH-(*S*)-H4CBD

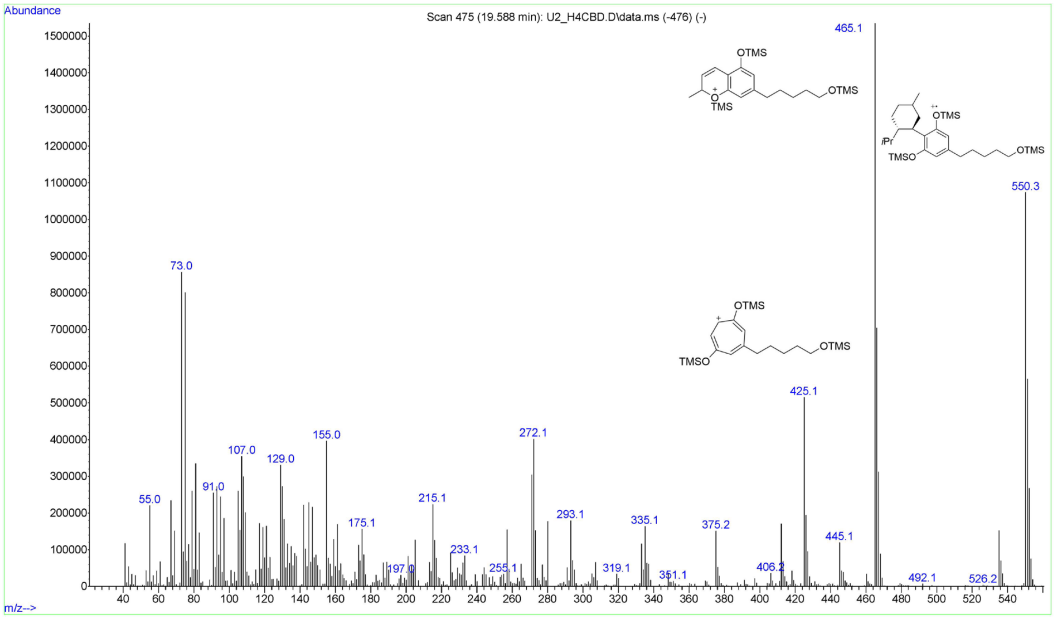

Figure S38: EI mass spectrum of the hydroxylated metabolite M35, hydroxylated on the side-chain. Hydroxylation position unknown.

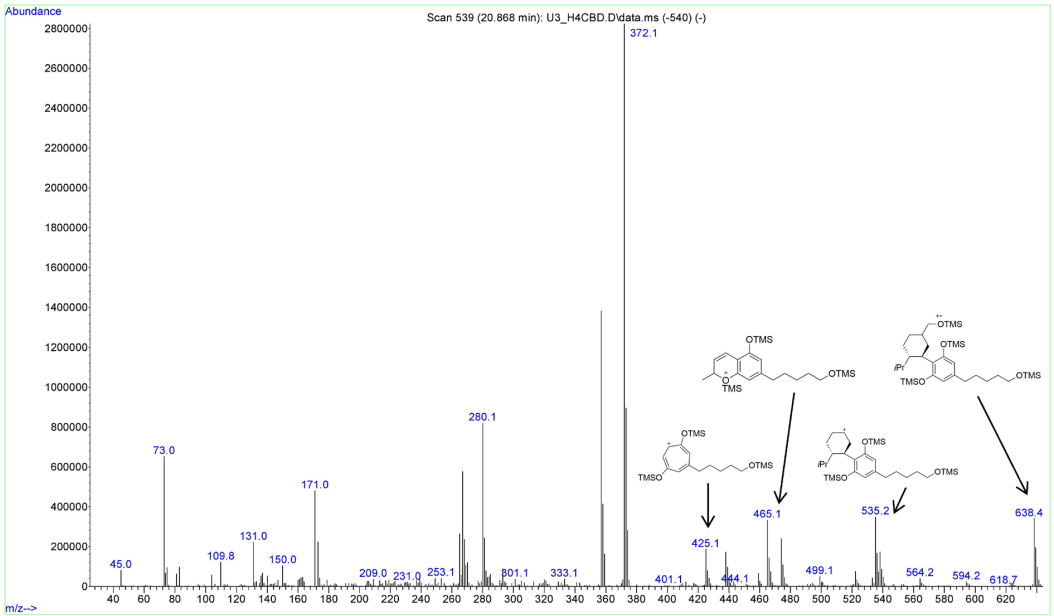

Figure S39: EI mass spectrum of the bishydroxylated metabolite M36, hydroxylated on C7 of the alicyclic moiety and on the side-chain. Position of the side-chain hydroxylation is unknown.

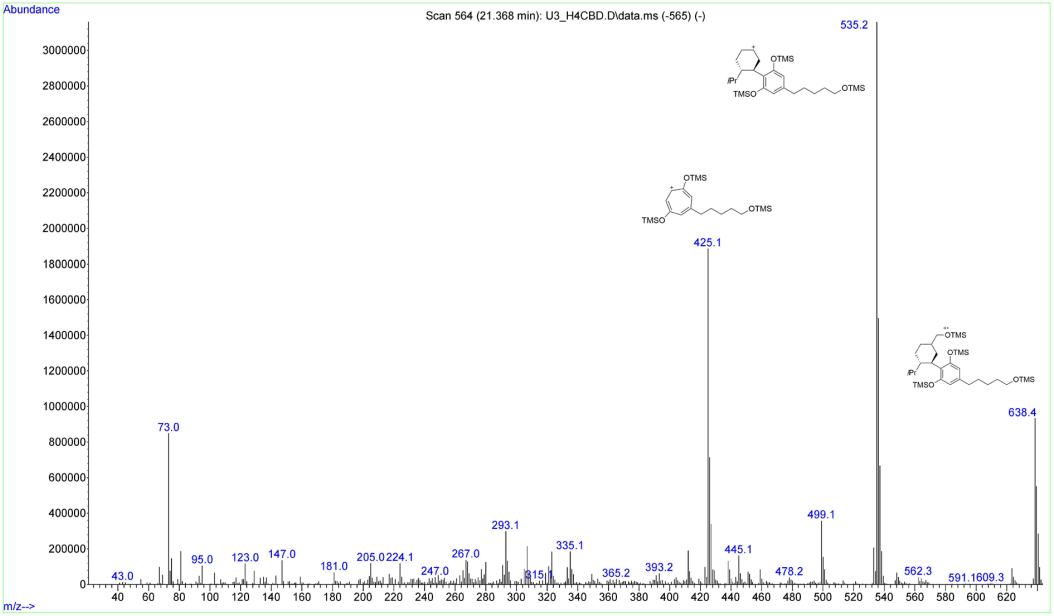

Figure S40: EI mass spectrum of the bishydroxylated metabolite M37, hydroxylated on C7 of the alicyclic moiety and on the side-chain. Position of the side-chain hydroxylation is unknown.

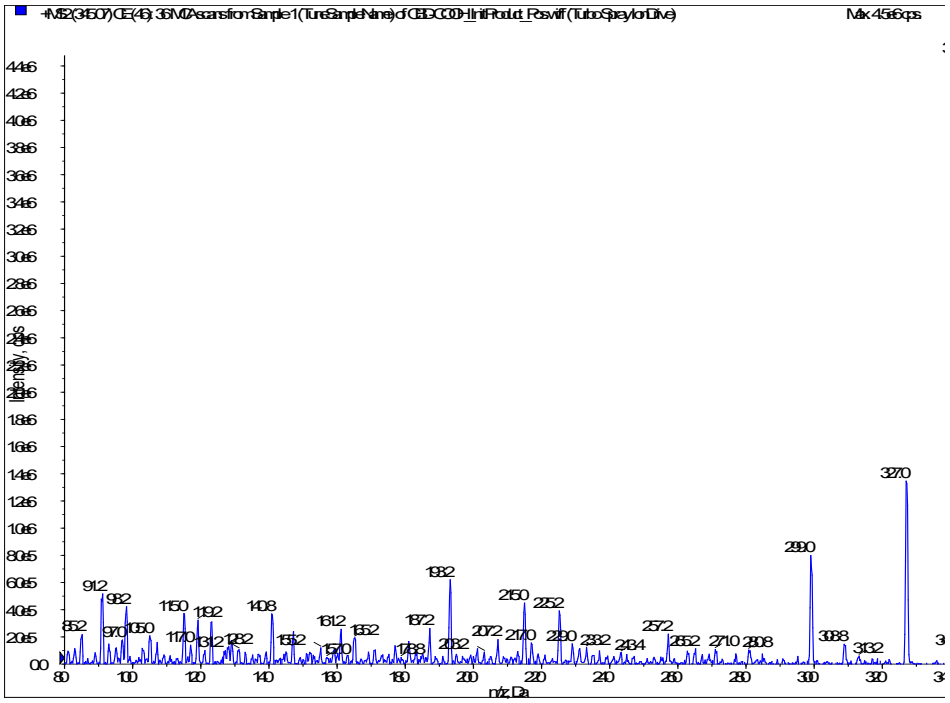

Figure S41: Product ion spectrum of 7-COOH-CBD at a collision energy of +46 V.

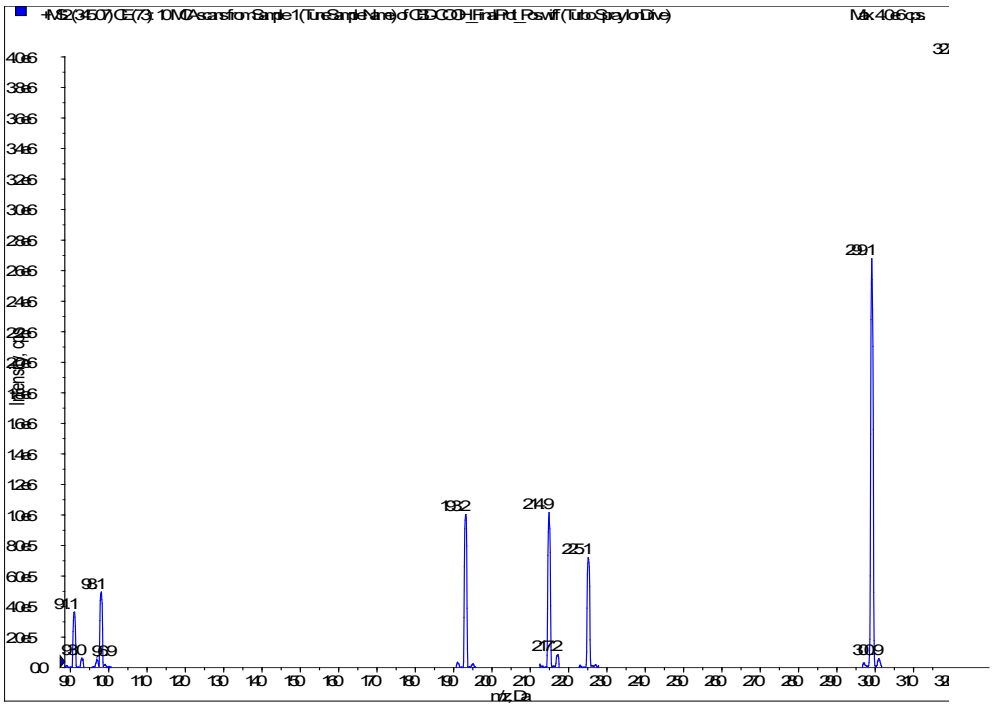

Figure S42: Product ion spectrum of 7-COOH-CBD at a collision energy of +73 V.

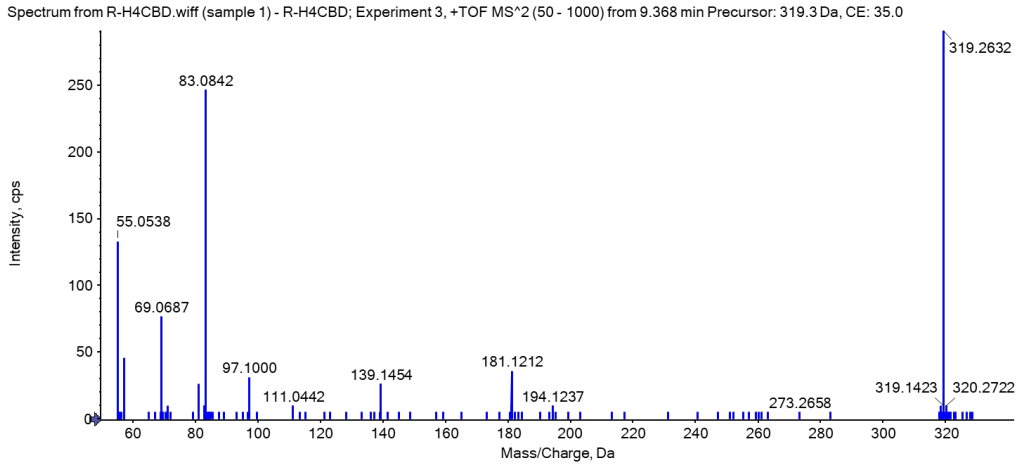

Figure S43: Product ion spectrum of (*S*)-H4CBD (reference standard).

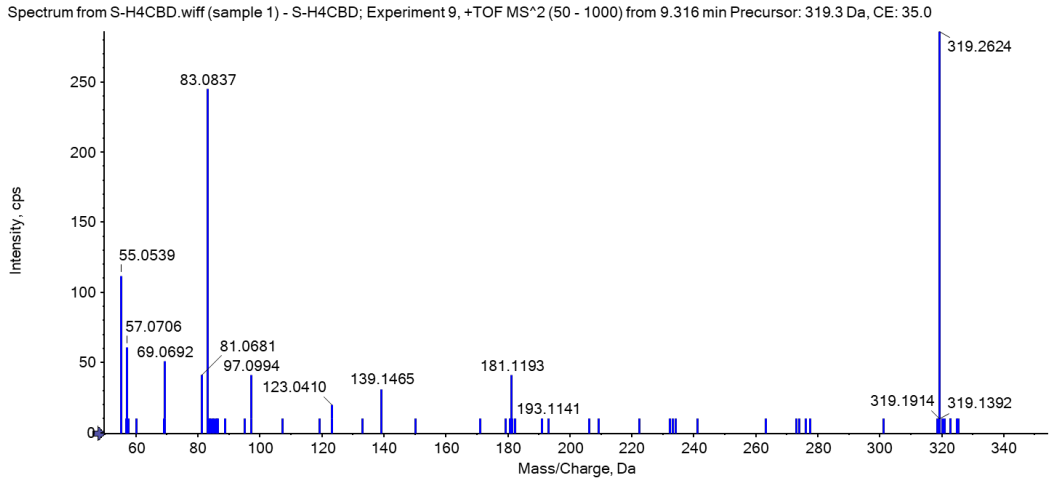

Figure S44: Product ion spectrum of (*R*)-H4CBD (reference standard).

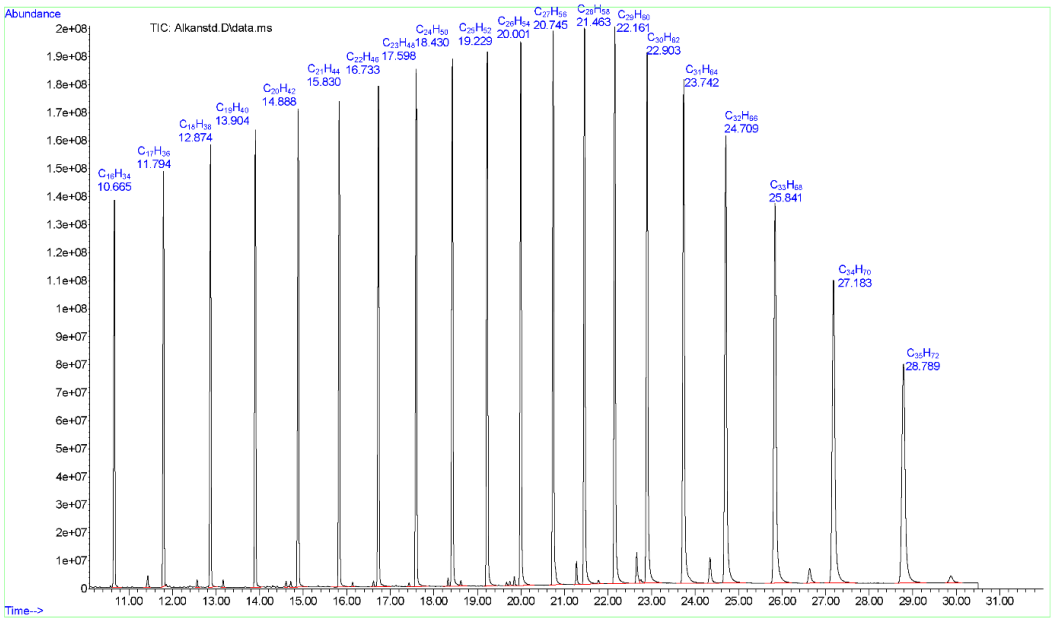

Figure S45: Chromatogram of an *n*-alkane standard (C7-C40) used for the determination of Kováts indices.

Supplementary Information

Rapid LC-QTOF-MS screening method for semi-synthetic cannabinoids in whole blood

Willi Schirmer[1, 2], Sara E. Walton[3], Wolfgang Weinmann[1], Stefan Schürch[2], Barry K. Logan[3, 4], Alex J. Krotulski[3]

[1]Institute of Forensic Medicine, Forensic Toxicology and Chemistry, University of Bern, Murtenstrasse 26, 3008 Bern, Switzerland

[2]Department of Chemistry, Biochemistry and Pharmaceutical Sciences, University of Bern, Freiestrasse 3, 3012 Bern, Switzerland

[3]Center for Forensic Science Research and Education, Fredric Rieders Family Foundation, Horsham, PA, 19044, United States

[4]NMS Labs, Horsham, PA, 19044, United States

Corresponding author:
Willi Schirmer, Institute of Forensic Medicine, Forensic Toxicology and Chemistry, University of Bern, Murtenstrasse 26, 3008 Bern, Switzerland
e-mail address: willi.schirmer@irm.unibe.ch

ORCID:
1st author orcid: 0009-0004-5579-2217
2nd author orcid: -
3rd author orcid: 0000-0001-8659-1304
4th author orcid: 0000-0001-5109-4623
5th author orcid: 0000-0003-2400-4711
Last author orcid: 0000-0003-1775-1882

Table of contents

S1: Recovery rates and matrix effects of the analytes from the liquid-liquid extraction protocol (LLE), measured in glass vials (left side) and from the solid-phase extraction protocol (SPE), measured in polypropylene vials (right side). Graphical illustration of the recovery rates from the LLE protocol (analyzed in glass vials) are shown in S3. Graphical illustration of the recovery rates from the SPE protocol are shown in S4.

Analyte	Recovery rates LLE glass vials / %	Matrix effects LLE glass vials / %	Recovery rates SPE / %	Matrix effects SPE / %
Δ^9-THCO	79 ± 7.3	76	69 ± 6.2	97
9β-OH-HHC	55 ± 4.8	49	82 ± 2.4	54
11-OH-Δ^9-THC	96 ± 10.5	39	75 ± 2.0	76
11-OH-Δ^8-THC	61 ± 7.7	45	86 ± 12.1	46
Δ^9-THCE	91 ± 1.3	36	75 ± 7.3	85
11-COOH-9*R*-HHC	62 ± 6.4	27	90 ± 1.1	33
11-COOH-Δ^9-THC	99 ± 8.3	28	64 ± 4.4	117
9α-OH-HHC	96 ±8.7	48	66 ± 4.4	95
CBD	65 ± 10.8	18	81 ± 5.8	79
CBG	94 ± 16.3	15	62 ± 6.8	126
Δ^9-THCB	103 ± 15.3	22	63 ± 3.6	96
CBN	111 ± 26.5	14	63 ± 2.2	84
Δ^9-THC	74 ± 16.0	11	68 ± 5.7	39
Δ^8-THC	95 ± 31.8	15	61 ± 2.4	43
9*S*-HHC	113 ± 30.5	12	53 ± 2.3	73
9*R*-HHC	0	N/A	69 ± 2.7	54
Δ^9-THCH	101 ± 29.9	31	72 ± 3.4	171
9*R*-HHCH	0	N/A	86 ± 1.8	85
Δ^9-THCP	0	N/A	45 ± 4.6	52
Δ^9-THC-O	0	N/A	57 ± 2.5	148
9*R*-HHCP	0	N/A	44 ± 3.0	52
9*R*-HHC-O	0	N/A	58 ± 1.7	74
Δ^9-THC-C8	0	N/A	31 ± 4.0	97
Δ^9-THC-OMe	0	N/A	28 ± 2.8	120

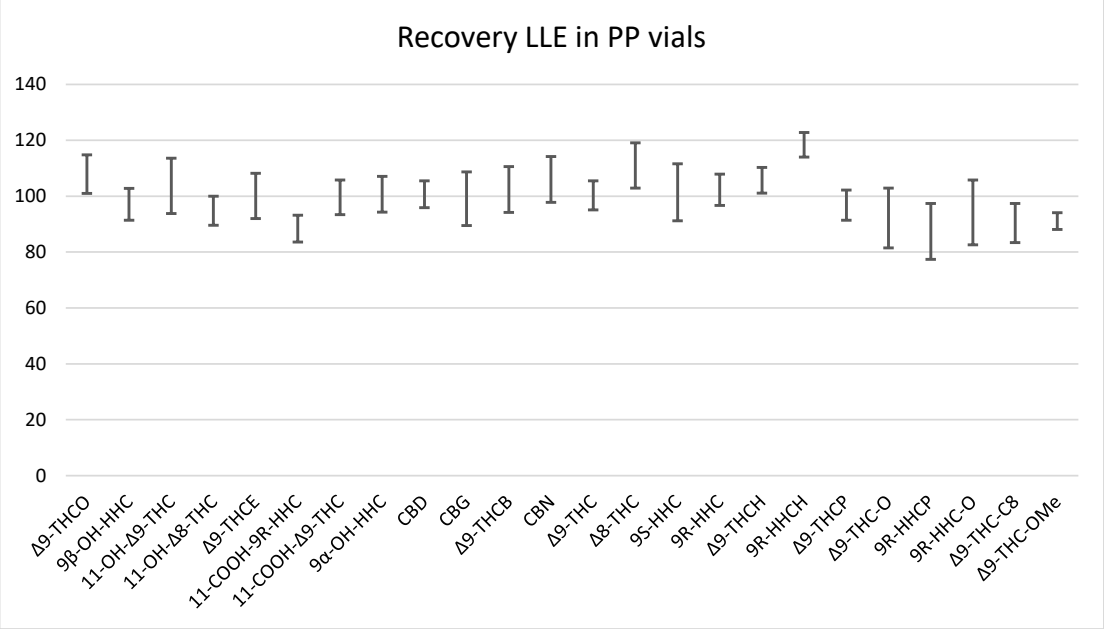

S2: Recovery rates of the analytes included in the screening panel. Analytes were spiked on blank blood and were extracted with a liquid-liquid-extraction (LLE) protocol. The solutions were measured using polypropylene (PP) vials. Recovery rates and error bars were determined from triplicates.

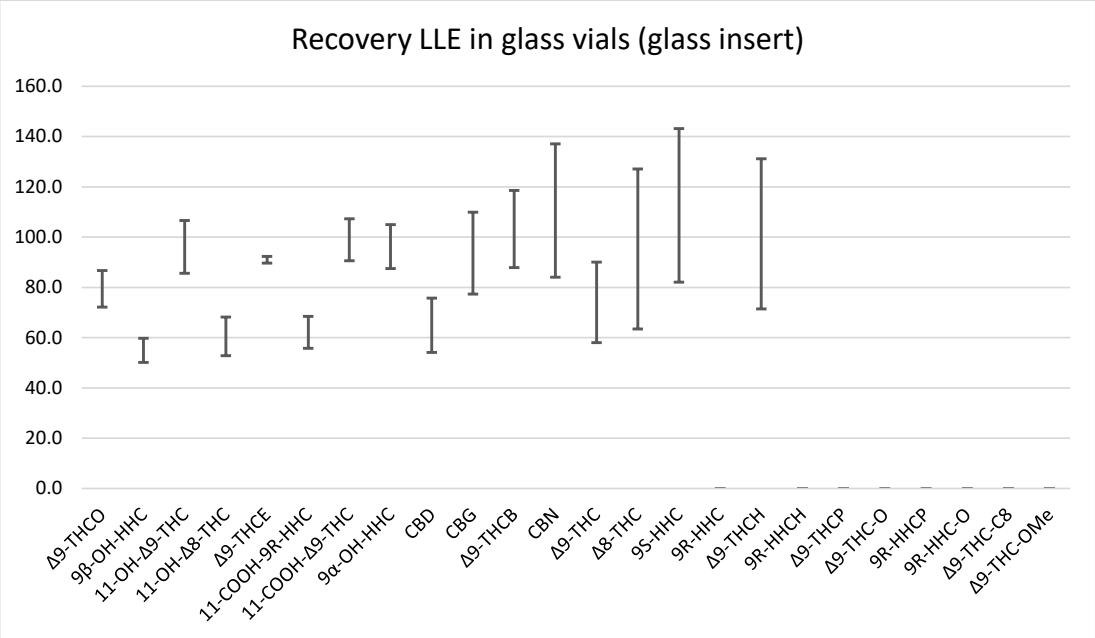

S3: Recovery rates of the analytes included in the screening panel. Analytes were spiked on blank blood and were extracted with a liquid-liquid-extraction protocol. The solutions were measured using glass vials. The recovery rates were in general lower than from PP vials and the late eluting compounds were not detected. Recovery rates and error bars were determined from triplicates.

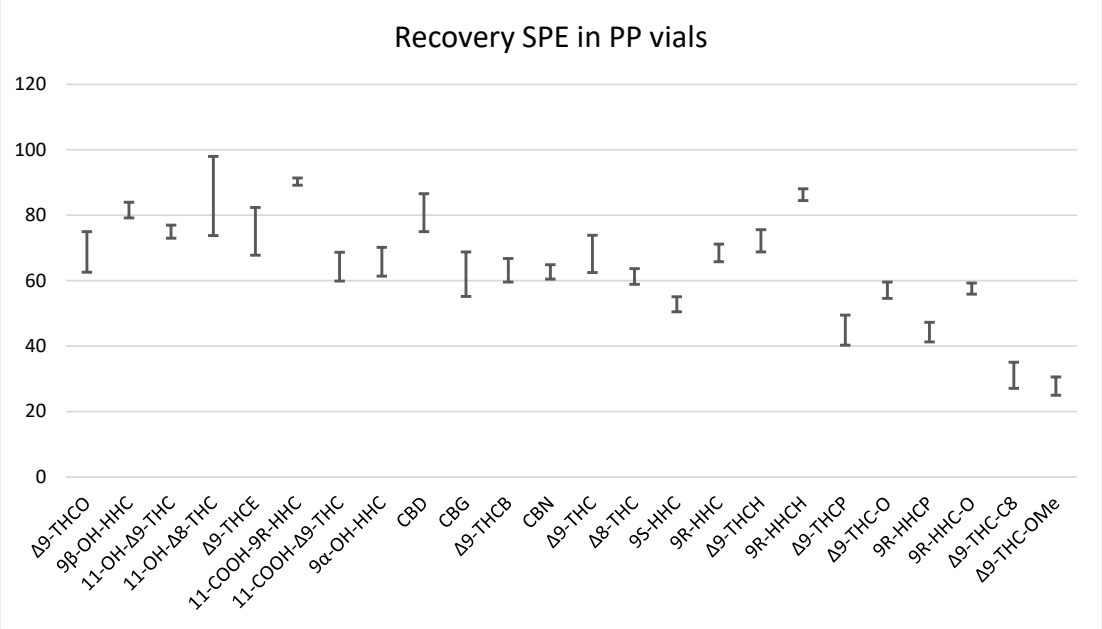

S4: Recovery rates of the analytes included in the screening panel. Analytes were spiked on blank blood and were extracted with a solid-phase-extraction (SPE) protocol. The solutions were measured using PP vials. Recovery rates seem to drop with the lipophilicity of the analytes. Recovery rates and error bars were determined from triplicates.

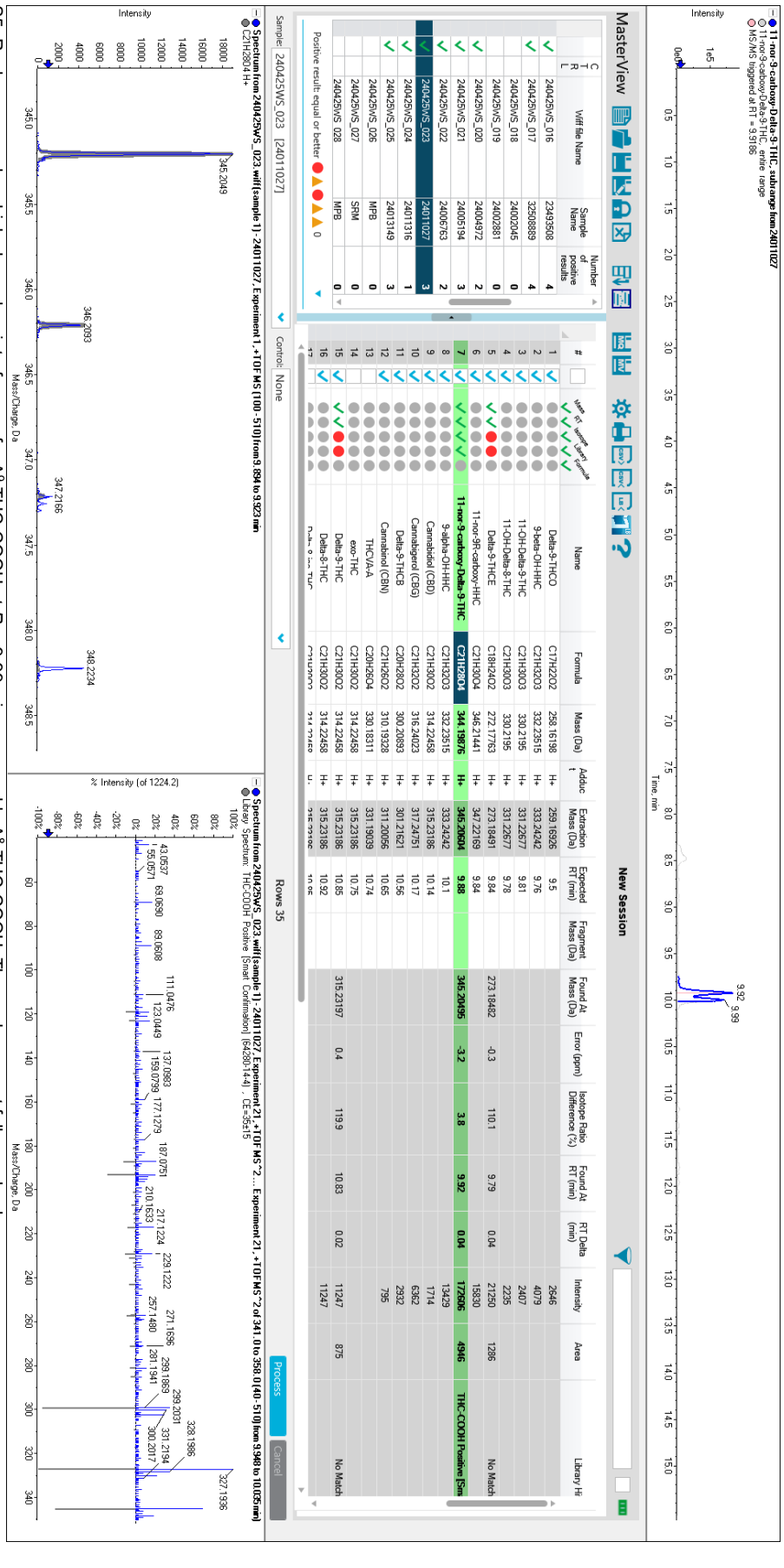

S5: Real case sample, which showed an interference for Δ^9-THC-COOH at R_t = 9.99 min, presumably Δ^8-THC-COOH. The peaks are not fully resolved.

S6: A real case sample with similar amounts of Δ^8-THC and Δ^9-THC. The peaks are not fully resolved.

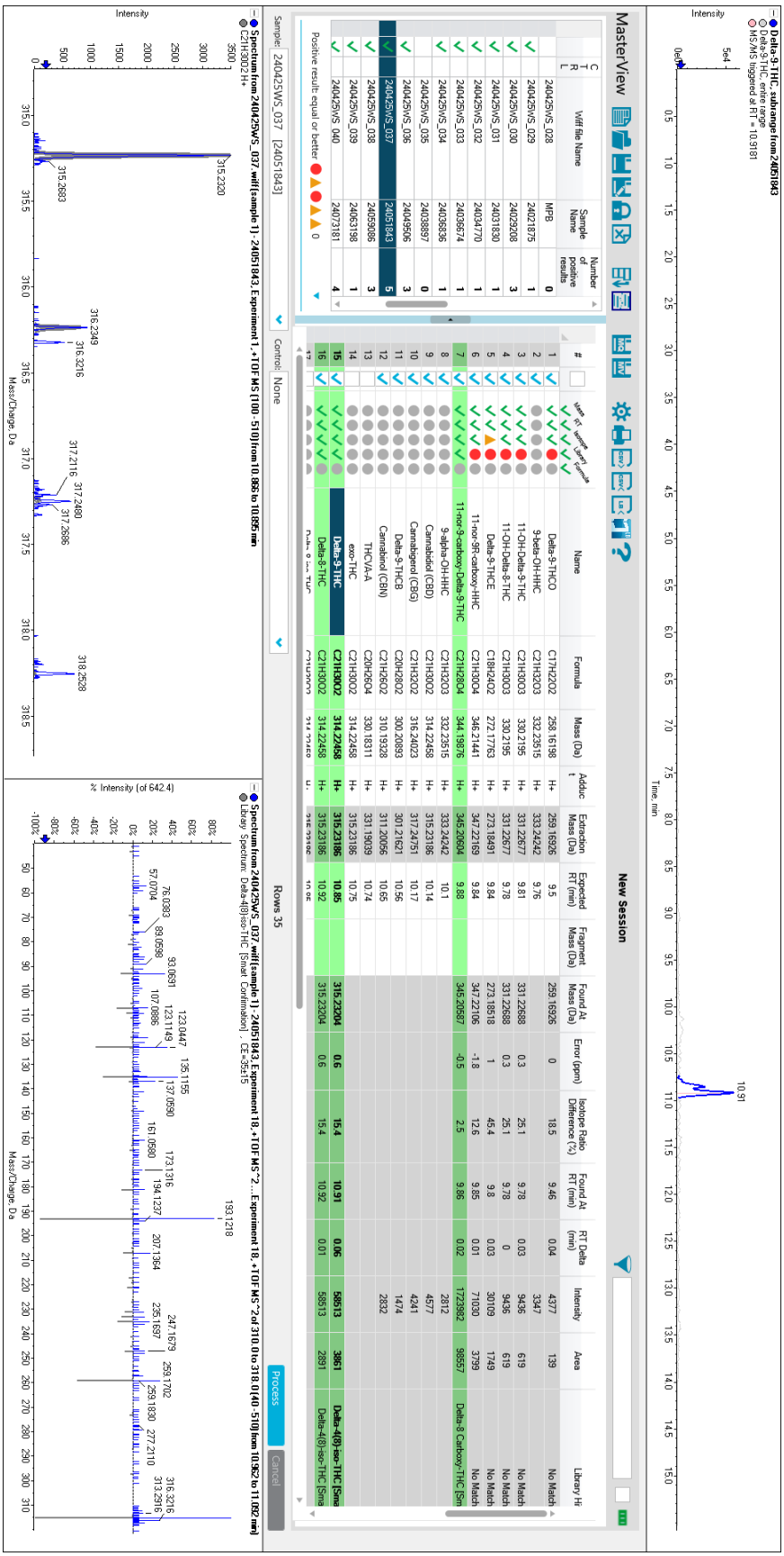

S7: Another real case sample showing more Δ^8-THC than Δ^9-THC. The isomers are not fully resolved.

S8: A real case sample containing HHC. Differentiation between the epimers (9*R*)- and (9*S*)-HHC is not possible as they are coeluting.

Declaration of consent

on the basis of Article 18 of the PromR Phil.-nat. 19

Name/First Name: Schirmer, Willi

Registration Number: 12-477-014

Study program: Chemistry and Molecular Sciences

Bachelor ☐ Master ☐ Dissertation ☑

Title of the thesis: Analytical characterization of semi-synthetic cannabinoids in Forensics: Detection, metabolism and synthetic origin

Supervisor: Prof. Dr. Wolfgang Weinmann
Prof. Dr. Stefan Schürch

I declare herewith that this thesis is my own work and that I have not used any sources other than those stated. I have indicated the adoption of quotations as well as thoughts taken from other authors as such in the thesis. I am aware that the Senate pursuant to Article 36 paragraph 1 litera r of the University Act of September 5th, 1996 and Article 69 of the University Statute of June 7th, 2011 is authorized to revoke the doctoral degree awarded on the basis of this thesis.
For the purposes of evaluation and verification of compliance with the declaration of originality and the regulations governing plagiarism, I hereby grant the University of Bern the right to process my personal data and to perform the acts of use this requires, in particular, to reproduce the written thesis and to store it permanently in a database, and to use said database, or to make said database available, to enable comparison with theses submitted by others.

Bern, 08.09.2025

Place/Date

Signature